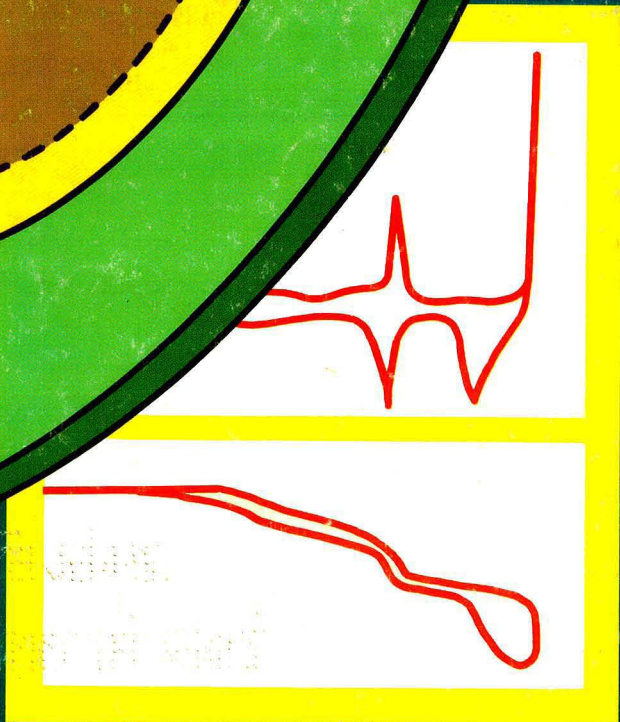
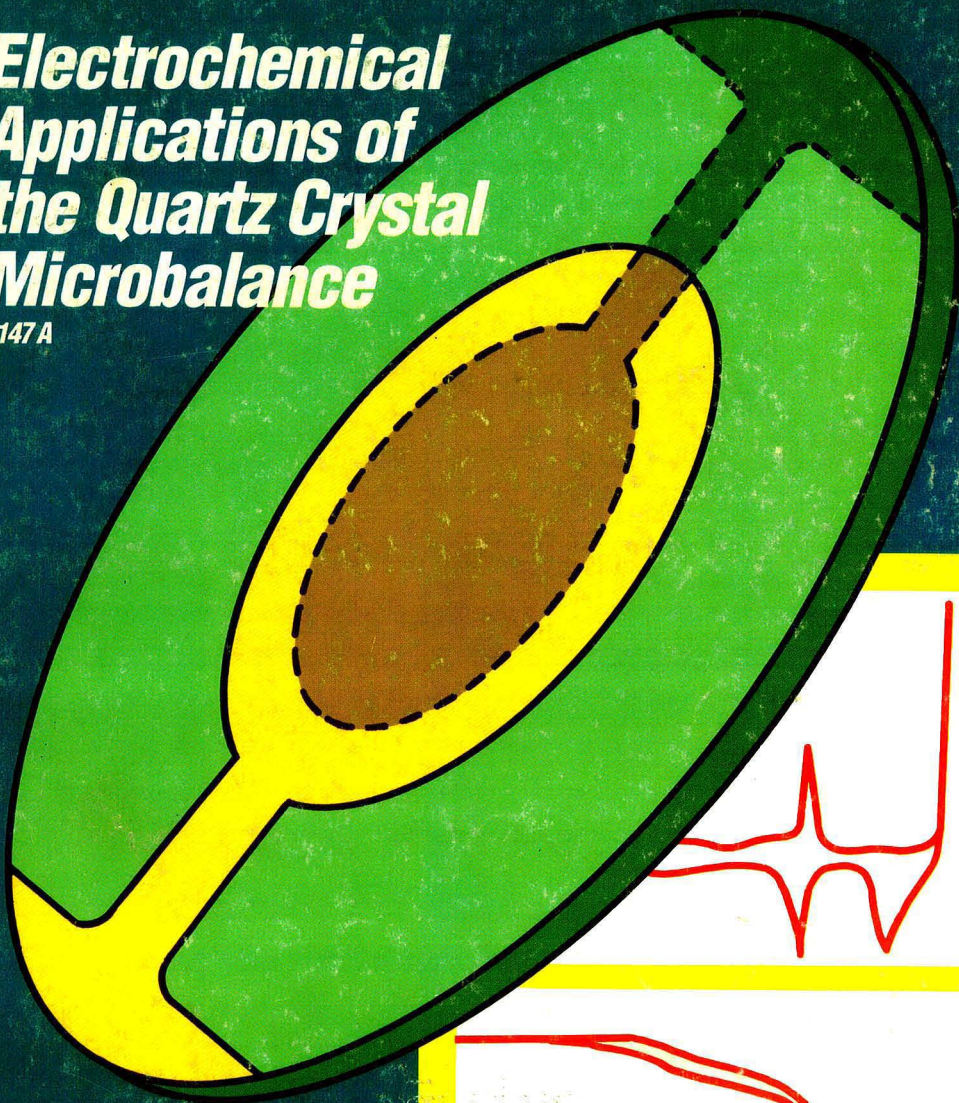


OCTOBER 15, 1989

Analytical CHEMISTRY

Electrochemical Applications of the Quartz Crystal Microbalance

1147A



It's A Dirty Job, But We Can Handle It.

*"The sample is
almost water..."*

*Just a little
dirty...but that's
today's river water
for you...*

*Tomorrow's
samples are in...
Great... Sewage,
sludges and solids.*

*Oh well... my Purge
& Trap system and
I can handle almost
anything."*

Seem familiar?...Very!

Real world samples place tough demands on your equipment. O I Analytical designs and manufactures the most complete line of systems for environmental analyses in the world. Recognizing the fact that sampling and detection systems are intimately coupled has resulted in designing these components to work as a system, not a collection of parts.

Anyone can offer pieces and parts, but O I Analytical provides an entire system backed by field support and on-site repair and training.



Samples:
Water, Sludges,
Soils & Air Tubes

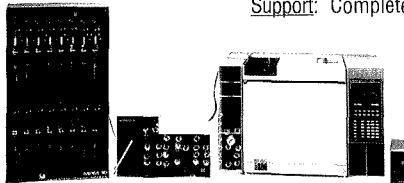
Automation:
16 Sample Discrete
Purging

Concentration:
Quantitative Trapping
Rapid Desorption
Trace Water removal

Separation:
Complete Systems
with the Worlds
Leading GC (HP)

Detection:
4420 Electrolytic Conductivity Detector (ELCD)
4430 Photoionization Detector (PID)
4440 ELCD/PID Tandem (no transfer lines)
4450 PID/FID Tandem (great for fuels analysis)

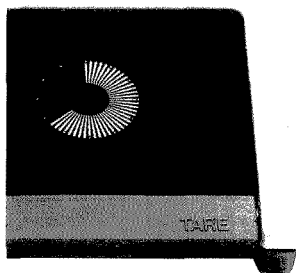
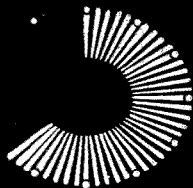
Support: Complete System Support and Training



The real world is full of surprises. Compatibility of Lab Equipment shouldn't be one of them. For the fundamental solution...Call (409) 690-1711

O I Analytical 

CIRCLE 122 ON READER SERVICE CARD



There's nothing like a new dimension to expand your view of the future. METTLER DeltaTrac® shows exactly what we mean.

It adds a unique visual dimension that makes the METTLER PM balance seem light-years ahead of all the rest.

That's because the DeltaTrac display is the fastest way to transmit information from the weighing instrument to the human brain. An automatic tracking device pinpoints precisely where you are in the weighing range — and does it with the speed of sight. No calculations needed.

No other lab balance is so simple to use, yet so advanced it's ready for the labs of tomorrow.

METTLER balances are available only from Fisher Scientific or VWR Scientific.

All products are backed by METTLER Service Plus®. Call 1-800-METTLER for information and put DeltaTrac in your future.

CIRCLE 96 ON READER SERVICE CARD

Mettler Instrument Corporation

Box 71

Hightstown, NJ 08520

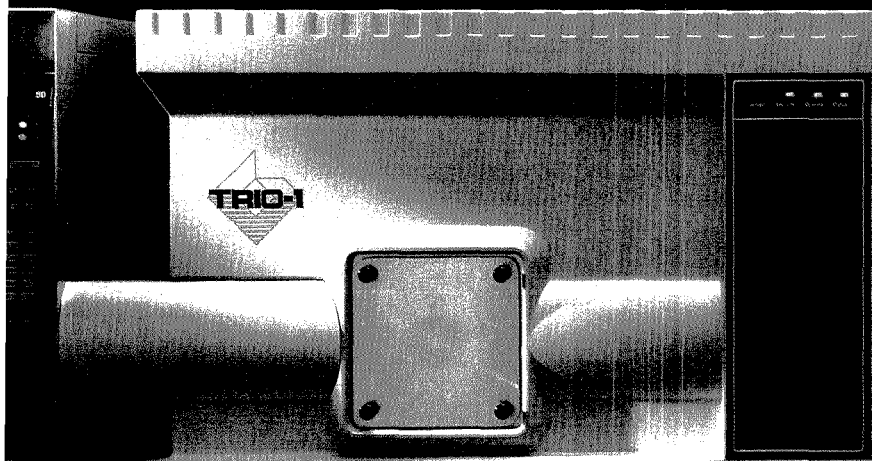
1-800-METTLER

(NJ 1-609-448-3000)

METTLER

We understand.
Precisely.

A Revelation in GC-MS.



The VG Trio-1

For when you've got better things to do...

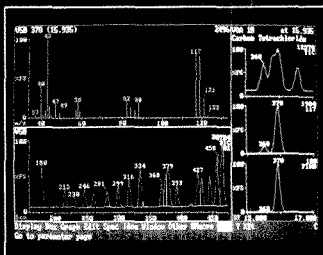
VG are opening the eyes of discerning chemists everywhere to the innovative VG Trio-1, the new standard in Benchtop GC-MS.

Offering unrivalled sensitivity within its class, the VG Trio-1 uses a research grade quadrupole analyser.

In designing the VG Trio-1 we wanted to produce a benchtop instrument with a difference. That's why we included full differential pumping* to ensure quality CI results every time. A first for Benchtop GC-MS.

Software teams working on both sides of the Atlantic have developed data handling facilities guaranteed to delight operators and laboratory managers alike. The VG Trio-1's unique LEARN facility and intelligent instrument control system provides total control of all GC-MS peripherals to guarantee high productivity in your laboratory. Walkaway automation is now a reality!

*Option



The VG Trio-1 'super computer' technology incorporates 32 bit RISC architecture and multiple parallel processing. All this adds up to a speed of data handling previously unheard of in GC-MS.

Open your eyes to these and many more exciting new features of the Trio-1 and you'll soon see why it is a revelation in GC-MS.



VG MASSLAB
automated mass spectrometry

CIRCLE 170 ON READER SERVICE CARD

A VG INSTRUMENTS GROUP COMPANY

UNITED KINGDOM. VG Masslab Ltd, Tudor Road, Altrincham, Cheshire WA14 5RZ, England. Tel: 061-941 3552. Telex: 669964.
USA. VG Instruments Inc, 32 Commerce Center, Cherry Hill Drive, Danvers, Massachusetts 01923. Tel: (617) 777 8024. Telex: 681909.
CANADA. VG Instruments Canada Inc, 5929 Transcanadienne, St. Laurent, Quebec H4T 1A1. Tel: (514) 744 5519. Telex: (5) 824614.
WEST GERMANY. VG Instrumente GmbH, Gustav-Nachtigal-Strasse 4, 6200 Wiesbaden. Tel: (6121) 71060. Telex: 4186556.
FRANCE. VG Instruments, 8 Rue de Mirechal du Latre de Tassigny, 78150 Le Chesnay. Tel: (1) 3955 5120. Telex: 695845.
ITALY. VG Instruments, Viale Dell'Assunta 101, 20083 Cerussico Sul Naviglio, Milano. Tel: (2) 924 2838. Telex: 340947.
THE NETHERLANDS. VG Instruments BV, PO Box 171, 1380 AD Weesp. Tel: (2940) 80484. Telex: 12097.
CHINA. VG Instruments, Room 7058, Xi Yuan Hotel, Erigoou, Xijiao, Beijing. Tel: 890721 Ext. 759. Telex: 222453.
HONG KONG. VG Instruments Asia Limited, 2404 Dominion Centre, 24/F, 43/59 Queens Road East. Tel: (5) 9612651. Telex: 62038.
KOREA. VG Instruments Korea Limited, Dongri Building, 58-5 Nonhyun-dong, Kangnam-Ku, Seoul. Tel: (01) 948 2883. Telex: 28523.
JAPAN. Jisco International Co. Ltd, 2-4-21 Senni-cho, Hachioji-City, Tokyo 193. Tel: 42686 1321. Telex: 2882515.

Registered in U.S. Patent and Trademark Office;
Copyright 1989 by the American Chemical Society

ANALYTICAL CHEMISTRY (ISSN 0003-2700) is published semimonthly by the American Chemical Society at 1155 16th St., N.W., Washington, DC 20036. Editorial offices are located at the same ACS address (202-872-4570; FAX 202-872-6325; TDD 202-872-8733). Second-class postage paid at Washington, DC, and additional mailing offices. Postmaster: Send address changes to ANALYTICAL CHEMISTRY Member & Subscriber Services, P.O. Box 3337, Columbus, OH 43210.

Claims for missing numbers will not be allowed if loss was due to failure of notice of change of address to be received in the time specified; if claim is dated (a) North America: more than 90 days beyond issue date, (b) all other foreign: more than one year beyond issue date, or if the reason given is "missing from files."

Copyright Permission: An individual may make a single reprographic copy of an article in this publication for personal use. Reprographic copying beyond that permitted by Section 107 or 108 of the U.S. Copyright Law is allowed, provided that the appropriate per-copy fee is paid through the Copyright Clearance Center, Inc., 27 Congress St., Salem, MA 01970. For reprint permission, write Copyright Administrator, Publications Division, ACS, 1155 16th St., N.W., Washington, DC 20036. **Registered names and trademarks, etc.,** used in this publication, even without specific indication thereof, are not to be considered unprotected by law.

Advertising Management: Centcom, Ltd., 500 Post Rd. East, Westport, CT 06880 (203-226-7131)

1989 subscription rates include air delivery outside the U.S., Canada, and Mexico

Members	1 yr	2 yr
Domestic	\$ 27	\$ 45
Canada and Mexico	56	103
Europe	83	157
All Other Countries	120	231
Nonmembers		
Domestic	49	83
Canada and Mexico	78	141
Europe	155	280
All Other Countries	192	354

Three-year and other rates contact: Member & Subscriber Services, ACS, P.O. Box 3337, Columbus, OH 43210 (614-447-3776 or 800-333-9511).

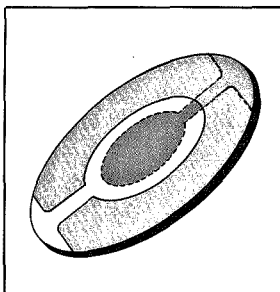
Subscription orders by phone may be charged to VISA, MasterCard, Barclay card, Access, or American Express. Call toll free 800-ACS-5558 in the continental United States; in the Washington, DC, metropolitan area and outside the continental United States, call 202-872-8065. Mail orders for new and renewal subscriptions should be sent with payment to the Business Management Division, ACS, P.O. Box 57136, West End Station, Washington, DC 20037.

Subscription service inquiries and changes of address (include both old and new addresses with ZIP code and recent mailing label) should be directed to the ACS Columbus address noted above. Please allow six weeks for change of address to become effective.

ACS membership information: Lorraine Bowlin (202-872-4567)

Single issues, current year, \$7.00 except review issue and LabGuide, \$12.00; **back issues and volumes and microform editions** available by single volume or back issue collection. For information or to order, call 800-ACS-5558 or write the Microform & Back Issues Office at the Washington address.

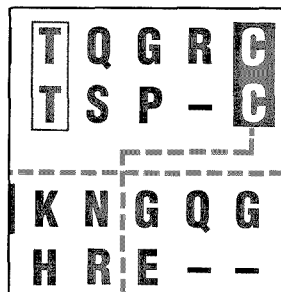
Nonmembers rates in Japan: Rates above do not apply to nonmember subscribers in Japan, who must enter subscription orders with Maruzen Company Ltd., 3-10 Nihonbashi 2-chome, Chuo-ku, Tokyo 103, Japan. Tel: (03) 272-7211.



REPORT

1147 A

On the cover. Quartz crystal microbalances are mass-sensitive detectors based on an oscillating quartz wafer. Mark R. Deakin of Florida State University and Daniel A. Buttry of the University of Wyoming discuss the theory and electrochemical applications of these devices



ANALYTICAL APPROACH

1173 A

The odyssey of angiogenin. Angiogenin induces blood vessel growth and is important in the process by which cells aggregate, differentiate, and form discrete tissues and organs. James F. Riordan and colleagues at Harvard Medical School describe their efforts to isolate and sequence this protein

BRIEFS

1128 A

EDITORS' COLUMN

1135 A

Readers are given a synopsis of ANALYTICAL CHEMISTRY's present-day editorial operation

NEWS

1145 A

Applicants and participants sought for 1990 Summer Internship Program. ▶ High-flying launch for small satellite

MEETINGS

1159 A

Conferences. ▶ Short courses

BOOKS

1161 A

Critical reviews. Recently released books on materials characterization, quadrupole storage mass spectrometry, Auger electron spectroscopy, preparative-scale chromatography, and HPLC are reviewed

FOCUS

1167 A

What happened to the ozone layer? From the ground, in the air, and above via satellite, the Earth's protective ozone layer is being thoroughly mapped and analyzed. An armada of analytical equipment and techniques has established that human activity has triggered a dramatic springtime drop in the ozone levels over Antarctica

NEW PRODUCTS & MANUFACTURERS' LITERATURE

1170 A

AUTHOR INDEX

2225

Articles

High-Sensitivity Peptide Mapping by Capillary Zone Electrophoresis and Microcolumn Liquid Chromatography, Using Immobilized Trypsin for Protein Digestion 2226

The use of immobilized trypsin makes it possible to reproducibly digest as little as 50 ng of protein, representing a decrease in sample size of ~3 orders of magnitude. Microcolumn HPLC and CZE can separate 100 ng and 2 ng of digested β -casein, respectively.

Kelly A. Cobb and Milos Novotny*, Department of Chemistry, Indiana University, Bloomington, IN 47405

Diffusion Coefficients of Gases in Liquids and Partition Coefficients in Gas-Liquid Interphases by Reversed-Flow Gas Chromatography 2231

The diffusion coefficients measured have the same order of magnitude as those calculated by using the Wilke-Chang formula. The partition coefficients allow the concentration to be calculated near the interphase.

N. A. Katsanos* and J. Kopolos, Physical Chemistry Laboratory, University of Patras, 26110 Patras, Greece

Determination of Trace Impurities in High-Purity Oxygen by Gas Chromatography with Photoionization Detection 2237

A simple and accurate GC system for the determination of parts-per-billion levels of Ar, N₂, Kr, CH₄, and Xe is described.

Hiroshi Ogino*, Yoko Aomura, Masatsugu Komuro, and Tetsu Kobayashi, Technical Research Laboratory, Toyo Sanso Co., Ltd., 3-3, Mizue-cho, Kawasaki-ku, Kawasaki-shi, Kanagawa 210, Japan

Conditions for Detecting Overlapped Peaks with Principal Component Analysis in Hyphenated Chromatographic Methods 2240

Simulated and real data are analyzed to illustrate a method that estimates the net signal determined from principal component analysis. The effects of relative concentration, spectral similarity, and chromatographic resolution are considered.

Paul J. Gemperline*, Department of Chemistry, East Carolina University, Greenville, NC 27858 and J. Craig Hamilton, Shared Research Resource Laboratories, School of Medicine, East Carolina University, Greenville, NC 27858

Determination of Selenium in Human Blood by High-Performance Liquid Chromatography with Fluorescence Detection 2244

Se in blood is determined as the diamiononaphthalene derivative using fluorescence HPLC. The method provides a 0.15-ng detection limit, a between-day standard deviation of 1% at the 20-ng level, and a 3% within-day standard deviation at the 1-ng level.

Garry J. Handelman, Chemistry Department, University of California, Santa Cruz, CA 95064, Paula Kosted, Chemistry Department, Montana State University, Bozeman, MT 59717, Sara Short, SRI International, Menlo Park, CA 94025, and Edward A. Dratz*, Chemistry Department, Montana State University, Bozeman, MT 59717

Theory of Cyclic Staircase Voltammetry for Electrode Kinetics 2249

Comprehensive working curves are presented for cyclic staircase voltammetry for the case of heterogeneous charge-transfer kinetics.

Mary M. Murphy, John J. O'Dea, Dieter Arn, and Janet G. Osteryoung*, Department of Chemistry, State University of New York at Buffalo, Buffalo, NY 14214

Long-Term Stability of Solid Standards for Radiochemical Analysis 2255

Analysis of natural and synthetic spiked -200 mesh solid standards shows no fractionation of the different-sized particles after standing undisturbed for five years. The RSD of the individual measurements is 0.2-1%.

Claude W. Sill, Idaho National Engineering Laboratory, EG&G Idaho, Inc., Idaho Falls, ID 83415

Electrocatalysis and Detection of Amino Sugars, Alditols, and Acidic Sugars at a Copper-Containing Chemically Modified Electrode 2258

A chemically modified glassy carbon electrode containing a crystalline Cu/Cl deposit electrocatalytically oxidizes various polyhydroxyl compounds. When used for constant potential detection in flow systems, the electrodes permit quantitation at subnanomole levels.

Sunil V. Prabhu and Richard P. Baldwin*, Department of Chemistry, University of Louisville, Louisville, KY 40292

Determination of Osmium and Osmium Isotope Ratios by Microelectrothermal Vaporization Inductively Coupled Plasma Mass Spectrometry 2263

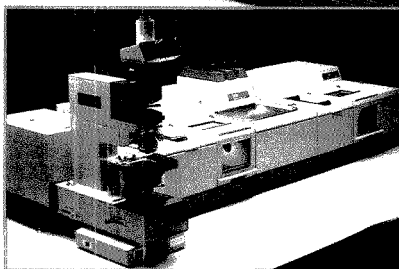
Os vaporized by a miniature heater in a merging chamber is analyzed by ICP/MS. Precision is better than 3%, and the detection limit is <100 fg.

Takafumi Hirata, Tasuku Akagi, Hiroshi Shimizu, and Aki-masa Masuda*, Department of Chemistry, Faculty of Science, The University of Tokyo, Hongo 113, Tokyo, Japan

* Corresponding author

Discover FT-IR 800

The new Nicolet System 800 shapes the future of FT-Spectroscopy



The System 800 represents the new generation in research tools. It is the synthesis of advances in optical, electronic and mechanical design. The System 800 combines an ultra-stable interferometer design with a unique dynamic alignment system, for superior data throughout the spectral range.

The System 800 provides the stability, signal-to-noise performance, and repeatability required for demanding applications. Whether your experiments involve long-term data acquisitions or rapid short-term dynamic spectroscopy applications, the 800 has the capabilities to solve your problems with confidence.

The System 800 incorporates the features demanded by leading research investigators throughout the world. Standard features include optical bench

communications, optical bench configuration monitoring and status, rapid spectral range conversion, ultra-quiet electronics train, highest throughput optical design, dynamic alignment, fully expandable optical path, ultra high-output sources, and simplified experimental design for multiple modulation techniques.

The System 800 supports the full range of experiments including FT-Raman, Emission, Microspectroscopy, GC/FT-IR, SFC/FT-IR, and more. Multiple beam paths allow several different experiments or applications to be configured simultaneously.

Nicolet sets the standard for research performance. Let us show you the future of FT-Spectroscopy.

Nicolet
INSTRUMENTS OF DISCOVERY

Belgium: 02-762-2511
Canada: 416-625-8302

France: 1-30-81-3081
Germany: 069-837001

Japan: 06-863-1550
Netherlands: 03403-74754

Switzerland: 056-834545
United Kingdom: 0926-494111

Nicolet Analytical Instruments / 5225-1 Verona Rd. / Madison, WI 53711 / (608) 271-3333 / FAX: (608) 273-5046

To complement these direct Nicolet offices, Nicolet maintains a network of representatives in countries throughout the world.

CIRCLE 110 ON READER SERVICE CARD

Photoreduction Fluorescence Detection of Quinones in High-Performance Liquid Chromatography 2267

A postcolumn photochemical reaction scheme provides sensitive (low-picogram range) and selective detection of anthraquinone and naphthoquinone derivatives. The anaerobic photoreduction reaction does not require the addition of any reagents to the eluent stream.

James R. Poulsen and John W. Birks*, Department of Chemistry and Biochemistry and Cooperative Institute for Research in Environmental Sciences (CIRES), Campus Box 449, University of Colorado, Boulder, CO 80309

Quantitative Analysis in the Presence of Spectral Interferents Using Second-Order Nonbilinear Data 2277

The abilities of nonbilinear rank annihilation, curve resolution, and multiple linear regression for quantitation in the presence of spectral interferents are compared.

Bruce E. Wilson and Bruce R. Kowalski*, Laboratory for Chemometrics, Department of Chemistry, BG-10, University of Washington, Seattle, WA 98195

Visible Semiconductor Laser Fluorometry 2285

The detection limit of rhodamine 800 is 4×10^{-12} M. After covalent bonding to Nile blue or oxazine 750 with water-soluble carbodiimide, albumin protein is determined.

Totaro Imasaka, Atsushi Tsukamoto, and Nobuhiko Ishibashi*, Faculty of Engineering, Kyushu University, Hakozaki, Fukuoka 812, Japan

Laser Fluorometric Detection of Porphyrin Methyl Esters for High-Performance Thin-Layer Chromatography 2288

The 488-nm visible line of an Ar-ion laser is used as the excitation source for the detection of porphyrins in human urine. Detection limits are ~ 2 orders of magnitude better than those obtained using TLC plates.

Carmen W. Huie* and William R. Williams, Department of Chemistry, State University of New York, Binghamton, NY 13901

Radio Frequency Plasma Detector for Sulfur Selective Capillary Gas Chromatographic Analysis of Fossil Fuels 2292

The detector is linear and selective, and has a detection limit of 0.5 pg/s. The large quantity of coeluting hydrocarbons causes little quenching in the analysis of sulfur heterocycles from coal extracts and petroleum distillates.

R. J. Skelton, Jr., H.-C.K. Chang, P. B. Farnsworth, K. E. Markides, and M. L. Lee*, Department of Chemistry, Brigham Young University, Provo, UT 84602

Analysis of Two-Dimensional Nuclear Magnetic Resonance Spectra with Relayed Proton-Proton-Carbon Magnetization Transfer: A Step toward Automated Structure Elucidation 2298

Automated analysis of 2D NMR spectra correlating the chemical shifts of carbon-13 atoms with those of neighboring and remote protons yields connectivity matrices that facilitate spectral interpretation and recognition of molecular structures.

Urs Eggenberger and Geoffrey Bodenhausen*, Section de Chimie, Université de Lausanne, Rue de la Barre 2, CH-1005 Lausanne, Switzerland

Fiber-Optic Dipping Sensor for Organic Solvents in Wastewater 2306

Triphenyl methane dyes, in conjunction with permeable membranes, are used as optical sensors to detect organic solvents and ammonia in wastewater. A detection limit as low as 30 ppm is possible under favorable conditions.

F. L. Dickert* and S. K. Schreiner, Institute of Physical and Theoretical Chemistry, Erlangen University, Egerlandstrasse 3, D-8520 Erlangen, FRG and **G. R. Mages and Heinz Kimmel**, Siemens AG, Central Research and Development, ZFE F1 AMF 3, Paul-Gossen-Strasse 100, D-8520 Erlangen, FRG

Quantitative Estimation of Component Amplitudes in Multiexponential Data: Application to Time-Resolved Fluorescence Spectroscopy 2310

The individual component contributions to multiexponential data are estimated by a reiterative, linear least-squares algorithm, and the amplitude uncertainties are predicted from first principles.

A. L. Wong and J. M. Harris*, Department of Chemistry, University of Utah, Salt Lake City, UT 84112

Ion Trap Tandem Mass Spectrometry of Tryptamine. Tissue Extracts and Isotope Dilution Using Combined Radio Frequency and Direct Current Voltages 2316

RF/DC is needed for the determination of tryptamine in crude tissue extract and for isotope dilution analysis. An RSD of 10% is obtained at the 2-ng level.

R. J. Strife* and J. R. Simms, Corporate Research Division, Miami Valley Laboratories, The Procter & Gamble Company, P.O. Box 398707, Cincinnati, OH 45239-8707

Ionspray Mass Spectrometry/Mass Spectrometry: Quantitation of Tributyltin in a Sediment Reference Material for Trace Metals 2320

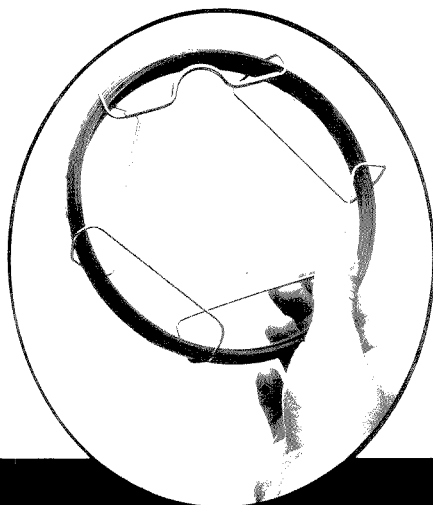
Tributyltin is determined by using flow injection into an ionspray tandem mass spectrometer. The detection limit is about 5 pg Sn absolute or 0.2 μ g Sn/g sediment.

K. W. M. Siu*, G. J. Gardner, and S. S. Berman, Division of Chemistry, National Research Council of Canada, Montreal Road, Ottawa, Ontario, Canada K1A 0R9

Now . . .

You Can Separate Complex Hydrocarbon Mixtures and Get . . .

- High Resolution
- High Efficiency
- Reproducibility



Our *Petrocol™ DH Column* is specifically designed and tested for detailed GC hydrocarbon analysis. You can separate closely eluting isomers and light hydrocarbon gases, or achieve detailed separations of highly complex mixtures.

Each 100M fused silica column is rigorously tested to ensure highly consistent polarity and film thickness. This testing includes retention index

measurements of key aromatic compounds (retention index tables are included with each column). Now you can be assured of consistent column-to-column performance.

For more information, call our Technical Service Department at 814-359-3041 and ask for our new *Petroleum/Chemical Applications Guide*.

Fused silica columns manufactured under HP US Pat. No. 4,293,415.

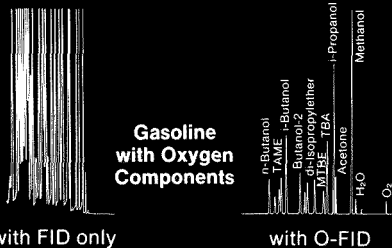
To Order, Call: 800-247-6628

TWX: 510-670-3600 FAX: 814-359-3044

CIRCLE 150 ON READER SERVICE CARD

 **SUPELCO**
SEPARATIONS TECHNOLOGIES GROUP
DIVISION OF ROHM AND HAAS

Selective Determination of Oxygen Components in Complex Mixtures



A Siemens SiCHROMAT® G.C. with Oxygen Specific (O-FID) Detector Makes it Simple

- Selectively determine oxygenates without difficult, time consuming, and expensive analysis
- Sensitivity <math><60 \text{ pg/sec}</math> — selectivity - Ideal for quantification of fuel additives or oxygen components in flavors, fragrances, and plastics

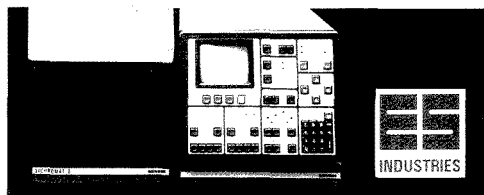
Introducing the Siemens SiCHROMAT Gas Chromatograph with O-FID Detector available exclusively in the U.S. from ES Industries.

For more information and/or to arrange for a demonstration call 1-800/356-6140, in NJ 609/983-3616 or write: 8 S. Maple Avenue, Marlton, NJ 08053.



ES INDUSTRIES

Expanding the Parameters of Gas Chromatography for Chromatographers



CIRCLE 40 ON READER SERVICE CARD

BRIEFS

Correspondence

Selectivity of Stearate-Modified Carbon Paste Electrodes for Dopamine and Ascorbic Acid 2323

Paul D. Lyne and Robert D. O'Neill*, Chemistry Department, University College Dublin, Belfield, Dublin 4, Ireland

Estimating Error Limits in Parametric Curve Fitting 2324

Marco S. Caceci, CEA-DRDD/SESD, B.P. 6, F-92265 Fontenay-aux-Roses Cedex, France

Technical Notes

Room-Temperature Phosphorescence of Polynuclear Aromatic Hydrocarbons on Matrix-Modified Solid Substrates 2328

L. M. Perry, A. D. Campiglia, and J. D. Winefordner*, Department of Chemistry, University of Florida, Gainesville, FL 32611

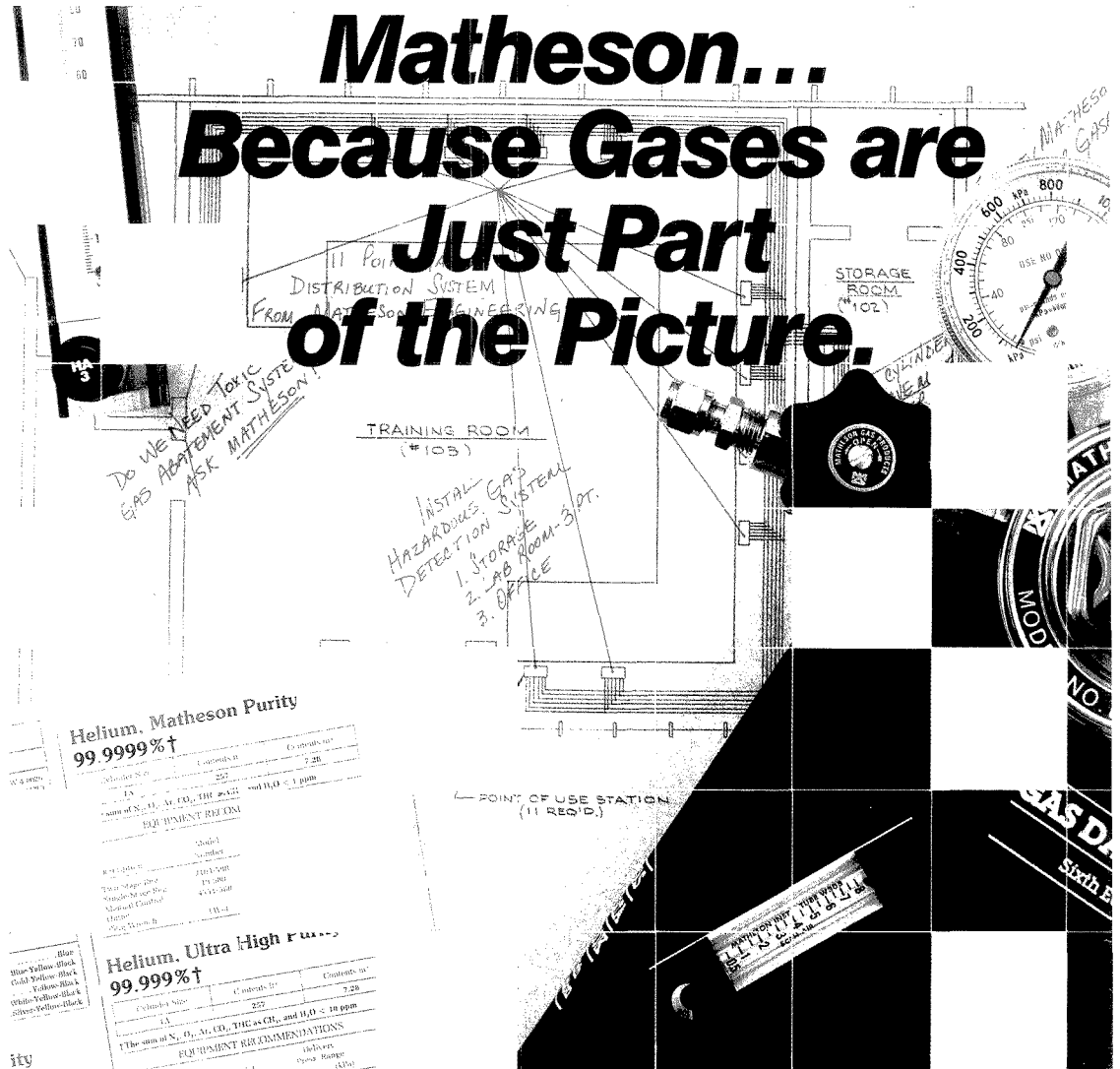
Apparatus for the Fabrication of Poly(chlorotrifluoroethylene) Composite Electrodes 2330

Jeffrey E. Anderson*, Dale Hopkins, John W. Shadrick, and Yee Ren, Department of Chemistry, Murray State University, Murray, KY 42071-3306

Hollow Fiber Membrane Probes for the in Situ Mass Spectrometric Monitoring of Nitrogen Trichloride Formation during Wastewater Treatment 2332

P. J. Savickas*, M. A. LaPack, and J. C. Tou, The Dow Chemical Company, Analytical Sciences, 1897 Building, Midland, MI 48667

Matheson... Because Gases are Just Part of the Picture.



Helium, Matheson Purity
99.9999% †

Cylinder Size	Contents, lb	Duration, hr
1A	257	7.26

†The sum of N₂, O₂, Ar, CO₂, H₂O, and H₂ ≤ 1 ppm

EQUIPMENT RECOMMENDATIONS

Model	Capacity
200	100
200	100
200	100
200	100

Helium, Ultra High Purity
99.999% †

Cylinder Size	Contents, lb	Duration, hr
1A	257	7.26

†The sum of N₂, O₂, Ar, CO₂, H₂O, and H₂ ≤ 10 ppm

EQUIPMENT RECOMMENDATIONS

Model	Capacity
200	100
200	100
200	100
200	100

You know Matheson as the pioneer in specialty gases; the reliable supplier of over 90 different gases in a variety of purities and sizes to suit your application.

But, did you know that Matheson offers you much more to meet today's laboratory requirements for increased efficiency and safety? Matheson engineers can provide you with gas distribution systems, hazardous gas detection instrumentation and toxic waste abatement systems customized to meet your lab's need.

Gases cannot be used alone. You need the right

Gas Distribution Systems,
select Reader Service No. 100

Toxic Waste Abatement,
select Reader Service No. 101

Gas Detection,
select Reader Service No. 102

Gases,
select Reader Service No. 103

regulators, flowmeters and other equipment to handle them properly. To select or install the right equipment to achieve maximum effectiveness, the exclusive full service back-up of Matheson is required.

Get the whole picture. Contact your Matheson office or use the Reader Service Numbers below.

Matheson[®]

World Leader in Specialty Gases & Equipment
30 Seaview Drive, Secaucus, NJ 07096-1587

Regulators,
select Reader Service No. 104

Flowmeters,
select Reader Service No. 105

Gas Handling Equipment,
select Reader Service No. 106

Publications,
select Reader Service No. 107

Maximum performance in a minimum of space

The new 701 KF Titrino

Even Karl Fischer would have been impressed...

The 701 KF Titrino is barely larger than this page. It is the most compact unit of its kind. This saves you expensive laboratory space. On the other hand no expense has been spared with regard to performance.

New features allow major advances...

Our newly developed control method allows extremely rapid, yet highly precise water determinations. The new drift criterion for improved endpoint recognition is largely responsible for this. The instrument is optimised for operation with any KF reagent.

Overflowing with technical refinements...

An RS 232 interface is standard, as are connections for a balance, printer and pen recorder. As a KF work station under computer control, the KF Titrino is just as flexible as it is in «stand-alone» operation. Talking of improved communication, the KF Titrino speaks English, deutsch, français and español. Olé.

KF water determination — quite simply with Metrohm

rinkmann

STRUMENTS, INC.
Montague Rd., Westbury, New York 11590
(516) 334-7500 (800) 645-3050

 **Metrohm**
Measurement in Chemistry
Worldwide with Metrohm

METROHM Ltd.
CH-9101 Herisau Switzerland
Phone 071 / 53 11 33
Telefax 071 / 52 11 14
Telex 88 27 12 metr ch

CIRCLE 96 ON READER SERVICE CARD



Publishing in ANALYTICAL CHEMISTRY

ANALYTICAL CHEMISTRY is unique because of the nature of the discipline of analytical chemistry, which consists of both the development and use of measurement techniques and the underlying science. The JOURNAL appeals to a broad audience; the readership is estimated to be about 105,000 and consists of those scientists who are involved in the basic research of measurement science as well as those who use analytical methodology to solve their measurement problems.

Most scientific journals currently serve only a research-oriented community. However, ANALYTICAL CHEMISTRY historically has attempted to meet the needs of two communities: the research-oriented and the applications-oriented. The origins of ANALYTICAL CHEMISTRY can be traced to the *Journal of Analytical and Applied Chemistry*, which merged with *JACS* in 1893. Analytical chemistry papers were published in *JACS* until 1907, when ACS began publication of the *Journal of Industrial and Engineering Chemistry*. This was divided into three editions (Industrial, Analytical, and News) in 1929. The *Analytical Edition*, which already had much in common with the current JOURNAL, became a separate publication in 1947 known as ANALYTICAL CHEMISTRY, and continued under the editorship of Walter Murphy. Over the years, the JOURNAL has flourished under the guidance of Murphy (1929–56), Lawrence Hallett (1956–65), Herbert Laitinen (1966–79), and George Morrison (1980 to the present).

Central to the goal of ANALYTICAL CHEMISTRY is a commitment to provide readers with the highest quality scientific information available as rapidly as possible. A critical reviewing process is used to ensure the quality of material published. Several thousand individuals are involved in the peer review of manuscripts submitted for consideration to ANALYTICAL CHEMISTRY. These individuals act as expert

consultants to the Editors, who are fully responsible for all material published. In addition, an Advisory Board, whose 16 members serve staggered three-year terms, is chosen by the Editor to provide input into the JOURNAL's operation. Members are chosen to represent various constituent groups in the research and reader communities. Although the Editors seek advice and help from individuals in the scientific community and from advisory groups, it is ultimately the Editor's responsibility to provide editorial direction and set editorial policy. Decisions normally are made based on a consensus of the Associate Editors and the Washington staff Editors.

The editorial offices of ANALYTICAL CHEMISTRY are located at ACS headquarters in Washington, DC. The Washington editorial staff works closely with the Editors on all aspects of the JOURNAL's editorial operation.

The Associate Editors of ANALYTICAL CHEMISTRY

In 1985 ANALYTICAL CHEMISTRY appointed Associate Editors to further improve the peer review system. These individuals, selected for their technical knowledge of various subdisciplines of analytical chemistry, are assigned manuscripts based on their areas of expertise. Each receives a weekly list of manuscripts received in the editorial office and the Associate Editor in charge. On overlapping areas, two Associate Editors are often involved in the editorial process. In addition, if an Associate Editor sees a manuscript on the list that has been assigned to another Associate Editor and wishes to have some input, (s)he simply informs the Associate Editor who has been given primary responsibility for the manuscript. The Editor/Associate Editors all have as much involvement as they wish in the peer review of manuscripts not directly assigned to them.

When an Editor/Associate Editor

submits a manuscript, the Editor is considered an author and not an editor. (S)he is not involved in any way with the peer review process; another Editor/Associate Editor handles the review and final disposition of the manuscript. The Editor/Associate Editors cannot examine the manuscript/reviewer records in the databases for their own papers.

How peer review of the technical section operates

Staff Editors in the Washington office are responsible for guiding manuscripts through the peer review process from the time of submission to acceptance or rejection. Once a manuscript is accepted, the Columbus editorial offices assume responsibility for the edit-

Editor

George H. Morrison
Cornell University

Associate Editors

Klaus Biemann, Massachusetts
Institute of Technology
(mass spectrometry)
Georges Guiochon, University of
Tennessee (separations)
Walter C. Herlihy, Repligen
(analytical biotechnology)
Robert A. Osteryoung, SUNY-Buffalo
(electroanalytical chemistry)
Edward S. Yeung, Iowa State University
(spectroscopy)

Washington Editorial Staff

Managing Editor

Sharon G. Boots

Associate Editors

Louise Vores, Mary Warner

Assistant Editors

Grace K. Lee, Alan R. Newman

Editorial Assistant

Felicia Wach

ing and typesetting. The publication is printed at Mack Printing Company in Easton, PA.

Washington staff Editors hold twice-weekly meetings to discuss all newly submitted manuscripts. They consult with the appropriate Editor/Associate Editors to determine the suitability of each manuscript for publication in ANALYTICAL CHEMISTRY. The Editor/Associate Editors, located throughout the United States, maintain daily contact with the Washington office by phone, FAX, and Federal Express. About 10% of the manuscripts are considered unsuitable and are returned to the authors without further review. The remaining 90% of the newly submitted manuscripts are handled jointly by a staff Editor and the appropriate Editor/Associate Editor.

Reviewers are selected by the Washington-based staff Editor, who frequently consults with the Editor/Associate Editor. Selection is based on the subject matter of the paper, the experts available in a given area, and our experience with the previous performance of the reviewer. References in the manuscript often provide the names of experts who might provide suitable reviews. Frequently authors provide the names of possible reviewers as well as individuals whom they do not wish to have review the manuscript because of a potential conflict. The recently (1988) updated reviewer database and the manuscript database are both searchable by key terms, and the Editors consult these databases when selecting reviewers.

Once the reviewers have been chosen, a copy of the manuscript and the names of the reviewers are sent to the appropriate Editor/Associate Editor, who may at this time decide to involve additional reviewers. At the same time, the manuscript is sent to the reviewers (usually two) selected by the Washington Editors. The Editor/Associate Editors, located outside the Washington office, assume ultimate responsibility for the technical review of the paper and its final disposition. A prime concern is the speed of the reviewing process; the reviewers are asked to return a postcard to the Washington editorial office indicating that they can review the manuscript within a two-week period. If they cannot review the manuscript for us, they are asked to return it immediately; and if they need additional time, they are asked to indicate this on the postcard when they return it. If the Washington office has not received the review within the allotted time, the reviewer is contacted by telephone. At this time the manuscript often is sent to an additional reviewer, if

it appears that this would provide a second review in a more timely manner. If six weeks have elapsed and we have been unable to obtain two substantive reviews, the Editor/Associate Editor handling the manuscript is asked whether (s)he would like to proceed with only one review. The reviewer database is dynamic, constantly changing and being updated. Because reviewers are expert consultants to the Editors of ANALYTICAL CHEMISTRY and not to the authors, anonymous review has been adopted. This leads to a strong editorial process whereby the Editors assume the final responsibility for each manuscript, and one that is not encumbered with interactions between the reviewers and authors. Reviewers are sent a copy of the Instructions to the Reviewers with each manuscript and

“The advancement of science requires the sharing of knowledge between individuals, even though doing so may sometimes entail foregoing some immediate personal advantage.”

are asked to judge the originality, technical quality, clarity of presentation, and significance to the field within the guidelines emphasized in the Instructions (see reviewer form on p. 1138 A and Instructions on p. 1139 A).

If the reviewers' comments suggest only minor changes, the staff Editor in Washington handles the revision and acceptance procedures. The Editor/Associate Editors are sent copies of the reviews and the accompanying letter to the author. Occasionally they indicate that when the manuscript returns they wish to become involved in additional review. All manuscripts whose dispositions are unclear, or where major revision is suggested, are sent to the Editor/Associate Editor. They read the reviews and the manuscript and prepare additional comments for incorporation into the revision letter, if necessary. All manuscripts that reviewers recommend be rejected are handled by the Editor/Associate Editor. If the reviews are orthogonal—a not infrequent oc-

currence—the Editor/Associate Editor makes the decision as to how to proceed. Often they may make the decision themselves; other times, they solicit the opinion of an additional person, most commonly a referee (this reviewer is sent copies of the other reviews).

If authors feel that the decision to reject their manuscript was unfair, they are free to ask for reconsideration. We make every effort to ensure that the review process is both rapid and fair; however, mistakes are sometimes made. Authors should explain clearly in their letter why they feel that the decision to reject their paper was not correct. The Editor/Associate Editors take seriously these rebuttals and act accordingly. Often the manuscript will be sent to new reviewers for additional opinions or returned to the original reviewers with a copy of the author's letter. Many rejected manuscripts are returned to authors with a request that they undertake additional work and resubmit the manuscript to us later. Although these types of manuscripts have formally been rejected, we actually encourage the authors to resubmit the paper once a more thorough investigation has been carried out.

How peer review of the A pages works

The review of the A-page features, INSTRUMENTATION, REPORT, A/C INTERFACE, ANALYTICAL APPROACH, and FOCUS, takes place in a manner similar to the review of articles published in the technical section, although it is more informal because of the nature of the articles. Most of the authors of A-page articles have been invited by the editorial staff to prepare the article. On occasion, an individual interested in preparing an article on a particular subject will write to us. At this time we may extend a formal invitation to this individual or we may indicate that this particular subject does not meet the needs of our editorial plan at the present time. Each proposed article is evaluated on an individual basis, and several experts are consulted before a final decision is reached. Because many of the A-page articles are tutorial, different criteria are necessary for evaluation. Of primary importance is to provide scientifically accurate, balanced reports that are written at a level that can be understood by most readers. Although the JOURNAL carries advertising, in no way do advertisers influence the editorial content of the JOURNAL. We make every effort to provide our readers with state-of-the-art coverage of subjects free from any bias toward a particular product.

Manuscript submission and ethical guidelines

In each January 1 issue we publish the "Manuscript Requirements" for the current year (see p. 1140 A). Authors should consult this when preparing a manuscript for the technical section. Careful preparation with regard to these requirements expedites processing. In addition, it is often helpful for authors to refer to recent issues of the JOURNAL and to pattern their manuscript (organizationally) after an article that they found to be particularly well written.

We actively encourage readers who are interested in writing A-page articles or "Perspectives" to write to us and include a brief outline of the proposed article with the letter.

ACS adopted "Ethical Guidelines to Publication of Chemical Research" in 1985 (see p. 1142 A). Each prospective author, reviewer, and editor is asked to follow these guidelines when participating in any aspect of the ACS publication program. If any author or reviewer feels that these guidelines have not been followed, (s)he is encouraged to contact the Editor.

Looking at the numbers

Table I presents the data for manuscripts since 1983. Note that the rejection rate has risen approximately 20% since 1986. This was caused primarily by a change in editorial policy regarding applications papers. Prior to 1987, applications papers were often accepted if the reviewers found them technically sound; a distinction was not necessarily made as to whether the particular method was a significant improvement over an already published method. In an effort to increase the technical quality of the JOURNAL, the Editors made a conscious decision to accept only those technically sound applications papers that offer either a unique application of or a significant improvement over existing analytical methods. This policy has led, in part, to the observed increase in the rejection rate. It is interesting to note that non-US contributions to ANALYTICAL CHEMISTRY have remained essentially the same since 1983. Approximately 27% of the published papers have non-US corresponding authors.

In the first full year (1986) that the Associate Editors were involved with the JOURNAL review process, records were begun that tracked the percentage of manuscripts received in each of the subdisciplines and their final disposition. Editor Morrison has routinely been responsible for all manuscripts that do not fall into the areas of exper-

No. of manuscripts	1983-86 (avg.)	1987	1988
Received	1130	1087	1048
Accepted	727	599	585
Rejected	400 (35%)	510 (47%)	578 (55%)
Published ^a	728	665	627

^a The number of papers published includes some manuscripts that were accepted in the previous year.

Subdiscipline	Year (by percent)		1988
	1986	1987	
Spectroscopy	27	29	36
Separations	27	28	22
Electrochemistry	15	18	18
Mass spectrometry	13	14	15
Biotechnology	—	1	1
Miscellaneous	17	10	8

^a Because many of the papers involve more than one technique, the assignment reflects the primary emphasis of the work.

tise of any of the Associate Editors. The percentages of manuscripts that were received that fall into each subdiscipline are shown in Table II. Note that an Associate Editor in Biotechnology was added to the staff in 1987. The manuscripts assigned to this Editor are usually not in the traditional areas that already existed, although many of the manuscripts in the biotechnology area are shared between two Associate Editors. When one considers only those 90% of the manuscripts that are actually peer-reviewed, the rejection rate for each of the subdisciplines is close to the average rejection rate for all papers in all categories.

In today's world of science publishing, speed is an important concern. Authors wish to see their work published as rapidly as possible without sacrificing quality. ANALYTICAL CHEMISTRY has always made an effort to publish manuscripts in six months or less (the average time from receipt of the manuscript to actual publication). Our record in this area has been and continues to be on a par with many ACS publications. Neither the centralized operation in Washington nor the addition of the Associate Editors in 1985 appears to have lengthened the publication time for ANALYTICAL CHEMISTRY. In addition, we continue to look for ways to improve the "speed of publication." We are now routinely asking reviewers

to return their comments by FAX. We have also just completed a six-month experiment using Federal Express to send manuscripts to the reviewers; the analysis of the cost versus increase in speed has not yet been completed. We are now asking reviewers to return postcards to us indicating their willingness to review the manuscript within a two-week period. All these changes were made in an effort to improve speed.

Our recordkeeping has also changed recently. Because authors often have not returned their revised manuscripts promptly, which biases the overall speed of publication, we are now considering all revisions returned after a three-month period as new submissions. Rejected manuscripts, if returned for reconsideration in revised form, are generally considered new manuscripts. This allows us to realistically compare our data with other scientific publications both within and outside ACS.

In concluding, I hope that I have answered many of the questions that you, the readers, have about our editorial operations. I urge you to let us know what you think of the publication, and especially, what we can do to make ANALYTICAL CHEMISTRY even more valuable to you professionally.

Sharon Boots



Published by the American Chemical Society
 1155 16th Street, N.W.
 Washington, D.C. 20036
 telephone (202) 872-4570
 FAX (202) 872-6325
 BITNET rmh96@cas
 telex 440159
G.H. MORRISON, EDITOR

AUTHOR:

TITLE:

PLEASE RETURN THE RATING FORM BY:

Recommendation

- Merits publication either as is or subject to minor revisions as indicated below.
- May eventually be publishable, but requires major revision as indicated below and re-evaluation.
 - I would like to re-evaluate the revised manuscript.
- Should not be published in ANALYTICAL CHEMISTRY for the reasons given below.
- Not appropriate subject matter for ANALYTICAL CHEMISTRY; recommend a different journal _____

Summary Rating

	Excel.	Good	Fair	Poor
Originality				
Technical quality				
Clarity of presentation				
Significance to field				

- The authors have addressed all necessary safety considerations (see "Instructions to the Reviewers").
- The authors need to address the safety considerations described in the comments below.

Signature _____

Date _____

Please do not include your recommendation for acceptance, revision, or rejection in the COMMENTS.
 (Only the comments below the dotted line will be returned to the author.)

COMMENTS (Use additional pages if needed)

ANALYTICAL CHEMISTRY

Instructions to the Reviewers

ANALYTICAL CHEMISTRY publishes results of original research in all areas of the discipline. Articles may contribute to any phase of analytical operations, such as sampling, chemical reactions, separations, instrumentation, measurements, and data processing. They need not refer to existing or even potential analytical methods but may be confined to the principles and methodology underlying such methods. Articles dealing with minor modifications of known analytical methods should offer either a unique application of or a significant improvement over existing analytical methods.

Research Articles, Correspondence, and Technical Notes are published. Correspondence may be brief disclosures of new analytical concepts of unusual significance or they may comment on the work of others. In such cases the authors of the work being discussed will, ordinarily, be allowed to reply. Technical Notes should be brief descriptions of novel apparatus or techniques that offer definite advantages over similar ones already available.

The subject matter should be judged on the basis of originality, significance to the field, technical content, and clarity of the presentation. The Editors do not expect reviewers to rewrite a manuscript. If you find that the manuscript is poorly written, please indicate this. In reviewing the enclosed manuscript(s), please consider the following:

- Is the scientific problem clearly stated and significant? Work of marginal significance, however competently carried out, should not be recommended for publication.
- Are materials and methods described in sufficient detail so that other workers could repeat the experiments?
- Are the interpretations of data sound, and are the conclusions justified?
- Is the manuscript excessively long? Are all the figures and tables necessary? Please provide specific suggestions for condensation, if appropriate.
- Does the abstract describe briefly but clearly the purpose of the research, the principal results, and the major conclusions?

- **Safety considerations.** Authors have been asked to describe all safety considerations, including any procedures that are hazardous, any reagents that are toxic, and any procedures requiring special precautions, in enough detail so that workers repeating the experiments can take appropriate safety measures. Have these safety considerations been adequately addressed?

As you prepare your comments, please remember that the author has most probably taken seriously the preparation of this manuscript. Your review should be written in such a way that any sensitivities the author may have toward criticisms of his/her work are anticipated by you prior to preparing your written comments.

If a manuscript requires modification, suggested revisions should be stated briefly. If rejection is recommended, the major reasons should be stated concisely and in a way that the author would find helpful. Authors whose papers are recommended for rejection should not be advised to submit their papers to another journal.

Please remember that the manuscript is a privileged communication. You may feel free to obtain help from a colleague in reviewing the manuscript or to refer it to someone in your own organization. However, if someone else is involved, please inform the editorial office. Reviewers are asked to refrain from communicating directly with the authors and from disclosing their identity without prior consent of the editorial office.

Reviewers perform a vital service to the JOURNAL and to the progress of chemical science. We greatly appreciate your efforts. It is also important, for the well-being of the field and in fairness to the authors, that the editorial process be concluded speedily.

We ask that you return your comments to us within two weeks. If this is not possible, please return the manuscript to us immediately.

We appreciate your help.

George H. Morrison, Editor
ANALYTICAL CHEMISTRY

MANUSCRIPT REQUIREMENTS

The following guide is published by the Editors of ANALYTICAL CHEMISTRY to aid authors in writing, and editors and reviewers in expediting review and publication of manuscripts.

SCOPE. The journal is devoted to the dissemination of knowledge concerning all branches of analytical chemistry. Articles either are entirely theoretical with regard to analysis or are reports of laboratory experiments that support, argue, refute, or extend established theory. Articles may contribute to any of the phases of analytical operations, such as sampling, chemical reactions, separations, instrumentation, measurements, and data processing. They need not refer to existing or even potential analytical methods in themselves, but may be confined to the principles and methodology underlying such methods. Articles dealing with minor modifications of known analytical methods should offer either a unique application of or a significant improvement over existing analytical methods.

In addition to regular research papers, *Correspondence* and *Technical Notes* are published. *Correspondence* may be brief disclosures of new analytical concepts of unusual significance. They may also represent important comments on the work of others, in which case the authors of the work being discussed will, ordinarily, be allowed to reply. *Technical Notes* should be brief descriptions of novel apparatus or techniques, requiring real ingenuity on the author's part, which offer definite advantages over similar ones already available.

Papers involving extensive use of computers will be judged by the usual criteria of originality, technical content, and value to the field. They should include a statement of the objectives and the procedural steps to the objective, and the results. However, *details* of procedural steps, including programs, should be omitted. Availability of the latter through commercial collections or by writing to the author should be clearly indicated in the text. Computational techniques for calculations of well-known analytical methods cannot be considered. **SUBMISSION OF MANUSCRIPTS.** Papers submitted to ANALYTICAL CHEMISTRY are considered with the understanding that they have not been published and are not under consideration elsewhere.

Four complete copies of the manuscript are required. All copy must be typed double- or triple-spaced on 22 × 28 cm (8½ × 11 in.) or A4 paper on one side only (if a printer is used, it must be high quality), with text, tables, and illustrations of a size that can be mailed to reviewers under one cover.

In addition, include with your manuscript: (i) any paper of yours that is in press or under consideration elsewhere and includes information that would be helpful in evaluating the work submitted to *Analytical Chemistry*; (ii) written permission from any author whose work is cited as a personal communication, unpublished work, or work in press but who is not an author of your manuscript.

Reviewers suggested by authors may be used at the discretion of the editors.

Send all copies of the manuscript with cover letter to ANALYTICAL CHEMISTRY, 1155 Sixteenth St., N.W., Washington, DC 20036.

TITLE. Use specific and informative titles with a high keyword content. Avoid trade names. Indicate, where applicable, compound or element determined, method, and special reagents (e.g., "Spectrophotometric Determination of Thallium in Zinc and Cadmium with Rhodamine B"). Do not use symbols, abbreviations, or series designations. Use one

complete title rather than a title and subtitle. Careful attention should be paid to the choice of words (e.g., *determination* or *analysis*, etc.) to reflect correct usage.

AUTHORSHIP. Give authors' names in as complete a form as possible. First names, initials, and surnames should be included. Omit professional and official titles. Give the complete mailing address of the place where the work was done and include the telephone number of the corresponding author. Add the current address of each author, if different, on the title page of the manuscript using a numerical superscript and footnote to indicate the difference. The corresponding author is indicated by an asterisk.

ABSTRACT. Abstracts are required for all manuscripts, but will not be published with *Correspondence* and *Technical Notes*. The abstract (80–200 words) should describe briefly and clearly the purpose of the research, the principal results, and the major conclusions. State the objectives of the study, the limits of detection, the degree of accuracy and precision, and the major unique reagents, times, and temperatures, but avoid the lengthy stepwise recipe. The abstract should be essentially independent of the main text. Remember that the abstract will be the most widely read portion of the paper and will be used by the various abstracting services.

TEXT. Consult the publication for general style. Write for the specialist. Do not include information and details or techniques that should be common knowledge to the specialist.

General Organization. Indicate the breakdown among and within sections with center heads and side heads. Results and Discussion follow Experimental Section. Keep all information pertinent to a particular section within that section (e.g., do not present results in the Experimental Section). Avoid repetition. Do not use footnotes for descriptive or explanatory information; include the information at an appropriate place in the text.

INTRODUCTION

The introduction should state the purpose of the investigation and its relation to other work in the same field, but should not include an extensive review of the literature. If the manuscript describes a new method, reasons should be given why it is preferable to older methods.

EXPERIMENTAL SECTION

Use complete sentences (i.e., do not use outline form). Be consistent in voice and tense.

APPARATUS. List only devices of specialized nature. Do not include equipment that is standard in an analytical laboratory and used in the normal way.

REAGENTS. List and describe preparation of special reagents only. Do not list reagents normally found in the laboratory and preparations described in standard handbooks and texts.

PROCEDURE. Since all procedures are intended as instructions for other workers, give adequate details of critical steps to permit the work to be repeated by a qualified analyst. Published procedures should be cited but not described, except where the presentation involves substantially new modifications. Omit details of procedures that are common knowledge to those working in the field.

Safety Considerations: Describe all safety considerations, including any procedures that are hazardous, any reagents that are toxic, and any procedures requiring

special precautions, in enough detail so that workers repeating the experiments can take appropriate safety measures.

RESULTS AND DISCUSSION

The results may be presented in tables or figures; however, many simple findings can be presented directly in the text with no need for tables or figures. The discussion should be concise and deal with the interpretation of the results. In most cases combining results and discussion in a single section will give a clearer, more compact presentation.

CONCLUSIONS

Use conclusions only when necessary for interpretation and not to summarize information already given in the text or abstract.

ACKNOWLEDGMENTS

Authors may acknowledge technical assistance, gifts, and the source of special materials.

LITERATURE CITED. References that are considered part of the permanent literature should be numbered in one consecutive series by order of mention in the text. However, the complete list of literature citations should be placed on a separate page, double-spaced, at the end of the manuscript. Reference numbers in the text should be placed in parentheses and on line. Repetition should be avoided by using the number corresponding to the original reference. Descriptive or explanatory (footnote) material should not routinely be given a reference number or included in the literature cited. This material should be included in the body of the text.

Use *Chemical Abstracts Service Source Index* abbreviations for journal names and include publication year, volume, and page number (inclusive pagination is recommended). Include *Chemical Abstracts* reference for foreign publications that are not readily available. List submitted articles as "in press" only if formally accepted for publication, and give the volume number and year if known. Otherwise use "submitted to" or "unpublished work" with place where work was done and date. Include name, affiliation, and date for "personal communications".

Please use the format given in the following examples.

- (1) Koile, Ross C.; Johnson, Dennis C. *Anal. Chem.* 1979, 51, 741-744.
- (2) Willard, Hobart H.; Merritt, Lynne L., Jr.; Dean, John A.; Settle, Frank A., Jr. *Instrumental Methods of Analysis*, 6th ed.; Van Nostrand: New York, 1981; Chapter 2.

CREDIT. On a separate page, give credit for financial support, meeting presentation information, and auspices under which work was done, including permission to publish. In the JOURNAL this information will immediately follow the received and accepted dates, and is not a part of the Acknowledgments.

FIGURES AND TABLES. Do not use figures or tables that duplicate each other or material already in the text. Straight line graphs will not normally be published; give the information in a table, or in a sentence or two in the text. Do not include tables or figures that have already been published.

Tables. Prepare tables in a consistent form, furnish each with an appropriate title, and number consecutively with Roman numerals in the order of reference in the text. Type each table on a separate page, and collate at the end of the manuscript.

Figures. Submit original drawings (or sharp glossy prints) of graphs and diagrams prepared on tracing cloth or plain white paper. If structures are given in the text, original drawings are to be provided. All lines, lettering, and numbering should be sharp and unbroken. If coordinate paper

is used, use nonphotographic blue cross-hatch lines. Use black India ink and a lettering set for all letters, numbers, and symbols. Do not use a typewriter to letter illustrations.

Design illustrations to fit the width of one journal column (8.3 cm). The width of original drawings should be twice the publication size. Letters and symbols should be about 4 mm high on the original (2 mm in reduced journal version). Lines should be drawn with a light (#1 Leroy for graph grids), medium (#2 Leroy for graph borders or reference lines), or heavy (#5 Leroy for graph curves or emphasis) thickness on the original. Lettering on copy should be in proportion. Label ordinates and abscissas of graphs along the axes and outside the graph proper.

Supply good prints of photographs. Sharp contrasts are essential. Label each figure on the back with the name of the corresponding author and the figure number.

Number all figures consecutively with Arabic numerals in the order of reference in the text.

If drawings are mailed under separate cover, identify by name of author and title of manuscript.

Color reproduction is possible provided the author bears all incremental charges. An estimate of these charges will be given upon request. A letter acknowledging the author's willingness to defray the cost of color reproduction should accompany the revised manuscript.

Figure Captions. Include, on one page, a list of all captions and legends for illustrations. Make the legend a part of the caption rather than inserting it within the figure. Keep captions as brief as possible and include detailed information in the text.

BRIEF. On a separate page, state in 30 words or less the significant results obtained, emphasizing precision and accuracy data when possible. Do not repeat the title. No Briefs are necessary for *Correspondence* or *Technical Notes*.

NOMENCLATURE. Nomenclature should conform with current American usage. Insofar as possible, authors should use systematic names similar to those used by the International Union of Pure and Applied Chemistry and the Chemical Abstracts Service. For CA nomenclature advice consult the Manager of Nomenclature Services, P.O. Box 3012, Chemical Abstracts Service, Columbus, OH 43210. A name generation service is available through the Registry Services Department, Chemical Abstracts Service, P.O. Box 3343, Columbus, OH 43210.

Avoid trivial names. Well-known symbols and formulas may be used (write out in title and abstract) if no ambiguity is likely. Define trade names and abbreviations at point of first use. First letter of trade names is capitalized.

Use SI units of measurement (with acceptable exceptions) and give dimensions for all terms. If nomenclature is specialized, as in mathematical and engineering reports, include a Nomenclature section at end of paper, giving definitions and dimensions for all terms. Type all equations and formulas clearly and number all equations in consecutive order.

For specialized nomenclature used by this JOURNAL, see "Guide for Use of Terms in Reporting Data in ANALYTICAL CHEMISTRY", "Spectroscopy Nomenclature", and "SI Units", which appear annually, with the "Manuscript Requirements", at the end of the technical section in the first issue of the year. From time to time, ANALYTICAL CHEMISTRY publishes special nomenclature guides promulgated by various organizations.

General information about American Chemical Society publications, including preparation of manuscripts, is given in *The ACS Style Guide* (1986), available from Distribution Office, American Chemical Society, 1155 16th St., N.W., Washington, DC 20036.

Ethical Guidelines to Publication of Chemical Research

The guidelines embodied in this document were adopted by the editors of the Books and Journals Division of the American Chemical Society in January 1985 and endorsed by the Society Committee on Publications.

PREFACE

The American Chemical Society serves the chemistry profession and society at large in many ways, among them by publishing journals which present the results of scientific and engineering research. Every editor of a Society journal has the responsibility to establish and maintain guidelines for selecting and accepting papers submitted to that journal. In the main, these guidelines derive from the Society's definition of the scope of the journal and from the editor's perception of standards of quality for scientific work and its presentation.

An essential feature of a profession is the acceptance by its members of a code that outlines desirable behavior and specifies obligations of members to each other and to the public. Such a code derives from a desire to maximize perceived benefits to society and to the profession as a whole and to limit actions that might serve the narrow self-interests of individuals. The advancement of science requires the sharing of knowledge between individuals, even though doing so may sometimes entail foregoing some immediate personal advantage.

With these thoughts in mind, the editors of journals published by the American Chemical Society now present a set of ethical guidelines for persons engaged in the publication of chemical research, specifically, for editors, authors, and manuscript reviewers. These guidelines are offered not in the sense that there is any immediate crisis in ethical behavior, but rather from a conviction that the observance of high ethical standards is so vital to the whole scientific enterprise that a definition of those standards should be brought to the attention of all concerned.

We believe that most of the guidelines now offered are already understood and subscribed to by the majority of experienced research chemists. They may, however, be of substantial help to those who are relatively new to research. Even well-established scientists may appreciate an opportunity to review matters so significant to the practice of science.

Formulation of these guidelines has made us think deeply about these matters. We intend to abide by these guidelines, strictly, in our own work as editors, authors, and manuscript reviewers.

GUIDELINES

A. ETHICAL OBLIGATIONS OF EDITORS OF SCIENTIFIC JOURNALS

1. An editor should give unbiased consideration to all manuscripts offered for publication, judging each on its merits without regard to race, religion, nationality, sex, seniority, or institutional affiliation of the author(s). An editor may, however, take into account relationships of a manuscript immediately under consideration to others previously or concurrently offered by the same author(s).

2. An editor should consider manuscripts submitted for publication with all reasonable speed.

3. The sole responsibility for acceptance or rejection of a manuscript rests with the editor. Responsible and prudent exercise of this duty normally requires that the editor seek advice from reviewers, chosen for their expertise and good judgment, as to the quality and reliability of manuscripts submitted for publication. In reaching a final decision, the editor should also consider additional factors of editorial policy.

4. The editor and members of the editor's staff should not disclose any information about a manuscript under consideration to anyone other than those from whom professional advice is sought. (However, an editor who solicits, or otherwise arranges beforehand, the submission of manuscripts may need to disclose to a prospective author the fact that a relevant manuscript by another author has been received or is in preparation.) After manuscripts have been accepted for publication, the editor and members of the editor's staff may disclose or publish manuscript titles and authors' names, but no more than that unless the author's permission has been obtained.

5. An editor should respect the intellectual independence of authors.

6. Editorial responsibility and authority for any manuscript authored by an editor and submitted to the editor's journal should be delegated to some other qualified person, such as another editor of that journal or a member of its Editorial Advisory Board. Editorial consideration of the manuscript in any way or form by the author-editor would constitute a conflict of interest, and is therefore improper.

7. Unpublished information, arguments, or interpretations disclosed in a submitted manuscript should not be used in an editor's own research except with the consent of the author. However, if such information indicates that some of the editor's own research is unlikely to be profitable, the editor could ethically discontinue the work. When a manuscript is so closely related to the current or past research of an editor as to create a conflict of interest, the editor should arrange for some other qualified person to take editorial responsibility for that manuscript. In some cases, it may be appropriate to tell an author about the editor's research and plans in that area.

8. If an editor is presented with convincing evidence that the main substance or conclusions of a report published in an editor's journal are erroneous, the editor should facilitate publication of an appropriate report pointing out the error and, if possible, correcting it. The report may be written by the person who discovered the error or by an original author.

B. ETHICAL OBLIGATIONS OF AUTHORS

1. An author's central obligation is to present an accurate account of the research performed as well as an objective discussion of its significance.

2. An author should recognize that journal space is a precious resource created at considerable cost. An author therefore has an obligation to use it wisely and economically.

3. A primary research report should contain sufficient detail and reference to public sources of information to permit the author's peers to repeat the work.

4. An author should cite those publications that have been influential in determining the nature of the reported work and that will guide the reader quickly to the earlier work that is essential for understanding the present investigation. Except in a review, citation of work that will not be referred to in the

reported research should be minimized.

5. Any unusual hazards inherent in the chemicals, equipment, or procedures used in an investigation should be clearly identified in a manuscript reporting the work.

6. Fragmentation of research reports should be avoided. A scientist who has done extensive work on a system or group of related systems should organize publication so that each report gives a well-rounded account of a particular aspect of the general study. Fragmentation consumes journal space excessively and unduly complicates literature searches. The convenience of readers is served if reports on related studies are published in the same journal, or in a small number of journals.

7. In submitting a manuscript for publication, an author should inform the editor of related manuscripts that the author has under editorial consideration or in press. The relationships of such manuscripts to the one submitted should be indicated.

8. It is in general inappropriate for an author to submit manuscripts describing essentially the same research to more than one journal of primary publication. However, there are exceptions as follows: (a) resubmission of a manuscript rejected by or withdrawn from publication in one journal; (b) submission of overlapping work to a second journal in another field, if workers in the other field are unlikely to see the article published in the first journal, providing that both editors are informed; and (c) submission of a manuscript for a full paper expanding on a previously published brief preliminary account (a "communication" or "letter") of the same work.

9. An author should identify the source of all information quoted or offered, except that which is common knowledge. Information obtained privately, as in conversation, correspondence, or discussion with third parties, should not be used or reported in the author's work without explicit permission from the investigator with whom the information originated. Information obtained in the course of confidential services, such as refereeing manuscripts or grant applications, should be treated similarly.

10. An experimental or theoretical study may sometimes justify criticism, even severe criticism, of the work of another scientist. When appropriate, such criticism may be offered in published papers. However, in no case is personal criticism considered to be appropriate.

11. The co-authors of a paper should be all those persons who have made significant scientific contributions to the work reported and who share responsibility and accountability for the results. Other contributions should be indicated in a footnote or an "Acknowledgments" section. An administrative relationship to the investigation does not of itself qualify a person for co-authorship (but occasionally it may be appropriate to acknowledge major administrative assistance). Deceased persons who meet the criterion for inclusion as co-authors should be so included, with a footnote reporting date of death. No fictitious name should be listed as an author or co-author. The author who submits a manuscript for publication accepts the responsibility of having included as co-authors all persons appropriate and none inappropriate. The submitting author should have sent each living co-author a draft copy of the manuscript and have obtained the co-author's assent to co-authorship of it.

C. ETHICAL OBLIGATIONS OF REVIEWERS OF MANUSCRIPTS

1. Inasmuch as the reviewing of manuscripts is an essential step in the publication process, and therefore in the operation of the scientific method, every scientist has an obligation to do a fair share of reviewing.

2. A chosen reviewer who feels inadequately qualified to judge the research reported in a manuscript should return it promptly to the editor.

3. A reviewer (or referee) of a manuscript should judge objectively the quality of the manuscript, of its experimental and theoretical work, of its interpretations and its exposition, with due regard to the maintenance of high scientific and literary

standards. A reviewer should respect the intellectual independence of the authors.

4. A reviewer should be sensitive to the appearance of a conflict of interest when the manuscript under review is closely related to the reviewer's work in progress or published. If in doubt, the reviewer should return the manuscript promptly without review, advising the editor of the conflict of interest or bias. Alternatively, the reviewer may wish to furnish a signed review stating the reviewer's interest in the work, with the understanding that it may, at the editor's discretion, be transmitted to the author.

5. A reviewer should not evaluate a manuscript authored or co-authored by a person with whom the reviewer has a personal or professional connection if the relationship would bias judgment of the manuscript.

6. A reviewer should treat a manuscript sent for review as a confidential document. It should neither be shown to nor discussed with others except, in special cases, to persons from whom specific advice may be sought; in that event, the identities of those consulted should be disclosed to the editor.

7. Reviewers should explain and support their judgments adequately so that editors and authors may understand the basis of their comments. Any statement that an observation, derivation, or argument had been previously reported should be accompanied by the relevant citation. Unsupported assertions by reviewers (or by authors in rebuttal) are of little value and should be avoided.

8. A reviewer should be alert to failure of authors to cite relevant work by other scientists, bearing in mind that complaints that the reviewer's own research was insufficiently cited may seem self-serving. A reviewer should call to the editor's attention any substantial similarity between the manuscript under consideration and any published paper or any manuscript submitted concurrently to another journal.

9. A reviewer should act promptly, submitting a report in a timely manner. Should a reviewer receive a manuscript at a time when circumstances preclude prompt attention to it, the unreviewed manuscript should be returned immediately to the editor. Alternatively, the reviewer might notify the editor of probable delays and propose a revised review date.

10. Reviewers should not use or disclose unpublished information, arguments, or interpretations contained in a manuscript under consideration, except with the consent of the author. If this information indicates that some of the reviewer's work is unlikely to be profitable, the reviewer, however, could ethically discontinue the work. In some cases, it may be appropriate for the reviewer to write the author, with copy to the editor, about the reviewer's research and plans in that area.

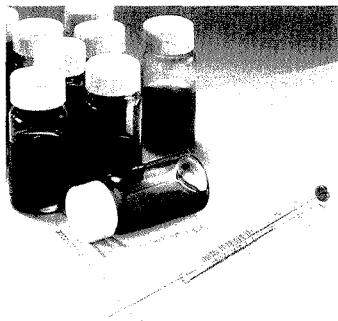
D. ETHICAL OBLIGATIONS OF SCIENTISTS PUBLISHING OUTSIDE THE SCIENTIFIC LITERATURE

1. A scientist publishing in the popular literature has the same basic obligation to be accurate in reporting observations and unbiased in interpreting them as when publishing in a scientific journal.

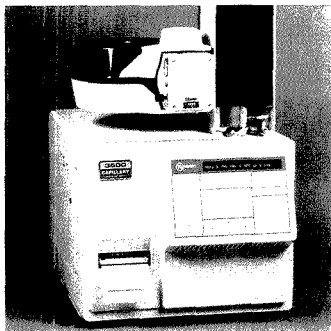
2. Inasmuch as laymen may not understand scientific terminology, the scientist may find it necessary to use common words of lesser precision to increase public comprehension. In view of the importance of scientists' communicating with the general public, some loss of accuracy in that sense can be condoned. The scientist should, however, strive to keep public writing, remarks, and interviews as accurate as possible consistent with effective communication.

3. A scientist should not proclaim a discovery to the public unless the experimental, statistical, or theoretical support for it is of strength sufficient to warrant publication in the scientific literature. An account of the experimental work and results that support a public pronouncement should be submitted as quickly as possible for publication in a scientific journal. Scientists should, however, be aware that extensive disclosure of research in the public press might be considered by a journal editor as equivalent to a preliminary communication in the scientific literature.

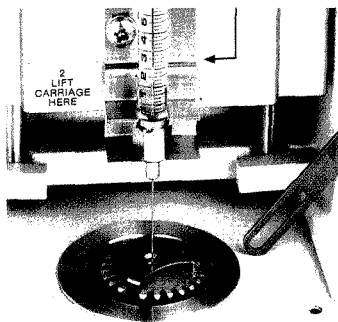
VARIAN ADVANCES THE TECHNOLOGY OF GAS CHROMATOGRAPHY. AGAIN.



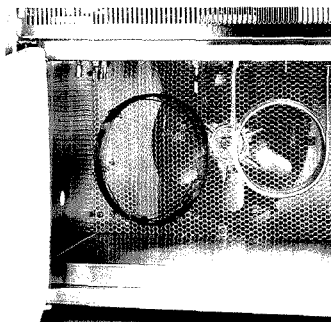
Our 3400 GC with four-method storage, and inboard data handling is ideal for routine and QA/QC work.



The 3500 is the most advanced capillary GC you can buy. With its patented small cell ECD, it's ideal for trace analysis.



3410 High Temperature GC to 500°C with unique SPI (Septum-equipped Programmable Injector) easily handles high boilers.



Our 3500 high level research GC with large column oven accommodating up to 4 detectors and 4 injectors.

From the development of the first preparative GC to discover why fruit flies were besieging strawberries to the development of our new high temperature GC, Varian has been an innovator in gas chromatography.

Our line of gas chromatographs includes systems ranging from routine use to fully automated, high-throughput research instruments. All are designed to give maximum performance with 530 micron as well as packed and capillary columns.

Varian research and development consistently advances new GC features designed to solve complex problems, are easy to use and deliver the best chromatographic results.

Varian also has a range of GC applications systems—natural gas, landfill gas, toxic air contaminants, pesticides, simulated distillation and more.

But instrumentation is only the beginning. At Varian we don't just sell a single instrument or system, we deliver a whole package. A package that includes technical support and superior service.

For further information, call **800-231-8134**. In Canada, call **416-457-4130**.

CIRCLE 72 ON READER SERVICE CARD

Varian is your full-line company for analytical instrumentation
UV-Visible-NIR
LIMS
Data Systems
Atomic Absorption
NMR
Liquid Chromatography
Gas Chromatography

GC WITH A FUTURE



1990 Summer Internship Program

The ACS Division of Analytical Chemistry is seeking applicants for the 1990 summer internship program. The program is aimed at introducing talented undergraduates to modern analytical chemistry. Chosen students will participate in fundamental and applied research in industrial, government, or academic laboratories.

Applications are screened and evaluated by the Division's Professional Status Committee, which acts as a broker in soliciting applications from students and positions from laboratories. Applications and reference letters for qualified students are then sent to participating laboratories, and these organizations select the individuals most suited to their needs. Salary and details of employment are negotiated by the organization and the student. Participating laboratories agree to employ one or more students for the summer.

To qualify for the program, students must have completed a minimum of two years of college, preferably including an instrumental analysis course or its equivalent, and display an interest in analytical chemistry. Ideally, students should be attending a four-year college and be between their junior and senior years at the start of the 1990 summer. The Division also welcomes applications from current graduate students in analytical chemistry and from college seniors graduating in 1990 who have applied to graduate school and intend to major in analytical chemistry.

The Division is also actively seeking participation from industrial, government, and academic laboratories. Information about the program and application forms for interested students are available from D. J. Curran, Chairman, Professional Status Committee, ACS Division of Analytical Chemistry, c/o Department of Chemistry, University of Massachusetts, Amherst, MA 01003. The deadline for receipt of student applications is Feb. 9.

For the 1989 program, 61 student applications were received; 14 students were placed with the 12 organizations listed below.

American Cyanamid Co., Stamford Research Labs, Stamford, CT

Valerie K. Miller, Moorhead State University, Moorhead, MN

Baxter Healthcare Corp., Parenterals Division, Round Lake, IL

Lena S. Issa, Saint Xavier College, Chicago, IL
Chemical Industry Institute of Toxicology, Research Triangle Park, NC

E.I. du Pont de Nemours & Co., Central Research and Development, Wilmington, DE

Cheryl L. Davis, Mary Washington College, Fredericksburg, VA

Hewlett Packard Co., Corvallis, OR

Denise E. Riley, Macalester College, Saint Paul, MN
Lovelace Inhalation Toxicology Research Institute, Albuquerque, NM

Bretton Freitag, Willamette University, Salem, OR
Karen D. Muscato, Mary Washington College

Merck Sharp & Dohme Research Labs, West Point, PA
Christopher J. Warren, King's College, Wilkes-Barre, PA
Miami University, Oxford, OH

Jarrod A. Marto, Centre College, Danville, KY
Pfizer Inc., Pfizer Central Research, Groton, CT

Margaret L. Crews, Mary Washington College

Phillips Petroleum Company, Bartlesville, OK

Paul T. Buckley, Northern Arizona University, Flagstaff
University of Minnesota, Minneapolis

Daniel W. Grossmann, Luther College, Decorah, IA

Robin N. Lubinski, Moorhead State University

University of Wisconsin, Madison

Andrew J. Thiel, Marquette University, Milwaukee, WI

Small Launch for Tiny Satellite

Reflecting the post-*Challenger* commitment to simpler and cheaper means of space research, Los Alamos National Laboratory researchers are designing a minisatellite that will be launched from a high-flying B-52 aircraft. The \$1.5 million project is scheduled for an April 1991 launch, only four years after such a mission was proposed.

The satellite, titled ALEXIS (Array of Low-Energy X-ray Imaging Sensors), will survey "ultrasoft" cosmic X-rays. Three pairs of telescopes on board the satellite will take measurements in the range of 70–110 eV, corresponding to X-rays from regions of hot, interstellar gas. "ALEXIS will allow us to map this background in our neighborhood of the galaxy," explains Bill Friedhorsky, mission project manager.

ALEXIS and its supporting spacecraft weigh about 240 lbs. and are approximately the size and shape of an office wastebasket. The satellite will be launched by the Air Force from a B-52 at about 40,000 ft. A three-stage booster will then power the satellite into a polar orbit 425 nautical miles above the Earth. Adds Friedhorsky, "You can put about twice the payload into orbit from a launch at altitude than you can with a launch from sea level."

In addition to scientists at Los Alamos, researchers from Sandia National Laboratory, the University of California-Berkeley, and the Astronautics company of Virginia are involved in the project.

For Your Information

Cray Research, Inc., will donate 2800 h of supercomputer time, worth ~\$4 million, to researchers working in all 11 National Science Foundation Science and Technology Centers. Computer time has been reserved on a Cray-2 supercomputer with up to 4.3 billion bytes of memory.

Concentrations of certain trace elements in blood can signal the onset of disease. A standard reference material containing certified concentrations of 13 trace elements in frozen bovine serum is available from NIST, Office of Standard Reference Materials, B311, Chemistry Bldg., Gaithersburg, MD 20899 (301-975-6776).

Acrodisc: The Difference is Clear.

Clearly the Widest Selection.

Gelman Sciences Acrodiscs® are available in a wide variety of membrane types, with 0.2 μ m or 0.45 μ m pore sizes and 13mm or 25mm diameters.

Clearly Identified.

Acrodiscs are printed with identifying information, and are color-coded to the product packaging. Convenient tube containers allow you to see their contents at a glance.

Clearly the Best Performance.

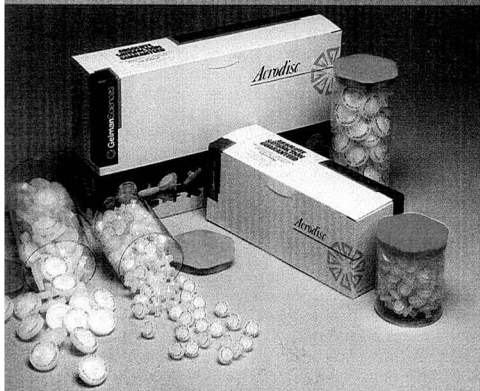
Gelman Sciences is so certain you'll be satisfied with the performance of its Acrodisc syringe filters, every package is covered by a free-replacement guarantee. So order Gelman Sciences Acrodiscs today through your local laboratory products distributor.

CIRCLE 58 ON READER SERVICE CARD



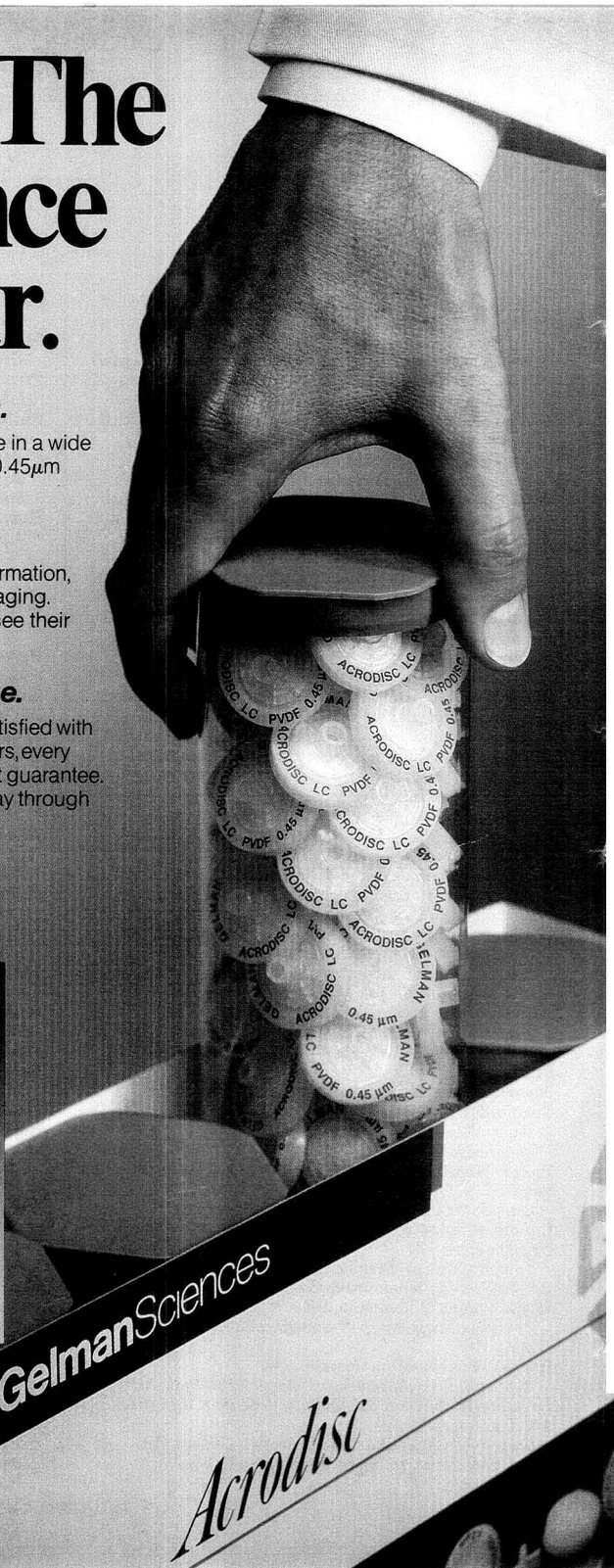
Gelman Sciences

600 S. Wagner Rd. • Ann Arbor, MI 48106-1448 • 313-665-0651

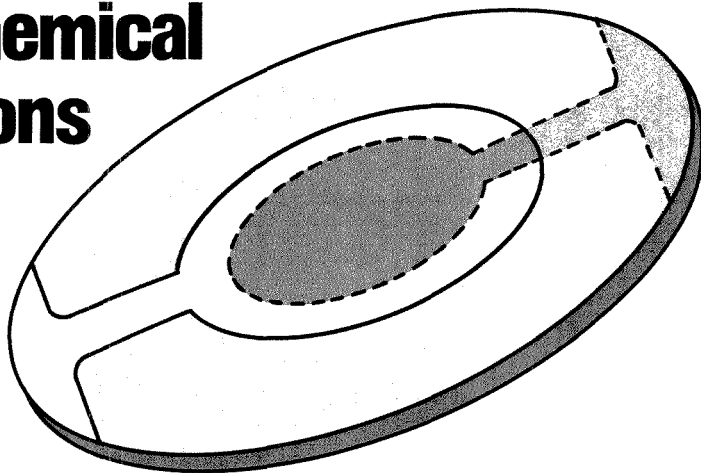


Gelman Sciences

Acrodisc



Electrochemical Applications of the Quartz Crystal Microbalance



Mark R. Deakin
Department of Chemistry
Florida State University
Tallahassee, FL 32306

Daniel A. Buttry
Department of Chemistry
University of Wyoming
Laramie, WY 82071

Charge-transfer reactions occurring at an electrode in solution often are affected dramatically by the character of the electrode-solution interface. Although these surface effects can be used to advantage in many areas, including analytical chemistry, we often lack a fundamental understanding of how interfacial chemistry affects electron transfer. To advance our knowledge of heterogeneous electron transfer, electrochemists attempt to couple surface-sensitive probes to conventional electrochemical experiments. Probes that can be used in solution, as charge transfer proceeds, are especially useful.

Recently the quartz crystal microbalance (QCM), a mass-sensitive detector based on an oscillating quartz wafer, was adapted for use in solution. QCMs have been used for many years as mass sensors in vacuum and gas-phase experiments. However, until about 10 years ago, it was believed that excessive viscous loading would pro-

hibit use of the QCM in liquids. In fact, operation in liquids is possible, and the response of the QCM is extremely sensitive to mass changes at the solid-solution interface. The QCM is not a very selective detector; it responds to any interfacial mass change. Still, it provides information that would be difficult to obtain with other methods.

A key attribute of the QCM is the quantitative nature of its response. When a monolayer or thin film on the QCM exhibits rigid-layer behavior, the QCM provides absolute information on the mass changes that occur at the solid-solution interface. Unlike surface acoustic wave (SAW) devices (1), the QCM requires no calibration when used for mass measurement under rig-

REPORT

id-layer conditions. However, the possibility of nonrigid behavior necessitates a careful evaluation of each system (2). As described below, quantitative frequency-mass correlations are difficult for thin, viscoelastic films, and only qualitative information is often obtained.

Recent advances in QCM instrumentation make it easy to apply this detector to liquid systems. This, coupled with the relatively low cost of the de-

vice (a complete, computerized system can be assembled for under \$10,000) and its submonolayer sensitivity, has increased interest in use of the QCM. As a sensitive detector useful in solution, the QCM may be applied to many analytical problems (3). In this REPORT we will concentrate on the use of the QCM in electrochemical research. Much of the following discussion, however, is appropriate for the general case: the detection of small mass changes in the region near the QCM-solution interface.

Theory

The microbalance is designed around a piezoelectric wafer sliced from a single crystal of quartz. As a piezoelectric material, the quartz wafer deforms slightly in the presence of an electric field. Quartz is not unique in this respect; a majority of the 32 crystal classes exhibit the piezoelectric effect. However, the electrical, mechanical, and chemical properties of quartz make it the most useful of the many possible piezoelectric materials. An extensive discussion of the use of quartz crystals in oscillator circuits is available (4).

When used in the QCM, the quartz wafer is sandwiched between two electrodes bonded to the wafer surface. These electrodes are used to induce an oscillating electric field perpendicular to the surface of the wafer. This oscillating electric field produces a mechan-

ical oscillation, a standing wave, in the bulk of the quartz wafer (Figure 1). The direction of crystal oscillation depends on the orientation of the crystal lattice in the electric field. In the QCM, the mechanical shear oscillation is predominant, and the displacements are parallel to the wafer surface. This shear wave oscillation is induced efficiently in AT-cut quartz wafers.

For a quartz wafer of a given thickness, the ease of inducing mechanical oscillation varies with the frequency of the oscillation. A resonant oscillation is usually achieved by including the wafer in an appropriately designed oscillator circuit. In such a circuit, the frequency of the electrical and mechanical oscillations centers at a characteristic fundamental frequency. Depending on the thickness of the wafer, this fundamental frequency is usually between 2 and 20 MHz. If the associated circuitry is designed to prevent oscillation at the fundamental frequency, oscillation may occur at an overtone frequency, an odd-integral multiple of the fundamental frequency. At these higher frequencies the mass sensitivity of the QCM increases. However, the bulk oscillations in the QCM cannot achieve the high frequencies found in some SAW devices. Thus the ultimate sensitivity of the QCM will be lower than that obtained from SAW devices oper-

ating in the GHz range (1).

The frequency of this coupled mechanical and electrical oscillation in the QCM depends on several factors. Factors that are normally constant include the physical properties of the quartz wafer (thickness, density, and shear modulus). Factors that sometimes are held constant include the density and viscosity of the phases adjacent to either side of the QCM wafer (gas or liquid), pressure differences across the wafer, and the temperature. Factors that often change are the mass of the attached electrode or the mass of an adsorbate or thin film attached to that electrode. These variations in mass are usually probed with the QCM.

For many cases, interfacial mass changes are related in a simple manner to changes in the QCM oscillation frequency, through the Sauerbrey equation (5).

$$\Delta f = -2\Delta m n f_0^2 / (A \sqrt{\mu_q \rho_q}) \quad (1)$$

In this formula, the change in the oscillation frequency (Δf) is equal to minus the change in interfacial mass (Δm) per unit area (A) times a constant. Thus the frequency decreases as the mass increases. The constant is evaluated with knowledge of the oscillation frequency of the fundamental mode of the QCM (f_0), the overtone number (n), the den-

sity of quartz ($\rho_q = 2.648 \text{ g cm}^{-3}$), and the shear modulus of quartz ($\mu_q = 2.947 \times 10^{11} \text{ g cm}^{-1} \text{ s}^{-2}$). One important ramification of this expression is that the QCM is sensitive to mass changes per unit area of oscillation. Mechanical oscillation of the crystal is at a maximum where the electrode pads overlap and diminishes rapidly in areas where the oscillator electrodes do not overlap, which leads to inaccuracies when measuring the oscillation area. Thus the QCM is most useful when probing processes that occur uniformly across the QCM surface—processes that can be represented as a change in mass per unit area.

The Sauerbrey equation is appropriate for many situations; however, there are limitations on its use. One assumption implicit in this expression is that the mass added or lost at the oscillator surface does not experience any shear deformation during oscillation. This is a good approximation for thin, rigid layers. For thicker, less rigid solids, however, a more complex theory is required. Use of the Z-match theory, which considers the acoustic impedance of a layer attached to the oscillator (6), makes the QCM more useful, but the density and shear modulus of the attached layer must be known.

The frequency of the QCM is also affected by contact with solution. Kanazawa and co-workers have shown that an exponentially damped shear wave is developed in solution at the surface of a submerged QCM (7), leading to an expression for the frequency change during submersion of the QCM,

$$\Delta f = -f_0^{3/2} [\eta_s \rho_s / (\pi \mu_q \rho_q)]^{1/2} \quad (2)$$

where η_s is the solution viscosity and ρ_s is the solution density. The penetration depth of this shear wave depends on $(\pi f_0 \rho_s / \eta_s)^{-1/2}$. For example, the characteristic decay length is approximately 250 nm in water at 25 °C when f_0 equals 5 MHz (7). Experiments by these authors and others (8) have related variations in the QCM frequency to changes in solution density or viscosity.

Use of the QCM in electrochemical experiments

The QCM has been coupled with both controlled-potential and controlled-current experiments by several research groups. In most electrochemical experiments, the quartz wafer with its attached electrodes is clamped between two O-rings. Only one side of the wafer and one electrode, which serves both as a part of the QCM oscillator circuit and as the working electrode in the electrochemical cell, are in contact with solution. This combined device of-

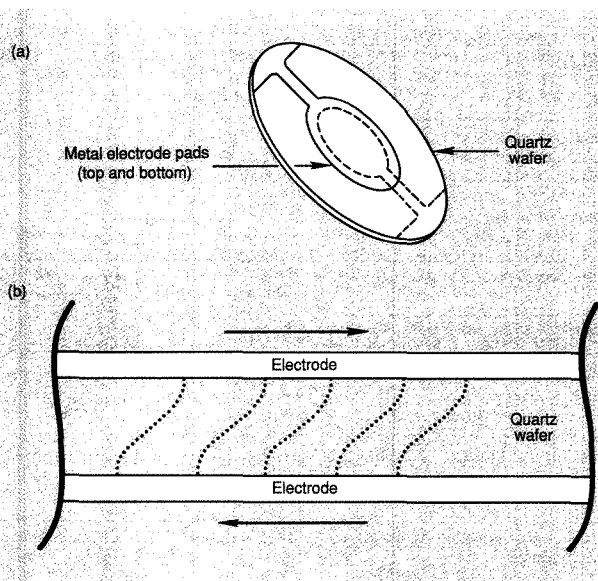
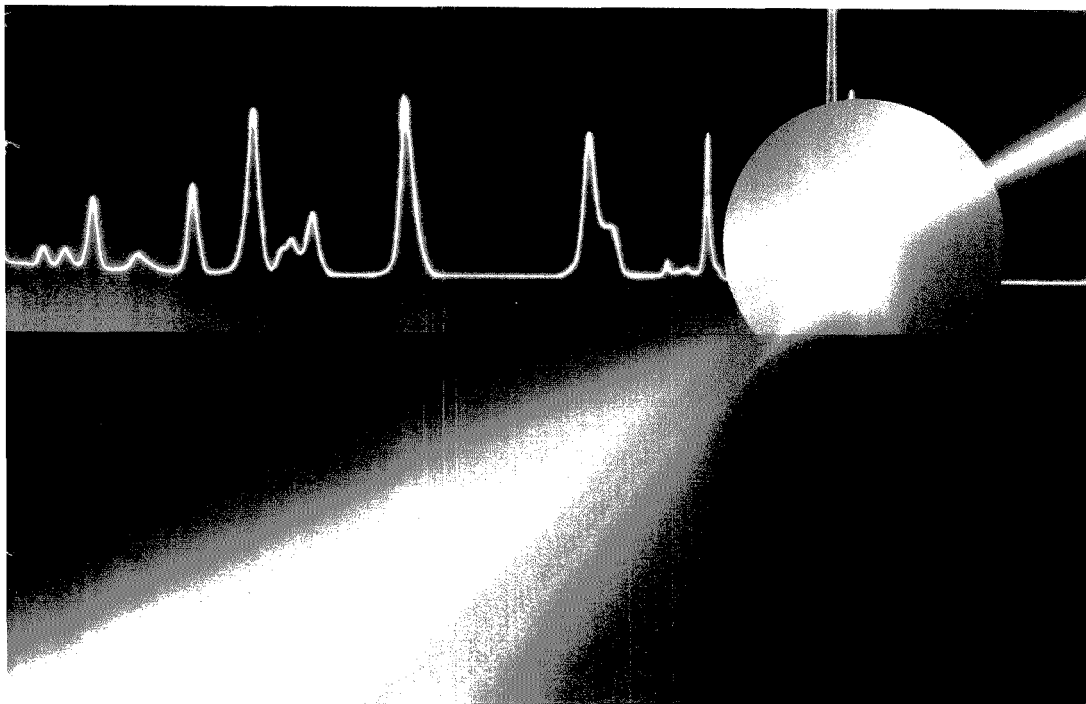


Figure 1. A typical QCM.

(a) Orientation of electrodes and (b) shear deformation during oscillation at the fundamental frequency (not to scale).

UV/VIS at its best -- from the world leader. Perkin-Elmer.



Only Perkin-Elmer — the world leader in UV/VIS spectroscopy — gives you price/performance at its best. The Lambda 6 UV/VIS System blends exceptional value, performance, and flexibility into one affordable system.

PERFORMANCE AT ITS BEST

Only the Lambda 6 System delivers proven performance at such an attractive price. Double-beam design, low stray light, and low noise guarantee accurate spectroscopic results for quantitative, multiwavelength, and kinetic analyses.

SOFTWARE AT ITS BEST

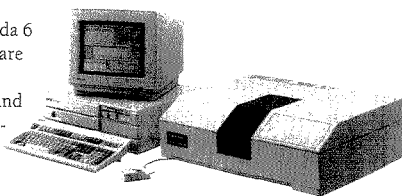
Our new UV Data Manager software is graphically oriented with pull-down menus, windows, an extensive HELP feature, and a mouse pointing device. It puts you in complete command of the instrument, accessories, and data processing routines without being a PC expert.

VERSATILITY AT ITS BEST

With the PC-controlled Lambda 6 System, data handling capabilities are never limited. Data can be quickly exported to third-party software. And with our powerful OBEY macrolanguage, you can write custom programs tailored to your lab needs.

FREE VIDEO OFFER

Send now for your free Lambda 6 System video — UV/VIS at its best. For more information and a free video, call 1-800-762-4000 or write Perkin-Elmer Corp., 761 Main Ave., Norwalk, CT 06859-0012 USA.



PERKIN ELMER

CIRCLE 129 ON READER SERVICE CARD

ten is referred to as the electrochemical QCM (EQCM).

As mentioned above, AT-cut quartz wafers are used to construct the QCM for solution work. The fundamental frequency of the QCM depends on the thickness of the wafer. A wafer with a thickness of 320 μm oscillates near 5 MHz and has sufficient mechanical strength for routine handling. Electrodes commonly are attached to the wafer by thermal evaporation of metals onto the quartz surface. For some metals a thin adhesion layer of Cr or Si is necessary.

The frequency of the QCM may be measured using either commercial or custom-designed frequency-counting equipment. With high-resolution counters such as the Philips PM6654 series, at 5 MHz, the frequency can be measured to within 0.1 Hz in 0.06 s. For a QCM oscillating at a fundamental frequency of 5 MHz, the sensitivity is about 18 $\text{ng cm}^{-2} \text{Hz}^{-1}$. With careful circuit design or signal averaging, noise levels for the EQCM are typically well below 1 Hz. It is possible, therefore, to measure very small mass changes. For example, a monolayer of Pb deposited on an Au surface has a mass of approximately 320 ng cm^{-2} , which corresponds to a frequency change of about 18 Hz. During a single scan the coverage can be measured to within 2% of a monolayer at a sampling rate of 10 Hz. Thus it is possible to measure submonolayer changes in the coverage of this species and many others on a time scale appropriate for electrochemical experiments.

Measuring monolayers on electrode surfaces. One of the first applications of the QCM to an electrochemical system was the measurement of the deposition of metal monolayers onto electrode surfaces (9). When a metal is reduced onto a foreign metal surface, the first monolayer often is deposited at potentials positive of the Nernstian potential for bulk deposition. This process is referred to as underpotential deposition (UPD) and is a convenient method for creating a single atomic layer of a metal. Early UPD experiments with the EQCM were performed *ex situ*. The metal monolayer was deposited in solution, washed, and dried, and the mass of the film was calculated from the EQCM response in air (9). More recently the EQCM has been used to monitor the UPD process in situ while the metal deposition is taking place (10).

Figure 2a shows the voltammetric response for the UPD of Pb on a polycrystalline film of Au (11). The peaks in the forward (negative going) scan correspond to the deposition of submonolayer amounts of Pb. The different

peaks are attributable to either varying crystal structure on the Au surface or to changes in the packing of Pb atoms on the surface. At approximately -0.5 volts versus SSCE (sodium-saturated calomel electrode) bulk deposition of Pb begins. On the return scan, bulk Pb is oxidized off of the surface followed by oxidation of the UPD layer. The simultaneous response of the EQCM attached to the Au film is shown in Figure 2b. The mass of the electrode increases as Pb is deposited on the electrode surface, and the frequency of the EQCM decreases. Each current peak in the forward voltammetric scan corresponds to a sudden decrease in the EQCM frequency. On the return scan, the mass of the electrode and the frequency of the EQCM return to their initial values.

The coverage (Γ) of Pb on the Au surface at any potential is calculated from the change in mass of the oscillat-

ing electrode. The frequency change during UPD is 18.0 Hz and corresponds to a mass increase of 0.32 $\mu\text{g cm}^{-2}$ or 1.5 nmol cm^{-2} for Pb ($f_0 = 5.03 \text{ MHz}$). This is the coverage expected for a hexagonal close-packed layer of Pb on Au. The resulting coverage data can be plotted against the integrated current to find the number of electrons transferred to each Pb atom on the electrode surface, the electroreduction valency (γ) for Pb. In 0.1 M HClO_4 , γ for the UPD of Pb on Au is found to be 2.0 and is approximately independent of potential. These data provide a convincing demonstration that the EQCM responds to changes in interfacial mass as predicted by the Sauerbrey equation.

The EQCM also has been used to measure the electroreduction of a monolayer of anions on an electrode surface. For example, both the voltammetric and EQCM response of a polycrystalline Au electrode to the electroreduction

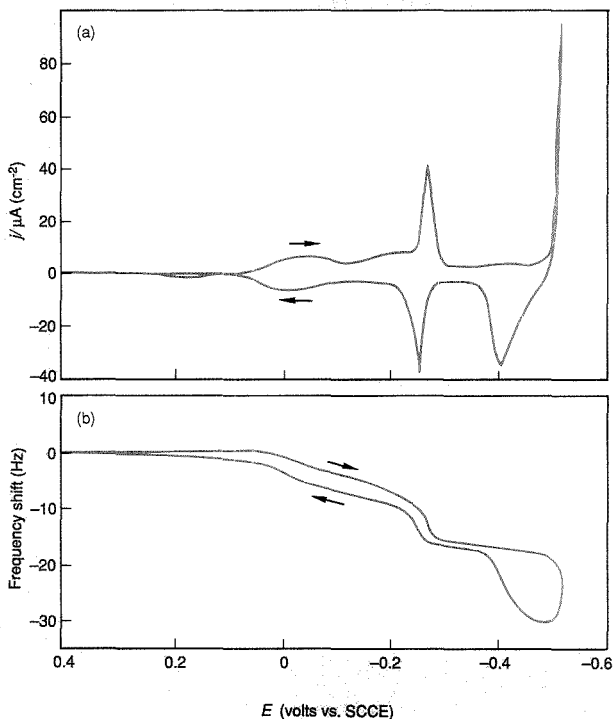


Figure 2. Cyclic voltammetry of the underpotential deposition of Pb (1.0 mM in 0.1 M HClO_4) on polycrystalline Au.

(a) Simultaneous current response and (b) frequency response of the EQCM. (Adapted with permission from Reference 11.)

of Br^- and I^- have been reported (12). The coverage of the ions can be determined directly from the EQCM response. Plots of charge versus coverage (Figure 3) indicate that the electro-sorption valencies for Br and I on Au in 50 mM NaClO_4 are -0.4 and -1.0 , respectively. Thus Br retains a partial negative charge on the electrode surface and I is totally discharged. These data are interesting in their own right, and they also demonstrate that electrolyte adsorption can influence the response of the EQCM. This should be considered when investigating adsorbed monolayers on electrode surfaces.

Measurement of mass changes in thin films on electrodes. Several authors have shown that the EQCM can be used to study the growth or dissolution of thin films on electrode surfaces. A few studies of thin metal films (13-16) have been reported, suggesting the utility of the EQCM as a monitor in plating or stripping baths. Although organic polymer growth suggests the possibility of nonrigid film behavior, Baker and Reynolds showed that for the growth of polypyrrole films the rig-

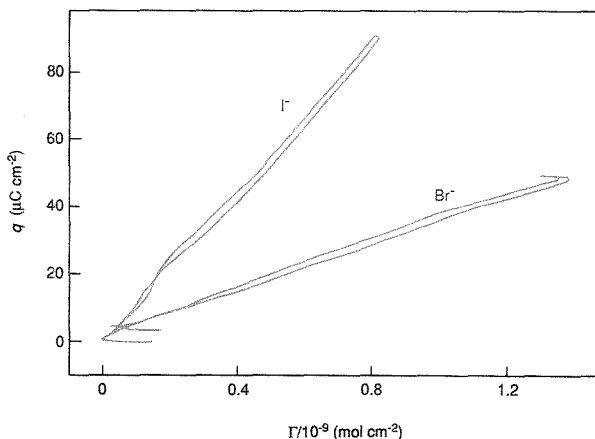


Figure 3. Electro-sorption of I^- and Br^- on polycrystalline Au. Integrated current versus coverage as measured with the QCM is plotted, with the slope proportional to γ . (Adapted with permission from Reference 12.)

When Buying TitraLab™ be Sure to Check your Fishing Tackle

TitraLab™ Titration Systems ensure you more time away from tedious routine tasks.

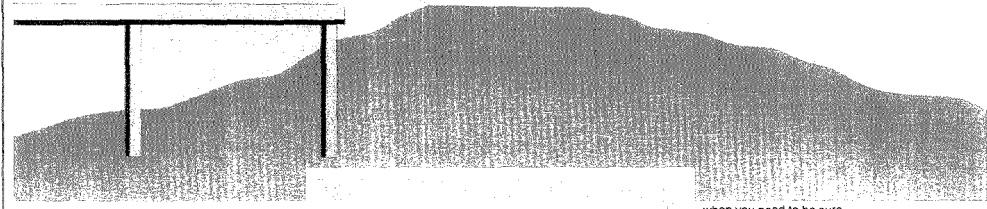
TitraLab automatically switches between electrodes and titrant/reagent burettes according to your methods. Time is saved and errors are eliminated.

Live titration curves on the screen make method development faster, and errors during routine operation can be seen immediately.

Time for instrument set-up is kept to a minimum by guided dialogue in plain English, German or French.

Check with your Radiometer product specialist to determine which TitraLab system will suit your needs, and find out about Radiometer's application support.

If you need precision and reliability in titration, be sure to contact your local Radiometer office and experience the convenience of TitraLab yourself.



- when you need to be sure ...

RADIOMETER ANALYTICAL A/S
KROGSHØJVEJ 49 · DK-2880 BACSVAERD · DENMARK
CIRCLE 138 ON READER SERVICE CARD

New!

American Chemical Society Announces An Intensive Three-Day Short Course . . .

SUPERCRITICAL FLUID EXTRACTION CHROMATOGRAPHY

Monday-Wednesday
December 4-6, 1989
Virginia Tech—Blacksburg, VA

An excellent course for those in need of practical laboratory experience in SFC/SFE

How You'll Benefit:

- Learn state-of-the-art techniques for performing SFE and SFC
- Gain hands-on experience working with chromatographs, column detectors, and extraction devices
- Use SFC to solve unique separation problems
- Couple SFE with SFC
- Interpret SFC data
- Learn ways to interface chromatography with detection devices
- AND MUCH MORE!

Course Instructor

Larry T. Taylor, Professor of Chemistry, Virginia Tech

For more information CALL COLLECT (202) 872-4508, ext. 1240. Or, use the coupon below to request a free descriptive brochure on this dynamic course.

American Chemical Society
Dept. of Continuing Education
Meeting Code VPI89120D
1155 Sixteenth Street, N.W.
Washington, DC 20036

Please send me a free brochure on the ACS Short Course, *Supercritical Fluid Extraction Chromatography* (SCFE8912) to be held December 4-6, 1989, at Virginia Tech in Blacksburg, VA.

Name _____
Title _____
Organization _____
Address _____
City, State, Zip _____

VPI89120D

REPORT

id-layer approximation holds (17). They were able to measure the mass of an electrodeposited film accurately over a relatively large thickness range, from 0 to 5 μm . As shown in Figure 4, these data were used to calculate the number of electrons transferred to each pyrrole molecule during film growth. Additionally, from measurements of the rate of film growth, they concluded that the polymerization process was second-order with respect to pyrrole concentration. Thus the EQCM was able to differentiate between the various possible mechanisms of film growth.

The EQCM is also well suited to the measurement of mass transport that can accompany redox processes occurring in thin films on electrodes (18, 19). Mass changes in the film associated with the gain or loss of any species are detected with the EQCM. Both ion and solvent transport have been measured directly in several systems, including thin inorganic polymers (20, 21), conducting polymers (22), and organic redox polymers (23, 24). The excellent sensitivity and large dynamic range of this device permit characterization of mass transport in films with thick-

nesses ranging from a few nanometers to many micrometers. The unraveling of the transport phenomena that occur during redox switching of such thin films has relevance to the ultimate rates at which charge may be injected or removed from these films. This ultimate rate of charge transport is an important factor in determining the utility of polymer-based devices in electronic, electrocatalytic, and sensor applications.

An example of the application of the EQCM to transport phenomena is its use to determine the extent of solvent transport during a redox event in a thin electroactive film. The EQCM provides unambiguous information about this process. Figure 5a shows the cyclic voltammogram for a thin film of nickel ferrocyanide (the nickel analogue of Prussian blue). The current peaks centered near 0.60 volts are attributable to the oxidation and reduction of the ion sites in the inorganic lattice. The changes in the EQCM frequency that occur during the redox switching of these ion sites in both H_2O and D_2O solutions are shown in Figure 5b. For this case, Cs^+ cations are the ionic species that are transported in and out of

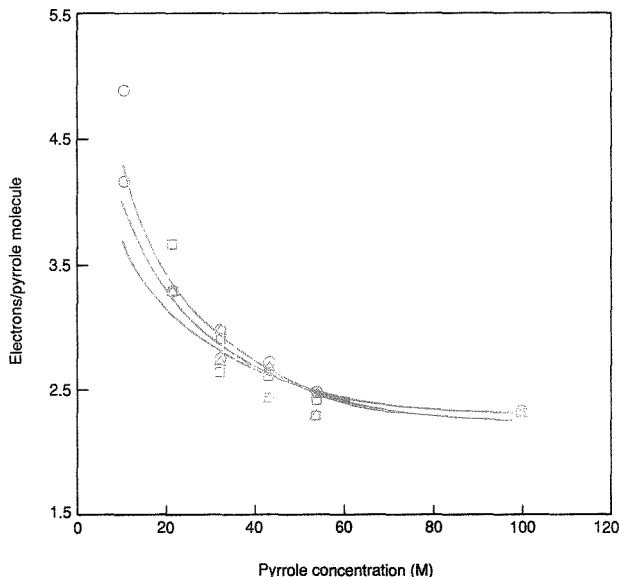


Figure 4. Electrons per pyrrole molecule as a function of pyrrole concentration with 50 (\circ), 65 (Δ), and 135 (\square) μg of poly(pyrrole tosylate) as deposited films.

(Adapted with permission from Reference 17.)

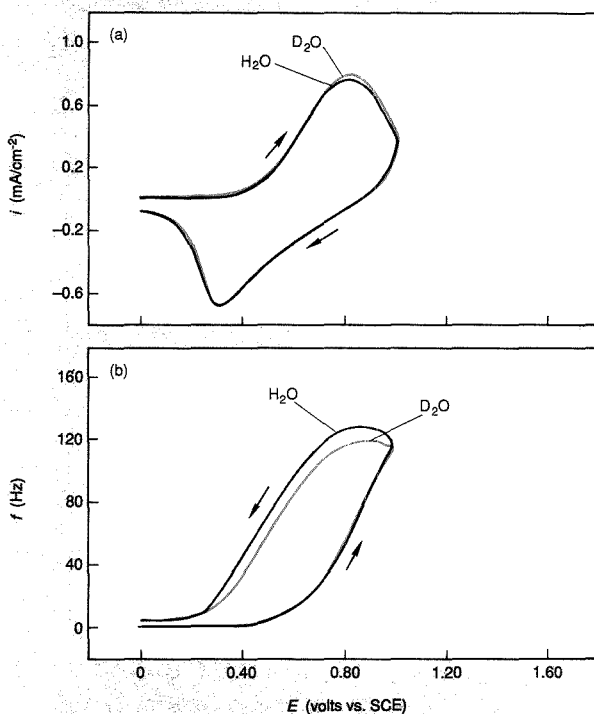


Figure 5. Cyclic voltammetry of a nickel ferrocyanide film in 0.1 M CsCl in H₂O and D₂O.

(a) Current response and (b) frequency response of the QCM. (Adapted from Reference 21.)

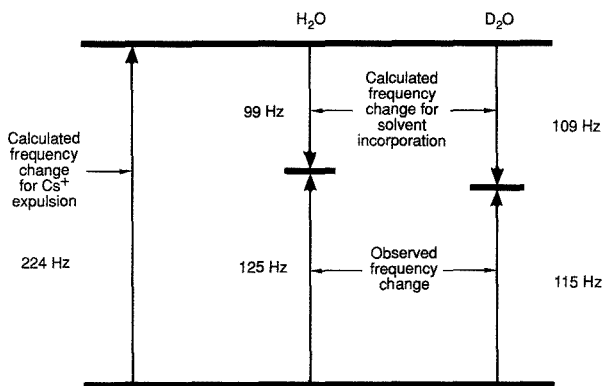


Figure 6. Schematic of the QCM frequency changes shown in Figure 5.

(Adapted from Reference 21.)

the film during electron injection and removal, respectively. Part of the mass loss during oxidation is attributable to Cs⁺ expulsion; reduction of the film leads to reincorporation of Cs⁺ into the film. Note, however, that the frequency changes observed for the H₂O and D₂O solutions are not the same, which suggests that solvent transport occurs during the oxidation and reduction of this film.

Because both the electrochemical charge and the mass changes are measured, independent calculation of the ion and solvent fluxes is possible, revealing that solvent transport occurs in the direction opposite to that for ion transport (Figure 6). The calculated frequency change for D₂O insertion is 10% larger than that for H₂O insertion, as expected based on the 10% difference in the molar masses of these species, and serves as a check on the assumptions inherent in the calculations (rigid-layer behavior and uniformity of the deposit). The important aspect of this study was the quantitative determination of the extent of solvent transport during a redox process for a thin film. It is especially significant that the measurement was made in the presence of simultaneous ion transport.

The analytical use of film-based EQCM devices is suggested by their extreme mass sensitivity and the ability to measure more than one property of the analyte. For example, it is possible to measure both the charge and mass of an electroinactive cation when it migrates into an electroactive polymer (18). A cation detector based on this principle has been demonstrated in a flow-injection system (19). This combined measurement scheme provided greater selectivity during ion detection. In addition to the electroanalytical use of the QCM, a number of research groups are investigating the nonelectrochemical use of the QCM in the liquid phase. For example, a recent report describes a glucose sensor using immobilized hexokinase (25). Most of the same considerations that pertain to use of the EQCM also apply to this type of thin-film sensor.

Both the elasticity (shear modulus) and the viscosity of the medium adjacent to the QCM electrodes can influence the nature of the QCM frequency response. In particular, the measurement of mass transport in thin films on the surface of the QCM can be affected by the viscoelasticity of the film. This effect is more important for thick polymer films than for thin, highly cross-linked films. A quantitative treatment of the influence of viscoelasticity is not yet available, but some strategies that allow for an evaluation of its impor-

tance in a given system have been discussed (22).

Future directions

At the present time, the challenges in the EQCM and QCM sensor fields are more chemical than instrumental. As discussed above, the response of these devices is nonspecific. Therefore the interfacial chemistry must be adjusted to give specific and reproducible measurements. In the sensor area the reproducible immobilizations of the desired chemical agents into thin films on the surface must be further developed. The vast amount of literature that has evolved in the modified electrode area (26) provides a wealth of information on the immobilization and stability of submonolayer to multilayer films on surfaces.

The EQCM has demonstrated its value as a tool for the elucidation of the mass transport processes that accompany redox processes in both monolayer and multilayer films on electrodes. It has also been demonstrated as a viable sensor technology. Applications that have yet to be investigated fully in-

clude its use in conjunction with spectroscopic and other probes of surface populations. Techniques for which such studies would be useful include surface-enhanced Raman spectroscopy, ellipsometry, and surface FT-IR. In such cases, the EQCM provides additional information to which any model of the interface must answer. As is the case with all such "hyphenated" techniques, this approach has advantages over single-method investigations. Such studies should be easily accessible with the EQCM; it offers relatively low cost and experimental simplicity.

The work by Dan Buttry described herein was supported in part by the Office of Naval Research.

References

- (1) Ballantine, D.; Wohltjen, H. *Anal. Chem.* **1989**, *61*, 704 A.
- (2) Buttry, D. In *In Situ Studies of Electrochemical Interfaces*; Abruna, H., Ed.; VCH Verlag Chemical, in press.
- (3) *Applications of the Piezoelectric Quartz Crystal Microbalance*; Lu, C.; Czanderna, A., Eds.; Elsevier: New York, 1984.
- (4) Bottom, V. E. *Introduction to Quartz Crystal Unit Design*; Van Nostrand Reinhold Co.: New York, 1982.
- (5) Sauerbrey, G. Z. *Z. Phys.* **1959**, *155*, 206.
- (6) Lu, C.; Lewis, O. J. *J. Appl. Phys.* **1972**, *43*, 4385.
- (7) Kanazawa, K. K.; Gordon, J. G. *Anal. Chim. Acta* **1985**, *175*, 99.
- (8) Muramatsu, H.; Tamiya, A.; Karube, I. *Anal. Chem.* **1988**, *60*, 2142.
- (9) Bruckenstein, S.; Swathirajan, S. *Electrochim. Acta* **1985**, *30*, 851.
- (10) Melroy, O.; Kanazawa, K. K.; Gordon II, J.; Buttry, D. *Langmuir* **1986**, *2*, 697.
- (11) Deakin, M.; Melroy, O. *J. Electroanal. Chem.* **1988**, *239*, 321.
- (12) Deakin, M.; Li, T.; Melroy, O. *J. Electroanal. Chem.* **1988**, *243*, 343.
- (13) Schumacher, R.; Muller, A.; Stockel, W. *J. Electroanal. Chem.* **1987**, *219*, 311.
- (14) Hinsberg, W.; Wilson, C.; Kanazawa, K. K. *J. Electrochem. Soc.* **1986**, *133*, 1448.
- (15) Hager, H.; Ruedisueli, R.; Buehler, M. *Corrosion* **1986**, *42*, 345.
- (16) Benje, M.; Eiermann, M.; Pitterman, U.; Weil, K. *Ber Bunsen-Ges Phys. Chem.* **1986**, *90*, 435.
- (17) Baker, C.; Reynolds, J. *J. Electroanal. Chem.* **1988**, *251*, 307.
- (18) Feldman, B.; Melroy, O. *J. Electroanal. Chem.* **1987**, *234*, 213.
- (19) Bruckenstein, S.; Wilde, C.; Shay, M.; Hillman, A.; Loveday, D. *J. Electroanal. Chem.* **1989**, *258*, 457.
- (20) Deakin, M.; Byrd, H. *Anal. Chem.* **1989**, *61*, 290.
- (21) Lasky, S.; Buttry, D. *J. Am. Chem. Soc.* **1988**, *110*, 6258.
- (22) Orata, D.; Buttry, D. *J. Am. Chem. Soc.* **1987**, *109*, 3574.
- (23) Varineau, P.; Buttry, D. *J. Phys. Chem.* **1987**, *91*, 1292.
- (24) Ward, M. J. *J. Phys. Chem.* **1988**, *92*, 2049.
- (25) Lasky, S.; Buttry, D. In *Chemical Sensors and Microinstrumentation*; Murray, R., Ed.; ACS Symposium Series; American Chemical Society: Washington, DC, 1989.
- (26) Murray, R. In *Electroanalytical Chemistry*; Bard, A. J., Ed.; Marcel Dekker: New York, 1984; Vol. 13, pp. 181-368.



Mark R. Deakin, an assistant professor at Florida State University, received his B.S. degree from Florida State University and his Ph.D. in analytical chemistry from Indiana University under the direction of R. Mark Wightman. He returned to FSU in 1987 after a postdoctoral appointment in the electrochemistry group at the IBM Research Laboratory in San Jose, CA. His research focuses on interfacial electrochemistry, including corrosion processes and the electrochemical deposition and dissolution of thin films on metal surfaces.



Daniel A. Buttry, an associate professor at the University of Wyoming, received his B.S. degree from the University of Colorado and his Ph.D. in electrochemistry from the California Institute of Technology. After spending a year at the IBM Research Laboratory in San Jose working on the application of surface EXAFS and the QCM to the characterization of electrochemical interfaces, he joined the faculty of the University of Wyoming in 1984. His research interests include fundamental studies of redox and other chemical processes in monolayer and multilayer films at surfaces, QCM and fiber-optic sensors, methods for reagent immobilization at surfaces, and interfacial chemistry in composite materials.

Get the whole picture from
the world's most cited
chemical publication

JOURNAL OF THE AMERICAN CHEMICAL SOCIETY

Editor: Allen J. Bard
University of Texas

Each biweekly issue of JACS gives you authoritative, original articles (plus concise communications hot off the press!) in every key arena of chemical research. What's more, JACS is the most competitively priced journal of its kind. Order your subscription today!

Call Toll Free 1-800-227-5558
Telex: 440159 ACPUI or
892582 ACPUB
Cable Address: JEICHEM

American Chemical Society
1155 16th Street, NW,
Washington, D.C. 20036
202-872-4363



FAX A P P E A L

Dear Reader:

If you have an urgent need for information on any of the products advertised in this issue, simply circle the appropriate inquiry numbers below and fax this form to us.

We will immediately relay your request to each of the advertisers involved and you will quickly receive data directly from them at no cost or obligation.

CIRCLE INQUIRY NO.	ADVERTISERS	PAGE NO.	CIRCLE INQUIRY NO.	ADVERTISERS	PAGE NO.
1	Advanced Graphics Software, Inc.	1160A	96	*Metrohm Ltd. Ecknauer & Schoch Werbeagentur ASW	1134A
3	*Alltech Chromad	1160A	98	*Mettler Instrument Corporation Gilbert, Whitney & Johns Inc.	1125A
26	*CDS Instruments Altman-Hall Associates	1163A	110	*Nicolet Analytical Instruments	1129A
28, 29	*Conostan Division/Conoco Specialty Products Robert Lamons & Associates	1178A	122	*O.J. Analytical	IFC
40	ES Industries Scientific Marketing Services, Inc.	1132A	129	*Perkin-Elmer Corporation Graystone	1149A
60	*Galileo Electro-Optics Corp. Legasse Associates Advertising, Inc.	1171A	125	*Phillips Scientific/Analytical Division Connors Publicity Ltd.	1166B
58	Gelman Sciences, Inc.	1146A	127	Plenum Publishing Corporation Plenum/Da Capo Advertising	1156A
65	*Hewlett-Packard Company Brooks Communications	OBC	138	Radiometer Analytical A/S	1151A
75	*Isotec, Inc. Kenyon Hoag Associates	1159A	152, 153	*Spectra-Physics	1166A
94	*Malvern Instruments, Inc.	1165A	150	*Supelco, Inc.	1131A
100-107	*Matheson Gas Products Kenyon Hoag Associates	1133A	172	*Varian Lanig Associates	1144A
			170	VG Masslabs Burgess Daring Advertising, Ltd.	1126A
			175	*Wheaton The Wheaton Agency	1175A

YOUR NAME _____ TITLE _____

ORGANIZATION _____

ADDRESS _____

CITY _____ STATE _____ ZIP _____

PHONE _____ FAX _____

Fax Operator: Please fax this form to JoAnn Ferrara at . . .

FAX NUMBER 203-454-9939



Plenum Books

CHEMISTRY RESEARCH & APPLICATIONS

MOSSBAUER SPECTROSCOPY APPLIED TO INORGANIC CHEMISTRY

Volume 3

edited by Gary J. Long and
Fernande Grandjean

A review from a previous volume:

"The book is well written, has been extremely well presented and . . . should soon become a standard text adopted by all Mossbauer laboratories."

—John Brooks, *Analytica Chimica Acta*

Applications on topics ranging from permanent magnets to biological mineralization. A volume in the Modern Inorganic Chemistry series.

0-306-43073-8/660 pp./ill./1989
\$115.00

PRINCIPLES OF CHEMICAL SENSORS

by Jiri Janata

Dr. Janata covers the principles of operation of chemical sensors in the four basic modes of transduction: thermal, mass, electrochemical, and optical.

0-306-43183-1/332 pp./ill./1989
\$39.50

SPECTROELECTROCHEMISTRY Theory and Practice

edited by Robert J. Gale

Provides detailed descriptions of the key practical and theoretical aspects of the modern spectroelectrochemical techniques that are likely to become routine aids in research and development.

0-306-42855-5/466 pp./ill./1988/\$85.00
text adoption price on orders of six or more copies: \$49.50

RECENT ADVANCES IN THIN-LAYER CHROMATOGRAPHY

edited by F.A.A. Dallas, H. Read,
R. J. Ruane, and I. D. Wilson

Discussions center around new developments in instrumentation, stationary phases, sorbents and modifiers, radial thin-layer chromatography, and practical applications of TLC.

0-306-42834-9/proceedings/262 pp./ill.
1988/\$59.50

Book prices are 20% higher outside the US & Canada

PLENUM PUBLISHING CORPORATION
233 Spring Street, New York, NY 10013-1578
Telephone orders: 212-620-8000/1-800-221-3369

CIRCLE 127 ON READER SERVICE CARD

INDUSTRIAL & ENGINEERING CHEMISTRY RESEARCH

PUBLISHED MONTHLY
Editor: Donald R. Paul
Univ. of Texas, Austin

Quality information that gives you the leading edge

Each month I&EC RESEARCH will help you meet today's intense challenges in chemical technology with...new ideas...new techniques...new procedures...and innovative research that could prove crucial to you and your work.

Don't miss a single issue! Subscribe today!

Call Toll free in the U.S. at 1/800-227-5558 for credit card orders, or write:
American Chemical Society
Marketing Communications Dpt.
1155 Sixteenth Street, NW
Washington, DC 20036

Telex: 440159 ACSPLU or 892582 ACSPLUBS
Cable address: JEICHEM

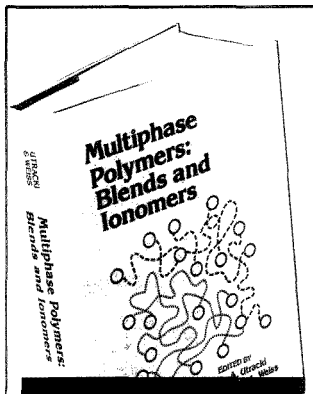
The American Chemical Society is interested in new software products!

Have you written a new program or a program to use with existing software for the IBM-PC or Macintosh that you think might have broad appeal in the scientific community?

If so, why not discuss it with the ACS? Call Susan Robinson at (202)872-4378 or write to her at the following address:

American Chemical Society,
1155 Sixteenth Street, NW,
Washington, DC 20036

ACS Software



Multiphase Polymers: Blends and Ionomers

Multiphase polymers encompass many types of polymer systems, each representing a distinct way of joining two or more polymers. This newly published volume focuses on two specific topics—polymer blends (including interpenetrating polymer networks) and ionomers. Similarly, both systems exhibit more than one phase, but the sizes of the dispersed phases are very different.

Key subject areas throughout the 21 chapters include:

- thermodynamics
- rheology
- interpenetrating networks
- new materials
- morphology
- solutions and plasticized systems

Both fundamental and applied aspects are considered. The chemistry, physics, processing, and final properties are treated.

Other subjects discussed include synthetic chemistry, theory, solution behavior, and morphological characterization. Current trends in the field are covered as are similarities and differences in problems associated with these materials and the approaches used to study them.

L.A. Utracki, Editor, National Research Council of Canada

R.A. Weiss, Editor, University of Connecticut

Developed from a symposium sponsored by the Division of Polymeric Materials: Science and Engineering of the American Chemical Society and by the Division of Macromolecular Science and Engineering of the Chemical Institute of Canada

ACS Symposium Series No. 395
512 pages (1989) Clothbound
ISBN 0-8412-1629-0 LC 89-6987
US & Canada \$99.95 Export \$119.95

ORDER FORM

American Chemical Society
Distribution Office, Dept. 30
1155 Sixteenth St., N.W.
Washington, DC 20036

or CALL TOLL FREE

800-227-5558

(in Washington, D.C. 872-4363) and use your credit card!

MEETINGS

Conferences

■ **Meeting on Modern Methods in the Analysis and Purification of Biopolymers: HPLC and Electrophoresis.** Dec. 4-5. Iselin, NJ. Contact: Janet Cunningham, Barr Enterprises, P.O. Box 279, Walkersville, MD 21793 (301-898-3772)

■ **Symposium on Electrochemical Techniques for Corrosion Measurement.** Dec. 4-6. Baltimore, MD. Contact: Ruth Rearick, EG&G Princeton Applied Research, CN 5206, Princeton, NJ 08543 (1-800-274-PARC)

■ **1st Pacific Polymer Conference.** Dec. 12-15. Maui, HI. Contact: J.C. Vogl, Polytechnic University, 333 Jay St., Brooklyn, NY 11201 (718-260-3069)

1990

■ **Meeting on Laser Applications to Chemical Analysis.** Feb. 5-8. Incline Village, NV. Contact: Optical Society of America, 1816 Jefferson Pl., N.W., Washington, DC 20036 (202-223-0920)

■ **Symposium on Hyphenated Techniques in Chromatography.** Feb. 22-23. Antwerp, Belgium. Contact: VCV, Section Analytical Chemistry, c/o R. Smits, BASF Antwerpen N.V., Scheldelaan, B-2040 Antwerp, Belgium

■ **International Conference on Tropospheric Ozone and the Environment.** March 19-22. Los Angeles, CA. Contact: Air and Waste Management Association, P.O. Box 2861, Pittsburgh, PA 15230 (412-232-3444)

■ **CHROMEXPO '90.** March 26. Washington, DC. Contact: Janet Cunningham, Barr Enterprises, P.O. Box 279, Walkersville, MD 21793 (301-898-3772)

■ **43rd Annual Conference of the Society for Imaging Science and Technology.** May 20-25. Rochester, NY. Contact: SPSE, 7003 Kilworth Lane, Springfield, VA 22151

■ **7th Symposium on Radiation Measurements and Applications.** May 21-24. Ann Arbor, MI. Contact: Helen Lum, 3034 Phoenix Memorial Laboratory, University of Michigan, Ann Arbor, MI 48109 (313-764-6214)

■ **38th ASMS Conference on Mass Spectrometry and Allied Topics.**

June 3-8. Tucson, AZ. Contact: Judith Watson, ASMS, P.O. Box 1508, East Lansing, MI 48826 (517-337-2548)

■ **Symposium on Optical Spectroscopic Instrumentation and Techniques for the 1990s: Applications in Astronomy, Chemistry, and Physics.** June 4-6. Las Cruces, NM. Contact: SPIE, P.O. Box 10, Bellingham, WA 98227 (206-676-3290)

■ **4th Annual Seminar on Analytical Biotechnology.** June 11-14. Arlington, VA. Contact: Janet Cunningham, Barr Enterprises, P.O. Box 279, Walkersville, MD 21793 (301-898-3772)

■ **14th Annual Conference of the International Precious Metals Institute.** June 17-21. San Diego, CA. Contact: Precious Metals Institute, Government Building, ABE Airport, Allentown, PA 18103 (215-226-1570)

■ **3rd International Symposium on Polymer Analysis and Characterization.** July 23-25. Brno, Czechoslovakia. Contact: Howard Barth, Du Pont Co., Experimental Station, E228/238, P.O. Box 80228, Wilmington, DE 19880 (302-695-4354)

Short Courses and Workshops

■ **Analytical Laboratory Services: Solving the Mysteries.** Nov. 1-2. Houston, TX; Nov. 15-16. Orlando, FL. Contact: Rose Ann Cochran, NUS, Analytical Updating Services, Park West Two, Pittsburgh, PA 15275 (412-788-1080)

■ **Workshop on Optical Emission Spectrochemical Analysis.** Nov. 14-16. Tewksbury, MA. Contact: Kathy Dickinson, ASTM, 1916 Race St., Philadelphia, PA 19103 (215-299-5480)

■ **Course on Fundamentals of Chromatographic Analysis.** Dec. 4-8. Kent, OH. Contact: Carl Knauss, Chemistry Dept., Kent State University, Kent, OH 44242 (216-672-2327)

These events are newly listed in the JOURNAL. See back issues for other events of interest.

Make

THE SOURCE
Your Source for
STABLE ISOTOPES

Isotec Inc. offers the scientific community one of the world's largest selections of stable isotopes and labelled compounds

18
15
13
**O
N
C
D**

- NMR Solvents
- Reagents
- Organics
- Inorganics
- Biologicals

You Get More From

THE SOURCE

- > 99% chemical purity
- High isotopic enrichment
- Competitive prices
- Fast delivery

Plus . . .

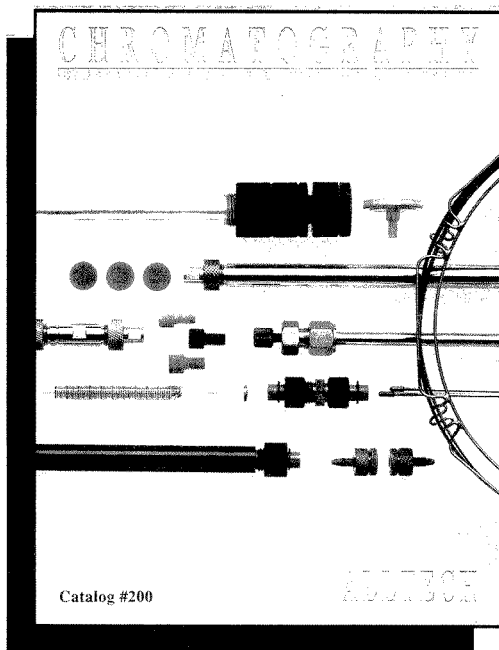
metal stable isotopes, helium-3 and other noble gas isotopes, other enriched stable isotopes, multiply-labelled compounds and custom synthesis

Call or write for your NEW complete price list today!

ISOTEC INC.
A Matheson, USA Company

3856 Benner Road, Miamisburg, OH 45342
(513) 859-1808 (800) 448-9760
Telex: 288278 Fax: (513) 859-4878

CIRCLE 75 ON READER SERVICE CARD



Alltech's NEW Catalog!

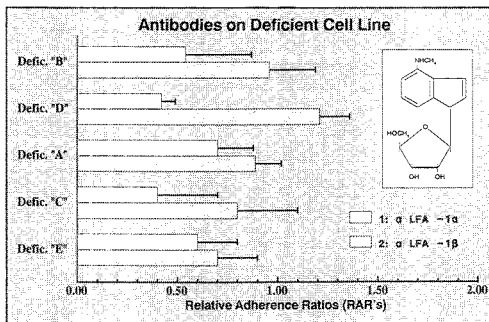
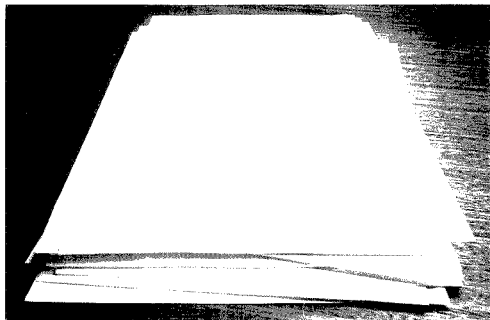
Now, more than ever, your most complete Chromatographic source. Over 700 pages of products and applications for GC, HPLC, TLC, Ion Chromatography, Sample Handling and Instrumentation.

Request Your Copy Today!



CIRCLE 3 ON READER SERVICE CARD

Make your data... greater.



No matter how interesting your scientific results are, they're not worth much unless you can communicate them to other people. That's where SlideWrite Plus comes in. You see, our powerful presentation graphics software for the IBM PC and compatibles can turn the data you worked so hard to capture into high impact

charts, graphs, slides and overheads — and do it all *in minutes*.

SlideWrite Plus gives you powerful graphing features, full drawing capability, flexible labeling with 16 fonts, and *extremely* high quality output on printers, plotters, and cameras. And that's just for starters. It's no wonder SlideWrite Plus tied for first

place in a recent *PC Week* poll!

Call us for a free demo diskette right now. We'll show you how SlideWrite Plus can help your results *get* results.

**Call for your FREE
full-featured trial diskette!
(408) 749-8620**

Advanced Graphics Software
333 West Maude Ave., Sunnyvale, CA 94086

SlideWrite Plus.™ We make your data look terrific.

CIRCLE 1 ON READER SERVICE CARD

Spectroscopy, Chromatography, Electrophoresis, and Materials Characterization Techniques

High Performance Liquid Chromatography. Phyllis R. Brown and Richard A. Hartwick. xii + 688 pp. John Wiley & Sons, 605 Third Ave., New York, NY 10158. 1989. \$75

Reviewed by David A. Hahn, The Upjohn Company, Kalamazoo, MI 49001

The editors of this book state in the preface that they hope to define the current state of the art in HPLC, explore the prospects and possible directions for future advances, consider other separation methods that might complement or supplant HPLC in the future, and provide a review of the basic theoretical concepts in HPLC—all in a single volume. Although these ambitious goals are not fully realized, this eclectic collection of topical overviews will be of interest to many chromatographers.

The book consists of 16 chapters, each a brief general review written by a well-known worker in the field. Topics include chromatographic theory (dynamics, solute retention, QSRRs); stationary phases (oxide, carbon, organic polymeric); separation approaches (size exclusion, affinity, chiral, field flow fractionation); and technique (high-speed LC, theory of derivatization, preparative LC, process LC, precision, multidimensional techniques). A brief assessment of future prospects is usually included. Overall, the quality of the individual contributions is good, although most tend to broad coverage at the expense of depth. Most chapters are well-referenced, with literature coverage through about 1986. The subject index is adequate.

As a whole, the book provides a partial picture of the state of the art in HPLC and some feel for possible directions for further research. However, the coverage is limited in some areas that are central to the current practice of HPLC, such as reversed-phase stationary phases and gradient elution.

Perhaps more importantly, there is no systematic coverage of research in molecular-level mechanisms of separation or chromatographic stationary-phase characterization, although these areas are briefly discussed in several chapters. In my view, an improved understanding of both processes and materials is critical to future developments in separations, potentially enabling a greater symbiosis with molecular recognition research. Molecular recognition concepts are mentioned in both the affinity chromatography and chiral separation chapters, but a more complete review of research in this area would have strengthened the volume.

The editors state that they hope that their book will be a "classic," in the sense that it will be valuable to users of chromatography and those who teach

“The volume will be of most value to chromatographers seeking a basic overview of an unfamiliar area.”

separation science 10 years from now as well as at present. Considering the intensity of research in separation science, it seems likely that both the selection of topics and most of the individual chapters will require updating long before 1999. Also, the accuracy of the contributors' views of the future remains to be determined. The volume will be of most value to chromatographers seeking a basic overview of an unfamiliar area. It might be useful as an ancillary text in a separations course but is limited by the lack of coverage in some areas.

Preparative-Scale Chromatography. Eli Grushka, Ed. 344 pp. Marcel Dekker, Inc., 270 Madison Ave., New York, NY 10016. 1989. \$100

Reviewed by R. M. Cassidy, Chemistry Department, University of Saskatchewan, Saskatoon, SK, Canada S7N 0W0

This book contains 15 contributions from 28 authors who are well known in the field of preparative chromatography. All of these contributions deal with very specific points and are presented in the format of a standard scientific manuscript prepared for publication in a scientific journal. In general, the manuscripts are well written and presented in a style that is clear and easy to read.

The introduction to the book does not make it entirely clear what the purpose of the publication is. The publication style and the wide range of subjects covered by the papers suggest that the contents may be the published proceedings from a conference. Each paper deals with one selected topic with no general overview other than that expected for a standard scientific publication. New data are presented and discussed in each contribution, but it is not clear if the papers have gone through a peer review process. Most of the contributions deal with packed-column technology, but the papers on instrumentation deal only with counter-current chromatography and continuous chromatography. This book claims "[it] closely examines different ways in which preparative-scale chromatography can be pursued—evaluating the advantages and disadvantages of each method," but falls somewhat short of this goal, partly because of its format. Consequently, this book cannot be recommended for the uninitiated.

For chemists with some background in preparative chromatography, however, this book does contain useful and

new information. Two papers discuss mathematical models for the prediction of peak shape for gas chromatography; one compares numerical simulations with experimental results, and the other simulates the effects of solute-solute interactions on peak shape. Another paper presents an experimental study of peak shapes obtained with ion exchange, reversed-phase, and adsorption packings. Experimental aspects of particle size, column width and length, sample size, sample injection, and flow velocity are covered by five of the papers; two detailed papers discuss various approaches for the isolation of albumin and oligonucleotides. Other subjects covered include the construction and evaluation of countercurrent chromatography (with two axes of rotation), continuous chromatography systems (with a brief review of options and the application of a column-array system to the kg/h production of sugars), and a short comparison of sample loadings in TLC for isocratic and step-gradient separations.

Nuclear Magnetic Resonance Spectroscopy. Frank A. Bovey. xiv + 653 pp. Academic Press, Inc., 1250 6th Ave., San Diego, CA 92101. 1988. \$50

Reviewed by Jim Haw, Department of Chemistry, Texas A&M University, College Station, TX 77843

Books on NMR spectroscopy are like California wines—there are quite a few of them these days, and each is best with certain foods or on certain palates. If you were laying down a collection of a dozen or so NMR books, the second edition of Bovey's *Nuclear Magnetic Resonance Spectroscopy* would be a good selection.

An updated version of a book originally published in 1969, the second edition also includes material by Lynn Jelinski and Peter Mirau. This book is best suited for the organic chemist or polymer scientist who already has some background in NMR spectroscopy; a beginning student, however, would find the organization and level of presentation to be daunting. The best parts of the book are the chapters on relaxation and NMR of macromolecules as well as lucid sections by Jelinski on experimental methods and NMR imaging.

With the continuing expansive growth of NMR spectroscopy and imaging, it seems that every scientific publisher wants several titles, and Bovey's second edition is one of a number of refurbished classics brought out to join new texts in meeting the need.

Many of these second editions are patchwork affairs, with new chapters on "new methods" sewn onto old fabric. Bovey's book occasionally suffers from this problem, although there is a partially successful effort to reference the relevant parts of new chapters within the old. In spite of this effort, there are some awkward sections that will certainly confuse the novice. One case in point is the discussion of the obsolescent technique of assigning ^{13}C solution-state spectra by off-resonance decoupling—which winds down by referring the reader to sections on 2D methods and spectral editing experiments. It would have been better to have either left out off-resonance decoupling entirely or to have used it as a historical perspective for motivating spectral editing. Some readers might be put off by the fact that many of the spectra reproduced in the figures were obtained at low fields or with CW excitation. The extensive references to original literature, however, are a plus.

The book's biggest weakness is its lack of cohesiveness—it is better read as a set of chapters on different aspects of NMR. It also suffers from an exclusively organic orientation. The contributions of NMR to the development of modern inorganic and organometallic chemistry cannot be understated, but there is little evidence of these contributions here. Chapters at the end of the book seek to introduce 2D NMR and NMR of solids; the success here is mixed, perhaps because they are considered "special" topics. Basic 2D methods and simple solid-state experiments like magic-angle spinning were

simulations, although a good PC-based spin simulation program might be even more useful. Synthetic organic chemists should also benefit from the discussions of scalar coupling and molecular shielding.

In conclusion, the 1988 vintage of Bovey is a respectable update of a classic. It has good complexity but perhaps a bit too much tannin for the novice palate. It goes well with polymers and organic spectral problems. With proper cellaring, it should retain its quality for another eight years or so.

A Guide to Materials Characterization and Chemical Analysis. John P. Sibilja, Ed. x + 318 pp. VCH Publishers, Suite 909, 220 East 23rd St., New York, NY 10010-4606. 1988. \$35

Reviewed by G. J. Scilla, IBM Watson Research Labs, Yorktown Heights, NY 10598

This book has evolved from an analytical facilities/capabilities guide published for internal use by the Corporate Analytical Sciences Laboratory of Allied Signal Incorporated, located in Morristown, NJ. The book covers a broad range of materials characterization techniques and is divided into the following topical chapters: molecular spectroscopy, mass spectroscopy, chromatography, electrochemistry, atomic spectroscopy, X-ray analysis, microscopy, surface analysis, thermal analysis, viscosity and molecular weights of polymers, physical properties of particles and polymers, physical testing, and scientific computation. The chapters are authored by current or recent members of the above-mentioned laboratory. Approximately 75 analytical techniques are covered.

The book is true to its title and is basically a guide to each of the techniques covered. As might be expected from any book that discusses such a broad range of material, no topic is treated in detail. Instead, the reader will find a brief summary of each of the techniques. Each summary includes a general statement of the technique's use, sample requirements, physical/chemical principles, applications (often with specific examples), limitations, and useful general references for further information. In some cases, the descriptions may be too general and may lack enough detail to be useful to someone with a strong background in materials characterization. In addition, there tends to be an emphasis on polymer-related topics. Despite these points, this book could be extremely useful as a starting point for those sci-

“ . . . best suited for the . . . scientist who already has some background in NMR . . . ”

coming into routine use 10 years ago, and we must dispel the illusion that one is doing something "different" by taking a set of data as a function of an evolution period or rotating the sample about an axis other than the vertical.

One reason to include Bovey's book in a collection of NMR tomes is the large amount of information in its tables and appendices. Representative of the level of detail in this book are the several hundred simulated spectra illustrating second-order effects for various spin systems. Synthetic chemists should benefit by ready access to these

entists and engineers who do not have an analytical background but need some guidance on which materials characterization techniques may be applicable to their projects and problems. The book may also be useful for the analytical professional as a quick reference for unfamiliar techniques.

Quadrupole Storage Mass Spectrometry. Raymond E. March and Richard J. Hughes. xx + 471 pp. John Wiley & Sons, 605 Third Ave., New York, NY 10158. 1989. \$70

Reviewed by R. G. Cooks, Department of Chemistry, Purdue University, West Lafayette, IN 47907

Throughout the 1970s, a small community of scientists worked diligently and with evident enjoyment on an exotic arrangement of electrodes known as the Paul ion trap. (Wolfgang Paul, its inventor, is the German scientist who was also responsible for the widely used quadrupole mass filter.) The efforts of the group included simulations of ion motion within these devices, studies on kinetics of ion-molecule reactions, and mass spectrometric studies using an external quadrupole mass filter attached to the Quistor. Among these workers were Ray March, who has teamed up with Richard Hughes to write this book, and John Todd, who has contributed a valuable opening summary chapter to it. In 1983, when George Stafford and his colleagues at Finnigan invented a new method of scanning the ion trap to produce mass spectra, the groundwork had already been laid for the rapid exploitation of the commercial quadrupole ion trap. The instrument has since been developed from a highly sensitive GC detector to a general-purpose mass spectrometer capable of chemical ionization, desorption ionization, and MS/MS experiments.

Analytical chemists in general, and not just mass spectroscopists, will need to become acquainted with this cousin of the quadrupole. Its rapid growth in popularity should be one motivation. The richness of the device for studies of thermochemistry and kinetics and for quantitative analysis also recommends such an effort. This book is an excellent place to start. It is also a valuable reference for those whose interests lie in other forms of MS. The first half of the book, and especially the chapters on the theory of quadrupole MS and the physics of the ion trap, are the principal strengths of the text. This relatively difficult material is presented with great clarity. Not only is the logic virtu-

ally faultless, but the insistence on good English, unambiguous symbols, and consistent units, together with well-chosen and well-reproduced diagrams, makes the book highly successful. The simulations of ion behavior are also exceptionally valuable.

The later chapters covering the commercial instruments are written from the difficult vantage point of being concurrent with a story that is changing rapidly. Within months of publication, a new version of the commercial trap was introduced; more recently still, the mass range has been extended by more than an order of magnitude beyond its original commercial limit of 650 daltons, while use of SIMS and other external ionization sources has been shown to allow biomolecule characterization. The extremely high sensitivity of the instrument is evident in these applications. Another consequence of writing a book on a rapidly developing subject is that citations to formal publications tend to be neglected in favor of conference proceedings. A heavy emphasis on such sources characterizes the last two chapters of this book.

However, this is such a fine effort

that one can only be grateful to the authors. Their work is likely to serve as a basis for all future treatments of the subject, and it will surely facilitate the further development and utilization of ion traps. The present rapid growth in use of ion traps suggests that such gratitude will be felt by a growing number of scientists.

New Directions in Electrophoretic Methods. James W. Jorgenson and Marshall Phillips, Eds. xi + 275 pp. American Chemical Society, 1155 16th St. N.W., Washington, DC 20036. 1987. \$65

Reviewed by John C. Ford, Department of Chemistry, Indiana University of Pennsylvania, Indiana, PA 15705

This book was developed from a 1985 symposium sponsored by the ACS Divisions of Agricultural and Food Chemistry and of Analytical Chemistry. The editors' stated intention "... was to acquaint chemists with state-of-the-art electrophoretic technology and its applications," and the topics were apparently chosen to provide the reader



GC-MS-FTIR

Sample inletting systems for solids, liquids & gases

Purge and trap concentrators for GC and GC/MS

- Models for R&D and environmental uses
- Improve sensitivity
- Ambient or cryogenic trapping
- Eliminate cold spots, contamination

Pyroprobes for GC, MS and FTIR

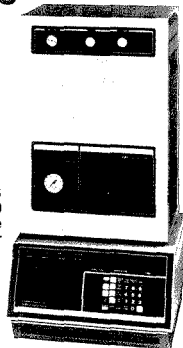
- Simplify solid analysis
- Improve quantitation
- Fast, accurate, repeatable
- Replaceable filaments

Pyrolysis • Purge & Trap • Oxidative Studies • Dynamic Headspace • Thermal Processing • Air Sampling

No matter what your sample problem, we've probably already solved it.

800-541-6593

CDS
Model 330
R&D Sample
Concentrator



CDS
INSTRUMENTS

A Product Line of Autoclave Engineers
7000 Limestone Road, Oxford, PA 19363
Fax: 215-932-4158 Telex: 83-5308

CIRCLE 26 ON READER SERVICE CARD

with a survey of the major issues of interest in the application of electrophoretic techniques. Overall, the editors have achieved their goal.

After an overview of electrophoretic technique, thorough discussions are presented on immobilized pH gradients in isoelectric focusing (IEF), rehydratable gels, and silver staining. These chapters provide a novice with an understanding of the constraints on the techniques of gel electrophoresis and IEF. This is important if one is trying to select a procedure to solve a specific analytical problem.

Similarly, standardization of a technique is particularly important to chemists concerned with QA/QC applications. A chapter dealing specifically with the choice of electrophoresis and electrofocusing standards thoroughly describes the situation and also details possible directions for intralaboratory standardization. Likewise, a chapter on the standardization of IEF procedures describes one laboratory's solution to this problem. This latter discussion is less satisfying than the former, as it does not address the problem from a global viewpoint but rather focuses on the standardization of the techniques and procedures employed by the authors' group; nonetheless, much valuable information is presented.

After a presentation of selected applications, the remainder of the book describes specific techniques such as capillary electrophoresis, isotachopheresis, and pulsed-field techniques. These point out the direction of current research on electrophoretic methodology and are of equal interest to novices and to those already applying electrophoresis. However, a caveat is appropriate here: These fields—and in particular, capillary electrophoresis—have progressed beyond the discussions presented in this volume. As is the case with most such symposium proceedings, the then-current papers are now somewhat dated.

As its origins would suggest, this is not a laboratory manual, and it is improbable that one could successfully apply a procedure based solely on the information here. Indeed, the amount of experimental detail presented varies from chapter to chapter. However, all of the chapters have ample references to the then-current literature, and numerous detailed manuals are available to describe electrophoretic techniques.

Two complaints might be made regarding the content of the book. First, although electrophoresis is closely associated with the separation of polypeptides and proteins and of nucleic acids, it is also applicable to a number of other problems. Unfortunately, this

text does little to indicate the full scope of the technique, because all but two of the 16 chapters deal directly or indirectly with the two classes of biopolymers mentioned above. Second, little or no discussion of the theoretical basis of electrophoresis is presented. This is particularly surprising in light of current developments concerning the reputation of large DNA fragments. These omissions are relatively minor, given the overall intent of the editors.

This book not only provides a survey of relatively recent developments for workers already using electrophoresis but also serves as an introduction to the technique (and its associated literature) for the chemist seeking to use electrophoresis to solve a specific problem. However, because of the shortcomings mentioned here, acquiring the book oneself is perhaps less satisfactory than reading the library's copy.

Auger Electron Spectroscopy. C. L. Briant and R. P. Messmer. 259 pp. Academic Press, 465 South Lincoln Dr., Troy, MO 63379. 1988. \$70

Reviewed by Robert Shaw, Division of Chemistry and Biological Science, Army Research Office, Research Triangle Park, NC 27709

This is volume 30 of the *Treatise on Materials Science and Technology*. Now, according to my dictionary, a treatise is a methodical discussion of the facts and principles of a field of study. The matchless volumes on atomic and molecular spectroscopy by Herzberg comprise a treatise. A complete and methodical discussion requires a single master (like Herzberg) whose vision encompasses an entire field, or a carefully orchestrated effort by several authors, each providing a separate, complementary piece of the complete picture.

The cover of this book carries the names of two editors; there is no single master. Inside we find the names of more editors—the "Treatise Editor" and his five-person editorial board. All of these, we must presume, have taken an active role in producing this volume. All of this editing should have produced a successful orchestration. It did not.

There is one outstanding chapter in this uneven book: the last and longest one, on Auger photoelectron coincidence spectroscopy, by G. A. Sawatzky. Its treatment is methodical and complete. The introduction is excellent, theory and experimental practice are described and explained, and several research examples are given. The writ-

ing style is engaging, and the material is presented so that it is accessible to those who are not experts in the field. This chapter deserves better company.

The surface segregation kinetics chapter seems incomplete to me. The introduction does not clearly define surface segregation. Does it include the formation of islands? What about defects? Surface steps? The section on sample preparation is too brief to be useful to someone who does not already know the subject, and there is no mention of damage to the surface caused by various cleaning techniques. This difficulty can be addressed by the use of a diffraction measurement in tandem with the Auger electron analysis, but I can find no discussion of this by the authors.

The chapter on local electronic structure information starts with a treatment neglecting electronic relaxation. In my opinion, this is misleading. The long section on fingerprint analysis is not convincing—one cannot predict when such analysis will fail. I disagree with the conclusion that Auger electron spectroscopy will be generally useful for the elucidation of adsorbate bonding; the extreme perturbation of the Auger transition is not conducive to measurements of bonding.

The metallurgical application chapter consists of a series of examples with no general development of the subject and is probably of no interest to those outside of a small circle of aficionados.

Finally, in a chapter on the historical development of Auger electron spectroscopy, there is a very narrowly focused description of the activities of a few people. In particular, this description ignores the development of betaray spectrometers for high-resolution measurements of photoelectron and Auger electron energies by Siegbahn and his colleagues in the 1950s. At times the article becomes merely an encomium for one particular instrument company and the people who work there—material in no way suitable for a scientific text. The authors of this chapter, and of the other chapters criticized here, are not to blame; they were simply responding to an invitation. The editors had the responsibility of putting this book together and ensuring its quality.

We are left with several questions. Some of the questions are merely interesting: What function, if any, did the editors play in the production of this book? Why do they call it a treatise? Some questions are much more important: Who should buy this book? My review copy arrived with a slip of paper listing a price of \$69.50 for about 250 pages.

Books Received

Lasers, Molecules, and Methods. Joseph O. Hirschfelder, Robert E. Wyatt, and Rob D. Coalson, Eds. xvii + 1022 pp. John Wiley & Sons, 605 Third Ave., New York, NY 10158. 1989. \$125

This is volume 73 in the series *Advances in Chemical Physics*. The topics covered in this 23-chapter book include multiple scales, linear and non-linear systems, Monte Carlo methods, laser-driven atomic excitations, line-shapes and semiclassical dynamics, and classical chaos. Most of the references span the 1960s through the 1980s.

X-Ray Spectroscopy in Atomic and Solid State Physics. J. Gomes Ferreira and M. Teresa Ramos, Eds. viii + 423 pp. Plenum Press, 233 Spring St., New York, NY 10013. 1988. \$85

This volume is the proceedings of the NATO Advanced Study Institute on X-Ray Spectroscopy in Atomic and Solid-State Physics held in September of 1987 in Vimeiro, Portugal. The sections of the book include Auger Electron Spectroscopy, X-Ray Fluores-

cence, Electron Energy Loss, and Instrumentation. Most of the references are from the 1980s. Abstracts, a list of the participants, and an index are included.

The Nuclear Overhauser Effect in Structural and Conformational Analysis. David Neuhaus and Michael Williamson. xxii + 522 pp. VCH Publishers, 220 East 23rd St., New York, NY 10010-4606. 1989. \$95

The topics covered in this 12-chapter book include steady-state NOE, kinetics, 1D and NOESY experiments, structure elucidation, and biopolymers. The references are from the 1970s and 1980s. Appendices, an index, and a list of symbols are included.

Gas Phase Inorganic Chemistry. David H. Russell, Ed. xv + 412 pp. Plenum Press, 233 Spring St., New York, NY 10013. 1989. \$80

Topics include reactions of atomic metal ions, nucleophilic addition reactions, structure-reactivity relationships, atomic clusters, photoelectron spectroscopy, and tandem MS. The references are from the 1970s and 1980s. An index is included.

Modern Aspects of Electrochemistry, No. 19. B. E. Conway, J. O'M. Bockris, and Ralph E. White, Eds. xi + 403 pp. Plenum Press, 233 Spring St., New York, NY 10013. 1989. \$65

The chapters are titled Transport Models for Ion-Exchange Membranes, Iron and Its Electrochemistry in an Active State, Theory of the Effect of Electrodeposition at a Periodically Changing Rate on the Morphology of Metal Deposits, Theory and Applications of Periodic Electrolysis, Electrocatalytic Properties of Carbon Materials, and Spin-Dependent Kinetics in Dye-Sensitized Charge-Carrier Injection into Organic Crystal Electrodes. Most of the references are from the 1970s and 1980s. An index is included.

Analysis of Polymers: An Introduction. T. R. Crompton. viii + 362 pp. Pergamon Press, Maxwell House, Fairview Park, Elmsford, NY 10523. 1989. \$41

This book covers the determination of elements and functional groups, fingerprinting, microstructure, thermal methods, fractionation, additives, volatiles, and general properties of polymers. The 1100 references are from the 1960s and 1970s. An index is included.

NO ONE UNDERSTANDS PARTICLE SIZING BETTER THAN MALVERN

Nearly 20 years of designing and making laser-based particle sizers have given Malvern an unrivalled understanding of the technology and of the needs of those concerned with characterizing small particles. The Malvern range is designed to meet those needs.

MasterSizer - the high resolution 0.1 - 60 micron particle sizer with automatic sample handling; the **SERIES 2600c** range of modular particle sizers for dry powders, emulsions and sprays up to 1880 microns; the revised **3600Ec** compact and cost effective sizer for emulsions or

powders in suspension up to 564 microns.

For submicron particles, the **SYSTEM 4700c** laser light scattering system and **AutoSizer IIc** offer particle sizing down to a few nanometres and molecular weight measurements for research or quality control applications; the new **Zeta-Sizer 3** is the very latest in microelectrophoresis for zeta potential measurements and in multi-

angle PCS particle sizing. We would like to tell you more about the system that's right for you. Please contact us now with details of your current or proposed application.



MALVERN

Malvern Instruments, Inc.,

10 Southville Road, Southborough, MA 01772.

Telephone: (508) 480 0200 Telex: 311397 Fax: (508) 460 9692

U.K. Malvern Instruments Ltd., Spring Lane South, Malvern, Worcestershire WR14 1AQ.

Telephone: (0684) 892456

Telex: 339679 MALINS G Fax: (0684) 892789

W. Germany Müttek GmbH, Arzbergerstrasse 10, D-8036 Herrsching.

Telephone: 08152 2046

Telex: 5270249 Fax: 08152 4374

CIRCLE 94 ON READER SERVICE CARD

Environmental Scientists

Lawrence Livermore National Laboratory, located in the San Francisco Bay area, is one of the Nation's premier research and development organizations. Our Nuclear Chemistry Division currently has challenging opportunities available for creative, dynamic scientists who have achieved national recognition for their scientific contributions to multidisciplinary environmental research.

The successful applicants will support a major new environmental initiative at the Department of Energy's Nevada Test Site that will be coordinated with a general expansion of research in environmental, waste, and geoscience areas. They will also provide complementary scientific skills and technical coordination for a multidisciplinary team assembled to address a broad range of environmental questions. Major responsibilities include: the design, conduct and publishing of field oriented research, identification of basic and applied research needs, short and long range technical planning, and communication/coordination with managers and scientists.

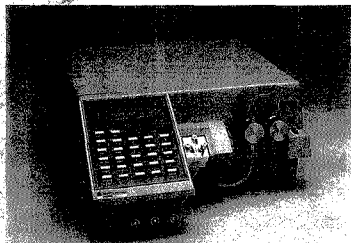
Requirements include a minimum of 5 years of professional experience, a demonstrated ability to design/direct multidisciplinary environmental research projects with both basic and applied objectives, excellent management abilities, and good communication/interpersonal skills. Research experience in regions of interior drainage typical of the Southwestern United States desirable, but not necessary. Some field work and travel required.

We offer a competitive salary and excellent benefits. For consideration, please forward your resume to: **Art Wong, Professional Staffing, Lawrence Livermore National Laboratory, P.O. Box 5510, L-725, Dept. KANAF904B, Livermore, CA 94550.** U.S. citizenship required. An equal opportunity employer.

University of California

**Lawrence Livermore
National Laboratory**

LC pumps with the best warranty in the industry:



LC Pump SP8800

5-Year Warranty

Ternary Gradient Version
Isocratic Version
Conforms to GLP
BioCompatible Option

For good reason.

Spectra-Physics quality.

For more information, call (800) 424-7666

Autolab Division M/S 62-75
3333 North First Street
San Jose, CA 95134-1995

Spectra-Physics

Discover the Quality

©1989 Spectra-Physics, Inc.

Zeolite Synthesis

Here in one volume is a complete progress report on the various aspects of zeolite synthesis on a molecular level. No other source covers this subject so completely!

This new title provides many examples that illustrate how zeolites can be crystallized and what the important parameters are that control crystallization. A variety of topics covered in this important book include: • crystallization techniques • gel chemistry • crystal signs and morphology • the role of organic compounds • novel synthesis procedures. With forty-two chapters, this valuable title offers a complete review of zeolite synthesis as well as the latest findings in this important field. Valuable new methods are highlighted such as VPI-5—the first 18-membered ring molecular sieve. In addition, examples of modern spectroscopic characterization of reactants and reaction intermediates are provided. Also covered is the chemistry of silicate solutions and reactant effects on crystallization products.

This essential volume contains benchmark contributions from many notable pioneers in the field including R.M. Barrer, H. Robson, and Robert Milton.

Mario L. Occelli, *Editor*, Unocal Corporation
Harry E. Robson, *Editor*, Louisiana State University

Developed from a symposium sponsored by the Division of Colloid and Surface Chemistry of the American Chemical Society

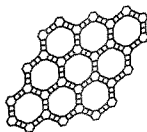
ACS Symposium Series No. 398 643 pages (1989) Clothbound
ISBN 0-8412-1632-0 LC 89-6884 US & Canada \$139.95 Export \$167.95

Order from: **American Chemical Society, Distribution Office, Dept. 33**
1155 Sixteenth St., N.W., Washington, DC 20036

or CALL TOLL FREE **800-227-5558**
(in Washington, D.C. 872-4363) and use your credit card!

Zeolite
Synthesis

Zeolite Synthesis



Over 600 pages

Circle 152 for sales rep. Circle 153 for literature.

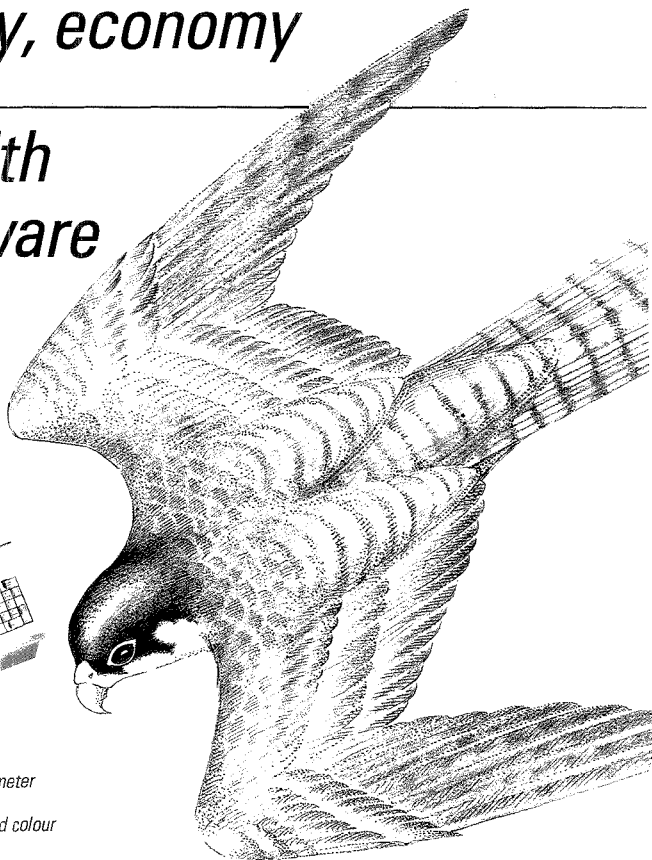
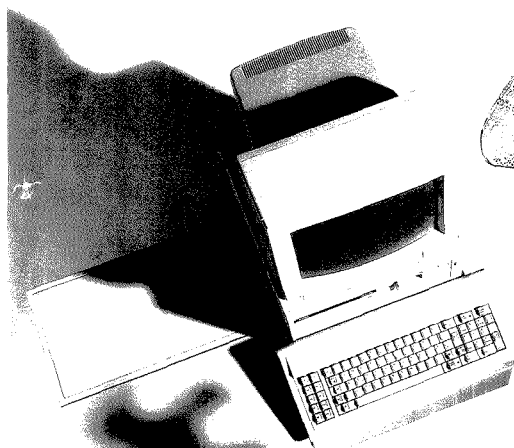


PHILIPS

Speed, accuracy, economy

Philips Analytical

New UV/VIS with Falcon PC software



*PU8710 scanning spectrophotometer
with Falcon software.
Available with or without PC and colour
plotter as required.*

Philips has introduced a new development in UV/VIS.
PU8710 – a scanning spectrophotometer at a really low price.

And it's so easy to use thanks to the specially designed
Falcon PC software. Now you can perform both simple and
complex data handling and method storage with total
confidence.

Falcon-Scan, Falcon-Quant and Falcon-Rate provide you

with an effortless step to sophistication in UV/VIS. The
colour plotter ensures accurate records, too.

PU8710 is the latest addition to the very successful PU8700
range which offers the best in easy-to-use scanning UV/VIS
instrumentation plus total customer support.

Swoop down on the best in UV/VIS. Contact us today and
we'll wing you full details.



PHILIPS ANALYTICAL - BIGGER IDEAS FOR BETTER ANALYSIS

For more information about the Philips Analytical UV/VIS spectrophotometry range, contact:

Philips Scientific Analytical Division York Street, Cambridge Great Britain CB1 2PX Tel. 0223 358866 Telex: 817331 Fax: 0223 312764

or **Austria:** (0222) 60101 – 1792 **Belgium:** (02) 525 62 75 **Denmark:** (01) 57 22 22 **Finland:** (90) 502 63 56 **France:** (1) 49 42 81 62

Germany: (0561) 501 384 **Italy:** (02) 64 49 12 **Netherlands:** (040) 783 901 **Norway:** (02) 68 02 00 **Spain:** (1) 404 22 00 **Sweden:** (08) 782 1591
Switzerland: (01) 488 22 11

CIRCLE 125 ON READER SERVICE CARD

UV26

We'll put all the latest advances in the chemical sciences right in your hands... And you won't need to lift a finger!

AMERICAN CHEMICAL SOCIETY STANDING ORDER PLANS

The ACS has a simple way to ensure that your library always has the chemistry titles your patrons require. It's called the ACS Standing Order Plans.

With ACS Standing Order Plans, you can save the time you'd otherwise spend on literature searches and purchase order details . . . and make certain that your library has the titles your patrons want—when they need them.

AS EASY AS 1-2-3

You can select from three Standing Order Plans—choose one or all or a combination . . . whatever best suits your patrons' needs!

1.

By Series:

Advances in Chemistry Series
ACS Symposium Series
ACS Monographs
Professional Reference Books
All ACS Series

2.

By Single Title:

ACS Abstract Books
ACS Directory of Graduate Research
College Chemistry Faculties

3.

By Subject:

Analytical • Agricultural/Agrochemical • Biological • Biotechnology • Carbohydrate • Cellulose/Paper/Textile • Colloid/Surface • Computers in Chemistry • Electronic Materials • Environmental/Chemical Health and Safety • Food/Flavor • Energy/Fuel/Petroleum/Geochemistry • Industrial/Chemical Engineering • Inorganic • Materials Science • Medicinal/Pharmaceutical • Nuclear • Organic • Polymer/Applied Polymer Science • Physical Chemistry

PLUS FIVE NEW SUBJECT AREAS . . . Chemical Information • Directories • History • Non-Technical • Toxicology!

You tell us which Standing Order Plan (or Plans) you'd like—1, 2, 3, or a combination. Your one-time order assures prompt, automatic delivery of each new title in the plan or plans you've chosen as soon as it's published. We'll send you an invoice with your shipment. You'll have thirty days to examine each new book and (if you decide for any reason) to return it for full credit. And you may modify or cancel your Standing Order Plan at any time. It's that easy!

Make sure your chemistry resources are always complete—don't overlook a single book from the world's most respected publisher in the chemistry field. Enroll in ACS Standing Order Plans today.

Write to American Chemical Society, 1155 Sixteenth Street, N.W., Washington, DC, 20036. Or call us TOLL FREE (800) 227-5558.

25 TO
CHOOSE
FROM!

After 25 years of monitoring the ozone layer, the British Antarctic Survey in 1982 measured an unusual springtime decline in the levels of ozone. Variations in ozone levels had been observed before, and they decided against sounding an alarm. Furthermore, the researchers were in the midst of upgrading their instrumentation. However, by October 1984 the Survey scientists were convinced they were observing a new, dramatic trend. Soon after they announced their observations (1), a flurry of research activity established the fact that chlorofluorocarbons (CFCs) were responsible for destroying Antarctica's protective layer of ozone (2, 3).

Today, ozone in Antarctica's upper atmosphere during the springtime is at

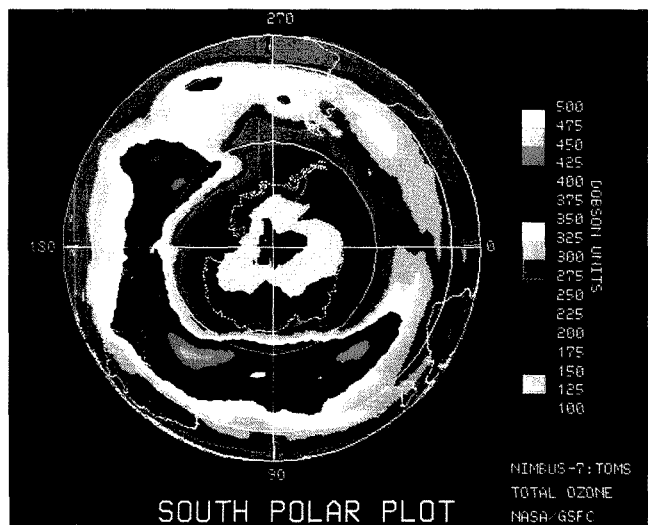
FOCUS

levels approximately one-half of the values observed in the mid-1970s. Early research suggests that a similar loss of ozone is occurring over the Arctic, although at a much slower rate (4).

Central to the discovery of the "ozone hole" and the mechanism of its formation has been data retrieved from scores of analytical instruments. Researchers collecting these data face a series of daunting problems. Not only must they collect measurements in distant polar regions, but their quarry, the ozone layer, lies in the stratosphere approximately 15-50 km above the Earth's surface. Furthermore, the atmospheric chemistry depends on light-initiated reactions and thus requires measurements covering day and night.

The analytical armada attacking this problem has engaged instrumentation situated on the ground, in space, and carried by balloon or airplane to altitudes of 20 km and higher. Backing them up are laboratory kinetics experiments and complex computer models

of the atmosphere that generate mechanistic pictures of the effects of CFCs on the planet's ozone layer.



This Southern Hemisphere plot of total ozone distribution for October 5, 1987, shows a region bounded in purple where the total ozone is less than 200 Dobson Units (DU). Within the purple area is a black region where the ozone is less than 125 DU. The lowest ozone value ever observed, 109 DU, is located in this black area near the South Pole. This plot also shows that the ozone hole area is larger than the Antarctic continent, a land area covering approximately 14 million km².

of the atmosphere that generate mechanistic pictures of the effects of CFCs on the planet's ozone layer.

It all began nearly a decade before the British discovery of the Antarctic ozone hole. F. Sherwood Roland and Mario Molina from the University of California at Irvine along with Richard Stolarski and Ralph Cicerone of the University of Michigan predicted that CFCs released into the atmosphere could reduce the ozone layer. "I always

believed in the prediction," says Stolarski, now at NASA's Goddard Space Flight Center in Greenbelt, MD, "but I never believed that it would be as clear-cut as the ozone hole."

Stolarski and the others feared that chemically inert CFCs could slowly rise through the atmosphere until they emerged above the ozone layer. There, high-energy UV light with wavelengths as short as around 200 nm could photochemically cleave CFC molecules, pro-

PHOTO COURTESY OF ARLEN J. KRUEGER, GODDARD SPACE FLIGHT CENTER

ducing chlorine free radicals. The chlorine radicals, in turn, initiate reactions that catalytically remove O₃.

The discovery of an ozone hole followed extensive ground-based UV measurements by the British scientists. That data came from Dobson spectrophotometers, which have been the standard instruments for determining total stratospheric O₃ since the 1950s. (The late Gordon M. B. Dobson of Oxford University pioneered work in this field, and his colleagues have honored his name with the unit of ozone concentration: 1 Dobson Unit (DU) = 10⁻³ atm-cm = 2.7 × 10¹⁶ molecules/cm².)

The instrument consists of a double or tandem monochromator with an optical wedge to balance light from two different wavelengths. To eliminate interference from atmospheric Rayleigh scattering, the spectrophotometer determines ozone from a ratio of wavelengths taken from the 300–350-nm range. Ratios have been selected that compare two close wavelengths that have very different absorptivities for O₃ absorption. For instance, the "A" wavelengths, one of the ratios selected, compares 305.5 with 325.4 nm (5).

Accurate data rely on careful calibration of the instrument. The total ozone value then depends solely on the optical wedge setting and the sun's height in the sky.

One reason the British researchers initially doubted their findings was that American scientists failed to spot the developing hole in the large database collected with the Nimbus 7 satellite. Subsequently that satellite has provided some of the best images of the hole.

Two instruments aboard Nimbus 7 have kept daily track of ozone levels (6). The Solar Backscatter Ultraviolet (SBUV) instrument is also a double monochromator that has been designed to operate over five decades of light levels. The instrument, explains Goddard's Arlin Krueger, measures the Earth's albedo—the fraction of solar light reflected back to space—by operating in two modes. Either it measures direct sunlight reflected from a diffuser of known reflectivity or it measures sunlight reflected from the Earth.

Measurements in the range of 310–340 nm are used to calculate column integral or total ozone amounts. Light in this range scatters from the troposphere and cloud tops, which are below the ozone layer, as well as from the Earth's surface. Like the Dobson spectrophotometer, the SBUV experiment eliminates errors from scatterers above the ozone layer and from other absorbing species by calculating total O₃ from

a ratio of wavelengths (7). The direct sun measurement furnishes the reference values.

The SBUV measurements in the 250–305-nm range are used to infer the O₃ concentration profile with altitude. These photons are strongly absorbed by O₃ and barely penetrate the Earth's atmosphere. Depending on the wavelength, what scatters back to space corresponds to different slices of the atmosphere, ranging from altitudes of 25–50 km.

Because the SBUV measurements include these strongly absorbed, very low albedo wavelengths, the instrument only views the nadir as the satellite follows a sun-synchronous orbit that passes near the Earth's poles (6). With the exception of the poles, the SBUV instrument only collects data at local noon. In addition, by using the precession of the satellite orbit tracks, a full global O₃ map can be produced in 13 days. However, significant total O₃ changes take place in a single day.

"The geographic patterns [of upper stratospheric ozone concentrations] are coherent from orbit to orbit," says Krueger. "However, the total ozone column amounts for the planet have much more horizontal structure." To keep track of these important changes, Nimbus 7 also carries the Total Ozone Mapping Spectrometer (TOMS). This single monochromator instrument measures a swath of the Earth's atmosphere on each orbit approximately 2700 km across, generating a daily global ozone map from the 14 orbits each day. Once again, a ratio of wavelengths from the 310–340-nm range is used to calculate the total O₃ integrals.

Currently only the TOMS is still working on Nimbus 7, although a new SBUV instrument onboard a National Oceanic and Atmospheric Administration (NOAA) satellite collects data. Krueger says that American-built TOMSs are scheduled to be launched onboard Soviet (1991), American (1993), and Japanese (1995) satellites.

Stratospheric O₃ has also been measured in situ. Balloon-borne detectors have profiled ozone partial pressures to altitudes of 30–32 km. These measurements have relied on a variety of analytical techniques including UV absorption, chemiluminescence, and electrochemistry.

The research chemiluminescent detector, developed by the Service d'Aéronomie du Centre National de la Recherche Scientifique in France, is based on the reaction of ethylene and O₃, which produces light with a 450-nm maximum (8). The electrochemical detector, which measures O₃ amperometrically (9), is quite inexpensive and is

flown routinely at many locations, including the South Pole. Ozone oxidizes iodide to triiodide, which is then reduced back to iodide (10).

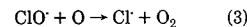
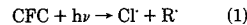
Additional in situ measurements have been collected during NASA-sponsored airplane flights over the North and South polar regions. Two planes, a DC-8 and an ER-2 (a modified U-2 spy plane) jam-packed with instrumentation, have measured a host of chemical species (11). The DC-8 reaches altitudes of about 10 km, whereas the ER-2 soars to about 19 km.

Once again, UV and chemiluminescent techniques are used to determine O₃. These detectors directly measure O₃ levels in outside air pumped through the instruments.

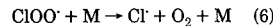
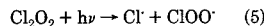
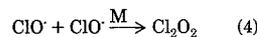
On the other hand, a sophisticated differential absorption light detection and ranging (lidar) system from NASA-Langley, onboard the DC-8, simultaneously determines O₃ and aerosol distributions from 2 to 20 km above the aircraft. Laser light of four wavelengths—300, 314, 600, and 1064 nm—is beamed out a zenith-facing quartz window. Backscattering of the laser light provides the data. Accuracy for these long-range ozone measurements runs around 10%, compared with 5% for NASA-Langley's chemiluminescent detector and 3% for NOAA's dual-beam UV photometer that is flown on the ER-2.

Finally, two FT near-IR (2–15 μm) interferometers, from the Jet Propulsion Laboratory (JPL) and the National Center for Atmospheric Research, can detect a variety of chemical constituents, including O₃. The accuracies on these values range from 3 to 25%.

Although ozone measurements illustrate the effect, they do not identify the means. Evidence of CFC involvement came with the detection of ClO, a key intermediate in the catalytic loss of O₃ (Equations 1–3).



Equation 3 applies in the normal stratosphere. In the perturbed Antarctica stratosphere, other reactions occur (Equations 4–8):



or



The ER-2 flights carried a sophisticated resonance fluorescence detection system to measure ClO and BrO. The bromine species, also a product of industrial chemicals, are now known from this experiment and laboratory kinetic studies to play a significant role in the ozone hole formation by reacting with ClO and other chlorine oxides to regenerate ozone-destroying Cl.

In the ClO/BrO experiment, led by Harvard atmospheric chemist James Anderson, 200 m/s air flowed into an open duct on the plane's port wing and was slowed to 20 m/s as it was fed into the flow-through detection system. Added NO rapidly converts ClO and BrO to atomic halogen. Vacuum-UV light from a low-pressure plasma discharge lamp induces resonance scattering in the atoms.

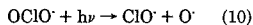
Early experiments relied on three redundant detection systems, situated along the flow system, to follow the conversion of ClO to Cl. "Because the in-flight flow conditions were uncharacterized, a redundant system was developed to monitor the kinetics of the ClO and NO reaction to verify proper flow and proper reaction kinetics," explains Darin Toohey, a member of Anderson's group. Nowadays the third detector is dedicated to Br.

This system takes about 10 ms to convert ClO to Cl, which is then easily detected at 119 nm. Bromine, on the other hand, is determined from an ensemble of lines ranging from 118 to 130 nm. It is difficult to make these measurements because bromine concentrations present in the atmosphere are small. Thus, resonant scattering from bromine is much smaller than nonresonant scattering off air molecules. Halogen concentrations are measured to pptv levels with an accuracy of 25% and a precision of 5%. Additional evidence of halogen species, including CFCs, comes from the near-IR detectors onboard the DC-8.

Data on halogen oxides have also been collected by ground-based detectors. Researchers from the State University of New York at Stony Brook have measured ClO by observing the molecule's rotational emission line at 278.63 GHz (corresponding to the transition $J = 15/2 \rightarrow 13/2$). To determine this very weak signal, the spectrometer collects data in successive 20-min observations, then bins and averages the information over several days. Background interference from an O₃ peak just 4 MHz from the ClO signal must also be mathematically removed. Despite these difficulties the instrument has detected ClO at pptv levels to altitudes of 20 km and higher (12).

Another halogen oxide, OCIO, is a

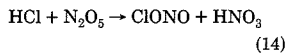
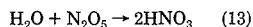
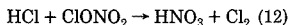
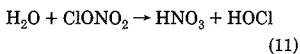
byproduct of one important catalytic cycle (Equation 9). Since it photolyzes nearly as quickly as it forms (Equation 10), OCIO is best detected at night.



Using light from a full moon, a ground-based spectrometer has indeed measured OCIO from absorptions in the 403–428-nm range. Furthermore, because a moon low on the horizon only illuminates a limited volume of the upper atmosphere, readings at these times determine OCIO in selected regions (13). Other species, including O₃, have also been measured by moonlight.

Indicting CFCs as the ozone-destroying molecule, however, requires that atmospheric NO_x concentrations remain low. Otherwise, ClO reacts with NO₂ to form ClONO₂, which is inert toward O₃. Ozone mechanisms must also account for HCl, which also ties up chlorine in an ozone-inert molecule.

Measurements reveal that NO_x levels inside the ozone hole are 2–10 times lower than outside the region. HCl levels are also quite low inside the hole. The lost nitrogen and HCl have been traced to heterogeneous reactions on the polar stratospheric clouds (Equations 11–14). These clouds form in the dry Antarctic air only during the cold winter months. To a lesser extent, these clouds also form over the Arctic.



The nitric acid generated in these reactions sticks to ice crystals while the gaseous chlorine products escape. Both Cl₂ and HOCl can then easily photolyze in the spring to regenerate Cl. Ground instruments can determine NO₂ by observing several absorption lines in the span of 403–453 nm (14). Multiple wavelengths aid in eliminating errors from other absorbing species. Red light, 605–685 nm, identifies another nitrogen species, NO₃ (Equation 15) (15).



Measurements of NO and NO₂ as NO_x have also been collected from detectors onboard balloons and planes. All the NO₂ is initially photolyzed to NO, then ozone is added to produce a chemiluminescent reaction that determines NO₂ to pptv concentrations. A

slight variation of this approach uses an Au catalyst heated to 300 °C to reduce nitrogen species prior to the chemiluminescent detection. The catalyst converts NO₂, NO₃, N₂O₅, HNO₃, and ClONO₂ to NO.

Water, which plays a role in a number of key reaction steps, was measured on both the DC-8 and ER-2 planes with NOAA's Lyman alpha hygrometer. A 121.6-nm source converts some of the water vapor into excited hydroxyl radicals that fluoresce at 309 nm. This hygrometer measures less than 1 ppmv water vapor with an accuracy of 6%.

In analyzing each of these pieces of the puzzle, researchers have clearly established the role of CFCs in the ozone hole. Although all the mechanistic details are not known, enough has been learned to prompt world leaders to call for a ban on CFCs. Even if that ban goes into effect now, the ozone hole will be around for some time. Several of the CFCs being released today will not be scrubbed from the Earth's atmosphere until well into the twenty-first century. "The real issue," says Stolarski, "is that we have to be careful not to use the atmosphere as a dumping ground."

Alan R. Newman

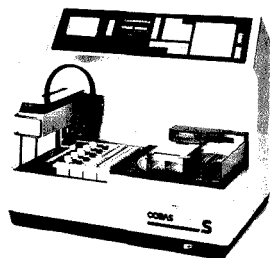
References

- (1) Farman, J.; Gardiner, B. G.; Shanklin, J. D. *Nature* 1985, 315, 207–10.
- (2) Zurer, P. *C&EN* November 2, 1987, 22–26.
- (3) Zurer, P. *C&EN* November 30, 1987, 25–27.
- (4) Hofmann, D. J.; Deshler, T. L.; Amedeu, P.; Matthews, W. A.; Johnston, P. V.; Kondo, Y.; Sheldon, W. R.; Byrne, G. J.; Benbrook, J. R. *Nature* 1989, 340, 117–21.
- (5) Farman, J. C. *Philos. Trans. R. Soc. London* 1977, B279, 261–71.
- (6) Heath, D. F.; Krueger, A. J.; Roeder, H. A.; Henderson, B. D. *Opt. Eng.* 1975, 14, 323–41.
- (7) Dave, J. V.; Mateer, C. L. *J. Atmos. Sci.* 1967, 24, 414–27.
- (8) Amedieu, P.; Barat, J. *Rev. Sci. Instrum.* 1981, 52, 432–37.
- (9) Komhyr, W. D. *Ann. Geophys.* 1969, 25, 203–10.
- (10) Schulze, F. *Anal. Chem.* 1966, 38, 748–52.
- (11) Airborne Arctic Stratospheric Expedition, National Aeronautics and Space Administration; Ames Research Center, Moffett Field, CA, December 1988.
- (12) de Zafra, R. L.; Jaramillo, M.; Parrish, A.; Solomon, P.; Connor, B.; Barrett, J. *Nature* 1987, 328, 408–13.
- (13) Solomon, S.; Mount, G. H.; Sanders, R. W.; Jakoubek, R. O.; Schmeltekopf, A. L. *Science* 1988, 242, 550–54.
- (14) Mount, G. H.; Sanders, R. W.; Schmeltekopf, A. L.; Solomon, S. *J. Geophys. Res.* 1987, 92, 8320–28.
- (15) Sanders, R. W.; Solomon, S.; Mount, G. H.; Bates, M. W.; Schmeltekopf, A. L. *J. Geophys. Res.* 1987, 92, 8339–42.

Suggested reading

- Graedel, T. E.; Crutzen, P. J. *Sci. Am.* 1989, 261, 58–68.

NEW PRODUCTS



Cobas Mira S automated chemistry analyzer features robotic sample, reagent, and cuvette handling; reagent cooling; and bar-code scanning. Roche Diagnostic Systems 401

IR. Model 711 nondispersive IR analyzer monitors chemical components in process applications, including gas-phase analysis of CO, CO₂, or NH₃. Features include a vibration-insensitive, solid-state detector and sample compartment temperature control. Teddy Analytical Instruments 404

Surface analysis. CSIRO UMIS-2000 characterizes surface materials including coatings and surface-modified layers. A diamond indenter is forced into the surface under controlled load, and penetration displacement is recorded during the loading and unloading segments. Microscience 405

LC. Capillary detector 433 features a wavelength range of 190–800 nm and dual-wavelength recording. The detector increases the sensitivity of capillary LC, capillary zone electrophoresis, or SFC systems by a factor of 100–500 compared with on-column detection. Kontron Instruments 406

Raman. RDS200 Raman multichannel detection system consists of a cooled CCD detector coupled with a customized version of Spectra Calc software. Exposures from 30 ms to 9 h are possible, enabling detection of extremely weak spectra. Photometrics 407

Water analysis. VOC water analyzer is designed for continuous, unattended determination of low concentrations of volatile organic compounds in surface

and drinking water. All functions of the capillary GC-based system are performed automatically. Chrompack 408

XRF. Model 8600+ XRF spectrometer features an improved monochromator design, external collimation, and self-aligned mechanics. The system includes encoded cassettes for unattended operation. Applied Research Laboratories/Fisons Instruments 409

Autosampler. Model 728B autosampler is composed of biocompatible materials in key sample transfer areas. The unit, which can inject up to 192 times from 64 different samples, can be controlled by an integrator, data system, or computer. Alcott/Micromeritics 410

Oxygen. Model 840 dissolved oxygen meter, designed for laboratory or field applications, features automatic pressure/altitude correction and adjustable salinity correction. The instrument locks in readings when stable values are achieved. Orion 411

Detector. Model 200 variable-wavelength LC detector features a wavelength range of 190–800 nm, digital absorbance readout, automatic zero operation, and sensitivity to 0.0005 AUFS. Flow cells for capillary, microbore, analytical, and preparative applications are available. Linear Instruments 412

Generator. OEM-6A power generator, designed for plasma etching and sputtering applications, produces more than 650 W of power at 13.56 MHz. The 25-pin interface bus uses optoisolated digital and ground-isolated analog inputs and outputs. ENI 413

Software

Data acquisition. MBC-MI MacInstruments data acquisition and control software is designed for Macintosh Plus, SE, and II computers. Features include automatic statistical calculations and the ability to view and acquire up to four channels of data automatically. MetraByte 415

Waveforms. Snap-Generator is a

menu-driven software package that generates analog waveforms using a D/A converter. Waveform types include standard functions (sine, cosine, square, triangular, and ramp) or those defined by the user. HEM Data Corp. 416

Manufacturers' Literature

Vacuum pumps. Brochure describes direct-drive vacuum pumps designed for filtering, drying, cryogenics, refrigeration, and degassing. Construction features, specifications, and accessories are discussed. 4 pp. Precision Scientific 418

Polymers. *Polymer Profiles*, Vol. 8, No. 1, includes information on viscosity measurement of thermoplastics and application software. 6 pp. Haake/Fisons Instruments 419

LC. Bulletin describes Aminex columns for carbohydrate, alcohol, organic acid, and organic base separations. Optimization of chromatographic conditions is discussed. 8 pp. Bio-Rad Laboratories 420

Langmuir-Blodgett. Brochure highlights the KSV 5000 Langmuir-Blodgett monolayer system. Practical applications, software capabilities, and specifications are discussed. Oriol 424

UV-vis. Data sheet discusses the Lambda 4B UV-vis spectrophotometer, which features application-specific software packages for kinetics, spectral processing, and quantitation of protein and nucleic acid samples. Perkin-Elmer 421

Carbon. Brochure describes the Model 555 total organic carbon analyzer, designed for laboratory measurement of organic carbon in natural and waste water. Features, applications, and principles of operation are discussed. Ionics 423

For more information on listed items, circle the appropriate numbers on one of our Readers' Service Cards

Catalogs

Liquid handling. Catalog features disposable laboratory products for pipetting, dispensing, measuring, and storing liquids. Included are pipet tips, test tubes, transfer pipets, cuvettes, and microtitration plates. 28 pp. Bio-Rad Laboratories 425

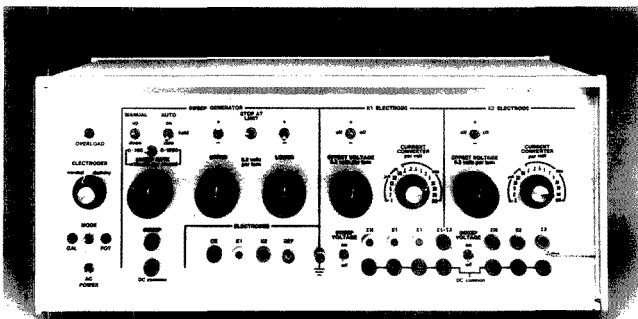
Research products. Catalog features immunoassay kits and magnetic separation particles. Chemical and physical properties and technical information are included. Advanced Magnetics 428

Peptides. 1989 catalog lists bioactive peptides, small peptides and substrates, polyamino acids, and books. Sequence data, technical references, and tables also are included. Sigma Chemical Co. 426

Laboratory Products. Catalog includes dispensers, desiccators, glassware, electrodes, and products for sample analysis, collection, processing, and storage. 54 pp. Markson Science 422

Laboratory equipment. Catalog includes autoclaves, balances, centrifuges, chromatography supplies, membrane filters, diluters, pH meters, titrators, cryoware, baths, and biotechnology instrumentation. 192 pp. Ace Scientific Supply Co. 427

IR. Catalog includes IR cells for liquid sampling; beam condensers for micro IR analysis; sample preparation and desiccant kits; and accessories for solid sampling, gas sampling, and multiple internal reflectance. 60 pp. Perkin-Elmer 429



Model 366 bi-potentiostat, designed for studies of kinetics and reaction mechanisms, can control two working electrodes operating at different potentials and can monitor the currents generated at the electrodes. EG&G Princeton Applied Research 402

Reaching Perfection in MS and SEM.



*"A man's reach should
exceed his grasp..."*
Robert Browning

Galileo detectors for Mass Spectrometry and Electron Microscopy.

What silicon chips did for computers, Galileo high-performance detectors are doing for GC/MS, MS and SEM analysis.

Whether your projects involve environmental or pharmaceutical analysis, analysis of organic compounds or general spectroscopy applications, a Galileo detector will speed sample identification while providing accurate and precise analysis.

When research projects require frequent sample analysis over a long period of time, you'll want the latest and best technology backing you up. Galileo is the innovator in analytical instrument detectors. If you demand high performance and are concerned about down time, rapid analysis, dynamic range and cost, insist on Galileo scientific detectors. You'll wonder how you ever got along without us.

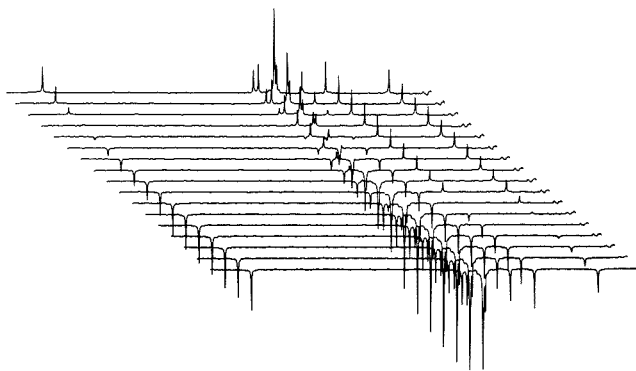
Write us and ask how to ensure that your instruments have Galileo scientific detectors.

Galileo Electro-Optics Corp.
Scientific Detector Products Group
P.O. Box 550, Dept. AA
Sturbridge, MA 01566
(508) 347-9191


GALILEO
Galileo Electro-Optics Corp.

CIRCLE 60 ON READER SERVICE CARD

Search spectra online



C13-NMR/IR Now available on STN®

Now there's a new way to identify chemical substances online through their CNMR or IR spectra. Discover the Carbon 13 Nuclear Magnetic Resonance/Infrared file and see how invaluable it can be in your research!

The file and its sources

In C13-NMR/IR you'll find almost 120,000 spectra for 90,000 compounds. Data are drawn from significant journals, spectral catalogs, and unpublished spectra from BASF and other industrial labs.

The workshop Not familiar with searching spectra online? Our workshop shows

you how to

- find spectra by searching a substance name or molecular formula
- predict a C13 spectrum or shift
- find exact or similar structures
- find substances using CAS Registry Numbers

How to get started The C13-NMR/IR file is available only through the STN International network. If you're already an STN user, arrange access to C13-NMR/IR by calling Customer Service at 800-848-6538 or 614-447-3600. If you aren't yet using STN, return the enclosed coupon.

Yes! I'd like more information about C13-NMR/IR on STN International. Please rush me my FREE information package.

Name _____

Organization _____

Address _____

Phone _____

Mail to: STN International, c/o Chemical Abstracts Service,
Dept. 38389, P.O. Box 3012, Columbus, OH 43210 U.S.A.

In Europe, contact STN International c/o FIZ Karlsruhe, P.O. Box 2465,
D-7500 Karlsruhe 1, Federal Republic of Germany. Telephone: (+49)
7247/808-555.



STN is operated in North America by Chemical Abstracts Service, a division of the American Chemical Society; in Europe, by FIZ Karlsruhe; and in Japan, by JICST, the Japan Information Center of Science and Technology.

The Odyssey of Angiogenin: A Protein That Induces Blood Vessel Growth

Daniel J. Strydom, James W. Fett,
and James F. Riordan

Center for Biochemical and Biophysical
Sciences and Medicine and
Department of Pathology
Harvard Medical School
Boston, MA 02115

Proteins are a marvelously diverse group of molecules that have fascinated biochemists for decades. They come in all sizes, shapes, and colors, and their functions span virtually the entire spectrum of life processes. It is difficult to imagine a biological reaction that is not somehow connected with one or more proteins. Their functional diversity is reflected in their structures: They can be incredibly complicated or simple polypeptides. By definition, proteins are polymers of up to 20 different amino acids that can be combined in an infinite number of ways, but nature often requires the addition of non-amino-acid components that extend the complexity even more. Researchers estimate that 1% of the human genome is actively transcribed into ~100,000 different proteins.

The history of protein chemistry, which spans 150 years, is a testament to advances in analytical chemistry. Early on it became clear that proteins were not typical organic compounds that could be purified by crystallization and characterized by melting point and C,H,N analysis. Until the early 1950s proteins were not considered to be discrete molecular entities and there was considerable controversy regarding their polypeptide nature. Sanger's sequencing of insulin was therefore much more than elegant deductive puzzle solving based on paper chromatography (1). It established the fundamental principles of protein structure.

Since then, achievements have mounted steadily as new analytical developments have been made, particularly in the area of chromatography

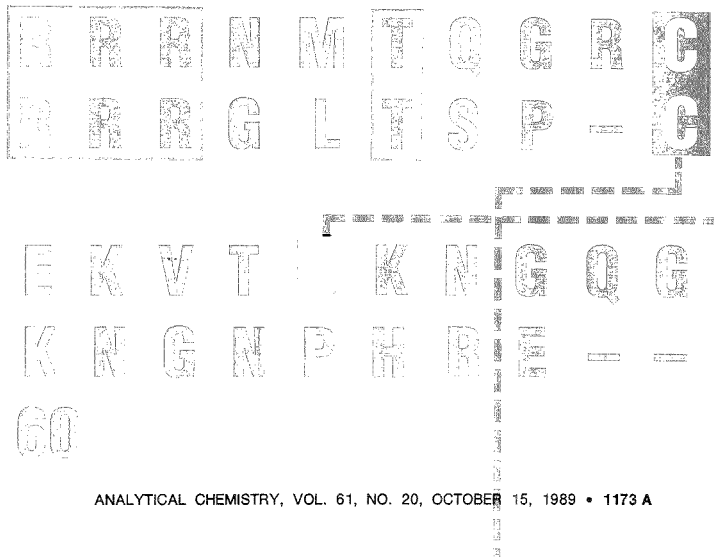
(adsorption, ion-exchange, size exclusion, bioaffinity, and reversed-phase), polyacrylamide gel electrophoresis, and capillary electrophoresis. Proteins that previously were inaccessible because of their extremely low abundance (a reflection of their highly specialized, highly localized, or highly potent action) are now being described almost routinely. Thus an entire generation of new proteins has emerged, bringing with it an exciting new era in developmental biology.

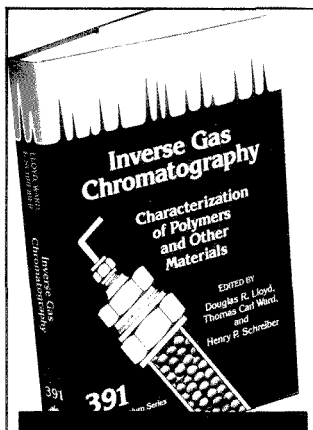
Organogenesis

Some 15 years ago our laboratory became interested in the biochemical problem of organogenesis—the process by which cells aggregate, differentiate, and form discrete tissues and organs (2). As a specific example of this process, we investigated the molecular mechanisms involved in angiogenesis—the development of a hemovascular network. Blood vessel proliferation takes place during embryonic growth; wound repair; in the development of

the lining of the uterus, ovarian follicles, and the placenta; and in a number of pathological states, particularly the growth of tumors (3). The proliferation of blood vessels in the vicinity of tumors was described more than a century ago and since then has generated much speculation and experimental effort. However, when our work was initiated little was known about the nature of molecular messengers involved in this process. In fact, the existence of such "factors" was not yet fully established. If, however, these molecules could be identified and characterized, their modes of action with target cells, mechanisms of action, and the processes that regulate their function could be investigated.

Early work on tumor blood vessel growth suggested that angiogenesis was mediated by a diffusible substance(s) (4, 5). It was also found that experimental tumors cannot grow beyond a certain small size and may not be able to spread (i.e., metastasize) when deprived of a blood supply (3).





Inverse Gas Chromatography

Characterization of Polymers and Other Materials

No other single reference covers this relatively new subject area so completely! As an extension of conventional gas chromatography, inverse gas chromatography (IGC) has many advantages—simplicity, speed of data collection, accuracy, and low operating costs.

This one volume offers an in-depth look into the most recent advances in theoretical and practical aspects of this approach. Twenty-two chapters provide information on:

- instrumentation and methodology
- characterization of vapor-polymer systems
- polymer-polymer systems
- surfaces and interfaces
- analytical applications
- application of IGC in coal characterization and food science

This valuable title discusses the application of IGC to the thermodynamic and acid-base interaction of components in polymer systems, and the technological advances in the field.

Douglas R. Lloyd, *Editor*, University of Texas
Thomas Carl Ward, *Editor*, Virginia Polytechnic Institute and State University

Henry P. Schreiber, *Editor*, Ecole Polytechnique

Clara C. Pizana, *Assistant Editor*

Developed from a symposium sponsored by the Division of Polymeric Materials, Science and Engineering of the American Chemical Society and the Macromolecular Science & Engineering Division of the Chemical Institute of Canada

ACS Symposium Series No. 391
327 pages (1989) Clothbound
ISBN 0-8412-1610-X LC 89-6628
US & Canada \$69.95 Export \$83.95

O • R • D • E • R F • R • O • M

American Chemical Society
Distribution Office, Dept. 22
1155 Sixteenth St., N.W.
Washington, DC 20036

or CALL TOLL FREE

800-227-5558

(in Washington, D.C. 872-4363) and use your credit card!

Therefore containment of neoplastic growth through control of tumor-induced angiogenesis has been suggested as a therapeutic approach for cancer control. We reasoned that the growth medium in which tumor cells are cultivated should be a source of the secreted tumor-derived angiogenic substance(s). We realized, however, that biological messenger molecules could be extremely potent and hence might only exist in minuscule quantities. The progress of our studies depended on and closely paralleled the introduction of new techniques in the field of biochemical research.

Isolation of angiogenin

In our initial attempts to isolate angiogenic molecules, we used rat Walker carcinoma cells propagated in Petri dishes. This cell line was chosen because previously it had been studied extensively for this purpose and because it was available and easy to grow. The medium used to culture such cells contained the customary fetal calf serum (FCS) as a source of growth factors, which greatly complicated our purification efforts because the FCS contributed about a millionfold excess of contaminating proteins. To avoid this problem, we periodically replaced the growth medium with phosphate buffered saline (PBS) into which the cells were allowed to secrete proteins for several hours. We obtained a few liters of "conditioned" PBS per month which, after dialysis and lyophilization, yielded a few milligrams of crude but active material. Purification to homogeneity required a sensitive, selective assay.

The angiogenesis assay that we adopted is a modification of that developed by Knighton et al. (6). Samples to be tested are applied to the fertilized chicken egg chorioallantoic membrane. After three days, the membrane is examined microscopically for evidence of blood vessel growth. Figure 1 shows a control and a positive sample eliciting a typical "spoke wheel" pattern of vessel growth. We have refined the assay to allow statistical analysis of the data by using a simple positive or negative response as our measure of attribution in a Bernoulli trial (7). This allows the results to be analyzed as binomial distributions.

Although we were able to demonstrate angiogenic activity in the conditioned PBS, we soon realized that this approach would never provide sufficient material for characterization because virtually all that was produced was used for the assay. The only solution was large-scale cell culturing, and for this purpose we entered into a long-term collaboration with the Monsanto Co. (This arrangement was the first major academic-industrial relationship of its kind; its inception and development are a separate saga.)

Monsanto developed facilities for growing rat cells (in suspension cultures containing FCS) in reactors with capacities varying from 12 to 40 L (8). Working with such large volumes required extraordinarily stringent sterility precautions and, despite these precautions, created seemingly endless difficulties. Nevertheless, eventually we had enough material to corroborate the existence of proteins with angiogenic properties (2), and megascale cell

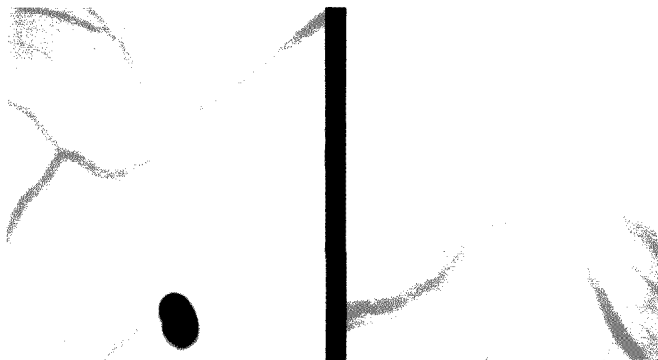


Figure 1. Induction of blood vessels on the chick chorioallantoic membrane by angiogenin.

The right panel shows a positive and the left panel a negative angiogenic response (control). The positive response was induced by 25 ng of angiogenin; the control was a 5- μ L sample of water applied near the black spot.

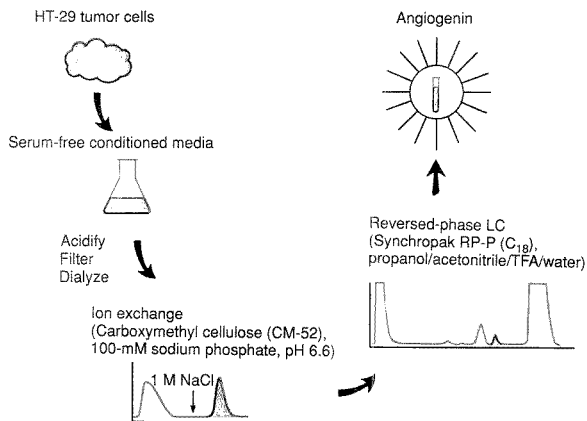


Figure 2. Purification scheme for tumor-derived angiogenin.
(For details, see Reference 7.)

culturing emerged as a viable commercial venture.

As we began making progress in the study, we reassessed the appropriateness of studying rat tumor cells. Several human cancer cell lines had become available, so we turned our attention to the colon carcinoma cell line HT-29. These cells require relatively large amounts of "contaminating" FCS, and we wondered whether it would be possible to cultivate them with little or no added serum. This turned out to be one of the most critical factors on the road to angiogenin. We discovered that HT-29 cells could be maintained in a viable state in the absence of added serum or other proteins (9). Under specifically defined, serum-free conditions, the cells do not proliferate but continue to secrete proteins into the medium for weeks. Scaling up this method by using cell factories gave us multiliter quantities of medium on a weekly basis and made our attempt to isolate an angiogenic molecule much more feasible.

Chromatography

Conventional chromatography was adequate for the first steps of fractionation, but each liter of the conditioned medium yielded only ~200 μ g of crude active material. Therefore, the last step in the isolation of angiogenin required the use of high-performance liquid chromatography (HPLC), which fortunately was emerging as a new, powerful means of separating proteins in the

early 1980s. Fractionation occurred on an octadecylsilane Synchropak RP-P column (10- μ m particle size, 250 \times 4.1 mm at a flow rate of 1 mL/min with either acetonitrile/trifluoroacetic acid/water or propanol/acetonitrile/trifluoroacetic acid/water gradients). Even after optimal conditions were established, it was several years before a single milligram of pure angiogenin was collected. The final scheme for purification (Figure 2) is deceptively simple and today is considered routine.

It is difficult to overemphasize the significance of technical and operational difficulties and the importance of their resolution to ensure success. The choice of the source for angiogenic material; the identification of a suitable human cell line with acceptable angiogenic activity; the mode of large-scale cell production; and the techniques for isolation, assay, and functional and chemical characterization of angiogenin were all problems that had to be surmounted and converted into opportunities.

Sequencing

A subtle example may convey some of the issues. Once cell culture methods had been established and were manageable on a laboratory scale, several months of full-time effort by three people were required to obtain 30 μ g of angiogenin—just enough for one sequencing experiment.

In a classical sequence study, the

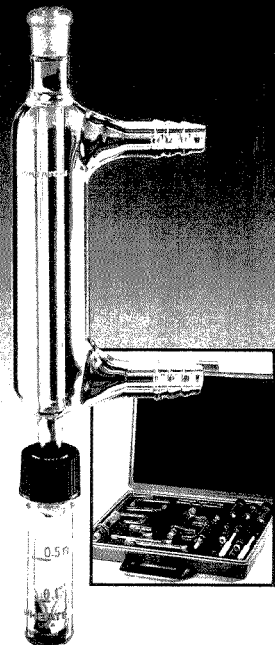
WHEATON MICRO KITS

**Microscale Glassware
Designed for Micro
Experimental Organic
Chemistry***

- Major cost reduction in chemicals and chemical waste disposal
- Eliminate danger of fire or explosion
- Expand the variety and sophistication of experiments
- Reduce experiment time and messy cleanup
- Increase student interest

For more information call toll-free 1-800/225-1437.

*Ref. *Microscale Organic Laboratory*, 1986, by Dana W. Mayo, Ronald M. Pike, Samuel S. Butcher.



WHEATON

Manufacturers Since 1888
1000 North Tenth Street
Millville, NJ 08332 USA
Call Toll-Free: 1-800/225-1437
Ext. 2768

CIRCLE 175 ON READER SERVICE CARD

protein is broken down by a series of chemical and enzymatic steps into sets of relatively short peptides whose individual sequences are determined and used to deduce the complete protein sequence. For angiogenin, however, this approach was precluded by a lack of material. Instead, we isolated an 18-amino acid peptide from an enzymatic digest of angiogenin, determined its sequence, and used that information to synthesize a 26-residue oligodeoxyribonucleotide whose sequence was complementary to the sequence of nucleotides in DNA that genetically code for part of that peptide. The 26-mer was labeled with ³²P so that it could be used as a probe.

Next, the messenger RNA molecules from human liver cells were isolated and used as the template for enzymatic synthesis of the corresponding DNA molecules, which then constitute a complementary DNA (cDNA) library. Using recombinant DNA methodology, we inserted cDNAs into a plasmid (circular extrachromosomal DNA molecules that can replicate in microorganisms) that was used to infect *E. coli* cells. The cells infected with the plasmid (carrying the cDNA that codes for angiogenin) were detected by hybridization with the 26-mer probe. Plasmids that bound the probe strongly were isolated and purified by cesium chloride gradient centrifugation. The cDNA inserts were removed with specific enzymes (restriction endonucleases) and sequenced by using the method of Maxam and Gilbert (10).

In the meantime, additional angiogenin was accumulated and we proceeded with classical protein sequencing. We determined the amino acid composition of the protein by using the newly developed PicoTag procedure (11), in which the protein is acid hydrolyzed to its constituent amino acids, which are converted into phenylthiohydantoin derivatives with C₆H₅NCS and quantitated by HPLC. Of the 123 constituent amino acids, one methionine and one tryptophan were sites for specific chemical cleavage of the intact protein. We intended to sequence the amino terminal of the protein by the Edman degradation method, cleave the remaining protein at the methionine and tryptophan residues, respectively, and sequence the resulting fragments. We were dismayed to discover that the α-amino group of the N-terminal residue was blocked and, hence, direct sequencing was impossible; the subsequent chemical cleavage reactions were equally uninformative.

Enzymatic hydrolysis of the native soluble protein with trypsin (which catalyzes the cleavage of peptide bonds following lysine and arginine residues) ultimately was chosen to avoid further problems, and this put us on the pathway to success. We were aided by the concomitant development of HPLC methods for protein and peptide purification, especially by reversed-phase LC. The scarcity of material made every analytical experiment a preparative one as well. Our strategy for tryptic peptide separation assumed a mixture

of both large and small peptides. Because large-pore-size reversed-phase supports should give better yields of large peptides (12-15), we chose a C₃ column to enhance this probability (16). Small peptides, as expected, were not retained and the breakthrough was rerun on a C₁₈ column. Pure peptides were obtained at the nanomole level without excessive background contamination from buffer, column materials, or handling.

We needed to determine amino acid composition at or below the 100-pmol level and simultaneously measure amino acid sequence at or below the 1-nmol level. (Today a 0.1-nmol level is routinely achieved.) Amino acid analysis on ion-exchange resins, using ninhydrin for detection, could be used at 50-pmol sensitivity. In fact, most of the amino acids could be determined semi-quantitatively at the 10-pmol level. However, the PicoTag method allows analyses to be performed by reversed-phase HPLC (at 254 nm) and interpreted at levels as low as 1-5 pmol.

Sequencing extremely low levels of protein required changes in the performance of the Beckman 890C sequencer, largely by the use of aldehyde-free reagents and implementation of the solvent purification/filtration systems of Frank (17). As material became available, the protein-sequencing studies assumed multiple objectives. Was angiogenin a known protein or closely similar in sequence to a known protein (i.e., was it an oncogene product [18])? Did it contain disulfide bonds? How

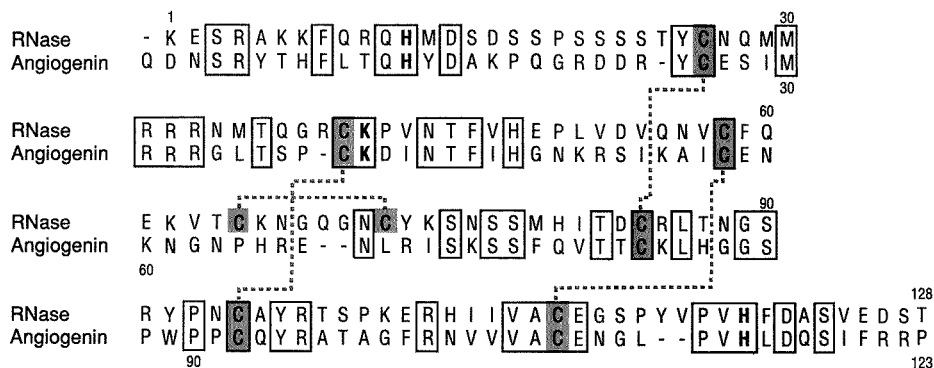


Figure 3. Alignment of the amino acid sequences of human pancreatic ribonuclease (35) and angiogenin. A, alanine; C, cysteine; D, aspartic acid; E, glutamic acid; F, phenylalanine; G, glycine; H, histidine; I, isoleucine; K, lysine; L, leucine; M, methionine; N, asparagine; P, proline; Q, glutamine; R, arginine; S, serine; T, threonine; V, valine; W, tryptophan; Y, tyrosine. Identities between the two sequences are boxed. The active site histidine and lysine residues are emphasized and the disulfide bridges between cysteine residues (shaded) are indicated by dotted lines.

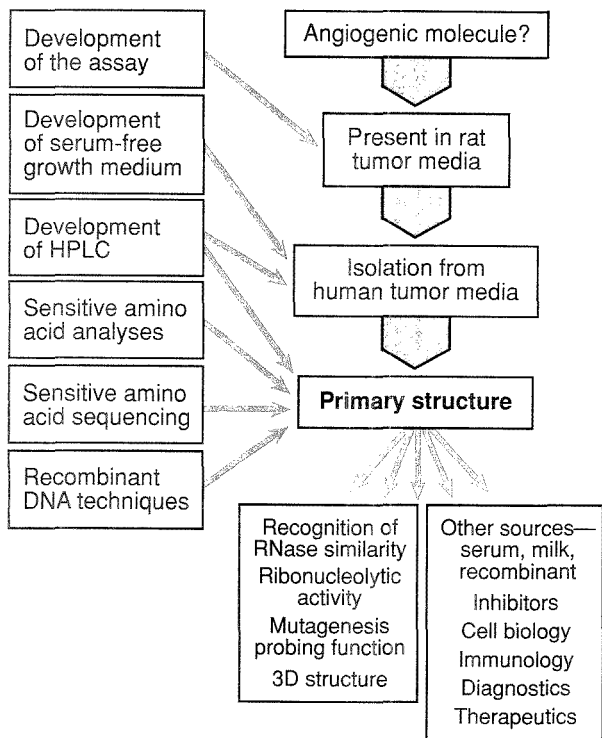


Figure 4. The odyssey of angiogenin.

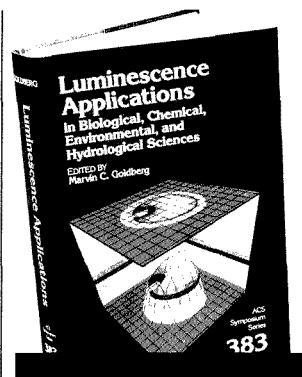
were they paired? Did it undergo post-translational modifications? The answers to these questions could provide insight into its mode of action.

Despite the challenges and frustrations of sequencing, the effort was worthwhile. As we soon discovered, the primary structure of angiogenin is homologous to that of ribonuclease A (19, 20). This was unexpected yet significant because RNase A is one of the most extensively studied of all proteins (21, 22). The sequences of these two proteins are 35% identical with only four gaps needed to optimize their alignment (Figure 3). The active site residues His-12, Lys-40, and His-119 of RNase are all preserved in angiogenin, as are three of its four disulfide bonds.

The RNase A homology emerged from a process of successive developments in biological assays, cell culturing, HPLC, amino acid analysis, sequencing, and, in the end, recombinant

DNA technology (Figure 4). It has proved to be pivotal to all of the detailed investigations of angiogenin that have been carried out in the past four years. It provided the incentive to determine whether angiogenin could also hydrolyze RNA (23-25), to identify a potent inhibitor (26-28), and to explore the relationship between the angiogenic and enzymatic activities of angiogenin by site-directed mutagenesis (29-31). It now appears that for angiogenin to induce neovascularization, it must be catalytically active as a ribonuclease and must be able to bind specifically to a cell membrane receptor. Details of the mechanism of blood vessel formation are still under investigation.

An analogous relationship was recognized some years ago between angiotensin-converting enzyme (ACE) and another pancreatic hydrolase, carboxypeptidase A, which ultimately led to



Luminescence Applications in Biological, Chemical, Environmental, and Hydrological Sciences

New techniques have made luminescence spectroscopy indispensable and crucial for fundamental investigations of the dynamics of chemical processes. This fact-filled book brings you up to date on new and original research on the uses of luminescence techniques.

You'll get a better understanding of the applications that allow research scientists to measure the interactive distance between molecules and the size and shape of molecules. Examine methods to determine electronic transition states and molecular lifetimes. Find out how to make use of the high sensitivity available for detection of fluorescing materials. Looks at natural environments as related to earth materials both in solid and liquid form, and gives information on reactions of these materials in both solid and water systems.

This multidisciplinary volume has 14 chapters and presents the important contributions in the fields of molecular biology, environmental science, methods of standardization, and molecular structure. It offers a unique look at research results and offers suggestions and examples of luminescence methodologies.

Marvin C. Goldberg, *Editor*, U.S. Geological Survey

Developed from a symposium sponsored by the Division of Environmental Chemistry of the American Chemical Society

ACS Symposium Series No. 383
252 pages (1988) Clothbound
ISBN 0-9412-1560-X LC 88-39131
US & Canada \$59.95 Export \$71.95

O · R · D · E · R · F · R · O · M

American Chemical Society
Distribution Office, Dept. 09
1155 Sixteenth St., N.W.
Washington, DC 20036

or CALL TOLL FREE

800-227-5558

(in Washington, D.C. 872-4363) and use your credit card!

**WE MAKE STANDARDS
BY THE BOOK.**



The metal content in each Canostan oil-based calibration standard is determined by chemical assay methods with results that are traceable to NIST standards (where applicable). This traceability means Canostan

products can serve as reference standards and provide a reliable benchmark for the determination of metals in organics. For a complete list of Canostan single and multi-element standards and special blends for the analysis

of metals in oils, write for our free brochure.



Canostan Division
Canaco Specialty Products Inc.
P.O. Box 1267
Ponca City, OK
Phone: (405) 767-3078
Fax: (405) 767-5843

CIRCLE 28 ON READER SERVICE CARD

**OUR STANDARDS
ENDURE THE TEST
OF TIME.**

Canostan oil-based calibration standards combine the convenience of blended standards and exceptional stability for the analysis of metals in oil. These metallo-organic sulfonates

remain stable in liquid form for more than a year—and individual concentrates have exhibited even longer shelf lives. For a complete list of single and multi-element standards that endure the



test of time, write or call for our free brochure.



Canostan Division
Canaco Specialty Products Inc.
P.O. Box 1267
Ponca City, OK 74603
Phone: (405) 767-3078
Fax: (405) 767-5843

CIRCLE 29 ON READER SERVICE CARD

the development of the extremely effective antihypertensive ACE inhibitors that are in widespread therapeutic use today (32). More recently, insights derived from studying pepsin and related aspartyl proteases are expected to be carried over to the design of specific HIV-1 protease inhibitors (33). Similarly, many therapeutic potentials have been postulated for both angiotensin and its inhibitors (31). These include wound healing, bone and tissue repair, and organ transplantation, on the one hand; and cancer, arthritis, and diabetic eye-damage therapy on the other.

If any of these reach fruition it will be partly because of the many years of effort that were devoted to the study of the structure and function of pancreatic ribonuclease largely during the 1950s and 1960s. In addition, we might still be waiting for the first clue to the angiotensin/ribonuclease homology were it not for the tremendous advances in protein purification and sequence technology that occurred during the late 1970s and early 1980s. We would not have embarked on this odyssey at all were it not for the early observations of a relationship between tumor growth and blood vessel proliferation (34); the suggestions by Baltzer, Needham, Speermann et al. that chemically discrete molecules induce organ formation (2); the experimental evidence of Folkman, Cotran, and others (3) that diffusible factors stimulate angiogenesis; and, last but not least, the generous support of our industrial colleagues.

The work described here was supported in part by funds from the Monsanto Co. and Hoechst, A.G. under agreements with Harvard University. We thank B. L. Vallee for advice and support and the staff of the Center for Biochemical and Biophysical Sciences and Medicine for many helpful discussions.

References

- (1) Sanger, F.; Tuppy, H. *Biochem. J.* 1951, 49, 481-90.
- (2) Vallee, B. L.; Riordan, J. F.; Lobb, R. R.; Higachi, N.; Fett, J. W.; Crossley, G.; Bühler, R.; Budzik, G.; Breddam, K.; Bethune, J. L.; Alderman, E. A. *Experientia* 1985, 41, 1-15.
- (3) Folkman, J.; Cotran, R. S. *International Review of Experimental Pathology* 1976, 16, 207-48.
- (4) Greenblatt, M.; Shubik, P. *J. Nat. Cancer Inst.* 1968, 41, 111-24.
- (5) Ehrmann, R. L.; Knoth, M. *J. Nat. Cancer Inst.* 1968, 41, 1329-41.
- (6) Knighton, D.; Ausprunk, D.; Tapper, D.; Folkman, J. *Br. J. Cancer* 1977, 35, 347-56.
- (7) Fett, J. W.; Strydom, D. J.; Lobb, R. R.; Alderman, E. M.; Bethune, J. L.; Riordan, J. F.; Vallee, B. L. *Biochemistry* 1985, 24, 5480-86.
- (8) Harakas, N. K.; Lewis, C.; Bartram, R. D.; Wildi, B. S.; Feder, J. In *Eukaryotic Cell Cultures*; Acton, R. T.; Lynn, J. D.,

- Eds.; Plenum Press: New York, 1984; pp. 119-33.
- (9) Alderman, E. M.; Lobb, R. R.; Fett, J. W. *Proc. Natl. Acad. Sci. USA* **1985**, *82*, 5771-75.
- (10) Maxam, A. M.; Gilbert, W. *Methods Enzymol.* **1980**, *65*, 499-560.
- (11) Bidlingmeyer, B. A.; Cohen, S. A.; Tarvin, T. L. *J. Chromatogr.* **1984**, *336*, 93-104.
- (12) Lewis, R. V.; Fallon, A.; Stein, S.; Gibson, K. D.; Udenfriend, S. *Anal. Biochem.* **1980**, *104*, 153-59.
- (13) Pearson, J. D.; Mahoney, W. C.; Hermodson, M. A.; Regnier, F. E. *J. Chromatogr.* **1981**, *207*, 325-32.
- (14) Wilson, K. J.; Van Wieringen, E.; Klausner, S.; Berchtold, M. N.; Hughes, G. J. *J. Chromatogr.* **1982**, *237*, 407-16.
- (15) Rivier, J.; Rivier, C.; Spiess, J.; Vale, W. *Anal. Biochem.* **1982**, *127*, 258-66.
- (16) Nice, E. C.; Capp, M. W.; Cooke, N.; O'Hare, M. J. *J. Chromatogr.* **1981**, *218*, 569-80.
- (17) Frank, G. *Hoppe-Seyler's Z. Physiol. Chem.* **1979**, *360*, 997-99.
- (18) Bishop, J. M. *Sci. Am.* **1982**, *246*, 80-90.
- (19) Strydom, D. J.; Fett, J. W.; Lobb, R. R.; Alderman, E. M.; Bethune, J. L.; Riordan, J. F.; Vallee, B. L. *Biochemistry* **1985**, *24*, 5486-94.
- (20) Kurachi, K.; Davie, E. W.; Strydom, D. J.; Riordan, J. F.; Vallee, B. L. *Biochemistry* **1985**, *24*, 5494-99.
- (21) Richards, F. M.; Wyckoff, H. W. In *The Enzymes*, 3rd ed.; Boyer, P. D., Ed.; Academic Press: New York, 1971; Vol. 4, pp. 647-806.
- (22) Blackburn, P.; Moore, S. In *The Enzymes*, 3rd ed. Boyer, P. D., Ed.; Academic Press: New York, 1982; Vol. 13, pp. 317-433.
- (23) Shapiro, R.; Riordan, J. F.; Vallee, B. L. *Biochemistry* **1986**, *25*, 3527-32.
- (24) St. Clair, D. K.; Rybak, S. M.; Riordan, J. F.; Vallee, B. L. *Proc. Natl. Acad. Sci. USA* **1987**, *84*, 8330-34.
- (25) Shapiro, R.; Weremowicz, S.; Riordan, J. F.; Vallee, B. L. *Proc. Natl. Acad. Sci. USA* **1987**, *84*, 8783-87.
- (26) Shapiro, R.; Vallee, B. L. *Proc. Natl. Acad. Sci. USA* **1987**, *84*, 2238-41.
- (27) Lee, F. S.; Auld, D. S.; Vallee, B. L. *Biochemistry* **1989**, *28*, 219-24.
- (28) Lee, F. S.; Shapiro, R.; Vallee, B. L. *Biochemistry* **1989**, *28*, 225-30.
- (29) Harper, J. W.; Vallee, B. L. *Proc. Natl. Acad. Sci. USA* **1988**, *85*, 7139-43.
- (30) Shapiro, R.; Fox, E. A.; Riordan, J. F. *Biochemistry* **1989**, *28*, 1726-32.
- (31) Riordan, J. F.; Vallee, B. L. *Br. J. Cancer* **1989**, *57*, 587-90.
- (32) Cushman, D. W.; Ondetti, M. A. *Prog. Med. Chem.* **1980**, *17*, 42-104.
- (33) Navia, M. A.; Fitzgerald, P. M. D.; McKeever, B. M.; Leu, C. T.; Heimbach, J. C.; Herber, W. K.; Sigal, I. S.; Darke, P. L.; Springer, J. P. *Nature* **1989**, *337*, 615-20.
- (34) Goldman, E. *Lancet* **1907**, *2*, 1236-40.
- (35) Eintema, J. J.; Wietzes, P.; Weickmann, J. L.; Glitz, D. G. *Anal. Biochem.* **1984**, *136*, 48-64.



James W. Fett (left) received his B.S. degree in biochemistry from Iowa State University in 1970 and his Ph.D. in physiological chemistry from the University of Wisconsin, Madison in 1974. Following a three-year instructorship at the Medical University of South Carolina, he joined the faculty of Harvard Medical School where he is currently an associate professor of pathology. His research interests focus on the biochemistry and molecular immunology of biological messenger molecules.

Daniel J. Strydom (center) received his Ph.D. from the University of South Africa in 1972 and pursued research in the protein chemistry of snake venom toxins at the Council for Scientific and Industrial Research, Pretoria. He joined the Center for Biochemical and Biophysical Sciences and Medicine at Harvard Medical School in Boston in 1978 and is an assistant professor in the department of pathology. His interests include protein sequencing and protein evolution.

James F. Riordan (right) received his B.S. degree in chemistry from Fairfield University and his Ph.D. in biochemistry from Fordham University in 1961. After completing a postdoctoral fellowship at Harvard Medical School, he was appointed to the faculty there and is now a professor of biochemistry in the Center for Biochemical and Biophysical Sciences and Medicine. His research interests include the enzymology of zinc-dependent peptide hydrolases, especially angiotensin-converting enzyme; the role of metals in biological systems; the biochemistry of alcohol; and the mechanism of action of angiotensin and other blood vessel-inducing proteins.

Chemical Structure Software for Personal Computers

Unique—A user's guide to available software!



For the first time—be able to compare quickly and easily all available software dealing with chemical structures. Focus on the basic details and functions of over 70 software packages. Find out what is available and what packages are best designed to fit your needs and resources. Learn about

- cost
- commercial source
- hardware required
- basic functions of each software program

In this timely user's guide, cover programs that have been grouped according to function: structure drawing, graphics terminal emulation, structure management, molecular modeling, special applications, and more.

Explore the various packages available with *Chemical Structure Software for Personal Computers* and make informed choices when selecting software.

Daniel E. Meyer, Editor, *Advanced Research Technologies, Inc.*

Wendy A. Warr, Editor, *ICI Pharmaceuticals*

Richard A. Love, Associate Editor, *American Chemical Society*

ACS Professional Reference Book

107 pages (1988) Clothbound

ISBN 0-8412-1538-3 LC 88-8153

US & Canada \$49.95 Export \$59.95

107 pages (1988) Paperbound

ISBN 0-8412-1539-1 LC 88-8153

US & Canada \$39.95 Export \$47.95

Order from: *American Chemical Society*

Distribution Office, Dept. 07

1155 Sixteenth St., N.W.

Washington, DC 20036

or CALL TOLL FREE

800-227-5558

and use your credit card!

LABORATORY SERVICE CENTER

1-Bromonaphthalene • Caffeic Acid • Dehydroascorbic Acid • Dibenzoylmethane
Dichloroacetic Acid • Diethyl Adipate • Dihydroxyacetone • Dimezone
3,4-Dimethoxycinnamic Acid • Disodium Succinate • Hydrocinnamic Acid
2-Hydroxy-iso-Butyric Acid • Meldrum's Acid • 2-Mercaptobenzimidazole
Methyl Acetamide • Methyl Acetate • Methyl-n-Propyl Ketone • Mucic Acid
Nitroso-R-Salt • Potassium Tetraoxalate • Pyruvic Acid • Rhodanine
Sodium Butyrate • Sodium & Potassium m-Periodate • Sodium Thioglycolate
Thenoyltrifluoroacetone • Thymolphthalein • Triphenylphosphine • Xylitol

Write for our Products List of over 3,000 chemicals

Tel: 516-273-0900 • TOLL FREE: 800-645-5566

Telefax: 516-273-0859 • Telex: 497-4275

EASTERN CHEMICAL
A Division of UNITED-GUARDIAN, INC.

P. O. Box 2500
DEPT. AC
SMITHTOWN, N.Y. 11787

Laboratory Service Center (Equipment, Materials, Services, Instruments for Leasing), Maximum space — 4 inches per advertisement. Column width, 2-3/16"; two column width, 4-9/16". Artwork accepted. No combination of directory rates with ROP advertising. Rates based on number of inches used within 12 months from first date of first insertion. Per inch: 1" — \$155; 12" — \$153; 24" — \$150; 36" — \$145; 48" — \$140.

CALL OR WRITE JANE GATENBY

ANALYTICAL CHEMISTRY

500 Post Road East

P.O. Box 231

Westport, CT 06880

203-226-7131/FAX: 203-454-9939

NMR ANALYSIS

MULTINUCLEAR LIQUID or
MULTIFIELD SOLID STATE
SPECTRAL DATA SERVICES, INC.
818 Pioneer
Champaign, IL 61820
(217) 352-7084

HELP WANTED ADS

ROP display at ROP rates. Rate based on number of insertions within contract year. Cannot be combined for frequency.

Unit	1-Ti	6-Ti	12-Ti
1" (25 mm)	\$180	\$160	\$150
	24-Ti	48-Ti	72-Ti
	\$140	\$130	\$125

CALL OR WRITE JANE GATENBY

ANALYTICAL CHEMISTRY

500 Post Road East

P.O. Box 231

Westport, CT 06880

203-226-7131

FAX: 203-454-9939

NEED AN ARTICLE FROM AN EARLIER ISSUE?

GET IT FROM CAS DOCUMENT DELIVERY SERVICE®

Does your research depend on locating an article published in this journal a few years back? The CAS Document Delivery Service can provide copies of articles from all ACS journals from initial publication to the present.

You'll also find CAS DDS an excellent source for documents related to chemistry and allied disciplines drawn from the more than 10,000 scientific and technical publications received at Chemical Abstracts Service each year.

Order articles, patents, and reports back to

1975 (1970 for Soviet material). Most orders are on their way within 24 hours. Call for more information. Ask about our FREE 1989 Directory of Publications.

Chemical Abstracts Service®

2540 Olentangy River Road

P.O. Box 3012

Columbus, OH 43210

Phone: (toll-free) 800-848-6538, ext. 3670
or 614-447-3670

Chemical Abstracts Service is a division of the American Chemical Society.

INDEX TO ADVERTISERS IN THIS ISSUE

CIRCLE INQUIRY NO.	ADVERTISERS	PAGE NO.	CIRCLE INQUIRY NO.	ADVERTISERS	PAGE NO.
1	Advanced Graphics Software, Inc.	1160A	172	*Varian Lanig Associates	1144A
3	*Alltech Chromad	1160A	170	VG Masslabs Burgess Daring Advertising, Ltd.	1126A
26	*CDS Instruments Altman-Hall Associates	1163A	175	*Wheaton The Wheaton Agency	1175A
28, 29	*Conostan Division/Conoco Specialty Products Robert Lamons & Associates	1178A	<i>Directory section, see page 1180A.</i>		
40	ES Industries Scientific Marketing Services, Inc.	1132A	<i>* See ad in ACS Laboratory Guide.</i>		
60	*Galileo Electro-Optics Corp. Legasse Associates Advertising, Inc.	1171A	<i>** Company so marked has advertisement in Foreign Regional edition only.</i>		
58	Gelman Sciences, Inc.	1146A	<i>Advertising Management for the American Chemical Society Publications</i>		
65	*Hewlett-Packard Company Brooks Communications	OBC	CENTCOM, LTD		
75	*Isotec, Inc. Kenyon Hoag Associates	1159A	<i>President</i>		
-	Lawrence Livermore National Laboratory Nationwide Advertising Service, Inc.	1166A	Thomas N. J. Koerwer		
94	*Malvern Instruments, Inc.	1165A	<i>Executive Vice President Senior Vice President</i>		
100-107	*Matheson Gas Products Kenyon Hoag Associates	1133A	James A. Byrne Benjamin W. Jones		
96	*Metrohm Ltd. Ecknauer & Schoch Werbeagentur ASW	1134A	Clay S. Holden, Vice President		
98	*Mettler Instrument Corporation Gilbert, Whitney & Johns Inc.	1125A	Robert L. Voepel, Vice President		
110	*Nicolet Analytical Instruments	1129A	Joseph P. Stenza, Production Director		
122	O.J Analytical	IFC	500 Post Road East P.O. Box 231 Westport, Connecticut 06880 (Area Code 203) 226-7131 Telex No. 643310 FAX: 203-454-9939		
129	Perkin-Elmer Corporation Graystone	1149A	ADVERTISING SALES MANAGER		
125	*Phillips Scientific/Analytical Division Connors Publicity Ltd.	1166B	Bruce E. Poorman		
127	Plenum Publishing Corporation Plenum/Da Capo Advertising	1156A	ADVERTISING PRODUCTION MANAGER		
138	Radiometer Analytical A/S	1151A	Jane F. Galenby		
152, 153	*Spectra-Physics	1168A	SALES REPRESENTATIVES		
150	*Supelco, Inc.	1131A	Philadelphia, PA ... Patricia O'Donnell, CENTCOM, LTD., GSB Building, Suite 405, 1 Belmont Avenue, Bala Cynwyd, Pa. 19004. Telephone: 215-667-9666, FAX: 215-667-9353		

AMERICAN CHEMICAL SOCIETY PRESENTS

A TOTALLY NEW CONCEPT IN LABORATORY TRAINING

A Full Curriculum of Coordinated Short Courses in Modern Laboratory Operations

Nine Dynamic Courses to Improve Your Skills in . . .

Analytical Instrumentation

- Atomic Absorption, ICP, and ICP-Mass Spectrometry (AAMS8911)
Learn fundamental instrumentation and state-of-the-art techniques
- Gas Chromatography (MTGC 8911)
Become familiar with basic and advanced GC techniques in this intensive two-day course
- High Performance Liquid Chromatography (HPLC8911)
Improve your instrumentation and laboratory techniques with this advanced course in the applications of HPLC
- Mass Spectrometry (GC/MS) in Environmental Analyses (MSEA8911)
Focus on key aspects of GC/MS in environmental laboratory operations

Business Skills and Laboratory Management

- Business Fundamentals for Scientists (LBUS8911)
A practical business course that teaches the fundamentals of financial and personnel management
- Life Cycle Management of Laboratory Data (LIFE8911)
Adopt a systems approach to handling laboratory data

Laboratory Applications

- Air Toxics Analysis (ENAA8911)
Learn state-of-the-art techniques for measuring toxic air pollutants
- Analysis of Water and Waste Samples by U.S. EPA Methods (ENAW8911)
Master applied environmental measurement of pollutants in liquid and solid samples
- Quality Assurance in Laboratory Analysis (QUEA8911)
Build a successful QA/QC program that will meet even the most stringent regulatory guidelines

NOVEMBER 30—
DECEMBER 1, 1989
CHERRY HILL, NJ

Register Today for
These Dynamic ACS
Short Courses!

For a FREE brochure describing the Modern Laboratory Operations Short Courses program in Cherry Hill, NJ, November 30-December 1, 1989, send in the coupon below or call (800) 227-5558 and press 3.

American Chemical Society
Dept. of Continuing Education
Meeting Code LOP8911
1155 Sixteenth Street, N.W.
Washington, DC 20036

YES! Please send me a free brochure describing the Modern Laboratory Operations Short Courses program in Cherry Hill, NJ, November 30-December 1, 1989.

Name _____

Title _____

Organization _____

Address _____

City, State, Zip _____

EDITOR: GEORGE H. MORRISON

ASSOCIATE EDITORS: Klaus Biemann,
Georges Guiochon, Walter C. Herlihy,
Robert A. Osteryoung, Edward S. Yeung

Editorial Headquarters

1155 Sixteenth St., N.W.
Washington, DC 20036
Phone: 202-872-4570
Telefax: 202-872-6325

Managing Editor: Sharon G. Boots

Associate Editors: Louise Voress,
Mary Warner

Assistant Editors: Grace K. Lee,
Alan R. Newman

Editorial Assistant: Felicia Wach

Director, Operational Support: C. Michael
Phillippe

Production Manager: Leroy L. Corcoran

Art Director: Alan Kahan

Designer: Amy Meyer Phifer

Production Editor: Elizabeth E. Wood

Circulation: Claud Robinson

Editorial Assistant, LabGuide: Joanne Mullican

Journals Dept., Columbus, Ohio

Associate Head: Marianne Brogan

Journals Editing Manager: Joseph E. Yurvati

Associate Editor: Rodney L. Ternos

Staff Editor: Sharon K. Hatfield

Advisory Board: Bernard J. Bulkin, Michael S.
Epstein, Renaat Gijbels, Peter R. Griffiths,
Thomas L. Isenhour, Nobuhiko Ishibashi,
James W. Jorgenson, Peter C. Jurs, Mary A.
Kaiser, David L. Nelson, Lawrence A. Pachla,
Ralph E. Sturgeon, George S. Wilson, Mary J.
Wirth, Andrew T. Zander, Richard N. Zare
Ex Officio: Sam P. Perone

Instrumentation Advisory Panel: James B.
Callis, Bruce Chase, R. Graham Cooks, L. J.
Cline Love, Sanford P. Markey, Ronald E. Ma-
jors, Linda B. McGown, Gary W. Small, R. Mark
Wightman

Published by the
AMERICAN CHEMICAL SOCIETY
1155 16th Street, N.W.
Washington, DC 20036

Publications Division

Director: Robert H. Marks

Journals: Charles R. Bertsch

Special Publications: Randall E. Wedin

Manuscript requirements are published in the
January 1, 1989 issue, page 91. Manuscripts
for publication (4 copies) should be submitted
to ANALYTICAL CHEMISTRY at the ACS Washing-
ton address.

The American Chemical Society and its editors
assume no responsibility for the statements
and opinions advanced by contributors. Views
expressed in the editorials are those of the
editors and do not necessarily represent the
official position of the American Chemical
Society.

- Akagi, T., 2263
Anderson, J. E., 2330
Aomura, Y., 2237
Arn, D., 2249

Baldwin, R. P., 2258
Berman, S. S., 2320
Birks, J. W., 2267
Bodenhausen, G., 2298

Caceci, M. S., 2324
Campiglia, A. D., 2328
Chang, H.-C. K., 2292
Cobb, K. A., 2226

Dickert, F. L., 2306
Dratz, E. A., 2244

Eggenberger, U., 2298

Farnsworth, P. B., 2292

Gardner, G. J., 2320
Gemperline, P. J., 2240

Hamilton, J. C., 2240
Handelman, G. J., 2244
Harris, J. M., 2310
Hirata, T., 2263
Hopkins, D., 2330
Huie, C. W., 2288

Imasaka, T., 2285
Ishibashi, N., 2285

Kapolos, J., 2231
Katsanos, N. A., 2231
Kimmel, H., 2306
Kobayashi, T., 2237
Komuro, M., 2237
Kosted, P., 2244

Kowalski, B. R., 2277

LaPack, M. A., 2332
Lee, M. L., 2292
Lyne, P. D., 2323

Mages, G. R., 2306
Markides, K. E., 2292
Masuda, A., 2263
Murphy, M. M., 2249

Novotny, M., 2226

O'Dea, J. J., 2249
Ogino, H., 2237
O'Neill, R. D., 2323
Osteryoung, J. G., 2249

Perry, L. M., 2328
Poulsen, J. R., 2267
Prabhu, S. V., 2258

Ren, Y., 2330

Savickas, P. J., 2332
Schreiner, S. K., 2306
Shadrick, J. W., 2330
Shimizu, H., 2263
Short, S., 2244
Sill, C. W., 2255
Simms, J. R., 2316
Siu, K. W. M., 2320
Skelton, R. J., Jr., 2292
Strife, R. J., 2316

Tou, J. C., 2332
Tsukamoto, A., 2285

Williams, W. R., 2288
Wilson, B. E., 2277
Winefordner, J. D., 2328
Wong, A. L., 2310

High-Sensitivity Peptide Mapping by Capillary Zone Electrophoresis and Microcolumn Liquid Chromatography, Using Immobilized Trypsin for Protein Digestion

Kelly A. Cobb and Milos Novotny*

Department of Chemistry, Indiana University, Bloomington, Indiana 47405

Procedures for the reduced-scale analysis of proteins by peptide mapping have been developed, allowing peptide maps to be obtained from picomole to femtomole quantities of protein. The use of trypsin immobilized on agarose gel and placed in a small reactor column has made it possible to reproducibly digest as little as 50 ng of protein. This represents a decrease in sample size of approximately 3 orders of magnitude from conventional tryptic digestion schemes. Separations of tryptic digests were accomplished by using either microcolumn high-performance liquid chromatography (HPLC) or capillary zone electrophoresis (CZE). Separations of 100 ng (4 pmol) of tryptic digest samples of β -casein were achieved with microcolumn HPLC, while separations of approximately 2 ng (80 fmol) of β -casein tryptic digest (from a total sample size of 50 ng) were possible with CZE. Peptide maps from phosphorylated and dephosphorylated forms of β -casein were readily distinguishable using both separation methods, demonstrating an ability to detect a single amino acid modification in a protein. Relative standard deviations of peak retention or migration times were less than 3% for microcolumn HPLC and less than 1% for CZE.

INTRODUCTION

Analytical methods used for protein identification and characterization have occupied longstanding roles of importance in biochemical and physiological investigations. Peptide mapping represents one of the most powerful and successful tools available for the study of proteins. The technique of peptide mapping involves the enzymatic or chemical cleavage of a protein into a number of smaller peptide fragments, followed by separation and detection of the peptides to yield a so-called peptide map. This peptide map then serves as a unique fingerprint of the protein and can accurately reveal very subtle differences between individual proteins. Applications for which peptide mapping has proven to be particularly valuable include the detection of posttranslational amino acid modifications (1, 2), the identification and localization of genetic variants (3, 4), and the quality control and monitoring of genetically engineered protein products (5, 6). Since the introduction of peptide mapping (7), the mode of peptide separation has developed from slab gel electrophoresis and thin-layer chromatography (8, 9) to high-performance liquid chromatography (HPLC) (10-14) and, most recently, to capillary zone electrophoresis (CZE) (15).

An important aspect of all methods used for the analysis of proteins is the ability to obtain reliable results from extremely small quantities of sample. Very often, proteins of interest, such as those occurring in physiological fluids, are only available in submicrogram quantities. To fully characterize a protein, a combination of techniques may need to be utilized, including protein separation and isolation, peptide mapping, and amino acid analysis and/or sequencing. The separation and isolation of picomole to femtomole quantities

of protein, using reduced-diameter chromatographic columns, have been demonstrated (16, 17). Analysis of amino acids resulting from the total hydrolysis of femtomole amounts of protein has been reported (18). Edman degradation-type sequencing procedures can routinely be performed on picomole quantities of protein (19), and sensitivity improvements in this area are anticipated. In comparison to the aforementioned techniques, conventional peptide mapping routines have been somewhat lacking in terms of compatibility with extremely small sample sizes. Although impressive HPLC separations of picomole quantities of tryptic digests have been reported (16, 20), the initial enzymatic hydrolysis procedures have required nanomole to micromole quantities of protein. The goal of the work reported here has been to develop an overall approach for the peptide mapping of picomole or smaller quantities of protein. To accomplish this, we have addressed both the sample preparation requirements as well as the peptide separation methods. A novel means of obtaining tryptic digests from low-nanogram quantities of protein is described, which utilizes trypsin immobilized on a solid substrate and placed in a small reactor column. Separations of the resultant protein digests are accomplished with either microcolumn HPLC or capillary electrophoresis, both of which exhibit high separation efficiencies, improved mass sensitivity in conjunction with concentration-sensitive UV absorbance detectors, and compatibility with very small sample sizes (21, 22). The advantages and drawbacks of both separation methods for high-sensitivity peptide mapping are presented, and the reproducibilities of the procedures are assessed.

EXPERIMENTAL SECTION

Reagents. β -Casein, dephosphorylated β -casein, *N*-[tris(hydroxymethyl)methyl]glycine (Tricine), and tris(hydroxymethyl)aminomethane (Tris) were purchased from Sigma Chemical Co. (St. Louis, MO). HPLC-grade acetonitrile and trifluoroacetic acid were obtained from Fisher Scientific (Fair Lawn, NJ). Immobilized TPCK-trypsin on an agarose gel substrate was obtained from Pierce (Rockford, IL). Ammonium bicarbonate was reagent grade (Mallinckrodt, Inc., Paris, KY). Distilled water was used for the preparation of buffers and mobile phases. All buffers and mobile phases were filtered through 0.2- μ m Nylon-66 membrane filters (Alltech Associates, Deerfield, IL) and degassed prior to use.

Preparation of Tryptic Digests. Reactor columns were prepared from thick-walled Pyrex tubing, 30 cm \times 1 mm i.d. One end of the column was tapered to an inside diameter of 0.5 mm, and a small piece of silanized glass wool was placed in the tapered end. TPCK-trypsin immobilized on agarose gel was rinsed several times with 0.05 M ammonium bicarbonate buffer (pH 8.2). A slurry of the gel in ammonium bicarbonate buffer was added to a small reservoir attached to the top of the reactor column and allowed to flow into the column. After the column was filled with gel, it was rinsed with several column volumes of buffer prior to use. Solutions of protein were prepared in 0.05 M ammonium bicarbonate buffer at concentrations ranging from 0.1 to 0.3 mg/mL. An aliquot of the protein solution (0.2-1.0 μ L) was added to the top of the reactor column and eluted through with ammonium bicarbonate buffer at atmospheric pressure. Effluent from the reactor column was collected in a 500- μ L vial and lyo-

philized. Dried samples were stored at -20°C until use. Samples were dissolved in $0.5\text{--}2.0\ \mu\text{L}$ of distilled water immediately prior to separation by either microcolumn HPLC or CZE.

Microcolumn HPLC Separations. Fused silica capillary columns (Polymicro Technologies, Phoenix, AZ) were slurry-packed with a C_{18} stationary phase ($5\text{-}\mu\text{m}$ Capcell Pak, Shiseido, Tokyo, Japan), using a previously described procedure (23). Column dimensions were $100\ \text{cm} \times 250\ \mu\text{m}$ i.d. A Varian Model 8500 syringe pump (Varian Instrument Division, Palo Alto, CA) was used to provide pulseless flow at constant pressure. A $\mu\text{LC-10}$ UV-absorbance detector (ISCO, Lincoln, NE) with a $1\ \text{mm}$ path length flow cell was operated at $215\ \text{nm}$. A stop-flow injection technique (24) was employed to allow full utilization of very small sample volumes with minimal sample loss. A step gradient elution method (24) was used. The mobile phase consisted of aqueous acetonitrile containing 0.1% trifluoroacetic acid. The gradient of increasing acetonitrile was comprised of the following steps, given in percent acetonitrile and volume of the step, respectively: 15% , $18\ \mu\text{L}$; 18% , $19\ \mu\text{L}$; 21% , $20\ \mu\text{L}$; 24% , $23\ \mu\text{L}$; 28% , $25\ \mu\text{L}$; 32% , $25\ \mu\text{L}$; 37% , $25\ \mu\text{L}$; 42% , $39\ \mu\text{L}$; 47% , $68\ \mu\text{L}$; 52% , $48\ \mu\text{L}$. The flow rate employed for all chromatographic separations was $3.0\ \mu\text{L}/\text{min}$.

Capillary Electrophoresis Separations. The capillary electrophoresis system was constructed in-house, following the basic format described by Jorgenson and Lukacs (25). A dc power supply capable of delivering up to $30\ \text{kV}$ (Spellman High Voltage Electronics Corp., Plainview, NY) was used to provide the high voltage. Applied voltage for all separations shown was $22\ \text{kV}$. Fused silica capillaries (Polymicro Technologies, Phoenix, AZ) had inner diameters of $50\ \mu\text{m}$ and outer diameters of $190\ \mu\text{m}$ and were $100\ \text{cm}$ in length ($85\ \text{cm}$ separation length). On-column detection was performed by use of a variable wavelength UV-absorbance detector (UVIDEC-100-V, Jasco, Tokyo, Japan) with an in-house modified flow cell, operated at $215\ \text{nm}$. A short section of polyimide cladding on the fused silica capillary was removed to produce the optical window. The buffer system used for all CZE separations was composed of $0.04\ \text{M}$ Tris/ $0.04\ \text{M}$ Tricine (pH 8.1). Sample introduction was accomplished by hydrodynamic flow (26) with a height differential of $22\ \text{cm}$ for the ends of the capillary. The capillary was rinsed sequentially with $0.1\ \text{M}$ NaOH, distilled water, and buffer, for approximately $1\ \text{min}$ each, between the individual electrophoretic runs.

RESULTS AND DISCUSSION

A model protein was used in the development of the tryptic digest preparation scheme and the peptide mapping separations described here. The protein used was β -casein, whose primary structure is shown in Figure 1 (27). β -Casein is a well-characterized phosphoprotein and was chosen as a model for our microscale peptide mapping work because of its intermediate size (23982 daltons) and availability in both phosphorylated and dephosphorylated forms, which were used for comparative studies.

Protein Hydrolysis with Immobilized Trypsin. The most common means of cleaving a protein into smaller fragments for peptide mapping purposes has been the use of the proteolytic enzyme trypsin (28). Tryptic digestion is desirable due to the quantitative and very specific nature of the hydrolysis process (trypsin cleaves only at the C-terminal side of lysine and arginine residues). Reactions for the tryptic hydrolysis of proteins have traditionally been performed in solution, involving a homogeneous mixture of the protein and trypsin (29, 30). The protein and trypsin concentrations, protein-to-trypsin ratio, pH, temperature, and time of incubation are maintained at optimum levels for enzyme activity. Our initial attempts to develop a procedure for the tryptic digestion of very small amounts of protein were based on simple modifications of this conventional procedure. Successive dilutions of individual solutions of protein and trypsin were made, thereby allowing smaller amounts of both protein and trypsin to be obtained in the aliquots which were mixed. The ratio of protein to trypsin was maintained near the optimum level (approximately $50:1$ (w/w)). This approach was

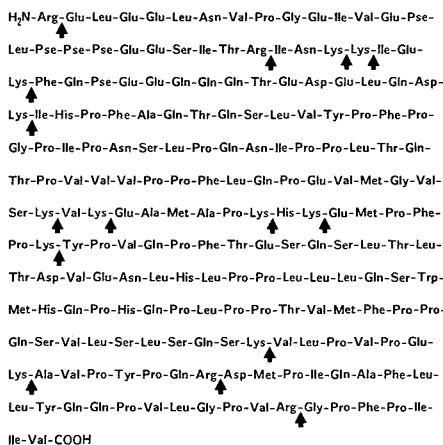


Figure 1. Primary structure of β -casein (A^2 variant). Arrows show theoretical cleavage sites when digested with trypsin. Pse indicates phosphoserine.

viable down to a level of a few micrograms of protein but eventually reached a point where the protein/trypsin mixture was so dilute that cleavage of the protein was frequently incomplete and reproducibility was poor. This was attributed to the fact that the trypsin concentration was far below its optimum, which significantly slowed the enzyme kinetics. A variation of this procedure involved the use of dilute protein solutions and more concentrated trypsin solutions, to allow the final concentration of trypsin to be near the optimum level. In this situation, however, it was impossible to maintain the proper ratio of protein to trypsin, and in fact, the amount of trypsin in the digest mixture approached or exceeded the amount of protein. This is an undesirable situation because trypsin will readily undergo autolysis, resulting in a final digestion mixture consisting primarily of peptide fragments from the trypsin.

Our final solution to the tryptic digestion of extremely small amounts of protein necessitated a complete departure from the conventional procedure. Rather than using trypsin in solution, we utilized trypsin immobilized on a solid substrate and loaded into a small column to form a fixed-bed reactor. An aliquot of a protein solution can then be applied to the top of the reactor column and eluted through with a buffer solution. As the protein comes into contact with the trypsin, it is cleaved at the lysine and arginine residues. The buffer used for elution must be volatile, to avoid the presence of a large amount of salt from the buffer following lyophilization of the samples. Additionally, a buffer pH near 8 is needed for optimal trypsin activity. An ammonium bicarbonate buffer was found to be well suited for this purpose.

Immobilized trypsin offers several advantages in comparison to trypsin in solution (31, 32). Immobilized trypsin is considerably more resistant to autolysis and therefore maintains its activity for prolonged periods of time. Individual reactor columns can be used for several weeks, provided a continual flow of buffer is maintained through the column. The resistance to autolysis also minimizes the occurrence of extraneous trypsin fragments in the protein digest samples. Use of the immobilized trypsin/reactor column format allows for easy regulation of the cleavage process by varying the flow rate of the eluent through the column and by using columns of different dimensions. The immobilized trypsin is also effective when used with very small volumes of dilute protein solutions. We have obtained reproducible tryptic digests of

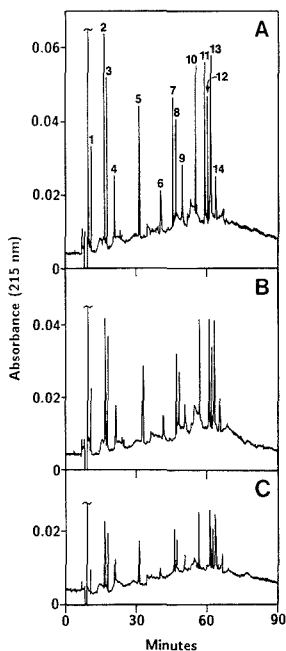


Figure 2. Tryptic digests of β -casein, separated by microcolumn HPLC. Chromatograms were obtained from three separate sample preparations of the following sizes: (A) 300 ng of protein digest; (B) 200 ng of protein digest; (C) 100 ng of protein digest. Numbered peaks in part A relate to Table I and bear no relationship to the numbers in Figure 4A or Table II.

β -casein from sample volumes as small as 0.2 μ L and from solutions as dilute as 4×10^{-8} M. Whereas the limit of tryptic digestion using the conventional procedure in solution was a few micrograms of protein, the immobilized trypsin scheme allows digestion of a few nanograms of protein (picomole to femtomole quantities).

Microcolumn HPLC for Peptide Mapping. Reversed-phase HPLC using conventional columns (4.6 mm i.d.) has become one of the most popular and successful methods for the separation of peptides in peptide mapping applications. A proven means of enhancing HPLC efficiency and sensitivity is miniaturization of the HPLC columns (21, 33). Reduced-diameter HPLC columns are also well suited for use with extremely small sample sizes. Microcolumn HPLC (250 μ m i.d. columns) in the reversed-phase mode was thus investigated as a separation method for our reduced-scale peptide mapping studies. Figure 2 shows three peptide maps from the separate tryptic digests of β -casein, ranging in size from 300 ng (12 pmol) to 100 ng (4 pmol) of total protein which was digested. For each of these separations, the lyophilized tryptic digest sample was dissolved in 2 μ L of water and the entire sample was used to obtain the chromatogram. Reproducibility of the tryptic digestion method is evidenced by the peak-to-peak comparison among the three sample sizes. The 100-ng sample is approaching the useful limit of detectability of our UV detector, without suffering the loss of smaller peaks into the base-line noise. The upward drift of the base line which is evident in the chromatograms in Figure 2 is due to the acetonitrile gradient used. The inherent absorbance of organic solvents at the low wavelengths needed for detection of peptide bonds, combined with slight changes in flow rate as the gradient progresses, results in the base-line drift. It is, in fact,

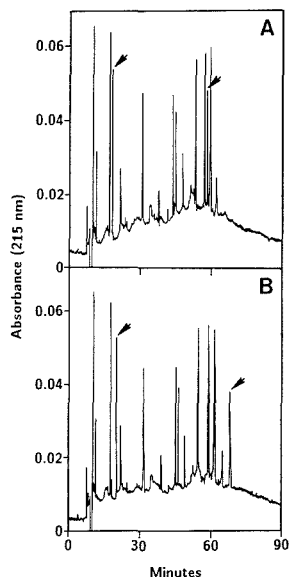


Figure 3. Comparison of tryptic digests from (A) phosphorylated and (B) dephosphorylated forms of β -casein, separated by microcolumn HPLC. Arrows point to the two peaks which exhibit different retention times between the two forms. Each chromatogram was obtained from a 300 ng protein digest sample.

the gradient elution that limits the sensitivity of the microcolumn HPLC separations. To keep the base-line drift to an acceptable level, the detector cannot be utilized at its highest sensitivity setting. Techniques such as base-line subtraction, which are frequently employed in conventional HPLC, are difficult to use with microcolumn HPLC (in which step gradients currently predominate) because of the irregularities in the step gradient profile. Anticipated improvements in the generation of mobile phase gradients for microcolumn HPLC may help to alleviate these problems and lead to improved sensitivity.

As previously mentioned, β -casein is a phosphoprotein, containing five phosphoserine residues (Figure 1). Upon digestion with trypsin, these five phosphoserine amino acids will be distributed among two peptides, with four phosphoserine residues in one peptide and one phosphoserine in another. β -Casein can also be obtained in a dephosphorylated form, in which the phosphoserine residues are replaced by serine residues. The peptide maps of the two forms of β -casein should be distinguishable due to differences in retention behavior of the two peptides containing either phosphoserine or serine. Such a comparison is illustrated in Figure 3, which shows the microcolumn HPLC peptide maps of phosphorylated and dephosphorylated forms of β -casein. As expected, there are two peaks exhibiting different retention times between the two forms, while the remaining peaks show essentially identical patterns. Reversed-phase HPLC separates components primarily on the basis of hydrophobicity, with the most hydrophobic components having the longest retention times. The removal of phosphate groups from a peptide should increase the hydrophobicity, and hence the retention time, of that peptide. Such behavior is noted in the chromatograms in Figure 3, in which two peaks are shifted to longer retention times in the dephosphorylated form of the protein. These separations demonstrate the ability of microcolumn HPLC peptide mapping to detect the phospho-

Table I. Reproducibility of Retention Times for Microcolumn HPLC Peptide Mapping^a

peak no.	retention time, min (<i>n</i> = 5)		
	\bar{x}	<i>s</i>	RSD, %
1	10.76	0.183	1.701
2	16.36	0.139	0.849
3	17.64	0.240	1.360
4	20.88	0.317	1.518
5	31.60	0.940	2.975
6	40.52	0.661	1.631
7	45.96	0.787	1.712
8	47.24	0.682	1.444
9	50.04	0.730	1.459
10	56.00	0.817	1.459
11	60.24	1.157	1.926
12	61.48	1.089	1.773
13	62.60	0.909	1.452
14	65.08	1.272	1.951

^a \bar{x} , mean; *s*, standard deviation; RSD, %, relative standard deviation. Peak numbers relate to Figure 2A.

rylation of a single amino acid in a protein. Similar capabilities should exist for other types of amino acid modifications, such as glycosylation.

Because peptide mapping is primarily a comparison-based technique, a high degree of reproducibility is required of the separation method employed. The deviations in retention times of 14 major peaks from β -casein tryptic digests were calculated, using five different chromatograms obtained from varying sample sizes. The reproducibility data are summarized in Table I, and it can be seen that the relative standard deviation is less than 2% for all peaks except one. The variations in retention times are attributed primarily to the step gradient elution technique and the inability to precisely reproduce the gradient from run to run.

Capillary Zone Electrophoresis for Peptide Mapping. CZE is a relative newcomer to the field of separation science, but it has proven to be an extremely powerful technique, particularly for the separation of biomolecules. Highly efficient and sensitive separations of proteins (34), nucleotides (35), peptides (36), and amino acids (37) have recently been achieved with CZE. In free-solution CZE (without the use of micellar modifiers or gels), separation is based on the difference in electrophoretic mobilities of the analytes in an applied electric field. Electrophoretic mobilities are directly related to the charge densities of the analytes (38). Substances with very subtle differences in charge densities can be resolved by CZE by manipulating such parameters as buffer composition and pH, applied voltage, and capillary dimensions.

The inherently high separation efficiencies of CZE, coupled with its compatibility with small sample sizes, have made CZE a natural choice for separation of complex mixtures in our high-sensitivity peptide mapping work. Figure 4 shows three electropherograms obtained from separate tryptic digests of β -casein. The tryptic digests range in size from 150 ng (6 pmol) to 50 ng (2 pmol) of starting protein. However, unlike the microcolumn HPLC separations which utilized the entire sample, the CZE separations shown in Figure 4 have been obtained from only a small fraction of the individual digests. Hydrodynamic injection volumes were calculated from the known injection times and the measured velocity of the hydrodynamic flow, as previously described by Rose and Jorgenson (39). From a total sample volume of 500 nL, a maximum of 20 nL was used to obtain each of the CZE separations. This corresponds to 6 ng (250 fmol), 4 ng (166 fmol), and 2 ng (83 fmol) of protein digest actually separated in Figure 4 (A, B, and C, respectively). Thus, we see sensitivity improvements of nearly 2 orders of magnitude for CZE in comparison to microcolumn HPLC. This improved sensitivity is

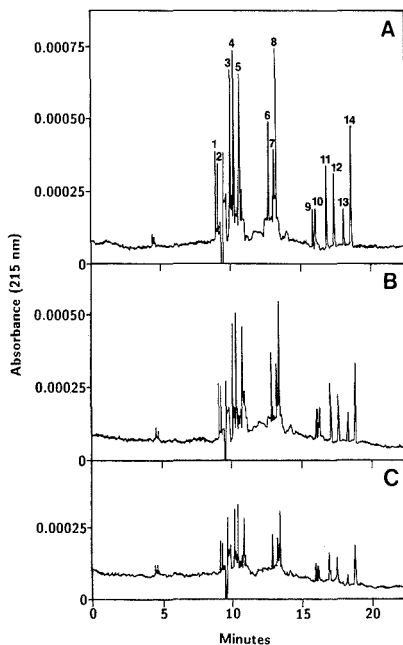


Figure 4. Tryptic digests of β -casein, separated by CZE. Electropherograms were obtained from three separate sample preparations of the following sizes: (A) 150 ng of protein digest (ca. 6 ng introduced into capillary); (B) 100 ng of protein digest (ca. 4 ng introduced into capillary); (C) 50 ng of protein digest (ca. 2 ng introduced into capillary). Numbered peaks in part A relate to Table II and bear no relationship to the numbers in Figure 2A or Table I.

attributed to several factors. First, the UV detector in the CZE separations can be utilized at its highest sensitivity setting without significant noise and base-line instability. The absence of gradient elution and organic solvents in the buffer system employed for CZE results in a much lower background absorbance, thereby overcoming the primary limitation of the microcolumn HPLC separations. Second, the higher efficiencies of CZE separations result in sharper, taller peaks, which are, in turn, detectable at lower levels. Third, mass sensitivity of the 50 μ m i.d. capillaries used in our CZE separations is inherently greater than that of the 250 μ m i.d. columns used for microcolumn HPLC (in conjunction with concentration-sensitive detectors, such as UV absorbance).

The sensitivity of CZE separations is limited primarily by the small sample volumes which can be utilized. This sample volume restriction necessitates the use of concentrated samples, from which only a few nanoliters will actually be used for the separation. Although we now have the capability to prepare tryptic digests from small volumes of dilute protein solutions, the resultant protein digest must be dissolved in a finite volume (typically 500 nL or greater) of liquid to allow reliable sample injections to be made. Therefore, it was impossible to utilize the entire tryptic digest sample in obtaining the peptide map, as was done with microcolumn HPLC. Injection volumes greater than about 20 nL were found to result in inferior electropherograms, apparently due to distortion of the electric field profile (40).

A comparison of the peptide maps of phosphorylated and dephosphorylated forms of β -casein was done with CZE (as previously described for microcolumn HPLC), and the resulting electropherograms are shown in Figure 5. Again, two

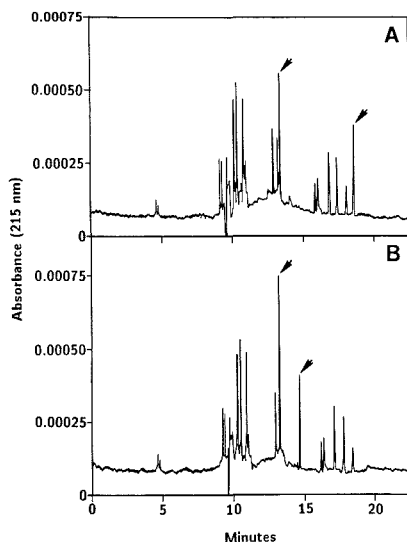


Figure 5. Comparison of tryptic digests from (A) phosphorylated and (B) dephosphorylated forms of β -casein, separated by CZE. Arrows point to the two peaks which exhibit different migration times between the two forms. Each electropherogram was obtained from a 100 ng protein digest sample, with ca. 4 ng introduced into the capillary in each case.

peaks exhibit shifts in retention time between the two forms, consistent with the distribution of phosphoserine residues in the tryptic peptides. Because electrophoretic mobilities of the peptides are strongly dependent on charge density, any modification that changes the charge density of certain peptides should be evident in the peak pattern of the peptide map. Dephosphorylation effectively reduces the net negative charge of the peptides containing phosphoserine residues, which is reflected in their increased mobility toward the cathodic electrode at the detector end of the capillary. Hence, reduced migration times of two peaks are observed in the dephosphorylated peptide map.

Reproducibility of migration times for 14 major peaks from CZE peptide maps of β -casein was evaluated, and results are given in Table II. Relative standard deviations are less than 1% for all peaks, indicating a slight improvement in comparison to the data for microcolumn HPLC in Table I. This improved reproducibility is attributed to the absence of gradient elution in CZE and the greater simplicity of the experimental procedure. The small deviations in migration times which are encountered in CZE separations are likely due to variations in the electroosmotic flow from run to run.

It is important to emphasize the experimental conditions that were employed for all CZE separations in this study. We have purposely maintained the simplest conditions in terms of the buffer system and capillary treatment. The buffer consisted of a binary mixture of Tris and Tricine, at pH 8.1, with no added modifiers. At this pH, a complex mixture of peptides can be expected to contain both positively and negatively charged peptides, depending on the overall isoelectric point of the peptide. The separation of both positively and negatively charged species in a single electrophoretic run is made possible due to the presence of a strong electroosmotic flow which exists within the capillary (41). This electroosmotic flow is a result of the negative zeta potential at the walls of the fused silica capillaries, thereby making the bulk osmotic flow toward the negative (or ground) electrode. It is possible

Table II. Reproducibility of Migration Times for CZE Peptide Mapping^a

peak no.	migration time, min (<i>n</i> = 5)		
	\bar{x}	<i>s</i>	RSD, %
1	9.02	0.057	0.632
2	9.14	0.049	0.536
3	10.06	0.042	0.417
4	10.30	0.054	0.524
5	10.75	0.051	0.474
6	12.75	0.051	0.400
7	13.20	0.033	0.250
8	13.28	0.029	0.218
9	15.90	0.077	0.484
10	16.10	0.068	0.422
11	16.87	0.078	0.462
12	17.44	0.071	0.407
13	18.13	0.087	0.480
14	18.68	0.086	0.460

^a \bar{x} , mean; *s*, standard deviation; RSD, %, relative standard deviation. Peak numbers relate to Figure 4A.

to eliminate or substantially reduce the electroosmotic flow by coating the walls of the capillary with an uncharged material, and several workers (36, 42) have found this to be effective in reducing the adsorption of positively charged analytes to the capillary walls. We have chosen to work with uncoated capillaries and have made no attempt to reduce or eliminate the electroosmotic flow. In spite of the negatively charged capillary walls, the peptides do not appear to be adsorbing to the capillary walls, as evidenced by the absence of any significant peak tailing or broadening. Thus, resolution of complex mixtures of peptides can be accomplished by CZE without the use of buffer additives or capillary coatings, maintaining the desirable simplicity of the separation method.

CONCLUSIONS

We have developed an overall procedure for high-sensitivity peptide mapping, allowing reproducible peptide maps to be obtained from low-nanogram quantities of protein. This work serves to bring the sample requirements for peptide mapping to a level comparable to that of microscale protein isolation and amino acid analysis. A critical component of successful peptide mapping is the initial sample preparation. The use of immobilized trypsin in a small-bore reactor column has allowed us to obtain complete and reproducible tryptic digests from as little as 50 ng (2 pmol) of protein. This represents a decrease of approximately 3 orders of magnitude from quantities digested by the conventional procedures in solution.

Both microcolumn HPLC and CZE have been successful in the resolution of tryptic digests of picomole quantities of protein, with each method exhibiting unique advantages and disadvantages. Microcolumn HPLC is capable of excellent resolution of peptides through the use of gradient elution. Although time of analysis by microcolumn HPLC was significantly longer than by CZE (70 min vs less than 20 min), improvements in separation time could likely be made by using micropellicular stationary phases, as recently demonstrated by Horvath and co-workers for conventional HPLC (43). The sensitivity of CZE peptide mapping was found to be 1–2 orders of magnitude more sensitive than that of microcolumn HPLC, primarily due to the absence of gradient elution and organic modifiers, resulting in lower background absorbance. The overall procedure for CZE peptide mapping was found to be significantly less complex and time-consuming than the microcolumn HPLC procedure employed in this study, supporting the growing popularity of this separation method. Although we have employed β -casein as a model protein in the present study, the general procedures described should be applicable to other proteins as well. However, some

experimental details may need to be reoptimized for different proteins.

LITERATURE CITED

- (1) Huberman, A.; Aguilar, M. B. *J. Chromatogr.* **1988**, *443*, 337-342.
- (2) L'Italien, J. J. *J. Chromatogr.* **1986**, *359*, 213-220.
- (3) Pohl, G.; Kallstrom, M.; Bergsdorf, N.; Wallen, P.; Jornvall, H. *Biochemistry* **1984**, *23*, 3701-3707.
- (4) Takahashi, N.; Takahashi, Y.; Ishioka, N.; Blumberg, B. S.; Putnam, F. W. *J. Chromatogr.* **1986**, *359*, 181-191.
- (5) Garnick, R. L.; Solli, N. J.; Papa, P. A. *Anal. Chem.* **1988**, *60*, 2546-2557.
- (6) Borman, S. *Anal. Chem.* **1987**, *59*, 969A-973A.
- (7) Ingram, V. M. *Nature (London)* **1956**, *178*, 792-794.
- (8) Cleveland, D. W.; Fischer, S. G.; Kirschner, M. W.; Laemmli, U. K. *J. Biol. Chem.* **1977**, *252*, 1102-1106.
- (9) Stephens, R. E. *Anal. Biochem.* **1978**, *84*, 116-126.
- (10) Hancock, W. S.; Bishop, C. A.; Prestidge, R. L.; Hearn, M. T. W. *Anal. Biochem.* **1978**, *89*, 203-212.
- (11) Cox, M. J.; Shapira, R.; Wilkinson, K. D. *Anal. Biochem.* **1986**, *154*, 345-352.
- (12) Leadbeater, L.; Ward, F. B. *J. Chromatogr.* **1987**, *397*, 435-443.
- (13) Vensel, W. H.; Fujita, V. S.; Tarr, G. E.; Margolash, E.; Kayser, H. J. *Chromatogr.* **1983**, *266*, 491-500.
- (14) Fullmer, C. S.; Wasserman, R. H. *J. Biol. Chem.* **1979**, *254*, 7209-7212.
- (15) Jorgenson, J. W.; Lukacs, K. D. *HRC CC, J. High Resolut. Chromatogr. Chromatogr. Commun.* **1981**, *4*, 230-231.
- (16) Lu, H.-S.; Lai, P.-H. *J. Chromatogr.* **1986**, *368*, 215-231.
- (17) Flurer, C.; Borra, C.; Beale, S.; Novotny, M. *Anal. Chem.* **1988**, *60*, 1826-1829.
- (18) Beale, S. C.; Hsieh, Y.-Z.; Savage, J. C.; Wiesler, D.; Novotny, M. *Talanta* **1988**, *36*, 321-325.
- (19) Hunkapiller, M. W.; Hewick, R. M.; Dreyer, W. J.; Hood, L. E. *Methods Enzymol.* **1983**, *91*, 399-413.
- (20) Stone, K. L.; Williams, K. R. *J. Chromatogr.* **1986**, *359*, 203-212.
- (21) Novotny, M. *Anal. Chem.* **1988**, *60*, 500A-510A.
- (22) Ewing, A. G.; Wallingford, R. A.; Olefirowicz, T. M. *Anal. Chem.* **1989**, *61*, 292A-303A.
- (23) Gluckman, J.; Hirose, A.; McGuffin, V. L.; Novotny, M. *Chromatographia* **1983**, *17*, 303-309.
- (24) Hirata, Y.; Novotny, M. *J. Chromatogr.* **1979**, *186*, 521-528.
- (25) Jorgenson, J. W.; Lukacs, K. D. *J. Chromatogr.* **1981**, *218*, 209-216.
- (26) Rose, D. J.; Jorgenson, J. W. *Anal. Chem.* **1988**, *60*, 642-648.
- (27) Dumas, B. P.; Brignon, G.; Grosclaude, F.; Mercier, J.-C. *Eur. J. Biochem.* **1972**, *25*, 505-514.
- (28) Regnier, F. E. *LC-GC* **1987**, *5*, 392-398.
- (29) Canfield, R. E. *J. Biol. Chem.* **1963**, *238*, 2691-2697.
- (30) Smith, D. G. *Methods Enzymol.* **1961**, *11*, 214-231.
- (31) Guilbault, G. *Analytical Uses of Immobilized Enzymes*; Marcel Dekker, Inc.: New York, 1984; Chapter 2.
- (32) Weetall, H. H. *Anal. Chem.* **1974**, *46*, 602A-615A.
- (33) Karlsson, K.-E.; Novotny, M. *Anal. Chem.* **1988**, *60*, 1662-1665.
- (34) Lauer, H. H.; McManigill, D. *Anal. Chem.* **1986**, *58*, 166-170.
- (35) Cohen, A. S.; Terabe, S.; Smith, J. A.; Karger, B. L. *Anal. Chem.* **1987**, *59*, 1021-1027.
- (36) McCormick, R. M. *Anal. Chem.* **1988**, *60*, 2322-2328.
- (37) Liu, J.; Cobb, K. A.; Novotny, M. *J. Chromatogr.* **1989**, *468*, 55-65.
- (38) Grossman, P. D.; Wilson, K. J.; Petrie, G.; Lauer, H. H. *Anal. Biochem.* **1988**, *173*, 265-270.
- (39) Rose, D. J.; Jorgenson, J. W. *J. Chromatogr.* **1988**, *438*, 23-34.
- (40) Jorgenson, J.; Lukacs, K. D. *Science* **1983**, *222*, 266-272.
- (41) Jorgenson, J. W.; Lukacs, K. D. *Anal. Chem.* **1981**, *53*, 1298-1302.
- (42) Hjerten, S. *J. Chromatogr.* **1985**, *347*, 191-198.
- (43) Kalghatgi, K.; Horvath, C. J. *Chromatogr.* **1988**, *443*, 343-354.

RECEIVED for review April 27, 1989. Accepted July 31, 1989. This research was supported by Grant No. PHS R01 GM 24349 from the National Institute of General Medical Sciences, U. S. Public Health Service, and a grant-in-aid from Dow Chemical Company.

Diffusion Coefficients of Gases in Liquids and Partition Coefficients in Gas-Liquid Interphases by Reversed-Flow Gas Chromatography

N. A. Katsanos* and J. Kaposol

Physical Chemistry Laboratory, University of Patras, 26110 Patras, Greece

Diffusion coefficients of two gases (propene and ethene) in three liquids (hexadecane, heptane, and water) have been determined in a very simple way by using the new technique of reversed-flow gas chromatography. In the same experiment the partition coefficient of each gas between the liquid and the carrier gas (nitrogen) was measured simultaneously, and from this the respective Henry's law constant was calculated. The determination of both physicochemical quantities above was based on the extension of a previous mathematical model. The diffusion coefficients measured have the same order of magnitude as those calculated by using the Wilke-Chang formula. The Henry's law constants, however, are found much smaller than those calculated from a nomogram. This is attributed to the fact that the partition coefficients found pertain to the gas-liquid interphase layers rather than to the bulk phases.

INTRODUCTION

Gas chromatography has widely been accepted both as a separation method and as a method for physicochemical

measurements, the latter being based on the distortion of the chromatographic elution bands caused by various physicochemical processes, like gas diffusion along the column. Recently, however, gas chromatography instrumentation has been used to sample the above processes as a function of time and then analyze the result of this sampling to calculate physicochemical quantities, like reaction rates. This is done by using the so-called reversed-flow gas chromatography (RF-GC) technique, a flow perturbation method developed in 1980 (1) and reviewed in 1984 (2) and also recently (3-5). It is based on narrow extra chromatographic sample peaks (cf. Figure 1) superimposed on the normal elution curves and created by reversing the direction of the carrier gas flow for short time intervals, at various times during the experiment. In its simplest form the method employs a chromatographic column filled with a catalyst (1, 6-11), or with a usual chromatographic material (12, 13), or both (14, 15). In all but one (13) of these cases the phenomena being studied were surface catalyzed reactions to determine fractional conversions of reactants to products, reaction orders, and reaction rate constants, from which Arrhenius activation parameters were calculated. The feeding of the catalytic bed with reactant(s) was done either by simple chromatographic injection at a middle point along the column (1, 6, 9, 10) or by gaseous diffusion along an empty column connected perpendicularly

* To whom all correspondence should be addressed.

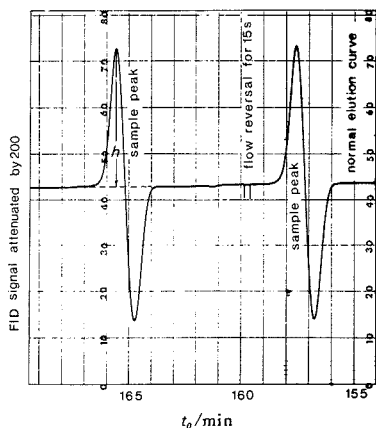


Figure 1. A reversed-flow chromatogram with two sample peaks obtained during the diffusion of propene into nitrogen (corrected volume flow rate $\bar{V} = 0.33 \text{ cm}^3 \text{ s}^{-1}$), at 323.2 K and 1 atm.

to the chromatographic column, usually at its middle point (9, 12, 14–16).

In another group of applications of RF-GC, the role of the chromatographic column (empty or packed with conventional chromatographic material) was confined to the mere creation of sample peaks by reversals of the direction of the carrier gas flowing through it, and for this reason it was termed "sampling column". The physical or chemical phenomenon under study, being a slow rate process or an equilibrium state, was physically separated from the chromatographic movement by "placing" it in the "diffusion column" mentioned above (cf. Figure 2), which is connected perpendicularly to the sampling column. A gas diffusion current is created along the diffusion column, carrying a solute from the region where the rate process or the equilibrium state are taking place (region of the liquid in Figure 2) to the junction $x = l'$ of the two columns. This gives rise to a so-called *diffusion band* comparable to the old chromatographic elution band. In the absence of other processes, the diffusion band can be used to measure accurately the diffusion coefficient of the solute into the carrier gas (17–19), or other quantities pertaining to it (20, 21). When a rate process or an equilibrium state involving one or more solutes is taking place inside the diffusion column, the diffusion band is distorted by that process and this distortion, rather than the distortion of an elution band, is used to measure various physicochemical quantities, like adsorption equilibrium constants (22), rates of drying of catalysts (23), mass transfer and partition coefficients across phase boundaries (24–28), adsorption, desorption and reaction rate constants (29, 30), activity coefficients in solutions (31–33), interaction of the solid components in a solid adsorbent (34), thermodynamic functions of polymer–solvent systems (35), solubility and interaction parameters in liquid mixtures (36), and finally obstructive factors and porosity in solid beds (37).

In the present work the distortion of a diffusion band, mentioned above and followed by the RF-GC sampling technique, is used to measure the diffusion coefficient of a solute gas into a liquid, together with the relevant partition coefficient (or the Henry's law constant) of the solute gas between the carrier gas and the liquid.

THEORY

The general chromatographic equation describing the elution curve of the sample peaks, like those of Figure 1, has been published elsewhere (2, 12, 14, 16, 18, 19, 24). The height h

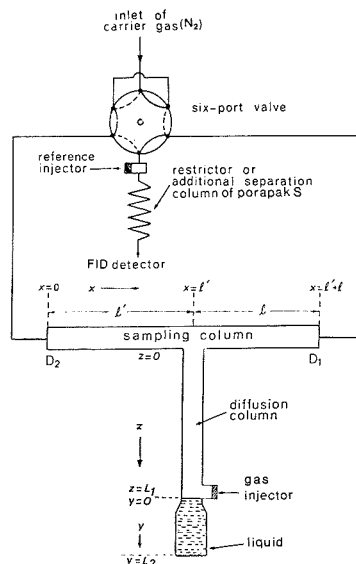


Figure 2. Schematic representation of the cell and the gas connections to measure diffusion and partition coefficients of gases in liquids by the reversed-flow technique.

of each sample peak above the ending base line is proportional to the concentration $c(l', t_0)$ of the solute in the sampling column at $x = l'$ at time t_0 (cf. Figure 2)

$$h = 2c(l', t_0) \quad (1)$$

The above concentration depends on (a) the partition coefficient K of the solute between the liquid and the carrier gas filling the diffusion column, (b) the diffusion coefficient D_L of the solute inside the liquid phase, and (c) the diffusion coefficient D_G of the solute into the carrier gas, since it is longitudinal diffusion along column L_1 which carries the solute from the surface of the liquid to the junction $x = l'$.

The mathematical equation giving $c(l', t_0)$ as an analytic function of the time t_0 contains K , D_L , and D_G as parameters and thus permits the determination of K and D_L from the variation of h with time. This equation can be derived with the help of the coordinates of Figure 2, by solving the diffusion equation (Fick's second law), first in the gaseous region z , then in the liquid region y , and finally linking the two solutions by using appropriate boundary conditions at $z = L_1$ and $y = 0$.

Gaseous Region z . In this region the diffusion equation is

$$\partial c_z / \partial t_0 = D_G \partial^2 c_z / \partial z^2 \quad (2)$$

where $c_z = c_z(z, t_0)$. This is solved under the initial condition

$$c_z(z, 0) = \frac{m}{a_G} \delta(z - L_1) \quad (3)$$

where m is the amount of solute injected at $z = L_1$, a_G the cross sectional area in the columns L_1 and $l' + l$, and δ the Dirac delta function, describing an instantaneous pulse injection. The boundary conditions at $z = 0$ are

$$c_z(0, t_0) = c(l', t_0)$$

and

$$D_G(\partial c_z / \partial z)_{z=0} = v c(l', t_0) \quad (4)$$

where v is the linear velocity of the carrier gas in the sampling column.

The details of the solution of eq 2, subject to the boundary conditions 4, have been given elsewhere (27). The result (eq 13 of ref 27), in the form of Laplace transform with respect to time (parameter p_0), is

$$C_z = C(l', p_0) \cosh q_1 z + (v/D_G q_1) C(l', p_0) \sinh q_1 z - \frac{m}{a_G D_G q_1} \sinh q_1 (z - L_1) u(z - L_1) \quad (5)$$

where

$$q_1^2 = p_0/D_G \quad (6)$$

and $u(z - L_1)$ the unit step function. The capital letters C_z and C denote the t_0 Laplace transformed functions of c_z and c , respectively.

Liquid Region y . The diffusion equation in this region reads

$$\partial c_y / \partial t_0 = D_L \partial^2 c_y / \partial y^2 \quad (7)$$

where $c_y = c_y(y, t_0)$. This partial differential equation is solved by applying first Laplace transformations with respect to t_0 (parameter p_0), under the initial condition $c_y(y, 0) = 0$

$$d^2 C_y / dy^2 - q_2^2 C_y = 0 \quad (8)$$

where C_y is the transformed function of c_y and q_2^2 is given by the relation

$$q_2^2 = p_0/D_L \quad (9)$$

Then, y Laplace transformation (transform parameter s) is applied to eq 8, giving, after rearrangement

$$\bar{C}_y = C_y(0) \frac{s}{s^2 - q_2^2} + C_y'(0) \frac{1}{s^2 - q_2^2} \quad (10)$$

where \bar{C}_y is the double Laplace transform of c_y with respect to t_0 and y , $C_y(0)$ the value of C_y at $y = 0$, and $C_y'(0) = (dC_y/dy)_{y=0}$. The inverse transformation of eq 10 with respect to s leads to

$$C_y = C_y(0) \cosh q_2 y + \frac{C_y'(0)}{q_2} \sinh q_2 y \quad (11)$$

The boundary condition at $y = L_2$ is $(\partial C_y / \partial y)_{y=L_2} = 0$, because there is no flux across this boundary. Thus, differentiating eq 11 with respect to y , substituting L_2 for y and setting the result equal to zero, one obtains

$$C_y'(0) = -C_y(0) q_2 \tanh q_2 L_2 \quad (12)$$

Equation 12 has been derived from eq 8 in the same way as eq 19 from eq 11 in ref 28, although there the meaning of q_2 is quite different from here.

Linking the Solutions in the Regions z and y . Now, eq 5, holding in region z is linked with eq 12, valid in region y , using the boundary conditions at $z = L_1$ and $y = 0$

$$K = C_y(0)/C_z(L_1) \quad (13)$$

$$a_G D_G (\partial C_z / \partial z)_{z=L_1} = a_G' D_L (\partial C_y / \partial y)_{y=0} \quad (14)$$

where the equilibrium 13 is assumed rapidly established with a partition coefficient K , and a_G' is the cross sectional area of region y . Calculation of $C_z(L_1)$ and $(\partial C_z / \partial z)_{z=L_1}$ from eq 5 and substitution into eq 13 and 14, using also eq 12 gives

$$C(l', p_0) = \frac{m}{a_G D_G q_1} \left[\sinh q_1 L_1 + \frac{v}{D_G q_1} \cosh q_1 L_1 + K \frac{a_G' D_L q_2}{a_G D_G q_1} \tanh q_2 L_2 \left(\cosh q_1 L_1 + \frac{v}{D_G q_1} \sinh q_1 L_1 \right) \right]^{-1} \quad (15)$$

Approximations. Certain approximations are needed in eq 15 to effect its inverse Laplace transformation with respect to p_0 . The first is analogous to that adopted previously (28), viz., omission of $\sinh q_1 L_1$ compared to $(v/D_G q_1) \cosh q_1 L_1$, and also omission of $\cosh q_1 L_1$ compared to $(v/D_G q_1) \sinh q_1 L_1$. Then, eq 15 becomes

$$C(l', p_0) = \frac{m}{V} \left[D_G q_1 \sinh q_1 L_1 \left(\frac{\cosh q_1 L_1}{D_G q_1} + K \frac{a_G'}{a_G} \cdot \frac{D_L^2 q_2^2}{D_G^2 q_1^2} \cdot \frac{\tanh q_2 L_2}{D_L q_2} \right) \right]^{-1} \quad (16)$$

where $V = va_G$ is the volumetric flow rate of the carrier gas.

Equation 16 applies when there is no gaseous volume above the liquid other than that (V_G) of column L_1 (cf. Figure 2). When such a volume V_G' exists in vessel y above the liquid, another term must be added on the right-hand side of eq 16

$$C(l', p_0) = \frac{m}{V} \left[D_G q_1 \sinh q_1 L_1 \left(\frac{\cosh q_1 L_1}{D_G q_1} + \frac{a_G'}{a_G} \cdot \frac{\tanh q_1 L_3}{D_G q_1} + K \frac{a_G'}{a_G} \cdot \frac{D_L^2 q_2^2}{D_G^2 q_1^2} \cdot \frac{\tanh q_2 L_2}{D_L q_2} \right) \right]^{-1} \quad (17)$$

where L_3 is the length of volume V_G' . The above relation results from a combination of eq 16 with eq 4 of ref 30.

Other approximations are

$$(1) \quad D_G q_1 \sinh q_1 L_1 \approx D_G q_1 q_1 L_1 = L_1 p_0 \quad (18)$$

$$(2) \quad \frac{\cosh q_1 L_1}{D_G q_1} = \frac{1}{L_1} \left(\frac{1}{p_0} + \frac{2}{p_0 + \beta} + \frac{2}{p_0 + 4\beta} + \frac{2}{p_0 + 9\beta} + \dots \right) \approx \frac{1}{L_1} \left(\frac{1}{p_0} + \frac{2}{\beta} + \frac{2}{4\beta} + \frac{2}{9\beta} + \dots \right) = \frac{1}{L_1} \left(\frac{1}{p_0} + \frac{2}{\beta} \sum_{n=1}^{\infty} n^{-2} \right) = \frac{1}{L_1} \left(\frac{1}{p_0} + \frac{\pi^2}{3\beta} \right) \quad (19)$$

where

$$\beta = \pi^2 D_G / L_1^2 \quad (20)$$

Equation 19 is derived by taking the inverse Laplace transform of $\cosh q_1 L_1 / D_G q_1$ in the form of an elliptic ϑ_3 function (38), transforming back to obtain the first series of terms above, then omitting the time parameter p_0 compared with the gaseous diffusion parameter β , and finally evaluating the sum $\sum_{n=1}^{\infty} n^{-2}$ as equal to $\pi^2/6$, since it is the Riemann zeta function of argument 2, $\zeta(2)$

$$(3) \quad \frac{\tanh q_1 L_3}{D_G q_1} \approx \frac{q_1 L_3}{D_G q_1} = \frac{L_3}{D_G} \quad (21)$$

$$(4) \quad \frac{\tanh q_2 L_2}{D_L q_2} \approx \frac{2}{L_2} \left(\frac{1}{p_0 + \alpha} + \frac{1}{p_0 + 9\alpha} + \frac{1}{p_0 + 25\alpha} \right) \approx \frac{2}{L_2} \left(\frac{1}{p_0} + \frac{1}{p_0} + \frac{1}{p_0 + 25\alpha} \right) \quad (22)$$

where

$$\alpha = \pi^2 D_L / 4L_2^2 \quad (23)$$

Equation 22 is the result of taking the inverse transform of $\tanh q_2 L_2 / D_L q_2$ in the form of an elliptic ϑ_2 function (38), retaining only the first three terms in the series, transforming back to obtain the three terms in the first parentheses, and then omitting the diffusion parameter in the liquid α and 9α compared to p_0 in the first two terms. This approximation

is based on the very small value of α , since D_L is usually 4 orders of magnitude smaller than D_G .

Using the above approximations (1), (2), (3), and (4), and the definitions 6 and 9, eq 17 reduces to

$$C(l', p_0) = N_2(p_0 + 25\alpha) \left[\left(p_0 + \frac{X+Y}{2} \right) \left(p_0 + \frac{X-Y}{2} \right) \right]^{-1} \quad (24)$$

where

$$N_2 = \frac{3mD_G}{\bar{V}L_1^2(1 + 3V_G'/V_G)} \quad (25)$$

$$X = \frac{3\beta + 72K\alpha V_L/V_G}{\pi^2(1 + 3V_G'/V_G)} + 25\alpha \quad (26)$$

$$\frac{X^2 - Y^2}{4} = \frac{75\alpha(\beta + 16K\alpha V_L/V_G)}{\pi^2(1 + 3V_G'/V_G)} \quad (27)$$

V_G' is the gaseous volume in vessel y above the liquid, $V_G = a_G L_1$ (gaseous volume in column z), $V_L = a_G' L_2$ (volume of the liquid in vessel y), K is the partition coefficient, defined by eq 13, and α and β are diffusion parameters given by eq 23 and 20, respectively.

When $V_G' = 0$, the same eq 24 would be obtained from eq 16, the only difference being that in eq 25–27 ($1 + 3V_G'/V_G$) = 1.

Inverse Transformation of Equation 24. The concentration $c(l', t_0)$ as an analytic function of time is found by taking the inverse Laplace transform of eq 24

$$c(l', t_0) = \frac{N_2}{2} \left[\left(1 + \frac{Z}{Y} \right) \exp\left(-\frac{X+Y}{2} t_0\right) + \left(1 - \frac{Z}{Y} \right) \exp\left(-\frac{X-Y}{2} t_0\right) \right] \quad (28)$$

where

$$Z = X - 50\alpha \quad (29)$$

This equation, combined with eq 1, describes the height h of the sample peaks as a function of time for a distorted diffusion band. It has the same form with eq 34 of ref 27 derived for a stirred liquid, and with eq 30 of ref 28 valid for a solid filling section y , although the physical meaning of the functions X , Y , and Z is different in those cases. It must be pointed out that eq 28 describes only the descending part of the diffusion band curve (after the maximum), because the approximation 18 excludes the ascending branch.

Calculation of D_L and K from the Experimental Data. In the absence of liquid in section y of the diffusion column, the descending branch of the diffusion band is linear with a slope $-3\beta/\pi^2(1 + 3V_G'/V_G)$, as can be seen from eq 17 by setting the height of the liquid $L_2 = 0$ and taking the inverse transformation of the remaining terms, using the same approximations as before (eq 18, 19, and 21)

$$c(l', t_0) = N_2 \exp\left[-\frac{3\beta}{\pi^2(1 + 3V_G'/V_G)} t_0\right] \quad (30)$$

From the value of $\beta = \pi^2 D_G / L_1^2$ (eq 20), the diffusion coefficient in the gas phase D_G can be calculated.

In the presence of liquid in vessel y the descending branch of the curve is described by the sum of two exponential functions, according to eq 28. The exponential coefficients $(X+Y)/2$ and $(X-Y)/2$ can be determined by means of a suitable computer program or, if these two coefficients are sufficiently different, by applying the method described elsewhere (27, 28), viz., by finding first the slope $-(X-Y)/2$

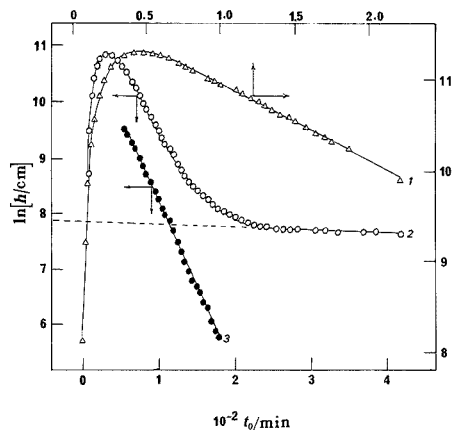


Figure 3. Diffusion bands obtained with 1 cm^3 of propene injected into the cell at 323.2 K . Curve 1 was obtained with L_2 containing no liquid, and curve 2 with L_2 containing 32 cm^3 hexadecane. Line 3 (plotted as $\ln h - 1$) was obtained by subtraction of the extrapolated (dashed line) last linear part of curve 2 from the experimental points of the same curve after the maximum.

and the intercept $\ln h_0$ of the last linear part of $\ln h$ vs t_0 plot (diffusion band), and then replotting the initial data of the nonlinear part after the maximum as $\ln [h - h_0 \exp\{-(X-Y)t_0/2\}]$ vs t_0 . An example of this kind is given in Figure 3. From the slope of the new straight line thus obtained, one finds $-(X+Y)/2$.

There are two ways to calculate D_L and K from the diffusion band: either by using the two exponential coefficients $(X+Y)/2$ and $(X-Y)/2$, and the diffusion parameter β , or by employing the above exponential coefficients and the respective preexponential factors $N_2(1+Z/Y)$ and $N_2(1-Z/Y)$ of eq 28, found from the intercepts of the $\ln h$ vs t_0 plots, mentioned above. In both ways the gaseous volumes V_G' and V_G , the volume of the liquid V_L , and the height of the liquid L_2 are required.

First Way. The sum of the two exponential coefficients $(X+Y)/2$ and $(X-Y)/2$ gives the value of X , i.e. the right-hand side of eq 26, while their product Π equals $(X^2 - Y^2)/4$, i.e. the right-hand side of eq 27. If eq 26 is solved for $K\alpha V_L/V_G$ and the result is substituted into eq 27, one obtains a quadratic equation in α

$$1250\alpha^2 - 25 \left[\frac{3\beta}{\pi^2(1 + 3V_G'/V_G)} + 2X \right] \alpha + 3\Pi = 0 \quad (31)$$

This on solution gives the value of $\alpha = \pi^2 D_L / 4L_2^2$, from which D_L is computed as L_2 is a known length. The α value found is then substituted back in eq 26 or 27 to find K .

Second Way. From the sum of the two exponential coefficients $(X+Y)/2$ and $(X-Y)/2$ one finds the value of X , while their difference gives the value of Y . From the ratio ρ of the two preexponential factors of eq 28

$$\rho = \frac{1 - Z/Y}{1 + Z/Y}$$

one calculates the value of Z

$$Z = \frac{1 - \rho Y}{1 + \rho} \quad (32)$$

The fact that arbitrary units are used for the height h of the sample peaks, from which the diffusion band is constructed,

Table I. Lengths and Volumes in the Cell Used To Obtain the Diffusion Bands, Together with the Values of the Diffusion Parameter $\beta = \pi^2 D_G/L_1^2$ for Ethene at 295.2 K (β_1) or Propene at 323.9 (β_2)

cell no.	L_1/cm	L_2/cm	V_G/cm^3	V_G'/cm^3	V_L/cm^3	$10^4\beta_1/\text{s}^{-1}$	$10^4\beta_2/\text{s}^{-1}$
1	43.7	13.5	7.90	2.37	32.00	8.5979	8.1280
2	94.2	13.5	17.26	2.37	32.00		1.5987
3	84.7	21.7	15.85	1.56	48.75		1.7059 ^a
4	54.7	13.5	9.95	1.10	30.85	5.1824	
5	54.7	6.76	9.95	1.10	16.97	5.1824	
6	43.7	4.18	7.91	3.01	10.28	8.5979	
7	43.7	6.76	7.91	1.10	16.97	8.5979	
8	43.7	3.83	7.91	22.56	9.40	8.5979	

^a At 298 K.**Table II. Exponential Coefficients and Preexponential Factors of Equation 28, Calculated from the Diffusion Bands Obtained with Two Gases and Three Liquids, Using the Cells of Table I**

expt	cell	$10^6[(X - Y)/2]/\text{s}^{-1}$	$10^4[(X + Y)/2]/\text{s}^{-1}$	$\ln [N_G(1 - Z/Y)]$	$\ln [N_G(1 + Z/Y)]$
Gas/Liquid System: Propene/Hexadecane at $T = 323.9$ K					
4	1	1.3829	6.1473	7.77291	13.55725
10	1	1.2371	5.1018	7.91231	12.28082
14	2	1.1963	1.8867	7.61077	10.28745
17 ^a	3	0.6021	1.5723	6.93908	10.40671
Gas/Liquid System: Ethene/Heptane at $T = 295.2$ K					
9	1	0.9076	6.5919	7.83946	10.63950
41	4	0.8027	3.3742	6.72342	10.59356
43	5	1.6792	4.1910	6.57070	9.11779
45	6	3.3258	5.3798	6.95760	8.69417
46	7	2.2633	4.5830	6.22208	8.98232
Gas/Liquid System: Ethene/Water at $T = 294.2$ K					
49	8	3.3734	6.0987		
51	8	3.8820	7.8125		

^a The temperature in this experiment was 296.4 K.

does not influence the value of Z , since it is calculated from the ratio ρ of two intercepts pertaining to the same substance and the same experiment, so that any unknown proportionality factors cancel out.

Equation 32 combined with eq 29 gives the value of α as

$$\alpha = \frac{1}{50} \left(X - \frac{1 - \rho}{1 + \rho} Y \right) \quad (33)$$

Table III. Diffusion Coefficients (D_L) of Two Gases into Three Liquids, Partition Coefficients (K), and Henry's Law Constants (H^*) for the Distribution of Each Gas between the Liquid and the Carrier Gas, Calculated in the First Way and the Second Way (See Theory Section)

expt	cell no. ^a	$10^6 D_L/\text{cm}^2 \text{s}^{-1}$		K		H^*/atm	
		1st Way	2nd Way	1st Way	2nd Way	1st Way	2nd Way
Gas/Liquid System: Propene/Hexadecane at $T = 323.9$ K							
4	1	5.58	4.63	40.8	21.7	2.23	4.19
10	1	4.90	5.50	36.4	42.7	2.49	2.13
14	2	4.98	6.89	23.1	27.0	3.92	3.36
Mean value ^b \pm S.E.:			5.41 \pm 0.33		31.9 \pm 3.7		3.05 \pm 0.36
17 ^c	3	6.19	8.09	20.5	25.9	4.43	3.51
Gas/Liquid System: Ethene/Heptane at $T = 295.2$ K							
41	4	3.04	4.36	31.0	44.0	5.34	3.75
43	5	1.65	3.41	35.4	41.3	4.67	4.00
45	6	1.30	3.08	49.8	46.4	3.32	3.56
46	7	2.12	3.60	21.2	30.6	7.78	5.40
Mean value ^b \pm S.E.:			2.82 \pm 0.37		37.5 \pm 3.4		4.73 \pm 0.52
Gas/Liquid System: Ethene/Water at $T = 294.2$ K							
49	8	1.21	-	306	-	4.38	-
51	8	1.40	-	345	-	3.89	-

^a See Table I. ^b These, together with their standard errors (S.E.), are calculated from the results obtained for each parameter in both ways, at the same temperature. ^c The temperature in this experiment was 296.4 K.

from which D_L is found, since $\alpha = \pi^2 D_L/4L_2^2$.

The value of K can now be calculated without using the value of the diffusion parameter β , by solving eq 26 for β and substituting it in eq 27. The result is

$$K = \frac{X - 25\alpha - \prod/25\alpha}{24\alpha V_L/V_G} \pi^2 (1 + 3V_G'/V_G) \quad (34)$$

EXPERIMENTAL SECTION

Chemicals. The gases used (ethene, propene) were obtained from Matheson Gas Products. Hexadecane and heptane were Fluka "purum" products.

The carrier gas was nitrogen of 99.99% purity from Linde (Athens, Greece).

Apparatus. The experimental setup is schematically outlined in Figure 2. It was basically that described elsewhere (4) except for the following. A six-port valve was used, with two alternate ports connected by means of a short $1/16$ -in. tube, as shown in the figure. The sections l , l' , and L_1 of the sampling cell were stainless steel $1/4$ -in. tubes with lengths $l = l' = 60$ cm and $L_1 = 43.7$ – 94.2 cm. The liquids were placed in a glass vessel of 17.5 mm i.d. at its lower part and of 4 mm i.d. at its upper part, which was connected to the stainless steel column L_1 with a $1/4$ -in. Swagelok union. The gaseous volume between the liquid's surface and column z was 1.10– 3.01 cm³.

The gas volume V_G in column V_1 was 7.90– 17.26 cm³. These volumes were measured by filling the columns with water at a certain temperature, weighing them, and using the density of the water at that temperature. All geometrical characteristics of the cells used in the experiments are given in Table I.

With heptane as liquid, an additional separation column was used (50×4 mm i.d., filled by Porapak S 50/80 mesh). The pressure drop along this column was 57 cmHg.

Procedure. After the injection of 1 cm³ of each gas at atmospheric pressure and the wait for the monotonously rising concentration-time curve to appear in the detector signal, the chromatographic sampling procedure was started by reversing the direction of the carrier gas flow for 15 s, which is a shorter time period than the gas hold-up time in both column sections l and l' . Examples of sample peaks created by the flow reversals have already been given in Figure 1. First, the diffusion coefficient of the two gases into the carrier gas was determined, by using an empty glass vessel. Then, by using the glass vessel filled with a liquid, the diffusion and the partition coefficients of the two gases into the liquid were estimated.

In all experiments, the pressure drop along $l + l'$ was negligible. It is estimated as less than 1 mmHg.

The carrier gas flow rate (corrected at column temperature and for pressure drop) ranged from 0.321 to 0.370 cm³ s⁻¹.

RESULTS AND DISCUSSION

The equations derived in the theory section were applied by conducting experiments with three liquids, namely, hexadecane, heptane, and water, and two gases, namely, propene and ethene. The diffusion parameters β of eq 20 are given in Table I for all cells. The exponential coefficients $(X + Y)/2$ and $(X - Y)/2$ (equal to -slopes) of the $\ln h$ vs t_0 plots, and the logarithms of the respective preexponential factors $\ln [N_2(1 + Z/Y)]$ and $\ln [N_2(1 - Z/Y)]$, all obtained experimentally, are listed in Table II. From the data of Tables I and II, the diffusion coefficients of the gases into the liquids, the partition coefficients, and the Henry's law constants, all calculated in the "first way" and the "second way", as previously described in the theory section, are listed in Table III. The roots for α of eq 31, when substituted into eq 26 or 27 to find K , give a negative and a positive value for the partition coefficient. Since negative values of K are physically meaningless, only the positive values and the D_L values corresponding to those are listed in Table III. The Henry's law constants $H^i = p/x$, where p is the partial pressure of the solute in the gas phase and x its mole fraction in the liquid, were calculated by using the approximation

$$H^i = \frac{p}{x} \approx \frac{c_2(L_1)RT}{c_2(0)M_L/d} = \frac{RTd}{KM_L} \quad (35)$$

where d is the density of the liquid, M_L its molar mass, and K is substituted from eq 13. The temperature in the experiments was as indicated in Table III. The number of significant figures in the tables is based on their standard errors as calculated from regression analysis. It is difficult to estimate the final error of the diffusion and the partition coefficients, since they come out as a result of a complex series of calculations, as was described in the theory section.

The dispersion of the diffusion coefficient values around their mean value is not big, given that the experiments were conducted under widely varying conditions as regards the lengths L_1 and L_2 of the cell, and the volume of the liquid V_L . The same applies to the partition coefficients K and the Henry's law constants H^i . It must be pointed out that there are not significant differences between the values found by using two completely different ways of calculation, which are based on different experimental data, namely, the "first way" on the diffusion parameter β , and the "second way" on the preexponential factors of eq 28, as found from the intercepts of linear plots. This indicates the internal consistency of the theory.

The diffusion coefficients found by the present method seem to be of the correct order of magnitude, as shown by comparing their values with those calculated using the Wilke-Chang formula (39). The values for the system ethene/water compare well with those reported by others (40).

The Henry's law constants H^i , calculated from a nomogram (41), are 37 and 15.5 atm for ethene at 295.2 K and propene

at 323.9 K, respectively. These values are bigger than the mean values found in the present work. This obviously reflects the high values of the partition coefficient K determined here, which for the system propene/hexadecane are an order of magnitude bigger than those found previously (27) at similar temperatures, using the same general technique but with an agitated liquid. A possible explanation of this difference is found by considering the definition of K , which in ref 27 represents the ratio $C_L^*/C_2(L_1)$ of the bulk liquid concentration of solute to that in the gas phase, while here with a quiescent liquid it gives the ratio $c_2(0)/c_2(L_1)$ of the liquid concentration of the solute at $y = 0$, i.e., at the interphase, to that in the gas phase. If this explanation is correct, the method of finding K described here can be used to calculate concentrations near the liquid-gas interphase. In other words, K is not an ordinary distribution coefficient of a solute between a gas and a liquid, but a coefficient probably pertaining to the interphase layers of the liquid and the gas. This is expected to be more pronounced for the partition of a hydrocarbon in a gas/water interphase, and this is actually borne out by the big values of K in the system ethene/water.

Registry No. Ethene, 74-85-1; propene, 115-07-1; hexadecane, 544-76-3; heptane, 142-82-5; water, 7732-18-5; nitrogen, 7727-37-9.

LITERATURE CITED

- Katsanos, N. A.; Georgiadou, I. *J. Chem. Soc., Chem. Commun.* **1980**, 242-243.
- Katsanos, N. A.; Karaiskakis, G. *Adv. Chromatogr.* **1984**, *24*, 125-180.
- Katsanos, N. A.; Karaiskakis, G. *Analyst* **1987**, *112*, 809-813.
- Katsanos, N. A. *J. Chromatogr.* **1988**, *446*, 39-53.
- Katsanos, N. A. *Flow Perturbation Gas Chromatography*; Dekker: New York, 1988.
- Katsanos, N. A. *J. Chem. Soc., Faraday Trans. 1* **1982**, *78*, 1051-1063.
- Karaiskakis, G.; Katsanos, N. A.; Georgiadou, I.; Lycourghiotis, A. *J. Chem. Soc., Faraday Trans. 1* **1982**, *78*, 2017-2022.
- Kotiniopoulos, M.; Karaiskakis, G.; Katsanos, N. A. *J. Chem. Soc., Faraday Trans. 1* **1982**, *78*, 3379-3382.
- Karaiskakis, G.; Katsanos, N. A. *Proceedings of the 3rd Mediterranean Congress on Chemical Engineering*; Feria de Barcelona: Barcelona, Spain, 1984; p 68.
- Katsanos, N. A.; Kotiniopoulos, M. *J. Chem. Soc., Faraday Trans. 1* **1985**, *81*, 951-959.
- Ioffe, B. V.; Katsanos, N. A.; Kokovina, L. A.; Marinitsev, A. N.; Stolyarov, B. V. *Kinet. Katal.* **1987**, *28*, 805-810.
- Karaiskakis, G.; Katsanos, N. A.; Lycourghiotis, A. *Can. J. Chem.* **1983**, *61*, 1853-1857.
- Dalass, E.; Karaiskakis, G.; Katsanos, N. A.; Gounaris, A. *J. Chromatogr.* **1985**, *348*, 339-346.
- Katsanos, N. A.; Karaiskakis, G.; Niotis, A. *Proceedings of the 8th International Congress on Catalysis*; Dechema Verlag-Chemie: West Berlin, 1984; Vol. 11, pp 143-154.
- Dalass, E.; Katsanos, N. A.; Karaiskakis, G. *J. Chem. Soc., Faraday Trans. 1* **1986**, *82*, 2897-2909.
- Katsanos, N. A.; Karaiskakis, G.; Niotis, A. *J. Catal.* **1985**, *94*, 376-384.
- Katsanos, N. A.; Karaiskakis, G. *J. Chromatogr.* **1982**, *237*, 1-14.
- Katsanos, N. A.; Karaiskakis, G. *J. Chromatogr.* **1983**, *254*, 15-25.
- Karaiskakis, G.; Katsanos, N. A.; Niotis, A. *Chromatographia* **1983**, *17*, 310-312.
- Karaiskakis, G.; Niotis, A.; Katsanos, N. A. *J. Chromatogr. Sci.* **1984**, *22*, 555-558.
- Karaiskakis, G. *J. Chromatogr. Sci.* **1985**, *23*, 360-363.
- Karaiskakis, G.; Katsanos, N. A.; Niotis, A. *J. Chromatogr.* **1982**, *245*, 21-29.
- Karaiskakis, G.; Lycourghiotis, A.; Katsanos, N. A. *Chromatographia* **1982**, *15*, 351-354.
- Karaiskakis, G.; Katsanos, N. A. *J. Phys. Chem.* **1984**, *88*, 3674-3678.
- Katsanos, N. A.; Karaiskakis, G. *J. Chromatogr.* **1987**, *395*, 423-435.
- Karaiskakis, G.; Agathonos, P.; Niotis, A.; Katsanos, N. A. *J. Chromatogr.* **1986**, *364*, 79-85.
- Katsanos, N. A.; Dalass, E. *J. Phys. Chem.* **1987**, *91*, 3103-3108.
- Katsanos, N. A.; Agathonos, P.; Niotis, A. *J. Phys. Chem.* **1988**, *92*, 1645-1650.
- Katsanos, N. A. *Catal. Today* **1988**, *2*, 605-612.
- Kapalos, J.; Katsanos, N. A.; Niotis, A. *Chromatographia* **1989**, *27*, 333-339.
- Katsanos, N. A.; Karaiskakis, G.; Agathonos, P. *J. Chromatogr.* **1986**, *349*, 369-376.
- Agathonos, P.; Karaiskakis, G. *Chromatographia* **1988**, *25*, 453-454.
- Agathonos, P.; Karaiskakis, G. *J. Chem. Soc., Faraday Trans. 1*, in press.
- Niotis, A.; Katsanos, N. A.; Karaiskakis, G.; Kotiniopoulos, M. *Chromatographia* **1987**, *23*, 447-448.

- (35) Agathonos, P.; Karaiskakis, G. *J. Appl. Polym. Sci.* **1989**, *37*, 2237-2250.
- (36) Kolladima, A.; Agathonos, P.; Karaiskakis, G. *Chromatographia* **1988**, *28*, 29-33.
- (37) Katsanos, N. A.; Vassilikos, Ch. *J. Chromatogr.* **1989**, *471*, 123-137.
- (38) Oberhettinger, F.; Badli, L. *Tables of Laplace Transforms*; Springer-Verlag: Berlin, 1973.
- (39) Danckwerts, P. V. *Gas-Liquid Reactions*; McGraw-Hill: New York, 1970; p 15.
- (40) Huq, A.; Wood, T. *J. Chem. Eng. Data* **1968**, *13*, 256-259.
- (41) Blackadder, D. A.; Nedderman, R. M. *A Handbook of Unit Operations*; Academic: New York, 1971; p 145.

RECEIVED for review November 14, 1988. Resubmitted April 28, 1989. Accepted July 3, 1989. The authors thank Professor A. Jannussis for his help in certain mathematical manipulations and for stimulating discussions. They also thank Mrs. M. Barkoula for technical assistance.

Determination of Trace Impurities in High-Purity Oxygen by Gas Chromatography with Photoionization Detection

Hiroshi Ogino,* Yoko Aomura, Masatsugu Komuro, and Tetsu Kobayashi

Technical Research Laboratory, Toyo Sanso Co., Ltd., 3-3, Mizue-cho, Kawasaki-ku, Kawasaki-shi, Kanagawa 210, Japan

A gas chromatographic system used for the analysis of trace impurities in high-purity oxygen (99.99-99.9999% (v/v)) is described. This system consists of a gas chromatograph equipped with a photoionization detector (PID), a gas sampler, a precolumn filled with a catalyst, and a computerized integrator with an interface. The analytical reproducibilities (relative standard deviation, $n = 15$) for Ar (0.50 ppm), N₂ (0.10 ppm), Kr (4.0 ppm), CH₄ (6.0 ppm), and Xe (0.30 ppm) were 1.7%, 4.8%, 0.5%, 0.6%, and 4.2%, respectively. The detection limits were as follows: Ar, 0.03 ppm; N₂, 0.04 ppm; Kr, 0.01 ppm; CH₄, 0.01 ppm; and Xe, 0.01 ppm. These limits are in a practical concentration range (sub parts per million to several tens of parts per million) in high-purity oxygen.

INTRODUCTION

Recently, the purity of oxygen used in certain semiconductor manufacturing processes is becoming more important. Gas analysis in the sub-parts-per-million range plays an increasing role in these industries. Several papers have been published on the analytical method for the determination of impurities, such as Ar and N₂, in oxygen by gas chromatography (1, 2). In these methods, a gas chromatograph equipped with a thermal conductivity detector (TCD) was used to determine any inorganic gases. However, their sensitivity is not sufficient to determine accurately such impurities at less than parts per million levels. It is hard to achieve a good separation of Ne, Ar, N₂, Kr, and Xe in a large volume of oxygen with a molecular sieve (5A or 13X) column, even if the column is operated at low temperature (e.g., -72 °C) (3). Also, the filaments of the TCD could be irreversibly damaged or interfered with by the huge amount of oxygen. Therefore, when a TCD for trace determination of inorganic gases is used, a preconcentration technique and the elimination of oxygen should be required. There are many problems, such as recovery of trace components and so on, inherently associated with the preconcentration technique. The latter was applied, consequently, to determine accurately trace impurities in high-purity oxygen.

Fortunately, a photoionization detector (PID) with a high sensitivity for inorganic gases, which is based on the emission

from a direct current discharge in helium gas, is commercially available (4, 5).

There have been no published reports on the determination method of a series of impurities of less than 1 ppm in high-purity oxygen by gas chromatography. To determine the concentration of such impurities in high-purity oxygen would be important and interesting for semiconductor industries.

This paper describes a simple and accurate gas chromatographic system for the determination of trace levels of impurities, such as argon, nitrogen, krypton, methane, and xenon, in high-purity oxygen.

EXPERIMENTAL SECTION

Apparatus and Materials. A diagram of the equipment setup for this experiment is shown in Figure 1. The experimental apparatus basically consists of a gas sampler, precolumn (oxygen adsorber), and gas chromatograph (Hitachi, GC-263-30, Tokyo, Japan) equipped with a PID. This system, including the gas sampler, can be programmed with a computerized integrator (Shimadzu, C-R4A, Kyoto, Japan) through an interface (Shimadzu, PRG-102A) and is able to analyze and automatically report its results every 20 min. Analytical results are computed by an absolute calibration method from the peak areas. Operating conditions of the GC and detectors used in this experiment are listed in Table I.

To remove oxygen as the major component from a sample gas, a precolumn was installed between the gas sampler and analytical column. The precolumn was a 1.5 m × 3 mm i.d. stainless steel tube and was filled with a copper-based catalyst Nikki Chemical, N-211, 30/80 mesh, Tokyo, Japan). This catalyst was selected after several catalysts were evaluated as to whether they could absorb all the oxygen in the sample gas and whether the catalyst could be regenerated easily and repeatedly. The precolumn was heated and controlled with a temperature control unit (Yokogawa, UT-10, Tokyo, Japan). High-purity helium (Toyo Sanso, [A] grade, 99.9999%) was employed without further purification as the carrier and discharge gas. In an attempt to evaluate and demonstrate the performance of this system, several oxygen gases of various purity levels, obtained from different manufacturers, were analyzed. Most of the experiments were conducted with reference gas mixtures having the following composition: 11 ppm each of Ar and N₂ in He and 9.7, 140, and 1400 ppm each of Ne, Ar, Kr, and Xe in He. All reference gases were prepared by the gravimetric method. Mass flow controllers (STEC, MS-400, Kyoto, Japan) were used to prepare the low-concentration samples in oxygen gas from their reference gases and high-purity oxygen if necessary.

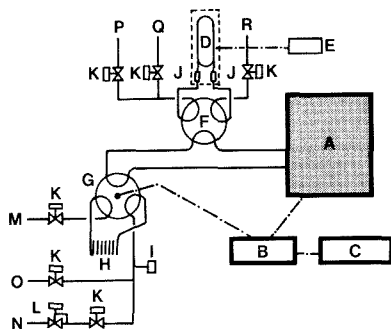
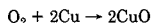


Figure 1. Schematic diagram of apparatus for determination of impurities in high-purity oxygen: A, GC; B, interface; C, integrator; D, precolumn (catalyst); E, heating controller; F, manually operated six-port rotary valve; G, air-actuated six-port rotary valve; H, sample loop; I, pressure transducer; J, line filter; K, stop valve; L, back-pressure control valve; M, sample inlet; N, sample gas outlet; O, vacuum pump for line purge; P, hydrogen gas inlet; Q, helium gas inlet; R, H₂ (or He) outlet.

Activation of the Precolumn. The oxygen elimination of the precolumn is based on the following reaction:



Also, the precolumn is regenerated with hydrogen via the following reaction:



First, valve F was manually switched to the activation position (as shown in Figure 1) and then high-purity hydrogen (Toyo Sanso, [A] grade, 99.9999% (v/v)) gas was passed through at ca. 150 mL/min to purge any air remaining in the precolumn. The precolumn temperature was then raised and held at 100 °C for 30 min. Finally, the temperature was raised to 140 °C and held with hydrogen flowing for 60 min. After the activation, the precolumn was purged with high-purity helium through inlet Q of Figure 1. Valve F was switched back to the analytical position. The activated precolumn was then connected in series with the GC.

RESULTS AND DISCUSSION

Characteristics of the Catalyst. The capacity of oxygen adsorption of the catalyst is strongly dependent on the heating temperature. Its capacity at room temperature was too small. Therefore, it was necessary to heat the precolumn at a constant temperature. However, the high temperature of over ca. 200 °C was unsuitable for the determination of hydrocarbons such as methane because such compounds could be decomposed on the catalyst. Considering the capacity of the oxygen adsorption and the thermal stability of methane with the catalyst, the temperature of the precolumn was maintained at 140 ± 2 °C. At this temperature, there was no evidence supporting any decomposition of methane. To confirm this point, the same oxygen gas was analyzed independently by the use of a Fourier transform infrared spectrophotometer (JEOL, JIR-3510, Tokyo, Japan) equipped with a 10 m optical path length gas cell. The analytical result for methane obtained by the present method was compared with that of the FT-IR. There was only a negligible difference, within experimental error, between the present and FT-IR methods: 0.90 ± 0.01 ppm for GC-PID and 0.85 ± 0.05 ppm for FT-IR.

In order to determine the capacity of oxygen adsorption, 3.7 mL of oxygen was repeatedly injected into the GC using the automatic gas sampler. The injected oxygen was carried to the precolumn by the carrier gas and was completely eliminated with the catalyst in the precolumn. The residual gases were then separated with an analytical column and

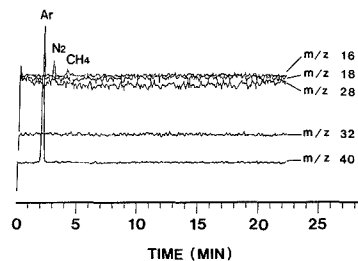


Figure 2. GC-MS selected ion profiles for residual gases passed through the precolumn. GC-MS operating conditions: column, MS-5A, 60/80 mesh, 3 m × 3 mm i.d. stainless steel tube; carrier gas (He), 30 mL/min; sample size, 5.38 mL; oven temperature, 100 °C; GC-MS transfer line temperature, 150 °C; ion source temperature, 200 °C; filament current, 3.20 mA; electron energy, 70 eV; gain, 2.0.

Table I. Operating Conditions of the GC, PID, and TCD

GC	
analytical column	MS-5A, 60/80 mesh, 3 m × 3 mm i.d. stainless steel tube
reference column ^a	MS-5A, 60/80 mesh, 3 m × 3 mm i.d. stainless steel tube
column temp	50 °C
carrier gas	He, 48 mL/min
PID	
discharge gas	He, 37 mL/min
PID temp	100 °C
applied potential	750 V
discharge current	150 μA
sample loop	1.70 mL
TCD	
current	180 mA
detector temp	100 °C
sample loop	4.47 mL

^a Installed for TCD.

detected with the PID. The precolumn (1.5 m × 3 mm i.d. stainless steel tube), which contained ca. 12 g of catalyst, could adsorb ca. 250–280 mL of oxygen at 140 °C even after several regenerations. This means that if a sample loop of 2 mL was used, analyses of more than 100 runs can be done without any additional regenerations of the catalyst.

The GC-MS (Shimadzu, QP-300) analysis of the residual gases was undertaken to confirm the adsorption efficiency of oxygen with the precolumn. The result showed that the selected ion monitoring profile, 32 *m/z* for oxygen, did not show any profile for the presence of oxygen, as shown in Figure 2. The oxygen, that is, could be preferentially and completely eliminated with the catalyst in the precolumn, which was operated under the proposed conditions described below. The activation and regeneration were performed by a method identical with that previously described.

Optimum Conditions of PID. The sensitivity of the PID is known to be dependent on the flow rate of helium as a discharge gas, the applied potential of discharge, the temperature of the detector, the purity of helium, and so on (4, 5). In order to confirm these effects and determine the optimum conditions of PID, a series of experiments were conducted using a reference gas having 11 ppm each of Ar and N₂ to He. The operating conditions of the GC are given in Table I.

Figure 3 shows the relation between the PID response and the flow rate of helium as the discharge gas. The response decreased almost exponentially with increasing flow rate of helium gas in the range examined in this experiment. The following experiments were carried out at ca. 40 mL/min,

Table II. Analytical Results of Determination of Impurities in Oxygen Gases with Different Purity Levels

sample	purity ^a	impurities, ppm				
		Ar	N ₂	Kr	CH ₄	Xe
A	99.9%	425 ^b	9.58 ± 0.89	10.32 ± 0.04	1.14 ± 0.13	nd ^c
B	99.99%	1.88 ± 0.03	0.24 ± 0.02	16.17 ± 0.04	24.66 ± 0.04	1.22 ± 0.01
C	99.995%	0.52 ± 0.01	20.61 ± 0.20	<0.01	0.05 ± 0.01	nd
D ^d	99.9995%	0.53 ± 0.01	0.24 ± 0.02	<0.01	0.08 ± 0.01	nd

^aGuaranteed purity. ^bObtained by GC-TCD. ^cNot detected (<0.01 ppm). ^dHigh-purity oxygen (TOYO SANSO, GO-55).

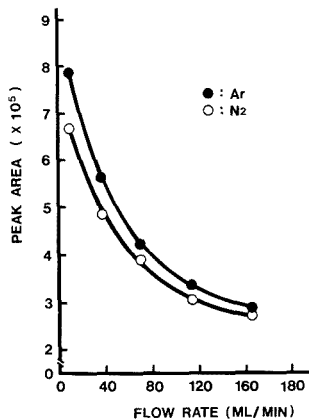


Figure 3. Effect of flow rate of discharge gas on the PID response. Other conditions are given in Table I.

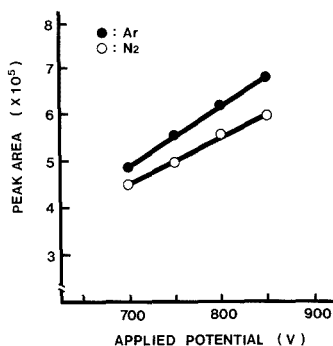


Figure 4. Effect of the applied potential of discharge on the PID response. Other conditions are given in Table I.

taking into account the sensitivity of the detector and the capability of the flow controller.

It is interesting to note that the response profile of the PID vs the flow rate, as reported in the literature (4), has a maximum value, but it did not in the present study.

Figure 4 shows the relation between the PID response and the applied potential of the discharge. The response for both components increased linearly as the discharge potential was increased. Figure 5 shows the relation between the PID response and the detector temperature. The response decreased linearly with increasing temperature. In these experiments, the detector temperature was controlled at 100 °C, which was sufficiently high to protect against any condensation of gases on the inside wall of the detector. According to the preliminary examined results, the optimum conditions of the PID were determined as shown in Table I.

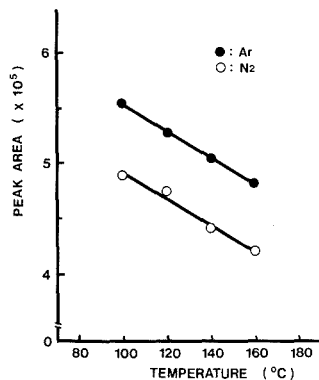


Figure 5. Effect of the detector block temperature on the PID response. Other conditions are given in Table I.

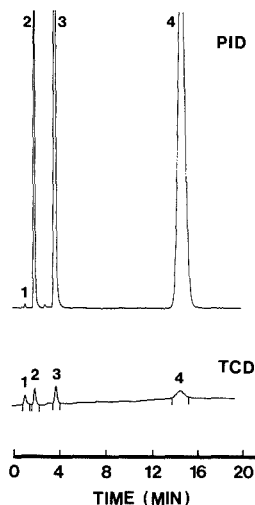


Figure 6. Typical gas chromatograms obtained with the PID and TCD: 1, Ne; 2, Ar; 3, Kr; 4, Xe. Both operating conditions are given in Table I.

Chromatogram and Quantitative Features. Typical gas chromatograms of the reference gas obtained with the PID and a TCD are shown in Figure 6. Both chromatograms clearly showed that the PID has a higher sensitivity than that of the TCD, except for neon, and is suitable for detecting trace impurities in high-purity oxygen.

The calibration curves were linear up to 200 ppm under the proposed conditions, and their linear ranges were dependent on the nature of the individual components. The relative

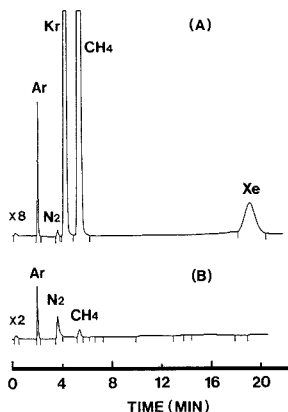


Figure 7. Typical gas chromatograms from practical purity oxygen gas stored in a cylinder: A, 99.99% oxygen; B, 99.9995% oxygen (GO-55). Operating conditions are given in Table I.

sensitivities ($A_r = 100$) were calculated from the calibration curves obtained in the range 0–10 ppm: 1, 73, 229, 247, and 355 for Ne, N_2 , CH_4 , Kr, and Xe, respectively. The quantitative performance of the system was conducted by repeated injections of 1.7 mL of an oxygen gas containing Ar (0.50 ppm), N_2 (0.10 ppm), Kr (4.0 ppm), CH_4 (6.0 ppm), and Xe (0.30 ppm). The results indicated that the reproducibilities (relative standard deviation, $n = 15$) were 1.7%, 4.8%, 0.5%, 0.6%, and

4.2% for Ar, N_2 , Kr, CH_4 , and Xe, respectively. The detection limits, which were calculated from the minimum peak areas of the integrator detection, were 2.0, 0.03, 0.04, 0.01, 0.01, and 0.01 ppm for Ne, Ar, N_2 , Kr, CH_4 , and Xe, respectively; the detection limit of neon was obtained from a reference gas containing 9.7 ppm Ne in He. Typical gas chromatograms and analytical results for several commercially available cylinder oxygen gases, with different purity levels, are given in Figure 7 and Table II. It is interesting that the profiles of the impurity distributions in samples showed considerable variation. Thus, analytical results suggest that the impurity distributions might apparently be due to the different manufacturing processes for oxygen. It is more important that we pay attention not only to Ar and N_2 but also to other gases and the distribution of concentrations of each impurity in order to evaluate the impurity of oxygen.

ACKNOWLEDGMENT

We thank T. Suzuki for his technical assistance and S. Iida for his useful help.

Registry No. Ar, 7440-37-1; N_2 , 7727-37-9; Kr, 7439-90-9; CH_4 , 74-82-8; Xe, 7440-63-3; O_2 , 7782-44-7.

LITERATURE CITED

- (1) Verzele, M.; Verstappe, M.; Sandra, P. *J. Chromatogr.* **1981**, *209*, 455-457.
- (2) Karlsson, B. M. *Chromatographia* **1975**, *8*, 155.
- (3) Lard, E. W.; Horn, R. C. *Anal. Chem.* **1960**, *32*, 878, 879.
- (4) Yamane, M. *J. Chromatogr.* **1964**, *14*, 355-367.
- (5) Kawazue, K.; Kamo, T.; Takata, Y.; Shikama, N. *Bunseki Kagaku* **1985**, *34*, 309-313.

RECEIVED for review July 14, 1989. Accepted July 14, 1989.

Conditions for Detecting Overlapped Peaks with Principal Component Analysis in Hyphenated Chromatographic Methods

Paul J. Gemperline*

Department of Chemistry, East Carolina University, Greenville, North Carolina 27858

J. Craig Hamilton

Shared Research Resource Laboratories, School of Medicine, East Carolina University, Greenville, North Carolina 27858

The purpose of this paper is to describe the effect of spectral similarity and chromatographic resolution on the limit of detection for severely overlapped peaks using principal component analysis of data from hyphenated chromatographic techniques. A method is reported here for estimating the net signal due to minor components when overlapped with major components. The effects of relative concentration, spectral similarity, and chromatographic resolution are each considered independently. Simulated and real data are analyzed to illustrate the method.

INTRODUCTION

Many hyphenated chromatographic methods exist which can rapidly measure the spectra of chemical components

eluting from chromatographic columns, the most common being gas chromatography/mass spectrometry (GC/MS), gas chromatography/infrared spectroscopy (GC/IR), and high-performance liquid chromatography/ultraviolet spectroscopy (HPLC/UV). Recently, a significant amount of research has been conducted using principal component analysis of data matrices produced by these techniques (1-10). Most workers in the field have focused on the mathematical resolution of overlapped peaks. Another equally important aspect is the determination of the number of spectrally unique components present in an overlapped peak. The number of spectrally unique components is usually determined by the number of statistically significant principal components present. McCue and Malinowski (2) used criteria developed by Malinowski (11, 12) to determine the number of spectrally unique components present in the ultraviolet spectra of unresolved liquid chromatographic fractions. Since then, refinements and additional techniques have been reported for determining the

* Author to whom correspondence should be sent.

number of significant principal components in data matrices (13-16).

Under certain circumstances, too few components may be detected in an overlapped peak. Consider a minor component, Y, overlapped with a major component, X. If the concentration of Y is reduced while the concentration of X remains constant, errors will occur when the net signal due to Y drops below some threshold value determined by experimental error. This paper reports a technique for estimating the net signal due to a minor component when overlapped with a major component in cases such as these. Although the estimates of the net signal are only accurate within 1 order of magnitude, there are two important benefits to be derived from its application. First, the technique clearly illustrates how chromatographic resolution, spectral similarity, and relative concentration ratios affect the magnitude of the eigenvalues produced during the decomposition of a data matrix. Secondly, the net analytical signal can be estimated over a wide range of different degrees chromatographic resolution without extensive experimentation. This knowledge, coupled with a knowledge of experimental error, can be used to judge whether or not a minor component will be detectable.

THEORY

The degree of chromatographic resolution between two overlapped components, X and Y, the similarity between the UV spectra of X and Y, the concentration of X and Y, and the signal to noise ratio all work in concert to determine the net signal of both components. When standards are available, it is a simple matter to experimentally determine the limit of detection of Y when overlapped with X by holding the chromatographic resolution constant, holding the concentration of the major component, X, constant, and varying the concentration of Y. In this case, the concentration of Y is reduced until the second eigenvalue from the decomposition of the data matrix becomes so small that Y is no longer detectable.

In the absence of standards, it is only possible to estimate the limit of detection of a minor component, Y, when overlapped with X. In a series of simulated studies, the relationship shown in eq 1 has been discovered that can be used to estimate the net signal of component Y to within an order of magnitude when overlapped with X. Equation 1 takes into

$$\lambda_2 = h^2 \beta_1 \beta_2 \lambda^* + \lambda_2^\circ \quad (1)$$

account the effect of chromatographic resolution, peak height, spectral similarity, and experimental error on the magnitude of the net signal. The term, λ_2 , in eq 1 is defined as the net signal for the minor component Y when overlapped with X. It is an estimate of the second eigenvalue obtained from the principal component decomposition of the covariance matrix, $Z = A'A$, where A is the matrix whose rows are spectra taken at equally spaced intervals during the elution of the two overlapped components. The term, λ^* is the signal obtained for component Y when it is not overlapped at all. Its value is estimated from the first eigenvalue obtained from the principal component analysis of the data acquired during the elution of a single pure peak of component Y. The term, λ_2° , is the contribution of experimental error to λ_2 , represented by the second error eigenvalue. It is the value of the second eigenvalue one would expect in the absence of a second component. The presence of a second component will be detected when the actual value of λ_2 is significantly larger (about 3 to 4 times larger) than λ_2° . This threshold level has been observed to work well in this application. False detection of the minor component has been occasionally observed for threshold levels lower than the above level. The false positive results were probably due to shifting base lines. The above criterion is only used to judge the detection limit of overlapped compo-

nents. Other methods such as Malinowski's RE criterion (11) or Malinowski's F test (16) should be used to determine the number of components in experimental data matrices.

The term h in eq 1 is the height of the elution profile of Y relative to X. The elution profiles are the vectors, h_x and h_y . The absorbance matrices of the pure components can be expressed as the outer vector product of the elution profiles with the corresponding molar absorptivity vectors normalized to unit area, v_x and v_y

$$A_{\text{total}} = A_x + A_y = h_x v'_x + h_y v'_y \quad (2)$$

The height ratio is related to the concentration ratio of X and Y according to

$$h = \frac{c_x \|v_x\|}{c_y \|v_y\|} \quad (3)$$

where $\|v_x\|$ is the Euclidian norm of the corresponding unnormalized vector v_x

$$\|v_x\| = (v'_x v_x)^{1/2} \quad (4)$$

Note that when X and Y have highly similar spectra and molar absorptivities the ratio $\|v_x\|/\|v_y\|$ is approximately equal to one.

The term β_1 in eq 1 represents the fraction of λ^* remaining when Y is overlapped with X at a specific chromatographic resolution and peak height ratio. The term, β_2 represents the fractional reduction of λ^* as a function of the similarity between the UV spectra of X and Y.

Two methods for estimating the expected error eigenvalue may be used. The first makes use of the reduced eigenvalues, REV, proposed by Malinowski in 1987 (15). The reduced eigenvalues of the error eigenvalues, REV° , are constant and may be predicted according to

$$REV^\circ = l\sigma^2 \quad (5)$$

where

$$l = r(c-n) / \sum_{j=n+1}^c (r-j+1)(c-j+1) \quad (6)$$

According to eq 5 and 6, the expected values of the reduced eigenvalues depend only on the experimental error, σ , and the degrees of freedom. The experimental eigenvalues are related to the reduced eigenvalues according to

$$REV_j = \lambda_j / (r-j+1)(c-j+1) \quad (7)$$

Any eigenvalue, λ_j , that is not an error eigenvalue will have REV_j values significantly larger than those predicted by eq 5. In the absence of two components, the expected value of the error eigenvalue, λ_2° , can be estimated from eq 5 and 6 by using $j=2$ and prior knowledge of the experimental error, σ

$$\lambda_j^\circ = (r-j+1)(c-j+1)l\sigma^2 \quad (8)$$

A second method for estimating the expected error eigenvalue is to use values of λ_3 from actual two-component data matrices, where λ_3 is assumed to be an error eigenvalue. An estimate of the second error eigenvalue can be obtained by making an adjustment to λ_3 to account for the difference in the number of degrees of freedom according to eq 9 with $j=2$.

$$\lambda_j^\circ = REV_{j+1} (r-j+1)(c-j+1) \quad (9)$$

The fraction of λ^* remaining after considering chromatographic overlap, β_1 , is calculated according to

$$\beta_1 = \lambda_2 / h'_y h_y \quad (10)$$

where λ_2 is the second eigenvalue obtained from the decomposition of the matrix containing the two vectors h_x and h_y ,

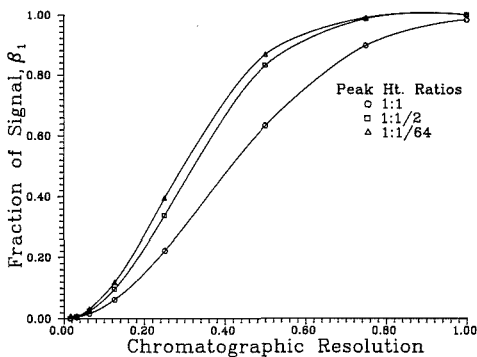


Figure 1. Effect of chromatographic resolution on net signal.

each representing the elution profiles of the pure components at equal heights. The dot product in the denominator, $\mathbf{h}'_y \mathbf{h}_y$, is the total signal due to Y when not overlapped at all.

The fraction of λ^* remaining after considering spectral similarity, β_2 , is calculated in a fashion similar to β_1 according to

$$\beta_2 = \lambda_2 / \mathbf{v}'_y \mathbf{v}_y \quad (11)$$

Here the vectors \mathbf{v}_x and \mathbf{v}_y represent the molar absorptivity spectra of X and Y normalized to unit area and λ_2 is the second eigenvalue obtained from the decomposition of the matrix containing the two vectors, \mathbf{v}_x and \mathbf{v}_y . The similarity between pairs of spectra is defined as $\cos(\theta)$, where θ is the angle between the vectors, calculated according to

$$\cos(\theta) = \mathbf{v}'_x \mathbf{v}_y / \|\mathbf{v}_x\| \|\mathbf{v}_y\| \quad (12)$$

This measure of similarity is independent of the shape of the spectra. For superimposable spectra, the angle between the two vectors will be zero, giving a similarity of one. Spectra that have no overlapped area at all are orthogonal and will have a similarity of zero. This definition of spectral similarity is related to Lorber's definition of selectivity, $\zeta_j = 1 - \cos(\theta)$ (17). His method of calculation may be used to extend these calculations to more than two components.

EXPERIMENTAL SECTION

Gaussian elution profiles were used to simulate chromatograms of two overlapped peaks. The retention times of the two peaks were adjusted to cover a wide range of chromatographic resolution (0.125 to 1.0). Peak heights of the two peaks were adjusted to cover the range of ratios from 1:1 to 1:1/128. Pairs of experimentally determined UV spectra of acetophenone, nitrobenzene, biphenyl, benzophenone, toluene, cumene, and phenylcyclohexane were used in a matrix multiplication step with the Gaussian elution profiles to produce the simulated two-component data matrices. Experiment error was simulated by adding uniformly distributed random numbers in the range of 5×10^{-4} , corresponding to a simulated measurement error of about 5×10^{-6} absorbance unit.

Experimental data for use in the two-component overlap studies were obtained by using mixtures of acetophenone and nitrobenzene in a wide range of concentration ratios. The standard solutions were run on a 25 cm \times 4.6 mm C18 analytical column using a mobile phase of 95/5 methanol/water, giving a chromatographic resolution of about $R_s = 0.5$.

RESULTS AND DISCUSSION

Calculations using simulated overlapped chromatographic peaks (Gaussian) were used to investigate the relationship between chromatographic resolution and β_1 . These results are summarized in Table I and Figure 1. Peak separation was adjusted to give pairs of overlapped peaks having precisely known resolution. Equation 7 was used to calculate the values

Table I. Value of β_1 As a Function of Chromatographic Resolution and Peak Height

chromatographic resolution	1:1	1:1/2	1:1/16	1:1/64
1.00000	0.98174	0.99955	0.99966	0.99966
0.75000	0.89461	0.98526	0.98885	0.98889
0.50000	0.63212	0.82926	0.86420	0.86463
0.25000	0.22119	0.33755	0.39252	0.39340
0.12500	0.06058	0.09583	0.11708	0.11746
0.06250	0.01550	0.02473	0.03064	0.03075
0.03125	0.00390	0.00623	0.00775	0.00778
0.01563	0.00001	0.00002	0.00775	0.00778

Table II. Spectral Similarity of Example Spectra

spectral similarity	β_2	mixture
0.2893	0.2965	acetophenone-nitrobenzene
0.4557	0.1611	acetophenone-benzophenone
0.5945	0.0859	acetophenone-biphenyl
0.7146	0.0416	nitrobenzene-benzophenone
0.5374	0.1134	nitrobenzene-biphenyl
0.7661	0.0277	benzophenone-biphenyl
0.9737	0.0003	toluene-cumene
0.8935	0.0057	toluene-phenylcyclohexane
0.9164	0.0035	cumene-phenylcyclohexane

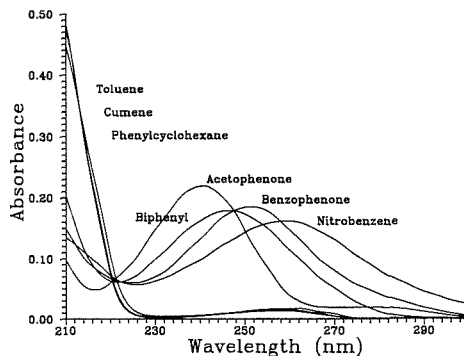


Figure 2. Normalized UV spectra of acetophenone, nitrobenzene, biphenyl, benzophenone, toluene, cumene, and phenylcyclohexane.

of β_1 . The curves for peak height ratios of 1:1, 1:1/2, and 1:1/64 are shown in Figure 1. Rapid convergence to the curve for 1:1/64 is observed as the height of the minor peak is decreased. Thereafter, no significant changes in the shape of the curve are observed. Since actual peaks are usually skewed, not Gaussian, slightly different results are expected for experimental data.

Table II shows the similarity between several pairs of UV spectra and the corresponding values for β_2 . Plots of these spectra may be found in Figure 2. In order to illustrate the relationship between spectral similarity and β_2 , calculations using simulated spectra (Gaussian-shaped absorption bands) were used to generate a plot of β_2 as a function of spectral similarity (see Figure 3). For reference, the location of some of the pairs of spectra in Table II is shown on the curve. Recall that β_2 does not depend on the shape of the spectra. The plot shows that the fraction of net signal for component Y is decreased sharply at a spectral similarity greater than 0.20.

The results from Tables I and II can be used to estimate the net signal for a minor component, Y, when overlapped with X. Suppose a certain set of chromatographic conditions gives a resolution of 0.25 between nitrobenzene (major component) and acetophenone (minor component). Furthermore, suppose

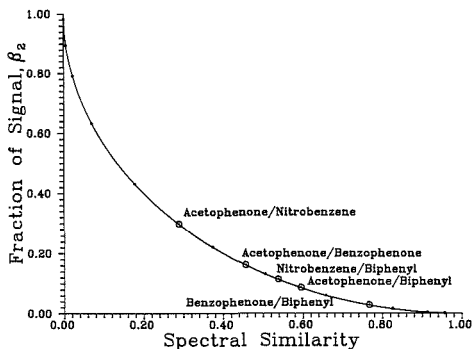


Figure 3. Effect of spectral similarity on net signal.

the signal due to a certain pure acetophenone peak and pure nitrobenzene peak is $\lambda^* = 7.09$ and 7.09 , respectively (the two pure peaks have equal heights). Finally, suppose the expected measurement error is 5×10^{-4} absorbance unit for a 32×30 data matrix, giving a value of 2.2×10^{-5} for λ_2^* according to eq 8. When nitrobenzene is overlapped with acetophenone at a height ratio of $1:1/2$, an estimate of the net signal due to acetophenone may be calculated by using $\beta_1 = 0.338$ and $\beta_2 = 0.297$

$$\lambda_2 = [(1/2)^2 \times 0.338 \times 0.297 \times 7.09] + (2.2 \times 10^{-5})$$

$$\lambda_2 = 0.178$$

Factor analysis of a simulated data matrix under the above conditions gives an actual value of $\lambda_2 = 0.199$, corresponding to a 40-fold reduction in the original acetophenone signal. The value estimated by eq 1 is low by about 11% but is within an order of magnitude of the actual value. At a peak height ratio of $1:1/64$, the estimated value of λ_2 is 0.00022 compared to the actual value of 0.00034 . In this case the actual net signal has been reduced by over 4 orders of magnitude. The estimated value is about 41% low; however, it is still within the correct order of magnitude. Simulations involving other pairs of spectra under varying degrees of chromatographic resolution give estimates having the correct order of magnitude with errors ranging from 0% to 50%.

The eigenvalues from factor analysis of the experimental data obtained from mixtures of acetophenone and nitrobenzene were used to test the relationship expressed in eq 1. The resolution between the acetophenone and nitrobenzene peaks was about $R_s = 0.5$. The results of the calculations are shown in Table III. In part A of Table III, values of $\lambda^* = 14.52$, $\beta_1 = 0.86$, and $\beta_2 = 0.297$ were used. In part B of Table III, values of $\lambda^* = 16.76$, $\beta_1 = 0.86$, and $\beta_2 = 0.297$ were used. An average value of $REV_3 = 2.83 \times 10^{-7}$ was calculated from experimental values of λ_3 . This value was used to estimate values of λ_2^* in Table III according to eq 9.

Fair agreement was observed between the observed values of λ_2 and the expected values of λ_2 . At ratios lower than $1/50$ the observed values of λ_2 level off, indicating a greater contribution from random experimental error.

The expected values of λ_2 reported in Table III can be used to estimate the minimum concentration of a minor component that can be reliably detected. The results in part A and part B of the table show that the smallest second eigenvalue that can be reliably detected should be about 3 to 4 times greater than 0.0002 . For nitrobenzene as the minor component or acetophenone as the minor component, the lowest concentrations meeting these criteria are those obtained from the mixtures having the concentration of the minor component reduced to $1/100$ of the concentration of the major component.

Table III. Observed and Expected Values of λ_2 for Experimental Data

Part A: Varying Nitrobenzene Concentration						
concn, mg/mL		expected	matrix	obsd	obsd	expected
acetoph	nitroben	height of nitroben	size	λ_1	λ_2	λ_2
0.0000	0.10036	1	29×30	14.52	0.0004	0.0002*
0.10258	0.01004	$1/10$	36×30	17.75	0.0536	0.0374
0.10258	0.00201	$1/50$	38×30	16.82	0.0029	0.0018
0.10258	0.001000	$1/100$	38×30	16.88	0.0015	0.0007
0.10258	0.00005	$1/200$	36×30	17.48	0.0009	0.0004
0.10258	0.00002	$1/400$	36×30	16.91	0.0007	0.0003

Part B: Varying Acetophenone Concentration						
concn, mg/mL		expected	matrix	obsd	obsd	expected
acetoph	nitroben	height of acetoph	size	λ_1	λ_2	λ_2
0.10258	0.00000	1	27×30	16.76	0.0010	0.0002*
0.01026	0.10036	$1/10$	32×30	16.35	0.0617	0.0431
0.00205	0.10036	$1/50$	31×30	15.04	0.0021	0.0019
0.00103	0.10036	$1/100$	36×30	15.88	0.0010	0.0008
0.00051	0.10036	$1/200$	38×30	14.78	0.0007	0.0004

* Estimated error eigenvalue. Observed eigenvalues should be 3 to 4 times greater than this value in order for minor components to be detected.

The corresponding expected eigenvalues are 0.0007 and 0.0008 for nitrobenzene and acetophenone, respectively. Analysis of the experimental data for the mixtures in Table III supports the detection limit estimated above. The second component was not reliably detected in the standards where the concentration of the minor component was reduced to $1/200$ or $1/400$ of the concentration of the major component.

CONCLUSIONS

The techniques reported here can be used to estimate the net signal due to a minor component in an overlapped peak. The presence of a second component will be detected when its net signal is significantly larger than a minimum value determined by experimental error in a data matrix with the same dimensions. These results can be used to judge the approximate conditions of peak height, resolution, and spectral similarity under which minor components will be reliably detected when overlapped with other peaks without resorting to lengthy, time-consuming sequences of experiments.

LITERATURE CITED

- (1) Knorr, F. J.; Futrell, J. H. *Anal. Chem.* **1979**, *51*, 1236-1241.
- (2) McCue, M.; Malinowski, E. R. *Appl. Spectrosc.* **1983**, *37*, 463-469.
- (3) Sharaf, M. A.; Kowalski, B. R. *Anal. Chem.* **1981**, *53*, 518-522.
- (4) Sharaf, M. A.; Kowalski, B. R. *Anal. Chem.* **1982**, *54*, 1291-1296.
- (5) Osten, D. W.; Kowalski, B. R. *Anal. Chem.* **1984**, *56*, 991-995.
- (6) Borgen, O. S.; Kowalski, B. R. *Anal. Chim. Acta* **1985**, *174*, 1-26.
- (7) Gemperline, P. J. *J. Chem. Inf. Comput. Sci.* **1984**, *24*, 206-212.
- (8) Gemperline, P. J. *Anal. Chem.* **1986**, *58*, 2656-2663.
- (9) Vandeginste, B. G. M.; Derks, D.; Kateman, G. *Anal. Chim. Acta* **1985**, *173*, 253-264.
- (10) Lacey, R. F. *Anal. Chem.* **1986**, *58*, 1404-1409.
- (11) Malinowski, E. R. *Anal. Chem.* **1977**, *49*, 606-612.
- (12) Malinowski, E. R. *Anal. Chem.* **1977**, *49*, 612-617.
- (13) Shrager, R. I.; Hender, R. W. *Anal. Chem.* **1982**, *54*, 1147-1152.
- (14) Rossi, T. M.; Warner, I. M. *Anal. Chem.* **1986**, *58*, 810-815.
- (15) Malinowski, E. R. *J. Chemom.* **1987**, *1*, 33-40.
- (16) Malinowski, E. R. *J. Chemom.* **1988**, *2*, 49-60.
- (17) Lorber, A. *Anal. Chem.* **1986**, *58*, 1167-1172.

RECEIVED for review April 25, 1989. Accepted July 17, 1989. Acknowledgment is made to the donors of the Petroleum Research Fund, administered by the American Chemical Society, and to Burroughs Wellcome Co. for partial support of this research. This work was presented at the Second Hidden Peak Symposium on Computer-Enhanced Analytical Spectroscopy, Snowbird, UT, June 1-3, 1988.

Determination of Selenium in Human Blood by High-Performance Liquid Chromatography with Fluorescence Detection

Garry J. Handelman¹

Chemistry Department, University of California, Santa Cruz, California 95064

Paula Kosted

Chemistry Department, Montana State University, Bozeman, Montana 59717

Sara Short

SRI International, Menlo Park, California 94025

Edward A. Dratz*

Chemistry Department, Montana State University, Bozeman, Montana 59717

Selenium was determined in human whole blood or red cells by high-performance liquid chromatography (HPLC) using a new internal standard. The method provides a 0.15-ng detection limit, a between-day standard deviation of 1% at the 20-ng level, and a 3% within-day standard deviation at the 1-ng level. Samples were wet-ashed, and a selenium-diaminonaphthalene derivative was formed, followed by addition of tetraphenylphthalene internal standard, reverse-phase HPLC separation (10 min/run), and fluorescence detection. The detection limit was reduced by discrimination of fluorescence excitation of the selenium complex from the background using long-wavelength excitation (480 nm), removal of stray light in the excitation beam, and other optimizations described. Representative aliquots of frozen and thawed whole blood samples were obtained by using a nitric acid predigestion at ambient temperature. Procedures to validate the method included standard addition and neutron activation analysis.

INTRODUCTION

Selenium is now known to be important both as an environmental contaminant (1) and an essential trace element (1). Investigation of these roles requires sensitive and reliable analytical methods for the determination of Se in complex biological materials. This has proved a challenging problem, especially when only small samples of tissue are available. Each of the methods developed for analysis of selenium in biological materials (reviewed in ref 2 and 3) has certain limitations.

Neutron activation analysis (NAA) is highly specific for Se, but the Na and Cl ions present in some tissue samples cause a large noise background. Se in whole blood samples is substantially lost if dialysis is employed to eliminate Na and Cl ions from the sample. Graphite furnace atomic absorption (GF-AA) has not given reliable results with whole blood due to interference from the high iron content (4, 5).

Several of the procedures useful for selenium analysis are not routinely available. NAA is done at only a few centers worldwide. GF-AA, when equipped with the Zeeman back-

ground corrector needed to correct for spectral interferences, is too costly for many laboratories.

Analysis of the fluorescent diaminonaphthalene (DAN) derivative of selenite ion in cuvettes has found wide application (6-8). The DAN-Se derivative yields a strong fluorescent signal when excited at 376 nm, but excess DAN reagent is present in the assay cuvette, which produces a background fluorescence equivalent to about 2 ng of Se (6, 7).

The method described here utilizes high-performance liquid chromatography (HPLC) equipment, which is commonly available, to resolve the DAN-Se analyte from free DAN and other background-producing materials. There is no detectable blank from the DAN reagent with use of the HPLC method if instrumental variables are properly selected. The HPLC method has a between-day coefficient of variation (CV) of 1% at the 20-ng level, and analyses can be reliably carried out down to 1.0 ng of Se. The method is effective for the whole blood matrix, red blood cells, or desiccated bovine liver (which behaves in a similar manner to that of other soft tissue materials). The chromatographic procedure described here differs from previous HPLC methods for Se (9-13) by its having lower background, its applicability to difficult biological matrices, and in the use of an internal standard, which greatly facilitates analytic procedures, decreasing the practical detection limit and improving reproducibility.

EXPERIMENTAL SECTION

Apparatus. The HPLC consisted of a Perkin-Elmer Model 100 pump, with integral pulse dampener, a Rheodyne Model 7125 injector with 20- μ L loop, an Alltech reverse-phase C18 \times 10 μ m, 25 cm \times 0.46 cm column with guard column, and a Perkin-Elmer Model 650-LC fluorescence detector. This fluorescence detector is currently marketed as the Hitachi Model F-2000. For some experiments, an Alltech Adsorbosphere C18 \times 5 μ m, 25 cm \times 0.46 cm column was utilized. The mobile phase was 100% MeOH, and the flow rate was 1.4 mL/min. The detector was set at 480-nm excitation, 20-nm band-pass, and 580-nm emission, 20-nm band-pass. A 420-nm high-pass optical filter (Schott GG-420) was placed in the excitation beam to remove stray light of wavelength $<$ 420 nm; however, a 450-nm high-pass optical filter was equally effective. The detector was set at the "fast" (0.5 s) time constant.

Retention times were monitored with a Spectra-Physics integrator. Peaks were recorded on a Hewlett-Packard Model 7130 chart recorder. Quantitation was done by determining peak height ratios of the DAN-Se peak and the internal standard peak. Se standards were dispensed with positive displacement micropipettors (SMI, American Scientific Products).

¹Present address: Department of Biochemistry, Tufts University, Health Sciences Campus, Boston, MA 02111.

Reagents. Perchloric acid was GF Smith, 70%, double-distilled, ACS reagent grade. Some lots of perchloric acid were found to contain waxy residues that extracted into cyclohexane. These lots were preextracted with cyclohexane before use in the analytical procedure. Sulfuric acid was GF Smith, 98%, Vycor distilled. Methanol and 2-propanol, both HPLC grade, were from Fisher Chemical Co. Sodium selenite was from Alfa Inorganics. Stock solutions for routine use were prepared by dilution with 0.1 N HCl. Selenium standard solution (Fisher) for atomic absorption (1 mg of Se per milliliter of H₂O, as SeO₂) was also evaluated and found to give equivalent results. Tetraphenyl-naphthalene (TPN, also called rubrene) and DAN-HCl were from Aldrich Chemical Co. Cyclohexane, HPLC grade, was from Fisher. Some lots were redistilled from sodium hydride (14) and stored under argon, as is further described in Procedures. Other materials were reagent grade.

Procedures. Blood was collected from the antecubital vein with the use of K₃EDTA anticoagulant. Some whole blood samples were diluted directly into 10 volumes of 70% HNO₃. Other aliquots were stored in small plastic tubes at -120 °C. When these aliquots were thawed, they were also diluted with 10 volumes of nitric acid. Before the digestion step, all samples were incubated in nitric acid at ambient temperature for at least 8 h. Some measurements were also made on saline-washed human red blood cells.

The samples were acid-digested by a method modified from the procedure of Alifhan (7). All digestion operations were carried out in a well-ventilated fume hood. One milliliter of the sample dilution in nitric acid was placed in a 16 × 125 mm disposable borosilicate glass test tube. Two glass beads and 0.4 mL of a 20:1 HClO₄/H₂SO₄ mixture were added, and the tubes were placed in an electrically heated, 7.5 cm deep digestion block preheated to 80 °C. The entire digestion block was wrapped with several layers of aluminum foil to facilitate control of block temperature in the strong draft of the fume hood. The samples were heated from 80 to 120 °C over 1 h, and then from 120 to 150 °C over 1 h. The tops of the tubes were then wrapped in several thicknesses of aluminum foil to minimize recondensation of HNO₃ vapors. The tubes were heated from 150 to 180 °C over 30 min and held at 180–200 °C for 1 h.

The tubes were cooled, 0.25 mL of saturated ammonium oxalate was added, and the tubes were heated at 100 °C in a boiling water bath for 10 min. The tubes were cooled again, 0.75 mL of 6 M HCl was added, and the tubes were heated at 100 °C in the boiling water bath for an additional 10 min, to reduce selenate present to selenite (7).

After cooling, 1 mL of 50% formic acid, 0.5 mL of 0.1 M Na₂EDTA/2.5% hydroxylamine 0.6 mL of 25% NaOH were added. A separate Pasteur pipet was placed in each tube, and the tubes were aspirated vigorously to remove ammonia formed from the ammonium oxalate added at the previous step. The pH was then adjusted to 1.2 (±0.1) with a pH meter, using 10% NaOH and 6 M HCl. The digest was then transferred, along with two 1-mL rinses with pH 1.0 HCl, to 16 × 125 mm screw-cap borosilicate glass tubes.

DAN reagent was prepared daily by boiling 1 mg/mL DAN-HCl in pH 1.0 HCl for 10 min under subdued incandescent light. A 1.0-mL aliquot of the DAN reagent was added to the sample digests, and the tubes were capped with Teflon-lined plastic caps (Thomas Scientific, No. 2390-H32), the contents mixed well, and the tubes placed in a dark 65 °C water bath for 40 min for synthesis of the DAN-Se derivative. All subsequent operations were carried out under subdued incandescent light.

The internal standard solution was prepared by dissolving the TPN in cyclohexane, measuring its absorbance at 526 nm, and diluting this stock solution with cyclohexane to obtain a working stock solution with an absorbance of 0.0004 at 526 nm. Care should be taken that the fluorescence of TPN does not create absorbance measurement artifacts.

After incubation, the tubes were cooled in a room-temperature water bath. Each tube received 1 mL of cyclohexane, containing TPN, and 2 mL of additional cyclohexane, and the tubes were tightly capped. The tubes were shaken vigorously by hand for 60 s and centrifuged to separate the phases, and the cyclohexane layer was collected in an 8-mL borosilicate glass vial. The cyclohexane was evaporated by placing the tubes in a 40 °C water

bath and passing a stream of nitrogen over them, and the residue was dissolved in 60 μL of 1:1 methanol/2-propanol. The injection loop was first rinsed with methanol/2-propanol, and the sample was analyzed by HPLC.

Explanation of Steps in the Analytical Procedures. The small amount of sulfuric acid was added to the digestion reagent to protect against the digest being evaporated to dryness (8). Taking the sample to dryness can cause volatilization of selenium and is one of the major potential losses of selenium associated with wet digestion procedures (15).

Nitric acid was found to interfere with formation of the DAN-Se derivative, and therefore digestion conditions were chosen to drive off and eliminate nitric acid during heating at 180–200 °C.

The ammonium oxalate step was employed to eliminate nitrite from the digest (16). Nitrite can interfere directly with the synthesis of the DAN-Se derivative (17) and has been reported to accumulate during the digestion procedure (17). Nitrite ion also forms a fluorescent derivative with the DAN reagent, with excitation and emission maxima of 364 and 412 nm, respectively (18). This DAN-nitrite derivative was synthesized at pH 1.0 and analyzed by HPLC. The DAN-nitrite peak is not detected at the excitation and emission wavelength settings used in the present method.

Addition of H₂O₂ was evaluated as an alternative method for eliminating the nitrite (8). Traces of H₂O₂ were found to interfere with DAN-Se formation, but oxalate did not. Since H₂O₂ may not be completely eliminated once added to the digest, it was not employed in this procedure.

Formic acid provides buffering to allow the pH of 1.2 to be more easily attained during pH adjustment. Hydroxylamine was added to stabilize the DAN reagent against oxidation during the derivatization step (19). EDTA chelates Fe, Cu, and other trace metals derived from the red blood cells (RBC), which may otherwise interfere with the formation of the DAN-Se derivative (20).

BHT (butylated hydroxytoluene) is added to the cyclohexane for two reasons. First, if cyclohexane is initially purchased under nitrogen atmosphere is left exposed to the air without BHT protection, the DAN-Se derivative is unstable in the aged cyclohexane, and losses of DAN-Se of up to 25% per hour are noted. Second, the DAN-Se may be substantially decomposed at the cyclohexane evaporation step, unless BHT is present. We hypothesize that the BHT inhibits peroxide formation in the cyclohexane (21) and also provides an inert hydrophobic layer during the evaporation step to protect the DAN-Se from air oxidation. Even when BHT-supplemented, bottles of cyclohexane open to the air for more than 90 days begin to show traces of DAN-Se decomposing activity.

Some lots of cyclohexane showed DAN-Se decomposing activity when initially opened, even with immediate BHT addition. For these lots, it was necessary to redistill the cyclohexane over sodium hydride (14), add BHT, and store the purified product tightly sealed under argon. The cyclohexane could be used for up to 30 days after redistillation if these precautions were followed. The TPN dilutions in cyclohexane used for internal standard are also stable when stored under argon.

After formation of the DAN-Se in the 65 °C water bath, it is stable for up to 8 h if stored at ambient temperature in the dark in the derivatization reagent. However, after the sample has been extracted into cyclohexane, the cyclohexane should be evaporated within 5 min and replaced with 1:1 methanol/2-propanol. Both DAN-Se and TPN are stable in the dark in 1:1 methanol/2-propanol for at least 2 h.

The nitric/perchloric acid digestion procedures often do not completely digest lipids in the sample (2, 8). Lipids may be carried through the cyclohexane extraction to the final HPLC step. For reliable results with whole blood analyses, it was necessary to dissolve the digested extract in 1:1 methanol/2-propanol for injection into the HPLC. This may be due to the superior ability of methanol/2-propanol to solubilize lipids. When Se standards were analyzed, 100% MeOH worked reliably. When whole blood is analyzed, it is important for accuracy that the injection loop and syringe be rinsed with methanol/2-propanol.

RESULTS

Analysis of Human Whole Blood and RBC. Either

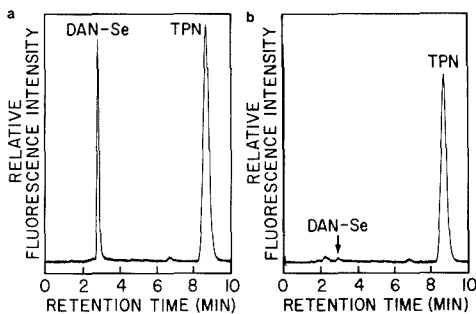


Figure 1. (a) HPLC analysis of Se in 100 μ L of normal human RBC: column, C18, 10 μ m, 25 \times 0.46 cm; mobile phase, 100% MeOH, 1.4 mL/min; excitation, 480 nm; emission, 580 nm; 420-nm high-pass barrier filter in excitation beam. (b) Reagent blank, all other conditions as in Figure 1a. The small peak marked "DAN-Se" is contributed by traces of Se in the reagents employed.

Table I. Between-Day Comparison of Eight Whole Blood Samples

sample	day 1	day 2	day 3	mean (\pm CV, %), (ng of Se/100 μ L)
1	18.4	18.5	18.0	18.3 (1.5)
2	16.2	16.1	16.0	16.1 (0.82)
3	19.7	19.5	19.7	19.6 (0.51)
4	19.5	19.3	19.0	19.3 (1.35)
5	17.1	17.3	17.7	17.4 (1.55)
6	15.2	15.2	15.1	15.2 (0.36)
7	19.8	19.8	20.1	19.9 (0.87)
8	20.3	20.5	20.9	20.5 (1.67)

* Mean between-day standard deviation, 1.1%.

whole blood or washed red cells were digested and analyzed for selenium content. A sample HPLC chromatogram of the selenium determined in a 100- μ L aliquot of RBC is shown in Figure 1a. The reagent blank is shown in Figure 1b. The blank equals 0.25 ng of Se.

Sampling Technique Required for Frozen Human Whole Blood Samples. It was found repeatedly that aliquots of frozen and thawed human whole blood were not homogeneous for Se. The Se content of replicate 100- μ L aliquots of thawed material frequently varied by as much as 25%. Fresh material, both whole blood and saline-washed RBC, showed high reproducibility. The reproducibility problem was fully overcome by predigesting frozen and thawed whole blood with nitric acid. To analyze a sample of frozen whole blood, the blood sample container is weighed, the sample is transferred to a screw-cap test tube, and the original sample container is reweighed. Then the volume of the blood sample is determined by using the whole blood density of 1.06 grams/cm³, which was taken from literature values (22) and confirmed experimentally.

Ten volumes of 70% HNO₃ are added to the sample in the screw-cap test tube, and the mixture is allowed to digest at room temperature overnight. Aliquots (1 mL) of this dilution are digested for Se analysis. Replicate analyses from this HNO₃ dilution gave highly reproducible results, as described below.

Between-Day Coefficient of Variation. Whole blood from eight subjects from the New York, NY, area who were enrolled in a nutritional study was analyzed in duplicate on three different days. Aliquots for the analyses were taken from the initial dilution of the whole blood in 70% HNO₃. The results are shown in Table I. The between-day coefficient of variation for these samples was 1.1%. Similar precision

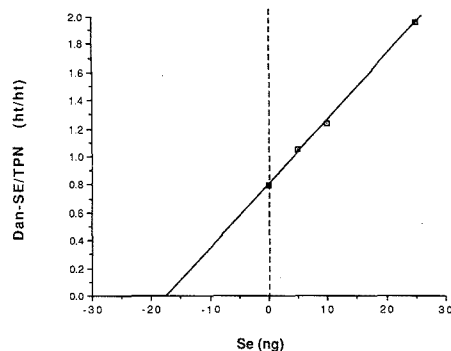


Figure 2. Determination of Se in a 100- μ L sample of whole blood by standard addition. The aliquot was spiked with 5, 10, and 25 ng of Se (as sodium selenite) and the Se value of the blood sample determined by extrapolation to the x axis.

was found with analyses of washed RBC (data not shown).

Within-Day Coefficient of Variation. Analyses in replicate ($n = 8$) were carried out on a single day on one of the above whole blood samples, and a within-day CV of 1.2% was determined. In experiments with washed RBC, the within-day CV varied from 1.4% to 2.0% ($n = 4$ for each experiment).

Calibration Curves. The method was determined to be linear through at least 40 ng of Se/determination. A separate calibration curve was prepared with Se (as sodium selenite) for each batch of samples. The calibration curve consisted of a blank and 10, 20, and 40 ng of Se. Each Se standard level was analyzed twice to establish this standard curve. Least-squares analysis (23) on six consecutive standard curves was carried out. The Pearson correlation coefficient (r) was 0.999 for the standard curves. The mean CV from the least-squares analysis for Se determination at the 20-ng level was 2.3%.

Analysis of Standard Reference Material. Bovine liver, National Bureau of Standards SRM No. 077, was analyzed by this procedure after desiccation of the material at 60 $^{\circ}$ C for 2 h. The certified Se value for this material is 1.1 (± 0.1) μ g/g. In the first determination a value of 1.04 (± 0.01) was obtained with the present method ($n = 4$). In a second determination, a value of 1.05 (± 0.02) was obtained ($n = 2$).

Matrix Effects. Matrix effects were evaluated by the method of standard addition. Samples prepared from 100 μ L of whole blood were predigested with nitric acid and spiked with 5, 10, and 25 ng of Se (as sodium selenite). The results of this analysis are shown in Figure 2. By extrapolation to the x intercept, the blood sample was determined to contain 17.4 ng of Se. Analysis of this sample by the standard procedure described above yielded 17.1 ng. The difference between the two procedures is 1.6%, which is within the experimental error of this method. Therefore, the whole blood matrix does not significantly interfere with the analysis of added selenite.

Comparison with Neutron Activation Analysis. Six samples of whole blood from normal adult subjects from the Bozeman, MT, area were analyzed by both the standard HPLC procedure described above and by neutron activation analysis (NAA) of Se-77 (24) at the University of Missouri Research Reactor Facility, Columbia, MO. For NAA, it was necessary to analyze whole blood without dialysis, because a substantial fraction of the Se (up to 25%) is lost from whole blood through the dialysis membrane (personal communication, September 1988, Dr. Steven Morris, University of Missouri, Columbia, MO). However, the Na, Cl, and other elements in the whole blood create background noise equivalent to 2 ng in a 0.1-mL blood sample, or a 10% noise level.

Table II. Determination of Se in Whole Blood at Trace Levels

Se in sample, ng	Se found, ng (n = 4)	Se in sample, ng	Se found, ng (n = 4)
2.0	1.99 ($\pm 3.3\%$)	0.2	0.219 ($\pm 18\%$)
1.0	0.980 ($\pm 2.2\%$)	0.1	0.098 ($\pm 16\%$)
0.4	0.445 ($\pm 14\%$)		

As a result, the precision of the NAA method with whole blood is significantly less than that of the HPLC method.

The mean Se value determined by the HPLC procedure was 21.5 (± 0.36) ng/100 μ L, and the Se value determined by the NAA procedure was 21.8 (± 1.35) ng/100 μ L, for a 1.5% difference. The correlation coefficient (*r*) between the two procedures was 0.98. This finding supports the conclusion that the HPLC procedure is measuring the entire Se content of the sample.

Detection Limit. The small peak in the reagent blank (Figure 1b) is due to traces of Se in the reagents employed in the procedure. The Se blank was 0.25 ng, with a standard deviation of 0.05 ng. Therefore, the detection limit (estimated as 3 times the standard deviation of the blank) was 0.15 ng.

AR-grade sulfuric acid was used initially for the digestion procedure, and a blank of 1.5 ng of Se was observed. The blank decreased to 0.25 ng when Vycor-distilled sulfuric acid was used. Studies of individual reagents indicate that 40% of this 0.25 ng is contributed by the Vycor-distilled sulfuric acid. The detector base-line noise had a peak-to-peak value with the 10- μ m HPLC column of 0.12 ng of Se.

Experiments with a Higher Resolution C18 \times 5 μ m HPLC Column. To further characterize the behavior of the assay with trace amounts of Se, analyses were carried out using a C18 \times 5 μ m, 25 cm \times 0.46 cm HPLC column with integral cartridge guard column, which gives a considerably sharper DAN-Se peak than the C18 \times 10 μ m HPLC column used elsewhere in this method. In these experiments, the final extract for HPLC analysis was dissolved in 40 μ L of 1:1 methanol/2-propanol instead of 60 μ L. From a whole blood sample with previously determined Se content, dilutions of whole blood were made with HNO₃ to yield Se concentrations from 0.1 to 2.0 ng of Se/mL of HNO₃. One-milliliter aliquots of these dilutions were analyzed, and the results are shown in Table II.

Effects of Fluorescence Detector Excitation and Emission Settings. Initially, HPLC of the DAN-Se derivative was attempted using the conventional excitation and emission wavelengths of 376 and 520 nm, respectively. With these settings, the DAN reagent alone, even in the absence of Se, produced a large peak that overlapped the DAN-Se peak on the chromatogram (data not shown). This substantial reagent peak remained even when the DAN was purified before use by 4 \times extraction with cyclohexane. Other detector wavelengths were therefore explored.

Figure 3 compares the excitation and emission spectra of the DAN reagent blank with the spectra of the DAN-Se derivative (prepared from 20 ng of Se, the middle of the working range of this method). The DAN-Se excitation at 376 nm is only twice that of the blank. However, the DAN-Se derivative also has a substantial excitation band in the 450–500-nm region, and the blank in that region drops close to zero. The suitability of the 450–500-nm region is further enhanced because the Xe light source employed has its greatest energy output in the 450–500-nm region. When the HPLC analysis was carried out using 480-nm excitation and 580-nm emission, with use of a 420- or 450-nm high-pass filter in the excitation beam, the contribution of the DAN reagent peak was reduced to near zero, as is seen in Figure 1b. Nazarenko and Ermakov

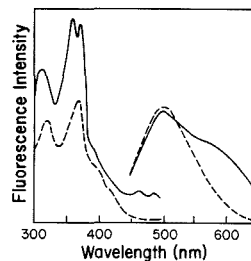


Figure 3. Excitation and emission spectra (without spectral correction) of DAN-Se from 20 ng of Se (solid line) and of the DAN blank (dashed line). The DAN-Se shows substantial fluorescence excitation at 480 nm, where the excitation of the blank drops to near zero.

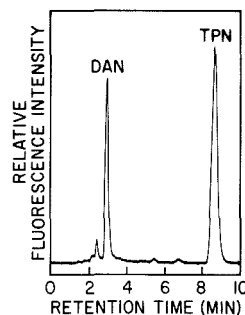


Figure 4. Effect on the reagent blank of removal of the high-pass filter from the excitation beam. The large DAN peak, with a retention time very similar to that of the DAN-Se peak, is due to stray light in the excitation beam. HPLC conditions were the same as in Figure 1b except for the absence of the high-pass filter.

(25) also reported that the fluorescence signal of DAN became very low with excitation wavelengths greater than 400 nm.

The HPLC fluorescence detector used in this work has a single-grating excitation monochromator, and stray light was a potential source of difficulty. Figure 4 shows a chromatogram of the reagent blank excited at 480 nm without the high-pass excitation filter. The chromatographic peak observed under these conditions results from excitation of the DAN reagent, due to stray light in the 300–400-nm range passed by the monochromator. Both the use of the 480-nm excitation wavelength and the high-pass 420-nm excitation filter to remove stray light were necessary to obtain the low blank values found in this work.

The TPN excitation spectrum extends from 440 to 530 nm, and emission spectrum from 550 to 620 nm (spectra not shown). Excitation and emission wavelengths used for the DAN-Se complex are well within these regions of the TPN spectra.

Contaminants in the DAN Reagent. Most commercial samples of DAN reagent were found to be acceptable without further purification. Some batches of DAN contained a component that eluted at a retention time equal to 7 times the DAN-Se retention time. The size of this peak (which eluted as a broad peak due to its prolonged retention time) varied among the different batches of DAN. The peak height of this component varied from 1 to 3 ng of Se equivalent. This component could not be removed by 4 \times extraction of the DAN reagent with cyclohexane. Interference from this contaminant, if present, was avoided by careful timing of each injection. It was possible to space the analyses out so that the broad peak from the previous injections consistently eluted between the DAN-Se and TPN peak, interfering with neither peak.

Effects of Conditions Used to Reduce Selenate to Selenite. Full reduction of selenate to selenite could be accomplished by placing the sample in a boiling water bath in 3 M HCl for periods of 5 to 20 min; 10 min is routinely used in the method as described.

The selenate and selenite content of samples may be distinguished by DAN-Se measurements before and after reduction of selenate with 3 M HCl. Such Se speciation may be of interest in studies of environmental waters (26, 27). Therefore we investigated the effect of the conditions used to form the DAN-Se derivative (65 °C, pH 1.0 HCl, 40 min) on reduction of selenate. No detectable conversion of selenate to selenite occurred under these conditions, and the analysis method may therefore be adaptable to Se speciation studies (26, 27).

DISCUSSION

This method was developed to exploit the superior sensitivity and selectivity provided by HPLC over that of fluorescence measurements carried out in cuvettes, as well as to gain the reliability of internal standard quantification. The individual components analyzed can be resolved as distinct peaks on the HPLC chromatogram, whereas in the classical DAN-Se fluorescence procedure in cuvettes there can be uncertainty about the relatively large contribution of background components to the fluorescence signal.

The method presented is compatible with the high lipid content of the whole blood or RBC matrix. Lipids often are not fully decomposed by perchloric acid digestion (2, 8). To prevent interference by residual lipid carried through to the HPLC step in whole blood digests, it is necessary to dissolve the final extract of the whole blood digests in 1:1 methanol/2-propanol.

Sample charring can be an important source of loss of volatile Se derivatives during digestion (15), but charring was not observed with the conditions employed in this work. If larger samples are to be digested, it may be useful to add additional perchloric acid, as recommended by Alfthan (8). The digests were gradually heated to the perchloric acid boiling point as recommended by Olson et al. (15) to avoid Se losses during digestion, and this procedure was found to be very satisfactory.

The HPLC step requires about 10 min per sample and adds approximately 25% more time for the analysis compared to the classical fluorometric technique. However, the HPLC method is capable of greater sensitivity and reproducibility. The use of the internal standard removes the need for rigorous control of volumes except at two steps: pipetting of sample and pipetting of internal standard. The steps of cyclohexane extraction, evaporation, and HPLC analysis are simplified on a routine basis by the use of the TPN internal standard.

The difficulties from relatively high blank values in the previously described procedures for Se analysis using DAN-Se derivatives (≥ 2.0 ng of Se equivalent) are likely to be due to the excitation of the DAN reagent at 376 nm. Even with highly purified reagent, some DAN extracts into the cyclohexane layer. The present method avoids direct excitation of the DAN reagent by exciting the DAN-Se fluorescence at 480 nm.

Several modifications may further lower the detection limit of this method. As discussed in Results, more highly purified reagents may be employed. For samples containing much less organic matter, the digestion might be carried out in one-tenth the volume of reagents used here, thereby lowering the blank to 0.025 ng.

We have been able to improve the signal-to-noise ratio by using a C18 \times 5 μ m analytical column with integral guard column and by dissolving the sample in 40 μ L of solvent for injection on the HPLC column, instead of the 60 μ L routinely

employed. Results obtained with these modifications are shown in Table II. The present method achieves a detection limit of 0.15 ng of Se in the sample, and lower limits can be attained by using the 5- μ m column and other modifications described above. This level of sensitivity compares favorably with that of current methods of Se analysis at trace levels.

In publications on trace element analysis, the detection limit is often reported in parts-per-billion (ppb). This convention, however, may not be appropriate with procedures, such as the present method, that are readily capable of analyzing samples of different weights or volumes. For such procedures, it is more useful to refer to the absolute detection limit. Biochemists interested in determining traces of Se, either in tissues from Se-deficient animals or in small tissue samples, are especially concerned with the absolute detection limit of a method. For these reasons, we describe below the working detection limit for several current procedures as nanograms of Se contained in the sample.

The conventional fluorometric procedure in cuvettes, when carried out with thorough purification of the DAN reagent, achieves a detection limit of 0.5 ng (8). NAA, using the Se-77 isotope, has a detection limit of 3 ng (24). Hydride generation-atomic absorption spectrophotometry (HG-AA), with a liquid-nitrogen trap and elution of the SeH₂ vapor into the detector as a sharp spike, attains a 0.5-ng detection limit (26).

GF-AA, with Zeeman background corrector and other features to optimize sensitivity, can achieve a 0.04-ng detection limit (28). This method has the additional merit of not requiring sample digestion, thereby eliminating the blank contributed by Se found in the strong-acid digestion reagents. However, the GF-AA procedure has been limited to small sample sizes (5–20 μ L of blood plasma), whereas the other methods described here can increase the working sensitivity by analyzing samples as large as 1 mL of whole blood or plasma. GF-AA has not given reliable results with whole blood samples (4, 5), as described in the Introduction.

Recently, Nakagawa et al. (13) described an HPLC method for Se using a new fluorescent derivative of Se with penicillamine and 7-fluoro-4-nitrobenz-2,1,3-oxadiazole. This method has excellent absolute sensitivity (the instrumental detection limit is 0.015 ng of injected Se). However, the method entails several sample dilutions, so that only $1/300$ of the Se in the sample reaches the detector flow cell (compared to one-third of the Se in the sample in the present method). As a result, the method of Nakagawa et al. (13) has a working detection limit of 5 ng of Se in the sample.

The HPLC method presented here combines an established method for conversion of Se in biological samples to selenite with a new HPLC method for measurement of the selenite. Prior workers have confirmed the reliability of the nitric acid/perchloric acid digestion procedure (8) for determination of selenium in whole blood (8) and a variety of animal and plant materials (15, 29, 30), including validation by neutron activation analysis (19, 30). The data reported here extensively document the accuracy and sensitivity of the HPLC method employing fluorescence detection. The high Fe, Cu, and organic matter content of whole blood makes this material a demanding matrix for Se determinations (5, 8, 20), and the success of the procedure described herein suggests it will be competent to handle less challenging materials, such as tissue proteins. Therefore, the method should have applicability to a wide range of biological samples. The highest sensitivity modifications might be useful in pediatric, forensic, or biochemical applications where small samples may be available and subnanogram sensitivity is required.

ACKNOWLEDGMENT

The helpful comments and insights of Kenneth Bruland are gratefully acknowledged. Mary Porter provided con-

structive comments on the manuscript. We thank Steven Morris for the reference determination of selenium in whole blood samples by neutron activation analysis.

LITERATURE CITED

- (1) National Research Council (U.S.), Subcommittee on Selenium. *Selenium in Nutrition*, revised ed.; National Academy Press: Washington, DC, 1983.
- (2) Raptis, S. E.; Kaiser, G.; Tolg, G. *Fresenius' Z. Anal. Chem.* **1983**, *316*, 105-123.
- (3) Lewis, S. A. *Methods Enzymol.* **1988**, *158*, 391-403.
- (4) Tada, Y.; Yonemoto, T.; Iwasa, A.; Nagakawa, K. *Bunseki Kagaku* **1980**, *29*, 248-253.
- (5) Alftan, G.; Kumpulainen, J. *Anal. Chim. Acta* **1982**, *140*, 221-227.
- (6) Parker, C. A.; Harvey, L. G. *Analyst* **1962**, *87*, 558-565.
- (7) Watkinson, J. H. *Anal. Chem.* **1986**, *38*, 92-97.
- (8) Alftan, G. *Anal. Chim. Acta* **1984**, *165*, 187-194.
- (9) Wheeler, G. L.; Lott, P. F. *Microchem. J.* **1974**, *19*, 390-405.
- (10) Schwedt, G.; Schwarz, A. *J. Chromatogr.* **1978**, *160*, 309-312.
- (11) Vezina, D.; Bleau, G. *J. Chromatogr.* **1988**, *426*, 385-391.
- (12) Shibata, Y.; Morita, M.; Fuwa, K. *Anal. Chem.* **1984**, *56*, 1527-1530.
- (13) Nakagawa, T.; Aoyama, E.; Hasegawa, N.; Kobayashi, N.; Tanaka, H. *Anal. Chem.* **1989**, *61*, 233-236.
- (14) Keese, R.; Muller, R. K.; Toube, T. P. *Fundamentals of Preparative Organic Chemistry*; Wiley: London, 1982.
- (15) Olson, O. E.; Palmer, I. S.; Whitehead, E. I. *Methods Biochem. Anal.* **1973**, *21*, 39-78.
- (16) Hasunuma, R.; Ogawa, T.; Kawanishi, Y. *Anal. Biochem.* **1982**, *126*, 242-245.
- (17) Lott, P. F.; Cukor, P.; Moriber, G.; Solga, J. *Anal. Chem.* **1963**, *35*, 1159-1163.
- (18) Sawicki, C. R. *Anal. Lett.* **1971**, *4*, 761-775.
- (19) Allaway, W. H.; Cary, E. E. *Anal. Chem.* **1964**, *36*, 1359-1362.
- (20) Michael, S.; White, C. L. *Anal. Chem.* **1976**, *48*, 1484-1486.
- (21) Farkas, A.; Passaglia, E. *J. Am. Chem. Soc.* **1950**, *72*, 3333-3337.
- (22) Davidsohn, I.; Nelson, D. A. In *Clinical Diagnosis by Laboratory Methods*, 15th ed.; Davidsohn, I., Henry, J. B., Eds.; Saunders: Philadelphia, 1976; Chapter 4.
- (23) Caulcutt, R.; Boddry, R. *Statistics for Analytical Chemists*; Chapman and Hall: London, 1983.
- (24) Morris, J. S.; Smith, M. F.; Morrow, R. E.; Heimann, E. D.; Hancock, J. C.; Gali, T. *J. Radioanal. Chem.* **1982**, *69*, 473-494.
- (25) Nazarenko, I. I.; Ermakov, A. N. *Analytical Chemistry of Selenium and Tellurium*; Wiley: New York, 1972; Chapter 4.
- (26) Cutter, G. A. *Anal. Chim. Acta* **1978**, *98*, 59-66.
- (27) Shimoiishi, Y.; Toei, K. *Anal. Chim. Acta* **1978**, *100*, 65-73.
- (28) Morisi, G.; Patriarca, M.; Menotti, A. *Clin. Chem.* **1988**, *34*, 127-130.
- (29) Vaessen, H. A. M. G.; van Ooik, A. Z. *Lebensm.-Unters. Forsch.* **1987**, *185*, 468-471.
- (30) Vijan, P. N.; Wood, G. R. *Talanta* **1976**, *23*, 89-94.

RECEIVED for review January 4, 1988. Resubmitted March 13, 1989. Accepted July 24, 1989. The work was partially supported by NIH Grants R03EY-05400 and R01EY-06913.

Theory of Cyclic Staircase Voltammetry for Electrode Kinetics

Mary M. Murphy, John J. O'Dea, Dieter Arn, and Janet G. Osteryoung*

Department of Chemistry, State University of New York at Buffalo, Buffalo, New York 14214

Cyclic staircase voltammograms have been calculated and compiled in the form of working curves for peak currents and peak potentials. All potentials and currents are normalized, making independent knowledge of n , D , and $E_{1/2}$ desirable. Kinetic information and in favorable cases rate constant values can be obtained by using these curves. If quasi-reversible behavior can be seen experimentally, peak separations can be used to estimate a rate constant. Measurement of the reverse peak current from a zero of current to calculate the peak current ratio is more convenient and reliable than the usual measurement from an extrapolated forward base line.

Staircase voltammetry (SCV) was introduced about 30 years ago as a digital counterpart to the widely used analog technique linear scan voltammetry (LSV). (For simplicity, we will use these abbreviations to include not only the linear but also the cyclic experiments.) These two very similar techniques have been compared recently, both theoretically and experimentally, in a series of papers by R. A. and J. G. Osteryoung and co-workers (1-4). A considerable amount of theoretical and experimental work has also been developed by others for the staircase technique (5-13). However, none of the previous theoretical work for SCV complicated by electrode kinetics has provided a thorough, systematic presentation of how all of the experimental quantities commonly measured in a cyclic voltammogram vary with the kinetic parameters and with a change in the characteristic time of the experiment over a wide range of values. We have carried out the necessary computations and present the results here in a series of working curves.

An introduction to cyclic voltammetry (LSV) has been provided in several recent articles (14, 15). In LSV the current response to a continuously changing potential is measured.

Typically the potential is $E = E_i - vt$, where E_i is the initial potential and v is the scan rate, up to the switching potential, E_{sp} , after which $E = E_{sp} + vt$. Although potential and time are inextricably linked by the scan rate in LSV, in SCV there are two parameters, step height (ΔE) and width (τ), permitting independent variation of the time scale. The SCV potential profile can be described in a way similar to that of LSV as $E = E_i - (j-1)\Delta E$ or $E = E_{sp} + (j-1)\Delta E$ for $(j-1)\tau \leq t \leq j\tau$, where j is the step number.

The fact that potential and time can be varied independently for SCV leads to a number of advantages over LSV. In LSV the ratio of faradaic to charging current decreases as $v^{-1/2}$ with increasing scan rate. This makes it difficult to vary scan rate over a meaningful range. In SCV, potential is held constant over the length of each step (for the period of time τ). Since charging current drops off exponentially with time while the desired faradaic signal only decays as $t^{-1/2}$, judicious choice of minimum step width can result in measurement of almost purely faradaic current. This property of pulsed waveforms, such as SCV, often allows the use of faster scan rates as long as background current is due primarily to charging current.

A potential step is also more readily implemented under control by digital computer than is a ramp. (In fact modern instruments offering "LSV" usually are employing a staircase waveform.) Finally, the widely used numerical methods based on integral equations describing the boundary value problem of interest are more conveniently applied to SCV than to LSV, because the discretized waveform in LSV is an approximation whereas in SCV it is exact.

The experimental quantities that are typically measured in a cyclic voltammogram are the cathodic and anodic peak potentials and their corresponding peak heights. A typical reversible staircase voltammogram is illustrated in Figure 1. The values shown are used to determine peak separations ($E_{pa} - E_{pc}$) and peak current ratios (i_{pa}/i_{pc}). Working curves

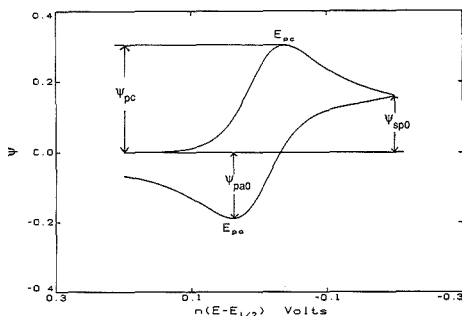


Figure 1. A cyclic staircase voltammogram for reversible electron transfer ($\log \kappa\tau^{1/2} = 2$), $n \Delta E = 5$ mV, $\alpha = 0.5$, and ψ is the dimensionless current (eq 4).

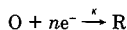
for peak currents, peak potentials, peak current ratios, and peak separations presented here provide information concerning the range and limitations for applying SCV to the study of a system complicated by slow electron transfer. A subsequent paper will deal with the other first-order kinetic cases of preceding (CE), following (EC), and catalytic (EC') reactions.

Also, since peak current ratios are measured in order to provide information concerning reversibility of an electrochemical system, and since most methods of determining this ratio are time-consuming and have associated experimental problems, we looked to other possibilities for obtaining equivalent information more directly. As seen in Figure 1, the biggest difficulty in calculating the peak current ratio lies in determining the correct base line for measuring the reverse (anodic) peak current. Traditionally, the decay of the forward (cathodic) current is chosen as the base line for anodic peak measurement. However, to apply this method, one should obtain two voltammograms, one linear, one cyclic, both plotted out on a recorder with a time base. Alternatively the potential can be held at E_{ap} until the current falls to zero before commencing the reverse scan. Graphical or algebraic methods are also employed which rely only on the current-potential information of the conventional cyclic voltammogram. These include subtracting a base line extrapolated from the falling portion of the forward branch and the semiempirical method of Nicholson (16). Although the latter was developed to obtain the peak current ratio for LSV for a particular type of EC reaction, it has achieved much wider use because it is simple. In the present work we have calculated the anodic peak current based on the extended forward scan ($E < E_{ap}$) and investigated in detail the range over which Nicholson's equation applies to this case. We also present complete calculations for the case in which the reverse peak height is measured with respect to the zero of current.

THEORY

The theory presented here for staircase voltammetry is based on previous work done by O'Dea et al. (17) for square wave voltammetry.

For a simple reversible system complicated by electrode kinetics



the Erdey-Gruz and Volmer equation can be applied as a boundary condition

$$i(t) = nFA\kappa\epsilon^\alpha [D_O^{1/2}C_O(0,t) - \epsilon D_R^{1/2}C_R(0,t)] \quad (1)$$

where

$$\kappa = k_a^\circ / D_O^{(1-\alpha)/2} D_R^{\alpha/2} \quad (2)$$

and

$$\epsilon = \exp(nF(E - E_{1/2})/RT) \quad (3)$$

and the other symbols have their usual electrochemical significance.

To further simplify eq 1 and make it independent of experimental constants such as A (electrode area), the current $i(t)$ is made dimensionless by using the following relationship:

$$i(t) = \psi(t)nFAC_0(D_O/\pi t)^{1/2} \quad (4)$$

where $\psi(t)$ is the dimensionless current to be calculated.

If eq 4 is substituted into eq 1 and surface concentrations are converted to their integral forms, the following relationship is obtained:

$$\psi(t) = \kappa\epsilon^\alpha \left[\pi^{1/2}\tau^{1/2} - ((1 + \epsilon)/\pi^{1/2}) \int_0^t \psi(u)/(t - u)^{1/2} du \right] \quad (5)$$

In order to evaluate the integral in eq 5, the step function method presented by Nicholson and Olmstead (18) was applied; this provides a means of replacing the integral in eq 5 with a finite sum. With rearrangement, the final equation is

$$b(m) = (\pi^{1/2}/2(1 + \epsilon)) - \sum_{i=1}^{m-1} b_i S_k' / (1 + (\pi l)^{1/2}/2\kappa\tau^{1/2}\epsilon^{-\alpha}(1 + \epsilon)) \quad (6)$$

where l is the number of subintervals per step, $S_k' = k^{1/2} - (k - 1)^{1/2}$, b_i is the approximation to $\psi(t)$ at $t = m\tau/l$, and $k = m - i + 1$. Equation 6 was then coded into FORTRAN. All theoretical results were calculated on a Masscomp 5500 series computer.

The cyclic staircase waveform is characterized by a number of evenly spaced steps. The number of steps in the staircase waveform is determined solely by the potential range chosen and the step height. In the present case, a symmetrical waveform is chosen with a potential window of $400/n$ mV and a step height of $5/n$ mV, which yields a staircase waveform consisting of 162 discrete steps.

Since there is a significant period of time during which the potential is held constant (along each tread of the staircase), it is possible to sample the current at any point along the step. Sampling current at various stages along the staircase step results in voltammograms differing in shape and amplitude. A number of investigators have examined this dependence on sampling time, and it has been shown that these characteristics can yield kinetic information (3, 7, 8, 12, 13). As mentioned above, all currents were computed at the end of the step in this study.

In the step function method used for these calculations, each constant potential step is divided up into a number of evenly spaced subintervals over each of which the value of the function, ψ , is approximated by a constant. As the number of subintervals per step (l) is increased, the approximation approaches the true value of ψ . Errors in the approximation are not cumulative. Increasing the number of subintervals, thus decreasing the width of each subinterval, increases accuracy but does so at the price of increased computational time.

The current at the end of the step according to eq 6 is the value obtained for ψ on the last subinterval on each constant potential step. However, the computation is begun by choosing $b_1 = 0$. Therefore it provides a high estimate to the true value. To counterbalance this tendency, and thus to decrease significantly the number of subintervals needed to achieve high precision (ψ values that differ by $< 0.5\%$), therefore decreasing the total time of the calculation, the

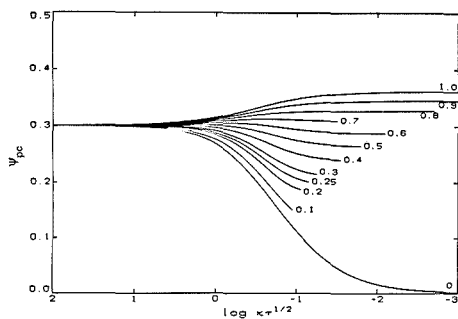


Figure 2. Cathodic peak height (ψ_{pc}) versus $\log(\kappa\tau^{1/2})$ for α values as indicated.

current at the end of the step was approximated by the current at the end of the next subinterval, the potential being held constant. Rapid convergence was achieved by using this method with little change in value (<1%) after 5 subintervals/step. The number of subintervals used in this study was 15.

The resulting voltammogram is a set of 162 discrete normalized current points at specified potentials. To obtain the conventional measures of forward (cathodic) peak potential and current, a parabola was fit to the three largest currents, and the peak potential and current were chosen as the position and amplitude of the maximum of the parabola. The anodic peak was defined in the same way. Measurement of the anodic peak current involved calculating an additional series of voltammograms of the same number of steps but without changing the direction of the potential steps. The cathodic current was referenced to the zero of current, and the anodic current was referenced to the base line obtained through extension of the cathodic curve or to the zero of current.

The data presented were calculated for the case in which the potential is changed from $200/n$ to $-200/n$ mV relative to the reversible half wave potential. Because the potential scale is chosen to be $n(E - E_{1/2}^*)$ the voltammograms are independent of the number of electrons transferred. Peak characteristics are plotted as a function of $\log \kappa\tau^{1/2}$ (where κ is defined by eq 2 and τ is the period or stepwidth of the staircase ($=1/f$)) for various values of α . All curves shown consist of data accumulated for anywhere from 60 to 101 individual voltammograms. The entire range of $\kappa\tau^{1/2}$ values (5 orders of magnitude) could not be determined for all α values due to the fact that a peak could not always be found within the limitation set by the potential range. Also, it should be noted that dimensionless peak current values, peak positions, and peak separations all depend on the step height chosen, but the trend in variation is the same for step heights other than the normalized value $n\Delta E = 5$ mV used here. This is an experimentally convenient value that yields adequate resolution consistent with reasonably rapid experiments.

The value of α in these calculations is varied from zero to unity. Note that α , the transfer coefficient, is an empirical parameter that is related to but in general not equal to the symmetry factor for the energy barrier to charge transfer. A good general description of the symmetry factor is provided by Bockris et al. (19). Delahay (20) and Parsons (21) provide a more thorough discussion of how α is influenced by chemical and electrochemical factors.

RESULTS AND DISCUSSION

Three distinct types of behavior can be seen in Figure 2, which displays the normalized peak current, ψ_{pc} , as a function of $\log \kappa\tau^{1/2}$. Similar trends have been noted for the net peak

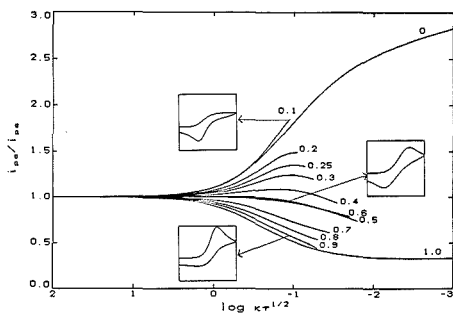


Figure 3. Peak current ratio, i_{pa}/i_{pc} , as a function of $\log(\kappa\tau^{1/2})$ for various α values. Insets show individual voltammograms for α values of 0.1, 0.5, and 0.9 when $\kappa\tau^{1/2}$ is about 0.11.

in square wave voltammetry (17). Reversible, quasi-reversible, and irreversible behavior can all be discerned clearly from the plot of ψ_{pc} as the dimensionless rate constant is varied from 100 to 0.001.

In the first region the values of κ or τ are so large that reversible, fast electron transfer occurs. For SCV, this range encompasses all values of $\log(\kappa\tau^{1/2}) \geq 0.5$. In this region, the system is under diffusion control and all peak positions ($n(E_p - E_{1/2}^*)$), peak heights (ψ), and peak separations ($n(E_{pa} - E_{pc})$) appear at their reversible values, independent of the values of α , κ , and τ .

The intermediate or quasi-reversible range is characterized by a combination of diffusion and charge-transfer control and is an area of particular interest due to the major changes occurring there. For SCV, this encompasses the range $0.5 \geq \log(\kappa\tau^{1/2}) \geq -1.0$. The dimensionless current for the forward (cathodic) peak decreases for $\alpha \leq 0.6$ but increases for values greater than 0.6 as the characteristic time of the experiment decreases. The insets provided in Figure 3 illustrate three individual voltammograms for three different α values for the case where $\kappa\tau^{1/2} = 0.11$, well into the quasi-reversible region. Small values of α correspond to a large energy barrier for the cathodic reaction and thus ψ_p is suppressed, whereas for large values of α , mutatis mutandis, the forward current is enhanced.

The last region is the irreversible region where the value of ψ_{pc} depends on the value of α but not on the value of the dimensionless rate constant over the range $-1.0 \geq \log(\kappa\tau^{1/2}) \geq -3.0$. Since ψ_{pc} is independent of $\log \kappa\tau^{1/2}$ in this region, limiting values of ψ_{pc} should be seen for all α values. However, a cathodic peak is seen in this region only for $\alpha = 0$ and for α greater than about 0.3. For $0 < \alpha \leq 0.3$ the voltammogram was shifted out of the computational range. (There is no intrinsic problem with computing voltammograms in this range. They were simply not done because the very large amount of computation represented here required a systematic approach which for practical reasons excluded more negative potentials.) As $\log \kappa\tau^{1/2} \rightarrow -\infty$, ψ_{pc} approaches a limiting value which depends on the value of α . For $\alpha = 0$, $\psi_{pc} \rightarrow 0$. For $0.1 \leq \alpha \leq 1.0$ the limiting value of ψ_{pc} is given by $\psi_{pc} = 0.08688 + 0.4422\alpha - 0.1717\alpha^2$.

A common criterion for reversible, diffusion-controlled behavior is that the product $i_{pc}\tau^{1/2}$ not vary with pulse width (or analogously in LSV, $i_{pc}/v^{1/2} = \text{constant}$). This is equivalent to the criterion $\psi_{pc} = \text{constant}$. Figure 2 shows that for intermediate values of α this is a very weak criterion, as normalized peak current is a weak function of kinetic parameter. For example, for $\alpha = 0.6$, values of ψ_{pc} may be larger or smaller than the reversible value, $(\psi_{pc})_{rev}$, but the maximum difference, $[(\psi_{pc})_{rev} - \psi_{pc}]/(\psi_{pc})_{rev}$, is less than 5%. This is no larger than

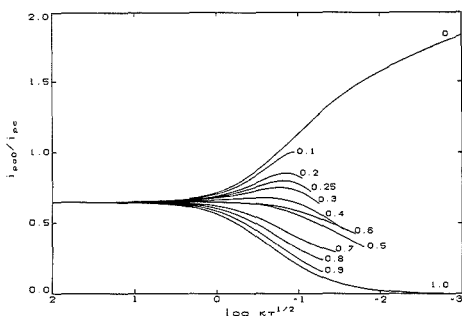


Figure 4. Simplified peak current ratio, $(i_{pa})_0/i_{pc}$, as a function of $\log k\tau^{1/2}$ for various α values.

the error commonly observed in routine experiments.

The ratio of peak currents, i_{pa}/i_{pc} , where i_{pa} is measured against an extended forward base line, is displayed for various values of α as a function of $\log k\tau^{1/2}$ in Figure 3. As for LSV, a ratio of unity for SCV indicates reversible electron transfer. For $\alpha \geq 0.5$ the ratio decreases with a decrease in the magnitude of $k\tau^{1/2}$. The variation in peak current ratio for $0.4 \geq \alpha \geq 0$ is harder to categorize, as the ratio passes through a maximum at about $\log(k\tau^{1/2}) = -1$ for alpha values of 0.2–0.4. The fact that the peak current ratio for $\alpha \approx 0.1$ is always equal to or greater than the ratio for the limiting case of $\alpha = 0$ is an incongruity which is difficult to rationalize, although the shapes of the voltammograms for $\alpha = 0$ and $\alpha = 0.1$ in the range discussed here are becoming increasingly different. For values of α larger than 0.1, the peak current ratio is significantly smaller than for $\alpha = 0$.

Note that the peak current ratios for $\alpha = 0.5$ and $\alpha = 0.6$ in Figure 3 are nearly coincident throughout the entire range of rate constants employed. The peak current ratio for these two alpha values is equal to the reversible value, unity, over a very wide range that extends to about $\log(k\tau^{1/2}) = -1$. Thus for the peak current ratio as well as for the normalized peak current, constancy over a range of τ for intermediate values of α is a very weak criterion for diffusion control and reversibility.

Another aspect of the i_{pa}/i_{pc} curves (Figure 3) worth noting regards the practice of assuming that $\alpha = 0.5$ in lieu of knowing the real value. If this is done in the range where $i_{pa}/i_{pc} < 1$, then an experimental determination of the normalized rate constant, κ , using the working curve presented here would be significantly smaller, by as much as an order of magnitude or more, than the true value, if in fact the real experimental alpha value were larger than 0.5.

Use of an extended forward base line to determine the base line for the anodic peak current presents additional work both for the person doing theoretical work and for the experimenter. Therefore, we looked to other possibilities for determining a diagnostically useful peak current ratio. The most obvious simplification is to measure the anodic current from a zero current base line ($(i_{pa})_0$, Figure 1) instead of from the extended cathodic base line, and then to consider the ratio $(i_{pa})_0/i_{pc}$.

The results of Figure 3 for i_{pa}/i_{pc} can be contrasted with those of Figure 4, which presents in the same format the ratio $(i_{pa})_0/i_{pc}$ based on measurements from the zero of current as illustrated in Figure 1. The ratio $(i_{pa})_0/i_{pc}$ is quantitatively different from i_{pa}/i_{pc} but should contain the same information. The current ratios of Figure 4 are smaller, as expected. The trends in the two ratios are generally the same. For $\alpha = 0.1$ the value of $(i_{pa})_0/i_{pc}$ is less than it is for $\alpha = 0$, which is the expected result, since it fits a regular trend of decreasing current ratio with increasing α . However, the ratio for $\alpha =$

0.6 is actually larger than for $\alpha = 0.5$ for $\log k\tau^{1/2} < -0.7$ and even begins to overlap with the ratio for $\alpha = 0.4$ at the smallest values of the rate parameter.

The ratio i_{pa}/i_{pc} was originally chosen to characterize cyclic voltammograms because its value is unity for uncomplicated systems. It is not clear that the extra effort and extra uncertainty associated with either measurement or computation of this quantity are warranted by attaching special significance to unity. In fact for $\alpha = 1$ the ratio $(i_{pa})_0/i_{pc}$ approaches zero as $k\tau^{1/2}$ approaches zero, certainly a physically reasonable and perhaps even more pleasing limiting value.

A second alternative to the direct measurement of i_{pa} is to compute the ratio i_{pa}/i_{pc} from other measurements following the treatment of Nicholson for following reactions (16). Nicholson's method requires the values $(i_{pa})_0$ and i_{pc} plus the additional term, $(i_{sp})_0$, which is the value of the reverse (anodic) current measured from the zero of current at the switching potential (Figure 1). Values of i_{pc} , $(i_{pa})_0$, and $(i_{sp})_0$ are then used to calculate the conventional peak current ratio (16)

$$i_{pa}/i_{pc} = (i_{pa})_0/i_{pc} + 0.485(i_{sp})_0/i_{pc} + 0.086 \quad (7)$$

This semiempirical equation was originally developed for linear scan voltammetry for the particular case where a reversible electrochemical reaction is followed by an irreversible chemical reaction ($E_r C_r$). Two further requirements were that $k\tau$ values (where k is the rate constant for the chemical step and τ is the time from $E_{1/2}$ to the switching potential) be in the range of 0.05–1.25 and that the switching potential should be 60/n mV more negative than the cathodic peak potential. Under these conditions, the equation should be accurate to within 1%.

Because of the appeal of this approach eq 7 has been applied to many more systems than that for which it was developed. Of particular interest in relation to this study is the fact that some investigators have used Nicholson's equation to calculate the peak current ratio for cyclic staircase voltammetry (2) and for reversible systems (2, 22–24). We have compared directly the value of the peak current ratio obtained by using the extended base line method and the value obtained by using Nicholson's method for all values of α and $k\tau$ discussed above. The result is that for electrode kinetics, the only region where Nicholson's method (eq 7) can be applied with any confidence is the reversible region, which contains no kinetic information. Furthermore, we were unable to find a simple equation which would predict i_{pa}/i_{pc} from $(i_{pa})_0$, $(i_{sp})_0$, and i_{pc} over an extended range. Therefore, it is suggested that the peak current ratio $(i_{pa})_0/i_{pc}$ (Figure 4) be used, since it is a simple, direct relationship more conveniently and more accurately obtainable both theoretically and experimentally than i_{pa}/i_{pc} .

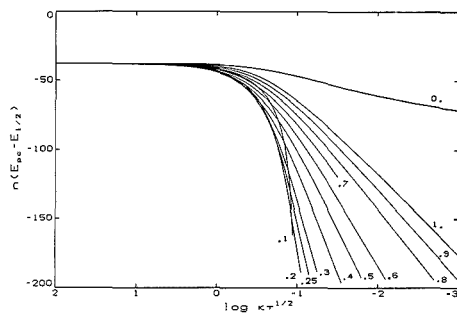
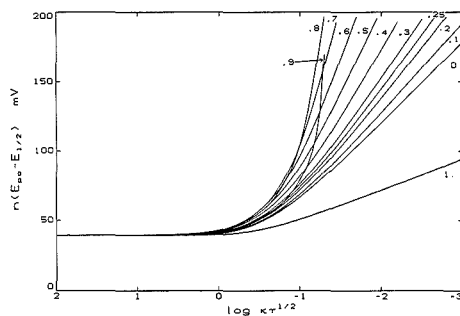
In principle the curves of Figures 2, 3, or 4 could be used together with a value of α and i_{pc} or i_{pa}/i_{pc} for various τ to determine κ , and thus (given D_O and D_R) k_a° . However the dependence of these current functions on the kinetic parameter is generally weak, so except in favorable cases this approach cannot be expected to yield accurate results. Representative peak current values for $\alpha = 0.5$ are provided in Table I.

The peak potential data (Figures 5–7) calculated for the electrode kinetics case are not as straightforward as the current data presented above. The limiting values of $\alpha = 0$ and $\alpha = 1$ show the smallest variation in both cathodic (Figure 5) and anodic (Figure 6) peak potential from the reversible values with a change in dimensionless kinetic parameter. Except for the cathodic peak potential for $\alpha = 0.1$ and the anodic peak potential for $\alpha = 0.9$, there is a gradual but regular trend in peak shifts with α . For these two cases, however, there is a particularly large change in peak position with small changes in $k\tau^{1/2}$ when the value of the latter is approximately 0.1. In general, small α values show the largest shift negative for the

Table I. Dimensionless Peak Current Values for $\alpha = 0.5$

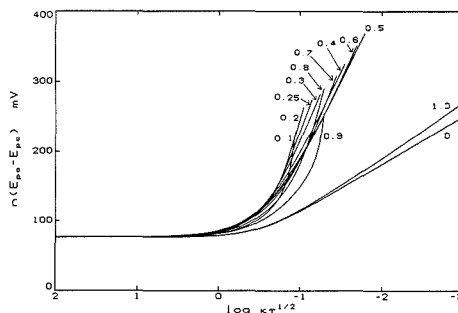
$\log \kappa\tau^{1/2}$	ψ_{pc}^a	ψ_{pc}^b	ψ_{po}^a	ψ_{pa}^b
2	0.3008	0.1945	0.1610	0.3014
1	0.3013	0.1950	0.1614	0.3020
0	0.3021	0.1960	0.1659	0.3037
-0.2	0.3000	0.1938	0.1686	0.3017
-0.4	0.2957	0.1886	0.1728	0.2968
-0.6	0.2892	0.1796	0.1789	0.2879
-0.8	0.2817	0.1673	0.1876	0.2758
-1.0	0.2750	0.1526	0.1996	0.2612
-1.2	0.2702	0.1367	0.2150	0.2452
-1.4	0.2671	0.1206	0.2335	0.2289
-1.6	0.2654	0.1044	0.2519	0.2125
-1.8	0.2646	0.08796	0.2636	0.1959

^a As described in Figure 1. ^b Measured from an extended forward base line.

**Figure 5.** Cathodic peak position, $n(E_{pc} - E_{1/2})$, versus $\log \kappa\tau^{1/2}$ for various α values.**Figure 6.** Anodic peak potential, $n(E_{pa} - E_{1/2})$, for various α values.

cathodic peak potential with decreasing $\kappa\tau^{1/2}$. The opposite trend holds for anodic peak potentials, where for an α value of 0.9 the shift is positive at the largest value of $\kappa\tau^{1/2}$ and then fans out in a regular manner with decrease in $\kappa\tau^{1/2}$ and decrease in α value. The limiting slopes from Figures 5 and 6 for most α values over the range $\log \kappa\tau \leq -0.9$ are presented in Table II. A plot of cathodic slopes/59 mV vs α and (-) anodic slopes/59 mV vs $(1 - \alpha)$ yields curves of the form $\text{csch}(\alpha)$ and $\text{csch}(1 - \alpha)$, respectively.

Due to the opposing nature of the potential shifts for the cathodic and anodic parts of the cyclic staircase curve, the peak separation data (Figure 7) do not display simple trends. Except for the limiting α values of 0 and 1 all peak separations are clustered together in the range of $\kappa\tau^{1/2}$ corresponding to the quasi-reversible region. This provides the possibility of being able to determine κ within less than an order of magnitude error, without knowing α , for all $\kappa\tau^{1/2}$ values studied.

**Figure 7.** Peak separation, $n(E_{pa} - E_{pc})$, for various α values.**Table II. Slopes for $n(E_p - E_{1/2})$ vs $\log \kappa\tau^{1/2}$ (mV/decade)**

α	$n(E_{pc}^a - E_{1/2}^f)$	$n(E_{pa}^b - E_{1/2}^f)$	$\frac{n(E_{pa} - E_{pc})}{(n\Delta E_p)^c}$
0	12.3	-56.21	-68.51
0.1	^d	-62.24	^d
0.2	299.0	-69.76	-399.1
0.25	238.1	-74.28	-315.7
0.3	197.9	-79.52	-270.2
0.4	147.8	-92.88	-231.1
0.5	116.9	-112.6	-224.9
0.6	97.24	-143.0	-235.0
0.7	77.04	-194.0	-268.3
0.8	73.08	-291.8	-353.6
0.9	64.72	^d	^d
1	56.25	-21.68	-77.93

^a From Figure 5. ^b From Figure 6. ^c From Figure 7. ^d Slope $\rightarrow \infty$.

Limiting slopes of ΔE_p vs $\log \kappa\tau^{1/2}$ are compiled also in Table II for most α values. Reversible peak separation (ca. 76/n mV for the 5/n mV step height employed) is obtained for all α values when $\kappa\tau^{1/2} \geq 1$. For α values in the range 0.1–0.9, the maximum value of $\log \kappa\tau^{1/2}$ that can be determined is approximately -1.5. For very small ($\alpha = 0.1$) or very large ($\alpha = 0.9$) values of transfer coefficient, the peak separation increases dramatically with small decrease in $\kappa\tau^{1/2}$ at about $\kappa\tau^{1/2} = 0.1$.

In the mid-1960s, Nicholson (25) presented a working curve for electrode kinetics for cyclic voltammetry that showed a simple correlation between peak separation ($n\Delta E_p$) and rate constant. The working curve covered the range from reversible to nearly irreversible behavior for $\alpha = 0.5$. In that paper, Nicholson commented that the curve was found to be nearly independent of α in the range $0.3 < \alpha < 0.7$. He further noted that as the value of the rate parameter decreased, and ΔE_p increased from 105/n mV to 200/n mV, the variation in ΔE_p as α changed from 0.3 to 0.7 increased from 5% to 20%.

The peak separation data of Figure 7 and Table II suggest a similar relationship for SCV. That is, peak separations seem to be nearly independent of α for values of α in the range 0.3–0.7. To investigate this correspondence in more detail, we chose a value of $n\Delta E_p$, found the corresponding $\kappa\tau^{1/2}$ value for $\alpha = 0.5$, and compared it to the $\kappa\tau^{1/2}$ values obtained by using the same value of $n\Delta E_p$ for α values of 0.3, 0.4, 0.6, and 0.7. The maximum relative percent difference increased from 2.5% to 19.5% when $n\Delta E_p$ increased from 116.0 to 189.6 mV. Thus it appears that the approach of Nicholson can be used with the data of Figure 7 or Table II with the same limitations to determine kinetic parameters from peak separations in SCV. Representative values of $n(E_{pc} - E_{1/2})$ and $n(E_{pa} - E_{1/2})$ are provided in Table III for $\alpha = 0.5$.

The curves presented here are useful for understanding the behavior of a kinetic system when investigated by cyclic

Table III. Peak Potential Values for $\alpha = 0.5$

$\log \kappa \tau^{1/2}$	$n(E_{pc} - E_{1/2}), \text{ mV}$	$n(E_{pa} - E_{1/2}), \text{ mV}$
2	-37.60	39.26
1	-37.96	39.29
0	-43.35	40.92
-0.2	-47.79	42.75
-0.4	-55.22	46.21
-0.6	-66.36	51.43
-0.8	-81.73	58.44
-1.0	-100.9	66.93
-1.2	-122.5	76.57
-1.4	-145.4	86.92
-1.6	-168.8	97.77
-1.8	-192.3	109.0

staircase voltammetry. A further question is their utility for determining values of rate parameters. All of the curves have a range ($\log \kappa \tau^{1/2} \geq 0.5$) over which reversible behavior is obtained. If the behavior cannot be shifted out of this range by changing τ , it is not possible to extract kinetic information. On the other hand, if this region is not accessible, it is difficult to obtain a value of the reversible half-wave potential, without which Figures 5 and 6, which display shifts in E_{pc} and E_{pa} with respect to $E_{1/2}$, cannot be used.

If both peaks are present, and if the value of n is known, the curves of Figure 7 (Table I) can be used, assuming $\alpha = 0.5$, to obtain an approximate value for $\log \kappa$. This may be refined and the assumption of $\alpha = 0.5$ checked by examining the dependence of $(i_{pa})_0/i_{pc}$ on $\log \tau^{1/2}$ according to Figure 4.

If rather slower experiments can be done to reach the limiting values of ψ_p (Figure 2), these can be used to obtain the value of α . However this requires in addition that the normalizing factor $nD^{1/2}$ (eq 4) be known so that ψ_p can be calculated from i_p . It is important to realize that the range from reversible to irreversible behavior ($+0.5 \geq \log \kappa \tau^{1/2} \geq -1.5$) spans 4 orders of magnitude in time scale. It is most unlikely that comparable experiments can be done over such an extended range. Considering the rather weak dependence of ψ_p or α for larger values of α , the requirement that $nD^{1/2}$ be known to use Figure 2 quantitatively is a serious limitation.

Since this presentation is limited to information about the peaked portion of the voltammetric curve, we have effectively ignored the changes in the nature of the overall curves with a change in kinetic parameters, from which it is possible to obtain additional kinetic information. That implies, however, a level of sophistication not readily accessible to or desired

by many experimenters. Peak current and peak potential measurements, which are directly obtainable from cyclic voltammograms, for a series of staircase experiments where only time is varied, can yield kinetic information concerning the value of the heterogeneous rate constant and in some cases the parameter α .

ACKNOWLEDGMENT

The authors gratefully acknowledge a donation of equipment from MASSCOMP and helpful discussions with M. Seralathan.

LITERATURE CITED

- Seralathan, M.; Osteryoung, R.; Osteryoung, J. J. *Electroanal. Chem.* **1986**, *214*, 141.
- Bilewicz, R.; Osteryoung, R. A.; Osteryoung, J. *Anal. Chem.* **1986**, *58*, 2761.
- Seralathan, M.; Osteryoung, R. A.; Osteryoung, J. G. *J. Electroanal. Chem.* **1987**, *222*, 69.
- Wikel, K.; Bilewicz, R.; Osteryoung, R.; Osteryoung, J. *Anal. Chem.* **1989**, *61*, 965-972.
- Ryan, M. D. *J. Electroanal. Chem.* **1977**, *79*, 105.
- Christie, J. H.; Lingane, P. J. *J. Electroanal. Chem.* **1965**, *10*, 176.
- Miaw, L. H. L.; Boudreau, P. A.; Pichler, M. A.; Perone, S. P. *Anal. Chem.* **1978**, *50*, 1988.
- Zipper, J. J.; Perone, S. P. *Anal. Chem.* **1973**, *45*, 452.
- Surprenant, H. L.; Ridgway, T. H.; Reilly, C. N. *J. Electroanal. Chem.* **1977**, *75*, 125.
- Stefani, S.; Seeber, R. *Anal. Chem.* **1982**, *54*, 2524.
- Schachterle, S. D.; Perone, S. P. *Anal. Chem.* **1981**, *53*, 1672.
- Ferrier, D. R.; Schroeder, R. R. *J. Electroanal. Chem.* **1973**, *45*, 343.
- Ferrier, D. R.; Chidester, D. H.; Schroeder, R. R. *J. Electroanal. Chem.* **1973**, *45*, 361.
- Kissinger, P. T.; Heineman, W. R. *J. Chem. Educ.* **1983**, *60*, 702.
- Mabbott, G. A. *J. Chem. Educ.* **1983**, *60*, 697.
- Nicholson, R. S. *Anal. Chem.* **1966**, *38*, 1406.
- O'Dea, J. J.; Osteryoung, J.; Osteryoung, R. A. *Anal. Chem.* **1981**, *53*, 695.
- Nicholson, R. S.; Olmstead, M. L. In *Electrochemistry: Calculations, Simulation and Instrumentation*; Mattson, J. S., Mark, H. B., MacDonald, H. C., Eds.; Marcel Dekker: New York, 1972; Vol. 2, Chapter 5.
- Bockris, J. O'M.; Reddy, A. K. N. *Modern Electrochemistry*; Plenum Press: New York, 1970; Vol. 2, p 917.
- Delahay, P. *Double Layer and Electrode Kinetics*; Wiley-Interscience: New York, 1965; Chapters 7-9.
- Parsons, R. In *Advances in Electrochemistry and Electrochemical Engineering*; Delahay, P., Ed.; Wiley-Interscience: New York, 1961; Vol. 1, Chapter 1, p 29.
- Keszthelyi, C. P. *Electrochim. Acta* **1981**, *26*, 1261.
- Chum, H. L.; Rabockai, T.; Dockal, E. R.; Benedetti, A. V. *J. Electroanal. Chem.* **1979**, *98*, 283.
- Hussey, C. L.; King, L. A.; Wilkes, J. S. *J. Electroanal. Chem.* **1979**, *102*, 321.
- Nicholson, R. S. *Anal. Chem.* **1965**, *37*, 1351.

RECEIVED for review April 10, 1989. Accepted July 14, 1989. This work was supported in part by the National Science Foundation under Grant No. CHE8521200.

Long-Term Stability of Solid Standards for Radiochemical Analysis

Claude W. Sill

Idaho National Engineering Laboratory, EG&G Idaho, Inc., Idaho Falls, Idaho 83415

The long-term stability of -200 mesh solid standards for use in radiochemical analysis has been questioned because of possible fractionation of the different sized particles on standing. Several such standards prepared by spiking -200 to +325 mesh soils with known quantities of various radionuclides were available in this laboratory that, because of some unique circumstance, were known to have been undisturbed for 5 to 15 years. Some standards prepared from naturally occurring uranium ores and mill tailings and then analyzed carefully and repeatedly for ^{230}Th were also available. Small quantities of each standard were carefully removed from a thin layer at the top, middle, and bottom of the sample and analyzed for the radionuclide present by the most sensitive and precise analytical methods available. The relative standard deviations of the individual measurements were generally in the range of 0.2 to 1%. Little or no statistical differences among the three fractions from any of the samples were present at the 95% confidence level.

In a previous publication (1), the present author presented a procedure for the preparation of standard soils containing known concentrations of any artificial nonvolatile radionuclide by spiking natural soil with a standard solution of the desired radionuclide. The soil was passed through standard sieves of both 200 mesh (75 μm opening) and 325 mesh (45 μm opening) and the spike was added to the -200 to +325 mesh fraction. At the time of preparation, these standards were not detectably inhomogeneous with the smallest sample sizes and most sensitive analytical conditions that could be employed. During the subsequent 15 years, many such standards have been prepared by the same procedure for ^{90}Sr , ^{239}Pu , ^{60}Co , etc. for use in internal quality control and have also been analyzed by several different laboratories. Not a single instance of inhomogeneity, instability, or deviation from the calculated value has been observed. The only change recommended even now would be to include about 1% of a surfactant (2) (Aerosol no. 200, American Chemical Enterprises, Inc., St. Louis, MO) to improve flowability and prevent formation of powder balls, particularly with soils having a high percentage of particle sizes smaller than 325 mesh.

Several authors have questioned the long-term stability of such standards because of possible segregation of the different sizes of particles. Referring in part to the previous procedure, Bowen and Volchok (3) state "In neither of the two foregoing references was the long term integrity of the final product tested." After discussing the published experiences of others in this respect, the same authors conclude "It appears, therefore, that both the Sill and Hindman (1974) and NBS (1978) procedures for making standards do indeed provide for long shelf lives." Recently, Olson and Bernabee (4) renewed the controversy with the unequivocal statement that "One of the important findings learned from the study is that -200 mesh material does not remain homogeneous on standing." However, their experimental evidence for this statement

was not persuasive for several reasons (5), particularly because of the relatively poor precision with which their analytical measurements were made and the way in which their standards were prepared.

Several of the spiked standards prepared previously were still available in the author's laboratory. Unfortunately for the present purpose, many of them have been used so frequently by so many others that the time since they might last have been mixed significantly cannot be stated with any certainty. However, a few were still available whose previous storage history was known with confidence because of some unique circumstance. In addition, several -200 mesh standards of uranium ores and mill tailings that had been analyzed carefully and repeatedly for ^{230}Th were also available. Many of them had never been out of the present author's personal possession and had been stored untouched for up to 24 years since their last use. It is the purpose of the present paper to present the results of careful reanalysis of these aged standards in profile and the evidence as to the length of time since they could have been mixed or disturbed in any way. It was particularly important that the measurements be as precise and reliable as possible so that the conclusions would not be obscured by imprecise data.

EXPERIMENTAL SECTION

Procedure. The wide-mouth bottle containing the standard was carefully removed from its storage area and uncapped without allowing any movement of the material inside. By use of a microspatula with its tip bent into an "L" shape, a thin layer of the standard was removed as carefully and uniformly as possible over the entire surface without tilting the container. With an "L"-shaped teaspoon, the bulk material was removed about half way to the bottom, again without tilting the container, and another sample was carefully removed with the microspatula over the entire area. The bulk material was again removed with the teaspoon and a third sample was taken with the microspatula from the remaining material barely covering the bottom of the jar.

With standards containing γ emitters, the layer removed was about 6 mm thick to obtain enough sample to permit the high precision desired to be obtained in reasonable counting times. Identical weights of the top, middle, and bottom layers were placed directly into counting bottles, packed down until the heights were exactly the same, and counted in contact with the same lithium-drifted germanium detector (GeLi) for the same length of time. The photopeaks were also integrated over identical energy intervals. Results were expressed in terms of counts per minute (cpm) because only comparative results were necessary and counting efficiencies were not available for the conditions used. Each result given below is accompanied by an uncertainty expressed as the standard deviation showing the precision with which each measurement was made. Every statistical uncertainty incurred anywhere in the entire measurement process has been propagated to the final result.

For analyses of uranium ores and mill tailings for ^{230}Th by chemical separation and α spectrometry, layers only about 2 mm thick were removed to give about 5 g of total material for analysis. From 0.25 to 1 g of sample was fused with potassium fluoride in the presence of ^{234}Th tracer to guarantee complete sample dissolution and exchange with tracer and analyzed for ^{230}Th as described elsewhere (6). All three layers of each sample were always counted in the same counter to minimize errors due to

uncertainties in the counting efficiencies. Again, all statistical uncertainties are included in the standard deviations given.

RESULTS AND DISCUSSION

Cesium-137 Standard. About 2600 g of this standard had been prepared by the spiking procedure described (1) and had been stored in two completely filled 1-qt fruit jars, the contents being about 15 cm high and 7 cm in diameter. All material used since its preparation has been taken from bottle number 1, while bottle number 2 has remained on the storage shelf untouched until now, 55 months after its original preparation. Exactly 25.000 g was counted for 48 h to obtain about 4.4×10^5 total counts in the photopeak, giving a relative standard deviation of each count of 0.14%. For the top, middle, and bottom layers, the results obtained were 151.8 ± 0.2 , 151.5 ± 0.2 , and 151.2 ± 0.2 cpm, respectively, which are not statistically different from each other at the 95% confidence level.

Lack of any detectable difference in specific activity in 4.5 years between two 25-g aliquots in layers 6 mm thick out of 1300 g, separated from each other by 15 cm, and measured with a relative standard deviation of 0.14% justifies a conclusion that "no" separation has occurred. Furthermore, it is highly unlikely that such standards will ever be used in practical work under as sensitive and precise conditions as those used in this comparison.

Cobalt-60 Standard. This standard was made up at the same time and stored under the same conditions described above for the cesium standard. The analysis was also carried out as described for cesium except that a 50-g aliquot had to be used to give even half the total number of counts because of a lower activity and counting efficiency. The results for the top, middle, and bottom layers were 72.07 ± 0.17 , 71.98 ± 0.17 , and 71.77 ± 0.17 cpm, respectively, using the 1173-keV peak, and 64.68 ± 0.15 , 64.41 ± 0.15 , and 64.59 ± 0.15 cpm, respectively, using the 1333-keV peak. As with the cesium results, there is no statistical difference among the results.

Americium-241 Standard. In November 1983, a soil standard containing $(1.307 \pm 0.007) \times 10^3$ pCi/g of ^{241}Am was prepared by spiking as described (1) for use in γ spectrometry. This sample was stored in a single large bottle only three-quarters full and used frequently so that the time since the bottle might have been inverted or otherwise disturbed cannot be determined with any certainty. Fortunately, 100.0 g of the standard was diluted gravimetrically with 2400 g of diluent soil to give a 25-fold dilution, or 52.3 ± 0.3 pCi/g, and was never used or made available to others. The solid material occupied a volume 15.0 cm high by 11.8 cm in diameter and had been undisturbed for 65 months before the present fractions were removed.

About 23 g was removed from each of the three levels, and 21.216 g of each was packed reproducibly in identical Petri dishes and counted on the Ge(Li) spectrometer for 50 h. By use of the 59.5-keV photopeak, the counting rates of the top, middle, and bottom layers were 77.86 ± 0.20 , 77.85 ± 0.20 , and 77.99 ± 0.20 cpm, respectively. Obviously, no separation was detected with measurements made with a relative standard deviation of 0.26%. As was found in the previous work (1), these results also show that -200 mesh homogeneous solids can be diluted gravimetrically without producing either detectable particle inhomogeneity or long-term instability. The higher-level standard from which the dilution was made was prepared by diluting 93.0 g of spiked material to 2665.1 g with soil for a dilution of 28.7-fold. With the subsequent 25-fold dilution, the standard being tested for fractionation resulted from a total dilution from the original spiked material of 716-fold without any evidence of particle inhomogeneity having been produced.

Pitchblende Ore Standard. In 1964, about 15 kg of pitchblende ore known to be primary unaltered material in

secular equilibrium was thoroughly ground, passed through a 200 mesh screen, blended for 24 h, and packaged in pint and half-pint fruit jars. Ten analyses for total uranium were made on five separate bottles by an accepted volumetric procedure. By use of accepted values of the half-lives and abundances, the activity of the ^{238}U chain was calculated from the mass concentration to be $(2.73 \pm 0.02) \times 10^3$ pCi/g. During the ensuing 25 years, this material has been analyzed extensively by several different laboratories for all significant members of both the ^{238}U and ^{235}U chains without any evidence of inhomogeneity or deviations from the calculated values being observed. Several of the half-pint bottles of standard were still stored in a warehouse in the same large compartmented packing crate, covered with dust, in which the packaged material had been shipped to the author's laboratory originally. The storage conditions lend considerable confidence that the samples had not been disturbed since they were received. One of these bottles of standard was used in the present tests.

Samples of only 0.25 g from each layer were fused with potassium fluoride in the presence of ^{234}Th tracer and analyzed for ^{230}Th by high-precision α spectrometry (6). Each sample was counted until about 1.2×10^5 counts had been accumulated in the ^{230}Th peak. The results for top, middle, and bottom layers were (2.76 ± 0.03) , (2.80 ± 0.03) , and $(2.80 \pm 0.03) \times 10^3$ pCi/g, respectively. All results are statistically identical at the 95% confidence level to each other and to the known value of the standard within a relative standard deviation of about 1%. The solid material in the small half-pint bottle was 56 mm in diameter and 3 cm between the top and bottom fractions. Because of the long standing time, the small sample size, and the relatively large distance between layers, and the high precision of these measurements, it is highly unlikely that anyone will ever have a problem with separation of the material.

Diluted Pitchblende Ore. In August 1975, some of the pitchblende ore standard mentioned above was diluted gravimetrically with low-blank soil for the Environmental Protection Agency (EPA) to provide a less-radioactive standard for use in their quality control cross-check program. The value calculated from the dilution and the known value of the ore standard given above was 254 ± 2 pCi/g. A bottle containing about 400 g of this material, the contents being 9.5 cm high by 6.9 cm in diameter, was retained by the author for his own use. However, the material was never used or made available to others.

The diluted pitchblende ore standard was analyzed for ^{230}Th in the same way as the more radioactive standard described above except that 0.5-g samples and 24-h counting times were used to give about 9×10^4 total counts in the ^{230}Th peak to keep the relative standard deviation around 1%. The results for top, middle, and bottom layers were 251 ± 2 , 250 ± 2 , and 259 ± 2 pCi/g, respectively. There is a small but statistically positive difference at the 95% confidence level between the top and bottom fractions but not between the top and middle fractions. It is suspected that this difference was caused by a slight curl that was noticed on the mounted filter from the bottom layer which would increase the counting efficiency. However, even if the difference is real, it could not be more than a few percent and is not significant for a 14-year old sample, with 0.5-g aliquots taken from layers only 2 mm thick and separated by 9.5 cm. This sample demonstrates again "That solids can be made to act almost like liquids with respect to homogeneity and dilution..." (1). It is interesting to note that Donovan et al. (7) obtained 251 ± 1 pCi/g for the mean and experimental standard deviation of two to five analyses of this same material obtained from EPA. Although the age, size, and storage conditions of their sample are unknown, there

is no significant difference discernible in the results.

Climax Sand Tailings Standard. In July 1975, several kilograms of uranium mill tailings was ground to pass a 200 mesh screen, blended for 48 h to ensure homogeneity, and analyzed ten times for ^{230}Th in the presence of ^{234}Th tracer by total dissolution and high-resolution α spectrometry. The most precise analytical result obtained at that time was 266 ± 3 pCi/g (590 ± 7 dpm/g) (8). Most of this material was turned over to EPA for use in their quality control cross-check program. About 700 g was retained by the author but was never used until the present investigation. The solid material in the container was 10.5 cm high by 8.2 cm in diameter. The analytical measurements for the top, middle, and bottom layers were 274 ± 3 , 274 ± 3 , and 282 ± 3 pCi/g, respectively. The top and middle fractions might be slightly higher statistically at the 95% confidence level than the original measurements. This agreement is very gratifying considering the 12-year difference in time and expertise, different instruments, different tracers, etc. However, the bottom fraction might be slightly higher statistically than either the top or middle fractions as was observed with the diluted pitchblende sample. For the same reason, it is felt that this is another analytical artifact. However, the difference is negligible for fractions of a 14-year old sample separated by 10.5 cm and measured with a relative standard deviation of about 1%. Donovan et al. (7) also analyzed this sample and obtained a value of 263 ± 1 pCi/g for the mean and experimental standard deviation of two to five analyses.

Diluted Climax Sand Tailings Standard. Also in July 1975, part of the above tailings standard was diluted gravimetrically with low-background soil to provide a lower-activity standard for EPA. The dilution factor was 0.1290 \pm 0.0001 of the tailings standard above or a calculated activity of 34.3 ± 0.4 pCi/g from the dilution plus 0.9 pCi/g for the ^{230}Th in the soil used for dilution for a total of 35.2 ± 0.4 pCi/g. Again, about 400 g of the standard was retained in the author's laboratory but was never used until now. The solid material in the bottle was 9.0 cm high by 6.9 cm wide. The analytical results obtained for the top, middle, and bottom layers using 1-g samples and 24-h counting times were 35.0 ± 0.3 , 36.0 ± 0.3 , and 35.5 ± 0.3 pCi/g, respectively. There is no evidence of fractionation of the particles over a distance of 9 cm in 14 years when measured with a precision of 1% relative standard deviation. These results also show again the excellent results that can be obtained by gravimetric dilution. Donovan et al. (7) also analyzed this sample with a result of 34 ± 1 pCi/g for the mean and experimental standard deviation of two to five measurements.

Particle Size Measurements. To determine how large a difference there might be in the specific activity of the different sized particles, 10 g of the higher ^{241}Am standard containing $(1.307 \pm 0.007) \times 10^3$ pCi/g mentioned above was dry screened through a 500-mesh ($25 \mu\text{m}$ opening) standard sieve. Equal weights of both fractions and the standard soil were counted in contact with the Ge(Li) detector under identical counting conditions. The -500 mesh fraction contained only 16.4% of the total mass and gave a counting rate in the 59.5-keV ^{241}Am photopeak of 120.5 ± 0.9 cpm/g. The +500 mesh fraction, which is also -200 mesh from the original preparation, contained 77.1% of the mass and gave a counting rate of 110.2 ± 0.9 cpm/g. The counting rate of the standard actually obtained was 118.3 ± 0.9 cpm/g. The specific activities have thus increased by $1.9 \pm 1.1\%$ for the -500 mesh fraction and decreased by $6.8 \pm 1.0\%$ for the +500 mesh fraction compared to the standard. The 6.5% of the mass unaccounted for was presumably caused by dusting of the fine fraction during the severe screening required and the mechanical losses to the screen and pan. Regardless of whether

the loss is assigned to the -500 mesh fraction, or ignored and the calculation made for the actual mass recovered, the composite counting rate of the original sample can be calculated to be about 112.6 ± 0.7 cpm/g. The material balance is about 5% low, probably due to a slight difference in the actual peak areas integrated in the high Compton continuum around the 59.5-keV peak. However, the conclusion that there is very little effect of particle size on the counting rate is obvious.

To determine whether or not fractionation might be enhanced by wet screening, 5,000 g of the same ^{241}Am standard soil was washed thoroughly through a 500 mesh screen with 95% ethanol. The -500 mesh fraction contained 23.6% of the mass and gave a counting rate of 109.2 ± 0.4 cpm/g. The +500-mesh fraction contained 74.3% of the mass and gave a counting rate of 55.1 ± 0.3 cpm/g. The measured rate of the standard was 71.6 ± 0.5 cpm/g for the same counting conditions. These measurements were made in a plastic holder about 6 mm above the detector to improve the precision of counting and are lower than those given above because of the consequent decrease in the counting efficiency. The specific activities are significantly different than those obtained with dry sieving, the -500 mesh fraction being $52.5 \pm 0.9\%$ higher and the +500 mesh fraction being $23.0 \pm 0.9\%$ lower than the untreated standard. The 2.1% missing is again due to experimental error in the measurements. The ethanol used in screening contained a slight residue on evaporation to dryness but no detectable activity. The composite counting rate of the standard can be calculated to be 68.1 ± 0.4 cpm/g, again giving a material balance that is about 5% low.

The dry-screening results show why spontaneous segregation of particles is neither observed nor expected from dry samples. In the first place, there is very little material present that is smaller than 500 mesh. Other soils might be somewhat different, but the soil used in these tests is thought to be fairly average. Secondly, with use of material whose largest particles are already as small as 200 mesh, there is not a very large range of particle sizes available to induce separation. If complete separation of the -500 mesh fraction from the -200 to +500 mesh fraction produces a maximum change in specific activity of only 7%, spontaneous fractionation should never be detectable over time.

The 44% relative increase in the -500 mesh fraction resulting from wet-screening with alcohol demonstrates quantitatively an important fact that can be confirmed visually. If a +200 or +325 mesh fraction of soil is shaken with a little water, a suspension of very finely divided particles is easily visible after the heavier particles have settled that will readily pass through a 500 mesh screen. This behavior indicates that many 200 mesh particles are not individual particles but are actually 200 mesh aggregates of much smaller particles that can be broken up easily on mixing with liquids. This fact is also partially responsible for an apparent anomaly in the present work. The ^{241}Am soil standard used in these screening tests was prepared originally by screening soil through both 200 and 325 mesh sieves and spiking 100 g of the -200 to +325 mesh fraction. In other words, the spike was added to a fraction from which all particles smaller than 325 mesh had been removed. Yet, most of the activity per gram ends up in the -500 mesh fraction added later in the 2572 g of -200 mesh soil diluent. Apparently, when the soil was slurried with water prior to adding the radioactive spike solution, the 200 mesh aggregates were dispersed, giving some -500 mesh particles on which the activity was subsequently dried. The number of -500 mesh particles containing activity was also undoubtedly increased by the extensive grinding required to get all the spiked material back through a 200 mesh screen after drying and ignition.

From the data presented, it is clear that the separation of different sized particles from -200 mesh dry standards over years of time is certainly less than the precision with which such differences can be measured using the most precise measurement techniques available. This of course requires that the standard be homogeneous to begin with and does not contain high specific activity particles. Perhaps the most important recommendation in the previous procedure (1) is to ensure that the spike activity is uniformly distributed over a very large number of particles by physically stirring the spiked mud continuously until dried to immobility, permitting no separation of liquid phases that could evaporate and form "hotspots". However, it would probably be prudent to shake solid standards moderately each time they are used as an added precaution.

Registry No. ^{137}Cs , 10045-97-3; ^{60}Co , 10198-40-0; ^{241}Am , 14596-10-2; ^{230}Th , 14269-63-7.

LITERATURE CITED

- (1) Sill, C. W.; Hindman, F. D. *Anal. Chem.* **1974**, *46*, 113-118.
- (2) Trahey, N. M., Department of Energy, New Brunswick Laboratory, Argonne, IL, private communication, 1982.
- (3) Bowen V. T.; Volchok, H. L. *Environ. Int.* **1980**, *3*, 365-376.
- (4) Olson, D. G.; Bernabee, R. P. *Health Phys.* **1988**, *54*, 451-459.
- (5) Sill, C. W. *Health Phys.* **1989**, *57*, 207-208.
- (6) Sill, C. W. *Waste Manage.*, in press.
- (7) Donivan, S.; Hollenbach, M.; Costello, M. *Anal. Chem.* **1987**, *59*, 2556-2558.
- (8) Sill, C. W. *Health Phys.* **1977**, *33*, 393-404.

RECEIVED for review June 19, 1989. Accepted July 21, 1989. Work performed under the auspices of the U.S. Department of Energy, DOE Contract No. DE-AC07-76ID01570.

Electrocatalysis and Detection of Amino Sugars, Alditols, and Acidic Sugars at a Copper-Containing Chemically Modified Electrode

Sunil V. Prabhu and Richard P. Baldwin*

Department of Chemistry, University of Louisville, Louisville, Kentucky 40292

Chemically modified electrodes (CMEs) produced by deposition of a Cu/Cl-containing crystalline species onto glassy carbon exhibited stable electrocatalytic oxidation of numerous polyhydroxyl compounds including carbohydrates, amino sugars, alditols, and aldonic, uronic, and aldaric acids. In cyclic voltammetry, the electrocatalysis appeared as an irreversible anodic wave that occurred only at hydroxide concentrations of at least 10^{-3} M and was centered at +0.5 V vs Ag/AgCl. The CMEs were readily adapted for constant-potential amperometric detection of these compounds in flow injection analysis and liquid chromatography. When used in this fashion, the electrodes provided detection limits in the nanomole-to-picomole range and were compatible with a relatively wide range of anion-exchange chromatography mobile phases. Examples of possible applications included the separation and quantitation of amino sugar mixtures, antibiotics, and mono- and disaccharides in tobacco.

INTRODUCTION

The development of novel electrode materials for use in the detection of carbohydrate compounds is currently an area of very active investigation. The most important of the approaches reported to date have utilized either metallic electrode substrates, such as platinum (1-3), gold (4-8), and nickel (9-11), or surface-attached metal electrocatalysts, such as cobalt phthalocyanine (CoPC) (12-14), to obtain enhanced carbohydrate oxidation over that seen at conventional carbon electrodes. Thus far, all of these electrodes have been shown to enable direct detection of carbohydrates, without derivatization, at the nanomolar level or below; and the platinum and gold systems form the basis of the commercially available liquid chromatography/electrochemical detection (LCEC) units currently recommended for carbohydrate analysis. The primary drawbacks common to these electrode systems are (1) their requirement for strongly alkaline solution conditions

in order for appreciable carbohydrate oxidation to occur and (2) the need for a pulsed potential waveform in order for stable and reproducible operation to be maintained over an acceptable length of time.

Very recently, our group has described the construction and use of a new Cu-based chemically modified electrode (CME) whose performance in carbohydrate oxidation and detection appears to be superior to these systems in nearly every respect (15). For example, the Cu CME was shown to provide detection limits on the order of 1-5 pmol for most mono- and disaccharides. Furthermore, because the detection was performed at a constant potential with no need for specialized pulse sequences to enhance electrode stability, the CME was completely compatible with the simple constant-potential LCEC units already in common usage among chromatographers. In this work, we have characterized more fully the nature of the Cu CME surface and have extended its range of application beyond the simple sugars previously considered. In particular, the Cu CME has been shown to offer sensitive and selective constant-potential detection for alditols, acidic sugars, and amino sugars as well.

EXPERIMENTAL SECTION

Reagents. Carbohydrates and related compounds were purchased from Sigma or Fisher, and stock solutions were prepared fresh daily in deionized water. Just prior to use, the stock solutions were adjusted to the desired concentration and pH by addition of the appropriate hydroxide-containing diluent. Mobile phases used for flow injection and liquid chromatography were prepared from carbonate-free NaOH and thoroughly degassed deionized water.

Sugar samples were obtained from flue-cured McNair No. 944 tobacco leaves (provided by Brown & Williamson Tobacco Corp. Research and Development, Louisville, KY) by extracting a known weight of tobacco with a 40:60 acetonitrile/deionized water solvent adjusted so that the tobacco concentration was approximately 0.1 g/L. The extraction was allowed to continue for 60 min with frequent manual stirring during this period. The sample used for injection onto the chromatograph was obtained by passing

the acetonitrile/water solution through a 0.22- μ m Millex-GS filter to remove particulates and diluting with deionized water to bring the sugar concentrations down into the linear range of the CME/LCEC method.

Electrodes. Electrode modification procedures were similar to those described in a previous communication (15). A freshly polished thin-layer glassy carbon electrode (Bioanalytical Systems, West Lafayette, IN) was immersed in a 0.050 M CuCl_2 solution for 5 min. At this point, a white deposit appeared on the glassy carbon surface and the CME was ready for use. During exposure to the CuCl_2 , it was necessary to immerse the entire electrode assembly, including the metallic leads, in order for the catalytically active deposit to develop. Although this remains to be verified, it appears likely that the initial surface modification results from interaction of the Cu(II) solution with metallic Cu from the electrode contacts to form a Cu(I) salt such as CuCl . Initial exposure of the electrode to strong base, used previously (15) to condition the glassy carbon surface prior to deposition of the copper film, was not essential for the formation of an electrocatalytically active CME in flow experiments but did appear to enhance the electrode's cyclic voltammetry response. The activity of the modified electrode could be restored to that of the original glassy carbon by polishing with alumina.

Apparatus. Cyclic voltammetry was performed with a Bioanalytical Systems Model CV-1B potentiostat with a Model MF1000 glassy carbon working electrode (modified or unmodified), an Ag/AgCl (3 M KCl) reference electrode, and a platinum wire auxiliary electrode. Flow injection and liquid chromatography experiments were carried out with either a Waters Model M-45 or a Beckman Model 110B pump, a Rheodyne (Berkeley, CA) Model 7125 injector with a 20- μ L sample loop, an SSI Model LP-21 pulse dampener, and an IBM Model EC/320 electrochemical detector. All chromatographic separations utilized either a 25-cm-long, 4-mm-i.d. Dionex CarboPac PA1 or a 15-cm-long, 4-mm-i.d. Dionex HPIC AS6A-5 μ anion-exchange column maintained at room temperature.

Surface imaging and X-ray fluorescence measurements were performed with an International Scientific Instruments Model SS60 scanning electron microscope equipped with an energy dispersive EDAX Model 9900 detector.

RESULTS AND DISCUSSION

Electrochemistry. In our initial report (15), the Cu CME itself was shown to exhibit one principal redox wave in strongly alkaline solution. It was suggested that this wave, which occurred at +0.45 V vs Ag/AgCl and was seen only on the initial cyclic voltammetry (CV) scan for each CME, might correspond to a Cu(II)/Cu(III) oxidation process similar to that obtained earlier by Miller (16) at a metallic copper electrode under similar conditions. The catalytic oxidation of glucose and other simple mono- and disaccharides at the CME was observed as a long-lived increase in the current at this potential that was directly proportional to the sugar concentration employed and to the square root of the potential scan rate (up to 50 mV/s). In the course of this work, analogous electrocatalytic currents were seen for a variety of polyhydroxyl compounds in addition to the carbohydrates originally reported. Representative examples are illustrated in Figure 1, which shows CVs obtained at the Cu CME for 1.0 mM solutions of glucose, glucitol, gluconic acid, glucuronic acid, glucaric acid, and glucosamine. All the CVs were quite similar, containing a broad oxidation in the +0.4–+0.6-V region. The exact peak potentials seen for each compound varied slightly; but other than this, the CVs were virtually the same. Similar electrocatalyses obtained at the CME for an extensive series of carbohydrates and related polyhydroxy compounds are summarized in Table I. Included in this compilation are not only larger oligosaccharides up to maltoheptose (no larger polysaccharides were examined) but also all alditols, aldonic acids, uronic acids, aldaric acids, and amino sugars examined. None of these compounds exhibited any significant current in CV when an unmodified working electrode was employed in place of the Cu CME.

Table I. Electrochemical Behavior of Polyhydroxyl Compounds at the Cu CME

compound	CV peak potential, V vs Ag/AgCl	FIA detection limits, ^a ng
I. Monosaccharides		
glucose	+0.50	0.2
galactose	+0.52	0.2
fructose	+0.53	0.2
ribose	+0.53	0.2
xylose	+0.50	0.2
arabinose	+0.40	0.2
II. Disaccharides		
lactose	+0.60	0.4
maltose	+0.60	0.7
sucrose	+0.60	0.7
trehalose	+0.60	0.7
III. Oligosaccharides		
maltotriose	+0.60	0.6
maltotetrose	+0.60	1
maltopentose	+0.60	1
maltohexose	+0.60	2
maltoheptose	+0.60	2
IV. Amino Sugars		
glucosamine	+0.53	0.3
galactosamine	+0.50	0.3
<i>N</i> -acetylglucosamine	+0.60	0.9
<i>N</i> -acetylgalactosamine	+0.60	0.9
V. Alditols		
methanol	NR ^b	NR ^b
ethylene glycol	NR ^b	NR ^b
glycerol	+0.40	0.2
erythritol	+0.45	0.2
ribitol	+0.45	0.1
glucitol	+0.45	0.2
VI. Aldonic Acids		
gluconic acid	+0.45	0.3
galactonic acid	+0.43	0.3
gulono- γ -lactone	+0.45	0.2
gluconolactone	+0.45	0.2
VII. Uronic Acids		
glucuronic acid	+0.50	0.2
galacturonic acid	+0.50	0.3
VIII. Aldaric Acids		
tartaric acid	+0.60	0.3
glucaric acid	+0.50	0.3
galactaric acid	+0.50	0.3
IX. Antibiotics		
streptomycin sulfate	+0.60	6
kanamycin sulfate	+0.60	2
digitoxin	NR ^b	NR ^b
erythromycin	NR ^b	NR ^b

^a Potential applied, +0.50 V vs Ag/AgCl ; signal/noise, 3. ^b NR, no response.

A critical feature of these CVs, from an analytical viewpoint, was that the catalytic oxidations seen at the Cu CME all occurred reproducibly at modest positive potentials. In fact, the electrode was sufficiently well-behaved toward the compounds examined that CV could typically be continued for several hours (encompassing hundreds of individual cycles) with no decrease in the current levels obtained. An important consequence of these observations was that the CME was well-suited for stable, constant-potential detection of these compounds in liquid chromatographic and flow injection schemes. This is unlike the situation with electrodes such as Pt (1–3), Au (4–8), and CoPC-containing carbon paste (12–14), which, when used for carbohydrate detection in LCEC, require the application of a pulsed potential waveform for stable, long-term operation to be realized. As a result, it was an easy

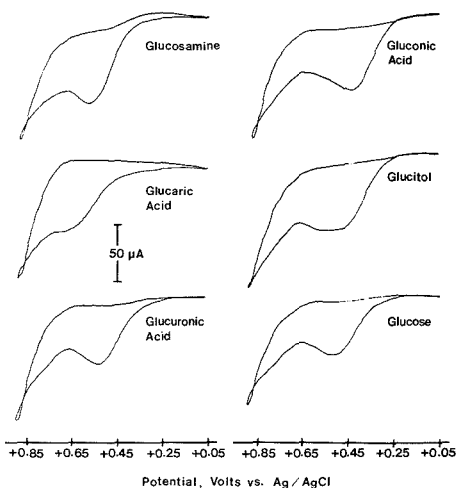


Figure 1. Steady-state cyclic voltammograms of 1.0 mM glucose, glucitol, gluconic acid, glucuronic acid, glucaric acid, and glucosamine at Cu CME: electrolyte, 0.15 M NaOH; scan rate, 20 mV/s.

matter to transfer the Cu CME to a thin-layer flow cell arrangement and characterize its performance as a detector element for polyhydroxyl compounds in flow injection analysis. The qualitative outcome of such flow experiments was exactly what would be expected on the basis of the voltammetric behavior seen in Figure 1. In particular, hydrodynamic voltammograms obtained under flow conditions for compounds from each of the families of carbohydrate derivatives were nearly identical, exhibiting oxidation currents starting at potentials in the neighborhood of +0.2 V vs Ag/AgCl and reaching maximum levels between +0.5 and +0.6 V. This is essentially the same hydrodynamic current-voltage behavior as that seen previously for glucose and other simple sugars at the Cu CME (15). The quantitative results of the flow experiments, shown as the detection limits (signal/noise = 3) obtained at the CME for the same compounds, are also provided in Table I. In nearly all cases, promising detection limits, nearly always below the nanogram level, were obtained. An applied potential of +0.5 V vs Ag/AgCl was chosen for use, even for compounds whose CV peak potential was somewhat more positive, because the high background currents due to solvent oxidation at higher potentials more than offset any increase in analyte current that could be so obtained. Finally, the stability of the CME's response in the flow system, though not perfect, appeared to be adequate for routine quantitative applications. For example, 60 repeated injections of 1.0×10^{-5} M gluconic acid over a period of approximately 1 h produced only an 8% decrease in the peak height observed at +0.5 V. Furthermore, the relative standard deviation of these measurements was only 4.9%. In general, the Cu CMEs did show a gradual decrease in response during continuous usage over extended periods—with the rate of the decrease dependent largely on the mobile phase flow rate in effect. However, as long as their response was periodically recalibrated, the electrodes could typically be placed in the flowstream and used continuously for periods as long as a few days before renewal of the modified surface was required.

The common trait shared by the compounds in Table I is that they all contain multiple hydroxyl groups. In fact, in the case of the alditols, the hydroxyl group is the only functional group present. Thus, it was reasonable to consider in particular the role played by this functionality in the electroca-

Table II. FIA Response of Cu CME to Various Alditols*

compound	no. of hydroxyls	current, nA for 10^{-5} M	% response with respect to glucitol
methanol	1	4.5×10^{-5}	0.02
ethylene glycol	2	2.3×10^{-4}	0.11
glycerol	3	0.098	47
erythritol	4	0.16	75
ribitol	5	0.17	83
glucitol	6	0.21	100

* Potential applied, +0.50 V vs Ag/AgCl.

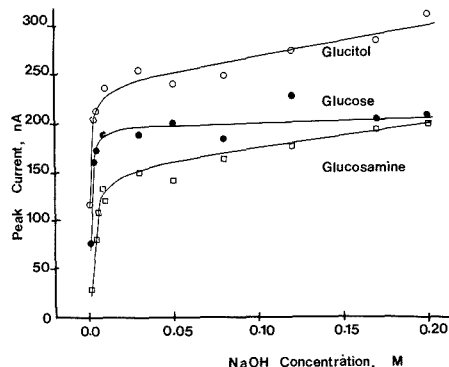


Figure 2. Plots of peak current at Cu CME vs NaOH concentration for FIA of glucose (●), glucitol (○), and glucosamine (□): potential, +0.48 V vs Ag/AgCl; flow rate, 0.5 mL/min.

talysis. This was first done by examining the homologous series of alditols from methanol up to glucitol. The results obtained for this group under flow injection conditions are summarized in Table II. Interestingly, the electrocatalytic current (per mole) was at a maximum for glucitol and steadily decreased down to glycerol, which still produced roughly half the current that was seen for the compounds containing six hydroxyl groups. Further decreases in molecular size down to ethylene glycol and then methanol resulted in a drastic decrease in catalytic response. Thus, it appears that the presence of at least three contiguous hydroxyl groups in the target compound was a necessary condition for the Cu CME response to approach a useful level. Of course, some exceptions to this generalization did occur among the various compounds examined. For example, glyceraldehyde, tartaric acid, and 2-deoxyribose all exhibited excellent electrocatalytic activity and low detection limits despite lacking three adjacent hydroxyls.

One definite requirement of the Cu CME—which is shared by all of the various electrode systems used thus far for carbohydrate detection—was the requirement for strongly alkaline solution conditions in order for the electrocatalysis to proceed efficiently. The extent of this requirement for the Cu CME is given explicitly in Figure 2, which shows the peak current response in flow injection as a function of pH for glucose, glucitol, and glucosamine. The pH was varied in these experiments by decreasing the NaOH concentration and keeping the ionic strength constant ($\mu = 0.4$) by appropriate addition of NaCl. For each of the compounds examined, excellent signals could be maintained for NaOH concentrations down to 10^{-3} M before significant decreases in the current levels started to occur; similar behavior was observed for the aldaric, uronic, and aldonic acids as well. This pH dependence turned out to be somewhat less limiting than what has been previously seen with Pt, Au, and CoPC electrodes, which functioned well only down to OH⁻ concentrations of 0.01 M.

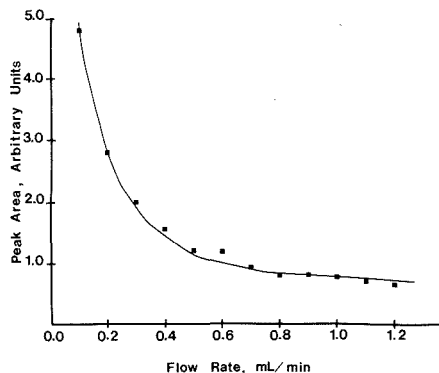


Figure 3. Plot of peak current vs mobile phase flow rate at Cu CME: potential, +0.48 V vs Ag/AgCl; glucose concentration, 10 μ M; mobile phase, 0.15 M NaOH.

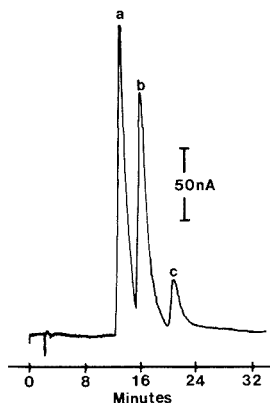


Figure 4. Chromatogram of 30 μ M galactosamine (a), 30 μ M glucosamine (b), and 100 μ M *N*-acetylgalactosamine (c): mobile phase, 10 mM NaOH; stationary phase, Dionex Carbobac PA1 column; potential, +0.50 V vs Ag/AgCl; flow rate, 0.5 mL/min.

As will be seen below, this ability to function usefully at lower pH values was important because it served to allow greater freedom to the chromatographer for the selection of an effective mobile phase.

Figure 3 illustrates the effect of variation in mobile phase flow rate on the Cu CME response for glucose in flow injection. The exponential decrease observed here for increasing flow rates contrasts sharply with the direct dependence typically seen at unmodified electrodes (17–20). At this point, the specific reasons for decreased CME response at higher flow rates are not known. One possibility, of course, is that the rate of the catalytic reaction between the CME and the polyhydroxy solute is simply too slow to produce large currents for the faster flow rates. In any case, the choice of flow rate to be used in any instance involves a compromise between electrode sensitivity and sample throughput. The flow rates that gave optimum results in chromatographic experiments described below and therefore were employed in all subsequent work were in the 0.3–0.7 mL/min range.

Liquid Chromatography. The most interesting feature of the Cu CME was the prospect that it provided for direct constant-potential monitoring of a wide range of important compounds not ordinarily considered for LCEC. In its initial use for detection of simple sugars, the CME had proven to

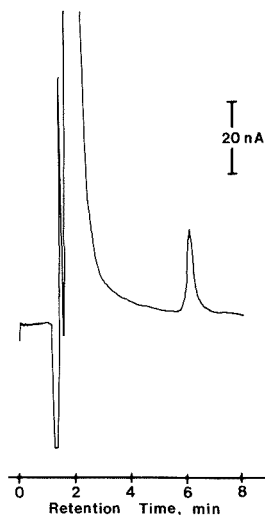


Figure 5. Chromatogram of 0.20 mM kanamycin: mobile phase, 0.15 M NaOH; stationary phase, Dionex AS6A-5 μ HPLC column; other conditions, same as in Figure 4.

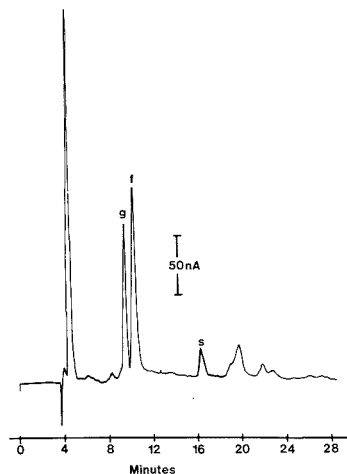


Figure 6. Chromatogram of flue-cured McNair No. 944 tobacco leaf extracted in $\text{CH}_2\text{CN}/\text{H}_2\text{O}$: mobile phase, 0.15 M NaOH; stationary phase, Dionex Carbobac PA1 column; flow rate, 0.3 mL/min; other conditions, same as in Figure 4.

be not only extremely sensitive but also quite stable and very easy to operate (15). It was hoped that these properties would also be displayed for all of the families of related compounds listed in Table I. That this was in fact the case is demonstrated at least in part by the chromatograms contained in Figures 4–6. It is important to note that no response was obtained for any of these carbohydrate-related compounds when unmodified glassy carbon electrodes were employed.

LCEC results obtained for a mixture of amino sugars containing galactosamine, glucosamine, and *N*-acetylgalactosamine are shown in Figure 4. The separation, carried out with an anion-exchange column and 0.010 M NaOH as mobile phase, has presented particular problems for previous LCEC efforts because the relatively low OH^- concentration needed

Table III. LCEC Assay for Tobacco Leaf Extract

method	glucose		fructose		sucrose	
	mean, %	SD, %	mean, %	SD, %	mean, %	SD, %
Cu CME ^a	3.7	0.2	5.2	0.02	1.4	0.2
LC/RI ^b	3.7	0.5	5.0	0.5	1.4	0.4

^a Reported results represent the mean and standard deviation of two separate assays obtained via LCEC with the Cu CME. Conditions were the same as in Figure 6. ^b From liquid chromatography/refractive index detection results provided by Brown & Williamson Tobacco Corp. Research and Development, Louisville, KY, and based on more than 50 separate assays.

for the separation of these compounds is not well-suited for electrocatalytic detection at Pt or Au electrodes (21). Rather, postcolumn addition of concentrated base was required in order to avoid severe tailing caused by poor adsorption/desorption characteristics of the amino sugars on these electrode materials. However, the Cu CME was able to operate quite efficiently at these lower OH⁻ concentrations (see Figure 2) and had no difficulty quantitating the amino sugars at quite low levels. Detection limits obtained for the above compounds under these chromatographic conditions were 5 ng for galactosamine, 8 ng for glucosamine, and 0.1 μg for *N*-acetyl-galactosamine.

Chromatograms obtained for a standard solution of the antibiotic kanamycin and for the glucose-, fructose-, and sucrose-containing extract from a tobacco leaf are shown in Figures 5 and 6, respectively. Kanamycin is an antibiotic composed of three variously substituted monosaccharide units. Although none of the three rings possesses the intact structure of an actual sugar residue, an excellent response was still obtained at the CME, with a detection limit of 5 ng able to be reached. The tobacco leaf sample employed was obtained from standard flue-cured McNair No. 944 tobacco that had been soaked for 60 min in a 40:60 acetonitrile/water mixture. Despite the possible complexity of the resulting extract, the anion-exchange chromatogram produced with 0.15 M NaOH as mobile phase was relatively simple, exhibiting well-resolved peaks with the same retention times as glucose, fructose, and sucrose. Quantitation of these species by comparison to a calibration curve generated from standard solutions gave the assay results shown in Table III. The results derived from CME/LCEC approach compared very favorably with those from liquid chromatography/refractive index detection techniques, also summarized in the table.

Nature of the Cu CME. In order to obtain further insight into the Cu CME and its mechanism of action, the physical and chemical nature of the CME surface was examined by X-ray fluorescence and scanning electron microscopy. These experiments were carried out for glassy carbon surfaces at three different stages of the modification procedure: (A) after alumina polishing and rinsing with water, (B) after treatment with 0.15 M NaOH and rinsing with water, and (C) after exposure to 0.050 M CuCl₂ to form the working CME.

As would be expected for what essentially were just clean carbon surfaces, micrographs obtained for surfaces A and B were nearly featureless. The NaOH-treated surface was noticeably rougher than the freshly polished surface; but at magnifications of up to 5000, no further differences were apparent. For the CME, however, the growth of the green deposit noticeable visually following the CuCl₂ treatment appeared clearly as well-defined hexagonal crystalline structures, 1–2 μm in diameter, seemingly embedded randomly into and across the glassy carbon surface (see Figure 7). X-ray fluorescence spectra for the first two surfaces also were nearly featureless, with no real differences to be seen between the two. The spectrum for the freshly polished surface is shown

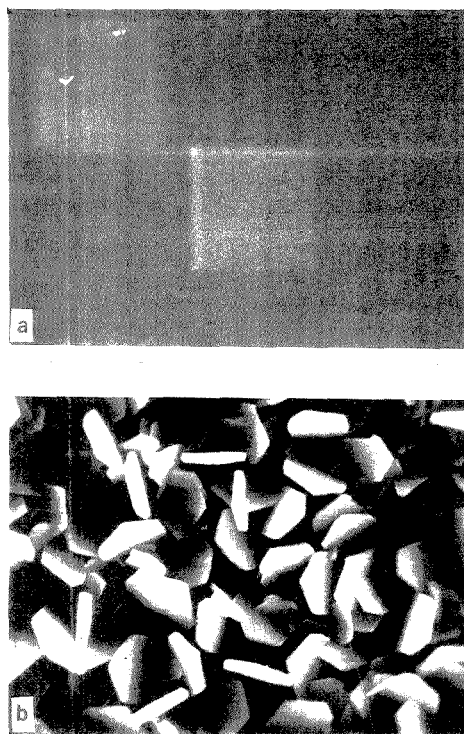


Figure 7. Scanning electron micrographs of clean glassy carbon electrode (a) and Cu CME (b). Magnification: 4900.

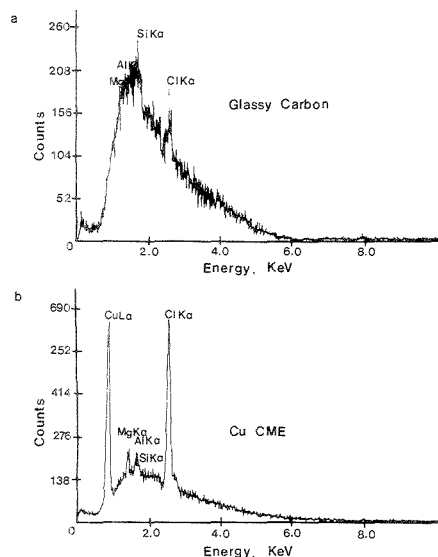


Figure 8. X-ray fluorescence spectra of clean glassy carbon electrode (a) and Cu CME (b).

in Figure 8a. For the fully treated CME, however, distinct Cu and Cl peaks were seen. The only additional peaks present were small ones occurring at energies corresponding to Al and

Si and presumably representing surface contaminants left from the initial alumina polishing process.

At this point, a definitive identification of the Cu/Cl surface microstructure has not been possible. X-ray diffraction spectra obtained for the crystals either intact on the glassy carbon surface or scraped off and collected for separate analysis have not yet been able to be matched with diffraction patterns of known Cu- and Cl-containing crystalline species. At present, more extensive characterization of the modification mechanism and specific surface structure of the Cu CME is continuing, and it is hoped that these investigations may lead to an improved understanding of the chemistry involved in its formation and operation. In the meanwhile, it is apparent that the CME offers impressive capabilities for the constant-potential flow detection of a wide variety of polyhydroxy compounds and an improved compatibility with a useful range of anion-exchange chromatography mobile phases.

ACKNOWLEDGMENT

We thank P. Luo for providing useful insights regarding the electrode modification procedure and J. R. Richardson and G. A. Lager for advice and assistance in carrying out X-ray diffraction characterization of the Cu CME surface.

LITERATURE CITED

- (1) Hughes, S.; Johnson, D. C. *Anal. Chim. Acta* **1981**, *132*, 11-22.
- (2) Hughes, S.; Johnson, D. C. *J. Agric. Food Chem.* **1982**, *30*, 712-714.

- (3) Hughes, S.; Johnson, D. C. *Anal. Chim. Acta* **1983**, *149*, 1-10.
- (4) Neuberger, G. G.; Johnson, D. C. *Anal. Chem.* **1987**, *59*, 203, 204.
- (5) Edwards, P.; Haak, K. K. *Am. Lab.* **1983**, (April), 78-84.
- (6) Rocklin, R. D.; Pohl, C. A. *J. Liq. Chromatogr.* **1983**, *6*, 1577-1590.
- (7) Neuberger, G. G.; Johnson, D. C. *Anal. Chem.* **1987**, *59*, 150-154.
- (8) Neuberger, G. G.; Johnson, D. C. *Anal. Chim. Acta* **1987**, *192*, 205-213.
- (9) Schick, K. G.; Magearu, V. G.; Huber, C. O. *Clin. Chem.* **1978**, *24*, 4480-450.
- (10) Buchberger, W.; Winsauer, K.; Breitwieser, C. H. *Fresenius' Z. Anal. Chem.* **1983**, *315*, 518-520.
- (11) Reim, R. E.; Van Effen, R. M. *Anal. Chem.* **1986**, *58*, 3203-3207.
- (12) Santos, L. M.; Baldwin, R. P. *Anal. Chem.* **1987**, *59*, 1766-1770.
- (13) Santos, L. M.; Baldwin, R. P. *Anal. Chim. Acta* **1988**, *206*, 85-96.
- (14) Tolbert, A. M.; Baldwin, R. P.; Santos, L. M. *Anal. Lett.* **1989**, *22*, 683-702.
- (15) Prabhu, S. V.; Baldwin, R. P. *Anal. Chem.* **1989**, *61*, 852-856.
- (16) Miller, B. J. *Electrochem. Soc.* **1969**, *116*, 1675-1680.
- (17) Swartzfager, D. C. *Anal. Chem.* **1976**, *48*, 2189-2192.
- (18) Weber, S. G.; Purdy, W. C. *Anal. Chim. Acta* **1978**, *100*, 531-544.
- (19) Meschi, P.; Johnson, D. C. *Anal. Chim. Acta* **1981**, *124*, 303-320.
- (20) Prabhu, S. V.; Anderson, J. L. *Anal. Chem.* **1987**, *59*, 157-163.
- (21) Olechno, J. D.; Carter, S. R.; Edwards, W. T.; Gillen, D. G. *Am. Biotechnol. Lab.* **1987**, (Sept.-Oct.), 38-50.

RECEIVED for review May 19, 1989. Accepted July 21, 1989. This work, which was presented in part at the 197th National Meeting of the American Chemical Society in Dallas, TX, was supported by the National Science Foundation through EPSCoR Grant 86-10671-01 and by Burdick & Jackson Research Grant BJ8807.

Determination of Osmium and Osmium Isotope Ratios by Microelectrothermal Vaporization Inductively Coupled Plasma Mass Spectrometry

Takafumi Hirata, Tasuku Akagi, Hiroshi Shimizu, and Akimasa Masuda*

Department of Chemistry, Faculty of Science, The University of Tokyo, Hongo 113, Tokyo, Japan

A new merging introduction technique has been developed for Os analysis with inductively coupled plasma mass spectrometry (ICP-MS). The sample was placed in a microheater cell in a merging chamber and vaporized OsO₄ was carried to the ICP with a blank matrix mist flow sprayed from a nebulizer. In the merging introduction, the best operational parameters could be obtained by the usual optimization using a standard solution. The ¹⁸⁷Os/¹⁸⁸Os ratio and the Os abundance were measured simultaneously by spiking ¹⁹²Os. The precisions of the ratio and abundance measurements using 0.8 ng of Os were 5 and 4%, respectively. The detection limit of Os by this method was lower than 100 fg, which is almost one-twelfth of that obtained by conventional nebulization introduction.

Mass spectrometry using inductively coupled plasma as an ion source (ICP-MS) is a new technique for elemental and isotopic analysis. However, nebulizers commonly used in ICP-MS transport only 2-3% of a sample solution into the ICP. Several techniques have been developed to enhance the efficiency of sample introduction to the ICP torch; e.g., the use of a recirculating nebulizer, a microconcentric nebulizer

(1), direct insertion (2), electrothermal vaporization (ETV) techniques (3, 4), and vapor generation introduction (5-8).

The ¹⁸⁷Re-¹⁸⁷Os isobaric pair is a promising isotopic system in the fields of geo- and cosmochemistry. However, the difficulty in Os isotopic analysis, due mainly to the high ionization potential of Os and the low abundance in common silicate rocks, has limited the use of this system. Methods with high performance in obtaining detection limits, including secondary ion mass spectrometry (9-11), accelerator mass spectrometry (12), and resonance ionization mass spectrometry (13), have been applied to Os isotopic analysis. With ICP-MS, we have succeeded in measuring the Os isotope ratios for natural metallic samples containing Os at parts per million (ppm) levels (14). A further enhancement of sensitivity is, however, required in order to measure the isotope ratio of Os for silicate rocks.

In this study, we put forward a new introduction technique using a miniature heater placed in a merging chamber (abbreviated to "microheater/merging introduction"). This method assures the effective introduction of Os to the ICP torch.

EXPERIMENTAL SECTION

The ICP-MS used in this study is a VG PlasmaQuad type I. The operational conditions are listed in Table I. Ion optical

Table I. Instrumental Operation Conditions

1. ICP Settings	incident power 1.35 kW reflected power <5 W argon gas flow rates cooling 13 L/min auxiliary 1.1 L/min nebulizer 0.8 L/min
2. Sample Injection	ETV introduction heater Ni-Cr wire diameter 0.35 mm current 0.5-0.7 A power 6-8 W temperature 60-90 °C
3. Nebulizer	nebulizer type; cross flow solution uptake rate 0.6 mL/min (pumped)
4. Interface	aperture diameter 0.9 mm skimmer diameter 1.0 mm load coil-aperture spacing 10 mm
5. Measurement Parameters	dwelt time 100 μ s no. of channels 50 per mass no. of scans 600

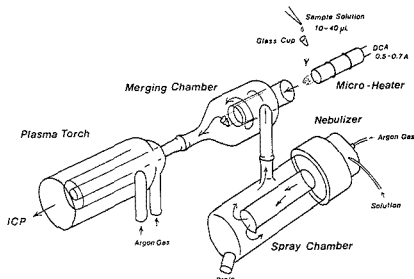


Figure 1. Schematic diagram of microheater/merging chamber. Twenty microliters of sample solution was loaded onto the glass cup, and evaporated OsO_4 was carried to the ICP torch with mist from the spray chamber.

settings were adjusted to optimize the signal of ^{208}Pb ion introduced by the nebulization of Pb standard solution, just before the sample heating for vaporization. Water was kept nebulized during the whole measurement to minimize change in the ion lens setting (15).

The sample preparation and calculation of Os isotope ratios were done after the method described in our earlier papers (14, 16). We have succeeded in developing a technique to measure Os isotope ratios and Os amounts at the same time (16), which was adopted in the present study. This technique is based on the assumption of a linear relation between mass discrimination factor and mass number. The principles of this technique are briefly described in the Appendix. After an addition of ^{192}Os spike, 10 mg of an iron meteorite was decomposed by 3 mL of aqua regia (1:1 mixture of 7 N HNO_3 and 6 N HCl) at 80 °C in a closed glass ampule (16). After decomposition, 1 mL of HClO_4 was added to the solution to oxidize Os. Osmium tetroxide was vaporized by distillation at 70-80 °C and was trapped in 1-2 mL of pure water. A very small fraction (20-40 μL) of the sample solution was loaded onto a Pyrex glass cup, and then the glass cup was set in a microheater (Figure 1). Next, the microheater cell was inserted into a merging chamber (Figure 1) with the ICP off. After adjustment of the ion optics, the solution in the glass cup was heated up to 70 °C by a Ni-Cr filament and OsO_4 was gently vaporized. The evaporated OsO_4 was mixed with spray mist in the merging chamber and was finally carried to the ICP.

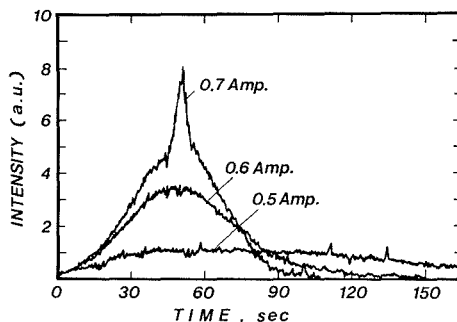


Figure 2. Effect of heating rates on signal intensity of ^{192}Os . The Os amount loaded was 100 pg (5 ppb, 20 μL).

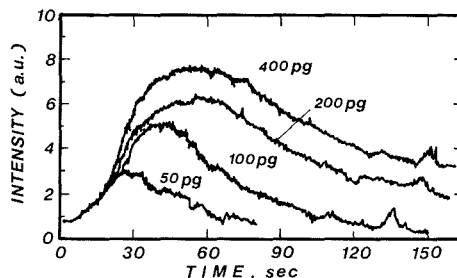


Figure 3. Effect of sample amount on signal intensity of ^{192}Os . The volume of Os solutions was 20 μL . The heater current was 0.6 A.

RESULTS AND DISCUSSION

The intensity and stability of Os signals are dependent on the current of the microheater, the Os concentration, and the volume of sample solution.

The dependence of signal intensity and stability on heating rate (heater current) is shown in Figure 2. In this experiment, the amount of Os loaded was constantly 100 pg (5 ppb, 20 μL). Higher heater current yielded a peak with a higher count rate and shorter duration, while lower heater current raised a peak with a lower count rate and longer duration. But the count rate at 0.7 A was not as large as expected from those at 0.5 and 0.6 A. Namely, integrated counts at 0.7 A were lower than those at 0.5 and 0.6 A. The reduction of integrated signal intensity at 0.7 A may be related to a large amount of water vapor generated at this current. It is likely that the water vapor condensed into dew in the merging chamber and that Os was trapped by the condensed water. This is one of the possible explanations for the signal reduction under consideration. Another possible explanation for the signal reduction is drift in the tuning condition of the ion lens due to an introduction of a large amount of vapor produced at 0.7 A. Moreover, as shown in Figure 2, a spiky signal was observed at a heater current of 0.7 A. The solution temperatures at heater currents of 0.6 and 0.7 A were approximately 70 and 90 °C, respectively. The spiky signal was due to the boiling of sample solution at a high temperature of 90 °C. These results indicate that a heater current of 0.7 A is not suitable. The heater current was set at 0.6 A for the later experiments.

The effects of Os amount on Os signal intensity are shown in Figure 3. Osmium amounts introduced by the microheater/merging introduction technique were 50, 100, 200, and 400 pg. In this experiment, the volume of Os solutions loaded and the heater current were adjusted to 20 μL and 0.6 A, respectively. The maximum intensity for each run was almost proportional to the loaded amount when the amount was less

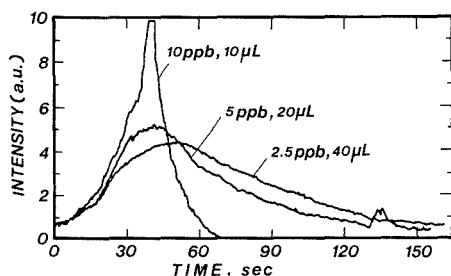


Figure 4. Effect of volume of sample solution on signal intensity of ^{192}Os . The absolute amount of Os loaded was 100 pg. The heater current was 0.6 A.

Table II. Comparison of the Absolute Detection Limits of Osmium between the Microheater/Merging Introduction and the Nebulization Introduction

	introduction technique	
	microheater/ merging	nebuliza- tion
signal intensity of $^{192}\text{osmium}$, counts/s per 100 pg of Os	11658	869
background, counts/s	11.4 ± 3.3	13.6 ± 2.9
detection limit, pg	$0.085 (3\sigma)$	$1.0 (3\sigma)$

than 100 pg. Saturation of the signal height was observed with a sample amount of more than 200 pg, for which the profiles have a plateau region lasting for more than 10 s. Taking both sensitivity and stability into account at the same time, a sample amount between 100 and 200 pg is desirable.

Finally, the dependence of signal stability and intensity on sample volume was investigated. Here, the amount of Os loaded was constantly 100 pg. The heater current was 0.6 A. The obtained time profiles are shown in Figure 4. A spiky time profile was observed when the volume of sample solution was 10 μL . This spiky signal was due to the boiling of the solution. On the other hand, the larger volume of sample solution gave a signal of lower intensity lasting for a longer time, which was due to lower temperature. Consequently, a sample solution volume of 20 μL was adopted for further measurements.

A comparison of the sensitivity and detection limit was made between the conventional nebulization and the microheater/merging introduction techniques employed here. In the test of detection limits, 100 pg (5 ppb, 20 μL) of Os was introduced by both the microheater/merging and the nebulization introduction techniques. The heater current was set at 0.6 A in the microheater/merging introduction. The mass spectra obtained by both techniques are shown in Figure 5a,b. The sensitivities and detection limits of these techniques are summarized in Table II. With the microheater/merging introduction technique, the ^{192}Os count rate of 11658 counts/s per 100 pg of Os was obtained with 20-s integration. On the other hand, the ^{192}Os count rate of 869 counts/s per 100 pg of Os was obtained with the conventional nebulization introduction. Therefore, the enhancement factor of the count rates with the microheater/merging introduction technique was 13 times, compared with the nebulization introduction method. The detection limits were defined as 3 times the standard deviation of the count rates of blank tests. The standard deviations of the count rates of blank tests were obtained by 10 sets of repeated measurements using blank solution in both introduction techniques. The detection limit of Os obtained by the microheater/merging introduction is 0.085 pg, which is almost one-twelfth of that obtained by the

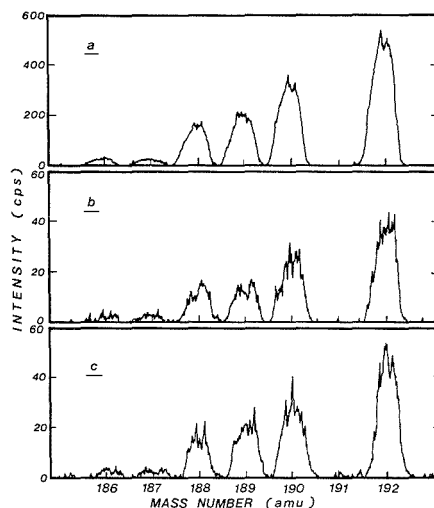


Figure 5. Mass spectra of osmium for 100 pg (5 ppb, 20 μL) of osmium obtained by (a) microheater/merging introduction with water nebulization, (b) conventional nebulization introduction, and (c) microheater/merging introduction without water nebulization. The same conditions (lens biases and plasma gas flow rates) were used in the three measurements. The heater current was 0.6 A for experiments a and c.

Table III. Results of Isotopic Ratio and Abundance Measurements of Osmium in Tlacotepec Iron Meteorite^a

	$^{187}\text{Os}/^{186}\text{Os}$	abundance, ppm	Os amt used, ng
continuous nebulization method	1.037 ± 0.006	39.17 ± 0.21	400
microheater/merging technique	0.995 ± 0.050	41.0 ± 1.5	0.8^b
literature data			
Herr et al. (17)	1.004 ± 0.018	39.6 ± 2.2	
Luck and Allegre (11)	0.980 ± 0.004	53.7 ± 0.4	

^a Errors are $1\sigma_m$. ^b Eight-time repetition of measurement using sample solution containing 100 pg of Os each time.

nebulization introduction (Table II).

In this study, nebulized water was introduced simultaneously with Os vapor. No shifts in the lens settings could be observed between the merging introduction and the conventional nebulization introduction. This result may be due to the very small volume of Os vapor released, which does not cause any change in the plasma. One can keep the operational settings unchanged for the measurement procedure. This is a great advantage of the microheater/merging introduction technique, because one need not consume the valuable sample on the cup to tune the lens. On the other hand, at the measurement without water introduction, the excellent enhancement of signal could not be observed, as shown in Figure 5c. The Os amount, the sample volume, and the heater current of this measurement (Figure 5c) were identical with those of Figure 5a. This obvious difference in signal intensity between with and without the water introduction may be caused by the shift of ion lens tuning.

Table III lists two sets of Os data from the Tlacotepec iron meteorite; one is by the microheater/merging introduction technique and the other is by nebulization introduction. The solutions used for the analyses were identical for both intro-

duction techniques. The abundance data obtained show a good agreement between the two introduction techniques. In addition, the isotopic ratio of $^{187}\text{Os}/^{186}\text{Os}$ obtained by the microheater/merging chamber method is consistent with that obtained by nebulization introduction within the analytical uncertainty. The precision of the values obtained by the microheater/merging chamber method was somewhat poorer than that obtained by nebulization introduction. However, it should be noted that the amount of Os used for the latter method was 400 ng, approximately 500 times larger than that used for the former one. Furthermore, it is seen in Table III that our values of the Os isotopic ratio and abundance are close to those obtained by Herr et al. (17). The small differences between the data obtained by Luck and Allegre (11) and those by Herr et al. (17) and us may be due to heterogeneous distribution of Os and Re.

The merging introduction technique, in which the sample is released from a merging chamber, may be applied to other sample introduction techniques. The combination of microheater and merging introduction can successfully reduce the absolute detection limits of Os to better than one-twelfth that of the nebulization introduction. Finally, it is noted that the technique developed here can be applied not only to ICP-MS, but also to ICP atomic emission spectrometry (ICP-AES).

APPENDIX

The calculation of Os abundance and the $^{187}\text{Os}/^{186}\text{Os}$ ratio is as follows (16). The isotopic composition A_m^C , in the mixture of sample and spike solution, is expressed by

$$A_m^C = A_m^N X + A_m^S M \quad (1)$$

where A_m^N and A_m^S are the isotopic compositions of ^mOs (here m refers to mass number of each Os isotope except 187) in sample and spike, respectively. These isotopic compositions (16) are constants. X and M are the amounts of Os in sample and spike, respectively. X is an unknown value to be determined here. The specific isotopic count rate (F_m) of isotope ^mOs is defined as

$$F_m = I_m/A_m^C \quad (2)$$

In eq 2, I_m is the observed count rate (peak area) of ^mOs and A_m^C is obtained from eq 1 by substituting proper values for X . The best value of X is determined so as to bring the mass discrimination factors (F_m) to be the closest to a linear function of the mass number.

The F_m defined above is used in the correction of mass discrimination. The corrected isotope ratio of $^{187}\text{Os}/^{186}\text{Os}$ is given by

$$^{187}\text{Os}/^{186}\text{Os} = (I_{187}/I_{186})(F_{186}/F_{187}) \quad (3)$$

where F_{187} is the value obtained from the linear line drawn in the final determination of X .

Registry No. Os, 7440-04-2; ^{187}Os , 15766-52-6; ^{186}Os , 13982-09-7.

LITERATURE CITED

- (1) Lawrence, K. E.; Rice, G. W.; Fassel, V. A. *Anal. Chem.* **1984**, *56*, 289-292.
- (2) Salin, E. D.; Horlick, G. *Anal. Chem.* **1979**, *51*, 2284-2286.
- (3) Nixon, D. E.; Fassel, V. A.; Kniseley, R. N. *Anal. Chem.* **1974**, *46*, 210-213.
- (4) Gregoire, D. C. *J. Anal. At. Spectrom.* **1988**, *3*, 309-314.
- (5) Bazan, J. M. *Anal. Chem.* **1987**, *59*, 1066-1069.
- (6) Russ, G. P., III; Bazan, J. M.; Date, A. R. *Anal. Chem.* **1987**, *59*, 984-989.
- (7) Tao, H.; Miyazaki, A.; Bansho, K. *Anal. Chem.* **1988**, *60*, 1762-1765.
- (8) Dickin, A. P.; McNutt, R. H.; McAndrew, J. I. *J. Anal. At. Spectrom.* **1988**, *3*, 337-342.
- (9) Luck, J. M.; Birck, J. L.; Allegre, C. J. *Nature* **1980**, *283*, 256-259.
- (10) Allegre, C. J.; Luck, J. M. *Earth Planet. Sci. Lett.* **1980**, *48*, 148-154.
- (11) Luck, J. M.; Allegre, C. J. *Nature* **1983**, *302*, 130-132.
- (12) Fehn, U.; Teng, R.; Eimore, D.; Kubik, P. W. *Nature* **1986**, *323*, 707-710.
- (13) Walker, R. J. *Anal. Chem.* **1988**, *60*, 1231-1234.
- (14) Masuda, A.; Hirata, T.; Shimizu, H. *Geochem. J.* **1986**, *20*, 233-239.
- (15) Hirata, T.; Shimizu, H.; Akagi, T.; Sawatari, H.; Masuda, A. *Anal. Sci.* **1988**, *4*, 637-643.
- (16) Hirata, T.; Shimizu, H.; Akagi, T.; Masuda, A. *ICP Inf. Newsl.* **1988**, *13*, 731-735.
- (17) Herr, W.; Hoffmeister, W.; Hirt, B.; Geiss, J.; Houtermans, F. G. Z. *Naturforsch.* **1961**, *16A*, 1053-1058.

RECEIVED for review January 23, 1989. Accepted July 3, 1989. This work was supported in part by a Grant-in-Aid for Scientific Research from the Ministry of Education, Science and Culture, Japan.

Photoreduction Fluorescence Detection of Quinones in High-Performance Liquid Chromatography

James R. Poulsen¹ and John W. Birks*

Department of Chemistry and Biochemistry and Cooperative Institute for Research in Environmental Sciences (CIRES), Campus Box 449, University of Colorado, Boulder, Colorado 80309

A simple, reagent-free photochemical reaction detector for quinones including, but not limited to, the K vitamins is presented. Quinones are photoreduced to dihydroquinones via hydrogen abstraction from the high-performance liquid chromatography (HPLC) mobile phase in a postcolumn photoreactor. An advantage over previous reaction-detection methods for quinones is the simplicity of this system. No postcolumn reagent addition pumps are required. Additionally, the reaction is accomplished in a very short reactor which minimizes band broadening and analysis time. Detection limits for many quinone derivatives are in the low picogram range with good selectivity. In this paper, the photochemistry of the detection scheme and its optimization for use in HPLC are discussed. As a sample application, the detector of vitamin K₁ in a plant extract (*Capsella bursa pastorius*) without pre-fractionation is included. A new photoreactor housing for carrying out anaerobic reactions in low-dispersion, PTFE photoreactors is described.

INTRODUCTION

Recently, we reported a reaction-detection scheme for quinone analytes, the photocatalytic chemiluminescence (PCCL) detector, which exhibits better sensitivity than UV detection with very high selectivity (1, 2). These compounds are of interest because of their use in modern wood pulping processes (3, 4), as oxidation products of polycyclic aromatic hydrocarbons in the environment (5, 6), and as important biogenic compounds found in electron transport systems of plants, bacteria, and animals. Quinone derivatives are vital to photosynthesis in plants and bacteria, as well as, for blood clotting in animals (7, 8). Detection of quinones in the complex matrices in which they typically are found presents severe challenges to most conventional techniques.

On-line, postcolumn, photochemical reactions for high-performance liquid chromatography (HPLC) provide a useful way of transforming analytes to compounds with enhanced detectability (9, 10). Quinones are good candidates for this form of detection as they are nonfluorescent and their UV detection, while quite sensitive, lacks the selectivity necessary for application to complex mixtures. Both the selectivity and sensitivity of quinone detection can be improved via photochemical reaction detection.

Anaerobic photoreduction of quinones produces highly fluorescent dihydroquinones. This reaction has been applied to the detection of "hydrogen atom donor" (HAD) analytes by Gandelman and Birks (11, 12). HAD compounds typically have an electron-withdrawing element (O or N) bound to a carbon with α -hydrogens (13, 14). For photoreduction/fluorescence detection (PRF), an anthraquinone sensitizer is added to the HPLC mobile phase and HAD compounds are detected through the fluorescence of the photoreduced anthraquinone derivative. Although background photoreduction

of the anthraquinone sensitizer ultimately limits the sensitivity, PRF improves the detectability of many compounds that lack strong chromophores.

Photoreduction/fluorescence detection of quinones (PRFQ) is relatively free from interference caused by photochemically generated background fluorescence, because no light-absorbing compound is added to the mobile phase. In fact, relative to the stray light from the excitation source of the fluorometer, the photoreduction/fluorescence background is negligible. The intense fluorescence of dihydroxyanthracenes allows the detection limits for most anthraquinone derivatives to be improved by at least an order of magnitude relative to UV detection. Naphthoquinones are detected sensitively as well.

PRFQ responds to a wider range of quinones than the detection scheme based on quinone-sensitized photooxidation (PCCL). Some substituents decrease the response of a quinone to PCCL, presumably by lowering the reactivity of its triplet state (15). Some quinones substituted with these groups respond in the photoreduction mode (e.g., the K vitamins). PCCL detection requires the analyte to cycle through the photooxidation reaction sequence many times in order to achieve high sensitivity (1, 2). On the other hand, PRFQ detection only requires the analyte to complete the photoreduction reaction sequence once. For this reason, nonproductive pathways that deactivate the excited state, destroy the free radical intermediates, or destroy the analyte are more problematic to the photooxidation-based detection scheme. Excitation efficiency is improved by the use of a 254-nm lamp with PRFQ. Relative to PCCL, PRFQ is less selective, because compounds that are natively fluorescent can interfere.

In a similar, though more complex, photochemical reaction-detection scheme, Lefevre et al. report sensitive detection of vitamin K₁ homologues (16). They were able to monitor clinically observed levels of these vitamins. Electrochemical reduction of K vitamins followed by fluorescence detection has been applied to their detection as well (17, 18). Alternatively, the K vitamins can be reduced chemically and detected by fluorescence (16, 19, 20). Sodium borohydride and tetramethylammonium octahydrododecaborate have been delivered in solution to effect the reduction reaction (19, 20). Solid-phase reactors (SPR) filled with borohydride reagents could improve this method of detection for K vitamins as SPRs would eliminate the stability problems of the dissolved reagents and the expense of the postcolumn pumps. Table I reviews the available HPLC detection methods for the K vitamins.

Because vitamin K₁ (2-methyl-3-phytyl-1,4-naphthoquinone) is extremely hydrophobic, its determination after extraction from matrices that contain lipophilic interferences is quite challenging. To determine normal levels of K₁ in serum samples with a UV absorption detector, a sequential adsorption and reversed-phase HPLC procedure was developed (22). Obviously, this procedure lengthens the analysis time over a single chromatographic separation coupled to a more selective detector. The low level of K vitamins in biological samples generates interest in reaction detection methods that increase the sensitivity along with the selectivity

¹ Current address: Henkel Research Corp., 2330 Circadian Way, Santa Rosa, CA 95407.

Table I. Detection of K Vitamins in HPLC

reaction scheme	analytes	reactor ^f	aerobic	reagents	d.l., pg	$\lambda_{ex}/\lambda_{em}$	ref
photoreduction/ fluorescence of quinones (PRFQ)	K ₁ K ₃	PTFE DOTR-17s	no	no	30 20	243.5/>370	this work
photoreduction/ fluorescence	K ₁	PTFE GSFR-146s	no	ascorbic acid ^a acetate buffer	150	320/420	16
electrochemical reduction/ fluorescence	K ₁ analogues K ₁ -ep ^g	ECD ^d	no	NaClO ₄ ^e	25-60 60	320/420	17, 18
chemical reduction/ fluorescence	K ₁	PTFE GSFR-89s	no	NaBH ₄ ^b	≈150	320/420	16
chemical reduction/ fluorescence	K ₁	PTFE DOTR-51s	no	(CH ₃) ₄ NB ₃ H ₈ ^b	150	325/420	19, 20
electrochemical reduction/oxidation	K ₁	ECD ^d	yes	acetate buffer ^c	50	-	21
UV absorption	K ₁	none	yes	no	550	248 nm	22

^a Reagent(s) can be spiked into the mobile phase or added postcolumn. ^b Reagent(s) added postcolumn. ^c Reagent(s) spiked into mobile phase. ^d Model 5100-A coulometric electrochemical cell, Coulochem, E.S.A., Bedford MA, USA. ^e Phylloquinones 2,3-epoxide. ^f Key: DOTR, deformed open tubular reactor; GSFR, gas segmented flow reactor; ECD, electrochemical detector.

of the detection step. Lambert et al. report a range of 62-980 pg/mL and a median of 247 pg/mL for vitamin K₁ in blood as a result of a study of 50 healthy, fasting adults (20).

In this paper the anaerobic photochemistry of quinones and its optimization for the on-line detection of these compounds in HPLC is discussed. In addition to simplifying the instrumentation, this mode of detection is expanded to include quinones other than the K vitamins. The detection of vitamin K₁ in a plant extract is used to demonstrate the enhanced capabilities of PRFQ relative to UV detection. Since any HPLC system equipped with fluorometric detection can be simply and economically adapted to perform this reaction, the PRFQ scheme is accessible to more laboratories than schemes requiring exotic reagents or additional pumping systems. The equipment requirements of the PRFQ, a nitrogen tank to purge the system, and a photoreactor, which can be built for under 300 dollars, are small in comparison to standard HPLC components. PRFQ should be adaptable to gradient chromatography, because the reaction has little solvent dependence, provided that a HAD is present, and no reagent background or decomposition problems.

EXPERIMENTAL SECTION

Chemicals. Quinone samples were obtained from Aldrich Chemicals, Alfred Bader Library of Research Chemicals, Sigma, Analabs, Fisher, Eastman, and Pfaltz and Bauer. These were used as received after checking the purity by HPLC with UV detection.

HPLC Apparatus. A schematic diagram of the HPLC system used for PRFQ detection appears in Figure 1. The HPLC system consisted of a Kratos Spectroflow-400 pump, a Rheodyne 7125 injector (20- μ L loop), a Du Pont Zorbax ODS column (5- μ m packing, 25 cm \times 4.6 mm), a Shimadzu CR-3A integrating recorder, a Kratos FS-970 filter fluorometer, and/or a Kratos Spectroflow-773 variable wavelength UV detector. The inlet line to the HPLC pump was stainless steel. A PTFE line would allow oxygen to enter the system. The chromatographic eluents were mixtures of methanol and water (Burdick and Jackson, HPLC grade), 80% to 100% methanol by volume. When vitamin K₁ or quinones with more than three rings were analytes, a mobile phase of 60% methanol and 40% isopropyl alcohol (Fisher, HPLC grade) was used. The solvent reservoir was equipped with a gas dispersion tube so that the mobile phase could be sparged with "oxygen-free" or USP grade nitrogen (General Air). Part of the nitrogen flow was diverted to a dispersion tube inside the photoreactor housing.

Photochemical Reactors and Reactor Housing. Reactors, prepared from 30-gauge PTFE tubing (0.30-mm i.d. with 0.15 \pm

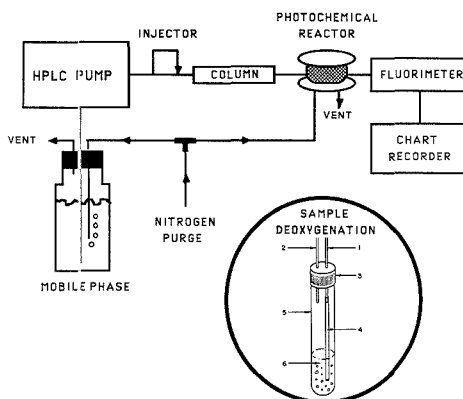


Figure 1. Schematic diagram of the PRFQ system; (insert) diagram of the sample deoxygenation device; (1) nitrogen inlet, (2) nitrogen outlet, (3) Teflon-lined cap, (4) disposable PTFE bubbler tubing, (5) screw-top test tube, (6) sample.

0.05-mm wall thickness) purchased from Small Parts, Inc., were plumbed and crocheted by the method of Poulsen et al. (23). A water-filled housing was designed for use with pencil lamps that allowed the temperature of the photoreactor to be regulated by an external circulation pump while maintaining an anaerobic environment (Figure 2). The body of the housing was an acrylic plastic tube (7.6-cm i.d., 0.6-cm wall thickness, 7.5 cm long), while a concentric quartz tube (1.5-cm i.d., 0.1-cm wall thickness, 8.5 cm long) held the reactor in place and kept the lamp dry. Pencil lamps were supported by the quartz tube and positioned with a rubber ring that fit around the lamp casing. The photoreactors were connected to metal HPLC tubing inside the reactor so that no PTFE tubing was exposed to air. An immersion pump circulated ice-cold water through coiled copper tubing (1/4-in. o.d., \approx 100-cm long) that was in contact with the nitrogen-flushed water inside the reactor housing.

Light Sources. A Pen-Ray low-pressure mercury-vapor lamp with an emission maximum of 254 nm (lamp Model 11 SC-1, power supply Model SCT-1, UV Products, Inc., San Gabriel, CA) produced the best results. A Pen-Ray lamp equipped with a phosphor (Model 11 SC-1L), with an emission maximum at 366 nm, was investigated as well.

Sample Degassing. A home-made device was designed for sample deoxygenation (Figure 1 insert). Stainless-steel capillaries

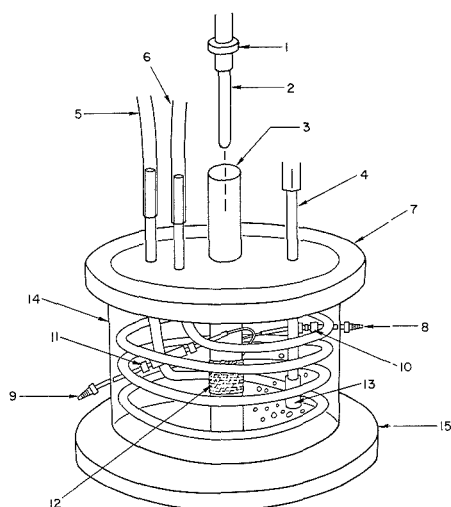


Figure 2. Diagram of the PRFO photoreactor housing: (1) rubber ring for positioning the lamp within the quartz tube, (2) 254-nm pencil lamp, (3) quartz tube, (4) nitrogen inlet, (5) coolant inlet, (6) coolant outlet, (7) top of housing, (8) photoreactor inlet [from HPLC column], (9) photoreactor outlet [to fluorometer], (10) adapter [Vaco fittings] stainless-steel to PTFE capillary tubing, (11) adapter [modified Swage-lok fittings] PTFE to stainless-steel capillary, (12) crocheted PTFE photoreactor, (13) gas dispersion tube [Pyrex], (14) body of the photoreactor housing [water filled], (15) bottom of housing.

($1/16$ -in. o.d., 0.030-in. i.d.) are inserted into two holes drilled in the cap of a screw-top test tube (10 cm \times 1.5 cm). One serves as a nitrogen inlet and the other as a vent. Neither of the metal tubes is in contact with the sample at any point during the deoxygenation procedure, because they only extend ≈ 1.5 cm into the test tube. The nitrogen inlet is connected by a pressure fit to a piece of PTFE tubing (1.5-mm i.d. \times 8.5 cm long, catalog no. BB 311-15, Bolab, Inc., Lake Havasu City, AZ). This piece of tubing extends into the sample solution and serves as the bubbler. Samples are held under the nitrogen flow for ≈ 5 –10 min prior to injection. A flow of nitrogen through the head space is maintained while the syringe is being loaded. The PTFE bubbler tube is disposable to prevent sample contamination.

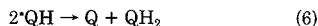
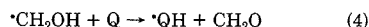
Detection Limit Calculations. Detection limits are reported as the amount of analyte that, when injected on column, produces a signal-to-noise ratio of three. Mobile phases that were well suited to their chromatographic separation were used in all cases. The noise was measured as the full peak-to-peak variation in the base line, recorded over a minimum of 20 time constants. The amount of analyte corresponding to the detection limit was calculated through linear regression of a minimum of three different analyte concentrations, all within a factor of 40 of the reported detection limit. Each analyte solution was injected a minimum of two times. Where necessary, the samples were degassed before injection.

Preparation of Plant Extracts. The extraction of vitamin K₁ from the herb shepherd's purse (*Capsella bursa pastorius*) was performed according to the following procedure. A dichloromethane extract of the herb (5.7 g, 16–20 Soxhlet cycles in a Whatman 2800 339 extraction thimble) was evaporated under nitrogen to a volume of ≈ 30 mL and then diluted to 80 mL final volume with methanol. An aliquot of this solution was filtered through a Millex HV 0.45- μ m and a Millex GV 0.22- μ m (Millipore Corp., Bedford, MA) syringe filter. The filtered extract was injected into the chromatograph.

PHOTOREDUCTION OF QUINONES

Quinone Photochemistry. Under the conditions for HPLC detection of quinones, the photoreduction reaction can be described in terms of a simple hydrogen abstraction

mechanism (24, 25). As the reaction sequence for photoreduction indicates,



Q = quinone analyte

$\cdot\text{QH}$ = semiquinone radical

QH₂ = dihydroquinone

the analyte is reduced to the corresponding dihydroquinone while oxidizing methanol to formaldehyde. Methanol is used as the HAD substrate in the photochemical reaction schemes, because it is effective as a mobile phase modifier for quinone separations and as a hydrogen atom donor. The quinone analytes are present at extremely low concentrations, while the hydrogen atom donor (mobile phase) is very concentrated.

After excitation (reaction 1), the molecules rapidly decay to their lowest excited singlet state (S_1) by internal conversion. The energy difference between the S_1 and T_1 is small, ca. 4 kcal/mol for anthraquinone, which allows a strong spin-orbit coupling of the states to occur (26). A large majority of the S_1 sensitizer molecules undergo intersystem crossing to the triplet manifold and subsequent internal conversion to the lowest excited triplet (T_1) state (reaction 2). Reported triplet yields for anthraquinone are between 0.90 (27) and 1.0 (28). Hence, the reactivity of the lowest triplet state determines the photochemical reactivity of quinones (26, 27, 29), and the quantum yield for the photoreduction reaction (ϕ_{pr}) is independent of the excitation wavelength (25).

While it is generally accepted that hydrogen abstraction reactions occur through the lowest triplet state, this does not mean that the T_2 or S_1 states are unreactive. The lifetimes and thermal populations of these states simply are insufficient to account for the high efficiency of hydrogen abstraction reactions by strong ($\phi_{pr} \geq 0.5$) sensitizers (26).

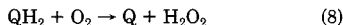
T_1 of the quinone rapidly abstracts a hydrogen atom from the HAD to produce a semiquinone radical and an α -hydroxy alkyl radical (reaction 3). In the final step of this sequence, two semiquinone radicals disproportionate to generate a dihydroquinone and a molecule of the parent quinone. Disproportionation of the semiquinone radicals takes place at rates that are within an order of magnitude of a diffusion limited reaction (30, 31). Depending on the relative rates of reactions 4 and 5, the quantum yield for the photoreduction of anthraquinone by good donors varies from 0.5 to 1.0 (25, 31). When the quantum yield is greater than 0.5, it also is affected by the concentration of anthraquinone (25). At low sensitizer concentration, reaction 5a competes more effectively with reaction 4 and the photoreduction yield decreases. The concentration dependence and lack of "diol" formation (reaction 5b) support the cyclic nature of the mechanism over a free-radical chain reaction mechanism (25, 32). Radicals formed from solvents that are poor donors can react with the semiquinone radical and lower ϕ_{pr} (31)



Substituent groups on the parent quinone will affect both the rate of photoreduction and the fluorescence properties of the reduced compound (15, 24, 30, 32–34). Orthoquinones (e.g., 9,10-phenanthrenequinone) (35), benzophenone, and

other aromatic carbonyl compounds sensitize similar hydrogen abstraction reactions (36).

The photoreduction sequence only will occur under anaerobic conditions (37). If oxygen is introduced after the photoreduction is complete, the dihydroquinone will be oxidized back to the parent quinone with the production of hydrogen peroxide (31, 33, 37)

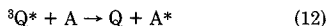
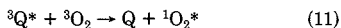


When oxygen is present during the reaction, it reacts with the semiquinone (reaction 9) and the α -hydroxy alkyl radicals (30, 31)



A photooxidation sequence that ultimately produces H_2O_2 and regenerates the quinone follows the reaction of oxygen with these radicals (24, 31, 33, 38).

Hydrogen abstraction (reaction 3) is the predominant relaxation pathway for quinone triplets in solutions with high HAD concentrations (26, 30, 31). Other pathways, such as those given in reactions 10–13, are unable to compete with reaction 3 under these conditions (N_2 -sparged, HPLC-grade solvents). However, the rates of energy transfer to quenchers that have triplet states lower in energy than T_1 of the quinone are very high (30).



In comparison to the PRF detection scheme of Gandelman et al. (11, 12), the donor concentration when quinones are detected through photoreduction is increased by about 9 orders of magnitude, relative to the detection limit for a good HAD analyte. At very low donor concentrations, the photochemistry of quinones can no longer be explained with simple hydrogen transfer mechanisms (28, 39–41). For example, the photochemical background reaction in PRF was greater than would be predicted for the level of HAD impurities in HPLC grade acetonitrile (12). In aqueous solution, the evidence points to the formation of a photosolvate between the triplet quinone and water (28, 39–41). This photosolvate can react with a ground-state sensitizer to form a hydroxylated semiquinone radical and a semiquinone radical. A long-lived transient observed during flash photolysis of anthraquinone sulfonates in acetonitrile indicates that it may be possible for photoadducts to form in solvents other than water (41). Many other mechanisms for these background reactions have been proposed.

Regardless of the mechanism, the background reactions of the sensitizer in the absence of HAD substrate limit the sensitivity of both the aerobic and anaerobic detection schemes for HAD analytes (12). Donor-limited background reactions do not come into play when quinones are detected by PRFQ. In the absence of the large photochemical background signals, the ultimate sensitivity of the detector is much higher. Furthermore, nonradiative deactivation of the reactive triplet states ($\text{T}_1 \rightarrow \text{S}_0$) in PRF detection competes with hydrogen abstraction and decreases the efficiency of the photoreduction reaction (reactions 12 and 13). With a triplet lifetime on the order of 100–200 ns in anaerobic aqueous solutions and quenching rates by HAD analytes of $\approx 2.1 \times 10^7 \text{ M}^{-1} \text{ s}^{-1}$ (e.g., 2-propanol), the quantum yield of photoreduction will be quite low in PRF (28, 30, 41). On the other hand, under the conditions for quinone detection virtually all of the triplet states will decay via hydrogen abstraction (26).

Hydrogen Abstraction. When alkyl amines serve as the substrate, the hydrogen abstraction step is best described as

an electron transfer rapidly followed by a proton transfer (13, 14, 42, 43). For strong sensitizers such as acetophenone, benzophenone, naphthoquinones, and anthraquinones reacting with alcoholic substrates, isotope effects and the lack of a large dependence on the ionization potential of the HAD suggest that electron abstraction and proton transfer occur simultaneously (43, 44). However, some controversy about the mechanism of hydrogen abstraction remains, particularly in the case of the photoreactions between weak sensitizers and alcohols (33, 42–44).

Differentiation between these two limiting mechanisms—abstraction of a hydrogen atom in a single step, or the sequential transfer of an electron followed by a proton—is difficult. The net reaction in either case is the same, a hydrogen atom from the alcoholic substrate is transferred to the quinone sensitizer. The reaction pathways available to the radicals produced by this reaction will determine the identity of the final products.

Both the concerted and sequential descriptions of hydrogen abstraction require an electronic charge-transfer interaction between the sensitizer's lowest triplet state and the HAD substrate (14). Since an n, π^* triplet state is more electrophilic than a π, π^* triplet, the compounds that are most efficient in abstracting hydrogen atoms and/or electrons will have a lowest triplet state with predominantly n, π^* character (13, 14, 30, 34, 45, 46). The intrinsic reactivity of the π, π^* triplet state toward concerted hydrogen abstraction is 2 to 4 orders of magnitude less than the n, π^* triplet (45).

The reactivity of quinone triplet states also depends on the solvent composition. As the solvent polarity increases, the efficiency of the quinone photoreactions decreases (46). This effect is most pronounced when the n, π^* and π, π^* triplet states are close in energy (14, 15). Here, the T_1 and T_2 states will be mixed in character and less reactive than a pure T_1 (n, π^*) state. Increased solvent polarity causes the energy of the reactive triplet (n, π^*) to be raised while the less reactive triplet state (π, π^*) is stabilized (13–15, 46). In the extreme case, hypsochromic shifts of the n, π^* state can cause a change from a T_1 state with primarily n, π^* character in apolar solvents to one that is dominated by π, π^* characteristics at high solvent polarity (13–15, 46). The change in energy of the T_1 (n, π^*) of anthraquinone is ≈ 0.3 – 0.9 kcal/mol between polar and nonpolar solvents (13, 47). Other aromatic carbonyl compounds exhibit shifts of similar magnitude, so the splitting between two triplet states must be very small for an inversion to occur. However, the extent to which the two triplet states are mixed in character depends strongly on the energy separation (14, 15). Energy changes of this magnitude may significantly decrease the reactivity of a sensitizer in polar solvents. When the energy separation between the T_1 and T_2 states is large, a change in the solvent polarity will have little effect on the hydrogen abstraction rate (15).

Substituent groups on the quinone also affect the character of the lowest triplet state. Electron-donating groups destabilize the n, π^* triplet state while stabilizing the π, π^* triplet state (13–15, 34). For example, the lowest triplet state of 1,4-benzoquinone (T_1 n, π^*) increases in π, π^* character as methyl groups are added. The T_1 of duroquinone (tetramethyl-1,4-benzoquinone) has a π, π^* configuration (46). Electron-withdrawing groups have the opposite effect. Through conjugation effects, halogens can lower the energy of both triplet states (13, 15). Some substituents, for example amino or hydroxy, cause the T_1 state to assume a charge-transfer configuration (13–15, 30, 34). This type of triplet state is less reactive toward hydrogen abstraction than even the π, π^* triplet (30, 34). An acidic solution will protonate amino groups and return the T_1 state to an n, π^* or π, π^* configuration (30). Radiationless deactivation of α -hydroxyanthraquinones via

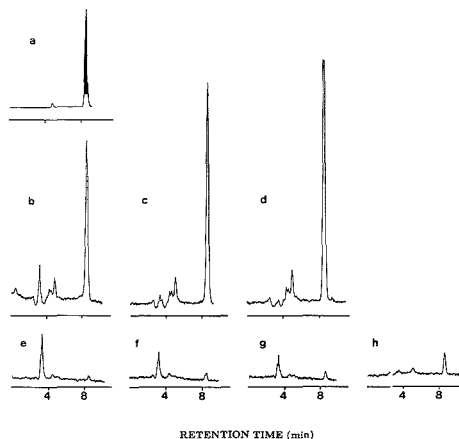


Figure 3. Photoreduction products of vitamin K_1 . Conditions: the HPLC mobile phase, 60:40 methanol:2-propanol was delivered at 1.30 mL/min. PRFQ detection: $\lambda_{ex} = 243.5$ nm, $\lambda_{em} > 370$ nm, $t_{run} = 16$ s. (a) Heart-cut of K_1 peak with the photoreactor lamp on (36 ng injected). The shaded portion of the K_1 peak was collected. (b-d) Photoproduct chromatograms with the photoreactor lamp on. The delay times between collection and injection were 1.5, 38, and 105 min for chromatograms b, c, and d, respectively. (e-h) Photoproduct chromatograms with the photoreactor lamp off. The delay times between collection and injection were 1, 14, 25, and 51 min for chromatograms e, f, g, and h, respectively.

photoenolization renders them particularly unreactive toward hydrogen abstraction (13, 34).

A description of hydrogen abstraction based on nuclear tunneling theory is able to account for the observation that the quantum efficiency of the reaction often decreases as the energy of the triplet state is increased (48). This occurs even though the rate of photoreduction may be higher for the sensitizers with higher energy T_1 states. Tunneling theory can accommodate charge-transfer type substrates as well as those described by "radical-like" hydrogen abstraction mechanisms (48).

Since a carbon-hydrogen bond is broken during the abstraction reaction, its strength will influence the rate of the reaction. The rate constant for hydrogen abstraction on by anthraquinone-2,6-disulfonate increases by more than an order of magnitude with IPA as the substrate in comparison to methanol (32). The ionization potential is important in determining the reactivity of a substrate when the reaction occurs through the charge-transfer mechanism.

RESULTS AND DISCUSSION

Photoreduction Product Stability. The disruption of the photoreduction reaction by oxygen makes the efficient deoxygenation of the HPLC mobile phase a requirement for PRFQ detection (reactions 8 and 9). In order to evaluate the rate that oxygen destroys the fluorescent products, heart-cuts of photoreduced quinone peaks were collected and reinjected into the HPLC system with the photoreactor turned off (after exposure to oxygen during collection). Only small amounts of fluorescent products were detected for vitamin K_1 (Figure 3). Virtually no air-stable fluorescent products were observed during a similar experiment with anthraquinone (7).

The first injections of the heart-cut peaks were performed as rapidly as possible. The decay of the fluorescent products and growth of the peak corresponding to the parent quinone were monitored by subsequent injections. It is evident that the rapid reaction of the photoreduced quinones with oxygen produces compounds (generally nonfluorescent) that are

converted to the parent quinone at a slower rate.

For vitamin K_1 , an early eluting peak ($t_R = 3.3$ min), which appears to consist of at least three components, slowly decays to regenerate vitamin K_1 . This is best evidenced in the photoproduct chromatograms run with the photoreactor lamp turned off (Figure 3e-h). No substantial change in the fluorescence intensity of the early eluting peak occurs between the chromatograms run with the photoreactor lamp turned on (Figure 3b-d) and those with the lamp off. This behavior indicates that the product is natively fluorescent. On the other hand, the vitamin K_1 peak ($t_R = 8.6$ min) in the lamp-off chromatograms (Figure 3e-h) is the result of photoreduction/fluorescence within the detector cell. The disappearance of the fluorescent product(s) coincides with an increase in the intensity of the vitamin K_1 peak and in those peaks caused by other reoxidation products which elute in the 4-5 min retention time range. These compounds are not natively fluorescent but do respond to PRFQ. Such behavior is not surprising in view of the complex photochemistry of vitamin K_1 .

Both the aerobic and anaerobic photochemical reactions of the biogenic K vitamins are complicated by the cyclization and/or degradation of their hydrophobic side chains (13, 49-54). Among the products that result from these photocyclization reactions of vitamin K_1 is a fluorescent naphthochromenol (16, 49, 50, 52). Diradical intermediates in the intramolecular abstraction reactions undergo a variety of rearrangements to produce a complicated mixture of side-products in addition to the naphthochromenol (13, 50-52). Since the photoreduced cyclization products generally are fluorescent, the anaerobic photoreduction/fluorescence detection schemes will work for the K vitamins (16). In fact, the cyclized photoreduction products often are more stable than the dihydroxy PAHs produced from quinones that are incapable of photocyclizing.

Under aerobic conditions, the reaction products include hydroperoxides, cyclic trioxanes, and side-chain fragments (aldehydes and ketones) resulting from the oxidative cleavage of the β,γ -double bond of the phytol or polyprenyl group (50, 51). Photooxidation reactions at the 2,3-position of the naphthoquinone moiety can take place as well (53). Metabolism of the K vitamins also generates these 2,3-epoxides in vivo (54). Strong "solvent" dependences of the photofluorescence reaction indicate that intermolecular hydrogen abstraction also may play a significant role in the photochemistry of K vitamins (49). Invariably, the best solvents are good HAD substrates.

It is likely that the relatively stable fluorescent product is generated by a photocyclization reaction. The nonfluorescent products with intermediate retention times probably result from cleavage of the phytol group or the formation of oxygenated vitamin K derivatives. Since these products are naphthoquinones, they are photoreduced to fluorescent dihydroxynaphthalenes in the photoreactor. Organic peroxides and epoxides also may be formed on exposure of the photoreduced vitamin K to air.

To demonstrate that these products were not artifacts generated during storage of the collected fraction, a heart cut of the K_1 peak was collected with the photoreactor lamp turned off. In both lamp-on and lamp-off chromatograms of this heart cut, only vitamin K_1 is detected. This indicates that flow-cell photoreduction does not convert a large amount of the analyte to photoproducts. However, the intensity of flow-cell photoreduction peaks increased dramatically when the flow-cell gaskets were replaced and the mounting assembly was tightened.

Results from a similar experiment with anthraquinone as the analyte were somewhat different (7). The photoproducts

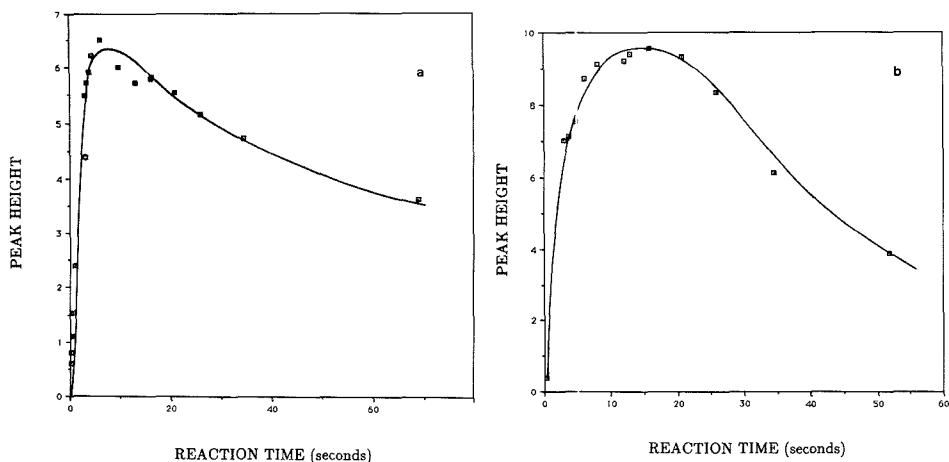


Figure 4. Reaction time optimizations for the PRFQ detection scheme. (a) Vitamin K₁ (2.8 ng/injection). The flow rate was varied with no reactor, a 1.1-m, and a 4.6-m long reactor to produce residence times from 0.2 to 69 s. Conditions: the HPLC mobile phase was 60:40 methanol-2-propanol, with the PMT set at 1000 V, λ_{ex} = 243.5 nm, and λ_{em} > 370 nm. (b) 9,10-Anthraquinone (1.1 ng/injection). The flow rate was varied with no reactor, a 1.1 m, and a 4.6 m long reactor to produce residence times from 0.2 to 52 s. Conditions: the HPLC mobile phase was 85:15 methanol:water with the PMT set at 1000 V, λ_{ex} = 257.5 nm, and λ_{em} > 370 nm.

showed virtually no native fluorescence after a brief exposure to air. A slow decay of a nonfluorescent, weakly retained compound to the parent quinone was observed. This compound was active toward PRFQ detection. As expected, the chromatograms of the anthraquinone photoreduction products were much simpler than those of vitamin K₁. These experiments demonstrated that the major fluorescent photoreduction products react rapidly with oxygen to form longer-lived nonfluorescent compounds. Most of these compounds eventually undergo further oxidation to regenerate the quinone. While reaction 3 describes the overall reaction, the mechanistic details are more complicated.

Similarly, no photoreduction/fluorescence peaks are observed for quinones when oxygen is present in the mobile phase. In fact, the principal disadvantage of the PRFQ detection scheme is the necessity of isolating the photoreactor from oxygen and purging the mobile phase. PTFE's permeability to oxygen is high enough that no PRFQ signal is observed when the photoreactor is exposed to air.

Oxygen is somewhat retained on the ODS column and elutes as a broad quench peak. Purging the sample with nitrogen prior to injection is essential if the analyte elutes in this region of the chromatogram. Increasing the water content of the solution to be injected decreases the magnitude and width of the oxygen quench peak, because the solubility of oxygen is lower in aqueous solutions. Retention of oxygen increases with the water content of the mobile phase, so it is difficult to separate poorly retained naphthoquinones and anthraquinones from the oxygen peak when the samples are not degassed. Alkylated (above ~C₃) naphthoquinones such as vitamin K₁ and anthraquinones without polar substituents are well resolved from the oxygen interference; hence, sample degassing is unnecessary for these analytes.

The lamp-off chromatograms in Figure 3 also demonstrate the low photoreduction background for PRFQ detection. The base-line noise is virtually unchanged by the small photoreduction/fluorescence background (lamp on).

Optimization. The dependence of the signal intensity on the reaction time is a significant factor in the optimization of any photochemical reaction-detection system. Generally, the optimal reaction time will be a compromise between the gain in sensitivity achieved by forcing the photoreaction to-

ward completion and the losses caused by photodegradation and band broadening. Analysis time and reactor back pressure are additional considerations.

The optimal reaction time for PRFQ is extremely short, 5–15 s, and allows relatively high flow rates to be used without causing a large back pressure in the photoreactor. Furthermore, photodegradation of the reduced analytes in the anaerobic system is not severe, so the signal does not decrease sharply beyond the optimal reaction time. This is a major improvement in PRFQ relative to previous work with high-intensity arc lamps (11, 16). Photodecomposition and polymerization are major concerns with high-intensity sources. Band broadening in PRFQ photoreactors is kept low by their design and small volume (23). Hence, the flow rate corresponding to a desired reaction time is limited primarily by the HPLC column rather than the dispersion and back pressure of the photoreactor. Background noise increases slightly with increasing photoreactor residence time. However, the noise contribution from the fluorometer is much greater than that of the photoreduction/fluorescence background.

To obtain reaction time optimization, two reactors, 1.1 m (0.09 mL) and 4.6 m (0.38 mL) in length, were used. The results are given in Figure 4. Flow rates were varied in each of these to achieve the desired residence times. To access extremely short times "no reactor" is used. In this case, the detector cell and lamp serve as both the "photoreactor" and fluorescence excitation source. The residence time in the detector cell (5 μ L) varied from 1.0 to 0.2 s, depending on the flow rate (0.30–1.6 mL/min), (note that this experiment was performed after the fluorescence flow-cell gaskets were replaced). While the highest intensity occurs in the 5–15 s residence time region, a loss of only 15–20% is observed at a 25-s reaction time.

Recognition of the photoreduction/fluorescence taking place within the detector cell is extremely important in interpreting chromatograms, as the fluorescent peaks resulting from photoreduction will decrease in intensity but not completely disappear when the photoreactor is turned off. Furthermore, this implies that a higher intensity source, such as a laser, could achieve sensitivities comparable to the PRFQ with the detector flow cell playing the added role of the photoreactor. A laser used for this purpose also would avoid the disadvan-

tages of arc lamps irradiating conventional photoreactors. Heat production by arc lamps causes the reaction temperature to be a difficult variable to control.

The sensitivity in reactor/flow combinations producing equal residence times consistently was better at the higher of the two flow rates. This behavior was most obvious in the case of 9,10-antraquinone. Oxygen permeable gaskets in the fluorometer flow cell are the most probable explanation for this observation. Oxygen diffusing through the gasket will react with the photoreduced quinones to produce nonfluorescent compounds (reaction 8). Because the photoreduced anthraquinone derivatives react with oxygen faster than those of the naphthoquinones, particularly phylloquinone, the effect is more pronounced in the former case.

To optimize the fluorescence excitation wavelength, several naphthoquinone and anthraquinone derivatives were injected into the system and trapped in the detector cell by stopping the pump and closing a valve located after the cell. A residence time of 10.6 s in the photoreactor was used in this optimization. With a $\lambda_{\text{em}} > 470$ nm filter in place, the photoreduced analyte's excitation spectrum was scanned from 220 to 420 nm. After subtraction of the "blank spectrum" caused by the wavelength dependence of the lamp intensity (stray light), the optimal excitation wavelength regions of 240–249 and 252–260 nm for naphthoquinone and anthraquinone derivatives, respectively, were selected and subjected to closer scrutiny. The optimal λ_{ex} suggested that an emission filter with a shorter cut-off should be used. Emission filters having cut-offs of 370 and 389 nm were about equal in performance.

As previously mentioned, the flow cell allows the entry of oxygen and causes the photoproducts to oxidize back to nonfluorescent compounds. This is observed as a decline in the fluorescence intensity once the flow is stopped. Photodegradation reactions of the analytes may occur within the flow cell under stopped-flow conditions as well. In order to lower the uncertainty this causes in the optimization of the excitation wavelength, chromatograms of a mixture of quinones were run and the λ_{ex} was varied in 0.5-nm increments through the optimal wavelength regions indicated by the stopped-flow experiments. The best performance, in terms of signal-to-noise ratio, was found at excitation wavelengths of 243.5 nm for naphthoquinones and 257.5 nm for anthraquinones. The variation in signal-to-noise ratio for naphthoquinones over the range from 240 to 249 nm and for anthraquinones over the range from 252 to 260 nm typically was less than a factor of 2.5. Since these optima were selected for response to a variety of substituted quinones, the best excitation wavelength for a particular analyte is likely to differ slightly from the "average" optimum.

Selectivity. The selectivity of PRFQ is limited by the fact that natively fluorescent compounds, at least those that are not destroyed in the photoreactor, will produce a response. Photoreduction fluorescence detection is more selective than UV detection. In addition, the sample can be run with the lamp off to screen for compounds that are natively fluorescent, followed by a run with the lamp on to quantify the quinone analytes. As previously mentioned, the reaction is so rapid that quinones will respond as a result of their photoreduction and subsequent fluorescence within the fluorometer detector cell. To completely eliminate responses from quinones, the mobile phase must contain oxygen. However, even in the deoxygenated mobile phases each analyte will exhibit a characteristic change in peak intensity when the photoreactor lamp is turned off and thereby provide a confirmation of the peak's identity. This "lamp on/off" approach has been used with considerable success in conjunction with other photochemical reaction detection systems (9, 10). Many natively fluorescent compounds produce less fluorescence when the

photoreactor is turned on; presumably, this is caused by their photodegradation.

The selectivity of PRFQ was compared to PCCL detection using a cardboard extract which contained low levels of 9,10-antraquinone (1). Despite its higher sensitivity, PRFQ had insufficient selectivity to detect the anthraquinone residue in this matrix. Coextracted phenolic compounds, also residues from the delignification process, probably cause the large number of interfering fluorescent peaks. While PRFQ detection does not compare favorably with the PCCL scheme for the detection of anthraquinone residues in paper extracts, it is much more capable of detecting biogenic quinones. For example, K vitamins, which respond poorly to PCCL, can be detected in difficult matrices by PRFQ.

Comparison of Light Sources. The key considerations in choosing a source for the photoreactor are its intensity and spectral distribution, absorptivity of the analytes over the range of the lamp output, the potential for high backgrounds caused by light-absorbing impurities in the solvents, and prevention of the destruction of the desired photoproduct. Quinones have strong absorption bands in the wavelength region near 254 nm, indicating that a low-pressure mercury lamp is an efficient source for their excitation. A clear advantage of the PRFQ detection mode over PCCL is the ability to use a 254-nm lamp without destroying the photoproduct. H_2O_2 , the photoproduct detected in PCCL, will photolyze when irradiated with 254-nm light. By use of a cooled reactor housing and short reaction times, the photodegradation exhibited by some of the analytes is minimized. Even the pencil lamps used for PRFQ will raise the temperature of the photoreactor housing if it is not equipped with an adequate heat sink. Reactor housings that relied upon the nitrogen flow for temperature regulation as well as oxygen removal consumed too much nitrogen and did not provide sufficient cooling capacity. Therefore, the water-filled housing was designed to alleviate this problem (see Figure 2). With ice-cold water circulated through the copper cooling-coil, the photoreactor was cooled below the ambient laboratory temperature. This improved both the sensitivity and reproducibility of PRFQ detection.

A broad-band (366-nm emission maximum), phosphor-coated Pen-Ray lamp produced low yields of fluorescent photoproducts. The yield of reduced quinones is even lower with the 366-nm lamp than would be expected if the only difference were absorption by the analytes. In fact, a majority of the analyte signal was caused by the 0.3-s residence time in the flow cell rather than the ≈ 30 -s photoreactor residence with the 366-nm Pen-Ray lamp. A probable explanation for this is the squared dependence of the disproportionation reaction (reaction 6). Any reaction that competes with disproportionation for the semiquinone radicals will be more important when the 366-nm lamp is used, because the probability of an encounter between two semiquinone radicals within their solution lifetime is decreased at lower concentrations.

Detection Limits. Detection limits for quinones are dependent on the substituent functional groups and the positions of these functionalities. In Tables II and III, PRFQ detection limits for some quinone compounds are presented. Detection of quinones with greater than three fused rings is improved by the addition of IPA to the mobile phase. This mobile phase additive decreases the retention and improves the sensitivity of detection especially in the case of pentacenequinone (Table III). 1-Aminoanthraquinone responds more sensitively when IPA is the HAD substrate relative to the methanol/water mobile phase. The enhanced reactivity of hydrogens α to secondary alcohols, relative to methanolic hydrogens, is well-known. Presumably this is the result of a weaker car-

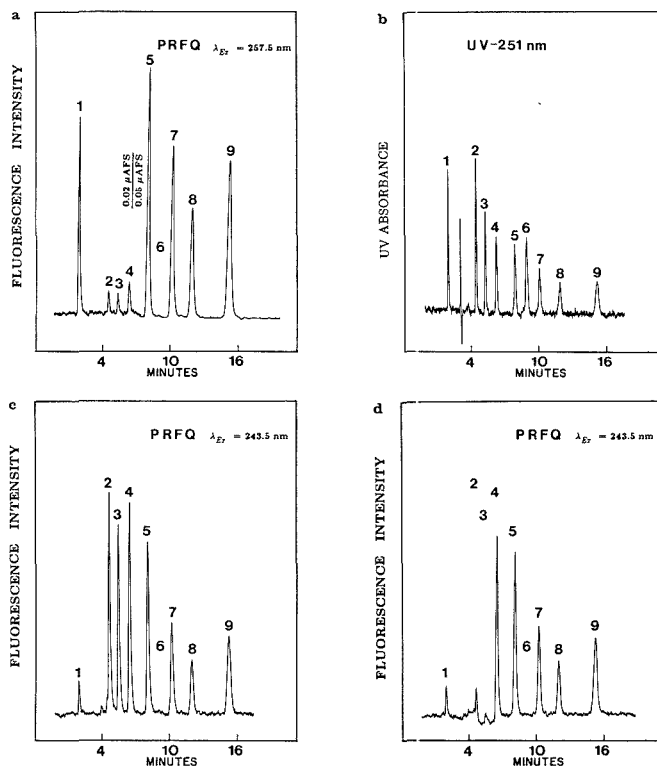


Figure 5. Separation of a quinone mixture. Conditions: the HPLC mobile phase, 89:11 methanol:water, was delivered at 0.80 mL/min. Peaks: (1) 9,10-antraquinone-2-sulfonate (0.59 pmol), (2) 1,4-naphthoquinone (2.4 pmol), (3) 2-methyl-1,4-naphthoquinone (vitamin K_2) (1.6 pmol), (4) 2,7-dimethyl-1,4-naphthoquinone (1.1 pmol), (5) 9,10-antraquinone (0.74 pmol), (6) 1,5-dichloro-9,10-antraquinone (1.1 pmol), (7) 2-methyl-9,10-antraquinone (0.50 pmol), (8) 2-ethyl-9,10-antraquinone (0.42 pmol), (9) 2-*tert*-butyl-9,10-antraquinone (0.55 pmol). (a) PRFQ detection, $\lambda_{ex} = 257.5$ nm. Detector conditions: $t_{run} = 14.6$ s, $\lambda_{em} > 389$ nm, PMT at 1100 V. The sample was degassed before injection. (b) UV detection ($\lambda = 251$ nm). (c) PRFQ detection, $\lambda_{ex} = 243.5$ nm. The sample was degassed before injection. Detector conditions: $t_{run} = 14.6$ s, $\lambda_{em} > 389$ nm, PMT at 1100 V. (d) PRFQ detection, $\lambda_{ex} = 243.5$ nm. The sample was not degassed before injection.

bon-hydrogen bond. This mobile phase is unsuitable for weakly retained analytes. The sensitivity toward 2-amino-antraquinone is not improved by IPA.

Figure 5 presents chromatograms of a mixture of nine quinones under different detection conditions. A 251-nm UV absorbance chromatogram is included for comparison. Improvements in sensitivity over UV detection are obvious. 1,5-Dichloroantraquinone (peak 6), which is present in the UV chromatogram, is not detected by PRFQ, because the fluorescence quantum yield of 1,5-dichloro-9,10-dihydroxy-anthracene is low. The heavy atom effect causes the rate of intersystem crossing to the triplet manifold to increase.

Linear calibration curves of 3 orders of magnitude or more are observed for vitamin K_1 , 9,10-antraquinone, and many other quinone analytes (1). Nonlinearity at very high concentrations, typical of fluorescence detection, is observed in PRFQ as well. Although PRFQ detection is much more sensitive than UV detection, the reproducibility of the UV detector is better. Once again, this primarily is caused by the fluorometer itself, rather than the photoreduction reaction.

Detection of Nitro-PAHs. Nitro-PAH compounds also are detected by PRFQ (see Table II). This response may be caused by either or both of two possible mechanisms. In the first, the nitro-PAH is converted to a quinone, which subsequently is photoreduced (55). Quinone formation from nitro-PAHs is more efficient under aerobic conditions but has

been observed in anaerobic systems. Photoreduction of the nitro-PAH to the corresponding amino-PAH is the second possibility (56, 57). Either reaction pathway will cause a large increase in the fluorescence intensity. While the detection limits are not as spectacular as those achieved by chemically reducing these compounds to amino-PAHs and detection via peroxyoxalate chemiluminescence (58), or fluorescence (59), they are comparable to UV absorption. Once again, selectivity is enhanced. Although the trend in response ratios between the two excitation wavelengths qualitatively agrees with the production of naphthoquinone from 1-nitronaphthalene and anthraquinone from 9-nitroanthracene, these ratios are smaller than would be expected were the quinones the sole photoproducts. It is likely that photoreduction to the amino-PAH is responsible for at least part of the increase in fluorescence. Under aerobic conditions, 9-nitroanthracene is converted to anthraquinone very efficiently in HPLC photoreactors (1).

Application to Vitamin K_1 Detection. As mentioned previously, PRFQ improves vitamin K_1 detection relative to both PCCL and UV detection (Table IV). The on-column detection limits for vitamin K_1 by photoreduction/fluorescence detection reported here are improved by a factor of 5 over those of Lefevre et al. (16). PRFQ compares favorably with all other HPLC detection methods for vitamin K_1 in terms of sensitivity (see Table I). One would expect comparable selectivity between the schemes that detect reduction products

Table II. PRFQ Detection Limits^a

compound	t_r , min	detection limit, pmol ($S/N = 3$)	
		$\lambda_{ex} =$	$\lambda_{ex} =$
		243.5 nm	257.5 nm
1,4-naphthoquinone 2,3-epoxide	3.1	0.20	1.2
2-methoxy-1,4-naphthoquinone	3.4	0.17	1.5
1,4-naphthoquinone	3.6	0.20	2.9
menadiene (vitamin K ₂)	4.3	0.29	2.5
2,7-dimethyl-1,4-naphthoquinone	5.2	0.26	1.6
2,6-dimethyl-1,4-naphthoquinone	5.2	0.25	1.5
2,3-dimethyl-1,4-naphthoquinone ^c	5.5	0.22	1.7
9,10-phenanthrenequinone	3.9	0.19	0.21
9,10-anthraquinone-2-sulfonate	1.6	0.21	0.050
2-hydroxymethyl-9,10-anthraquinone	3.9	0.32	0.077
2-methyl-1-nitro-9,10-anthraquinone	4.9	5.9	2.1
2-amino-9,10-anthraquinone ^b	3.7	0.058	0.038
1-amino-9,10-anthraquinone ^b	5.1	1.7	0.82
9,10-anthraquinone	6.6	0.078	0.026
1,5-dichloro-9,10-anthraquinone	7.8	3.4	1.4
1-(3-methoxyphenoxy)-9,10-anthraquinone ^b	8.1	0.18	0.055
2-methyl-9,10-anthraquinone	8.7	0.078	0.021
2-ethyl-9,10-anthraquinone	10.6	0.10	0.027
2-chloro-9,10-anthraquinone	11.1	0.55	0.10
1,4-dimethyl-9,10-anthraquinone ^c	13.8	0.77	0.19
2-tert-butyl-9,10-anthraquinone	14.6	0.12	0.037
9-anthrone	5.4	0.078	0.042
1-nitronaphthalene	4.7	0.69	2.8
9-nitroanthracene	7.6	0.16	0.077
1-nitropyrene	12.2	0.15	0.22

^aOn column detection limits under the following conditions: HPLC mobile phase, 85:15 methanol-water, delivered at 1.20 mL/min. PRFQ detection: $t_{R_{ex}} = 17.5$ s, $\lambda_{em} > 370$ nm, PMT biased at 1180 V with a 2.5-s time constant. t_r is the uncorrected retention time. ^bNot detected by PCCL at 1 μ g level. ^cPoor response to PCCL (1, 2).

Table III. PRFQ Detection Limits^a

compound	t_r , min	detection limit, pmol ($S/N = 3$)	
		$\lambda_{ex} =$	$\lambda_{ex} =$
		243.5 nm	257.5 nm
2-amino-9,10-anthraquinone	2.7	0.085	0.049
1-amino-9,10-anthraquinone	3.1	0.58	0.23
benz[a]anthracene-7,12-dione	4.6	0.18	0.064
6,13-pentacenequinone	6.1	≤ 0.8	≤ 0.5

^aOn column detection limits under the following conditions: HPLC mobile phase, 60:40 methanol:2-propanol, delivered at 1.20 mL/min. PRFQ detection: $t_{R_{ex}} = 17.5$ s, $\lambda_{em} > 370$ nm, PMT biased at 1180 V with a 2.5-s time constant. ^b t_r is the uncorrected retention time.

of vitamin K₁ by fluorescence, since they are all limited by interference from natively fluorescent compounds. We did not test vitamin K₁ epoxide in this system, as it was not readily available; however, its analogue, 1,4-naphthoquinone 2,3-epoxide, is detected sensitively.

To demonstrate the advantages of PRFQ over UV detection, a Soxhlet extract of the herb *Capsella bursa pastoris*, also known as shepherd's purse, was prepared. This herb is known to contain vitamin K₁ and was available at a local health-food store (Alfalfa's Market) for this reason. From the chromatograms (Figure 6), it is obvious that the PRFQ easily detects the vitamin K₁ and what appears to be a homologue with a shorter hydrocarbon side chain, while the UV chromatogram is swamped with interferences. A second possibility for the homologue peak is K₁ epoxide, which also is found in plants. The UV detector was highly attenuated in order to

Table IV. Detection Limits for Vitamin K₁^a

	detection limit, pmol ($S/N = 3$)			
	PRFQ ^b 4.5-m reactor	PRFQ ^b 4.5-m reactor	PCCL ^c 27-m reactor	UV 247 nm
	100% CH ₃ OH	0.22	60/40	60/40
phylloquinone (vitamin K ₁)	0.22	0.055	78	1.8
V_r , mL	29.2	10.6	10.6	10.6

^aOn column detection limit under the following conditions: HPLC mobile phase, either 100% methanol or 60:40 methanol:2-propanol, delivered at 0.78 mL/min (PCCL) or 1.30 mL/min (UV and PRFQ). ^bPRFQ: $t_{R_{ex}} = 16$ s, $\lambda_{ex} = 243.5$ nm, $\lambda_{em} > 389$ nm. ^cPCCL: $t_{R_{ex}} = 158$ s, TCPO (0.95 g/L) and rubrene (32 mg/L) in acetone delivered at 0.33 mL/min, TRIS buffer (pH = 8.1, 0.5 mM) delivered at 0.15 mL/min (1, 2).

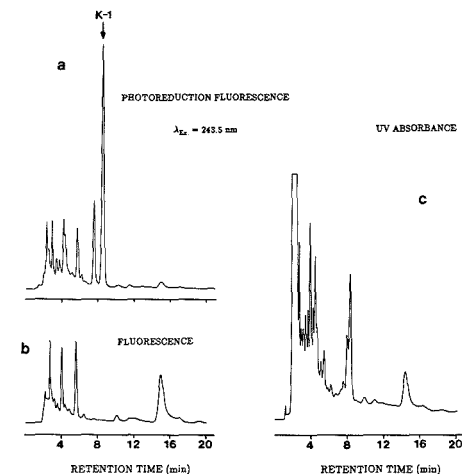


Figure 6. Chromatograms of a plant extract (*Capsella bursa pastoris*). Conditions: the HPLC mobile phase, 60:40 methanol:2-propanol, was delivered at 1.3 mL/min. In both chromatograms the PMT was set at 1000 V, $\lambda_{ex} = 243.5$ nm and $\lambda_{em} > 370$ nm. (a) PRFQ detection ($t_{R_{ex}} = 16$ s). (b) Fluorescence detection (oxygenated mobile phase, no reactor). (c) UV absorption detection at 247 nm. Vitamin K₁ is not detected (the vitamin K₁ peak is buried under the two interfering peaks in the 8–8.5 min retention time region).

bring the chromatogram on scale, so the vitamin K₁ in the sample would produce no detectable peak at this sensitivity, even if the interfering components in the matrix were absent. A fluorescence chromatogram, run with the lamp off and oxygen present in the mobile phase, shows that these two peaks disappear completely in the presence of oxygen (Figure 6b). With the photoreactor turned off and the mobile phase flushed with nitrogen, the height of the K₁ peak is decreased by about a factor of 8 but still is detected through photoreduction taking place within the detector cell. The K₁ standards also exhibited the same "lamp on/off" change in sensitivity.

A chromatogram also was run on a strong "tea" prepared from this herb. Even with PRFQ detection, vitamin K₁ and the "K₁ homologue" were not detected in this sample; indicating that eating this herb would be a more effective method of adding "K vitamins" to the diet than preparing it as a "tea".

ACKNOWLEDGMENT

Figure 1 (insert) and Figure 2 artwork was done by Maria Neary.

Registry No. 9,10-Anthraquinone-2-sulfonate, 84-48-0; 1,4-naphthoquinone, 130-15-4; 2-methyl-1,4-naphthoquinone, 58-27-5; 2,7-dimethyl-1,4-naphthoquinone, 482-70-2; 9,10-anthraquinone, 84-65-1; 1,5-dichloro-9,10-anthraquinone, 82-46-2; 2-methyl-9,10-anthraquinone, 84-54-8; 2-ethyl-9,10-anthraquinone, 84-51-5; 2-*tert*-butyl-9,10-anthraquinone, 84-47-9; 1,4-naphthoquinone 2,3-epoxide, 5824-47-5; 2-methoxy-1,4-naphthoquinone, 2348-82-5; 2,6-dimethyl-1,4-naphthoquinone, 6290-94-4; 2,3-dimethyl-1,4-naphthoquinone, 2197-57-1; 9,10-phenanthrenequinone, 84-11-7; 2-hydroxymethyl-9,10-anthraquinone, 17241-59-7; 2-methyl-1-nitro-9,10-anthraquinone, 129-15-7; 2-amino-9,10-anthraquinone, 117-79-3; 1-amino-9,10-anthraquinone, 82-45-1; 1-(3-methoxyphenoxy)-9,10-anthraquinone, 122357-52-2; 2-chloro-9,10-anthraquinone, 131-09-9; 1,4-dimethyl-9,10-anthraquinone, 1519-36-4; 9-anthrone, 90-44-8; 1-nitronaphthalene, 86-57-7; 9-nitroanthracene, 602-60-8; 1-nitropyrene, 5522-43-0; benz[*a*]anthracene-7,12-dione, 2498-66-0; 6,13-pentacenequinone, 3029-32-1; phylloquinone, 84-80-0.

LITERATURE CITED

- Poulsen, J. R. Ph.D. Thesis, University of Colorado, 1988.
- Poulsen, J. R.; Birks, J. W., unpublished work, University of Colorado, Boulder, 1989.
- Holton, H. H.; Chapman, F. L. *Tappi* **1977**, *60*(11), 121.
- Hagglin, J. *Chem. Eng. News* **1984**, *62*(42), 20.
- Fox, M. A.; Olive, S. *Science* **1979**, *205*, 582.
- Rontani, J. F.; Rambeloarisoa, E.; Bertrand, J. C.; Giusti, G. *Chemosphere* **1985**, *14*, 1909.
- Wraight, C. A. *Photochem. Photobiol.* **1979**, *30*, 767.
- Function of Quinones in Energy Conserving Systems*; Trumpower, B. L., Ed.; Academic Press: New York, 1982.
- Poulsen, J. R.; Birks, J. W. In *Chemiluminescence and Photochemical Reaction Detection in Chromatography*; Birks, J. W., Ed.; VCH Publishers, Inc.: New York, 1988; pp 149-230.
- Birks, J. W.; Frei, R. W. *TrAC, Trends in Anal. Chem.* **1982**, *1*, 361.
- Gandelman, M. S.; Birks, J. W.; Brinkman, U. A. Th.; Frei, R. W. *J. Chromatogr.* **1983**, *282*, 193.
- Gandelman, M. S. Ph.D. Thesis, University of Colorado, 1983.
- Bruce, J. M. In *The Chemistry of Quinoid Compounds, Part 1*; Patai, S., Ed.; J. Wiley and Sons, Inc., Interscience Publ.: 1974; pp 494-507.
- Turro, N. J. *Modern Molecular Photochemistry*; W. A. Benjamin: New York, 1981; pp 362-408.
- Wagner, P. J. *Top. Current Chem.* **1976**, *66*, 1.
- Lefevère, M. F.; Frei, R. W.; Schotten, A. H. M. T.; Brinkman, U. A. Th. *Chromatographia* **1982**, *15*, 459.
- Langenberg, J. P.; Tjaden, U. R. *J. Chromatogr.* **1984**, *289*, 377.
- Kusube, K.; Abe, K.; Hiroshima, O.; Ishiguro, Y.; Ishikawa, S.; Hoshida, H. *Chem. Pharm. Bull.* **1984**, *32*, 179.
- Lambert, W. E.; De Leenheer, A. P.; Lefevère, M. F. *J. Chromatogr. Sci.* **1986**, *24*, 76.
- Lambert, W. E.; De Leenheer, A. P.; Baert, E. *J. Anal. Biochem.* **1986**, *158*, 257.
- Hart, J. P.; Shearer, M. J.; McCarthy, P. T. *Analyst (London)* **1985**, *110*, 1181.
- Lefevère, M. F.; De Leenheer, A. P.; Claeys, A. E. *J. Chromatogr.* **1979**, *186*, 749.
- Poulsen, J. R.; Birks, K. S.; Gandelman, M. S.; Birks, J. W. *Chromatographia* **1986**, *22*, 231.
- Wilkinson, F. J. *Phys. Chem.* **1962**, *66*, 2569.
- Tickla, A.; Wilkinson, F. *Trans. Faraday Soc.* **1965**, *61*, 1981.
- Carlson, S. A.; Hercules, D. M. *J. Am. Chem. Soc.* **1971**, *93*, 5611.
- Larncia, A. A.; Hammond, G. S. *J. Chem. Phys.* **1965**, *43*, 2129.
- Harriman, A.; Mills, A. *Photochem. Photobiol.* **1981**, *33*, 619.
- Hammoue, K.; Kajiwara, Y.; Miyake, T.; Nakayama, T.; Hirase, S.; Teranishi, H. *Chem. Phys. Lett.* **1983**, *94*, 276.
- Hulma, B. E.; Land, E. J.; Phillips, G. O. *J. Chem. Soc., Faraday Trans. 1* **1972**, *68*, 1992, 2003.
- Carlson, S. A.; Hercules, D. M. *Photochem. Photobiol.* **1973**, *17*, 123.
- Cooper, H. R. *Trans. Faraday Soc.* **1966**, *62*, 2865.
- Hammoue, K.; Yokoyama, K.; Miyake, T.; Kasuya, T.; Nakayama, T.; Teranishi, H. *Chem. Lett., Chem. Soc. Jpn.* **1982**, 1967.
- Pitts, J. N., Jr.; Johnson, H. W., Jr.; Kuwana, T. *J. Phys. Chem.* **1962**, *66*, 2456.
- Walker, P. J. *Chem. Soc.* **1963**, 5545.
- Beckatt, A.; Porter, G. *Trans. Faraday Soc.* **1963**, *59*, 2038.
- Hercules, D. M.; Surash, J. J. *Spectrochim. Acta* **1963**, *19*, 788.
- Wells, C. F. *Trans. Faraday Soc.* **1961**, *57*, 1703, 1719.
- Clark, K. P.; Stonehill, H. I. *J. Chem. Soc., Faraday Trans. 1* **1972**, *68*, 177, 1676.
- Clark, K. P.; Stonehill, H. I. *J. Chem. Soc., Faraday Trans. 1* **1977**, *73*, 122.
- Loeff, I.; Treinin, A.; Linschitz, H. *J. Phys. Chem.* **1983**, *87*, 2536.
- Inoue, H.; Kawabe, K.; Noboru, K.; Hida, M. *Bull. Chem. Soc. Jpn.* **1982**, *55*, 1874.
- Hammoue, K.; Kimoto, M.; Kajiwara, Y.; Nakayama, T.; Teranishi, H. *J. Photochem.* **1985**, *31*, 143.
- Hammoue, K.; Yokoyama, K.; Kajiwara, Y.; Nakajima, K.; Nakayama, T.; Teranishi, H. *Chem. Phys. Lett.* **1984**, *110*, 25.
- Formosinho, S. J. *J. Chem. Soc., Faraday Trans. 2* **1978**, *74*, 1978.
- Bunce, N. J.; Ridley, J. E.; Zerner, M. C. *Theoret. Chim. Acta (Berl.)* **1977**, *45*, 283.
- Handbook of Photochemistry*; Murov, S. L., Ed.; Marcel Dekker, Inc.: New York, 1973; p 11.
- Armat, L. G.; Formosinho, S. J.; Da Silva, A. M. *J. Photochem.* **1984**, *27*, 185.
- Leary, G.; Porter, G. *J. Chem. Soc. A* **1970**, 2273.
- Snyder, R. D.; Rappoport, H. *J. Am. Chem. Soc.* **1969**, *91*, 731.
- Wilson, R. M.; Walsh, T. F.; Gee, S. K. *Tetrahedron Lett.* **1980**, *21*, 3459.
- Nakai, T.; Tsuchida, E. *Methods Enzymol.* **1980**, *67*, 148.
- Vire, J. C.; Patriarche, G. J.; Christian, G. D. *Anal. Chem.* **1979**, *51*, 752.
- Willingham, A. K.; Matschiner, J. T. *Biochem. J.* **1974**, *140*, 435.
- Chapman, O. L.; Heckert, D. C.; Reasoner, J. W.; Thackaberry, S. P. *J. Am. Chem. Soc.* **1966**, *88*, 5550.
- Barthrop, J. A.; Bunce, N. J. *J. Chem. Soc., C* **1968**, 1467.
- Ou, A.; Testa, A. C. *J. Am. Chem. Soc.* **1974**, *96*, 1983.
- Sigva tson, K. W.; Birks, J. W. *J. Chromatogr.* **1984**, *316*, 507.
- MacCrehan, W. A.; May, W. E.; Yang, S. D. *Anal. Chem.* **1988**, *60*, 194.

RECEIVED for review December 14, 1988. Revised manuscript received June 14, 1989. Accepted June 16, 1989. This work was supported by grants from the U.S. Environmental Protection Agency (R-810717-01-0 & R-813912-01-0).

Quantitative Analysis in the Presence of Spectral Interferents Using Second-Order Nonbilinear Data

Bruce E. Wilson¹ and Bruce R. Kowalski*

Laboratory for Chemometrics, Department of Chemistry, BG-10, University of Washington, Seattle, Washington 98195

One of the most serious problems that can occur when a model is being used to predict the concentration of an analyte in an unknown sample is the presence of one or more chemical species that are unaccounted for in the calibration samples. With very few exceptions, the model being used to predict analyte concentration is invalidated by the presence of these spectral interferents, and in some cases it is not even possible to detect the invalidation of the model except when nonsensical predictions are obtained. One group of methods that have been used successfully for prediction in the presence of spectral interferents are the rank annihilation methods. This paper compares nonbilinear rank annihilation with three curve resolution methods on three data sets (simulated spectra, two-dimensional nuclear magnetic resonance, and tandem mass spectrometry) for their abilities to accurately predict the concentration of an analyte in the presence of one or more spectral interferents. Multiple linear regression is used as a referee method. It is shown that nonbilinear rank annihilation is the only one of the methods tested which has any potential for solving real chemical problems, inasmuch as the curve resolution methods are not consistently able to correctly solve even idealized cases (with no noise present).

One of the most serious problems that can occur in quantitative analysis is the presence of one or more spectral interferents—chemical species which affect the instrument response and which are unaccounted for in the calibration process. The usual result of the presence of an interferent is that the model used to predict the analyte concentration is invalidated (1-3). If the instrument or procedure used for quantitative analysis produces a single data point per sample (a zeroth-order instrument), then the model will be invalidated without any possibility for detecting the interferent. If, however, the instrument generates a vector of data per sample (a first-order instrument), then it is at least possible to detect the presence of the interferent and thereby know that the prediction model has been invalidated. In such a case, the analyst may then either try to recalibrate to allow for the interferent or else try to remove the interferent from the sample without affecting the concentration of the analyte (e.g. chromatography). These two methods are likely to be expensive and time-consuming, and neither is guaranteed to be successful at eliminating the effects of the interferent, particularly if the interferent cannot be identified. Neither method, however, is likely to be as expensive as the consequences of allowing a spectral interferent to go uncorrected in a routine quantitative analytical procedure.

A third alternative for dealing with the problem of spectral interferents—using a mathematical method to correct for the effects of the interferent—has been the subject of much recent research (4). For the most part, however, the results of these attempts have not demonstrated a potential for application in systems with more than two or three chemical components.

The primary reason for these disappointments was demonstrated by Osten and Kowalski to be an inherent ambiguity in the formulation of the problem (2). The general consequence of their work is that for most quantitative analysis procedures, it is not possible to determine the concentration of the analyte unless one of the instrument's signal channels responds solely to the analyte. It is not necessary that the identity of the unique signal channel be known, only that it exists. However, there is no a priori method of verifying the validity of this assumption and the performance of any method which depends on a unique signal channel will be extremely sensitive to the signal to noise of that signal channel.

One solution to the problem of spectral interferents, which has been successfully used with more complex multicomponent systems, was originally developed by Ho and co-workers (5). This method, which they called rank annihilation factor analysis (RAFA), is applicable to data from a certain type of instruments, including chromatography with multichannel detection (e.g. liquid chromatography/ultraviolet (LC/UV), gas chromatography/mass spectrometry (GC/MS)) and fluorescence excitation-emission matrices (EEM). The important characteristics of these instruments are that (a) each sample yields a matrix of data (as opposed to a single scalar or a vector of data), termed the response matrix, and (b) the rank of a response matrix for a pure chemical component is unity, in the absence of noise. Methods and the data thereby produced which meet these two requirements are classified as second-order bilinear (5-7). RAFA and the conceptual extensions developed by Lorber (8,9) and by Sanchez and Kowalski (10) have been successfully applied to fluorescence excitation-emission (5, 11, 12), thin-layer chromatography with multichannel ultraviolet (UV) detection (13), and liquid chromatography with photodiode UV detection (14-16).

Furthermore, by use of the generalized rank annihilation method (GRAM) developed by Sanchez and Kowalski (10), it is possible to quantitate for multiple analytes in the presence of spectral interferents by using a single calibration sample. The earlier rank-annihilation-based methods of Ho and co-workers and of Lorber allow quantitation in the presence of interferents, but they require the pure component response matrix for calibration and so can only quantitate for a single analyte at a time (although multiple analytes are possible simply by repeating the mathematics for each analyte). GRAM is also more powerful in that it provides the pure component profiles for all of the chemical components present in both the calibration and unknown samples. As an example, if the LC/UV response matrices were measured under exactly the same conditions for a mixture containing eight components at known concentrations and for an unknown which contained some or all of these eight components, then it would be possible to use GRAM to obtain the concentrations in the mixture of these eight analytes as well as their isolated UV spectra and elution profiles. These UV spectra can then be compared against library spectra for confirmation of the identities of the analytes as well as for a measure of the accuracies of the predicted concentrations.

The success applying rank annihilation, particularly GRAM, to real chemical problems is most remarkable in that quan-

¹Current address: Tennessee Eastman Company, P.C. Box 1972, Building 95A, Kingsport, TN 37662.

titration for the analytes of interest in the presence of unknown spectral interferences is possible, but without the requirement of a unique signal channel. Unfortunately, the bilinear data requirement of rank annihilation has prevented the method from being applied to two of the most powerful instrumental methods which can generate a matrix of data per sample: two-dimensional nuclear magnetic resonance (2D NMR) and tandem (two-dimensional) mass spectrometry (MS/MS). To address this problem, Wilson and co-workers (17) developed a method called nonbilinear rank annihilation (NBRA), which they applied to 2D J -coupled NMR spectra of a system consisting of three mono- and three disaccharides in D_2O . Unfortunately, NBRA requires the pure component spectra for calibration, so that the direct multicomponent analysis and qualitative analysis advantages of GRAM are lost. As with all methods which require the pure component calibration spectrum for calibration, NBRA is adversely affected by the presence of matrix effects. However, NBRA opens up a wealth of opportunity for using 2D NMR and MS/MS for direct analysis of mixtures in a manner not previously possible.

In this paper, the usefulness of NBRA for quantitative analysis in the presence of spectral interferences will be compared with that of three curve resolution methods: first zero, entropy minimization, and net analyte signal maximization. Multiple linear regression (MLR) will be used as a referee method to indicate the fundamental quality of the data as well as to demonstrate the effects of spectral interferences on typical multivariate calibration methods. It will be demonstrated that NBRA is the only method which is consistently capable of quantitating for an analyte of interest, even when using idealized mixture spectra (mathematical additions of pure component spectra with no noise present). The failure of the three curve resolution methods and of MLR to give the correct analyte concentrations in these idealized cases is conclusive evidence of the inappropriateness of these techniques for quantitative analysis of real chemical mixtures when spectral interferences are present.

THEORY

Nomenclature. The terminology used for classifying types of instruments and the data they produce is as suggested by Sanchez and Kowalski (3, 7) and is based upon the order of the tensor that can be used to represent the data generated by the instrument for a single sample. A pH meter and a single-wavelength spectrophotometer both generate a single datum for each sample, and so are classified as zeroth-order instruments. A spectrometer or sensor array (18) generates a vector of data (e.g. absorbance at multiple wavelengths) which can be represented as a first-order tensor, and so are both first-order instruments. Note that first order is also sometimes used in the literature to refer to instruments which have a linear response with concentration (i.e. a first-order polynomial); in this paper the term first order will always refer to instruments which produce a vector of data per sample or to the data thereby produced. Hyphenated chromatographic methods, such as LC/UV, and other so-called two-dimensional experiments, such as 2D-NMR and MS/MS, generate a matrix of data per sample and so are second-order instruments. However, not all hyphenated techniques are second order. For example, inductively coupled plasma atomic emission spectroscopy coupled with mass spectrometry (ICP-AES/MS) is a first-order method because one does not measure a mass spectrum of a specific atomic emission line or vice versa (19). In LC/UV, by comparison, one does measure the UV spectrum at a specific chromatographic retention time.

Within second order, a distinction is made between bilinear and nonbilinear data, based upon the mathematical rank of the response matrix for a pure component. For a bilinear second-order instrument, such as hyphenated chromatogra-

phy, the rank of a pure component response matrix is unity. For a nonbilinear second-order instrument, such as MS/MS and 2D-NMR, the rank of a pure component response matrix is larger than one. Another way of expressing the difference between bilinear and nonbilinear instruments is that for a bilinear instrument, the response function $R(x_1, x_2)$ is separable into the product of two independent response functions, $R_1(x_1)R_2(x_2)$, each a function of one variable only. For a nonbilinear instrument, $R(x_1, x_2)$ is not separable. In chemical terms, in LC/UV the elution profile and the UV spectra are independent of one another, but in MS/MS the daughter spectrum is a function of the parent ion mass. In both cases, linear superposition of spectra is assumed, so that the concentration enters into the response function only as a multiplicative constant.

For a second-order instrument, the term order is also used to refer to either of the two independent axes which make the data two dimensional. For example, in hyphenated chromatography, there is a chromatographic order (or axis) and a spectral order. A chemical component's elution profile is then also referred to as its pure component response in the chromatographic order.

Rank Annihilation. The basic concept behind rank annihilation (11) is that the bilinear response matrix N_k for a pure chemical component can be represented by

$$N_k = \mathbf{x}_k c_{k,N} \mathbf{y}_k^T + \mathbf{E} \quad (1)$$

where \mathbf{x}_k and \mathbf{y}_k are vectors which are the pure component response functions in each of the two orders, $c_{k,N}$ is the scalar concentration in some appropriate set of units so that \mathbf{x}_k and \mathbf{y}_k are normalized to unit length, and \mathbf{E} represents unmodeled experimental error. To the extent that \mathbf{E} can be neglected, N_k has rank one. A bilinear response matrix \mathbf{M} for a mixture containing K chemical components can then be written as the sum of K such pure component matrices

$$\mathbf{M} = \sum_{k=1}^K \frac{c_{k,M}}{c_{k,N}} N_k = \sum_{k=1}^K \mathbf{x}_k c_{k,M} \mathbf{y}_k^T = \mathbf{X} \mathbf{C}_M \mathbf{Y}^T \quad (2)$$

where $c_{k,N}$ is the concentrations of the k th chemical component in the mixture, \mathbf{X} is a matrix whose columns are the pure component column space responses (e.g. spectra), \mathbf{C}_M is a diagonal matrix whose elements are the concentrations in appropriate units so that the columns of \mathbf{X} and \mathbf{Y} are normalized, and \mathbf{Y} is a matrix whose columns are the pure component row space responses (e.g. chromatographic profiles). Note that the columns of \mathbf{X} and \mathbf{Y} are not necessarily orthogonal, as would be the case for the singular value decomposition (SVD) of \mathbf{M} . However, if the responses of the K components are linearly independent, then the rank of \mathbf{M} is nonetheless equal to K .

Following work by Ho and co-workers (5, 12) and by Lorber (8, 9), Sanchez and Kowalski developed GRAM (10), which is based on solving the generalized eigenproblem

$$\mathbf{NZ} = \mathbf{MZA} \quad (3)$$

where \mathbf{N} is the bilinear response matrix for a calibration sample containing one or more analytes with known concentrations, \mathbf{Z} is a matrix whose columns are the eigenvectors of this eigenproblem, \mathbf{M} is the bilinear response matrix for the unknown sample, and \mathbf{A} is a diagonal matrix containing the eigenvalues. These eigenvalues are the relative concentrations for the analytes present in both the calibration and unknown samples, in the form $\Lambda_{kk} = c_{p,N}/c_{p,M}$. Even more powerful, however, is the fact that \mathbf{Z} is the pseudoinverse of \mathbf{Y}^T —the pure chemical behavior in the column space (e.g. the pure chromatographic elution profiles).

For a second-order nonbilinear instrument, Wilson and co-workers (17) showed that nonbilinear rank annihilation can

be performed in a manner similar to the GRAM formulation in eq 3. In NBRA, the pure component response matrix N_p has a rank larger than one, so that there are multiple nonzero eigenvalues for the generalized eigenproblem $N_p Z = MZA$, resulting in a number of different concentration estimates. For MS/MS and absolute value mode 2D-NMR the correct concentration estimate is then the smallest of these concentration estimates, in analogy to choosing the solution on the outer bound in two-component self-modeling curve resolution (20).

Curve Resolution Methods. Another approach to the problem of spectral interferences utilizes a class of techniques known as curve resolution. In the form most relevant to this work, one iteratively subtracts the known pure component spectrum from a mixture spectrum until some optimization criterion is minimized or maximized, which then yields an estimate of the concentration of the analyte of interest in the mixture. The term curve resolution is more commonly applied to techniques which attempt to determine the pure component spectra of more than one component present in a series of mixtures. This second class of curve resolution is primarily used for problems of overlapping chromatographic elution profiles in qualitative analysis (4, 20-22), which is a somewhat different problem than that of a known pure component and a single mixture sample which contains one or more spectral interferences. Some of the concepts are applicable between the two types of curve resolution, but the specifics of the algorithms generally are not, so that the chromatographic overlap type of curve resolution will not be further discussed in this paper.

In the case where only the first-order spectra of the mixture containing a spectral interferent (\mathbf{m}) and the pure analyte of interest (\mathbf{n}_p) are available, there are basically two optimization criteria which can be used: (a) monitor $\mathbf{b} = (\mathbf{m} - \alpha\mathbf{n}_p)$ as a function of the scalar α until the first new zero in \mathbf{b} is observed and (b) minimize the information entropy of the difference spectrum (23-25). For second-order data where the pure component response is the matrix N_p and the mixture response is the matrix \mathbf{M} , then a third alternative is possible, which is to maximize the matrix net analyte signal of N_p with respect to the difference matrix $\mathbf{B} = \mathbf{M} - \alpha N_p$ (26).

Method of First Zero. The conceptually simplest of the three curve resolution methods is to monitor \mathbf{b} as a function of increasing α (starting at $\alpha = 0$) until an element of \mathbf{b} which was not zero becomes zero, assuming that the spectra are nonnegative. In practice, this method is best achieved by calculating concentration ratio estimates for each channel as $(\hat{c}_p)_i = c_{p,N}m_i/(n_p)_i$ for all $i = 1, \dots, I$ (the number of wavelengths), $(n_p)_i \neq 0$. The selected concentration estimate is then the smallest of these $(\hat{c}_p)_i$. As with the proposed non-bilinear rank annihilation methods, this method will give a concentration estimate which will tend to be biased low when noise is present. Because of the high degree of sensitivity to noise, this method is generally used within the context of other curve resolution techniques to define a range of concentrations in which to search (20-25, 27).

Entropy Minimization. Because the method of first zero is sensitive to the presence of noise and gives a result which is biased low, Sasaki and co-workers (23-25) proposed that the information entropy be the criterion which is minimized in curve resolution. They originally proposed this concept for use with self-modeling curve resolution (overlapped chromatographic peaks), but the idea is also applicable to the type of curve resolution discussed herein. For the difference spectrum \mathbf{b} , containing I channels (wavelengths) the information entropy is given by

$$H = \sum_{i=2}^{I-1} p_i \ln(p_i) \quad (4)$$

where \mathbf{p} is the normalized first derivative spectrum of \mathbf{b} . At least in theory, H is a unimodal function and for nonnegative spectra, the minimum must occur between zero and the largest concentration estimate from the first zero method: $\max_i \{c_{p,N}m_i/(n_p)_i\}$. As a result, the optimization should be fairly straightforward. As will be shown, the presence of random noise unfortunately causes the function to flatten out (cf. Figure 2) making it more difficult to determine the minimum precisely. Furthermore, the method appears to work fairly well for relatively slowly varying spectra, with a high degree of correlation between channels, but works poorly (if at all) when the spectra contain higher frequency Fourier components.

Net Analyte Signal Maximization. The third curve resolution method evaluated in this paper was suggested by Lorber (26) and is previously unpublished. This method works only for second-order data and involves the net analyte signal (28) generalized to second order

$$N_p^* = (\mathbf{I} - \mathbf{P}_B \mathbf{P}_B^T) N_p (\mathbf{I} - \mathbf{Q}_B \mathbf{Q}_B^T) \quad (5)$$

where N_p^* is the net analyte signal of N_p with respect to the previously defined difference matrix $\mathbf{B} = \mathbf{M} - \alpha N_p$; \mathbf{P}_B and \mathbf{Q}_B are orthonormal basis sets for the column and row spaces, respectively, of \mathbf{B} ; and \mathbf{I} is the identity matrix.

Because optimization processes are most readily solved when the optimization parameter is a scalar, $\xi = \|N_p^*\|_F / \|N_p\|_F$ is then defined, where $\|\cdot\|_F$ denotes the Frobenius matrix norm (square root of the sum of the squares of the elements of the matrix) (29). It will be shown that ξ is fairly well-behaved with a maximum at $\alpha = c_{p,M}/c_{p,N}$ (over the domain of chemically reasonable values of α) for systems where the row and column spaces of N_p are sufficiently distinct from those of the remaining components. Problems occur, however, when the spectra are sufficiently overlapped that the joint row and column spaces of the analyte of interest and one or more of the remaining components describe more variance in \mathbf{M} than is described by the row and column spaces of N_p^* . The problems occur not as a function of the total overlap between N_p and the remaining components, but rather as a function of the largest overlap between N_p and the individual remaining N_i .

Given that the net analyte signal is originally defined in terms of first-order data, it would seem reasonable that net analyte signal maximization curve resolution should work for first-order data. Unfortunately, such is not the case. In analogy with eq 5, define

$$\mathbf{n}_p^* = (\mathbf{I} - \mathbf{b}\mathbf{b}^T) \mathbf{n}_p \quad (6)$$

$$\xi_1 = \frac{\|\mathbf{n}_p^*\|}{\|\mathbf{n}_p\|} \quad (7)$$

where the subscript 1 denotes first-order net analyte signal, $\|\cdot\|$ denotes the usual Euclidian vector norm, and it is assumed that \mathbf{b} has been normalized to unit length. Using the definition that $\mathbf{b} = \mathbf{m} - \alpha\mathbf{n}_p$ and rearranging eq 4 and 5 give

$$\xi_1 = \|\mathbf{n}_p - (\mathbf{n}_p(\mathbf{m} - \alpha\mathbf{n}_p))\mathbf{b}\| / \|\mathbf{n}_p\| \quad (8)$$

$$= \|\mathbf{n}_p - (\mathbf{n}_p\mathbf{m} - \alpha\mathbf{n}_p\mathbf{n}_p)\mathbf{b}\| / \|\mathbf{n}_p\| \quad (9)$$

The quantity $(\mathbf{n}_p\mathbf{m} - \alpha\mathbf{n}_p\mathbf{n}_p)$ is equal to zero when $\alpha = (\mathbf{n}_p\mathbf{m})/(\mathbf{n}_p\mathbf{n}_p)$, which implies that ξ_1 will always have a maximum equal to 1.0 at that α value. Consequently, ξ_1 cannot be used for curve resolution purposes.

Multiple Linear Regression. The referee method, multiple linear regression, has been extensively described elsewhere (1, 30). In the classical formulation of MLR, \mathbf{R} is a matrix whose columns are the responses of the calibration

samples, C is a matrix whose columns are the concentrations of the chemical components in each of the calibration samples, and r_{un} is the response of the unknown sample. The concentrations of the analytes of interest in the unknown sample are then given by $c_{un} = CR_{un}^{-1}$, where superscript -1 denotes the generalized inverse $R^{-1} = (R^T R)^{-1} R^T$. Because the calibration sets used in this comparison contained few samples, the generalized inverse could be readily calculated without the usual collinearity problems.

In order to use second-order nonlinear data with entropy minimization and MLR, which are first-order data methods, the matrices were unfolded into long vectors. If the original matrix contained m rows and n columns, then the resulting vector contained $m \cdot n$ elements. For the 2D-NMR and MS/MS data, these vectors were shortened, and the computational requirements thereby decreased, by eliminating all elements of the vectors which were zero for all samples (both calibration and unknown).

EXPERIMENTAL SECTION

Simulated Spectra. In order to test the application of nonlinear rank annihilation in cases where sources of variation could be controlled, sets of response matrices ("spectra") were constructed for hypothetical pure components using sine and cosine functions. These spectra were mathematically added to generate mixture spectra. For the simulation experiments reported in this paper, none of the analytes has a unique signal channel, so that these simulation experiments are examples of quantitation problems involving completely overlapped, unknown spectral interferences.

For the first set of experiments, each pure component response matrix was constructed from two diads, x_i, y_j ,^T where each x_i contained 60 elements and each y_j contained 40, to generate a system with $m = 60$ rows and $n = 40$ columns. Initially, all four diads (two for each of two pure components) were constrained to be orthogonal; in later experiments the orthogonality constraint was removed by adding phase angles to the sine and cosine functions to generate specific amounts of component overlap. It should be clearly understood that this data set is used in analogy to a mixture of two pure chemical components, with each having a pure component spectrum of rank two.

Two-Dimensional J -Coupled NMR Data. The 2D-NMR spectra of arabinose, cellobiose, lactose, melibiose, sorbose, and xylose in D_2O were the same as those used in the previous paper by Wilson and co-workers (17).

Two-Dimensional Mass Spectra. All MS/MS experiments were performed on a VG-70-SEQ BEQ double focusing tandem mass spectrometer (VG Isotopes, Ltd., Winsford Cheshire, England), consisting of a magnetic sector, an electrostatic sector, and a quadrupole sector. Standards and solutions of warfarin, 3', 4', 5-, 6-, and 7-hydroxywarfarin, and of phenylbutazone were provided by Professor William Trager's research group (Department of Medicinal Chemistry, University of Washington). The warfarin and phenylbutazone standards were prepared by recrystallizing warfarin and phenylbutazone (Sigma Chemicals, St. Louis, MO) from spectral grade acetone (J.T. Baker Chemicals, Phillipsburg, NJ), drying the product, and dissolving known masses (ca. 1 mg) in 1.000 mL (by pipet) of spectral grade acetone. The hydroxylated warfarin compounds were prepared by synthesis, as described by Lewis and co-workers (31), recrystallizing from spectral grade acetone, and also dissolving known masses (ca. 1 mg) in 1.000 mL of spectral grade acetone. Mixture solutions consisting of (a) warfarin and phenylbutazone; (b) warfarin and 5- and 6-hydroxywarfarin; (c) warfarin and 4', 5-, and 6-hydroxywarfarin; and (d) warfarin, phenylbutazone, and all five hydroxywarfarins were prepared by volumetric addition (by pipet) of ca. 100 μ L of each of the appropriate standards.

Two-dimensional mass spectra of the samples were obtained by first measuring the electron impact (EI) one-dimensional spectrum of the seven-component mixture (d) at 70-eV impact using 1.0 μ L deposition on a ceramic direct insertion probe (DIP). From this spectrum, 10 ions at m/e 324, 308, 281, 265, 252, 249, 229, 213, 187, and 183 daltons were selected as daughter ions for which the granddaughter spectra would be acquired. This se-

lection was based on using the 10 most intense peak groups in the spectrum with m/e greater than 150 daltons. Once the daughter ions had been selected, the granddaughter spectrum for m/e 324 in the seven-component mixture was acquired by setting the appropriate instrumental parameters and integrating all of the peak intensities from the burn-off of a 7.5- μ L ceramic DIP deposition. Approximately 70 scans of the m/e 324 granddaughter intensities were collected for the seven-component mixture, with each scan requiring approximately 3 s. The m/e 324 granddaughter spectrum was then similarly acquired from a 4.35- μ L deposition of mixture d, a 2.95- μ L deposition of mixture b, and 1.00- μ L depositions of the hydroxywarfarins. No m/e 324 granddaughter spectrum of mixture a, warfarin, or of phenylbutazone was acquired, because m/e 324 does not appear in the EI spectra of these samples. This process was repeated for each of the remaining nine daughter ions, acquiring spectra for each sample for which the daughter ion had an intensity of at least 0.5% relative to the base peak in the EI spectrum. For the daughter ions occurring in warfarin and phenylbutazone, 1.00- μ L depositions were used; for the daughter ions occurring in mixture a, 1.70- μ L depositions were used; and for the remaining samples, the deposition volumes were as listed above for m/e 324.

The procedure for acquiring the full MS/MS spectrum of these samples is not one which would normally be used in a qualitative or quantitative analysis problem. It is time-consuming and tedious, and very few mathematical methods are capable of conveniently handling this much information. However, these spectra were acquired in this fashion in order to obtain a good data set with which to test nonlinear rank annihilation (NBRA) and to compare NBRA with other methods for solving the problem of spectral interferences. A number of issues must be addressed before true two-dimensional mass spectroscopy can be used in this fashion as a quantitative analysis tool; it is hoped that this work will inspire researchers in this area to work on these problems.

Computations. All computations were performed on a VAXstation II computer (Digital Equipment Corp., Maynard, MA). Rank annihilation was performed as described by Wilson and co-workers (32) using the *geig* routine in Ctrl-C (Systems Control Technology, Palo Alto, CA), which implements the combination shift QZ algorithm as described by Ward (33). Because of the sparsity of the 2D-NMR and MS/MS data matrices, orthonormal basis sets for the column and row spaces were computed where needed using the *svdrs* singular value decomposition, as given by Lawson and Hanson (34), which uses column and row permutations to obtain more stable decompositions of sparse matrices. The curve resolution computations were written in the C programming language, using Brent's rule optimization (35) for finding function minima and maxima.

RESULTS AND DISCUSSION

Effect of Random Noise. In order to compare the effects of white noise on the prediction errors, first zero curve resolution (FZ), entropy minimization curve resolution (EM), net analyte signal curve resolution (NAS), and nonlinear rank annihilation (NBRA) were used to predict the concentration of the first pseudocomponent in a simulated mixture containing one other pseudocomponent using 30 repetitions at each of 15 levels of simulated white noise. The results of these experiments are summarized in Figure 1. The effects of noise on the shape of the information entropy function and the shape of the net analyte signal function are shown in Figures 2 and 3, respectively. In Figures 1 through 3, the percent added noise refers to the standard deviation of the normally distributed simulated white noise, expressed as a percentage of the tallest peak in the spectrum.

As expected, the FZ curve resolution method shows the greatest susceptibility to white noise. This particular method is unique in that the performance of the method actually degrades with the addition of more unique signal channels. If, for example, the spectrum of the analyte of interest contains three unique signal channels each with a relative noise standard deviation of 2%, then there is a probability of 0.077 that the estimated concentration will be low by more than 4% and a probability of 0.004 that the estimate will be low by more

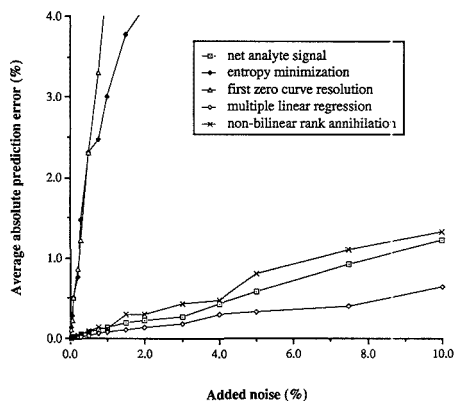


Figure 1. Comparative prediction errors as a function of added noise. The first zero curve resolution prediction error continues to increase to a maximum of 59% and the entropy minimization curve increases to a maximum of 18%.

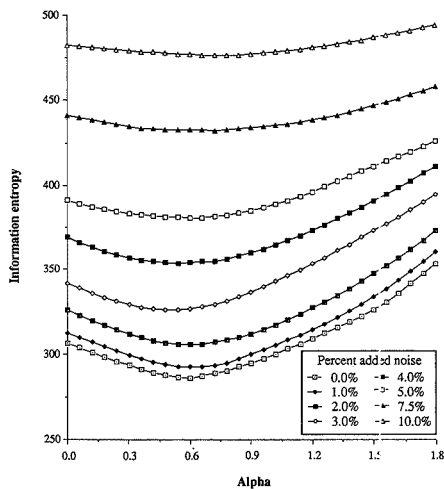


Figure 2. Effect of added noise on the information entropy function. The true concentration ratio (α_0) is 0.6.

than 6% (assuming normally distributed errors). If, however, the spectrum contains 15 unique signal channels, then the probability that the estimate is low by more than 4% increases to 0.293% and the probability that the estimate is low by more than 6% increases to 0.020.

The method second most susceptible to noise is entropy minimization curve resolution, the other first-order curve resolution method. Not only does the average prediction error increase substantially faster than NAS curve resolution, but the average predicted concentration is smaller than the true concentration for all levels of added noise. This bias is surprising, since none of the previously published reports of this technique give any indication of such a problem (23, 24, 36). As a possible explanation for this phenomenon, let \mathbf{m} , the mixture response vector, be modeled by $\mathbf{m} = \mathbf{m}_0 + \mathbf{e}$, where \mathbf{e} contains all of the error. The information entropy of the difference vector $\mathbf{b}_0 = \mathbf{m}_0 - \alpha\mathbf{n}$ will have a minimum at $\alpha = c_{k,M}/c_{k,N}$ while the difference vector $\mathbf{b}_e = \mathbf{e} - \alpha\mathbf{n}$ will have a

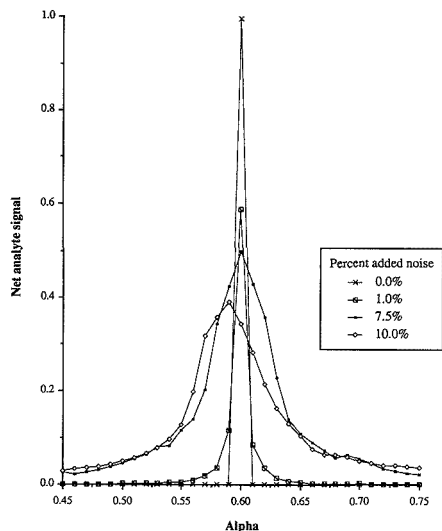


Figure 3. Effect of added noise on the net analyte signal function. The true concentration ratio (α_0) is 0.6.

minimum at $\alpha = 0$. Although the information entropy of a sum of vectors is not equal to the sum of the entropies of the individual vectors, the result is nonetheless two competing effects. One effect has a minimum at α equal to zero and should have an increasing influence as the amount of noise increases (\mathbf{e} becomes more important in determining \mathbf{m}), while the other effect has a minimum at $c_{k,M}/c_{k,N}$.

The net analyte signal curve resolution method performs very well in these experiments, with prediction accuracies slightly better than those of NBRA and without the systematic bias shown by NBRA. However, both the NAS and NBRA results are generally very good. Adding random noise to 10% of the tallest peak in the spectrum only results in a 1% prediction error, a good example of the benefits of effective signal averaging in multivariate methods. As discussed by Wilson and co-workers (17), the NBRA method is biased toward low concentration estimates for very similar reasons to those for the first zero curve resolution. In both cases, the method chooses the smallest from a series of concentration estimates. As the amount of noise increases, the spread of the concentration estimates increases, and the smallest estimate tends to get smaller.

The results from using MLR are, not surprisingly, more accurate than those from the other four methods. However, this is not a fair comparison, since the other four methods use only the pure component spectrum of the analyte of interest for calibration. MLR requires calibration information from all of the pure components in order to predict the concentration of the analyte of interest. This fact will be discussed in more detail below, where MLR will be used with incomplete calibration information.

Effect of Interferent Concentration. To test the effect of the concentration of the spectral interferent, one mixture spectrum (mix 1) was constructed with the concentrations equal to 1.8 for the first pseudocomponent (pure 1) and 4.0 for the second (pure 2), and a second spectrum (mix 2) was constructed with respective concentrations of 1.8 and 0.2. The five methods were then used to predict the concentration of pure 1, using 30 repetitions at 2% added noise. The results of these experiments are summarized in Table I.

Table I. Effect of Interferent Concentration on FZ, EM, NAS, NBRA, and MLR Predictions for Pseudocomponent Pure 1^a

	FZ		EM		NAS		NBRA		MLR	
	mean	std dev								
mix 1	1.630	0.086	0.567	0.331	1.801	0.006	1.798	0.007	1.800	0.003
mix 2	1.631	0.083	1.692	0.069	1.800	0.005	1.798	0.005	1.800	0.003

^aThe true concentration is 1.8. In mix 1 the interferent concentration is 4.0; in mix 2 the interferent concentration is 0.29.

Table II. FZ, EM, NAS, NBRA, and MLR Predictions from a Six-Component Sugar Mixture Using 2D-NMR Spectra^a

	true	FZ	EM	NAS	NBRA	MLR
arabinose	23.12	7.43	15.53	14.86	20.64	23.91
cellobiose	11.40	4.43	6.18	7.49	9.77	11.24
lactose	39.10	17.56	25.37	20.41	40.53	40.48
melibiose	17.80	8.40	11.89	21.33	17.19	18.30
sorbose	3.67	1.33	2.80	4.60	3.35	3.62
xylose	23.07	11.55	14.26	21.33	24.26	23.68

^aAll concentrations are in mg of solute per mL of D₂O.

Table III. FZ, EM, NAS, NBRA, and MLR Predictions from a Simulated Ideal Case Six-Component Sugar Mixture Using 2D-NMR Spectra^a

	true	FZ	EM	NAS	NBRA	MLR
arabinose	23.12	23.12	29.33	34.36	23.12	23.12
cellobiose	11.40	11.40	20.42	19.99	11.40	11.40
lactose	39.10	39.10	62.78	163.41	39.10	39.10
melibiose	17.80	17.80	26.89	26.59	17.80	17.80
sorbose	3.67	3.67	4.03	5.63	3.67	3.67
xylose	23.07	23.07	23.07	26.43	23.07	23.07

^aAll concentrations are in mg of solute per mL of D₂O.

Of the five methods, only the entropy minimization concentration prediction is biased by the interferent concentration. When the interferent concentration is large, the concentration predicted by EM is biased negatively from the true concentration, but when the interferent concentration is small, the EM prediction is near the true value. The negative bias when the interferent has a large concentration is due to the fact that the correlation (dot product) between these two spectra is less than zero. If the projection of the spectral interferent onto the spectrum of the analyte of interest was positive, then the bias in the predicted concentration would also be positive. Note also that the standard deviation of the concentration predictions for EM are substantially larger when the spectral interferent is present at the larger concentration. The reason for this is that the presence of the spectral interferent causes the information entropy function to flatten out, which in turn makes the minimum less sharp and increases the prediction error. When the interferent is present at a low concentration, the flattening effect is minimized and a more precise prediction can be obtained.

Application to 2D-NMR Data. Table II summarizes the results of applying the five methods to a mixture of six sugars in D₂O using 2D-NMR absolute value mode COSY spectra of the six pure sugars and the mixture. Because the NAS and EM predictions were substantially different from the true concentrations and the NBRA and MLR predictions, a "best

case" system was constructed by mathematically adding the pure component spectra to simulate the mixture spectrum under ideal circumstances. The results of applying the five methods to this idealized system are given in Table III.

As might be expected, the first zero method does not correctly predict the concentrations of the sugars in the real mixture. Because each sugar spectrum has unique regions, however, the first zero method is able to correctly predict the concentrations in the idealized mixture. The entropy minimization curve resolution method gives somewhat better prediction for the real mixture than does the first zero method, although the results are all biased low. However, EM curve resolution does not give the correct concentrations for the idealized mixture, with the exception of the xylose prediction. A comparison of the information entropy functions for the real and idealized cases for lactose shows that the information entropy function from the real mixture has a higher base line than does the function from the idealized mixture. The entropy function for the real mixture has a fairly distinct minimum, except that the minimum occurs at the wrong concentration. The function for the ideal case mixture, however, does not have a distinct minimum, but instead has a very broad valley. This type of behavior for the information entropy function, particularly in an ideal case, has not been previously reported in its application to the curve resolution problem (23, 24, 36). A possible explanation for the fact that this phenomenon has not been previously noted is that the first-order pseudospectra from vectorization of the COSY spectra have a lot of fine structure and, consequently, a relatively large number of high-frequency Fourier components. Previous applications of this method primarily used infrared and ultraviolet-visible spectra, which generally do not contain these higher frequency Fourier components.

The new analyte signal curve resolution method more accurately predicts the concentrations of the sugars in the mixture than do the other two curve resolution methods. However, NAS curve resolution does not correctly predict the concentrations of any of the sugars in the idealized mixture. Even xylose, which has the most distinct spectrum and which is the only one correctly predicted by EM curve resolution, is predicted incorrectly by NAS curve resolution.

The nonbilinear rank annihilation predictions for the real mixture are the most accurate of the methods with incomplete calibration information. NBRA is also the only method which exactly predicts the concentrations of the analytes of interest in the idealized mixture. Because of this fact, NBRA is the only one of the methods with any practical potential for quantitation with second-order nonbilinear data in the presence of spectral interferents.

As previously mentioned (1), the MLR referee method requires calibration information from all of the components

Table IV. MLR Prediction from a Six-Component Sugar Mixture Using One Component for Calibration^a

	arabinose	cellobiose	lactose	melibiose	sorbose	xylose
true conc	23.12	11.40	39.10	17.80	3.67	23.07
real mix	3948	2282	423.0	878.7	1821	506.5
ideal mix	10950	11160	1488	2713	4513	1162

^aOnly the pure component spectrum for the analyte of interest was used to construct the calibration model.

Table V. MLR Prediction from a Six-Component Sugar Mixture after Deleting the Lactose Spectrum from the Calibration

	arabinose	cellobiose	lactose	melibiose	sorbose	xylose
true conc	23.12	11.40	—	17.80	3.67	23.07
real mix	13.41	-8.96	—	25.33	3.75	30.73
ideal mix	22.47	13.55	—	20.59	3.94	23.86

Table VI. FZ, EM, NAS, NBRA, and MLR Predictions from a Mixture of Warfarin, Phenylbutazone, and 3', 4', 5-, 6-, and 7-Hydroxywarfarin Using MS/MS Spectra

	true	FZ	EM	NAS	NBRA	MLR
warfarin	0.0858	0.1028	0.0000	0.1116	0.0888	0.0871
ph butazone	0.1153	2.476	0.0822	0.1250	0.1118	0.1129
3'-OH warf	0.1337	5.576	0.0000	0.4045	0.1358	0.1312
4'-OH warf	0.2092	1.870	0.3185	0.4305	0.2111	0.2102
5-OH warf	0.1542	0.4946	0.2819	0.4046	0.1498	0.1597
6-OH warf	0.1720	0.1749	0.2146	0.7885	0.1668	0.1685
7-OH warf	0.1997	0.2301	0.2782	0.5743	0.1966	0.1946

Table VII. FZ, EM, NAS, NBRA, and MLR Predictions from an Ideal Case Mixture of Warfarin, Phenylbutazone, and 3', 4', 5-, 6-, and 7-Hydroxywarfarin Using MS/MS Spectra

	true	FZ	EM	NAS	NBRA	MLR
warfarin	0.0858	0.0858	0.0859	0.1063	0.0858	0.0858
ph butazone	0.1153	0.1153	0.1153	0.1158	0.1153	0.1153
3'-OH warf	0.1337	0.1377	0.1446	0.3973	0.1337	0.1337
4'-OH warf	0.2092	1.0291	0.2092	0.4137	0.2092	0.2092
5-OH warf	0.1542	0.4474	0.4402	0.3801	0.1542	0.1542
6-OH warf	0.1720	0.1720	0.1720	0.7687	0.1720	0.1720
7-OH warf	0.1997	0.1997	0.3394	0.5593	0.1997	0.1997

present in the mixture in order to predict the concentration of the analyte of interest. To demonstrate this fact, MLR was used to predict the concentration of the analyte of interest using only the analyte's pure component spectrum for calibration. These results are given in Table IV. Using only the pure component spectrum for calibration then allows for a direct comparison of MLR and the other four methods, using the same incomplete calibration information. Clearly, from the data presented in Table IV, under these sorts of circumstances MLR is outperformed even by the first zero curve resolution method.

As a more realistic example of using MLR when spectral interferents are present, the pure component spectra of arabinose, cellobiose, melibiose, sorbose, and xylose (but not lactose) were used to construct an MLR model. This model was then used to predict the concentrations of these five sugars in both the real and simulated best case mixtures. As shown in Table V, the MLR model does not give the correct concentrations for the idealized mixture and even predicts a negative concentration for cellobiose in the real mixture. This type of inaccurate prediction result in the presence of spectral interferents is typical for regression methods (1, 37), although this particular example is interesting because leaving lactose out of the calibration model actually improves the prediction for sorbose somewhat. The reason for the prediction of sorbose being relatively unaffected by the presence of lactose as a spectral interferent is that the chemical structures in lactose are also present in cellobiose and melibiose. Consequently, the regression coefficients for sorbose are already nearly orthogonalized to lactose and the prediction is relatively unaffected. By the same token, the presence of lactose as a spectral interferent has a very significant effect on the predictions for cellobiose and lactose.

Application to MS/MS Data. As a second basis for evaluation using real chemical data, the five methods were used to predict analyte concentrations from MS/MS spectra of (a) a mixture of warfarin and phenylbutazone; (b) a mixture of warfarin and 5- and 6-hydroxywarfarin; (c) a mixture of warfarin and 4', 5-, and 6-hydroxywarfarin; and (d) a mixture of warfarin, phenylbutazone, and 3', 4', 5-, 6-, and 7-hydroxywarfarin. The results for the real and idealized seven-component mixture (case d) are given in Tables VI and VII, respectively; the results from the other three cases are qualitatively similar and will not be further discussed herein. It should be pointed out that warfarin and phenylbutazone parent ions are isobaric at 308 daltons and that the hydroxywarfarin parent ions are all isobaric at 324 daltons.

The results of these experiments are, in general, not qualitatively different from those obtained by using the 2D-

NMR data. FZ curve resolution does not correctly predict any of the analytes in the real case and is accurate in the idealized case only for five of the seven components. The fact that FZ does not correctly predict the concentrations of 4'- and 5-hydroxywarfarin in the idealized case is because these two components do not have unique mass peaks. Similarly, EM curve resolution does not accurately predict any of the components in the real case and is correct for only three of the seven components in the idealized case.

As with the NMR data, the NAS curve resolution method is unable to correctly predict the concentrations of the analytes in the idealized mixtures, although in a few cases the predictions are fairly close. For most of the analytes, however, the NAS curve resolution predictions are substantially larger than the true values. Comparing the real and idealized case NAS functions shows that the functions for the real mixture have a lower base line than those for the idealized mixture, although the function peaks in both cases have similar widths. NAS function for the idealized mixture also shows multiple maxima and is broader than would be expected for a spectrum with no noise (based on the simulated spectra discussed above). For both real and idealized mixtures, the functional maxima are substantially displaced from the true concentrations.

The proposed explanation for the problems with the net analyte signal function is then as follows: Recall that the net analyte signal of N_p with respect to the difference matrix \mathbf{B} is given by the Frobenius norm of a projection matrix, $\xi = \|(\mathbf{I} - \mathbf{P}_p \mathbf{P}_p^T) \mathbf{N}_p (\mathbf{I} - \mathbf{Q}_p \mathbf{Q}_p^T)\|_F$, where \mathbf{P}_p and \mathbf{Q}_p span the column and row spaces, respectively, of \mathbf{B} . The scalar ξ then measures the magnitude of the part of N_p which is orthogonal to \mathbf{B} at the current value of α . If component p has a significant part of its row and column space in common with other components present in the mixture, then ξ will also have a minimum when that part of N_p has been subtracted off, which in turn leads to the result is that ξ can have multiple maxima. Further, if the portion of N_p which is orthogonal to all of the other components is small with respect to the portion in common with some or all of the other components, then the global maximum will be displaced from the true concentration ratio. Any local maximum which occurs at the true concentration ratio under these conditions will likely be obscured by larger maxima elsewhere. The presence of noise in the real spectrum then has the effect of blending the multiple maxima into a single maximum, which occurs at an α biased from the true concentration ratio.

Both the NBRA and MLR predictions are exact for the idealized mixtures. For the real spectra, the NBRA predic-

tions have an average error of approximately 2.5%, while the MLR prediction errors are somewhat smaller, about 1.8%. However, as demonstrated above, the NBRA predictions are based on far less calibration information than the MLR predictions. When forced to work with the same amount of information, MLR does not give results which are at all close to the true concentrations. However, the quality of the NBRA and MLR predictions demonstrate that the problems predicting the concentrations in the real and idealized mixtures using EM and NAS curve resolution are due to deficiencies in the methods, rather than to problems with the data itself.

CONCLUSIONS

Of the four methods available to counter the problem of spectral interferences in multivariate calibration using non-bilinear data, only NBRA is consistently able to predict analyte concentrations in idealized mixtures. The failures using idealized data of entropy minimization and net analyte signal curve resolution are conclusive evidence of the deficiencies of these methods for use with real chemical data for this type of problem. By comparison, NBRA is consistently able to accurately predict the concentrations of the analytes of interest in real and idealized cases. NBRA is the only method which can use incomplete calibration information and which was able to exactly solve all of the idealized cases—a necessary prerequisite for solving real chemical problems. Further, NBRA has been demonstrated under relatively demanding conditions—a seven-component real chemical mixture where the analyte of interest is obscured by a completely overlapped spectral interferent.

Even as poor as the EM and NAS predictions are, however, when MLR is forced to use the same calibration information, the curve resolution methods are considerably more accurate. MLR is capable of accurately predicting the concentration of the analyte of interest only when calibration information is available for all of the components present in the mixture. Consequently, NBRA is the only one of the methods tested which has any practical potential for quantitation in the presence of spectral interferences using second-order nonbilinear data.

ACKNOWLEDGMENT

The warfarin, phenylbutazone, and hydroxywarfarin standards were provided by Professor William Trager's research group in the Department of Medicinal Chemistry, University of Washington. The persistence of Rasmy Talaat and Bill Howald in acquiring the MS/MS spectra is gratefully acknowledged. The 2D-NMR spectra were acquired by Walter Lindberg.

LITERATURE CITED

- (1) Beete, K. R.; Kowalski, B. R. *Anal. Chem.* **1987**, *59*, 1007A–1017A.
- (2) Oster, D. W.; Kowalski, B. R. *Anal. Chem.* **1985**, *57*, 908–917.
- (3) Sanchez, E.; Kowalski, B. R. *J. Chemometrics* **1988**, *2*, 247–263.
- (4) Brown, S. D.; Barker, T. Q.; Larivee, R. J.; Wilk, H. R. *Anal. Chem.* **1988**, *60*, 252R–279R.
- (5) Ho, C. N.; Christian, G. D.; Davidson, E. R. *Anal. Chem.* **1980**, *52*, 1071–1079.
- (6) Hirschfeld, T. *Anal. Chem.* **1980**, *52*, 297A–312A.
- (7) Sanchez, E.; Kowalski, B. R. *J. Chemometrics* **1988**, *2*, 265–280.
- (8) Lorber, A. *Anal. Chem.* **1985**, *57*, 2395–2397.
- (9) Lorber, A. *Anal. Chim. Acta* **1984**, *164*, 293–297.
- (10) Sanchez, E.; Kowalski, B. R. *Anal. Chem.* **1986**, *58*, 496–499.
- (11) Ho, C. N.; Christian, G. D.; Davidson, E. R. *Anal. Chem.* **1978**, *50*, 1108–1113.
- (12) Ho, C. N.; Christian, G. D.; Davidson, E. R. *Anal. Chem.* **1981**, *53*, 92–98.
- (13) Grantlill, M. L.; Burns, D. H.; Callis, J. B.; Christian, G. D.; Anderson, N. H. *Anal. Chem.* **1983**, *55*, 1858–1862.
- (14) McCue, M.; Malinowski, E. R. *J. Chromatogr. Sci.* **1983**, *21*, 229–234.
- (15) Ramos, L. S.; Sanchez, E.; Kowalski, B. R. *J. Chromatogr.* **1987**, *395*, 165–180.
- (16) Sanchez, E.; Ramos, L. S.; Kowalski, B. R. *J. Chromatogr.* **1987**, *395*, 151–164.
- (17) Wilson, B. E.; Lindberg, W. A.; Kowalski, B. R. *J. Am. Chem. Soc.* **1989**, *111*, 3797–3804.
- (18) Carev, W. P.; Beebe, K. R.; Kowalski, B. R. *Anal. Chem.* **1987**, *59*, 1529–1534.
- (19) Meyer, G. A. *Anal. Chem.* **1987**, *59*, 1345A–1354A.
- (20) Oster, D. W.; Kowalski, B. R. *Anal. Chem.* **1984**, *56*, 991–995.
- (21) Lawton, W. H.; Sylvestre, E. A. *Technometrics* **1971**, *13*, 617–633.
- (22) Smit, H. C.; van der Heuvel, E. J. *Top. Curr. Chem.* **1987**, *141*, 63–90.
- (23) Kawata, S.; Komeda, H.; Sasaki, K.; Minami, S. *Appl. Spectrosc.* **1985**, *39*, 610–614.
- (24) Sasaki, K.; Kawata, S.; Minami, S. *Appl. Opt.* **1983**, *22*, 3599–3602.
- (25) Sasaki, K.; Kawata, S.; Minami, S. *Appl. Opt.* **1983**, *23*, 1955–1959.
- (26) Lorber, A. University of Washington, personal communication, 1987.
- (27) Friedrich, H. B.; Yu, Y. P. *Appl. Spectrosc.* **1987**, *41*, 227–234.
- (28) Lorber, A. *Anal. Chem.* **1986**, *58*, 1167–1172.
- (29) Golub, G. H.; van Loan, C. F. *Matrix Computations*; Johns Hopkins University Press: Baltimore, MD, 1985.
- (30) Weisburg, S. *Applied Linear Regression*, 2nd ed.; Wiley: New York, 1985.
- (31) Lewis, R. J.; Trager, W. F.; Chan, K. K.; Breckenridge, A.; Orme, M.; Rolard, M.; Scharey, W. J. *Clin. Invest.* **1974**, *53*, 1607–1617.
- (32) Wilson, B. E.; Sanchez, E.; Kowalski, B. R. *J. Chemom.*, in press.
- (33) Ward, R. C. *SIAM J. Numer. Anal.* **1975**, *12*, 835–853.
- (34) Lawson, C. L.; Hanson, R. J. *Solving Least Squares Problems*; Prentice-Hall, Inc.: Englewood Cliffs, NJ, 1974.
- (35) Press, W. H.; Flannery, B. P.; Teukolsky, S. A.; Vetterling, W. T. *Numerical Recipes*; Cambridge Press: Cambridge, 1986.
- (36) Jumarie, G. *Patt. Recog. Lett.* **1987**, *5*, 191–194.
- (37) Chatterjee, S.; Hadi, A. S. *Statist. Sci.* **1986**, *1*, 379–416.

RECEIVED for review April 19, 1989. Accepted June 19, 1989. B.E.W. acknowledges the support of a National Science Foundation Graduate Fellowship, a Center for Process Analytical Chemistry Fellowship, and a Summer Analytical Fellowship sponsored by the Analytical Chemists of Pittsburgh and the American Chemical Society Analytical Division. This work was partially supported by the Office of Naval Research under Contract No. N00014-84-K-0270.

Visible Semiconductor Laser Fluorometry

Totaro Imasaka, Atsushi Tsukamoto, and Nobuhiko Ishibashi*

Faculty of Engineering, Kyushu University, Hakozaki, Fukuoka 812, Japan

A visible semiconductor laser oscillating at 670 nm is used as a light source for fluorescence spectrometry. The detection limit of rhodamine 800 is 4×10^{-12} M, which is slightly better than that obtained by near-infrared semiconductor laser fluorometry. Several dyes with reactive sites, available in the deep-red region, are used as labeling reagents. Nile blue with a primary amino group is most efficiently bound to albumin with water-soluble carbodiimide, but the absorptor maximum is located at 640 nm and is less efficiently detected. Oxazine 750 is less reactive to protein due to its attached ethyl group but gives the largest signal. This is ascribed to good coincidence between the absorption maximum (670 nm) and the laser wavelength. Methylene blue with a tertiary amino group is also used for labeling protein by electrostatic adsorption.

Laser fluorometry provides an ultrasensitive means for chemical analysis. Recently, efforts have been much more concentrated on the determination of trace biological molecules. The detection limits achieved for the fluorescein isothiocyanate derivatives of amino acids are reported to be 0.009 amol in capillary zone electrophoresis (1). Even in indirect fluorometry 70 amol of nucleotides is detected by using sodium salicylate as a fluorescent reagent in the carrier (2).

A laser has great performance, but it has not yet been used as a light source in a commercial spectrometer. This is probably due to the large dimension and expensiveness of the laser. Furthermore, maintenance and operation costs may be additional problems in practical applications. On the other hand, a recently developed semiconductor laser is small and less expensive, and it is simply driven by an integrated circuit or a small battery. The output power of the semiconductor laser was recently reported to 38 W, which exceeds that given by a commercial high-power argon or krypton ion laser (3).

Based on near-infrared semiconductor laser fluorometry, ultratrace analysis has already been demonstrated (4). The detection limit reported for a polymethine dye is 5×10^{-12} M or 12 fg (5, 6). High-performance liquid chromatography based on near-infrared semiconductor laser fluorometry has also been demonstrated, and protein in human serum was determined after labeling it with a near-infrared dye by an electrostatic force (adsorption) (7, 8). The polymethine dye of indocyanine green forms a nonfluorescent species with H_2O_2 , so that an enzyme reaction producing H_2O_2 is monitored (9).

To our best knowledge, all the dyes fluorescent in the near-infrared region belong to a group of polymethine dyes. Three thousand of these molecules are commercially available, but they have no active sites to covalently bind to biological molecules such as protein. Furthermore, the fluorescence intensity of the polymethine dye decreases rapidly in an aqueous solution, which is considered to be due to formation of nonfluorescent dimers (10). The oscillating wavelength of the semiconductor laser used in fluorometry was limited to 750-1500 nm, and it was difficult to find a suitable organic dye for labeling by a covalent bond. It prevents wide use of

semiconductor laser fluorometry in practical work such as the fluorescence immunoassay.

In this study we report the first application of a visible semiconductor laser oscillating at 670 nm to fluorescence spectrometry to overcome the above problems. There are several stable and strongly fluorescent dyes with reactive sites useful for labeling in the deep-red region, e.g. thionine, oxazine, and similar analogues (11, 12). We bind these organic dyes to protein by a covalent or noncovalent bond and discuss their labeling and detection efficiencies.

EXPERIMENTAL SECTION

Apparatus. A block diagram of the experimental apparatus is shown in Figure 1. A sample is injected at the top of a column (Pharmacia Fine Chemicals, K 9/30, 9-mm i.d., 30 cm long) and is separated by a gel (Pharmacia Fine Chemicals, Shephadex G25) by flowing a phosphate buffer (pH 6.4) using a pump (Shimadzu, LC-5A). The eluent is detected by a commercial absorbance spectrometer (Jasco, Uvidec-100-IV), a commercial fluorescence spectrometer (Kyowa, KLF-3080), and a homemade fluorescence spectrometer using a visible semiconductor laser. Details of the laser fluorometric system constructed are shown in Figure 2. The semiconductor laser (NEC, NDL 3200) has an output power of 3 mW and an oscillating wavelength of 670 nm. The laser has a high slope efficiency (~ 1 W/A), and the diode current should be carefully controlled by not allowing the output power to exceed the maximum rating (4 mW). The laser power is regulated by an automatic power control circuit specified by the manufacturer (13). The laser beam is collimated by an objective lens for a microscope (Olympus, LWD MS Plan 50) mounted on a micrometer-controlled stage (Sigma, S-207S). It is focused into a homemade quartz flow cell (1-mm i.d., 10 mm long) or a conventional quartz cuvette for fluorescence spectrometry ($1 \times 1 \times 5$ cm³). Fluorescence from the sample is collected by a pair of glass lenses onto the slit of a monochromator (Jasco, CT-10). A R928 photomultiplier (Hamamatsu) is used for construction of an analytical curve for rhodamine 800 and is replaced by Model R636 (Hamamatsu) with a flatter spectral response for comparison of the fluorescence intensities in chromatography. The signal is amplified 500 times by a homemade amplifier and is directly displayed by a three-pen chart recorder (Rikadenki, R304).

For recording the emission spectrum of the semiconductor laser, a double monochromator (Jasco, CT-40D) was used to reduce stray light. The double monochromator was necessary to measure weak photoemission in the vicinity of the strong oscillating line. The absorption and fluorescence spectra were measured by a double-beam spectrophotometer (Shimadzu, UV-140-02) and a fluorescence spectrophotometer (Hitachi, MPF-4), respectively.

Reagents. Chemical structures of the organic dyes used in this study are shown in Figure 3. Rhodamine 800 (LC 8000) and oxazine 750 (LC 7271) were purchased from Lambda Physik. The other dyes, thionine (Lauth's Violet), Nile blue, and methylene blue, were supplied from Tokyo Kasei, Wako Pure Chemical Industries, and Kanto Chemical, respectively. Albumin (from egg, 018-09882) was obtained from Wako. A bifunctional reagent of water-soluble carbodiimide (1-ethyl-3-[3-(dimethylamino)propyl]carbodiimide hydrochloride) purchased from Dojindo Laboratories was used for the condensation reaction of COOH and NH_2 (or NHR). This reaction scheme is shown in Figure 4.

Procedure. For construction of the analytical curve, rhodamine 800 was diluted stepwise with ethanol. The fluorescence measurement was carried out by using a cuvette. Water-soluble carbodiimide, which has currently been used as a binding reagent for peptide (14, 15), was used to label protein with Nile blue, 27

* Author to whom correspondence should be addressed.

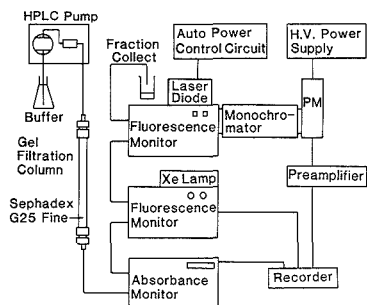


Figure 1. Experimental apparatus for determination of protein. Eluted species are simultaneously detected by three detectors.

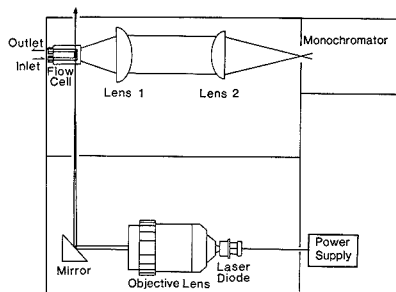


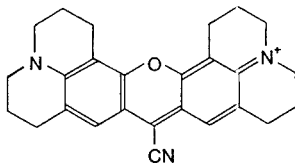
Figure 2. Structure of semiconductor laser fluorometer.

mg for oxazine 750) was dissolved in the 5-mL saturated dye solution at 0 °C by ultrasonic agitation. Several drops of 1 N HCl were added to the solution to adjust the pH to 4.5. Water-soluble carbodiimide dissolved in the phosphate buffer (pH 6.4) was added and the solution mixed gently overnight at 0 °C. For labeling protein with methylene blue, 90 mg of albumin was dissolved in

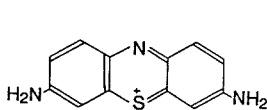
the 9 mL of phosphate buffer (pH 6.4). This solution was mixed with methylene blue dissolved in the phosphate buffer prepared at a specified concentration. The 0.1-mL sample solution was injected into the gel filtration column, and absorption and fluorescence signals were simultaneously recorded. The column was rinsed with concentrated NaOH and a copious amount of buffer to remove dyes that remained at the top of the column.

RESULTS AND DISCUSSION

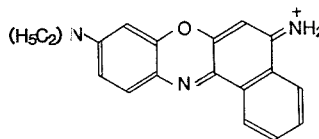
Analytical Curve of Rhodamine 800. In order to investigate the sensitivity of visible semiconductor laser fluorometry, an analytical curve was constructed for rhodamine 800. In this measurement the fluorescence wavelength of the monochromator was adjusted to 700 nm. The absorption maximum was located at 682 nm, which was close to the oscillating wavelength of the semiconductor laser (670 nm). The molar absorptivity is reported to be 8.95×10^4 for ethanol solution (11) and the fluorescence quantum yield to be 39% for dichloroethane solution; the value for ethanol solution is unknown but is estimated to be ~10% (16). The constructed analytical curve was straight from 10^{-11} M to 10^{-6} M. The signal was saturated above this range owing to concentration quenching. The detection limit was 4×10^{-12} M, which was limited by scattering of the exciting light. To investigate the source of noise, the emission spectrum of the semiconductor laser was measured by a monochromator. It was found that a broad background emission was appreciable at the wavelength of fluorescence detection. This is probably due to nonlasing photoemission from the semiconductor laser. The present detection limit is slightly better than the values achieved by near-infrared semiconductor laser fluorometry: 5×10^{-12} M by a digital photon counting system and 5×10^{-11} by an analog lock-in amplifier (5). It is worth mentioning that the present detection limit is achieved by a simple direct current amplifier with a time constant of <1 s. On the other hand, a comparable detection limit is obtained in near-infrared fluorometry only by a photon counting system with an accumulating period of 50 s. Improvement of sensitivity may be partly due to the better sensitivity of the photomultiplier at



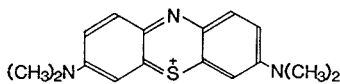
Rhodamine 800



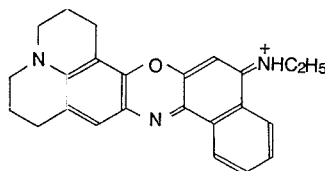
Thionine



Nile Blue



Methylene Blue



Oxazine 750

Figure 3. Chemical structures of organic dyes used for labeling protein.

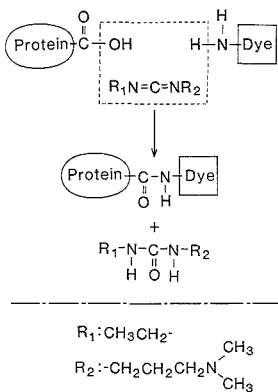


Figure 4. Binding reaction of protein and dye using water-soluble carbodiimide.

Table I. Characteristics of Organic Dyes in the Deep-Red Region

compound	absorption max, nm	molar absorptivity, (M cm) ⁻¹	fluorescence max, nm	saturated concn, M
thionine	600	1.20 × 10 ⁴	623	1.1 × 10 ⁻³
methylene blue	668	6.66 × 10 ⁴	683	1.1 × 10 ⁻¹
rhodamine 800	685	8.95 × 10 ⁴	700	3.1 × 10 ⁻⁴
nile blue	640	7.75 × 10 ⁴	672	2.8 × 10 ⁻⁴
oxazine 750	673	8.25 × 10 ⁴	691	1.5 × 10 ⁻⁴

700 nm and the better light collection efficiency in this experiment. Further improvement may be expected by placing a band-pass filter into a semiconductor laser beam to discriminate the oscillating line against nonlasing emission.

Characteristics of Organic Dyes. Characteristics of several organic dyes available in the deep-red region (~670 nm) are summarized in Table I. In the preliminary work the effort was concentrated on thionine, since it has two active sites of amino groups and its aqueous solution is used for oscillating the laser at around 850 nm by pumping it with a ruby laser (694 nm) (17). However, thionine was found to have an absorption band at 600 nm under moderate pH conditions and to have an absorption band at 670 nm only under strongly acidic conditions (~20 N H₂SO₄).

Methylene blue is strongly fluorescent, and the absorption maximum coincides almost exactly with the oscillating wavelength of the semiconductor laser. However, it has no active site for labeling protein. It is noted that methylene blue is 100 times more soluble in water than the other dyes. Rhodamine 800 may be also used for labeling protein, but it was strongly adsorbed on the Shephadex gel. Thus, it was not used for further investigation.

On the other hand, nile blue with a primary amino group has a rather short absorption maximum, though it is still possible to excite this molecule by using a 670-nm semiconductor laser. Oxazine 750 with a secondary amino group has an absorption maximum that exactly coincides with the oscillating wavelength of the semiconductor laser.

Fluorescence Labeling of Protein. The fluorescence intensity of albumin labeled with equimolar nile blue or oxazine 750 was measured by changing the concentration of water-soluble carbodiimide. The intensity increased and became constant at a 20-times excess of water-soluble carbodiimide. Further addition provided no signal increase. It

Table II. Fluorescence Intensity of Labeled Albumin^a

dye	detection at optimum ^b	laser excitation
nile blue	4.0	0.2 (700 nm) ^c
oxazine 750	1.3	2.0 (690 nm)
methylene blue	1.0	1.0 (683 nm)

^a Values are normalized to those for methylene blue.

^b Calculated from results obtained by lamp excitation.

^c Wavelength for fluorescence detection given in parentheses.

may be due to the decrease of the reactive sites for intermolecular binding; the reactive sites are consumed by the intramolecular reaction with increasing concentration of water-soluble carbodiimide.

The relative fluorescence intensities of labeled protein are summarized in Table II. Nile blue is most efficiently bound to albumin, since it has the most reactive NH₂ group. However, the fluorescence intensity measured by semiconductor laser fluorometry is rather small. This is ascribed to low excitation (11%) and detection (31%) efficiencies, which are due to a mismatch between the absorption maximum and the oscillating wavelength. Oxazine 750 is less reactive to protein because of the hindrance effect of the attached alkyl group and gives a smaller signal intensity at the optimum excitation wavelength. However, it gives the largest signal in semiconductor laser fluorometry, due to good coincidence between the absorption maximum and the laser wavelength. Methylene blue is efficiently adsorbed onto albumin, because of the high saturation concentration. The binding efficiency is much less, but it is still useful for labeling protein.

Labeling Efficiency. By collection of the eluted solution, the absorption spectrum of protein labeled with methylene blue was measured. From the ratio of the absorption intensities for methylene blue at 665 nm to albumin at 280 nm, the mole ratio of bound methylene blue to albumin was determined to be 0.04. The results for nile blue and oxazine 750 were similar to that for methylene blue. This fact indicates that the labeling efficiency is rather poor at present, since albumin has 47 COOH groups in the molecule (18). More efficient labeling may be accomplished by optimizing the reaction conditions (e.g. reaction period, pH, solvent, etc.) and by using a different bifunctional reagent. Further improvement may be effected by developing a labeling reagent with a functional group that directly binds to NH₂ groups in protein without using a bifunctional reagent, as in the case of fluorescein isothiocyanate. Since albumin has 67 amino groups and no intra- and intermolecular binding reactions occur, such a reagent may greatly improve the labeling efficiency in visible semiconductor laser fluorometry.

Sensitivity. From the ratio of the fluorescence intensities for methylene blue in the buffer solution to rhodamine 800 in ethanol, the concentration detection limit of methylene blue is estimated to be 10⁻¹¹ M. Assuming that no spectral change occurs for methylene blue bound to protein, the detection limit of albumin is calculated to be 2.5 × 10⁻¹⁰ M. Since the sample is diluted 10 times in a separation column, the detection limit of the sample injected is 2.5 × 10⁻⁹ M, corresponding to a mass detection limit of 0.25 pmol for albumin. This value is improved to 0.13 pmol for oxazine 750. It is noted that attomole detection limits for amino acids are reported in capillary zone electrophoresis by injecting 300 pL of 10⁻⁵ to 10⁻⁸ M solutions; the sample is detected by focusing a 8-mW laser beam into a detection volume of 3 pL (2). Thus, the mass detection limit may be substantially improved by decreasing the injection and detection volumes, since the semiconductor laser beam can be tightly focused and has a sufficient output power. In indirect spectrometry, stability of the output power is most important to obtain a large dynamic reserve. This value is

reported to be 10^3 for the HeCd laser with a power stabilization unit (2). In the case of a semiconductor laser, this value is readily improved to 2×10^4 by using an automatic power controller. Thus a semiconductor laser is essentially more suitable than other discharge-excited lasers.

Potential Applications. In near-infrared fluorometry there is no dye useful for labeling protein by a covalent bond. On the other hand, many organic molecules are present in the deep-red region. In fact, several dyes are currently used in biological assay. Nucleotides separated by electrophoresis are detected after staining them with methylene blue. This molecule is also used as an oxidation-reduction indicator (12). Therefore, visible semiconductor laser fluorometry will find many applications in the future. For example, a semiconductor laser may be useful in an optical fiber sensor system, since it requires a small light source with good beam-focusing capability. Recently, a frequency-doubled beam of the semiconductor laser was used in an oxygen sensor system (19, 20). However, its available output power is limited to 50 nW to 0.5 pW at present, which is due to the poor conversion efficiency of second harmonic generation. Covalently labeled protein with a deep-red dye may allow direct application of semiconductor laser fluorometry to an optical fiber immunological sensor. It is well-matched to the required compactness of the sensor and may be useful in practical biological assays.

Laser Fluorometric Detection of Porphyrin Methyl Esters for High-Performance Thin-Layer Chromatography

Carmen W. Huie* and William R. Williams

Department of Chemistry, State University of New York, Binghamton, New York 13901

A new detection method is presented for the determination of porphyrins present in biological materials. Separation is accomplished by high-performance thin-layer chromatography after esterification of individual carboxylic acid porphyrins. Detection is achieved by utilizing one of the visible lines of an argon-ion laser for fluorometric excitation. Good selectivity and detectability are demonstrated for the determination of porphyrin profiles in human urine. The detection limits for uro-, heptacarboxy-, hexacarboxy-, pentacarboxy-, copro-, and mesoporphyrin methyl esters are in the 18–35 pg range.

INTRODUCTION

The determination of porphyrins and porphyrin-related compounds is of great biomedical significance. For many years the measurement of total porphyrin content, as well as the relative concentrations of individual porphyrin components, is an essential tool for the confirmation and differential diagnosis of various kinds of porphyrias. Porphyrias are diseases characterized by excessive production and excretion of porphyrins due to defects associated with the enzymes of the heme biosynthetic pathways (1). These disorders may be inherited, such as those occurring naturally within the red blood cell and the liver, or they may be induced, due to exposure to certain toxicants, such as lead or polychlorinated biphenyls. More recently, porphyrins and metalloporphyrins are being actively investigated by chemists and biomedical

LITERATURE CITED

- (1) Cheng, Y. F.; Dovichi, N. J. *Science* **1988**, *242*, 562–564.
- (2) Kuhr, W. G.; Yeung, E. S. *Anal. Chem.* **1988**, *60*, 2642.
- (3) Sakamoto, M.; Welch, D. F.; Harnagel, G. L.; Streifer, W.; Kung, H.; Scifres, D. R. *App. Phys. Lett.* **1988**, *52*, 2220.
- (4) Imasaka, T.; Ishibashi, N. *Am. Biotech. Lab.* **1988**, *6*, 34.
- (5) Imasaka, T.; Yoshitake, A.; Ishibashi, N. *Anal. Chem.* **1984**, *56*, 1077.
- (6) Kawabata, Y.; Imasaka, T.; Ishibashi, N. *Talanta* **1986**, *33*, 261.
- (7) Saudki, K.; Imasaka, T.; Ishibashi, N. *Anal. Chim. Acta* **1986**, *187*, 353.
- (8) Saudki, K.; Imasaka, T.; Ishibashi, N. *Anal. Chem.* **1986**, *58*, 2649.
- (9) Imasaka, T.; Okazaki, T.; Ishibashi, N. *Anal. Chim. Acta* **1988**, *209*, 325.
- (10) Lenherd, J. R.; Parton, R. L. *J. Am. Chem. Soc.* **1987**, *109*, 5808.
- (11) *Laser-Grade Dyes (Data Sheet)*; Brackmann, U., Ed.; Lambda Physik GmbH: D-3400 Göttingen, West Germany, 1986.
- (12) *Indicator*; Bishop E., Ed.; Pergamon Press: Oxford, England, 1972.
- (13) *NEC Data Sheet (LD-7549A)*; NEC Corporation: April 1988.
- (14) *Dojindo Catalog*, 16th ed.; Kumamoto, Japan, 1988; p 71.
- (15) Williams, A.; Ibrahim, I. T. *J. Am. Chem. Soc.* **1981**, *103*, 7090.
- (16) Raue, R.; Harnisch, H.; Drexhage, K. H. *Heterocycles* **1984**, *21*, 167.
- (17) Stepanov, B. I.; Rubinov, A. N. *Soviet Phys. Usp.* **1968**, *11*, 304.
- (18) McReynolds, L.; O'Malley, B. W.; Nisbet, A. D.; Fothergill, J. E.; Givol, D.; Fields, S.; Robertson, M.; Brownlee, G. G. *Nature* **1978**, *237*, 723.
- (19) Okazaki, T.; Imasaka, T.; Ishibashi, N. *Anal. Chim. Acta* **1988**, *209*, 327.
- (20) Imasaka, T.; Hiraiwa, T.; Ishibashi, N. *Mikrochim. Acta*, in press.

RECEIVED for review April 25, 1989. Accepted July 11, 1989. This research is supported by Grants-in-Aid for Scientific Research from the Administration of Education of Japan and by Naito Foundation.

researchers worldwide for the purposes of imaging and photodestruction of cancerous tumors (2). On the other hand, a research group in China has recently shown some very interesting data suggesting the potential use of certain porphyrins for the diagnosis of the onset of some types of cancers (3).

In the early years the separation of porphyrins was usually performed by solvent fractionation methods (4, 5). These methods were laborious and were imprecise in the separation of various porphyrins. In the 1970s, various chromatographic methods have been employed extensively for the separation of porphyrins. Individual porphyrin esters have been successfully separated by thin-layer chromatography (TLC) (6, 7) or by normal-phase high-performance liquid chromatography (HPLC) (8). In the 1980s, the use of reversed-phase HPLC has become very popular since the separation of individual porphyrin carboxylic acids with good resolution and fast analysis time is possible (9, 10).

In the past few years TLC has undergone a renaissance with the development of high-performance TLC (HPTLC). It has become accepted as a sensitive technique for quantitative analysis due to the improvements in resolution and reproducibility (11, 12). The term high-performance stems from the use of 5- μ m HPLC packings on the thin-layer plates. Compared to conventional TLC plates, the decrease in particle size on HPTLC plates requires the application of smaller sample volumes. To minimize errors associated with sample spotting, the use of HPTLC plates equipped with preadsor-

bent area is essential. This preadsorbent area consists of weak sorbent such as kieselguhr or diatomaceous earth. Capillary forces move the development solvent and sample quickly to the interface zone, where the sample is concentrated as a narrow band as it reaches the normal adsorbent such as high-surface-area silica gel. Compared to HPLC, HPTLC is a more economical separation technique because multiple samples can be run simultaneously (13). In addition, with two-dimensional HPTLC, peak capacity can be much greater than with HPLC and more complex samples can be analyzed faster (14). With these advantages, the potential routine usage of HPTLC for the separation of porphyrins present in a variety of biological samples should be explored.

In order to make HPTLC a more attractive technique, the improvements in separation power have to be accompanied by similar advancements in detection power. Several unique properties of lasers such as spatial coherence and high power have been employed for the fluorometric detection of aflatoxins separated by TLC (15, 16). The ease with which the laser beam can be focused to a very small spot while maintaining sufficiently high intensity made it possible to achieve excellent detectability in these experiments. Also, high laser power has made it possible to utilize several nonlinear excited fluorescence techniques in TLC to provide selective detection of certain compounds (17). Moreover, the speed at which two-dimensional measurements can be made on TLC plates has been improved dramatically by the use of a high-speed laser-based acoustooptic scanner (18).

In recent years fluorometric detection after separation by TLC (19) or HPLC (20, 21) has become the method of choice for the study of porphyrias due to its inherent sensitivity and selectivity. However, it remains difficult to determine porphyrins individually at low levels in biological materials because a variety of potential interfering compounds oftentimes appear in the chromatograms while using ultraviolet (UV) radiation for fluorometric excitation (9, 10). In addition, impurities present in even "high-grade" solvents (10, 22) and on TLC plates (15, 17) may contribute relatively high background fluorescence under UV excitation, which prevent the best detection limits that could be achieved.

Excellent detectability and selectivity are very important criteria for the determination of porphyrins present in biological samples because, for examples, the differential diagnosis of various types of inherited porphyrias (23) and the detection of early stages of induced porphyrias require the ability to detect subtle changes of relative concentrations of individual porphyrin components with good reliability (24). Furthermore, improvements in porphyrin determination may lead to better understanding of the advancements in photosensitization processes accompanying the phototherapy of cancer (25) and to improved detection of early onsets of certain types of cancers (3).

In this paper, fluorometric detection of five porphyrin carboxylic acids present in human urine using one of the visible lines of an argon ion laser for excitation is performed after esterification of the free porphyrin acids and subsequent separation by HPTLC. Detectability in the low picogram quantities can be achieved without interferences for the determination of porphyrin profiles of the urine samples.

EXPERIMENTAL SECTION

Apparatus. The experimental arrangement used for laser fluorometric detection of porphyrin methyl esters was similar to the one illustrated in ref 17. Radiation from a Coherent Innova 90-4 argon ion laser was first passed through a 488-nm line filter before it was focused with a 90 mm focal length lens and directed at an angle of about 45° relative to the plate surface. The excitation and emission wavelengths were found to be optimum at 488 and 620 nm, respectively. Typical output power of the laser was 20 mW. To obtain a chromatogram, the thin-layer plate was

scanned in front of the focused laser beam at approximately 30 mm/min using a precision dc-motor-driven translational stage (Newport, Fountain Valley, CA, Model 850-41805-S).

Fluorescence signal was collected normal to the thin-layer plate with an $f/1.25$ mm focal length lens. The signal was then focused by a 80 mm focal length lens onto the entrance slit of a $f/4$ monochromator (MiniChrom 1 from PTR Optics, Waltham, MA). The monochromator was fitted with 2-mm slits and the band-pass was 12 nm. Further fluorescence isolation was provided by Corning 2-73 and 3-66 sharp cut-off filters. The signal was measured with the EMI 9558B photomultiplier tube operated at 900 V. The photocurrents were fed to a picoammeter (Oriental, Stratford, CT, Model 7072) and the output signal was filtered through a 1.0-s time constant before recording on a strip chart recorder.

Standards. Porphyrin standards were obtained from Porphyrin Products, Logan, UT. Each vial contains 10 nmol of eight, seven, six, five, four, and two carboxylic porphyrins as the corresponding methyl esters in the dry form. All of these porphyrins are of type I isomers, except the two carboxylic porphyrin (mesoporphyrin) which is of type IX. Standard solutions were prepared by dissolving the contents of each vial in HPLC grade chloroform (J. T. Baker, Inc., Phillipsburg, NJ). These solutions were kept in the dark at 4 °C and used within a few hours.

Specimens. Twenty-four-hour urine specimens collected with sodium carbonate (5 g/L of urine) and disodium ethylenediaminetetraacetate (3 g/L of urine) as preservatives were stored in the dark at 4 °C until analysis. In order to separate individual porphyrin components with good resolution on thin-layer plates using isocratic elution, the urinary porphyrins must be first esterified. To prepare porphyrin methyl esters, the procedures of Petryka and Watson were used (7). Briefly, 100 mL of urine was acidified with glacial acetic acid to pH 4. Preliminary concentration of the porphyrins by mixing 15 g of talc powder with the urine sample was necessary for the direct esterification of normal urine (8). After sedimentation of the talc with the adsorbed porphyrins, excess urine was removed. The talc powder was then mixed with 20 mL of boron trifluoride in 12% methanol and refluxed in hot water for 20 min. After the esterification procedures, 200 mL of chloroform was added to the talc, and the mixture was shaken and filtered. The talc was washed 3 more times with chloroform. The chloroform filtrate was then washed once with 1% ammonia and once with water. The chloroform fraction was then concentrated to 1 mL before use for spotting on the thin-layer plate.

Chromatography. Separations of various porphyrin methyl esters were performed on 5- μ m silica gel HPTLC plates with preadsorbent area (Whatman Labsales, Inc., Hillsboro, OR). The plates have a dimension of 10×10 cm and a layer thickness of 200 μ m. To minimize background fluorescence from impurities on the plates, the plates were first washed with methanol followed by an additional wash with the development solvent. The chromatography solvent systems described in the literatures for the separation of porphyrin esters in TLC were evaluated. Through systematic investigations we found that the solvent system containing 75:16:2 (v/v/v) of toluene-ethyl acetate-methanol provided the best resolution in our experiment. The development distance from origin to the solvent front was 8 cm. Before development, the silica gel plates were activated and stored in a desiccator at room temperature. Sample volumes ranging from 200 to 500 nL were spotted onto the plates with a 0.5- μ L syringe, followed by drying with a stream of nitrogen to minimize spot size.

RESULTS AND DISCUSSION

By examining the absorption spectra of various porphyrin methyl esters on TLC plates, one would observe that all of them have a major absorption band which centers around 400 nm (7). This is the so-called Soret band region from which the excitation wavelengths of all absorbance and fluorescence measurements using conventional light sources are chosen. Interestingly, a minor absorption band appearing in the visible region can be found which centers around 500 nm, and this happens to fall conveniently within the most intense emission region of an argon-ion laser. Therefore, it is possible to use

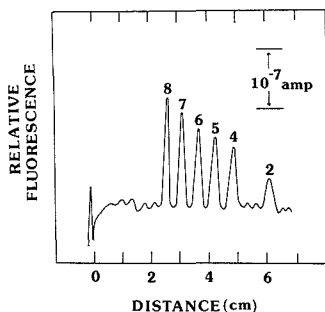


Figure 1. Chromatogram of porphyrin methyl ester standards. The spotted sample consisted of 0.060 pmol of each standard. The number on top of each peak denotes the number of methyl ester groups in the porphyrins: 8 to 4, uro-, heptacarboxy-, hexacarboxy-, pentacarboxy-, and coproporphyrin methyl esters; 2, mesoporphyrin methyl ester. See text for conditions used.

one of the visible lines of the argon-ion laser for fluorometric excitation of porphyrins. Although the laser line is not at the excitation maximum of the various porphyrin methyl esters, the high intensity of the laser will more than compensate for the sacrifice in the magnitude of the molar absorptivity since fluorescence signals are proportional to the light intensity incident onto the sample. More importantly, the spatial coherence of the laser allows all of the radiation to be efficiently utilized in a small area, which should result in improvement in sensitivity. Selectivity will also be improved by using visible laser fluorometry since only a small number of organic molecules present in biological samples absorb in the visible region and yield appreciable fluorescence signals (26, 27).

The excellent resolving power of HPTLC can be seen in Figure 1 in which the standards of six individual porphyrin methyl esters are well separated according to the number of methyl ester groups in the side chains. Uroporphyrin and coproporphyrin, named according to their major sources of occurrences, are important precursors in the biosynthetic pathways leading to the formation of heme. As mentioned earlier, quantitation of excreted porphyrins is a central feature of the diagnosis of porphyrin metabolism. In the case of urine, the porphyrins exist as mixtures of two major fractions, uroporphyrin and coproporphyrin. The overproduction and excretion of these two porphyrins in urine can be used to diagnose the existence of certain acute forms of porphyrias. More interestingly, the discovery of latent forms of porphyrias may be made by examining the relative concentrations of the minor components, namely, hepta-, hexa-, and pentacarboxylic acid porphyrins, which are byproducts of disorders occurring in heme biosynthesis and are present in trace amounts in healthy individuals.

The limits of detection for porphyrins with various numbers of methyl ester groups obtained in our experiment are listed in Table I. These values are similar to those reported for HPLC (20, 21) and about 1 to 2 orders of magnitude better than those reported for TLC (6, 23) in the determination of porphyrins by conventional fluorescence techniques. The improvements in the limits of detection in our method are made possible by the highly fluorescent nature of porphyrins and the enhancement in fluorescence signal derived from the increase in photon flux using a laser source. Unfortunately, large photon flux also contributes to very high background specular scatter from the plate surface, which limits further improvements in detectability. A gradual decrease in fluorescence intensity can be observed in Figure 1 starting from uroporphyrin to mesoporphyrin. This trend could be explained by the decrease in the magnitude of the molar

Table I. Detection Limits and Linearity

porphyrin methyl esters	detection limits, ^a pg	linearity	
		upper limits, ng	linear regression constants ^b
uro	18	1.4	0.996
hepta	19	1.3	0.995
hexa	21	1.2	0.993
penta	23	1.1	0.991
copro	25	1.0	0.993
meso	35	0.9	0.992

^aDetection limits based on $S/N = 3$. ^bLinear regression constants determined from detection limits up to the amounts listed for the upper limits. Each equals to 1.5 pmol of the corresponding porphyrin methyl ester.

absorptivity with the decrease in the numbers of methyl ester groups in the side chains (7, 28) and the increase in sample spot size as the porphyrin moves further away from the sample origin. It is also interesting to note that the silica gel layer is not homogeneous throughout the entire surface of the plate. This is an important factor since at the amplifier sensitivity used to detect low picogram quantities, the signal-to-noise ratio is primarily governed by background fluctuations resulting from plate irregularities. Typically, the layer thickness is more inhomogeneous near the edge of the plate, resulting in a higher degree of irregular base lines in these regions. Care should be taken to select plates that are free from scratches and have relatively homogeneous layer thickness. In Figures 1 and 2, the sharp drop in the signal at 0 cm (sample origin) is due to the laser beam crossing the boundary between the preadsorbent and silica gel layers.

Since our detection system is only capable of scanning the TLC plate in one dimension at a time, the laser beam was focused to a diameter of about 2 mm onto the plate surface to maximize the overlap between the laser spot and the various sample spots that were developed on the plate. Further increase in the laser spot size will degrade the resolution of the chromatogram. A better way to perform the experiment is probably to interface the scanning table to a computer so that two-dimensional scanning could be performed either along a mutually perpendicular direction or in "meander-scanning" mode (29), or better yet, a laser-based acoustooptic scanner may be used to scan the entire plate in just a few seconds (18).

Although high light intensity incident onto the sample is desirable for fluorescence detection, one has to be aware of the potential problem of photodecomposition or photo-oxidation of the sample, especially when the laser beam is focused to a very small spot and the compounds of interest are light sensitive (29, 30). We have done some preliminary investigations on this problem by recording the change in peak areas of the porphyrin methyl ester standards after repetitive scanning of the same sample spot at a particular laser power. We found that at a laser power of 20 mW and laser spot diameter of about 2 mm, there is less than 2% decrease in peak area for 0.060 pmol of uroporphyrin methyl ester after each consecutive scan over the same spot while scanning the plate at ~ 30 mm/min. Under the same experimental conditions a larger decrease in peak area is observed as the number of methyl ester groups in the side chains decreases; a $\sim 4\%$ decrease in peak area is detected for mesoporphyrin. At a laser power of 30 mW and keeping other experimental conditions the same, decreases in peak areas of $\sim 5\%$ and $\sim 8\%$ are recorded for uro- and mesoporphyrin methyl esters, respectively. Of course, the rate of photodegradation is also dependent on the scan rate of the scanning table, and higher laser power could be used at higher scan rate and if the sample spot is only scanned once. The restraint set on the lower limits

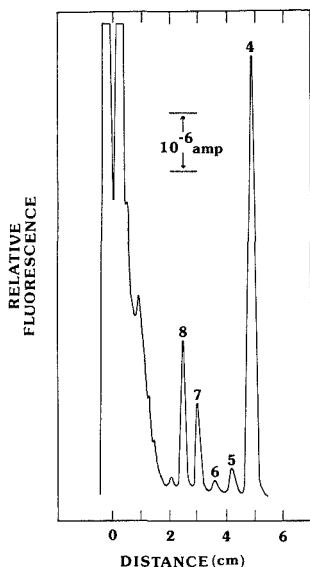


Figure 2. Chromatogram of urinary porphyrins from a healthy non-porphyrin male. As in Figure 1, the numbers 8 to 4 and 2 denote the number of methyl ester groups in the porphyrins. See text for conditions used.

of the scan speed at higher laser powers will limit the ability to employ a long detection time constant to improve detectability. Moreover, it is possible that the loss in fluorescence intensity due to photodecomposition or photooxidation processes is dependent on the wavelength used for excitation and the rates at which these processes proceed may be slower under visible excitation (30, 31). A more detailed study on the effects of the various important experimental parameters on the rate of photodegradation of porphyrins will be performed.

Calibration plots of porphyrin methyl ester standards indicated linear response from the limits of detection up to the values given in Table I. The corresponding linear regression constants are also tabulated. At higher concentrations, non-linearity may arise from self-quenching of porphyrin molecules and quenching through the interactions of porphyrins with the silica gel, involving the singlet state of the π electrons within the porphyrin ring. The linear dynamic range may also be limited by detector saturation from the large fluorescence signal at higher sample concentration and large background specular scatter from the TLC plates.

Figure 2 showed a chromatogram demonstrating the selectivity of using visible laser fluorometry for the determination of porphyrins present in biological fluids. Urinary porphyrins are converted to their corresponding methyl esters and separated on HPTLC plates as described in the Experimental Section. The urine sample was also spiked with the porphyrin methyl ester standards, and the retention times of the standards and the peaks which are marked as the corresponding porphyrin methyl esters (shown in Figure 2) were found to be identical. It is clear that uroporphyrin and coproporphyrin are major components excreted in urine, and the minor components, porphyrins with seven to five carboxylic groups, are detectable from a concentrated urine sample of a healthy male individual *vide infra*. Mesoporphyrin is not excreted in urine. A small peak that appears at about 2 cm in Figure 2 was found in every chromatogram of all urine

Table II. Urine Porphyrin Values

porphyrin methyl esters	typical values for this expt ^a amt excreted, $\mu\text{g}/24 \text{ h}$	range, $\mu\text{g}/24 \text{ h}$	
		normal male population ^b	patients with porphyria cutanea tarda ^b
uro	13	8-44	104-5177
hepta	7	0-12	43-1508
hexa	1	0-5	0-161
penta	3	0-4	0-305
copro	50	10-109	7-263

^a Values determined from chromatogram represented in Figure 2. ^b Reported in ref 9.

samples. This peak has also been reported in the literature and is postulated to have arisen from nonesterified uroporphyrin since it is known that the rate of esterification of the individual porphyrins depends upon the number of carboxylic groups per molecule, and in particular, complete esterification of the relatively small amounts of uroporphyrin in normal urine is very difficult to achieve (6, 8). Certain amounts of fluorescent background, probably due to non-porphyrin materials, can also be observed adjacent to the sample origin. The important feature to notice here is that there are no spurious peaks appearing in between the various urinary porphyrin peaks, which is rather difficult to achieve with UV excitation. The selectivity gained with visible excitation will help in obtaining more reliable excretion patterns of individual porphyrin components present in biological materials, which is probably the most important feature in clinical analysis of porphyrin-related diseases.

The urine porphyrin values calculated from the chromatogram represented in Figure 2 are expressed in Table II. These values are only an estimation since any losses due to incomplete extraction or esterification are not taken into account in our calculations. However, an appropriate mixture of standards could be added to the samples to determine these losses if absolute quantitation is desired. For comparison, this table also presents the rates of urinary excretion of porphyrins by 33 healthy non-porphyrin males and by 15 persons with porphyria cutanea tarda (inherited porphyria of hepatic origin). These data indicated that the urinary porphyrin contents of our samples are well within the range of the healthy male population. It is interesting to note that early onset of porphyria cutanea tarda could be detected by monitoring in particular the excretion of uroporphyrin and heptacarboxylic porphyrin, which showed modest to extreme increase for different individuals.

In summary, the excellent detectability and selectivity achieved in our experiment demonstrated the possibility of using visible laser-induced fluorescence in combination with HPTLC as a competitive and complementary technique to conventional fluorescence methods coupled with HPLC for the determination of trace amounts of porphyrins present in a wide variety of complex biological samples. In addition to the capabilities of having large sample throughput and of achieving superior resolution using two-dimensional development, gradient elution is also possible with HPTLC with the advent of automated multiple-development systems (32); in combination with recently improved reversed-phase HPTLC, it is possible to analyze urinary porphyrins directly without any sample preparation since gradient elution reversed-phase HPLC has already been used to achieve this goal. Limits of detection for free porphyrin carboxylic acids and the corresponding porphyrin methyl esters should be quite similar (20, 28). However, esterification procedures are still oftentimes used for efficient extraction of porphyrins from solid samples, e.g., faeces and red blood cells, before separa-

tions of individual porphyrins are performed (23, 33, 34), and some researchers preferred esterification methods due to the simplicity of isocratic elution (20).

Further significant improvement in the detectability of porphyrin methyl esters separated on TLC plates requires major reduction in the high background specular scatter, which may be achieved by using a pulsed laser and gated detection electronics (15). In our experiment it should be realized that only 20 mW of continuous wave radiation is necessary to produce relatively large fluorescence signal from porphyrin methyl esters, which could be easily generated from a low-cost, air-cooled argon-ion laser. Work is in progress in our laboratory to improve upon the detectability of various porphyrins present in human serum after separation by HPLC and the use of an optical fiber flow cell to optimize signal-to-noise ratio (27, 35). Hopefully, the ability to detect trace or ultratrace amounts of certain porphyrins in human serum would allow the detection of the early onset of certain types of cancers.

LITERATURE CITED

- Harris, J. W.; Kellermeyer, R. W. *The Red Cell*; Harvard University: Cambridge, MA, 1970; pp 3-63.
- Baum, R. M. *Chem. Eng. News* **1988**, *66*, 18-22.
- Xu, X.; Meng, J.; Hou, S.; Ma, H.; Wang, D. *J. Lumin.* **1988**, *40 & 41*, 219-220.
- Askevold, R. *Scand. J. Clin. Lab. Invest.* **1951**, *3*, 318-319.
- With, T. K. *Clin. Biochem.* **1968**, *2*, 97-104.
- Doss, M. Z. *Klin. Chem. Klin. Biochem.* **1970**, *3*, 197-207.
- Petryka, Z. J.; Watson, C. J. *J. Chromatogr.* **1979**, *179*, 143-149.
- Evans, N.; Jackson, A. H.; Mattin, S. A.; Towill, R. *J. Chromatogr.* **1976**, *125*, 345-355.
- Ford, R. E.; Ou, C. N.; Ellefson, R. D. *Clin. Chem.* **1981**, *27*, 397-401.
- Johnson, P. M.; Perkins, S. L.; Kennedy, S. W. *Clin. Chem.* **1988**, *34*, 103-105.
- Poole, C. F.; Khatib, S. In *Quantitative Analysis Using Chromatographic Techniques*; Katz, E., Ed.; Wiley: Chichester, 1987; Chapter 6.
- Donovan, J.; Gould, M.; Majors, R. E. *LC-GC* **1987**, *5*, 1024-1028.
- Issaq, J. H. *Chromatography* **1987**, *2*, 37-41.
- Zakaria, M.; Gonnord, M. F.; Guiochon, G. *J. Chromatogr.* **1983**, *271*, 127-130.
- Berman, M. R.; Zare, R. N. *Anal. Chem.* **1975**, *47*, 1200-1202.
- Bicking, M. K. L.; Kriseley, R. N.; Svec, H. J. *Anal. Chem.* **1983**, *55*, 200-204.
- Huff, P. B.; Sepaniak, M. J. *Anal. Chem.* **1983**, *55*, 1992-1994.
- Kawazumi, H.; Yeung, E. S. *Appl. Spectrosc.* **1989**, *43*, 249-253.
- Day, R. S.; Pimstone, N. R.; Eales, L. *Int. J. Biochem.* **1978**, *9*, 897-902.
- Sagen, E.; Romslo, I. *Scand. J. Clin. Lab. Invest.* **1985**, *45*, 309-314.
- Adams, R. F.; Slariv, W.; Williams, A. R. *Chromatogr. News!* **1976**, *4*, 24-27.
- Crosby, D.; Abaronson, N. *J. Chromatogr.* **1966**, *25*, 330-335.
- Day, R. S.; Pimstone, N. R.; Eales, L. *Int. J. Biochem.* **1978**, *9*, 897-904.
- Kennedy, S. W.; Wingfield, D. C. *Toxicol. Lett.* **1986**, *31*, 235-241.
- Reyftmann, J. P.; Moriere, P.; Goldstein, S.; Santas, R.; Dubertret, L.; Lagrange, D. *Photochem. Photobiol.* **1984**, *40*, 721-729.
- Leiner, M. J. P.; Hubmann, M. R.; Wolfbeis, O. S. *Anal. Chim. Acta* **1987**, *198*, 13-23.
- Sepaniak, M. J.; Yeung, E. S. *J. Chromatogr.* **1980**, *190*, 377-383.
- Doss, M. In *Progress in Thin-Layer Chromatography and Related Methods*; Niederwieser, A., Pataki, G., Eds.; Ann Arbor Science: Ann Arbor, MI, 1972; Vol. III, p 162.
- Belenki, B. G.; Gankina, E. S.; Adamovich, T. B.; Lobazov, A. Ph.; Nechaev, S. V.; Solonenko, M. G. *J. Chromatogr.* **1986**, *365*, 315-320.
- Sawicki, E.; Golden, C. *Microchem. J.* **1969**, *14*, 437-442.
- Andrade, J. D. *Surface and Interfacial Aspects of Biomedical Polymers*; Plenum: New York, 1985; Vol. 2, Chapters 1 and 2.
- Field, L. R.; Sanders, L. J. *Chromatogr. Sci.* **1980**, *18*, 133-136.
- Kennedy, S. W.; Wigfield, D. C.; Fox, G. A. *Anal. Biochem.* **1988**, *157*, 1-7.
- McCarroll, N. A. *Clin. Chem.* **1988**, *34*, 2390-2391.
- Roach, M. C.; Harmony, M. D. *Anal. Chem.* **1987**, *59*, 411-415.

RECEIVED for review May 30, 1989. Accepted July 26, 1989. This work was supported by BRSG 240-H0050 awarded by the Biomedical Research Support Grant from the U.S. Public Health Service.

Radio Frequency Plasma Detector for Sulfur Selective Capillary Gas Chromatographic Analysis of Fossil Fuels

R. J. Skelton, Jr.,¹ H.-C. K. Chang,² P. B. Farnsworth, K. E. Markides, and M. L. Lee*

Department of Chemistry, Brigham Young University, Provo, Utah 84602

Flame photometric detection is often used for sulfur selective gas chromatographic analysis. However, nonlinear response and quenching are significant drawbacks to this detector. Due to the relatively low abundances of sulfur compounds in extremely complex fossil fuels, capillary gas chromatography coupled with element selective radio frequency plasma detection was used to provide sulfur selective ($>10^3$) analysis of petroleum distillates and coal extracts. This detector was evaluated as a sulfur selective detector and was found to possess low limits of detection (0.5 pg/s) and good linear response (4 decades). Various numbers of phenyl groups attached to the base thiophenic ring had little effect on the intensity of the sulfur emission signal. Coelution of hydrocarbons was found to affect sulfur response only at high concentrations.

* Author to whom correspondence should be addressed.

¹ Current address: Shell Development Company, P.O. Box 1380, Houston, TX 77251.

² Current address: Department of Chemistry, Virginia Polytechnic Institute and State University, Blacksburg, VA 24061.

INTRODUCTION

Polycyclic aromatic compounds (PAC) are known to be major constituents in coal and petroleum products. Polycyclic aromatic hydrocarbons (PAH) are by far the most common PAC in these materials. However nitrogen-, oxygen- and sulfur-containing PAC are also often found in significant quantities. Because of the widespread interest in and use of fossil fuels, detailed study of their compositions has become an important task (1).

The sulfur content of these fuels is of major importance when one is considering environmental pollution during processing or usage. Sulfur gases that result from combustion or conversion processes are particularly noxious. Organic sulfur compounds from these processes have been classified according to functional groups: thiol (-SH), sulfide (-S-), disulfide (-S-S-), and thiophene. Many of these compounds have been identified in fossil fuels (2-8), but the major organosulfur compounds are thiophenic in nature, and many are known to possess mutagenic activities (9-12). In addition to pollution, organic sulfur compounds are known to affect storage stabilities of petroleum products, and they foul the

catalysts used in the cracking process.

The determination of these compounds has often been accomplished with gas chromatography (3-7). The flame photometric detector (FPD) is often used with gas chromatography because of its excellent selectivity for sulfur. This detector has existed for over 2 decades (13), and it continues to have widespread use. The FPD is well suited to the laboratory, because of its ease of use and reasonable cost. In addition, it can also be used as a phosphorus selective detector, greatly increasing the number of applications for which it is suited. These advantages have made this the detector of choice for sulfur selective detection after gas chromatography. Electrochemical techniques and the microwave induced plasma detector provide other means for sulfur detection (14); however, their use is limited by either complexity or expense.

Although the FPD is an excellent detector, it is not without drawbacks. The FPD is based on S_2 band emission in a cool, hydrogen-rich flame. Because the detector responds to a molecular band, the response is of the form $R = [S]^n$. The exponent n is theoretically 2, but the response to sulfur ranges between first and second order, depending on the heteroatom environment (15). The detector response is also quenched by coeluting water or hydrocarbons (16, 17). Dual-flame photometric detectors have been used to overcome these problems to a degree, but the single-flame versions are more common in the laboratory.

Recently, we reported the construction and initial evaluation of a multielement selective radio frequency plasma detector (18) that is similar to the helium afterglow detector reported by Rice et al. (19). Because this detector is based on atomic emission from a helium plasma, high sensitivity is coupled with good selectivity and linear response. This study was undertaken to determine the operational characteristics of this plasma for sulfur detection, including detector response dependence on molecular structure, quenching, linearity, and sensitivity. The detector was applied to the analysis of sulfur heterocycles occurring in coal extracts and petroleum distillates.

EXPERIMENTAL SECTION

Radio Frequency Plasma Detector. The radio frequency plasma detector has been previously reported (18) and will be only briefly described here. The detector consists of a helium radio frequency plasma doped with a small quantity of oxygen and contained inside a 1-mm-i.d. quartz tube. Research grade helium (99.9999%, Scott Specialty Gases, Plumsteadville, PA) was used with a flow of 70 mL/min. High-purity oxygen (<25 ppm N_2 , Matheson, Secaucus, NJ) was introduced in trace amounts via a narrow-bore capillary to maintain a very small, even flow. Flow rates measured by displacement indicated that the O_2 flow rate was approximately 0.03 mL/min.

A Macor ceramic (Corning Glass Works, Corning, NY) cell body was used to provide thermal and electrical insulation, as well as to support the stainless steel electrode. A radio frequency power supply (Model HPG-2, ENI Power Systems, Rochester, NY) was used to generate the plasma in the containment tube, directly between the electrode and grounded detector base. Power levels used were between 50 and 80 W, at approximately 335 kHz.

A 0.20-m-focal-length monochromator (Model H-20, Instruments, S.A., Metuchen, NJ) equipped with a 1200 g/mm grating and 0.5-mm slits was used to observe emission lines in the near-infrared portion of the spectrum. The instrument had a spectral band-pass of 0.5 nm. A 1-in.-diameter convex lens ($f = 10$ mm, Melles Griot, Irvine, CA) was used to focus the image of the plasma on the entrance slit of the monochromator. A colored 595-nm glass cutoff filter (Melles Griot) was used to remove ultraviolet and visible radiation. A red-sensitive photomultiplier tube (R2658, Hamamatsu, Middlesex, NJ) was used as a photodetector. Figure 1 shows the detector cell design and system schematic.

Gas Chromatography. The detector cell was mounted directly onto either a Lee Scientific Model 600 (Salt Lake City, UT) or

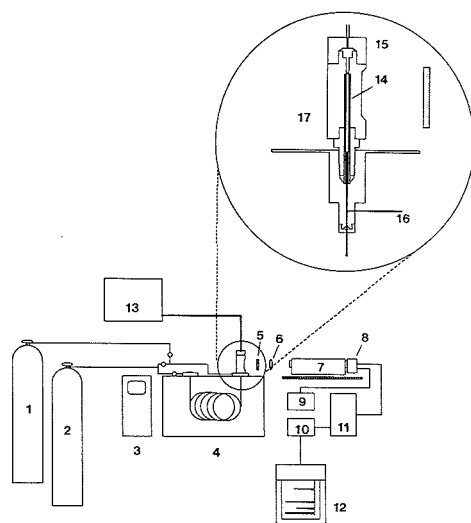


Figure 1. Schematic diagram of the GC-RPD system. Key: (1) oxygen, (2) 99.9999% helium, (3) GC controller, (4) oven, (5) UV filter, (6) plano convex lens, (7) monochromator, (8) photomultiplier, (9) PMT power supply, (10) low-pass filter, (11) electrometer, (12) chart recorder, (13) rf power supply, (14) quartz tube, (15) electrode assembly, (16) helium inlet, (17) Macor cell body.

a Hewlett-Packard 5890 gas chromatograph (Avondale, PA). Both cold on-column and split/splitless injection methods were used. Their use is cited in the appropriate text. Columns employed were 200- μ m-i.d. fused silica coated with methyl or biphenyl polysiloxane (SB-Phenyl-5 and SB-Biphenyl-30, Lee Scientific). A 1 m \times 320 μ m i.d. deactivated fused silica retention gap was used for on-column injections with a Carlo Erba cold on-column injector. A Hewlett-Packard single-flame photometric detector (Model 100AT) was used in conjunction with an HP 5880 gas chromatograph. Exact conditions are cited in the figure legends.

Fossil Fuel Samples. The coals were obtained from the Argonne National Laboratory. These premium coals had been previously ground (~100 mesh) and sealed under nitrogen in brown glass ampules. A quantity of each coal was extracted by stirring in 800 mL of pyridine under a nitrogen atmosphere for 72 h. The extracted material was separated by filtration through a 0.5- μ m Teflon filter. The solvent was removed by rotary evaporation, and the extracts were dried under vacuum for 24 h. The dry extracts were fractionated into different chemical classes by using liquid chromatography with neutral alumina as the adsorbent (20). The aromatic fraction was analyzed in this study. The sulfur heterocycles were further isolated from this fraction by using $PdCl_2$ coated silica to produce a sulfur heterocycle fraction (21).

Two petroleum distillates were analyzed. The first petroleum distillate was a 600-650 $^{\circ}$ F cut from a catalytically cracked crude petroleum. The second was a cut between 650 and 750 $^{\circ}$ F. The standards of benzo[b]thiophene, dibenzothiophene, and benzo[b]naphtho[2,1-d]thiophene used in this study were obtained from Aldrich Chemical Co., Milwaukee, WI. All samples were dissolved in benzene (J. T. Baker Chemical Co., Phillipsburg, PA). The concentrations of the fossil fuel application samples were adjusted to give ~1-100 ng amounts per peak of the solutes of interest. Extremely complex aromatic fractions of coal extracts were therefore used at ≥ 100 mg/mL total sample concentrations when sulfur selective detection was employed.

RESULTS AND DISCUSSION

Atomic emission has long been proposed as an ideal method for selective chromatographic detection. Atomic lines are often intense, affording good sensitivity. Also, the intensity of a

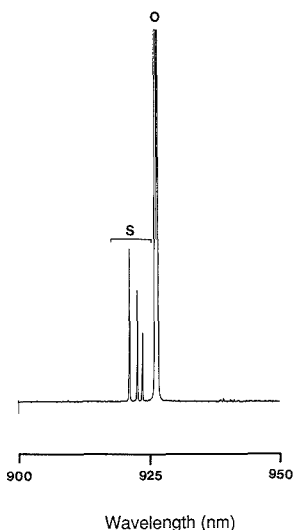


Figure 2. Spectrum of the helium plasma between 900 and 950 nm, indicating the sulfur emission lines at 921.3, 922.8, and 923.7 nm and the intense series of oxygen lines at 926 nm.

line depends on the concentration of atoms present in the flame or plasma, allowing for good quantitative analysis. Another major benefit is the possibility for detection of several elements at a time. The most common detector for gas chromatography based on this principle is the microwave induced plasma. This detector uses microwave radiation in a resonant cavity to create a helium plasma, which is then used for sample decomposition and excitation of the atomic species.

The radio frequency plasma detector was developed as an alternative system for providing detection on a similar basis (18, 19). Exploitation of the simple near-infrared spectral region allows the use of a low-cost monochromator. The radio frequency power supply is also easy to use, and no resonance cavities or wave guides are necessary. In the RPD system, an rf discharge between two electrodes exists in the containment tube. The direct discharge is self-seeding, unlike the microwave induced plasma. This means that a tesla coil is not required to ignite the plasma and that no venting is necessary to prevent the plasma from being permanently extinguished as the solvent passes. Small quantities of oxygen doped in the plasma scavenge carbon deposits and provide excellent excitation characteristics for the various nonmetallic elements. Figure 2 shows a spectrum of the near-infrared region around the sulfur emission lines at 921.3, 922.8, and 923.7 nm for an H_2S doped plasma.

Figure 3 shows the gas chromatographic results obtained for the analysis of the aromatic fraction of an Upper Freeport coal. The top chromatogram (A) is an FID trace of this fraction, indicating its great complexity. Chromatogram B was obtained by analysis of the same sample using a single-flame FPD as detector. The last chromatogram, also generated with the FPD, is of the isolated sulfur heterocyclic fraction of this sample. Because this fraction was rich in sulfur, quenching of the detector signal was quite low. Figure 4 shows the same samples analyzed with the RPD. The top chromatogram (A) was obtained by monitoring the H line at 656 nm, giving universal detection of the organics. Chromatogram B is the RPD trace obtained by monitoring at 921 nm for sulfur selective detection. Chromatogram C is the sulfur-rich fraction, again obtained with the sulfur selective

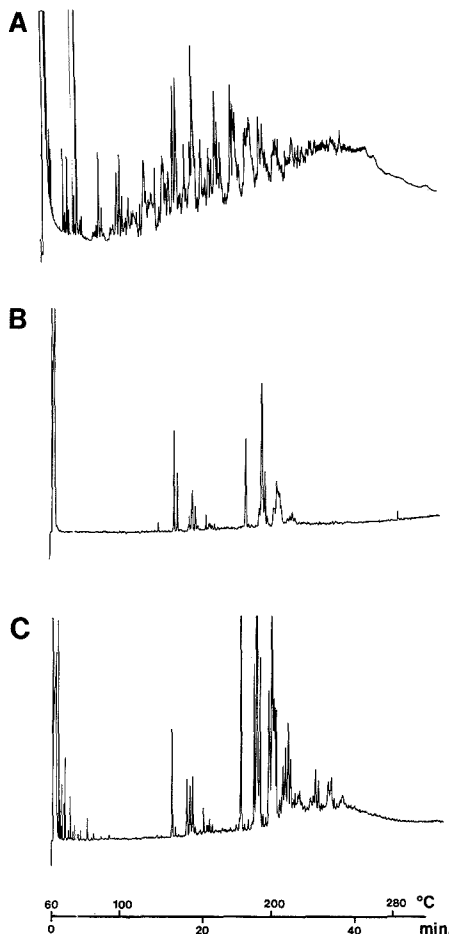


Figure 3. Gas chromatograms of the aromatic and isolated sulfur heterocyclic fractions of an Upper Freeport coal extract: (A) FID detection of the aromatic fraction, (B) single-flame FPD detection of the aromatic fraction, and (C) single-flame FPD detection of the isolated sulfur fraction. Chromatographic conditions: 10 m \times 200 μ m SB-Phenyl-5 capillary column and splitless injection.

plasma detector. Obviously there is less quenching with the RPD. Chromatograms 4B and 4C compare quite well. Peak intensities vary between the complete aromatic and isolated sulfur fractions, but this is expected due to the incomplete recovery of some sulfur compounds from the $PdCl_2$ during fractionation.

For better characterization of the detector response as a sulfur detector, the effect of molecular structure on detector response was determined by using three sulfur heterocyclic test compounds, benzo[*b*]thiophene, dibenzothiophene, and benzo[*b*]naphtho[2,1-*d*]thiophene. A solution was prepared in benzene such that the quantity of sulfur eluting into the detector was equivalent (4 ng) for each compound. On-column injection was used to prevent discrimination during injection. Figure 5 shows the chromatogram obtained. Results from integration show that the peak areas vary less than 5%. These results indicate that for this series of heterocycles, molecular size does not greatly affect detector response. This is an important attribute of the plasma detectors; only one com-

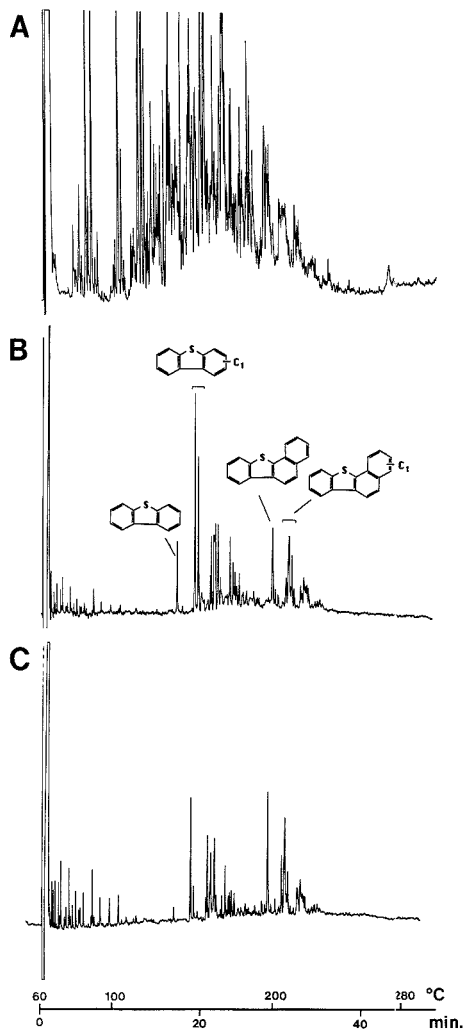


Figure 4. Gas chromatograms of the aromatic and isolated sulfur heterocyclic fractions of an Upper Freeport coal extract: (A) RPD with H detection at 656 nm of the aromatic fraction, (B) RPD with S detection at 921 nm of the aromatic fraction, and (C) RPD with S detection of the isolated sulfur fraction. Chromatographic conditions were the same as in Figure 3.

pond is needed to calibrate the system because the sample is decomposed in the plasma and only the quantity of sulfur present determines the response.

An exponential dilution flask (22) was employed to determine the effect of quenching on the detector. A gas mixture of 75 ppm H_2S in helium was fed through a low-volume tee into the detector, providing a steady sulfur signal of approximately 3 times the background current. The flow from a dilution flask was connected to this same tee. Hexane was injected into the dilution flask, such that the amount of hexane entering the detector decayed exponentially with time. The flow through this flask was monitored with a digital flow meter so that precise concentrations could be determined as a

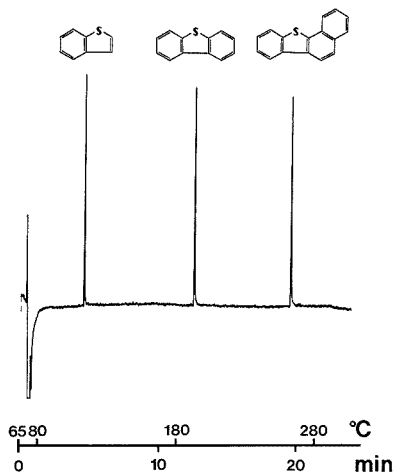


Figure 5. Gas chromatogram obtained with the RPD (921 nm) of three sulfur heterocycles (benzo[*b*]thiophene, dibenzothiophene, and benzo[*b*]naphtho[2,1-*d*]thiophene) showing the effect of molecular structure on detector response. Concentrations of the standard compounds were each adjusted to give equal amounts (4 ng) of sulfur entering the detector. Other conditions: cold on-column injection, 1-m phenyl deactivated retention gap followed by an 11 m \times 200 μ m i.d. SB-Biphenyl-30 capillary column, and temperature-programmed from 65 to 80 $^{\circ}C$ at 50 $^{\circ}C$ min^{-1} and then at 10 $^{\circ}C$ min^{-1} to 290 $^{\circ}C$ after a 1-min isothermal period.

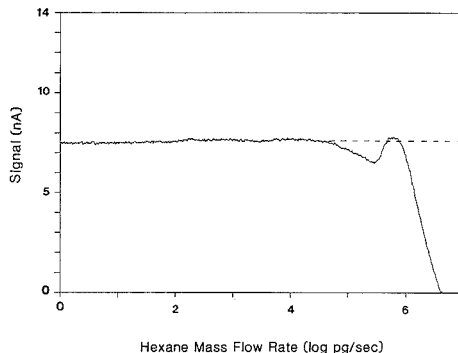


Figure 6. Plot of RPD sulfur signal intensity as a function of the amount of *n*-hexane entering the detector. The normal base line is indicated by a dashed line.

function of time. The signal was observed over the time of dilution to determine the effect of the hexane on detector signal. Figure 6 shows a plot of detector signal versus the log of the hexane mass flow rate entering the detector. The dashed line represents the normal signal. It is noticed that very high concentrations of hexane cause a negative deviation in signal as the plasma is overloaded and quenched. The second negative deviation at lower concentration is believed to be also due to quenching, with the area of normal base line separating these areas being caused by interference from molecular bands that occur in this range of hexane concentration. Coincident with the rounded peak in the signal, the plasma acquires an intense green color, indicating the presence of C_2 band emission. These deviations are not experienced except at very high concentrations and should not normally be of concern during a GC analysis.

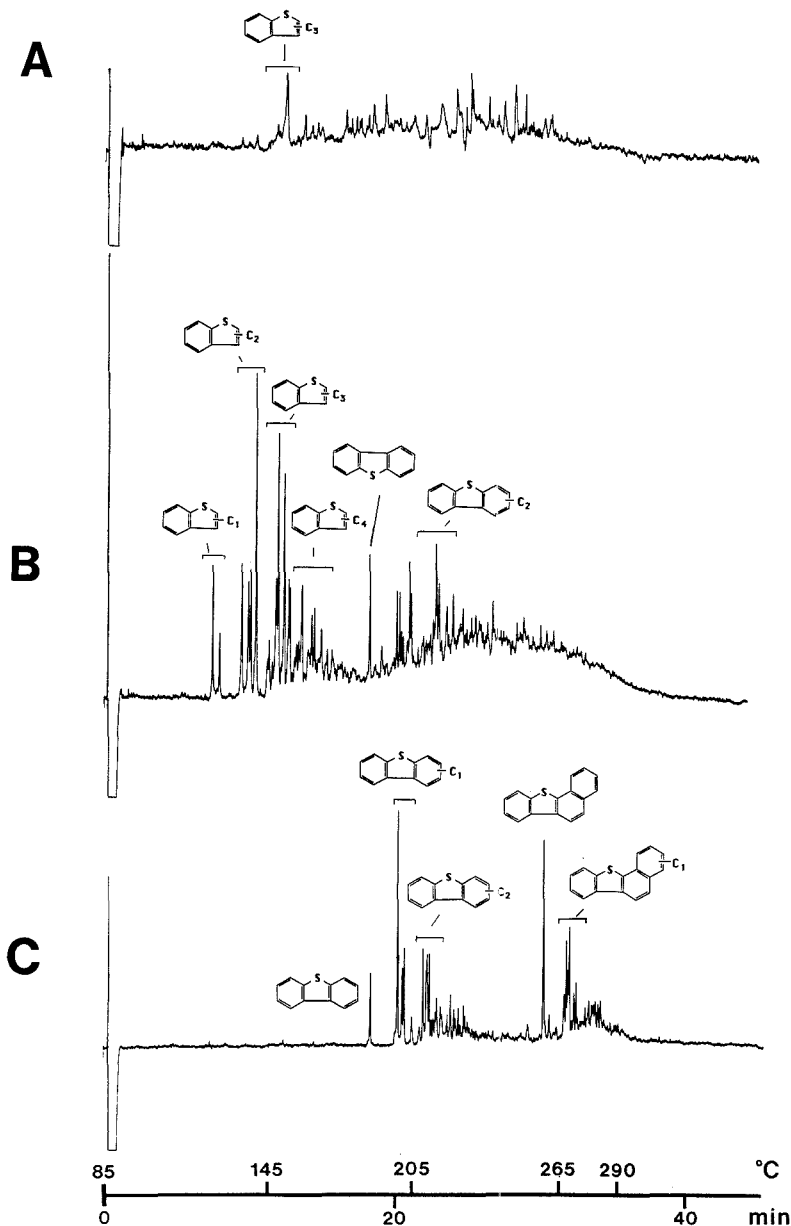


Figure 7. Sulfur selective (RPD at 921 nm) gas chromatograms of the aromatic fractions of several coal extracts: (A) North Dakota Lignite, (B) Illinois No. 6, and (C) Pocahontas No. 8 coals. Chromatographic conditions: 11 m \times 200 μ m i.d. SB-Biphenyl-30 capillary column, temperature-programmed from 85 to 290 $^{\circ}$ C at 6 $^{\circ}$ C min $^{-1}$ after a 1-min isothermal period, splitless injection.

Finally, the RPD system described was evaluated for sensitivity and selectivity. Again, exponential dilution was used to determine the sensitivity by allowing CS₂ to flow into the detector in an exponentially decaying concentration. Computations from the exponential decay curve allow direct calculation of the detection limit (concentration that gives a signal greater than twice the relative standard deviation of

the noise) and linearity. Selectivity for sulfur was also obtained by comparison of this exponential dilution curve to that obtained with hexane. Results from these experiments are shown in Table I. These results indicate that the RPD demonstrates excellent characteristics for sulfur detection after gas chromatography.

The detector was then utilized for qualitative detection of

Table I. Sulfur Detection Characteristics of the Radio Frequency Plasma Detector and the Single-Flame FPD

	RPD	FPD ¹
detection limit, pg/s	0.5	5-50
selectivity (R_s/R_c) ^b	>10 ⁸	10 ³
linearity, decades	4	nonlinear
resistance to quenching	good	poor

^aData taken from ref 23. ^b R_s is response per unit weight of sulfur; R_c is response per unit weight of carbon.

Table II. Class and Elemental Compositions of Argonne Premium Coal Samples (Moisture, Ash Free Basis)^a

coal	rank	C	H	S	O
Pocahontas No. 3	low volatile bituminous	91	4.7	0.9	3
Upper Freeport	med volatile bituminous	87	5.5	2.8	4
Illinois No. 6	high volatile bituminous	77	5.7	5.4	10
North Dakota	lignite	73	5.3	0.8	21

^aData taken from Argonne National Laboratory, Premium Coal Sample Repository, Argonne, IL and from Chang, H.-C. K. Ph.D. Dissertation, Brigham Young University, 1989, p 169.

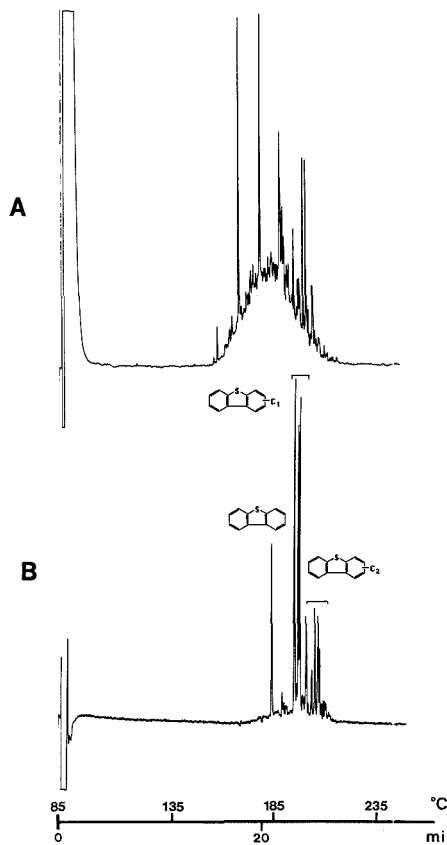


Figure 8. Gas chromatograms of a petroleum distillate (630-650 °F cut): (A) RPD with H detection at 656 nm and (B) RPD with S detection at 921 nm. Chromatographic conditions: 11 m X 200 μ m i.d. SB-Biphenyl-30 coated capillary column, temperature programmed from 85 to 280 °C at 5 °C min⁻¹ after a 1-min isothermal period, splitless injection.

sulfur compounds in several additional coal extracts. Three coals were analyzed: a Pocahontas No. 3, an Illinois No. 6, and a North Dakota lignite. Table II gives more detailed information on these coals, as well as on the Upper Freeport coal previously discussed (Figure 2). These coals were selected to represent different geological time periods, with the Pocahontas No. 3 coal being the oldest and the lignite the youngest.

Figure 7 shows the sulfur selective analyses of the aromatic fractions of these coals. There are obvious differences in the

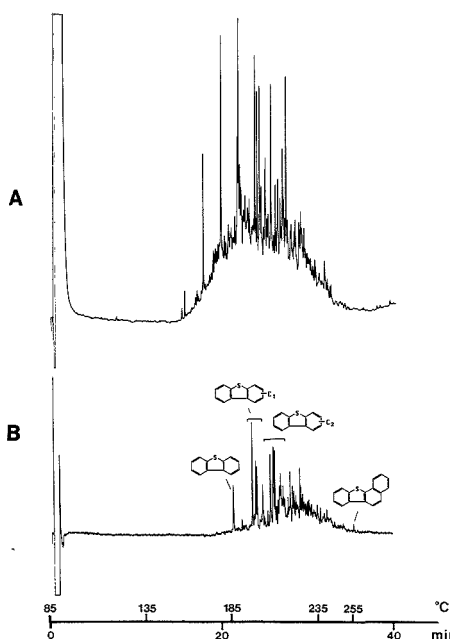


Figure 9. Same as Figure 8, except that the distillate was a 650-750 °F cut.

abundances and types of compounds present in these coals. The identified structures were determined by GC-MS and by retention time comparisons of individual compounds in the isolated sulfur fractions with standard compounds. Older coals such as the Pocahontas No. 3 coal were expected to have a higher relative concentration of multiring aromatic compounds than the younger ones. A more detailed discussion of the occurrence of these compounds is given in ref 24.

Figure 8 shows two chromatograms of a 600-650 °F petroleum distillate. Chromatogram A was obtained by monitoring H emission at 656 nm, affording universal detection of organic compounds. The great complexity of this sample is obvious, even though it is a narrow boiling range cut. Chromatogram B is a sulfur selective chromatogram of this sample. Dibenzothiophene and its methyl-substituted isomers were the major sulfur-containing components in this sample.

Figure 9 contains two chromatograms of a 650-750 °F petroleum distillate. This again is an extremely complex mixture of compounds. Chromatogram A was obtained, as in Figure 8, by monitoring H emission at 656 nm. Chromatogram B represents the sulfur selective chromatogram obtained from this same sample. Again, the chromatogram is quite complex, with a large number of alkylated dibenzothiophene isomers

observed. As expected, the compounds were of higher molecular weight, including alkylated dibenzothiophenes and benzo[b]naphtho[2,1-d]thiophene.

ACKNOWLEDGMENT

We thank Dr. W. Raymond West of Shell Development Co. for providing the petroleum distillates.

Registry No. S, 7704-34-9.

LITERATURE CITED

- Lee, M. L.; Novotny, M. V.; Bartle, K. D. *Analytical Chemistry of Polycyclic Aromatic Compounds*; Academic Press: New York, 1981.
- Ozogalla, C.-D.; Boberg, F. *Sulfur Rep.* **1983**, *3*, 121.
- Kong, R. C.; Lee, M. L.; Tominaga, Y.; Pratap, R.; Iwao, M.; Castle, R. N. *J. Chromatogr. Sci.* **1982**, *20*, 502.
- Kong, R. C.; Lee, M. L.; Iwao, M.; Tominaga, Y.; Pratap, R.; Tompson, R. D.; Castle, R. N. *Fuel* **1984**, *63*, 702.
- Nishioka, M.; Lee, M. L.; Castle, R. N. *Fuel* **1986**, *65*, 390.
- Arpino, P. J.; Ignatiadis, I.; De Rycke, G. J. *Chromatogr.* **1987**, *390*, 329.
- Nishioka, M. *Energy Fuels* **1988**, *2*, 214.
- Sornogyvari, A.; Zanzotto, L.; Sieben, D.; Auger, J. *Fuel* **1988**, *67*, 1269.
- Eastmond, D. A.; Booth, G. M.; Lee, M. L. *Arch. Environ. Contam. Toxicol.* **1984**, *13*, 105.
- Later, D. W.; Peiray, R. A.; Mahlum, D. D.; Wright, C. W.; Lee, M. L.; Weimer, W. C.; Wilson, B. W. *Polynuclear Aromatic Hydrocarbons: Formation, Metabolism and Measurement*; Cooke, M., Dennis, A. J., Eds.; Battelle Press: Columbus, OH, 1983; p 771.
- Peiray, R. A.; Stewart, D. L.; Tominaga, Y.; Iwao, M.; Castle, R. N.; Lee, M. L. *Mutation Res.* **1984**, *117*, 31.
- McFell, T.; Booth, G. M.; Lee, M. L.; Tominaga, Y.; Pratap, R.; Tedjamulia, M.; Castle, R. M. *Mutation Res.* **1984**, *135*, 97.
- Brody, S. S.; Chaney, J. E. *J. Gas. Chromatogr.* **1966**, *4*, 42.
- Genna, J. L.; McAninch, W. D.; Reich, R. A. *J. Chromatogr.* **1982**, *238*, 103.
- McGaughy, J. F.; Gangwal, S. K. *Anal. Chem.* **1980**, *52*, 2079.
- Pearson, C. D.; Hines, W. J. *Anal. Chem.* **1977**, *49*, 123.
- Bertrou, F.; Dreano, Y.; Sandra, P. *HRC CC, J. High Resolut. Chromatogr. Chromatogr. Commun.* **1984**, *7*, 679.
- Skelton, R. J., Jr.; Farnsworth, P. B.; Markides, K. E.; Yang, F. J.; Lee, M. L. *HRC CC, J. High Resolut. Chromatogr. Chromatogr. Commun.* **1988**, *11*, 75.
- Rice, G. W.; D'Silva, A. P.; Fassel, V. A. *Spectrochim. Acta* **1985**, *40B*, 1573.
- Later, D. W.; Lee, M. L.; Bartle, K. D.; Kong, R. C.; Vassilaros, D. L. *Anal. Chem.* **1981**, *53*, 1612.
- Nishioka, M.; Campbell, R. M.; Lee, M. L.; Castle, R. N. *Fuel* **1986**, *65*, 270.
- Skelton, R. J., Jr.; Farnsworth, P. B.; Markides, K. E.; Lee, M. L. *Anal. Chem.* **1989**, *61*, 1815.
- Poole, C. F.; Schuette, S. A. *Contemporary Practice of Chromatography*; Elsevier: New York, 1984; p 189.
- Chang, H.-C. K.; Skelton, R. J., Jr.; Markides, K. E.; Lee, M. L. *Anal. Chem.*, in press.

RECEIVED for review January 3, 1989. Revised manuscript received July 21, 1989. Accepted July 27, 1989. Financial support for this work was provided by the Gas Research Institute. Contract No. 5084-260-1129, and by the State of Utah Centers of Excellence program. Any opinions, findings, or recommendations expressed herein are those of the authors and do not necessarily reflect the views of GRI.

Analysis of Two-Dimensional Nuclear Magnetic Resonance Spectra with Relayed Proton-Proton-Carbon Magnetization Transfer: A Step toward Automated Structure Elucidation

Urs Eggenberger and Geoffrey Bodenhausen*

Section de Chimie, Université de Lausanne, Rue de la Barre 2, CH-1005 Lausanne, Switzerland

Procedures are described for automated analysis of two-dimensional NMR spectra correlating the chemical shifts of carbon-13 with the shifts of neighbor protons that are directly attached to the carbon-13 nuclei and with remote protons that have scalar couplings to the neighbor protons. The analysis yields connectivity matrices with quality factors that provide a measure for the reliability of the evidence. The connectivity matrices can be represented graphically either by drawing the pathways of magnetization transfer onto the molecular formula or by indicating the connectivities in conventional shift correlation spectra. Applications are shown to 2-thiophene-carboxylic acid, to 1-hexanol, to 2,6-dimethylcyclohexanol, and to (1*RS*, 2*SR*, 4*SR*, 5*RS*, 6*RS*)-6-*exo*-(2-nitrophenylthio)-spiro[bicyclo[2.2.2]octane-2,2'-oxirane]-5-*endo*-yl chloride.

INTRODUCTION

In the last few years, a variety of approaches have been proposed for computer-supported analysis of two-dimensional NMR spectra (1). So far, the majority of the efforts have been directed toward the analysis of homonuclear correlation spectra (COSY) and related experiments (2-17), while to our knowledge only one research group has attempted to extend the analysis to the correlation of proton and carbon spectra (18). In conventional heteronuclear shift correlation spectra

(19-23), one usually obtains a signal at frequency coordinates $(\omega_1, \omega_2) = (\Omega_H, \Omega_C)$ for each CH_n group in the molecule. This signal is normally devoid of multiplet structure, except perhaps for some uninformative broadening due to homonuclear proton-proton couplings. The analysis of such spectra can at best yield a table of chemical shifts, which is not very useful as input for automated analysis, unless one considers cross-referencing the proton and carbon shifts to a data base containing empirical relationships between shifts and chemical structures. To make better use of conventional proton-carbon correlation, the information can be combined with knowledge derived from proton-proton correlation (COSY spectra), as suggested by Szalma et al. (18). This approach undoubtedly deserves further attention. In our opinion however, the information contained in conventional heteronuclear correlation spectra is not sufficiently rich to make much progress with automated analysis. In order to enhance confidence in pattern recognition, one would prefer to see multiplets with specific structures, and groups of multiplets that span characteristic patterns in two-dimensional frequency space. Basically, one has to take recourse to experimental schemes that are more sophisticated than conventional heteronuclear shift correlation spectroscopy and that yield spectra which contain a greater wealth of information.

In this paper, we should like to broaden the scope of automated analysis by considering a two-dimensional experiment that involves relayed proton-proton-carbon magnetization

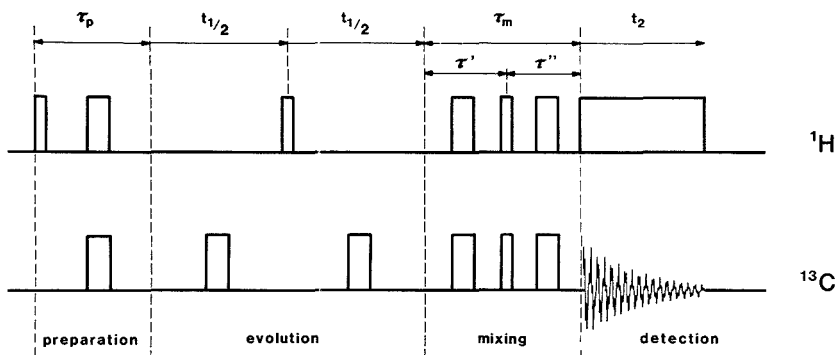


Figure 1. Experimental scheme for relayed $^1\text{H} \rightarrow ^1\text{H} \rightarrow ^{13}\text{C}$ NMR spectroscopy, which, depending on the phase-cycle, yields "pseudo-zero-quantum" (PZQ) and "pseudo-double-quantum" (PDQ) spectra. Narrow and wide pulses represent 90° and 180° pulses, respectively. The 90° proton pulse in the middle of the evolution period t_1 , may cause coherence transfer between protons that are in remote and neighboring positions with respect to a carbon-13 nucleus. The timing of the intervals and the cycling of the phases are discussed in the text.

transfer. This method yields information about both hetero- and homonuclear correlation in a single two-dimensional spectrum. The structure of the spectra allows a step-by-step analysis that is well suited for a computer. The frequency coordinates of the peaks obey simple rules, and the structures and relative signs of the multiplets can be easily interpreted. The experimental scheme used in this study (Figure 1) was originally described in simpler form by Bolton et al. (24) and was subsequently improved by Sørensen et al. (25), who dubbed it "pseudo-multiple-quantum spectroscopy", an expression that we should like to retain for the present study. In fact, the experiment does not involve any multiple-quantum coherences, but the signals appear at sums and differences of chemical shifts, i.e. at frequencies that are reminiscent of those found in multiple-quantum spectra. The proton magnetization is initially excited by a 90° pulse. In the preparation interval τ_p , which must be chosen to be equal to the inverse of the average one-bond proton-carbon coupling constant, $\tau_p = 1/(^1J_{\text{CH}})$, the phase of the transverse magnetization of a proton attached to a carbon-13 nucleus is reversed with respect to the phase of protons attached to carbon-12 nuclei. The latter are essentially unaffected by the τ_p interval (except perhaps for slight phase errors due to homonuclear couplings). The key element of the sequence is the 90° proton pulse in the middle of the evolution period t_1 , which can bring about coherence transfer through homonuclear J_{HH} couplings, in particular between remote protons and neighbor protons that are directly attached to a carbon-13 nucleus. The two 180° carbon-13 pulses in the middle of the two halves of the evolution period ensure that the protons are not affected by heteronuclear couplings, at least if the system is weakly coupled. The mixing interval, which transfers coherence from protons to directly attached carbon-13 nuclei, is analogous to the INEPT sequence (26). The intervals are chosen so that $\tau' = (2(^1J_{\text{CH}}))^{-1}$ and $\tau'' = (3(^1J_{\text{CH}}))^{-1}$ (27, 28). During the detection period the carbon-13 signal is acquired while the protons are decoupled. The phase of the 90° proton pulse in the middle of the evolution period t_1 is cycled through x , y , $-x$, and $-y$. If the signals of the four experiments are alternately added and subtracted, one obtains a pseudo-zero-quantum (PZQ) spectrum, while addition of all four signals leads to a pseudo-double-quantum (PDQ) spectrum (24, 25). The PDQ frequencies correspond to $\omega_1 = 1/2[\Omega(\text{H}_A) + \Omega(\text{H}_B)]$, while the PZQ frequencies are given by $\omega_1 = 1/2[\Omega(\text{H}_A) - \Omega(\text{H}_B)]$, i.e. half the sum or half the difference of two proton chemical shift frequencies. The basic four-step phase cycle of the 90° proton pulse is embedded in a 16-step

cycle, which also involves alternating the phase of the first proton pulse (suppression of axial peaks) and alternating the phases of the two 180° carbon-13 pulses in the evolution period.

STRUCTURE OF PSEUDO-MULTIPLE-QUANTUM SPECTRA

Figure 2 shows experimental pseudo-double-quantum and pseudo-zero-quantum (PDQ and PZQ) spectra of 2-thiophenecarboxylic acid, obtained with the sequence of Figure 1. Quaternary carbons (and of course heteroatoms) are not observable. The direct connectivity peaks (filled circles) in the PDQ spectrum appear at the same coordinates as in a conventional heteronuclear correlation spectrum, i.e. at $(\omega_1, \omega_2) = (\Omega_A, \Omega_X), (\Omega_M, \Omega_Y),$ and (Ω_Q, Ω_Z) . The remote connectivity peaks in the PDQ spectrum (open circles) appear at the average of the shifts of two protons, e.g. at $\omega_1 = 1/2(\Omega_A + \Omega_M)$, $1/2(\Omega_A + \Omega_Q)$, and $1/2(\Omega_M + \Omega_Z)$. Such signals provide evidence for the existence of homonuclear proton-proton couplings, since they stem from magnetization that has been transferred from a remote to a neighbor proton by the 90° pulse in the middle of the evolution period. In the PZQ spectrum, the direct connectivity peaks (filled circles) all appear on a horizontal axis at $\omega_1 = 0$. The remote peaks in the PZQ spectrum (open circles) appear shifted in ω_1 with respect to those in the PDQ spectrum, so that the ω_1 frequency differences between direct and remote signals observed in the PZQ spectrum are the same as those in the PDQ spectrum. Connectivities between remote peaks are indicated by dashed lines.

The patterns observed in Figure 2 are characteristic for neighborhood relationships in the chain $\text{C}_X\text{H}_A-\text{C}_Y\text{H}_M-\text{C}_Z\text{H}_Q$. Note that in this aromatic system the long-range $^4J(\text{H}_A\text{H}_Q)$ coupling cannot be neglected. One should therefore be careful in the interpretation of the expression "neighbor": although the fragments C_XH_A and C_ZH_Q are of course not neighbors in the structural sense, since there is no C_X-C_Z bond, they are neighbors in the spectroscopic sense, since there is a non-vanishing scalar coupling $J(\text{H}_A\text{H}_Q)$. In nonaromatic systems, long-range proton-proton couplings are usually much smaller than vicinal couplings, so that the concepts of structural and spectroscopic neighbors largely coincide in such systems.

In the simple example of Figure 2 the information about homonuclear proton couplings can easily be extracted. From the PZQ spectrum this is achieved by connecting pairs of remote resonances with ω_1 frequencies of opposite signs. Likewise, the remote resonances in the PDQ spectrum can be connected with dashed lines parallel to the ω_2 axis, since

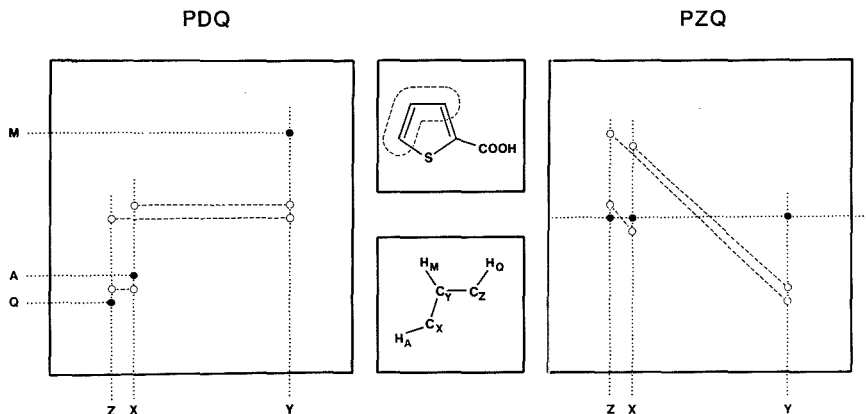


Figure 2. Experimental pseudo-double-quantum (PDQ) and pseudo-zero-quantum (PZQ) spectra of 2-thiophenecarboxylic acid. For clarity the remote peaks have been emphasized by circles, and the direct peaks have been enlarged to filled dots. The ω_2 (carbon-13) axis runs horizontally, the ω_1 (proton) axis vertically. The spectral width was 1000 Hz in ω_2 and 500 Hz in ω_1 . The spectra were recorded on a Bruker AM 400 spectrometer.

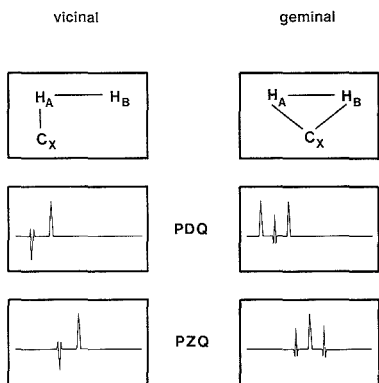


Figure 3. Schematic representation of cross sections through PDQ and PZQ spectra taken parallel to the ω_1 axis for vicinal and geminal fragments, featuring direct and remote connectivity multiplets, with in-phase and antiphase structures respectively, as explained in the text.

they appear pairwise at the same ω_1 frequencies.

MULTIPLIET STRUCTURES

It is important to distinguish between the multiplet structures of direct and remote connectivity signals and to study the special case of diastereotopic geminal protons, i.e. the case of CH_2 groups where the two geminal protons have different chemical shifts. In vicinal fragments (see left-hand side of Figure 3) one expects one direct connectivity signal in the PDQ spectrum, stemming from the process $\text{H}_A \rightarrow \text{H}_A \rightarrow \text{C}_X$ (in-phase multiplet at $\omega_1 = \Omega_A$), and one indirect connectivity signal due to the pathway $\text{H}_B \rightarrow \text{H}_A \rightarrow \text{C}_X$ (antiphase multiplet at $\omega_1 = 1/2(\Omega_A + \Omega_B)$). In the PZQ spectrum of a vicinal group, the direct connectivity pathway $\text{H}_A \rightarrow \text{H}_A \rightarrow \text{C}_X$ leads to an in-phase axial signal at $\omega_1 = 0$, while the indirect pathway $\text{H}_B \rightarrow \text{H}_A \rightarrow \text{C}_X$ leads to an antiphase multiplet at $\omega_1 = 1/2(\Omega_B - \Omega_A)$. Note that the PDQ and PZQ traces of the vicinal case can be brought to superposition by a simple frequency shift.

For geminal fragments with nondegenerate diastereotopic protons (see right-hand side of Figure 3), one expects two in-phase direct connectivity signals in the PDQ spectrum, one

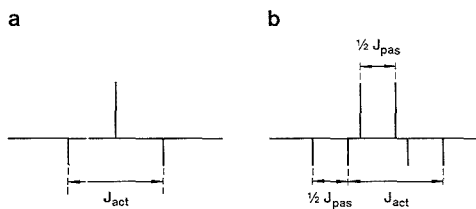


Figure 4. (a) Schematic representation of the antiphase structure of a remote connectivity multiplet. (b) Additional in-phase splitting of this multiplet by a passive proton-proton coupling.

from the process $\text{H}_A \rightarrow \text{H}_A \rightarrow \text{C}_X$ (at $\omega_1 = \Omega_A$), the other from $\text{H}_B \rightarrow \text{H}_B \rightarrow \text{C}_X$ (at $\omega_1 = \Omega_B$), and one indirect connectivity signal (antiphase multiplet) at $\omega_1 = 1/2(\Omega_A + \Omega_B)$, which is due to the superposition of the two pathways $\text{H}_A \rightarrow \text{H}_B \rightarrow \text{C}_X$ and $\text{H}_B \rightarrow \text{H}_A \rightarrow \text{C}_X$. In the PZQ spectrum of a geminal group, the two direct connectivity pathways $\text{H}_A \rightarrow \text{H}_A \rightarrow \text{C}_X$ and $\text{H}_B \rightarrow \text{H}_B \rightarrow \text{C}_X$ both contribute to a signal at $\omega_1 = 0$, while the indirect pathways $\text{H}_A \rightarrow \text{H}_B \rightarrow \text{C}_X$ and $\text{H}_B \rightarrow \text{H}_A \rightarrow \text{C}_X$ lead to two antiphase multiplets that are symmetrically disposed at $\omega_1 = \pm 1/2(\Omega_A - \Omega_B)$.

In the geminal case, remote resonances have the same sign as direct connectivity resonances, while in the vicinal case direct and indirect signals are of opposite sign. This is due to the fact that in the preparation period τ_p of the pulse sequence of Figure 1, the phase of the magnetization of protons directly connected to a carbon-13 nucleus is reversed. In the vicinal case, this affects only the H_A proton, while in the geminal case, both H_A and H_B protons have their phases reversed. Note that for the geminal case it is no longer possible to distinguish remote and direct signals simply by checking the sign of the peaks.

It should be mentioned that if the geminal protons are degenerate in chemical shift (isochronous because of chemical or magnetic equivalence), it is no longer possible to distinguish their number, i.e. CH , CH_2 , and CH_3 groups give the same signature in spectra obtained with the sequence of Figure 1. If a distinction between these groups is essential, complementary experiments such as insensitive nuclei enhanced by polarization transfer (INEPT) (26), the attached proton test (APT) (29), or distortionless enhancement by polarization transfer (DEPT) (30) have to be carried out.

For remote transfer in a three-spin system, be it a vicinal or a geminal fragment, we observe an antiphase $\{-1:+2:-1\}$ triplet in the ω_1 domain (see Figure 4a), arising from the convolution of two antiphase doublets. The peak separation in such remote multiplets is equal to $1/2J_{\text{act}}$, where the active coupling is the proton-proton coupling responsible for coherence transfer between remote and neighbor protons (i.e. $J_{\text{act}} = J_{\text{AB}}$ in the systems of Figure 3). Each additional passive coupling partner H_P causes a further in-phase splitting by $1/2J_{\text{pass}}$ (i.e. by $1/2J_{\text{AP}}$ or $1/2J_{\text{BP}}$) (Figure 4b), which in unfavorable cases may lead to partial cancellation and hence to a reduction of the sensitivity of the experiment. Such losses in sensitivity tend to be rather unpredictable. For the direct transfer pathways in three-spin systems one also expects triplets, but here all the lines are in-phase, so that one merely observes a broad resonance. As the resolution in ω_1 is generally low and all splittings are reduced by a factor 2, the multiplet patterns can be generalized in the following way: direct connectivity multiplets tend to merge to broad lines in positive absorption, while the remote connectivity multiplets take the form of a negative absorptive line with a small positive sidelobe on each side.

SEPARATION OF DIRECT AND REMOTE SIGNALS

Automated analysis could be greatly facilitated if direct and remote connectivity signals in experimental spectra can be distinguished from the outset. This can be achieved by using so-called low-pass J filters (31), which eliminate the magnetization of protons directly attached to carbon-13 nuclei by conversion into unobservable multiple-quantum coherence. This approach yields spectra where all direct connectivity signals have been removed, so that all information about direct connectivity is lost. We have therefore attempted to use an alternative approach to separate remote and direct connectivity signals, by inserting a preparation period τ_p in the pulse sequence as shown in Figure 1. In vicinal subsystems (see Figure 3), one obtains opposite signs for resonances arising from direct and remote subunits. This procedure retains all magnetization components and is therefore less wasteful, but it may suffer from the fact that partial signal cancellation occurs in unfavorable cases when remote and direct peaks accidentally coincide.

The effect of the preparation period is demonstrated in Figure 5, which shows cross-sections through PDQ and PZQ spectra of 2,6-dimethylcyclohexanol with resonances of the $C_1H_4OH_D$ group that is sandwiched between two tertiary carbon atoms C_2H_B and C_6H_B , which because of molecular symmetry have isochronous protons H_B and H_B . The experimental traces feature an in-phase direct connectivity peak due to the transfer $H_A \rightarrow H_A \rightarrow C_1$, and two antiphase remote connectivity multiplets, which appear on each side of the in-phase peak (but not in symmetrical positions), and which are due to the processes $H_D \rightarrow H_A \rightarrow C_1$ and $H_B \rightarrow H_A \rightarrow C_1$. The latter process leads to a more intense signal because of the superposition of two degenerate protons H_B and H_B . Note however that the amplitude ratio is not 1:2, presumably because cancellation effects are more pronounced for the pathways starting at H_B and H_B . In Figure 5a, the preparation delay is $\tau_p = 1/2J_{\text{CH}}$, as in the normal sequence of Figure 1, and the direct and remote peaks therefore have opposite signs (see Figure 3). In Figure 5b, $\tau_p = 0$ and the 180° pulses in the preparation period have been skipped, so that the protons are simply excited by a 90° pulse. In this case, the direct and remote peaks have the same signs. Figure 5c and Figure 5d show the weighted difference and sum of Figure 5a and Figure 5b. Ideally, a simple sum (with equal weights) should give only direct connectivity signals, while the difference (with opposite weights) should give only remote connectivity signals.

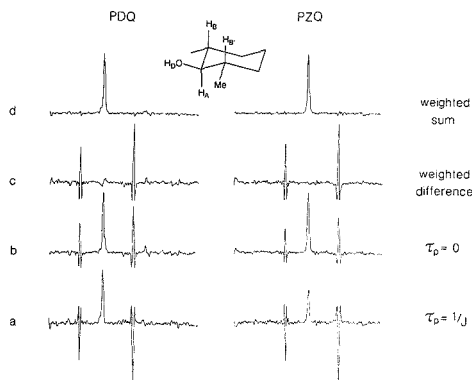


Figure 5. Cross sections taken parallel to the ω_1 axis of experimental PDQ and PZQ spectra of 2,6-dimethylcyclohexanol at the ω_2 frequency corresponding to the chemical shift of the C_1 carbon. (a) Preparation period with $\tau_p = 1/2J_{\text{CH}}$, as in the normal sequence of Figure 1, leading to direct and remote connectivity peaks with opposite signs. (b) If $\tau_p = 0$, the direct and remote peaks have the same signs. (c) Weighted difference and (d) weighted sum of (a) and (b).

In practice, it turned out that the weights had to be adjusted empirically, and that they depended on the carbon-13 shifts, presumably because of off-resonance effects. These artifacts could not be completely eliminated by using composite pulses (32), so that the idea of a clean separation of remote and direct correlation peaks could not be fully exploited in this study.

PROGRAM STRUCTURE AND ALGORITHMS

The analysis of the data is structured in three main blocks: (i) Fourier transformation and phase correction, (ii) reduction of the two-dimensional matrices to small records by "peak picking", and (iii) identification of neighboring fragments and storage in a suitably extendable file. The linear combinations of the free induction decays that are required to obtain the time-domain data matrices for the PDQ and PZQ spectra, the Gaussian weighting, the Fourier transformation, and the phase correction of the frequency-domain matrices were carried out on a VAX 8550 mainframe computer with a software package developed in Groningen and Utrecht by R. Scheek, R. Boelens and R. Kaptein. The raw data were transferred via tape from an Aspect 1000 data station to the mainframe computer. In the first step of data reduction, a peak picking routine is applied to a cross-section through the PZQ spectrum, taken parallel to the ω_2 axis at $\omega_1 = 0$. The resulting array of maximas serves as a reference table to construct a new reduced frequency-domain data matrix, which consists of interleaved PDQ and PZQ traces taken parallel to the ω_1 axes. Each of these traces is further reduced to two arrays containing lists of extrema, one array for positive peaks and one for negative peaks. The resulting set of arrays serves as a base for subsequent data handling. However, the matrix of the full PDQ and PZQ traces taken parallel to the ω_1 axis is kept in store for further inspection in cases of ambiguities.

The analysis of the reduced data can be divided in two parts. The first part allows one to identify the direct connectivities, i.e. to recognize the CH_n subunits. This is done by creating two dynamic lists, one for the ^{13}C shifts, the other for the 1H shifts, connected by pointers. This connectivity table may be regarded as a simple representation of a conventional heteronuclear shift correlation spectrum. The algorithm designed to extract these two cross-connected lists acts sequentially on the arrays of extrema mentioned above and determines the number of direct correlations, taking into account intensities and shapes of the positive peaks in the

PDQ trace. For geminal cases the positive maxima of the PZQ trace are also taken into account (see Figure 3). If there are two carbons that have accidentally the same ^{13}C shift, this leads to two entries in the ^{13}C list and up to four entries in the ^1H list.

The second part of the analysis aims at establishing the remote heteronuclear shift correlation map. The ^{13}C chemical shift list is scanned and the negative maxima of the PDQ and PZQ traces are examined and related to entries in the ^1H list. Each of the connectivities is labeled with a number that we call the *quality factor* Q_{AB} , which expresses the degree of reliability of the evidence. Evidence for a transfer $\text{H}_B \rightarrow \text{H}_A \rightarrow \text{C}_A$ may be found at five possible levels of confidence (q_{BA} factors given on the left side of Figure 6), and similarly there are five levels of confidence for the identification of the opposite transfer $\text{H}_A \rightarrow \text{H}_B \rightarrow \text{C}_B$ (q_{AB} factors in the central part of Figure 6). The likelihood that the A and B fragments are neighbors (in the sense that $J(\text{H}_A\text{H}_B) \neq 0$), is assumed to be given by the product $Q_{AB} = q_{AB}q_{BA}$. The numerical values in Figure 6 have been chosen empirically and could probably be refined on the grounds of statistical criteria. At this stage of development, they merely serve to define a "pecking order" and to remind us that some pieces of evidence are more reliable than others.

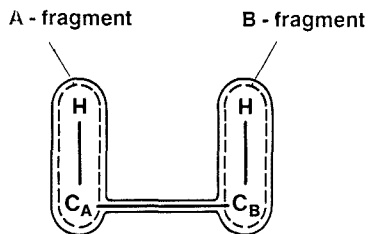
Finally, the whole network of direct and remote connectivities is summed up in the form of a connectivity matrix. Connectivities can also be represented graphically by drawing arrows in conventional heteronuclear two-dimensional correlation spectra. Examples of the resulting "spectral representation" of the connectivity matrix will be shown below. If the actual assignment is completed (a crucial step which at this stage cannot be carried out automatically and therefore remains the responsibility of the spectroscopist), remote connectivities that have been identified by pattern recognition can also be represented by drawing arrows onto the molecular formula to represent the pathways of magnetization transfer.

EXPERIMENTAL SECTION

In addition to the illustrative examples of 2-thiophenecarboxylic acid and 2,6-dimethylcyclohexanol shown in Figures 2 and 5, two other samples have been investigated to test our approach. Sample I consisted of a solution of 60 mg of 1-hexanol in 1 mL of CDCl_3 with 100 mg of $\text{Eu}(\text{DPM})_3$ as a shift reagent (33). Sample II consisted of a solution of 65 mg of (1*RS*,2*SR*,4*SR*,5*RS*,6*RS*)-6-*exo*-(2-nitrophenylthio)spiro[bicyclo[2.2.2]octane-2,2'-oxirane]-5-*endo*-yl chloride (34) in 0.5 mL of a 1:5 mixture of hexadeuterobenzene and deuteriochloroform. The spectra were recorded on a Bruker AM 400 spectrometer, using time-proportional phase increments (TPPI) to obtain pure absorption peak shapes (7, 35). The time domain data were transferred to a VAX 8550 cluster via magnetic tape. After assembling the PDQ and PZQ data matrices, Lorentz-Gauss transformation, zero-filling to $2\text{K} \times 2\text{K}$ data points, Fourier transformation, and phase correction, two real $1\text{K} \times 1\text{K}$ matrices were obtained for each sample. The Groningen-Utrecht software package is written in Fortran and some Fortran input/output routines have been added. All other programs and supporting routines are written in VAX-Pascal. The entire analysis takes less than 2 min for each sample on the CPU which is rated at 14 MIPS.

RESULTS

Figure 7 shows cross sections through PDQ and PZQ spectra of hexanol (sample I), demonstrating the wealth of information and the ease of interpretation of the spectra obtained by our method. Note the in-phase direct connectivity signals and the antiphase remote connectivity multiplets, which have the general appearance of the patterns shown in Figure 3. Some remote signals have been emphasized by dashed circles for clarity. If two PDQ traces correspond to neighboring carbons, these circled signals appear exactly at the same frequencies. Partial cancellations and overlaps sometimes may cause the antiphase multiplets to be attenuated. In traces c and f one



transfer B → A						transfer A → B					neighbourhood A ↔ B	
a	b	c	d	e	q_{BA}	a	b	c	d	e	q_{AB}	Q_{AB}
*					1.0	*					1.0	= 1.00
	*				1.0	*	*				0.9	= 0.90
		*			1.0	*		*			0.5	= 0.50
			*		1.0	*			*		0.4	= 0.40
				*	1.0	*				*	0.1	= 0.10
	*				0.9	*	*				1.0	= 0.90
		*			0.9	*		*			0.9	= 0.81
			*		0.9	*			*		0.5	= 0.45
				*	0.9	*				*	0.4	= 0.36
	*				0.9	*	*				0.1	= 0.09
		*			0.5	*		*			1.0	= 0.50
			*		0.5	*			*		0.9	= 0.45
				*	0.5	*		*			0.5	= 0.25
	*				0.5	*	*				0.4	= 0.20
		*			0.5	*		*			0.1	= 0.05
			*		0.4	*			*		1.0	= 0.40
				*	0.4	*	*				0.9	= 0.36
				*	0.4	*		*			0.5	= 0.20
	*				0.4	*			*		0.4	= 0.16
		*			0.4	*				*	0.1	= 0.04
			*		0.1	*	*				1.0	= 0.10
				*	0.1	*		*			0.9	= 0.09
				*	0.1	*			*		0.5	= 0.05
	*				0.1	*	*				0.4	= 0.04

Figure 6. Table of quality factors q_{BA} and q_{AB} and of their product Q_{AB} assigned to various cases that can be encountered in pattern recognition. The codes (a) to (e) represent the following cases: (a) intense remote connectivity signals found in both PDQ and PZQ spectra; (b) two remote peaks found, but one signal has low intensity; (c) one remote connectivity signal found in the PZQ spectrum only; (d) one remote connectivity signal found in the PDQ spectrum only; (e) no remote connectivity found.

observes a near-coincidence of direct and remote peaks, leading to some attenuation of the latter. Note that in this simple case the patterns observed in the PDQ and PZQ spectra appear almost identical except for a displacement along the frequency axis.

Figure 8 shows the molecular structure of hexanol (sample I) and its ^{13}C spectrum. The number of chemically equivalent protons attached to each carbon is not determined by our

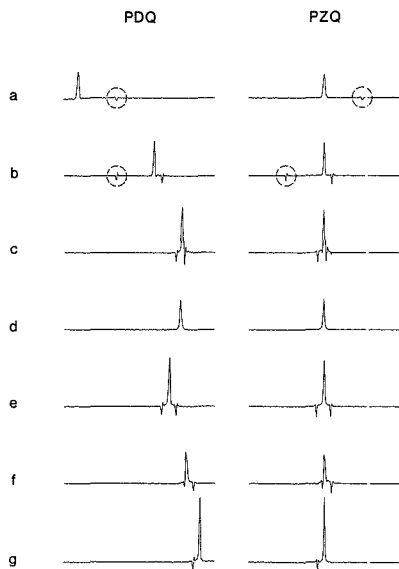


Figure 7. Cross sections taken parallel to the ω_1 axis through PDQ and PZQ spectra of hexanol (sample I). The seven ^{13}C chemical shift values spread along ω_2 (shown from top to bottom) are labeled in alphabetical order from low to high field. A set of 360 t_1 increments with 2K data points each were acquired, the spectral width was 4546 Hz in ω_2 and 2108 Hz in ω_1 , the final digital resolution was 4.4 Hz per point in ω_2 and 2.1 Hz per point in ω_1 .

method, hence the notation with " H_n " groups. The pattern recognition program identifies a chain of remote connectivities that yields a symmetrical connectivity matrix (top right). The

quality factors Q_{ab} , Q_{be} , Q_{ce} , Q_{ef} , and Q_{fg} are all equal to one (see table in Figure 6). No misleading long-range connectivities were found in this case. The short-range vicinal connectivities have been represented by drawing two-pointed arrows onto the chemical formula of hexanol. The connectivity matrix readily allows even the most inexperienced chemist to assign the carbon-13 spectrum (and hence the proton-carbon correlation spectrum) in the following manner: $a \leftrightarrow 1$, $b \leftrightarrow 2$, $c \leftrightarrow 4$, $e \leftrightarrow 3$, $f \leftrightarrow 5$, and $g \leftrightarrow 6$. This assignment is shown along the edges of the matrix: the alphabetic sequence is shown on top (and on the left), while the numerical sequence is shown below (and on the right). If the columns and rows of the matrix were reordered according to the numerical sequence, the matrix would have a band structure, with $Q_{xy} = 1$ in elements with $x = y \pm 1$. This band structure is characteristic of noncyclic molecules without branching and with negligible long-range proton-proton couplings.

A connectivity matrix such as the one shown in Figure 8 for sample I is not easily grasped at first glance. To ease its interpretation, this matrix can be transformed into the "spectral representation" of Figure 9 by drawing arrows onto a conventional heteronuclear shift correlation spectrum. The arrows indicate the connectivities that have been identified by pattern recognition. For example, the double-pointed arrow between peaks a and b indicates that remote peaks have been found arising from both processes $\text{H}_a \rightarrow \text{H}_b \rightarrow \text{C}_b$ and $\text{H}_b \rightarrow \text{H}_a \rightarrow \text{C}_a$, providing evidence that the C_aH_a and C_bH_b groups are neighbors, in the sense that there is a nonvanishing homonuclear coupling $J(\text{H}_a\text{H}_b)$. It is not necessary to record a conventional heteronuclear shift correlation spectrum to make a plot such as in Figure 9, since it is sufficient to consider the positive peaks in the PDQ spectrum, which have frequency coordinates that correspond to the proton and carbon shifts of the CH_n groups.

Figure 10 shows cross sections through PDQ and PZQ spectra of the bicyclic compound of sample II (see molecular formula in Figure 11). Note the modest signal-to-noise ratio,

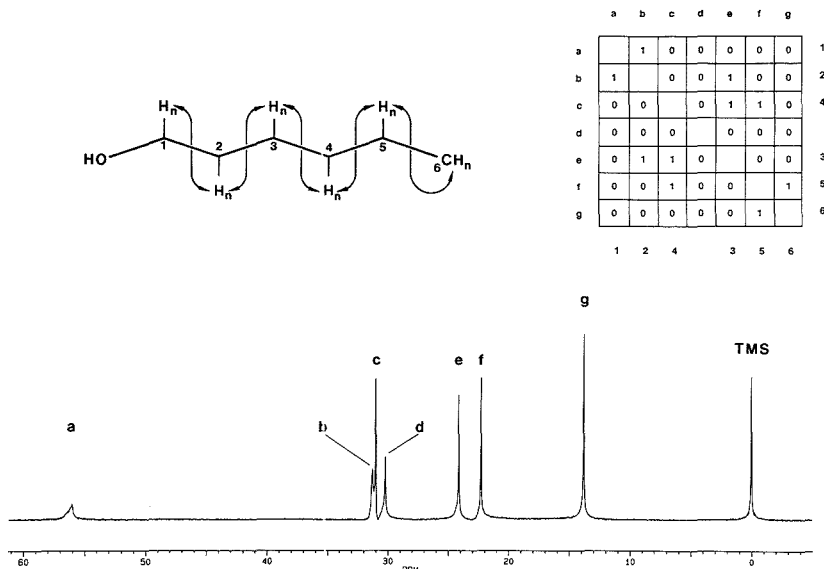


Figure 8. Molecular structure of hexanol (sample I) with conventional numbering of the carbon atoms, but without specifying the number of chemically equivalent protons attached to each carbon (hence the notation H_n). Below: ^{13}C spectrum obtained in the presence of the shift reagent $\text{Eu}(\text{DPM})_3$ with resonances labeled alphabetically from low to high field. Line d corresponds to the CH resonance of the DPM ligand. The connectivity matrix (top right) indicates the quality factors Q_{xy} found by automated analysis.

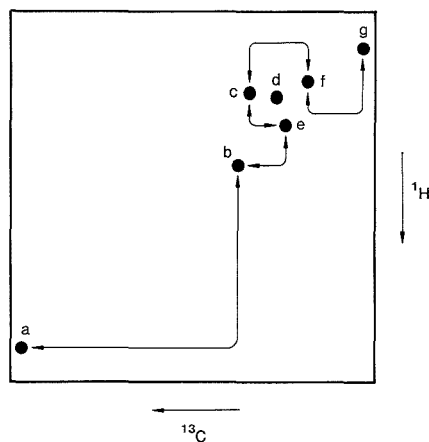


Figure 9. "Spectral representation" of the connectivity matrix found for hexanol (see matrix in Figure 8). The arrows indicate the connectivities that have been identified by pattern recognition.

which is due to the complexity of the coupling network and to the fact that only 65 mg of substance was available. By way of example, the remote connectivity peaks that reveal the neighborhood of $C_c (=C_6)$ and $C_d (=C_1)$ have been emphasized by dashed circles. Although some of the antiphase multiplets are severely attenuated, this did not prevent identification of connectivities. Note the patterns in the PDQ and PZQ spectra arising from the geminal CH_2 group of $C_f = C_3$, which may be compared with the schematic patterns of Figure 3. Unlike the simple situation of Figure 7, most of the patterns in the PDQ and PZQ spectra in Figure 10 *cannot* be brought to superposition by a mere shift in frequency. This is due to the complexity of the coupling network, to strong coupling, and to the presence of diastereotopic geminal protons in sample II.

Figure 11 shows the molecular structure of the bicyclic compound of sample II, its ^{13}C spectrum, and the connectivity matrix obtained by pattern recognition. The quality factors Q_{xy} vary from 0.04 to 1.0 in accordance with the table of Figure 6. In spite of the complexity of the proton coupling network, all neighboring subunits were identified as such, and, with the sole exception of the link C_e-C_f (C_6-C_3), the corresponding quality factors were all larger or equal to 0.1. Some long-range connectivities were found in addition, but the quality factors of these misleading connectivities were all smaller than 0.1, with the exception of the links C_e-C_h (C_6-C_7) and C_d-C_g (C_1-C_8), which have quality factors of 0.16 and 0.1, respectively. This is presumably because of insidious effects of strong coupling (36) between the two protons attached to C_6 . Further connectivity information with $Q_{xy} < 0.1$ can be used to obtain hints how fragments that are separated by quaternary carbons or heteronuclei can be linked together (e.g. in Figure 11, the connectivities $Q_{bf} = Q_{g3}$ and $Q_{df} = Q_{13}$).

In Figure 11, remote connectivities with $Q_{xy} > 0.1$ are represented by solid arrows drawn onto the molecular formula. A dashed arrow was used to represent a vicinal relationship that was identified with a disappointingly low quality factor of $Q_{ef} = Q_{43} = 0.05$. Double-pointed arrows indicate that the connectivities were found in both directions, single arrows (such as those emanating from the two H_f protons pointing to the H_1 proton) indicate that the reverse pathway could not be observed. The conventional heteronuclear shift correlation spectrum shown in Figure 12 was obtained by representing the direct connectivity peaks identified in the PDQ spectrum

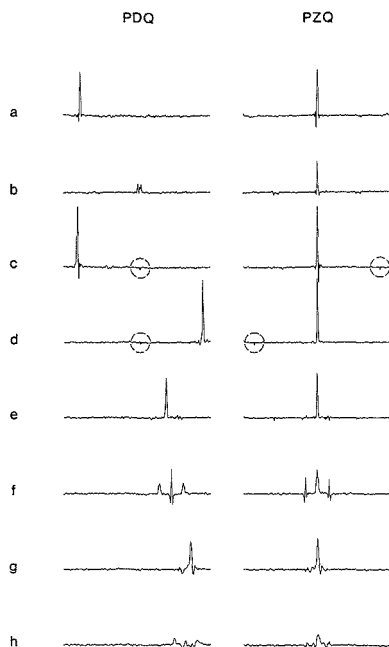


Figure 10. Cross sections taken parallel to the ω_1 axis through PDQ and PZQ spectra of the bicyclic compound of sample II (molecular formula see Figure 11). The traces are labeled alphabetically (from top to bottom) according to the order of their ^{13}C chemical shifts from low to high field. A set of 400 t_1 increments with 2K data points each were acquired, the spectral width was 6014 Hz in ω_2 and 1250 Hz in ω_1 , and the final digital resolution was 5.9 Hz per point in ω_2 and 1.2 Hz per point in ω_1 .

by filled dots. The arrows in Figure 12 indicate all connectivities that have been identified by pattern recognition with $Q_{xy} > 0.1$.

The complexity of the proton coupling network of sample II can be best appreciated by inspecting the double-quantum filtered homonuclear correlation spectrum (DQF-COSY), displayed in Figure 13. Note the complexity of the proton multiplets h and h' at 1.5 and 1.96 ppm, which correspond to the two protons attached to C_7 , and the ill-resolved multiplet g at 1.62 ppm which comprises the two protons attached to C_6 . It may seem remarkable that the heteronuclear relayed spectra could be readily interpreted in spite of these complications.

SCOPE FOR FURTHER INVESTIGATION

It may be necessary in some cases to study the effects of strong coupling by spectral simulations. This should allow one to identify misleading long-range connectivities as such. One could consider introducing a more interactive concept, where the program, after completing the analysis of the PDQ and PZQ spectra, would ask the operator for further chemical and spectroscopic information, and perhaps propose a type of experiment required to solve the remaining ambiguities. In particular, homonuclear correlation spectra (COSY and its many variants) might be useful, Overhauser effects might help to assemble fragments separated by quaternary carbons and heteroatoms, the attached proton test (APT) (29) and distortionless enhancement by polarization transfer (DEPT) (30) could yield information about the multiplicity of degenerate protons. Last but not least, information that is closely related to our connectivity matrices can in principle be obtained from

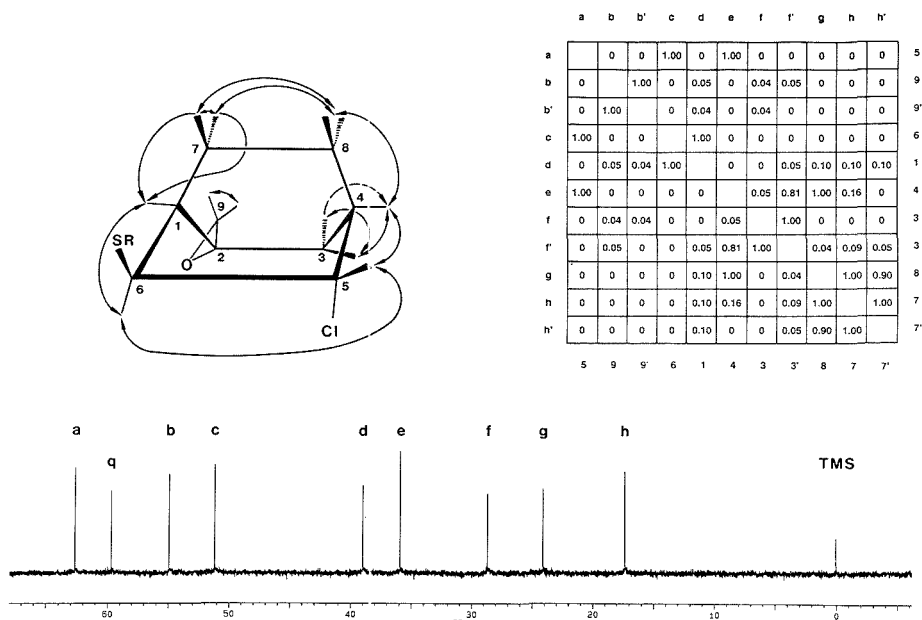


Figure 11. Molecular structure of sample II with conventional numbering of the carbon atoms, and ^{13}C spectrum with resonances labeled alphabetically from low to high field, except for the resonance q of the quaternary carbon C_9 , which does not appear in either PDQ or PZQ spectra. The connectivity matrix indicates the quality factors Q_{xy} . The main connectivities are represented by arrows in the molecular formula, following conventions explained in the text.

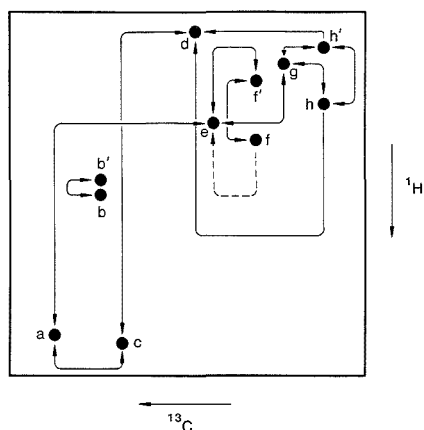


Figure 12. Spectral representation of the connectivity matrix found for the bicyclic compound of sample II. The arrows indicate the remote connectivities that have been identified by pattern recognition.

carbon-13 double quantum spectroscopy (INADEQUATE), if sensitivity considerations are not too forbidding (37).

CONCLUSIONS

Starting from a set of two complementary heteronuclear relayed magnetization transfer spectra, i.e. a pseudo-zero-quantum and a pseudo-double-quantum spectrum, the approach introduced in this paper performs the following tasks: (i) extraction of the conventional carbon-proton chemical shift correlation map, (ii) identification of remote correlation sig-

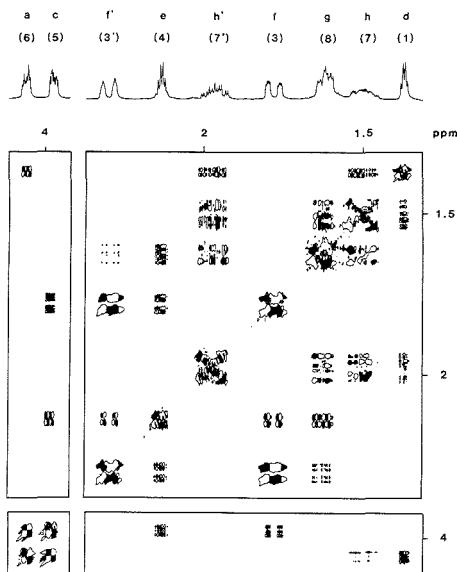


Figure 13. Homonuclear double-quantum filtered correlation spectrum (DQF-COSY) of sample II, recorded with an AM 400 spectrometer with 4K data points for each of the 1024 t_1 increments and a spectral width of 1250 Hz in both dimensions. Positive peaks have been filled in for clarity. The labels of the protons correspond to Figure 11.

nals, (iii) linking of the CH_n subunits through their remote connectivities, and (iv) determination of a correlation matrix

containing quality factors that express the reliability of the results. For ease of interpretation, the information about correlation may be displayed in the form of a *spectral representation* like in Figure 12. We hope that further research will allow us to use our correlation matrices in order to identify molecular fragments and ultimately to build up entire structural formulas of unknown compounds.

ACKNOWLEDGMENT

We are indebted to Martial Rey for valuable assistance with instrumentation, to François Claret and Pierre Vogel for providing a sample of the bicyclo[2.2.2]octane derivative, and Ruud Scheek, Rolf Boelens, and Robert Kaptein for their kind permission to use their software package.

LITERATURE CITED

- Ernst, R. R.; Bodenhausen, G.; Wokaun, A. *Principles of Nuclear Magnetic Resonance in One and Two Dimensions*; Clarendon Press: Oxford, 1987.
- Meier, B. U.; Bodenhausen, G.; Ernst, R. R. *J. Magn. Reson.* **1984**, *60*, 161.
- Neidig, K. P.; Bodenmüller, H.; Kalbitzer, H. R. *Biochem. Biophys. Res. Commun.* **1984**, *125*, 1145.
- Pfändler, P.; Bodenhausen, G.; Meier, B. U.; Ernst, R. R. *Anal. Chem.* **1985**, *57*, 2510.
- Pfändler, P.; Bodenhausen, G. *J. Magn. Reson.* **1986**, *70*, 71.
- Bolton, P. H. *J. Magn. Reson.* **1986**, *70*, 344.
- Mädi, Z.; Meier, B. U.; Ernst, R. R. *J. Magn. Reson.* **1987**, *72*, 584.
- Novič, M.; Oschkinat, H.; Pfändler, P.; Bodenhausen, G. *J. Magn. Reson.* **1987**, *73*, 493.
- Glaser, S.; Kalbitzer, H. R. *J. Magn. Reson.* **1987**, *74*, 450.
- Meier, B. U.; Mädi, Z.; Ernst, R. R. *J. Magn. Reson.* **1987**, *74*, 565.
- Hoch, J. C.; Hengyi, S.; Kjaer, M.; Ludvigsen, S.; Poulsen, F. M. *Carlsberg Res. Commun.* **1987**, *52*, 111.
- Engenberger, U.; Pfändler, P.; Bodenhausen, G. *J. Magn. Reson.* **1988**, *77*, 192.

- Grahn, H.; Delaglio, F.; Delsuc, M. A.; Levy, G. C. *J. Magn. Reson.* **1988**, *77*, 294.
- Novič, M.; Bodenhausen, G. *Anal. Chem.* **1988**, *60*, 582.
- Pfändler, P.; Bodenhausen, G. *J. Magn. Reson.* **1988**, *79*, 99.
- Meier, B. U.; Ernst, R. R. *J. Magn. Reson.* **1988**, *79*, 540.
- Pfändler, P.; Bodenhausen, G. *Magn. Reson. Chem.* **1988**, *26*, 888.
- Szalma, S.; Pelczer, I. *J. Magn. Reson.* **1988**, *76*, 416.
- Maudsley, A. A.; Ernst, R. R. *Chem. Phys. Lett.* **1977**, *50*, 368.
- Maudsley, A. A.; Müller, L.; Ernst, R. R. *J. Magn. Reson.* **1977**, *28*, 463.
- Freeman, R.; Morris, G. A. *Bull. Magn. Reson.* **1979**, *1*, 5.
- Müller, L. *J. Am. Chem. Soc.* **1979**, *101*, 4481.
- Bax, A.; Griffey, R. H.; Hawkins, B. L. *J. Am. Chem. Soc.* **1980**, *102*, 7188.
- Bolton, P. H.; Bodenhausen, G. *Chem. Phys. Lett.* **1982**, *89*, 139.
- Sørensen, O. W.; Ernst, R. R. *J. Magn. Reson.* **1983**, *55*, 338.
- Morris, G. A.; Freeman, R. *J. Am. Chem. Soc.* **1979**, *101*, 760.
- Burum, D. P.; Ernst, R. R. *J. Magn. Reson.* **1980**, *39*, 163.
- Wimberger, S.; Bodenhausen, G. *J. Magn. Reson.* **1986**, *69*, 264.
- Le Cocq, C.; Lallemand, J.-Y. *J. Chem. Soc., Chem. Commun.* **1981**, 150.
- Dodtrel, D. M.; Pegg, D. T.; Bendall, M. R. *J. Magn. Reson.* **1982**, *48*, 223.
- Koglar, H.; Sørensen, O. W.; Bodenhausen, G.; Ernst, R. R. *J. Magn. Reson.* **1983**, *55*, 157.
- Levit, M. H. *Prog. Nucl. Magn. Reson. Spectrosc.* **1986**, *70*, 518.
- Fribolin, H. *Ein- und zweidimensionale NMR-Spektroskopie*; Verlag Chemie: Weinheim, 1986.
- Claret, F.; Carrupt, P.-A.; Vogel, P. *Helv. Chim. Acta* **1987**, *70*, 1886.
- Marion, D.; Wüthrich, K. *Biochem. Biophys. Res. Commun.* **1983**, *113*, 967.
- Morris, G. A.; Smith, K. I. *Mol. Phys.* **1987**, *61*, 467.
- Bax, A.; Freeman, R.; Kempell, S. P. *J. Am. Chem. Soc.* **1980**, *102*, 4849.

RECEIVED for review April 25, 1989. Accepted July 14, 1989. This research was supported in part by a grant of Spectrospin AG, Fällanden, Switzerland, and by the Swiss National Science Foundation.

Fiber-Optic Dipping Sensor for Organic Solvents in Wastewater

F. L. Dickert* and S. K. Schreiner

Institute of Physical and Theoretical Chemistry, Erlangen University, Egerlandstrasse 3, D-8520 Erlangen, FRG

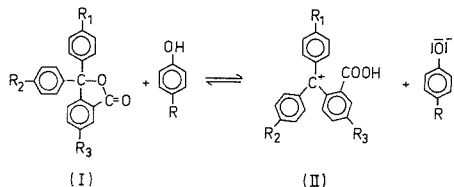
G. R. Mages and Heinz Kimmel

Siemens AG, Central Research and Development, ZFE F1 AMF 3, Paul-Gossen-Strasse 100, D-8520 Erlangen, FRG

Triphenylmethane dyes were used as sensor materials for the detection of organic solvents and gases (ammonia) in water via changes in optical absorbance. For this purpose these sensor layers were separated from the aqueous solutions by a gas-permeable membrane. The measurements were performed with a quartz fiber arrangement using optical detection in the visible range. The distinct vapor pressures of the organic solvents in water lead to an enhancement of the sensor selectivity in comparison to the analogous gas-phase studies. Down to approximately 30 ppm organic solvents in water can be analyzed in favorable cases.

Substituted 3,3-diphenylphthalides (I) form a highly colored triphenylmethane dye (II) by interaction with an acid component, e.g., a phenol (I). This reaction can be applied for the design of an optochemical sensor system for the detection of solvent vapors in the air (1, 2). The sensor materials are used in thin layers (thickness 0.2–0.6 μm) on a carrier for optical transmission measurements. The absorption of solvent vapors leads to a decrease in the optical absorbance due to

a shift of the following equilibrium toward the colorless phthalide (I).



These ideas are transferred to the development of a sensor arrangement for the detection of solvent traces in water, since huge amounts of wastewater are produced in the chemical industry that have to be continuously analyzed according to their organic ingredients.

For this purpose the sensor layers are separated from the water by a permeable membrane (3). The solvent is allowed to penetrate the membrane, and its vapor yields the same sensor effect as described for gas-phase measurements (1). A fiber optical system is used as a transducer for the light (4, 5). In this way the light of the emitter is transferred to the

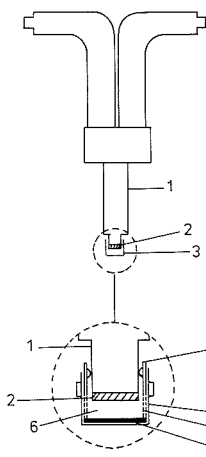
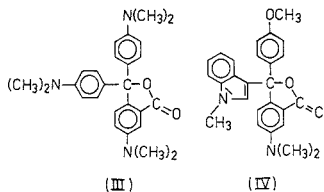


Figure 1. Bifurcated glass fiber bundle and sensor head: 1, wave guide end; 2, sensor layer; 3, metal cover with O-ring and mounting; 4, Teflon membrane; 5, windows; 6, gas volume; 7, mirror.

layer and then back to the detector element. Remote monitoring of poisons in water can be accomplished by this procedure. The phthalides are practicable sensor materials for several organic solvents, and many water pollution problems can be solved by using the proposed system.

EXPERIMENTAL SECTION

Sensor Materials. Two distinct phthalides, the crystal violet lactone (III) and a derivative with an indolyl ring (IV) which yields especially large sensor effects for ammonia, were selected from a large variety (6) of compounds because of their pronounced absorbance in the visible range (6). Again bisphenol A (I) (Fluka) was an acidic ingredient for the formation of the dyes (II). The linearity of the characteristic lines over the whole measuring range can be drastically improved by the addition of 4-nitrophenol (Merck), which is a stronger acid in comparison to bisphenol A. In this way no plateau formation is observed at low solvent content in the air. The stability of the layers was improved by 10 wt % poly(vinyl chloride) (Fluka).



Measurements. The central part (Figure 1) of the equipment is a statistically mixed bifurcated glass fiber bundle (Oriol, Model 77533). The sensor material was applied in a tetrahydrofuran solution (Merck) to the common end of the wave guide (Figure 1, (1)). Sensor layers (2) of 0.2–0.4 μm thickness are formed after solvent evaporation. The sensor layer was protected from the liquid phase by a metal cover (3). The penetration of solvent vapor is possible by means of Teflon windows (5) (foils of 100 μm thickness, (4)) at the sides of the sensor head. The gas volume (6) in front of the sensor layer was minimized to realize short sensor rise times. A mirror (7) was adjusted at the bottom of the cap. The light passes the sensor layer twice due to a reflection (Figure 1), and the sensitivity is enhanced in this way. A light-emitting diode (LED, $\lambda_{\text{max}} = 590 \text{ nm}$, Siemens) was taken as the light source. The rectangular signals (600 Hz) of a wave generator (Wavetec 164) were used as a power supply. The normal operation current for the LEDs was 5 mA. Improved stability

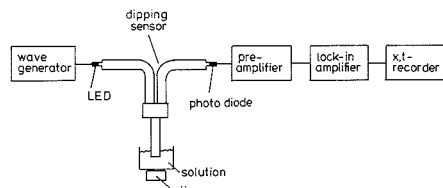


Figure 2. Measuring arrangement.

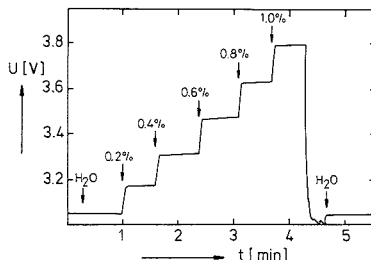


Figure 3. Dipping sensor output signal at 20 °C as a function of the addition of tetrahydrofuran (in volume percentages) to water at the marked time points. The sensor layer contained lactone (III) with equimolar 4-nitrophenol and a 7.5 excess of bisphenol A.

was achieved by applying an increased direct current of 20 mA for 2 days. A silicon photodiode was used as a detector followed by a self-built preamplifier. Modulation of the LED current (600 Hz) enables a lock-in amplifier (Ithaco 399) to be used and thus the stray light to be eliminated (Figure 2). The temperature stability of the sensor head was controlled with an accuracy of ± 0.1 °C by immersing it in a bath to realize constant vapor pressures.

RESULTS AND DISCUSSION

Sensor Effect and Reversibility. A typical sensor response, the output voltage of the lock-in amplifier, as a function of the addition of tetrahydrofuran at the marked time points can be seen in Figure 3. Crystal violet lactone (III) with an excess of phenols was chosen as the sensor material. Decreasing absorbance leads to an increase in the light intensity at the detector diode, and the lock-in amplifier output voltage is enhanced. The water vapor also penetrates the Teflon membrane and therefore causes a diminution of the sensor layer absorbance (1) in comparison to dry air. The addition of 0.2% by volume of the organic solvent yields steps that slightly increase in height in parallel with the amount of tetrahydrofuran in water. This sensor signal can easily be converted to absorbances, and the steps attain an equal height in these units. The sensor is removed from the solution after the measuring procedure and is then again immersed in pure water. In this way the starting condition is reestablished and the absorbance becomes identical with that before the measurements. Spikes are observed for sensor responses as a function of time if organic solvents are studied that are only slightly soluble in water, such as ethyl acetate.

Sensor Characteristics. Excellent linear characteristic lines are obtained if absorbances calculated from data as presented in Figure 3 are plotted versus the solvent content in water. For example, the addition of 1 vol % of tetrahydrofuran to water halves the initial absorbance and therefore appreciable effects are observed even for small amounts of organic solvents.

Time Behavior. The exact rise times of the sensor responses can be determined from measurements as demonstrated in Figure 3 if the time scale becomes expanded. The

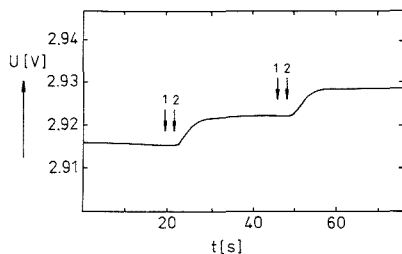


Figure 4. Dipping sensor time behavior upon addition of 0.2 vol % ethanol to water at 20 °C: 1, addition of ethanol; 2, mixing process completed.

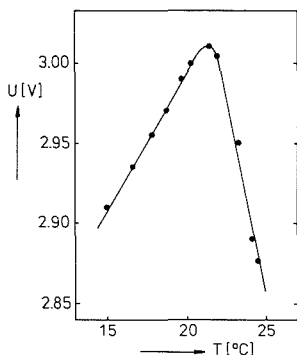


Figure 5. Dipping sensor output signal for pure water as a function of temperature.

results in Figure 4 indicate that the sensor response to an increase of 0.2% ethanol is established in less than 10 s if the rise time is defined via a signal coming up to 90% of the end point. This finding is very favorable for chemical sensors and the rise times are faster than those observed for gas-phase measurements with low solvent amounts and low humidity. The sensor material behind the membrane incorporates water according to the saturation vapor pressure. The rate-determining process for the sensor effect is the diffusion of solvent in the layers and not the formation of the lactone from colored triphenylmethane dye (7). The sensor films are soaked, and therefore a high mobility of particles is realized, leading to very favorable time behavior.

Temperature Dependencies. The sensor response is directly related to the vapor pressure of both water and the organic component. For this reason the temperatures of the solutions under investigation have to be exactly controlled, and defined conditions are established in this way. The effect of temperature on the sensor output for pure water is shown in Figure 5. A characteristic maximum is observed, which can be explained by two opposing effects. The vapor pressure increases in parallel with temperature. Thus a diminishing dye concentration in the layer is accompanied by a rise of voltage (Figure 5). Another effect, however, has to be included, namely the temperature dependence of absorption of solvent vapor in the sensor layers. This phenomenon obviously shows a larger temperature dependence than the vaporization process does, and therefore the signal decreases above 22 °C. These data for pure water are the ordinate intercepts of the sensor characteristics which describe solvent sensitivities at variable temperatures (Figure 6). The slopes of these straight lines increase with temperature, this behavior being due to the vapor pressure of the organic solvent in water. The absorption of ethanol in the sensor layers is favored by an increasing

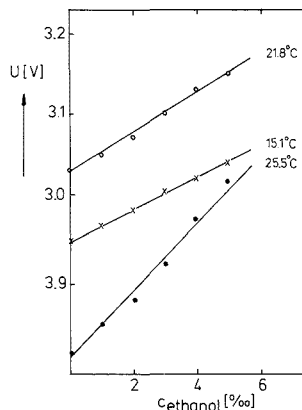


Figure 6. Dipping sensor output signal as a function of the addition of ethanol (in volume percentages) to water at variable temperatures.

temperature since the vaporization of the solvent is more strongly influenced than the desorption process. This phenomenon is quite plausible since ethanol and other organic solvents are more favorably adapted in their polarity to the sensor layers than water.

Detection Limits. The sensitivity for minute amounts of organic solvents in water can be inferred from the slope of the characteristic lines and the noise amplitude of the measuring signal. The noise level in typical measurements was 0.5 mV, which can be converted to 4×10^{-5} absorbance units (AU). The detection limits can be defined as twice this level. According to Figure 3 a limiting value of 15 ppm tetrahydrofuran can be detected in water by the proposed method.

The sensitivity of the dipping sensor arrangement to non-aqueous solvents is not only affected by the noise level, but temperature control also has to be discussed. The pressure of water and its absorption in the sensor layer are temperature dependent as shown in Figure 5. An accuracy of ± 0.1 °C in controlling the temperature of the water solution and the sensor element can easily be achieved. These variations lead to changes of $\pm 1.2 \times 10^{-4}$ and $\pm 4.1 \times 10^{-4}$ AU for the range of the positive and the negative slope of the curve in Figure 5. Additionally the temperature dependence of the organic solvent vapor pressure has to be included since different slopes for the characteristic lines in Figure 6 are observed. These changes in the slopes lead to a variation of 1.7×10^{-5} AU at a 0.5% content of ethanol in water if the temperature is altered by ± 0.1 °C. This effect is negligible in comparison to the noise level. The ordinate intercepts, however, of the characteristics (Figure 6) have to be included also in discussing temperature dependencies. These effects are larger than the noise level, as can be deduced from Figure 5. This temperature dependence of the water sensor response simulates up to 30 ppm tetrahydrofuran in water. If the temperature of the sample or of the sensor layer is less exactly controlled or defined, the sensitivity and the inaccuracy of the dipping sensor will of course increase.

Selectivity. A large number of different solvents were used to test the selectivity of this sensor equipment. The relative changes of absorbances that are caused by the addition of 0.5% organic solvent or ammonia to water are presented in Figure 7. A better visualization of the data is achieved by dividing all values by the minimum response of all chosen solvents observed for methanol.

The sensitivities differ by a factor of up to 30. Three different effects have to be considered for the explanation of

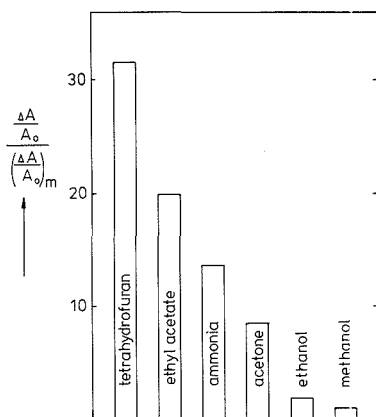


Figure 7. Dipping sensor sensitivities; relative changes of absorbance $\Delta A/A_0$ referred to the minimum response $(\Delta A/A_0)_m$ (methanol) for the addition of 0.5 vol % (ammonia; weight percentages) ingredients to water at 20 °C.

this finding. The first step for this sensor phenomenon is the absorption of solvent by the layers. These sensor materials exhibit amphiphilic properties since an ion reaction is used (reaction I-II), but on the other hand the carbenium ions (II) show a very effective charge delocalization. For this reason solvent molecules with relative nonpolar solvents such as ethyl acetate are also incorporated by the sensor layers. The extent of optical absorbance changes is determined by the interaction of the absorbed solvent with the network of hydrogen bonds that is formed from the phenolic acid (1). Sensor measurements with solvent vapors show that large sensor effects are observed for strong donors (8) or solvents that exhibit structure-breaking effects. For this reason tetrahydrofuran shows a pronounced sensitivity due to its oxygen donor atom. This effect is even surpassed by solvents with stronger donor properties (8) such as dimethylformamide, dimethyl sulfoxide, or hexamethylphosphoric acid triamide. In this case a direct interaction between the electron-deficient compound, namely the carbenium ion (9), and the donor molecule may occur and colorless 1:1 adducts are formed. Additionally, however, the donor molecules form hydrogen bonds with the phenolic ingredient. Therefore the phenol is removed from the equilibrium and the reaction (I-II) is shifted toward the covalent colorless species. Ammonia shows strong donor properties, but due to its small molecular weight no effective absorption occurs. The same effect can be responsible for the larger

sensitivity of tetrahydrofuran in comparison to that of diethyl ether. Ethyl acetate has less pronounced donor properties but may disturb the hydrogen network in a very effective manner. Methanol has an acid proton and can form hydrogen bridges with the phenols. Therefore the acidity of the layers is only slightly changed and methanol has a smaller effect than all the other applied solvents (1).

The different vapor pressures of the organic solvents in water have to be included in a discussion to explain the distinct sensitivities of the proposed dipping sensor arrangement. The extent of solvent absorption by the layers and the position of the carbenium ion formation equilibrium (I-II) are not able to explain the results in Figure 7 since ethanol and ethyl acetate vapors, for example, show a similar sensitivity as could be shown for gas-phase measurements (1). The different sensitivities presented in Figure 7 can easily be understood by a deviation of the vapor pressure from ideal behavior. This phenomenon is predominantly observed for organic solvents that are very dissimilar to water or even only slightly miscible with water. These facts apply to tetrahydrofuran and ethyl acetate, and the partial pressures of these solvents are elevated by a factor of up to 50 at infinite dilution in comparison to an ideal behavior (10). In going from acetone to ethanol and methanol, the activity coefficients decrease from roughly 6 to 3 to 2 (10). The partial pressures of the organic solvents in water depend very strongly on their polarity, and it can therefore be concluded that this is the main effect for the different sensor sensitivities as shown in Figure 7.

Registry No. III, 1552-42-7; IV, 121861-10-7; tetrahydrofuran, 109-99-9; ethyl acetate, 141-78-6; ammonia, 7664-41-7; acetone, 67-64-1; ethanol, 64-17-5; methanol, 67-56-1; water, 7732-18-5; 4-nitrophenol, 100-02-7; bisphenol A, 80-05-7.

LITERATURE CITED

- (1) Dickert, F. L.; Lehmann, E. H.; Schreiner, S. K.; Kimmel, H.; Mages, G. R. *Anal. Chem.* **1988**, *60*, 1377-1380.
- (2) Posch, H. E.; Wolfbeis, O. S.; Pusterhofer, J. *Talanta* **1988**, *35*, 89-94.
- (3) Bruckenstein, S.; Symanski, J. S. *Anal. Chem.* **1986**, *58*, 1766-1770.
- (4) Sepaniak, M. J.; Tromberg, B. J.; Vo-Dinh, T. *Prog. Anal. Spectrosc.* **1988**, *11*, 481-509.
- (5) Saar, L. A. *TRAC, Trends Anal. Chem. (Pers. Ed.)* **1987**, *6*, 85-90.
- (6) Dickert, F. L.; Vonend, M.; Kimmel, H.; Mages, G. R. *Fresenius' Z. Anal. Chem.* **1989**, *333*, 615-618.
- (7) Brandner, G.; Dickert, F. L.; Lehmann, E. *Ber. Bunsen-Ges. Phys. Chem.* **1987**, *91*, 740-745.
- (8) Gutmann, V. *The Donor Acceptor Approach to Molecular Interactions*; Plenum Press: New York, 1978; Chapter 2.
- (9) Blumenstock, H.; Dickert, F. L.; Hammerschmidt, A. *Z. Phys. Chem. (Munich)* **1984**, *139*, 123-132.
- (10) Gmehling, J.; Onken, U. *Vapor-Liquid Equilibrium Data Collection*; Friedrich Bischoff: Frankfurt, FRG, 1977.

RECEIVED for review May 8, 1989. Accepted July 6, 1989. This work was supported by Fonds der Chemischen Industrie.

Quantitative Estimation of Component Amplitudes in Multiexponential Data: Application to Time-Resolved Fluorescence Spectroscopy

A. L. Wong and J. M. Harris*

Department of Chemistry, University of Utah, Salt Lake City, Utah 84112

Quantitative information about individual component contributions to multiexponential data is obtained by a reiterative, regression algorithm that employs a linear least-squares determination of component amplitudes within a nonlinear least-squares search for the exponential decay times. Uncertainty in the parameter estimates, arising from uncertainty in the data and overlap in the response, is predicted from first principles. The analysis method includes weighting to account for the Poisson error distribution arising from shot-noise-limited signals, which increases the accuracy of the amplitude estimates. While the algorithm is applicable to a variety of kinetic methods, it is applied in the present work to the analysis of time-resolved fluorescence decay curves. A fluorescence decay curve, written as a row vector, D , is decomposed into two factors: A , a column vector containing the amplitude contribution of each component, and $[C]$, a matrix which contains temporal behavior of each component in its rows. The analysis uses linear least squares to obtain estimates of A , which increases the efficiency by reducing the number of parameters that are searched. The theory of error in linear least squares allows the uncertainty of the component amplitudes to be determined from the $[C]$ matrix, derived from best estimates of the temporal behavior of the sample.

Quantitative determination of individual component contributions in multicomponent spectroscopic data is a common and difficult analytical problem. For data that derive from first-order kinetic reactions, such as time-resolved fluorescence, metal ion complexation reactions, and the decay of radioisotopes, component contributions to the observed amplitude are particularly difficult to retrieve due to the similar temporal behavior of exponential decay curves. Computational approaches to reaction-rate methods of chemical analysis have been compared by Wentzell and Crouch (1) for reactions following first-order and pseudo-first-order kinetics, and the computational difficulties commonly encountered were described. Mieling and Pardue (2) have developed a multiple-linear regression procedure to obtain the amplitudes of sample components simultaneously reacting at different rates. The method was similar to that examined by Willis et al. (3) to follow complexation kinetics of alkaline-earth complexes. The approach modeled the product concentration as the sum of the integrated first-order rate law for each component plus any other sources of product that are time-independent. The expression that is fit to the data is a sum of an offset and two or three exponentials of known decay constant, where the amplitudes are extracted by linear regression.

Time-resolved fluorescence spectroscopy, where the decay of intensity following pulsed excitation is generally obtained by time-correlated single photon counting techniques, produces data that also follow exponential relationships (4, 5). Most data analysis schemes for time-resolved fluorescence (6-9) follow an approach similar to the method described

above for chemical kinetics, except that the sensitivity of fluorescence lifetimes to the sample matrix does not generally allow the decay constants to be known in advance. As a result, fitting the data requires a nonlinear least-squares method since the observed intensity depends exponentially on the unknown decay constants; these nonlinear parameters appear in the argument of the exponential time dependence.

In nonlinear least squares, optimal values for each parameter are found by directly searching a parameter space while minimizing the squared deviations between theory and experimental results. A sequence of error-reducing steps is chosen where the best direction is reappraised after each step. A complication arises with this approach for fitting multicomponent systems, which results in large increases in computation time and uncertainty in evaluating parameters. Since each resolvable component in the fluorescence decay signal is described by an amplitude and a lifetime or decay constant, the number of parameters that must be optimized grows twice as fast as the number of components in the system. As a result, a fluorescence decay signal containing three resolvable components requires that a six-dimensional parameter space be searched.

In this work, we present a more efficient approach to the resolution of multiexponential data, where the decay constants are unknown. The method combines a linear regression step to obtain the amplitudes, similar to that described for multicomponent chemical kinetic data (2, 3), within a nonlinear least-squares algorithm to determine the best fit decay constants. This approach was first used to resolve multicomponent fluorescence spectra from emission wavelength-decay time data matrices (10). We have modified the method to obtain single preexponential factors for each component and to account for the nonhomogeneous variance of shot-noise-limited data. Proper weighting of the observations is found to significantly influence the accuracy of the results. The theory of error in linear regression has allowed us to develop an analytical expression that predicts quantitatively the precision of determining individual component contributions. Synthetic data, generated with multiexponential decay curves, and experimental fluorescence decay transients, obtained by time-correlated single photon counting, were used to evaluate the efficiency and accuracy of weighted regression algorithm and its predictions of the uncertainty for the component amplitudes.

THEORY

Modeling Fluorescence Decay Data. In absence of excited state-excited state interactions, the decay of fluorescence after pulsed excitation follows first-order kinetics, and the response of an n -component sample is

$$d_j = \sum_{i=1}^n (a_i/\tau_i) \exp(-j\Delta t/\tau_i) * I_j \quad (1)$$

where the intensity, d_j , at time interval j is the sum of contributions of the n fluorophores emitting in the sample. The parameters τ_i and a_i are the lifetime and total intensity of the

*i*th component, respectively, and Δt is the time interval between data points. The asterisk, "*", represents convolution (17) of the exponential decay of fluorescence with the instrument response function, I_j . This fluorescence decay data can also be represented as a row vector, \mathbf{D} , where t is the number of time intervals over which the fluorescence is recorded. The data can be expressed as a product of a vector and a matrix

$$\mathbf{D} = \mathbf{A}[\mathbf{C}] + \mathbf{R} \quad (2)$$

where \mathbf{A} is a row vector of length n containing the amplitudes of the fluorophores in the sample and $[\mathbf{C}]$ is an $(n \times t)$ matrix containing the time decay behavior of the excited-state components in its rows. Since the observed data, \mathbf{D} , contains error associated with the observation, there is a difference between the observation and the theory, given by a vector of residuals, \mathbf{R} .

Combining Linear and Nonlinear Least Squares. An efficient method of utilizing linear least squares in the analysis of time-resolved fluorescence decays has been described (10), based on assuming uniform variance in the residuals, \mathbf{R} . Given a time-resolved data vector \mathbf{D} , the method factors this matrix into \mathbf{A} and $[\mathbf{C}]$ which provide quantitative and lifetime information, respectively. To analyze \mathbf{D} , a trial matrix $[\hat{\mathbf{C}}]$ of decay curves is constructed row by row, by convolution of the exponential decay of the *i*th component having an trial lifetime, $\hat{\tau}_i$, with the measured instrument response, I_j

$$\hat{c}_{ij} = I_j * (1/\hat{\tau}_i) \exp(j\Delta t/\hat{\tau}_i) \quad (3)$$

This approach requires the assumption that the excited states of each component decay by first-order kinetics, an excellent approximation for dilute solutions and high repetition rate excitation.

The unweighted, linear least-squares solution for the best estimate of the component amplitudes $\hat{\mathbf{A}}$ is given by (12, 13)

$$\hat{\mathbf{A}} = \mathbf{D}[\hat{\mathbf{C}}]'([\hat{\mathbf{C}}][\hat{\mathbf{C}}]')^{-1} \quad (4)$$

where $[\hat{\mathbf{C}}]'$ signifies the transpose of $[\hat{\mathbf{C}}]$ and the superscript "-1" represents the matrix inverse operation. A model data vector $\hat{\mathbf{D}}$ is calculated from the product of the estimated amplitudes, $\hat{\mathbf{A}}$, and the trial time decay matrix, $[\hat{\mathbf{C}}]$

$$\hat{\mathbf{D}} = \hat{\mathbf{A}}[\hat{\mathbf{C}}] \quad (5)$$

Optimal parameter values are those which minimize χ^2

$$\chi^2 = (1/\sigma^2) \sum_{j=1}^t (d_j - \hat{d}_{ij})^2 \geq (1/\sigma^2) \mathbf{R}'\mathbf{R} \quad (6)$$

which has a lower limit given by the residual error in the data, \mathbf{R} .

Minimization of χ^2 requires an algorithm to search for n -dimensional parameter space of unknown lifetimes. The Nelder Mead SIMPLEX algorithm (14, 15) utilizes an iterative procedure which moves a simplex, a geometric figure having plane faces and $n + 1$ vertices in an n -dimensional space, where the vertices represent points at which χ^2 has been evaluated. The major advantage of the present algorithm, which adds a linear least-squares step of eq 4 into a nonlinear least-squares search for the lifetimes, is the reduction in the number of parameters that must be optimized by the nonlinear search procedure. This reduction represents a 2-fold lowering in the dimensionality of the search compared to the more common approach in which both lifetime and amplitude parameters are searched (5). Some concern could be raised as to whether this approach is a single-factor-at-a-time optimization which could be subject to false optima. Fortunately, this is not the case since the best amplitude estimates are determined by eq 4 for each combination of the trial lifetimes. Unlike a single-factor-at-a-time approach, the amplitudes are not constrained during the optimization of the lifetimes but

are reoptimized upon each move of the simplex in the nonlinear parameter space.

Weighting Shot-Noise-Limited Data. Application of the linear least-squares method of eq 4 and minimization of the unweighted squared error, eq 6, require that the error in the data be described by an error distribution of constant variance (12, 13). In the case of shot-noise-limited, fluorescence decay data, typical of single photon counting experiments (4), the dependence of the signal variance on amplitude requires that the solution be modified to account for differences in the size of the residuals. Regression methods for exponential decay data have been shown to be sensitive to inhomogeneous variance (16), where the efficiency of extracting parameters is degraded if weighting is neglected. The expected variance of the individual observations, σ_j^2 , required to weight the observations is readily available for intensity measurements made by single photon counting (17). Under such conditions, the error is Poisson distributed, approaching a Gaussian distribution for a large number of counts (18). The variance, σ_j^2 , of the data in the *j*th time interval has an expected value equal to the mean number of counts for that interval (4). Although the mean number of counts is not known from single observation, if the number of counts is sufficiently large (≥ 100), the variance may be estimated (with $<20\%$ error) from the observed number of counts in the time interval, $\sigma_j^2 = d_j$. The residual error vector, \mathbf{R} , in eq 2, is modeled as a row of random numbers distributed about a zero mean, with standard deviation equal to the square root of the number of counts in corresponding element in the data vector, \mathbf{D} .

The linear least-squares solution for the component amplitudes is found by multiplying both sides of eq 2 by a factor $[W]$, such that the product of $(\mathbf{R}[W])$ is a vector of uniform variance

$$\mathbf{D}[W] = \mathbf{A}[\mathbf{C}][W] + \mathbf{R}[W] \quad (7)$$

A matrix, $[W]$, which accomplishes this goal is a t -by- t diagonal matrix where the nonzero elements w_{jj} are

$$w_{jj} = 1/\sigma_j = 1/(d_j)^{1/2} \quad (8)$$

Chi-square for weighted residuals also has a simple form, represented as

$$\chi^2 = \sum_{j=1}^t (d_j - \hat{d}_j)^2 / \sigma_j^2 \geq \mathbf{R}[W][W]'\mathbf{R}' \quad (9)$$

The least-squares solution of eq 7 for the vector of best estimated component amplitudes takes the same form similar to eq 2

$$\hat{\mathbf{A}} = \mathbf{D}[W][W]'\hat{\mathbf{C}}'([\hat{\mathbf{C}}][W][W]'\hat{\mathbf{C}}')^{-1} \quad (10)$$

Since the diagonal elements of the matrix $([W][W]')$ are equal to $1/\sigma_j^2 = 1/d_j$, see eq 8, then the product $[\mathbf{D}[W][W]'] = \mathbf{U}$, which is a unit row vector of length, t , where the elements are all equal to one. This substitution results in a simpler form for eq 10

$$\hat{\mathbf{A}} = \mathbf{U}[\hat{\mathbf{C}}]'([\hat{\mathbf{C}}][W][W]'\hat{\mathbf{C}}')^{-1} \quad (11)$$

Error Estimation. An additional benefit of a linear least-squares determination of the component amplitudes is that errors associated with their estimation can be predicted from first principles. These uncertainties are collected into a variance-covariance matrix, $[\mathbf{V}]$, the diagonal elements of which are the variances of the amplitude estimates, and the off-diagonal elements are the covariances between the estimates. For data of uniform variance the variance-covariance matrix is given by (12, 13)

$$[\mathbf{V}] = \sigma^2([\mathbf{C}][\mathbf{C}]')^{-1} \quad (12)$$

where σ^2 is the variance of the data, d_j , which for shot-noise-limited signals is approximated by the average photon counts in each time channel. Lifetime values of individual

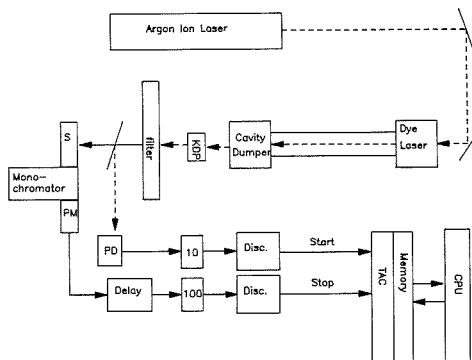


Figure 1. Block diagram of single photon counting fluorometer: PD, photodiode; PM, photomultiplier; TAC, digital time-to-amplitude converter; S, sample.

components in a mixture, known prior to the analysis or obtained through a nonlinear least-squares fit of the data, are used in eq 1 to construct $[C]$.

When \hat{A} is obtained from a weighted linear least-squared method, eq 11, the variance-covariance matrix is obtained by evaluating (13)

$$[V] = ([C][W][W][C])^{-1} \quad (13)$$

The estimated variance depends upon not only the component lifetimes, which are used to construct $[C]$, but also the particular data set that was observed, since the diagonal elements of $[W][W]$ are equal to $1/d_j$. Unlike linear least squares for constant variance data (19), weighted least squares requires that the error estimates be evaluated with each observed set of data since the relative intensity affects the weight of an observation; see eq 11.

EXPERIMENTAL SECTION

Modeling and data analysis on synthetic and experimental data were performed on a DEC 20/60 computer and a Compac 386 PC using FORTRAN. Subroutines from the IMSL and LINPACK libraries were called in the algorithms. Synthetic fluorescence decay curves were generated numerically by convoluting a Gaussian function of desired width with the decay law given in eq 3. Random noise vectors, \mathbf{R} , were derived from a Gaussian distribution, the mean of which was zero and standard deviation of which proportional to the square root of the signal. The final data vector \mathbf{D} was obtained according to eq 2, by adding the random noise to the fluorescence decay law generated by eq 1.

Time-resolved, fluorescence decay curves were experimentally obtained by using a pulsed laser fluorometer, shown in Figure 1. Excitation was accomplished by a mode-locked argon ion laser (Spectra Physics, Model 2000) synchronously pumping a rhodamine 6G dye laser (Spectra Physics, Model 375). The pulse rate of the dye laser output was maintained at 400 kHz by a cavity dumper (Spectra Physics, Model 454). The 604-nm emission from the dye laser was frequency doubled with a KDP crystal (Quantum Technology) and subsequently filtered with a Corning 7-54 UV-transmitting filter. The beam was then directed onto a sample, and fluorescence was detected at a 90° geometry using a photomultiplier. Data were recorded with Phillips discriminators (Model 6915) and LeCroy time-to-amplitude converter and multichannel analyzer (Models 4204 and 3588) controlled by a Leading Edge Model D personal computer via a GPIB interface.

The samples used were prepared by dissolving naphthalene (Aldrich Gold Label) in cyclohexane (Omnisolv). To avoid the uncertainty of preparing multicomponent samples, experimental data of multicomponent systems were generated by first recording transients of single-component samples with differing fluorescence lifetimes and then subsequently adding various transients together to obtain multicomponent fluorescence decay transients. Different

fluorescence lifetimes for the naphthalene samples were obtained by varying the concentration of oxygen in the sample, which acts as a quencher. Oxygen was removed by freeze-pump-thawing samples of naphthalene in cyclohexane to a base pressure of <15 mTorr. Data sets with different amplitude parameters were acquired by varying the collection time for individual samples, thus varying the total number of counts in a given data set. The generation of multicomponent data sets by adding together transients of single component systems together not only avoided the uncertainty in sample preparation but also guaranteed that the parameters describing the individual component behavior in those samples were accurately known.

The performances of each data analysis algorithm were compared by evaluating synthetically generated, fluorescence decay data. The number of iterations, required to reach a condition where χ^2 was changed by less than a designated value, was used as a criterion to judge the efficiency of each method, where an iteration is defined as a successful step in the SIMPLEX algorithm (14). The effects of ignoring proper weighting factors were determined by comparison of the two linear least-squares algorithms. Equations 4, 11, 12, and 13 were evaluated by solving for \hat{A} and $[V]$ using correct lifetime values and by a simplex search for the lifetimes for one-, two-, and three-component systems. The resulting estimates of component amplitudes and uncertainties obtained by unweighted and weighted least squares were compared. Initial starting parameters were kept constant in comparing these methods. The predictions of amplitude variances given by eq 13 and 14 were first evaluated by using synthetic data. Comparison of the predicted component amplitude variance, $\sigma_{a_i}^2$, to the observed variance, $s_{a_i}^2$, obtained by fitting N different synthetic data sets, tests the predicting capabilities of this expression. Different fluorescence decay data were generated by varying both lifetime and amplitude parameters and the number of components in each sample. A total of 10 different combinations of fluorescence decay parameters were used to generate 80 sets of data which were analyzed. The criterion used to determine whether the observed variance for synthetic data could be distinguished statistically from the value predicted by eq 12 or 13 is the F test (18). The ratio of observed to predicted variance, F , was compared to the critical level for 95% and 99% confidence.

To assess the capabilities of eq 12 and 13 to predict the uncertainty in amplitude estimates from laboratory data, fluorescence decays of naphthalene dissolved in cyclohexane were also evaluated by using two-component data sets. The fluorescence lifetime and amplitude were first determined for the single-component vectors which make up these two-component systems using the weighted least-squares algorithm. Taking these values to represent the "true" or best estimate of the concentration and lifetime parameters (σ_i, τ_i), we compared the component amplitudes estimated by linear least-squares analysis of the multicomponent data sets using the "true" lifetime values to build $[C]$. Results from 10 single-component decay transients of naphthalene produced nine reconstructed multicomponent data vectors which were analyzed, and the accuracy of the results was compared with the error predictions of eq 13.

RESULTS AND DISCUSSION

Three methods of quantitative analysis of multicomponent fluorescence decay data are evaluated in this study, representing two different approaches to obtaining the fit to a multiexponential model. A direct search approach, in which both the lifetime and amplitude parameters are optimized by using the nonlinear least squares (5, 18) to minimize the squared differences between the experimental data and the model, is compared to a second approach in which a linear least-squares step to determine the amplitudes is carried out within a nonlinear least-squares search for the optimum lifetimes. This second, linear least-squares approach is further expanded into unweighted and weighted least-squares methods, which are also compared.

A comparison of efficiency of the three data analysis methods is summarized in Table I, where the numbers of iterations required to converge on the optimal set of fitted parameters are compared. To illustrate the typical quality

Table I. Number of Iterations Required To Satisfy Convergence Criteria^a

% rel error of initial parameter estimate ^b	direct search algorithm	weighted linear least-squares algorithm	
		unweighted linear least-squares algorithm	weighted linear least-squares algorithm
One-Component System			
0	108	82	98
50	198	68	86
75	188	64	62
Two-Component System			
0	177	110	104
50	<50% convergence ^c	111	122
75	no convergence	144	120
Three-Component System			
0	196	110	120
50	no convergence	160	167

^a Each result is an average of fitting seven decay transients. Convergence was defined as an accepted SIMPLEX move which did not improve χ^2 by more than 1 part in 10^5 . ^b Relative error of the initial parameter estimate is the difference between the initial estimate and known value of fitting parameter divided by the known value. ^c Convergence within 250 SIMPLEX moves occurred less than half the time.

Table II. Relative Error of Amplitude Estimates from Weighted and Unweighted Least Squares^a

sample	τ_1 , ns	τ_2 , ns	τ_3 , ns	av amplitude error, %	
				weighted LS	unweighted LS
one component					
	100			0.35	0.35
	150			0.32	0.46
two component					
	100	125		3.4	2.1
	100	150		1.1	2.0
three component					
	75	150	250	1.6	1.2
	50	150	250	0.7	3.9

^a Average of four trials, 500-point synthetic decay transients where $\Delta t = 1.0$ ns. Lifetimes used in the amplitude determination were the correct values. Component amplitude factors, a_i , ranged from 1.0×10^5 to 3.0×10^5 counts/ns.

ber of components in the sample is greater than two. For one- and two-component samples, substituting a linear least-squares determination of the amplitudes, which reduces the number of parameters to be searched by the SIMPLEX algorithm by a factor 2, increases the efficiency of convergence, on average, by about a factor 2. From the results in Table I, weighting the linear least-squares fit for the Poisson-distributed error in the data does not appear to systematically affect the efficiency of convergence. Interestingly, the quality of fits as judged by the χ^2 values (eq 9) at the optimum as determined by unweighted and weighted linear least-squares searching shows only slight differences. χ^2 was consistently smaller for the weighted least-squares fit by 1.0% to 2.0%.

While the rate of convergence and the apparent quality of fit do not depend strongly on weighting, the accuracy of the amplitudes that are returned by the analysis is sensitive to proper weighting of the observations. This behavior is summarized in Table II, where the accuracies of the component amplitudes that result from unweighted versus weighted least-squares analysis are compared for one-, two-, and three-component synthetic data sets. The relative error in the amplitude estimates is 1.9 times greater on average when A is obtained by unweighted least squares, eq 4, rather than by proper weighting of the photon shot noise using eq 11. The largest improvement provided by properly weighting the data is observed when the fluorescence decay is dominated by amplitude from shorter-lived components. Over the fixed 500-ns observation time, short-lived components result in a greater dynamic range in the observed fluorescence intensity which creates a correspondingly greater range of measurement variance in the data.

An additional advantage of a linear least-squares determination of the component amplitudes is that the uncertainties of the parameters may be predicted from first principles, using eq 12 and 13 presented above. The variances of the amplitudes determined by the diagonal terms of $[V]$ from these equations were compared with the precision of fitting synthetic data sets, representing a wide range of concentration and decay time values. These comparisons are reported in Table III, along with the corresponding values of the F statistic used to determine whether the observed uncertainties systematically exceed the predictions. Interestingly, both the unweighted and weighted least-squares methods of estimating the amplitude precision are equally valid in predicting their corresponding errors, according to these results. Both algorithms produce F values that are outside the expected bounds for 95% confidence (not unlikely for 16 results), while only one set of the results just exceeds 99% confidence bounds. We conclude, therefore, that while unweighted linear least

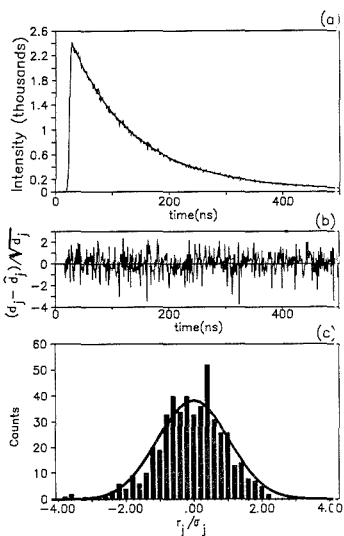


Figure 2. Synthetically generated two-component fluorescence decay curve. Decays were constructed from data 500 points, where $a_1 = 1.0 \times 10^5$ counts, $a_2 = 1.5 \times 10^5$ counts, $\tau_1 = 100$ ns, $\tau_2 = 150$ ns, and $\Delta t = 1.0$ ns. (a) fitted data, (b) weighted residuals, (c) histogram of weighted residuals and corresponding Gaussian distribution, having a zero mean, a unit standard deviation, and an area equal to the total number of counts.

of fit, Figure 2 shows an example two-component synthetic data transient, along with the predicted fit and weighted residuals obtained by the weighted linear least-squares algorithm. While all three methods perform adequately when the initial parameter estimates are close (or equal) to the true values, the direct search algorithm for amplitudes and lifetimes is much more sensitive to errors in the initial estimates. Prior information, therefore, is required for the direct search algorithm to successfully converge, particularly when the num-

Table III. Component Amplitude Variance Predicted (σ^2), Observed (s^2), and Compared by the F Test^a

A(1)/A(2)	$\tau(1), \tau(2)$	$\sigma^2(1)$	$\sigma^2(2)$	$s^2(1)$	$s^2(2)$	F(1)	F(2)
Unweighted Linear Least Squares ^b							
1:1	150, 200	0.9294	0.6865	0.6678	0.4917	0.72	0.72
1:1	90, 150	0.3850	0.2182	0.7946	0.3466	2.06	1.59
1:1	210, 280	0.9942	0.7517	1.3301	0.9679	1.34	1.29
2:3	100, 200	0.3206	0.1087	0.2664	0.0857	0.83	0.79
3:7	100, 200	0.2393	0.1129	0.1746	0.0625	0.73	0.55
3:7	200, 400	0.2501	0.1325	0.0680	0.0413	0.27	0.31
3:7	300, 600	0.3367	0.1993	0.1415	0.0548	0.42	0.27
3:7	150, 300	0.2284	0.1140	0.2008	0.1190	0.88	1.04
Weighted Linear Least Squares ^c							
1:1	150, 200	0.6160	0.3889	0.7188	0.5361	1.17	1.38
1:1	90, 150	0.2539	0.1026	0.6282	0.2497	2.47	2.43
1:1	210, 280	0.7601	0.5166	1.4292	1.0096	1.88	1.95
2:3	100, 200	0.1828	0.0607	0.1695	0.0409	0.93	0.67
3:7	100, 200	0.1945	0.0666	0.0964	0.0325	0.50	0.49
3:7	200, 400	0.2245	0.1010	0.0686	0.0531	0.31	0.53
3:7	300, 600	0.3156	0.1711	0.2586	0.1073	0.82	0.63
3:7	150, 300	0.1967	0.0778	0.1882	0.1119	0.96	1.44

^a A total of 10 decay profiles of 500 points were constructed synthetically for each combination of lifetime and amplitude. Experimental variance was based on the true value of the amplitude (not the average), resulting in 10 degrees of freedom. $F = s^2/\sigma^2$. Appropriate critical values (t_8) for the F test are $F_{0.05} = 1.83$, $F_{0.01} = 2.32$. ^b Component amplitudes found by using eq 4 and variances predicted by eq 12. ^c Component amplitudes found by using eq 11 and variances predicted by eq 13.

squares produced somewhat inferior results with respect to the amplitude accuracy compared to proper weighting of the shot noise (see above), amplitude reproducibility can be predicted reliably by using this simpler algorithm.

The principal advantage of unweighted linear least squares is that the variance-covariance matrix depends only on the lifetimes of the components in $[C]$, scaled by the average variance in the data vector given by the average number counts in each channel for shot-noise-limited data; see eq 12. As a result, this method requires that the $[V]$ be evaluated only once for a given system of component lifetimes, being independent of the relative amplitudes of the components. By contrast, the weighted least-squares strategy uses the measured data vector to define the weighting factors in $[W]$, which are included in the prediction of the amplitude errors in eq 13. Thus, this equation must be fully reevaluated, and not just rescaled, for every new observation of D , even when the lifetimes of the components do not change.

Since the uncertainty in the component amplitudes determined by linear least squares can be predicted accurately from first principles by evaluating $[V]$, this theory can be a powerful tool for modeling errors in the analysis of multiexponential data. For example, one can predict a priori how the error in determining the component amplitudes is affected by similarity of lifetimes of the components. Such a prediction provided by eq 13 is illustrated in Figure 3 for a two-component determination, where the relative standard deviations of the component amplitudes are plotted as a function of the ratio of the decay times for two different component amplitudes. Note that the preexponential factor in eq 1 is (a_i/τ_i) , so that a_i is the total number of counts independent of the lifetime of emission. The results show the effect of the time dependence and relative amplitude of the components on the error in determining the amplitudes. As the lifetimes approach the same value, the rows of $[C]$ become identical, and the uncertainty in extracting the amplitudes from a decay transient increases without bound. As the lifetime ratio increases, the uncertainty of extracting each component decreases since the time behavior of the components becomes more distinguishable.

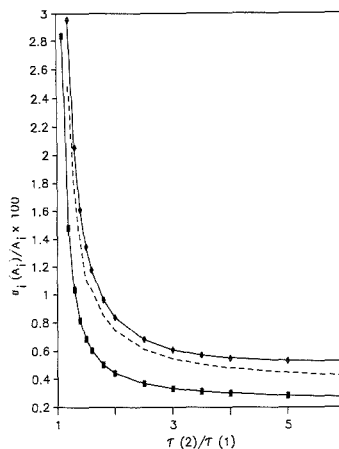


Figure 3. Predicted variance for two-component fluorescence decay curve as a function of lifetime ratios. Synthetic data constructed from a 500-point decay, where $a_1 = 2.0 \times 10^5$ counts, $a_2 = 1.0 \times 10^5$ counts, and $\Delta t = 1.0$ ns.

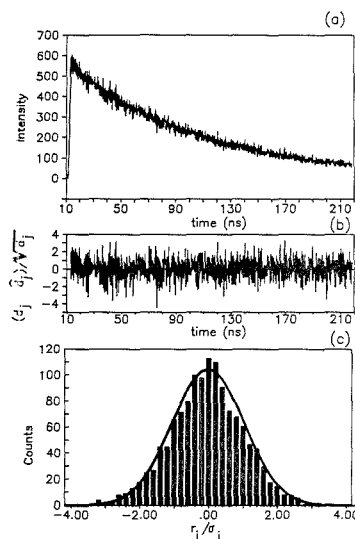


Figure 4. Experimental two-component fluorescence decay data fit to a biexponential model. Data derive from two samples of naphthalene, where $a_1 = 1.39 \times 10^4$ counts, $a_2 = 2.08 \times 10^4$ counts, $\tau_1 = 85.5$ ns, and $\tau_2 = 107.7$ ns: (a) fitted data, (b) weighted residuals, (c) histogram of weighted residuals and corresponding Gaussian distribution, having a zero mean, a unit standard deviation, and an area equal to the total number of counts.

When the amplitudes of the two components are equal, as shown by the dashed line of Figure 3, the errors in estimating the amplitudes are virtually identical. This is a somewhat surprising result, since one might anticipate that the longer-lived component could be determined with better precision since its intensity persists for a longer time when the first component has decayed away. The reason that the two components have equivalent amplitude error, however, is that the uncertainty of the amplitude determination is dominated by covariance. That is, the error one encounters in this analysis is related to partitioning the amplitude of the ob-

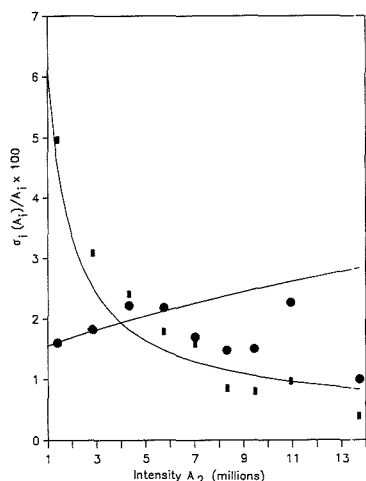


Figure 5. Relative error in component amplitude from weighted least-squares fitting of experimental data. The amplitude of component 1 was held constant, $a_1 = 4.28 \times 10^5$ counts, while the a_2 was varied as shown. The fluorescence lifetimes, τ_1 and τ_2 , were 107.7 and 85.5 ns, respectively. Circles and rectangles are the observed relative errors for single determinations of a_1 and a_2 , respectively, while the solid lines are the predicted relative standard deviations from the variance-covariance matrix, eq 13.

served signal between the two components. Since the actual magnitude of the two amplitudes is the same in this case, the relative errors are equal. When the amplitude of one of the components is larger, as shown in the solid lines in Figure 3, the relative uncertainty of estimating this component decreases due to its proportionally smaller shot noise, while the smaller-amplitude component exhibits larger uncertainty due to the added background noise from the larger component.

The final goal of this study is to test the data analysis methodology on laboratory fluorescence decay data. An example of a two-component transient, its fit to a biexponential model determined by the weighted least-squares algorithm, and the weighted residuals from the fit are shown in Figure 4. The relative errors in the component amplitudes estimated by the weighted least-squares algorithm are compared to the relative standard deviation predicted by eq 13 for 9 data sets, where the long-lived component amplitude was held constant and the short-lived component amplitude was varied. The results are plotted in Figure 5, showing the excellent agreement between the theoretical predictions and the observed errors. An F test indicates that all of the observed results fall well within the 95% confidence limits.

In summary, we have developed an efficient method for resolving multiexponential data in the case where the decay constants are unknown. The method adds a linear least-

squares step to the nonlinear least-squares search for the lifetime parameters. Adding the linear least-squares step to the algorithm was significantly more efficient in determining an optimal set of parameters than searching for both the amplitudes and lifetimes. In cases of three-component data, the linear least-squares algorithm could tolerate over 75% error in the initial parameter estimates while the latter method would not converge on a solution unless the initial estimates were very near the true value. While the overall efficiency of searching depends on the particular nonlinear least-squares algorithm chosen, the gain in efficiency and the insensitivity to initial parameter estimates provided by adding a linear least-squares step to the nonlinear search was found to be quite general. Similar improvements, as observed for the SIMPLEX search above, were observed when this step was added into a Marquardt algorithm (18, 20).

Correct weighting of shot noise in fluorescence decay data was found to have a minimal impact on the rate of convergence but significantly improved the accuracy of the estimated component amplitudes. The linear least-squares formalism also allows one to predict quantitatively the magnitude of the errors to expect in the amplitude estimates. This capability can be powerful for predicting the accuracy of kinetic methods of analysis for multicomponent samples. While the data and error analysis methods were evaluated by using time-resolved fluorescence decay data, the results are equally valid for optimizing the analysis and predicting amplitude errors for any method which produces a first-order kinetic response.

LITERATURE CITED

- Wentzell, P. D.; Crouch, S. R. *Anal. Chem.* **1986**, *58*, 2855.
- Mieling, G. E.; Pardue, H. L. *Anal. Chem.* **1978**, *50*, 1611.
- Willis, B. G.; Woodruff, W. H.; Frysinger, J. R.; Margerum, D. W.; Pardue, H. L. *Anal. Chem.* **1970**, *42*, 1350.
- O'Connor, D. V.; Phillips, D. *Time-correlated Single Photon Counting*; Academic Press, Inc.: Orlando, FL, 1984; Chapter 6.
- Lakowicz, J. R. *Principles of Fluorescence Spectroscopy*; Plenum: New York, 1983; Chapter 3.
- Marquies, S. *Rev. Sci. Instrum.* **1968**, *39*, 478.
- Grinvald, A.; Steinberg, I. Z. *Anal. Biochem.* **1974**, *69*, 583.
- Knight, A. E. W.; Selinger, B. K. *Spectrochim. Acta* **1971**, *27A*, 1223.
- Ware, W. R.; Doemeny, L. J.; Nemzek, T. L. *J. Phys. Chem.* **1973**, *77*, 2038.
- Knorr, F. J.; Harris, J. M. *Anal. Chem.* **1981**, *53*, 272.
- Bracewell, R. N. *The Fourier Transform and Its Applications*, 2nd ed.; McGraw-Hill: New York, 1978; Chapter 3.
- Draper, N. R.; Smith, H. *Applied Regression Analysis*, 2nd ed.; John Wiley & Sons: New York, 1981; Chapter 2.
- Deming, S. N.; Morgan, S. L. *Experimental Design: A Chemometric Approach*; Elsevier: New York, 1987.
- Nelder, J. A.; Mead, R. *Comput. J.* **1965**, *7*, 308.
- Deming, S. N.; Morgan, S. L. *Anal. Chem.* **1973**, *45*, 278A.
- Kalantar, A. H. *J. Phys. Chem.* **1986**, *90*, 6301.
- Schuyler, R.; Isenberg, I. *Rev. Sci. Instrum.* **1971**, *42*, 813.
- Bevington, P. R. *Data Reduction and Error Analysis for the Physical Sciences*; McGraw-Hill: New York, 1961.
- Frans, S. D.; Harris, J. M. *Anal. Chem.* **1985**, *57*, 2680.
- Marquardt, D. W. *J. Soc. Ind. Appl. Math.* **1963**, *11*, 431.

RECEIVED for review March 8, 1989. Accepted July 27, 1989. This work was supported in part by the Office of Naval Research and by a fellowship grant (to J.M.H.) from the Alfred P. Sloan Foundation.

Ion Trap Tandem Mass Spectrometry of Tryptamine. Tissue Extracts and Isotope Dilution Using Combined Radio Frequency and Direct Current Voltages

R. J. Strife* and J. R. Simms

Corporate Research Division, Miami Valley Laboratories, The Procter & Gamble Company, P.O. Box 398707, Cincinnati, Ohio 45239-8707

Novel applications of ion trap tandem mass spectrometry using a combined radio frequency and direct current voltage scan function (RF/DC) are reported. Tryptamine, as the bis(pentafluoropropionamide) derivative, is determined by gas chromatography/tandem mass spectrometry (GC/MS/MS) in the full product ion scan mode at the 50-pg level. RF/DC is shown to be necessary for the determination of this compound in crude biological extracts at the 5 ng/g level. The mass-selective storage effected by RF/DC prior to MS/MS reduces space charge contributed by matrix components. A space charge condition is also found in the isotope dilution analysis of tryptamine at low ratios of unlabeled analyte to internal standard (labeled compound). Too many ions are produced from the internal standard, since a long ionization pulse is required for the small amounts of analyte. The RF/DC method is useful here also. In initial trials, a linear correlation coefficient $r^2 = 0.9986$ was obtained with a relative standard deviation of 10% at the 2 ng (on-column) level and 60% at the 0.1 ng level. The low-level relative standard deviation can be improved by scan averaging.

Ion traps or quadrupole ion storage (Quistor) devices were originally described in the late 1950s. This work, other historical developments, and recent advances leading to commercial production of the ion trap detector (ITD, Finnigan-MAT) and the ion trap mass spectrometer (ITMS, Finnigan-MAT) have been summarized (1-3). A particularly noteworthy characteristic of the ITD is its sensitivity in the full-scan mode, especially when combined with capillary gas chromatography (GC/MS). Very similar spectra have been obtained at the 15-pg and 150-ng level for tricyclodecane (4).

The ITMS is a more versatile version of the ITD. It is capable of multidimensional experiments in time, the simplest of which is the mass spectrometry/mass spectrometry (MS/MS) mode of operation (2). In the MS/MS mode, the ITMS has been reported to effect collisionally activated dissociation (CAD) with 40-100% observed efficiency for precursor ions produced by electron ionization (2, 5). Very high sensitivity should be obtained in the GC/MS/MS mode of operation on the ITMS and early reports have shown this to be true. By use of a scan function based on radio frequency (rf) voltage only (designated RF-only), product ion spectra have been obtained on 15 pg (0.09 pmol) of diethyl ethyl phosphate with >95% apparent CAD efficiency (6).

A drawback of the RF-only mode of MS/MS operation is that all ions above a cut-off mass are stored prior to CAD. It is more desirable to store only the precursor ion of interest (mass-selective storage) because the ion trap has a finite storage capacity. By maximizing the stored population of the desired precursor ion, more signal would be obtained for the product ions formed by CAD. This is especially true for the analysis of a trace component in a crude extract. By definition,

most of the ions created will be due to the matrix and not the analyte.

Previously, we reported the use of combined rf and direct current (c.c) voltages (designated RF/DC) in a scan function effecting mass-selective storage prior to MS/MS (7). The steps of the scan function were also described in terms of the parameters a_z and q_z of the Mathieu equation and a partial stability diagram that shows whether or not ions will have stable trajectories and be stored. A prostaglandin standard was analyzed by GC/MS/MS with a full-scan product ion spectrum obtained on less than 75 pg of the compound (0.14 pmol with 50% apparent CAD efficiency). We have now extended our work with RF/DC to the analysis of crude biological extracts and have developed an approach for GC/stable-isotope-dilution MS/MS. We chose the analysis of tryptamine in brain extracts because methodology for a selected-ion-monitoring assay has been reported (8-10). Since no quantitative work has been performed on ion traps by stable-isotope-dilution MS/MS, the reported assay and brain levels would provide a reference base line. Also, we needed a model to develop simplified GC/MS/MS methods for drug disposition studies on analgesic amines, using ion trap technology.

EXPERIMENTAL SECTION

All chemicals were obtained from standard suppliers and distilled-in-glass grade solvents were used. Deuteriated tryptamine hydrochloride was synthesized according to a procedure for labeled 5-methoxytryptamine (11), with some modifications. The addition of oxalyl chloride was carried out under an argon atmosphere. After the specified reaction period, the vessel was purged with argon for 5 min and the acid chloride (in situ) was quenched with ammonia gas bubbled gently through the reaction medium. Tritiated tryptamine hydrochloride, formally 3-(1,1,2,2-[^3H]-2-aminoethyl)indole was obtained from New England Nuclear, Boston, MA, and standard dilutions were made in pure ethanol. Serial stock dilutions of tryptamine hydrochloride were also made in ethanol.

Derivatization to form the bis(pentafluoropropionamide) (designated tryptamine-PFP₂) was done by a literature method (8). However, after the reaction, the reagents were carefully evaporated at 0 °C under a nitrogen flow of 30 mL/min through a standard manifold (Model 18780, Pierce Chemical, Rockford, IL). Reconstitution was done in small volumes of hexane. Rat brain homogenate extracts were prepared by the method of Beck and Flodberg (9).

The prototype ITMS (Finnigan-MAT, San Jose, CA) has been previously described (2). Software included version 4.1 ITD and version 1.41 of the ITMS scan editor. Gas chromatography was carried out on a Hewlett-Packard Model 5890 (Avondale, PA) interfaced to the ITMS. The capillary GC column was a 15 m × 0.25 mm inner diameter DB-1 or DB-5 (J&W Scientific, Rancho Cordova, CA). The injector and transfer line temperatures were 250 °C. Splitless injection of 1- μL samples was used. The column was programmed from 130 to 250 °C at 10 °C/min.

RESULTS AND DISCUSSION

Methodology. The structure of tryptamine, positions of the radio- or stable-isotope labels (*), and derivatization

* Author to whom correspondence should be addressed.

Scheme I

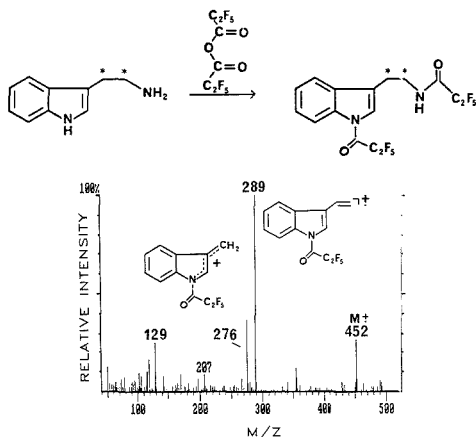


Figure 1. Full-scan mass spectrum obtained for 25 pg of tryptamine-PPF₂ by GC/MS in the rf-only mode, using automatic gain control (AGC). The structures of *m/z* 289 (rearrangement cleavage) and *m/z* 276 (simple cleavage) are derived from classical fragmentation rules.

scheme are summarized in Scheme I. [³H]₄tryptamine hydrochloride gave a single peak by thin-layer chromatographic analysis and radioscanning. This peak coeluted with standard tryptamine hydrochloride. When trial derivatizations to form tryptamine-PPF₂ were carried out, substantial radioactivity was lost during the evaporative step. The modified procedure described above gave better than 95% recovery of the derivative as determined by standard scintillation counting methods. The retention index of the derivative was about 1600 on the DB-1 column. The *k'* value was 9.3 and the peak width at half-height was 4 s during a typical analysis. The mass spectrum of the derivative, obtained on a "standard" quadrupole (rectangularly symmetric field) mass spectrometer (70 eV), was consistent with the derivative structure and previous reports (8, 9).

GC/MS and GC/MS/MS. A 25- μ g sample of tryptamine was derivatized and serially diluted to form standards of various concentrations. The full-scan mass spectrum obtained for just 25 pg of tryptamine-PPF₂ (RF-only, using automatic gain control or AGC software) by GC/MS is shown in Figure 1. The molecular ion is apparent at *m/z* 452 with two intense ions at *m/z* 276 and 289. These represent simple cleavage and rearrangement cleavage, respectively, to form a carbonium ion or a radical cation. The ion structures in Figure 1 are based on classical rules of fragmentation. Even at this low level of 25 pg, the spectral peak intensities agreed within 10% relative abundance when compared with spectra obtained at the 250-pg level. At this higher level, correct intensities were observed for the natural-abundance isotope peaks.

The spectrum in Figure 1 resembled spectra obtained at 20-eV ionization energy (8, 9) more than our spectrum obtained at 70 eV on a "standard" quadrupole. For instance, *m/z* 289 was the base peak on the ITMS (vs 58% relative abundance at 70 eV) with a large decrease in low-mass fragments like *m/z* 119 (18% vs 50% relative abundance). This suggests that the internal energy of the molecular ions is lower on the ITMS, especially since the residence times are longer in the trap than in a standard electron ionization source.

The chromatogram for *m/z* 289 (reconstructed) is shown in Figure 2. The signal/noise ratio is about 25:1. The signal intensity is a function of the number of ions produced. This is determined by the ionization time and the filament current.

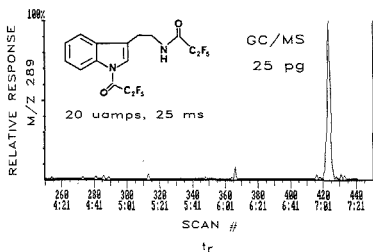


Figure 2. Structure and GC/MS analysis of tryptamine-PPF₂ derivative. The chromatographic trace is of the reconstructed profile for *m/z* 289, with 25 ms of 20 μ A ionization. Retention time, *t_r*, is given as minutes:seconds.

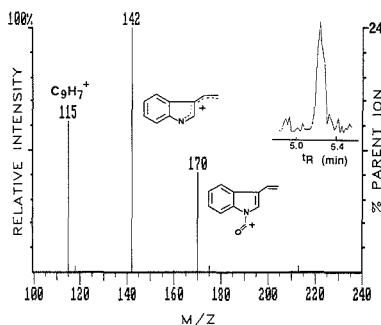


Figure 3. Daughter ion spectrum for *m/z* 289, obtained on 50 pg of tryptamine-PPF₂ by GC/MS/MS. The scan function was of the RF/DC type previously described by Strife et al. (7). The total product ion current as a function of time is shown inset.

The parameters noted in Figure 2 (25 ms at 20 μ A) can each be increased by at least a factor of 4. We are investigating the effect of these changes on ultimate sensitivity. It should be noted that in the RF-only mode for purified samples or standards, a scan function to mimic "selected-ion-monitoring" would not be expected to be advantageous. All ions are stored and the scanning is rapid (18 ms for 100 u).

The ion of *m/z* 289 was chosen as the parent ion for an MS/MS assay because of its intensity, structural specificity for tryptamine, and *m/z* value (12). An RF/DC scan function was created for selected ion storage of *m/z* 289, as previously described for other compounds (7). Dissociation to product ions was accomplished with a supplementary ac voltage having an amplitude of 250 mV, for 10 ms, with the *q_z* value of *m/z* 289 adjusted to 0.25. The product ion spectrum obtained by a full-scan GC/MS/MS analysis (*m/z* 80–250) of 50 pg of the derivative is shown in Figure 3. The structures of the product ions are based on MS/MS studies of the deuterated material, reported within. The apparent CAD efficiency was 50% with *m/z* 142 carrying 24% of the intensity of the precursor ion before it was dissociated. The chromatographic trace of total product ion current as a function of time (inset) showed a signal to noise ratio (*S/N*) of 5.

A significant advantage of the trap is that full-scan information is obtained in the GC/MS/MS mode without sacrificing sensitivity. Since the scanning of the formed product ions is rapid (18 ms per 100 u), there is no obvious advantage to developing a selected-reaction-monitoring scan function. Chromatograms for selected reactions are simply reconstructed post-run by the data system. In this case, since CAD was carried out at a *q_z* value of 0.25 for *m/z* 289, product ions with *m/z* values down to approximately 80 are stored.

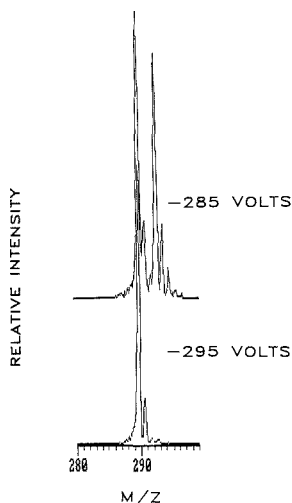


Figure 6. Real-time profiles for probe analysis of a mixture of tryptamine-PPF₂ and deuterated tryptamine-PPF₂. After an RF/DC sequence the contents of the trap were scanned (no MS/MS). Selective-mass range storage (upper) or selective mass storage (lower) are demonstrated as a function of dc pulse magnitude.

a slight increase of the magnitude of the dc pulse, selective mass storage was effected (Figure 6, lower trace).

Since the amount of deuterated tryptamine (IS) was constant in each analysis, about 10 ng on column, a constant ionization time was selected for it (1 ms). The time was optimized by trial and error to avoid space charging when only m/z 292 was stored. The ionization time for the unlabeled material was then scaled inversely, to a maximum time of 25 ms. For instance, 1 ng of tryptamine would be ionized for 10 ms. Thus, for several of the points of the isotope dilution curve, approximately the same number of ions are analyzed for the labeled and unlabeled substances.

A scan function to carry out alternating RF/DC MS/MS analyses during chromatography was created (Figure 7). After the first ionization pulse, m/z 289 is isolated by the RF/DC sequence, while m/z 292 and all other ions are rejected. MS/MS is carried out and the daughter ions of m/z 289 are observed. This process is then repeated with a second ionization pulse and slightly different rf and dc voltage values so that m/z 292 is isolated instead of m/z 289. The entire scan can be carried out in 125 ms, well within the chromatographic time frame.

In terms of practical operation of the ITMS, the entire scan function (Figure 7) is defined in a series of tables, one for each step of the experiment. A Forth program was created by using the screen editor of the version 1.41 software. The program calls the tables for m/z 289 analysis and parameters stored in the tables are loaded into the firmware controlling the trap. The scan function is run, and the data are collected in a particular file (steps noted as 1-4, Figure 7). Next, the tables for m/z 292 analysis, containing slightly different RF/DC parameters, are loaded. Similar steps follow, the data are collected in a different file, and the scan counter is decremented by one. Thus, at the end of a run, two data files exist with similar scan numbers and time scales. One file contains the full product ion spectra of m/z 289 as a function of time and the other contains the information for m/z 292. Specific reactions are reconstructed by using the data system. In initial

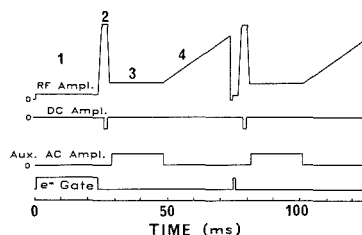


Figure 7. Scan function for isotope dilution given as relative voltage amplitude (ampl.) vs time. The sequence represents (1) ionization time for unlabeled material, (2) RF/DC sequence causing ejection of all masses except m/z 289, (3) resonant excitation by auxiliary (aux.) ac voltage to cause MS/MS, and (4) scanning of the resulting product ions. The detector is on only during period 4. The sequence repeats with slightly different parameters to analyze m/z 292 by MS/MS.

trials, a linear isotope dilution line was obtained by working with about 10 ng of internal standard (ionization time 1 ms) and 0.1 to 2 ng of unlabeled material. The isotope dilution line showed $r^2 = 0.9986$ for triplicate injections. Evaluation of the relative standard deviation at the 2 ng point gave a value of 10%. At the lowest level, much scatter was evident (relative standard deviation about 60%, $n = 6$). This variation is attributed in part to the slow speed of down-loading the information in the tables in an alternating fashion. Since the scan function has a maximum time of 125 ms, at least seven scans should be acquired per second. In practice, only two scans are actually acquired. Averaging of individual scans is done at the expense of chromatographic peak shape definition.

Other Internal Standards. Alternating scan functions are not necessary when structurally different internal standards are used, since such standards separate in the chromatographic time frame. A more detailed study of quantitative methodology on the ITMS in our lab (data not shown here) at similar levels of analyte gave relative standard deviation values of 2-5%, even at the 100-pg level. Similar linear correlations were obtained. Fifteen scans per second were averaged for the two analytes chosen in this case. We suggest that the more effective averaging and better definition of the chromatographic profile contribute to the lower relative standard deviation values. A small change in the firmware or programs to allow faster access to alternate scans would likely improve the isotope dilution result.

LITERATURE CITED

- Stafford, G. C., Jr.; Kelly, P. E.; Syka, J. E. P.; Reynolds, W. E.; Todd, J. F. *J. Int. J. Mass Spectrom. Ion Processes* **1984**, *60*, 85-98.
- Louris, J. N.; Cooks, R. G.; Syka, J. E. P.; Kelly, P. E.; Stafford, G. C. *Anal. Chem.* **1987**, *59*, 1677-1685.
- Brodbeck, J. S.; Louris, J. N.; Cooks, R. G. *Anal. Chem.* **1984**, *59*, 1278-1285.
- Yost, R. A.; McClennen, W.; Snyder, A. P. Presented at the 35th ASMS Conference on Mass Spectrometry and Allied Topics, Denver, CO, May 24-29, 1987.
- Strife, R. J.; Weber-Grabau, M.; Kelley, P. E. Presented at the 35th ASMS Conference on Mass Spectrometry and Allied Topics, Denver, CO, May 24-29, 1987.
- Johnson, J. V.; Yost, R. A. Presented at the 35th ASMS Conference on Mass Spectrometry and Allied Topics, Denver, CO, May 24-29, 1987.
- Strife, R. J.; Kelley, P. E.; Weber-Grabau, M. *Rapid Commun. Mass Spectrom.* **1988**, *2*, 105-109.
- Artigas, F.; Sunoi, C.; Tusell, J. M.; Martinez, E.; Gelpi, E. *Biomed. Mass Spectrom.* **1984**, *11*, 142-144.
- Beck, O.; Flobberg, G. *Biomed. Mass Spectrom.* **1984**, *11*, 155-158.
- Peura, P.; Faull, K. F.; Barchas, J. D. *J. Pharm. Biomed. Anal.* **1987**, *6*, 821-825.
- Shaw, G. J.; Wright, G. J.; Milne, G. W. A. *Biomed. Mass Spectrom.* **1977**, *4*, 348-353.
- Strife, R. J.; Simms, J. R. *Anal. Chem.* **1988**, *60*, 1800-1807.
- Corval, M. *Org. Mass Spectrom.* **1981**, *16*, 441-447.

RECEIVED for review March 14, 1989. Accepted June 14, 1989.

Ionspray Mass Spectrometry/Mass Spectrometry: Quantitation of Tributyltin in a Sediment Reference Material for Trace Metals¹

K. W. M. Siu,* G. J. Gardner, and S. S. Berman

Division of Chemistry, National Research Council of Canada, Montreal Road, Ottawa, Ontario, Canada K1A 0R9

Tributyltin (TBT) concentration in a sediment reference material for trace metals, PACS-1, was determined by using ionspray mass spectrometry/mass spectrometry. TBT was extracted into isooctane or 1-butanol, diluted with methanol containing 1 mM ammonium acetate, delivered to the ionspray tandem mass spectrometer by using flow injection, and quantitated by means of selected reaction monitoring of the daughter/parent pair of m/z 179/291. The minimum detectable amount of TBT was about 5 pg of Sn absolute or 0.2 μg of Sn/g of sediment. PACS-1 was found to contain tributyltin at a concentration of $1.29 \pm 0.07 \mu\text{g}$ of Sn/g of sediment.

INTRODUCTION

Organotin compounds have wide ranging chemical and toxicological properties. They find application in usages as diverse as poly(vinyl chloride) stabilizers, fungicides, pesticides, and marine antifoulants, to name just a few. The most important organotin in the marine environment is tributyltin (TBT), the active ingredient in antifouling paint. TBT is toxic to shellfish at ng of Sn/mL levels. As a result, the use of TBT as an antifoulant is now banned in many countries. Model studies have shown that TBT has a high tendency to adsorb on particulates and thus be available to benthic organisms (1, 2).

The two most common techniques for TBT determination are gas chromatography with flame photometric detection (GC-FPD) (3) and hydride generation-atomic absorption spectrometry (HG-AAS) (4, 5). Both methods require fairly extensive sample work up including extraction, cleanup, and derivatization. We have recently shown that ionspray mass spectrometry/mass spectrometry (ISMS/MS) to be an extremely sensitive technique for TBT determination, having a minimum detectable amount in the low picogram range (6).

Ionspray (IS) and its related technique, electrospray, are fairly new ion desorption techniques for atmospheric pressure ionization mass spectrometry (APIMS). As well, they are excellent methods for interfacing liquid chromatography (LC) or capillary zone electrophoresis to APIMS (7-9). In IS, the analyte solution—whether it is a flow injection analysis (FIA) carrier solution, a liquid chromatographic eluant, or an electrophoretic effluent—is allowed to flow through, at a rate of 1-500 $\mu\text{L}/\text{min}$, a very narrow-bore capillary tubing (50-200 μm) polarized to a high voltage (2-3 kV). A coaxial flow of nitrogen is installed to facilitate spraying, thus effecting a lower optimum polarizing voltage or a higher maximum operable flow rate than electrospray. Droplets emerging from the capillary tubing are electrically charged. These are pneumatically sheared off and/or electrically repelled into the surrounding gas once surface tension is overcome. As a droplet evaporates during its flight to the sampling plate (counter-

electrode), coulombic repulsion increases due to a decrease in its surface area. Ion evaporation takes place when coulombic repulsion overcomes ion solvation forces and results in ions being ejected into the surrounding gas. The most significant difference between ionspray and other introduction/ionization techniques for mass spectrometry is that, in IS, no ionization process exists; the analyte must be present as ions in solution otherwise it will not be seen. This means that the analyte must have an ionizable functional group or be able to form an ionic adduct in solution.

Polar organotin compounds, e.g. butyltin halides, acetates, etc., form pentacoordinated anionic adducts readily in solution (6, 10). These have been detailed in a recent study (6). In addition, cationic species may also be formed due to heterolytic cleavage of the tin-(pseudo)halide bond (6). When monitored by IS, tributyltin chloride shows an intense TBT^+ ion at m/z 291. This report describes application of IS to the quantitation of tributyltin in a sediment reference material for trace metals, PACS-1.

EXPERIMENTAL SECTION

Instrumentation. The ionspray tandem mass spectrometer has been described in detail elsewhere (11). Briefly, the LC/FIA side consisted of a reciprocating pump (Waters Model 590) capable of delivering from 1 $\mu\text{L}/\text{min}$ to 10 mL/min of mobile phase, and a valve injector (Rheodyne Model 7125 or 7520 for injection of 100 or 0.5 μL of samples, respectively). The injector was connected to the ionspray interface via a 1 m \times 50 μm i.d. fused-silica tubing. The carrier solution was methanol containing 1 mM ammonium acetate at a flow rate of 5 $\mu\text{L}/\text{min}$.

The ionspray probe was built in-house and consisted of two coaxial stainless steel capillary tubes, 33 and 22 gauge (ca. 100 and 400 μm i.d., respectively), polarized to 2.5 kV. Liquid chromatographic effluent/FIA carrier solution was routed to flow in the inner 33 gauge tubing. Nitrogen (40 psi, pressure controlled) flowed in the channel between the inner and the outer, 22 gauge tubing, acting as a nebulizer gas. With this setup, a stable ionspray was obtained by using a liquid flow rate as low as 1 $\mu\text{L}/\text{min}$ to as high as about 500 $\mu\text{L}/\text{min}$.

The MS used was an API mass spectrometer (SCIEX TAGA 6000 prototype). For ionspray, the corona discharge assembly and housing were detached. The ionspray probe tip was positioned about 1-2 cm from the interface plate (the ionspray counter-electrode) and about 1 cm off-axis from the sampling aperture. The interface plate was usually at ± 450 V. Other MS operating conditions were identical with those used for corona discharge ionization. For tandem MS runs, argon was used as the collision gas at a target gas thickness of about 1.3×10^{14} atoms cm^{-2} , which allowed on the average less than one collision event per ion. The laboratory-frame collision energy was 61 eV.

Reagents. Tributyltin chloride was purchased from a commercial source (Aldrich). Its purity was confirmed by high-performance liquid chromatography-inductively coupled plasma mass spectrometry (HPLC-ICP/MS). Solutions were made up usually in methanol and refrigerated when not in use. Solvents were "Distilled-in-glass" grade (Caledon). Acids were sub-boiled distilled from reagent grade stocks. All other chemicals were reagent grade or better.

The sediment reference material for trace metals was PACS-1 (National Research Council of Canada), which was collected from

¹NRCC 30533.

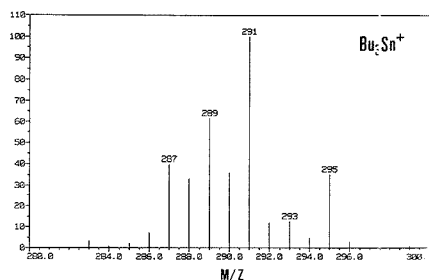


Figure 1. Ionspray mass spectrum of tributyltin chloride showing the isotopic distribution of TBT^+ . Bu = butyl.

the Esquimalt Harbour in British Columbia.

TBT Extraction. Four grams of PACS-1 plus the appropriate TBT spike was placed in a 50-mL borosilicate glass centrifuge tube, followed by 4 mL of 10 M hydrochloric acid and 8 mL of methanol. The centrifuge tube was placed in an ultrasonic bath and sonicated for 1 h. Four milliliters of isoctane was then added. The centrifuge tube contents were shaken vigorously for 3 min and then centrifuged at about 2000 rpm for 10 min. The isoctane phase was removed; 0.5 mL of it was diluted to 25 mL with methanol containing 1 mM ammonium acetate (the FIA carrier solution).

Alternatively, 4 g of PACS-1 was placed in a 50-mL centrifuge tube, together with 8 mL of 1-butanol. The suspension was sonicated for 1 h and centrifuged as previously described. The 1-butanol phase was removed, and 1 mL of it was subsequently diluted to 25 mL with methanol containing 1 mM ammonium acetate.

ISMS/MS Analysis. The usual sample size was 0.5 μ L. For quantitative analysis, the mass spectrometer was operated under selected reaction monitoring (SRM) of the parent/daughter pair, m/z 291/179. No liquid chromatographic separation was necessary due to the high selectivity in this mode.

RESULTS AND DISCUSSION

As noted earlier (6), TBT compounds respond under both the positive and negative ion detection modes in ionspray mass spectrometry. In the negative ion detection mode, TBT forms adduct anions, whose nature is dependent on matrix composition. This is deemed inconvenient as any analytical methodology based on these adducts would be too matrix dependent. On the contrary, in the positive ion detection mode, polar TBT compounds yield only one tin-containing ion, the TBT^+ ion. This is desirable for analytical purposes since the same tin ion is always formed irrespective of counterions, solvents, and matrix composition. No DBT^{2+} (dibutyltin) and MBT^{3+} (monobutyltin) have been seen. These ions are likely to have too high charge-to-size ratios (their solvation energies are likely too high) to evaporate effectively (11). When chloride ions are present, the singly charged adduct ion ($DBT-C$) $^+$ is observed albeit with sensitivity too low for pursuing.

An ionspray mass spectrum of tributyltin chloride is shown in Figure 1, showing the isotopic distribution of the TBT^+ ion. A daughter ion spectrum of m/z 291, the most abundant TBT isotope, is shown in Figure 2. The daughter ions, m/z 235, 179, and 123, are apparently formed via loss of one, two, and three butene molecules from the parent ion. Figure 3 shows selected reaction monitoring of the daughter/parent pair of m/z 179/291. The samples were tributyltin chloride standard solutions containing 30, 15, and 50 pg of Sn. Figure 4 shows the same selected reaction monitoring of PACS-1 extracts. By use of the method of standard additions, the TBT concentration in PACS-1 was determined to be 1.29 ± 0.07 μ g of Sn/g ($n = 5$). Results obtained by using the two different extraction procedures were indistinguishable.

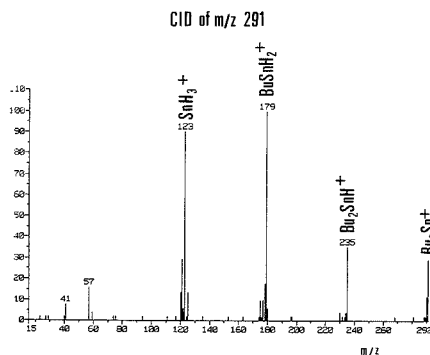


Figure 2. Collision-induced dissociation (CID) of m/z 291 from TBT^+ . Bu = butyl.

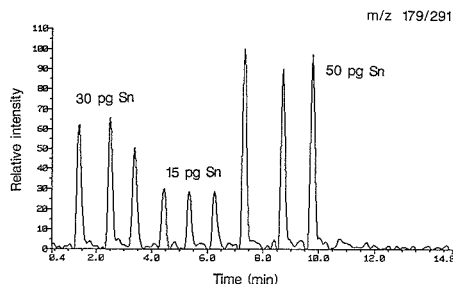


Figure 3. Flow injection analysis of TBT standard solutions: triplicate injections of 30, 15, and 50 pg of Sn. SRM of daughter/parent pair, m/z 179/291.

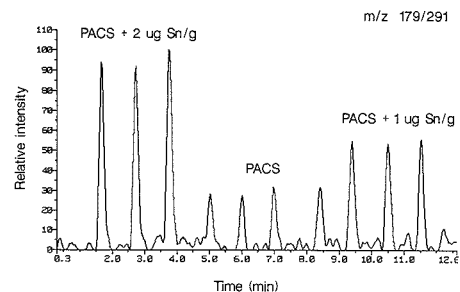


Figure 4. Flow injection analysis of PACS-1 extracts: determination by using standard additions method.

For quantitating TBT in real life samples, e.g. sediment extracts, the use of selected reaction monitoring rather than the less selective single ion monitoring is imperative, particularly when no prior separation is performed. For a sample as complex as a sediment extract, its ionspray mass spectrum is littered with peaks from low to high mass, including m/z 291, whether it contains TBT or not. In the SRM measurement, the non-TBT contribution in the m/z 291 signal was filtered out (any parent ion of m/z 291 that did not yield a daughter ion of m/z 179 was not counted), and the tandem mass spectrometer operated as a TBT specific detector. No interference from DBT and MBT was expected or observed. This tremendously simplified the sample work up since detection as specific as this required minimal processing. As it turned out, no liquid chromatographic separation, off line

Table I. TBT Determination in PACS-1^a
(μg of Sn/g of sediment)

ISMS/MS	GC-FPD	HPLC-ICP/MS
1.29 ± 0.07^b (5) ^c	1.13 ± 0.30 (15)	1.18 ± 0.15 (7)

^a Certified value: $1.27 \pm 0.22 \mu\text{g}$ of Sn/g (95% confidence interval). ^b Standard deviation. ^c Number in parentheses is the number of replicate analyses.

or on line, was needed after sediment extraction. That was convenient as some reversed-phase LC materials had been observed to cause degradation of TBT (12), bypassing LC avoided this potential problem.

The isooctane extraction isolated TBT as the chloride by virtue of the presence of a high concentration of hydrochloric acid. The TBT form extracted into 1-butanol is unknown. This mattered little as TBT compounds are polar and expected to dissociate into TBT^+ and a counterion in a polar solvent such as methanol containing 1 mM ammonium acetate. The dilution of the PACS-1 extract (in isooctane and 1-butanol) with the flow injection carrier solution served several purposes: (1) dilution placed TBT in a suitable matrix that promoted TBT ionization, (2) it provided a suitable medium where stable ionspray could take place, and (3) TBT concentration in PACS-1 is high, dilution lowered the concentration to a level convenient for analysis. Compared to that of standard solutions of TBT, the response of TBT spikes to PACS-1 was suppressed by a factor of about 2. This was attributed to matrix effects as signals of PACS-1 samples spiked with equal amounts of TBT before and after the extraction were indistinguishable, showing that the discrepancy was not due to nonquantitative TBT recovery. The recoveries for the isooctane and 1-butanol extractions were determined as $95 \pm 4\%$ and $97 \pm 6\%$, respectively. The rationale for using two rather different solvents was that they might extract different portions of the sediment matrix, and therefore one might exhibit less matrix suppression on the TBT signal than the other one. As it happened, the suppressions for both extractants were comparable. The nature of this interference is unknown; adduct formation, ion pairing, different solvation, etc., could all affect the concentration of TBT^+ in the gas phase, and hence its ionspray signal.

The TBT determination using ionspray tandem mass spectrometry was rapid. The most time-consuming portion was sample extraction/work up, which took about 1.5 h. The analysis itself was extremely fast; 10 injections could be made in a time as short as 12 min (Figure 4). The accuracy of this

method is demonstrated by comparing the TBT concentration in PACS-1 as determined by this method and by two other techniques, GC-FPD (13) and HPLC-ICP/MS (14) (Table I). Agreement among the three methods as well as with the certified value is good. The minimum detectable amount of TBT in sediment, as defined as the signal equivalent to two times the standard deviation of the blank, was about $0.2 \mu\text{g}$ of Sn/g of sediment, using the present sample work up. The relatively high relative detection limit was due to the 25-fold dilution made on the sediment extracts; most of the blank signal originated not from TBT but from electronic noise. The absolute detection limit was about 5 pg of Sn when matrix interference was absent, which is superior to that of Hg-AAS (20–50 pg of Sn (5)) and GC-FPD (30 pg of Sn (13, 15)). The ionspray relative detection limit is comparably inferior (0.6 pg of Sn/g for HG-AAS (4) and 30 ng of Sn/g for GC-FPD (13, 16), a consequence of dilution and small (0.5 μL) sample size.

ACKNOWLEDGMENT

We thank P. S. Maxwell and J. W. McLaren of this laboratory for GC-FPD and HPLC-ICP/MS analyses of PACS-1.

Registry No. Tributyltin chloride, 1461-22-9.

LITERATURE CITED

- Donald, O. F. X.; Weber, J. H. *Environ. Sci. Technol.* **1985**, *19*, 1104–1110.
- Rancall, L.; Weber, J. H. *Sci. Total Environ.* **1986**, *57*, 191–203.
- Maguire, R. J. *Environ. Sci. Technol.* **1984**, *18*, 291–294.
- Rancall, L.; Han, J. S.; Weber, J. H. *Environ. Technol. Lett.* **1986**, *7*, 571–576.
- Donald, O. F. X.; Rapsomanikis, S.; Weber, J. H. *Anal. Chem.* **1986**, *58*, 772–777.
- Siu, K. W. M.; Gardner, G. J.; Berman, S. S. *Rapid Commun. Mass Spectrom.* **1988**, *2*, 201–204.
- Whitehouse, C. M.; Dreyer, R. N.; Yamashita, M.; Fenn, J. B. *Anal. Chem.* **1985**, *57*, 675–679.
- Bruirs, A. P.; Covey, T. R.; Henion, J. D. *Anal. Chem.* **1987**, *59*, 2642–2646.
- Smith, R. D.; Olivares, J. A.; Nguyen, N. T.; Udseth, H. R. *Anal. Chem.* **1988**, *60*, 436–441.
- Neumann, W. P. *The Organic Chemistry of Tin*; John Wiley & Sons: New York, 1970; p 14.
- Siu, K. W. M.; Gardner, G. J.; Berman, S. S. *Org. Mass. Spectrom.*, in press.
- Siu, K. W. M.; McLaren, J. W.; Maxwell, P. S.; Gardner, G. J.; Berman, S. S. *Analytical Chemistry of Butyltins*; Oceans 88, Baltimore, MD, Nov 1988.
- Siu, K. W. M.; Maxwell, P. S.; Berman, S. S. *J. Chromatogr.* **1989**, *475*, 373–379.
- McLaren, J. W.; Siu, K. W. M.; Lam, J. W.; Maxwell, P. S.; Palepu, A.; Berman, S. S., submitted for publication in *Anal. Chem.*
- Aue, W. A.; Hastings, C. R. *J. Chromatogr.* **1973**, *87*, 232–235.
- Hattori, Y.; Kobayashi, A.; Takemoto, S.; Takami, K.; Kuge, Y.; Sugimae, A.; Nakamoto, M. *J. Chromatogr.* **1984**, *315*, 341–349.

RECEIVED for review April 3, 1989. Accepted July 19, 1989.

CORRESPONDENCE

Selectivity of Stearate-Modified Carbon Paste Electrodes for Dopamine and Ascorbic Acid

Sir: A number of distinct voltammetric methods have been developed recently to detect the overflow of monoamines in brain extracellular fluid (1-5). For techniques that are designed to measure dopamine, a major limitation has been the inability to distinguish between currents arising from the oxidation of catecholamine and those due to the oxidation of ascorbic acid (6-9). A stearic acid modification of graphite paste electrodes has been reported to overcome this restriction (10, 11), and they have frequently been used with linear sweep voltammetry and chronoamperometry in attempts to monitor base line and drug-induced changes in dopamine levels in vivo (10, 12-15). However, there are some anomalies in the reported findings (2, 9), in particular the estimation of the basal concentration of extracellular dopamine at approximately 2 orders of magnitude greater than the value of approximately 50 nmol/L measured with other electrochemical methods (16, 17) and microdialysis probes (18). We now investigate this problem, and find that the response of stearate-modified electrodes is altered by brain tissue to such an extent that they no longer discriminate between the oxidation currents of dopamine and ascorbate and consequently, in their present form, cannot be used to measure levels of dopamine unambiguously in vivo.

EXPERIMENTAL SECTION

The stearate-modified electrodes were prepared as described by Blaha and Lane (10) from 1.5 g of UCP 1-M graphite powder (Ultra Carbon Corp.) and 100 mg of stearic acid (Sigma Chemical Co.) dissolved in 1 mL of Nujol oil (Aldrich Chemical Co.), packed into a Teflon-coated silver wire. The working diameter of the disk electrode was 250 μm . The unmodified carbon paste electrodes were prepared in the same way, but without stearic acid. Cyclic voltammetric experiments were performed at 25 $^{\circ}\text{C}$, using a microcomputer based three-electrode system similar to that described previously (19), at 50 mV/s between 0 and 1000 mV vs Ag/Ag⁺ reference electrode (-15 mV vs SCE).

For clarity, however, and because the systems used were essentially chemically irreversible under these conditions, only the oxidation phase of the waves is shown. The background current, measured in the absence of substrate, was subtracted from each voltammogram before analysis. The substrates, dopamine (Sigma) and ascorbic acid (BDH), were used as supplied. The experiments were carried out in phosphate buffered saline (PBS), pH 7.4; NaCl (0.15 mol/L), NaH₂PO₄ (0.04 mol/L), and NaOH (0.04 mol/L). The effect of brain tissue on the response of stearate-modified electrode to oxidation of dopamine and ascorbate was determined in separate experiments by measuring their response in vitro before and after a 24-h contact period with brain tissue.

RESULTS AND DISCUSSION

The oxidation waves for dopamine and ascorbate at unmodified carbon paste electrodes are shown in Figure 1. As can be seen, there is no well-defined peak for either substrate and so that potential of maximum slope (20), $V_{S_{\text{max}}}$, is used to compare the position of the two waves on the voltage axis and as an index of changes in electron transfer kinetics for ascorbate and dopamine. The foot potential (the potential at which the current first reached 1 nA above the base line), V_f , is also used to compare the positions of the two waves on the potential axis.

Table I. Means \pm Standard Error of Mean ($n = 3$)^a

	dopamine	ascorbic acid
	$V_{S_{\text{max}}}$, mV	
CPE	140 \pm 3	565 \pm 45
SME	272 \pm 15	880 \pm 55
TMSME	77 \pm 9	275 \pm 10
	V_f , mV	
CPE	68 \pm 12	300 \pm 28
SME	140 \pm 10	487 \pm 22
TMSME	40 \pm 5	27 \pm 27

^a $V_{S_{\text{max}}}$ for each substrate was significantly different for every combination of electrode pairs (unpaired two-tailed *t* test); $P < 0.01$. CPE, unmodified carbon paste electrode; SME, stearate-modified carbon paste electrode; TMSME, stearate-modified electrode after 24-h tissue treatment. $V_{S_{\text{max}}}$, potential maximum slope for the waves; V_f , potential at which the oxidation wave has reached a current of 1 nA.

The introduction of stearic acid into carbon paste electrodes reduced the rate of charge transfer for both dopamine and ascorbate (Figure 1 and Table I), but, as expected (10, 11), the effect on the ascorbate anion was greater than that for the cationic dopamine species. Thus the modification increases the separation of the waves ($V_{S_{\text{max}}}$) for dopamine and ascorbate from 425 \pm 45 to 608 \pm 57 mV. However, after a 24-h period of contact with brain tissue, this separating power of stearate-modified electrodes in vitro was not only reversed but reduced to a value of 188 \pm 14 mV, which is less than that of unmodified carbon paste electrodes.

Furthermore, the positions of the foot potential for the two waves virtually coincide after the electrode had been modified by contact with the tissue, indicating that at any potential along the range 0-800 mV the electrode can no longer detect dopamine without interference from ascorbate (Figure 1 and Table I). The limit of detection for dopamine at the stearate-modified electrode before and after tissue treatment is of the order of 5 and 10 $\mu\text{mol/L}$, respectively. These values indicate that the electrode would not be able to detect dopamine in the concentration range observed in vivo with other techniques (16-18).

A further problem for the measurement of dopamine is posed by possible amplification of the signal in the presence of ascorbic acid due to electrocatalysis. This problem does not arise when ascorbate oxidizes at a less anodic potential than dopamine. However, shifting the ascorbate oxidation to higher anodic potentials, as was done with the stearate-modified electrode, enables the electrocatalytic process to take place (11). In the presence of ascorbate the oxidized form of dopamine, dopamine-*o*-quinone, oxidizes ascorbate present in the vicinity of the electrode, with the dopamine-*o*-quinone being reduced back to dopamine which can then be reoxidized at the electrode (21-23). We did not address this problem for the stearate-modified electrode in the present study, since after treatment with brain tissue electrochemical discrimination of the substrates is lost; this renders studies on electrocatalytic interference of the dopamine signal superfluous.

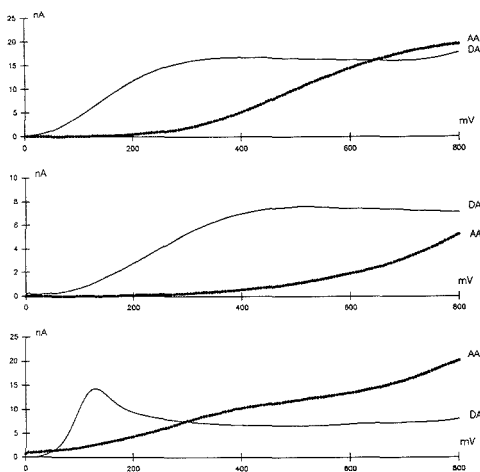


Figure 1. Sections of the voltammograms (see text) for dopamine (DA) and ascorbate (AA) in PBS, pH 7.4: (top) DA, 100 $\mu\text{mol/L}$; AA, 200 $\mu\text{mol/L}$; at an unmodified carbon paste electrode; (middle) DA, 20 $\mu\text{mol/L}$; AA, 200 $\mu\text{mol/L}$; at a stearate-modified carbon paste electrode; (bottom) DA, 100 $\mu\text{mol/L}$; AA, 500 $\mu\text{mol/L}$; at a tissue-treated stearate-modified carbon paste electrode.

The effect of brain tissue on the stearate-modified electrode is consistent with recent studies of similar action by brain tissue on unmodified carbon paste electrodes (24) and with reports for surfactant action on carbon paste electrodes (25). It has been proposed that in such cases the surfactant solubilizes the oil and other hydrophobic elements of the paste, leaving behind a "clean" graphite surface. We propose that a similar mechanism occurs *in vivo*. The stearate-modified electrode implanted in brain tissue is introduced to the hydrophobic environment of lipids and proteins. These take the role played by the surfactants mentioned above and remove the oil and other hydrophobic/lipophilic moieties of the electrode surface, the result being a modification of the electrode surface and an increase in the rate of electron transfer as shown (Figure 1 and Table I). A reduction in sensitivity is found at the tissue-treated electrodes compared to the electrodes before treatment, and is most likely a result of partial blockage of the electrode surface due to the adsorption of lipids and proteins (26).

A linear sweep voltammetric wave, attributed to dopamine oxidation at the stearate-modified electrode *in vivo*, has been reported by Lane et al. (14). The wave, centered at +100 mV vs Ag/AgCl, has a peak height of the order of 1 nA. This peak occurs at a potential (vs SCE) corresponding to large ascorbate oxidation at the tissue-treated electrode. A current of 1 nA for dopamine *in vitro* would correspond to a concentration of approximately 5 $\mu\text{mol/L}$ (10). Taking into account the restricted compartment environment of the electrode in the brain (27, 28), this concentration represents a gross under-

estimate of the concentration of dopamine needed to produce a current of this size. Considering the ratio of 10000:1 for ascorbate to dopamine concentrations in the striatum, it is likely that the current recorded *in vivo* is due almost entirely to ascorbate.

In conclusion, the results indicate that while stearate-modified electrodes have the desired properties for electrochemical discrimination of ascorbate and dopamine before they are implanted in brain tissue, these properties are lost after implantation. Taken together, the literature data and the present findings also suggest that these electrodes are neither selective nor sensitive enough to detect dopamine levels *in vivo*.

LITERATURE CITED

- (1) Marcerac, F.; Gonon, F. *Anal. Chem.* **1985**, *57*, 1778-1779.
- (2) Crespi, F.; Martin, K. F.; Marsden, C. A. *Neuroscience* **1988**, *27*, 885-896.
- (3) Stamford, J. A. *Anal. Chem.* **1986**, *58*, 1033-1036.
- (4) Kasser, R. J.; Renner, K. J.; Feng, J. X.; Brazell, M. P.; Adams, R. N. *Brain Res.* **1988**, *475*, 333-344.
- (5) Ewing, A. G.; Wightman, R. M. *J. Neurochem.* **1984**, *43*, 570-577.
- (6) Adams, R. N.; Marsden, C. A. In *Handbook of Psychopharmacology*; Plenum Press: New York, 1982; Vol. 15, pp 1-74.
- (7) *Voltammetry in the Neurosciences*; Justice, J. B., Jr., Ed.; Humana Press: Clifton, NJ, 1987.
- (8) *Measurement of Neurotransmitter Release In Vivo*; Marsden, C. A., Ed.; IERO Handbook Series; J. Wiley and Sons: Chichester, 1984; Vol. 6.
- (9) Marsden, C. A.; Joseph, M. H.; Kurk, Z. L.; Maidment, N. T.; O'Neill, R. D.; Schenk, J. O.; Stamford, J. A. *Neuroscience* **1988**, *25*, 389-400.
- (10) Blaha, C. D.; Lane, R. F. *Brain Res. Bull.* **1983**, *10*, 861-864.
- (11) Gelbert, M. B.; Curran, D. J. *Anal. Chem.* **1986**, *58*, 1028-1032.
- (12) Lane, R. F.; Blaha, C. D.; Harl, S. P. *Brain Res. Bull.* **1987**, *19*, 19-27.
- (13) Broderick, P. A. *Life Sci.* **1985**, *36*, 2269-2275.
- (14) Lane, R. F.; Blaha, C. D.; Phillips, A. G. *Brain Res.* **1986**, *397*, 200-204.
- (15) Glynn, G. E.; Yamamoto, B. K. *Brain Res.* **1989**, *481*, 235-241.
- (16) Gonon, F. G.; Navarre, F.; Buda, M. J. *Anal. Chem.* **1984**, *56*, 573-575.
- (17) Kelly, R. S.; Wightman, R. M. *Brain Res.* **1987**, *423*, 79-87.
- (18) Church, W. H.; Justice, J. B., Jr. *Anal. Chem.* **1987**, *59*, 712-716.
- (19) O'Neill, R. D.; Fillenz, M.; Albery, W. J.; Goddard, N. J. *Neuroscience* **1983**, *9*, 87-93.
- (20) Oldham, K. B. *J. Electroanal. Chem.* **1985**, *184*, 257-267.
- (21) Sternson, A. W.; McCreery, R.; Feinberg, B.; Adams, R. N. *J. Electroanal. Chem.* **1973**, *46*, 313-321.
- (22) Dayton, M. A.; Ewing, A. G.; Wightman, R. M. *Anal. Chem.* **1980**, *52*, 2392-2396.
- (23) Kovach, F. M.; Ewing, A. G.; Wilson, R. L.; Wightman, R. M. *J. Neurosci. Methods* **1984**, *10*, 215-227.
- (24) Ormonde, D. E.; O'Neill, R. D. *J. Electroanal. Chem.* **1989**, *261*, 463-469.
- (25) Albahadly, F. N.; Mottola, H. A. *Anal. Chem.* **1987**, *59*, 958-962.
- (26) Nelson, A.; Auffret, N. J. *Electroanal. Chem.* **1988**, *248*, 167-180.
- (27) Albery, W. J.; Goddard, N. J.; Beck, T. W.; Fillenz, M.; O'Neill, R. D. *J. Electroanal. Chem.* **1984**, *161*, 221-233.
- (28) Cheng, H.-Y. *J. Electroanal. Chem.* **1982**, *135*, 145-151.

Paul D. Lyne
Robert D. O'Neill*

Chemistry Department
University College Dublin
Belfield, Dublin 4
Ireland

RECEIVED for review April 28, 1989. Accepted July 20, 1989.
We thank EOLAS for a grant to P.D.L. under the Basic Research Awards scheme.

Estimating Error Limits in Parametric Curve Fitting

Sir: The recent article by Phillips and Eyring in this journal (1) presented an interesting solution, based on the sequential simplex method, to the problem of the estimation of errors in nonlinear parametric fitting. The authors did not mention

two other simple, powerful, and reliable methods, the jackknife and the bootstrap (2-6).

The need for simple and robust procedures to assess confidence limits in estimated parameters is widely perceived in

Table I. The Reference "Experimental" Data Set^a

<i>t</i>	<i>A</i>	<i>t</i>	<i>A</i>
1.5	0.111	9.0	0.325
1.5	0.109	12.0	0.326
3.0	0.169	12.0	0.330
3.0	0.172	15.0	0.362
4.5	0.210	15.0	0.383
4.5	0.210	18.0	0.381
6.0	0.251	18.0	0.372
6.0	0.255	24.0	0.422
9.0	0.331	24.0	0.411

^aThese "noisy" data (from ref 16) are simulated results of a first-order kinetics experiment. The absorbance (*A*) is a function of time (*t*). The function has the form $A = A_{\infty}(1 - \exp(-kt))$, where A_{∞} , the absorbance at $t = \infty$, and *k*, the rate constant, are the unknown parameters.

all physical sciences. The jackknife and the bootstrap algorithm can provide a particularly simple solution. Other methods (for example, likelihood and lack-of-fit, ref 7), which will not be discussed here, can also be used.

Relatively few explicit references to the jackknife and the bootstrap are found in the chemical literature. Some applications of the bootstrap have been determination of the confidence limits of correlation coefficients between elemental concentrations in meteorites (8), analysis of the correlation between blood lead content and blood pressure in policemen (9), determination of confidence bounds of means, errors, and correlation coefficients in air quality data (10), determination of confidence intervals for the timing of the DNA molecular clock in human filogenesys (11), and analysis and interlaboratory comparison of exponential fits in specific-heat measurements (12). The jackknife has found application in the estimation of confidence intervals for parameters associated with quantitative structure-activity relationships (13), in uncertainty analysis in reactor risk estimation (14), and in outlier detection and error estimation in geothermometer calibration (15).

Concise operational descriptions are presented here and are applied to a simple test problem in two parameters. Extension to problems with more parameters and/or variables is straightforward. Formal descriptions and proofs can be found in ref 3 and 6 and references therein.

The jackknife is a finite algorithm (it requires a finite and a priori computable number of calculations) while the bootstrap is not: the number of computations needed is proportional to the precision asked of the results. The bootstrap can provide a better representation of the geometry of the confidence regions, at the cost of a significantly larger computational load. Both can use any curve-fitting program.

Let us consider the now classic data set (from ref 16) reproduced in Table I.

The 18 "experimental" pairs (*A*, absorbance; *t*, time) simulate the results of a first-order kinetics experiment. They are to be fitted by the function

$$A = A_{\infty}(1 - \exp(-kt))$$

where A_{∞} , the absorbance at $t = \infty$, and *k*, the rate constant, are the unknown parameters to be determined.

Assuming that all points have identical statistical weight, that the error is normal (random with Gaussian distribution), and that it affects only the dependent variable *A*, use of any nonlinear least-square parametric curve fitting program gives

$$\hat{A}_{\infty} = 0.4043$$

$$\hat{k} = 0.1698$$

as extensively published. The fitting program used in this work was SIMP, a public domain implementation of the

Table II. Parameters Fitting the Full Data Set (Table I) and the 18 Jackknife Subsets of 17 Points Each^a

A_{∞}	<i>k</i>	SSR	
Full Set			
0.404 275 02	0.169 830 49	0.003 642 02	
Diminished Sets			
0.405 939 18	0.166 835 86	0.003 217 55	(point 1 deleted)
0.405 777 97	0.187 121 95	0.003 297 86	(point 2 deleted)
0.405 177 94	0.168 074 16	0.003 576 97	(point 3 deleted)
0.405 540 86	0.167 383 43	0.003 515 64	(point 4 deleted)
0.403 581 31	0.171 362 37	0.003 600 41	(point 5 deleted)
0.403 581 31	0.171 362 37	0.003 600 41	(point 6 deleted)
0.403 652 97	0.171 502 97	0.003 580 29	(point 7 deleted)
0.403 988 70	0.170 592 54	0.003 629 21	(point 8 deleted)
0.404 293 19	0.168 054 53	0.003 414 61	(point 9 deleted)
0.404 278 38	0.168 799 02	0.003 564 66	(point 10 deleted)
0.406 488 95	0.170 112 28	0.002 932 80	(point 11 deleted)
0.406 138 61	0.170 070 34	0.003 137 11	(point 12 deleted)
0.406 020 11	0.168 898 68	0.003 516 72	(point 13 deleted)
0.402 573 00	0.170 752 77	0.003 522 67	(point 14 deleted)
0.405 275 02	0.169 083 22	0.003 620 91	(point 15 deleted)
0.407 392 05	0.167 523 33	0.003 437 54	(point 16 deleted)
0.396 140 77	0.177 452 69	0.002 866 60	(point 17 deleted)
0.399 689 70	0.174 060 41	0.003 404 72	(point 18 deleted)
Mean			
0.404 196 11	0.169 946 83		
Standard Deviation			
0.002 592 61	0.002 594 33		

^aThe full data set and the one-minus subsets were fitted by a PC-DOS Pascal port of program SIMP (ref 17), a public domain implementation of the simplex algorithm.

Table III. Error Analysis of Data in Table I

method	error		ref
	A_{∞} , abs at $t = \infty$ value, 0.404	<i>k</i> , rate constant value, 0.170	
jackknife	0.0107	0.0107	a
bootstrap	0.0102	0.0103	a
sequential simplex	0.012	0.013	1
Marquardt	0.009	0.010	1
Newton	0.006	0.007	1

^aPresent work.

simplex algorithm (17) ported to Borland Pascal in the PC-DOS environment. The questions to be answered now are what is the error on the estimates of the parameters A_{∞} and *k* and what are the limits (e.g. at the 0.5, 0.9, 0.98 confidence level) on the possible range of these estimates?

THE JACKKNIFE

To estimate error by the jackknife method

1. Delete the first data point from the original data set.
2. Fit the "jackknifed" set to compute $\hat{A}_{\infty}^{(1)}$, $\hat{k}^{(1)}$.
3. Repeat steps 1 and 2 *n* times (where *n* is the number of data points) deleting now point 2, 3, ..., *n*, to obtain a set of *n* ($\hat{A}_{\infty}^{(i)}$, $\hat{k}^{(i)}$) parameter sets.
4. Compute the jackknife estimate of the standard error of parameter *p* (here, $p = A_{\infty}$, *k*) as

$$\sigma_j(\hat{p}) = \left[\frac{n-1}{n} \sum_{i=1}^n (\hat{p}^{(i)} - \hat{p}^{(1)})^2 \right]^{1/2}$$

where

$$\hat{p}^{(i)} = 1/n \sum_{j=1}^n \hat{p}^{(j)}$$

Application to the example data set produced the jackknife replicates in Table II, from which the standard errors reported in Table III were obtained, in good agreement with results

previously obtained by other methods.

The jackknife can be applied to small data sets, such as the one studied here, with no need to develop computer code. All that is needed is to run the fitting program n times, where n is the number of data points in the set. The fitting program can utilize, of course, any algorithm.

The jackknife can be programmed in the following way:

Instruct or modify the fitting program (called FITTER) to append the parameters it computes to a given result file.

Write a program (called KNIFE) to produce diminished data sets (input the data set and the ordinal number of the point to be deleted).

Write a program (possibly a batch/script file, called JACK) to call n times KNIFE and FITTER.

JACK will produce a file containing the n parameter sets obtained by fitting the n diminished sets of $(n - 1)$ data points. The variance of these parameters can be computed by any statistical package (or most pocket calculators). Multiplying the square root of the variance by $(n - 1)^{1/2}$ gives the standard error of each parameter.

Outliers can be easily detected by examining the sum of the squares of the residuals (SSR) of the jackknifed sets: if deleting a data point decreases significantly the SSR of the resulting reduced set, that point is probably in error. The decision to reject an outlier from the experimental set can then be made according to definite rules.

If the error on a parameter is known to obey a specific distribution (for example normal or Student's law), then tabulated values of the appropriate function can be used to translate standard error to confidence intervals. The variance-covariance matrix of the jackknifed results can be used to construct elliptical joint confidence regions, but this technique implicitly assumes Gaussian distribution and has been found unreliable (18), at least for a highly nonlinear function and a data set affected by large and probably inhomogeneous errors (19).

THE BOOTSTRAP

The bootstrap method studies the statistical properties of a set of parameter sets obtained by fitting a large number of simulated data sets. These simulated data sets (or bootstrap replicates) are simply obtained by random sampling (with replacement) of the "experimental" data set.

Operationally:

1. Copy a point at random from the original data set to a simulated data set.
2. Repeat step 1 n times, the number of samples in the original set, to produce a bootstrap replicate.
3. Fit the bootstrap replicate, computing $\hat{A}_\infty^{(i)}$, $\hat{k}^{(i)}$.
4. Repeat steps 1, 2, and 3 m times to obtain a set of m ($\hat{A}_\infty^{(i)}$, $\hat{k}^{(i)}$) sets.
5. Compute the bootstrap estimate of the standard error on parameter p (here, $p = A_\infty, k$) as

$$\sigma_B(\hat{p}) = \left[\frac{1}{m-1} \sum_{i=1}^m (\hat{p}^{(i)} - \bar{\hat{p}})^2 \right]^{1/2}$$

where

$$\bar{\hat{p}} = 1/m \sum_{i=1}^m \hat{p}^{(i)}$$

The bootstrap can be programmed in the following way: Instruct or modify the fitting program (called FITTER) to append the parameters it computes to a given result file.

Write a program (called STRAP) to produce a bootstrap replicate by copying n times a point at random from the original set to the replicate set.

Write a program (it can be a batch/script file, called BOOT) to call m times STRAP and FITTER.

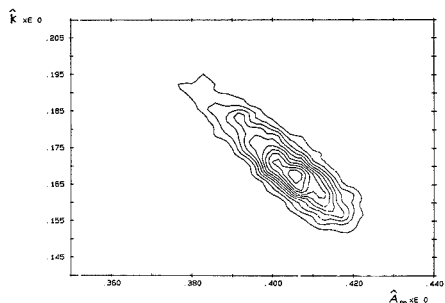


Figure 1. Contour plot of the density of distribution of the results of the fit of 2000 bootstrap replicates of the data set in Table I, in the absorbance-rate constant plane. The plot was obtained by mapping the values of the 2000 pairs of fitted parameters in a 64×64 grid. The grid was smoothed (Blackman window of period 4) in the two dimensions. The correlation between the two parameters and the skewness of their distribution are visually evidenced.

The output of BOOT will be a file containing the m parameter sets obtained by fitting m bootstrap replicates containing the same number of data points (n) as the original set. The best estimate of the error on each parameter is the square root of the sample variance (the sample standard deviation) of each parameter.

Application of the bootstrap ($m = 2000$) to the example data set gave error estimates in agreement with jackknife results (Table III). Jackknife error estimates can be proven to be larger than bootstrap estimates by a factor $[n/(n-1)]^{1/2}$ (4).

It is perhaps not sufficiently appreciated that function parameters are often strongly correlated. This can be evidenced, in this example, by the contour plot in the absorbance-reaction rate plane of the density (probability) distribution of the results of fitting 2000 bootstrap replicates (Figure 1). The knowledge, with higher certainty, of the value of one of the parameters will allow a more correct estimate of the value of the other. For example, if other measurements were to indicate that the value of A_∞ is exactly 0.380 (and not 0.403 ± 0.010 as determined), the best estimate of k would become 0.192 (and not 0.170 ± 0.010). This can be seen in Figure 1 or obtained from the least-squares linear regression of \hat{k} vs \hat{A}_∞ computed from the m bootstrap ($\hat{A}_\infty^{(i)}$, $\hat{k}^{(i)}$) pairs

$$\hat{k} = 0.5347 - 0.9012\hat{A}_\infty$$

Confidence intervals around best parameter estimates are usually assumed to be normal (symmetrical and shaped as Gaussians); the joint confidence curves are then elliptical in parameter space. While this is true in linear models, at least for large number of points and/or normal error distribution on these points, confidence intervals in nonlinear regression are in general nonnormal, even if the errors on the data are themselves normally distributed: their nonnormality is a consequence of the nonlinearity of the fitting function.

So, the histograms illustrating the bootstrap distribution of the probable values of the parameters A_∞ and k (Figures 2 and 3) are asymmetric, reflecting the asymmetry apparent in Figure 1 along the regression line of the contour plot.

Caution should then be used in applying standard tools of statistical analysis, such as the normal probability or Student's t distribution functions, to obtain confidence limits from standard error estimates. Rather, the whole set of bootstrap results should be used to observe the ranges within which the fitted parameters have a definite probability of being found.

From the results of 2000 bootstrap replicates it was possible to compute the asymmetric confidence intervals reported as fractiles in Table IV. The median (not the average) of the distributions is in excellent agreement with the results ob-

Table IV. Confidence Intervals of the Computed Parameters (from Bootstrap Analysis, $m = 2000$)^a

parameter	fractile						
	0.01	0.05	0.25	0.50 (median)	0.75	0.95	0.99
A_{∞}	0.3758	0.3847	0.3974	0.4042	0.4103	0.4180	0.4218
k	0.1498	0.1565	0.1641	0.1699	0.1773	0.1899	0.1996

^aThe fractiles were computed by program Asyst (Asyst Software Technologies, Inc.) on the fits of 2000 bootstrap replicates. Note that the median of the replicates is in agreement with the fit of the original data set. Since the distributions are skewed (Figures 2 and 3), the average values of the parameters in the replicates are slightly but significantly different from the median: $A_{\infty} = 0.4033$, $k = 0.1712$. The table can be used to indicate, for example, that there is a 90% probability that the true value of k lies between 0.1565 and 0.1899, but only a 1% probability that it lies above 0.1996.

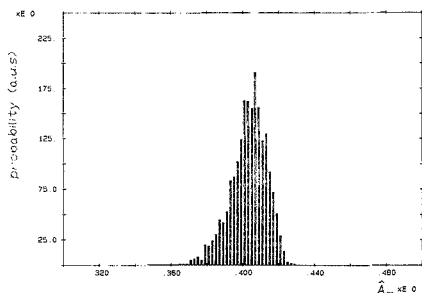


Figure 2. Histogram representing the distribution probability of A_{∞} , obtained from 2000 bootstrap replicates of the data set in Table I. Note that the distribution is skewed.

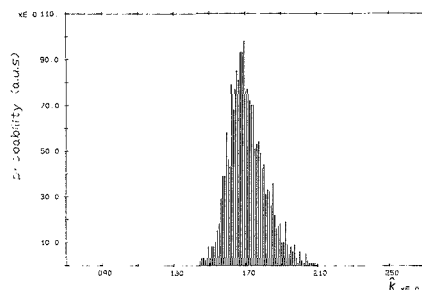


Figure 3. Histogram representing the distribution probability of k , obtained from 2000 bootstrap replicates of the data set in Table I. Note that the distribution is skewed. A finer grid was used than in Figure 2, resulting in "spikes" in the distribution, of no significance.

tained from the fit of the original data set.

Since the bootstrap method depends on the existence of random numbers, its results are not, in a strict sense, reproducible. There is a finite probability that the STRAP routine will produce "degenerate" replicates. So, in the example given, there is about a 4.57×10^{-22} probability that one replicate set will contain 18 times the same data point; such a data set cannot be fitted. It is often convenient then to trim the bootstrap results set and to perform statistics, for example, only using values within a given range about the mean.

The jackknife and—to an even larger extent—the bootstrap can be extremely demanding of computer resources. Producing and fitting the 2000 replicates of this example required more than 20 min on a 16-MHz PC-DOS machine based on 80386 and 80387 processors. On the other hand, the growing availability of inexpensive computer power, the high cost of software development, and the power of these methods make the jackknife and the bootstrap a practical solution and a valid alternative to possibly faster, but less powerful and far more complex methods.

In conclusion, the computation of error estimates and of confidence intervals is possible and relatively simple in nonlinear curve fitting, as it is in linear problems. The jackknife and the bootstrap require no exceptional code development effort and can be applied together with any curve fitting program. It is hoped that the methods illustrated here will be of use in those cases—more and more common given the present proliferation of computers and of computer-based instrumentation—in which data are processed by nonlinear curve-fitting methods.

LITERATURE CITED

- (1) Phillips, G. R.; Eyring, E. M. *Anal. Chem.* **1988**, *60*, 738–741.
- (2) Efron, B.; Gong, G. *Am. Statistician* **1983**, *37*(1), 36–48.
- (3) Miller, R. G. *Biometrika* **1974**, *61*, 1–16.
- (4) Efron, B. *Can. J. Statistics* **1981**, *9*(2), 139–172.
- (5) Efron, B. *Ann. Statist.* **1979**, *7*, 1–26.
- (6) Babu, G. I.; Bose, A. *Statistics Probability Lett.* **1989**, *7*, 151–160.
- (7) Donaldson, J. R.; Schnabel, R. B. *Technometrics* **1987**, *29*, 67–82.
- (8) Florenskii, P. V.; Petrenko, A. S. *Metacritika* **1987**, *46*, 172–177.
- (9) Weiss, S. T.; Munoz, A.; Stein, A.; Sparrow, D.; Speizer, F. E. *EHP, Environ. Health Perspect.* **1988**, *78*, 53–56.
- (10) Hanna, S. R. *JAPCA* **1988**, *38*(4), 406–412.
- (11) Hasegawa, M.; Kishino, H.; Yano, T. *J. Mol. Evol.* **1987**, *26*(1–2), 132–147.
- (12) Cray, S. B.; Fahey, D. A. *Phys. Rev. B: Condens. Matter* **1987**, *35*(4), 2102–2104.
- (13) Dietrich, S. W.; Dreyer, N. D.; Hansch, C.; Bentley, D. L. *J. Med. Chem.* **1980**, *23*(11), 1201–1205.
- (14) Modarres, M.; Cadman, T. *Nucl. Eng. Des.* **1985**, *85*(3), 385–399.
- (15) Powell, R. J. *Metamorph. Geol.* **1985**, *3*(3), 231–243.
- (16) Derring, S. N.; Morgan, S. L. *Anal. Chem.* **1973**, *45*, 278A–283A.
- (17) Cacceti, M. S.; Cacheris, W. P. *Byte Mag.* **1984**, *9*(5), 340–362.
- (18) Duncan, G. T. *Technometrics* **1978**, *20*, 123–129.
- (19) Fox, T. *Technometrics* **1980**, *22*, 28–33.

Marco S. Cacceti

CEA-DRDD/SES

B.P. 6

F-92265 Fontenay-aux-Roses Cedex

France

RECEIVED for review May 5, 1989. Accepted July 17, 1989.

TECHNICAL NOTES

Room-Temperature Phosphorescence of Polynuclear Aromatic Hydrocarbons on Matrix-Modified Solid Substrates

L. M. Perry, A. D. Campiglia, and J. D. Winefordner*

Department of Chemistry, University of Florida, Gainesville, Florida 32611

INTRODUCTION

Room-temperature phosphorescence spectrometry (RTP) is an established analytical technique used for the analysis of trace components in biological, pharmaceutical, and environmental samples (1). Although RTP analyses have been performed with analytes in the solid, liquid, and gaseous states, the simplest method of analysis is done with the analyte in the solid state on a solid support. Reports on solid surface RTP (SSRTP) appeared in the literature in 1896, but until the work of Roth, Schulman, and Walling, the full potential of this technique was not recognized (2-4). Since then, numerous studies have been reported, and recent publications by Vo-Dinh and Hurtubise have reviewed the RTP phenomena on solid substrates in detail (1,5).

Silica gel, sodium acetate, polymer salt mixtures, and filter paper are some of the supports that have been used for SSRTP (1,6-9). Although filter paper is the most commonly used support because of low cost and commercial availability, it suffers from two important drawbacks. It has a broad RTP emission band from 400 to 600 nm, the region where many organic compounds also phosphoresce, and its surface is not uniform. Both conditions can affect the precision and limit of detection (LOD) of the analytes. In addition, filter paper is susceptible to moisture, which causes quenching of the analyte signals and additional problems with reproducibility.

Analysis of polynuclear aromatic hydrocarbons (PAHs) has been accomplished by RTP on solid substrates (1, 9, 10). Selectivity, sensitivity, and small sample requirements make this technique conducive for trace analysis. In general, satisfactory analysis of nonpolar PAHs requires the use of a heavy atom or enhancement of the RTP signal. Phosphorescence enhancement by use of a heavy atom has been reported by several investigators (9, 11-13). Winefordner and Lue-Yen Bower investigated a series of heavy-atom enhancers for a variety of PAHs and determined Tl(I), overall, to be the most effective enhancer (9).

RTP emission for PAHs depends not only on the presence of a heavy atom but also on the environment for the phosphors. Immobilization in a rigid medium, association by hydrogen bonding, or entrapment of the phosphor are believed to be required to minimize collisional deactivation and loss of the phosphorescence signal (1, 5). Recent literature reports investigations of PAHs on matrix-modified filter paper (9, 14-16). Diethylenetriaminepentaacetic acid, cyclodextrin, and various inorganic salts, i.e., sodium citrate and malonate, are just a few of the many compounds used to modify the surface of filter paper for the inducement or enhancement of phosphorescence.

Previously, we reported nanogram detection of anthracene, a weak phosphor, by SSRTP (17). The solid substrate, Whatman No. 1, was pretreated with Tl(I). Measurements

were accomplished by using the surfactant salt thallium lauryl sulfate (TILS) and the inorganic salt TlNO_3 . The RTP signal of anthracene in the presence of TILS was approximately 2-fold greater than obtained for TlNO_3 . Additionally, the precision for the measurement of anthracene on Whatman No. 1 pretreated with TILS was observed to be 2 times better than the one observed for the TlNO_3 system. It was suggested that the long alkyl chains of the TILS protected the phosphor from collisional deactivation and possible moisture quenching. In this investigation, Whatman No. 1 pretreated with TILS was examined as a general surface for inducing RTP from several PAHs.

EXPERIMENTAL SECTION

Instrumentation. A Perkin-Elmer LS-5 luminescence spectrofluorometer (Perkin-Elmer, Norwalk, CT) coupled to a Model 3600 data station was used to collect all RTP spectra and intensity measurements. The spectrofluorometer was equipped with a xenon flash lamp as the excitation source. All phosphorescence data were collected by using a pulse delay time of 0.03 ms and a gate time of 9.0 ms. The excitation and emission monochromator slits were set at 10 and 5 nm, respectively. The sample compartment was continuously purged with dry nitrogen. A 360-nm cutoff filter was used where necessary to minimize second-order scatter.

Reagents. Naphthalene (Mallinckrodt, St. Louis, MO), 4-aminobenzoic acid (PABA) and carbazole (Eastman Kodak Co., Rochester, NY), and 1,2,3,4-dibenzanthracene (1,2,3,4-DBA) and pyrene (Aldrich Chemical Co., Milwaukee, WI) were of reagent grade and used as received. The PABA was used as a reference compound for comparison of RTP figures of merit. Thallium lauryl sulfate (TILS) was prepared in our lab by a procedure previously described (17). Absolute ethanol (Florida Distillers Co., Lake Alfred, FL) and "Nanopure" demineralized water (Barnstead System, Sybron Corp., Boston, MA) were used as the solvents.

Procedures. TILS was prepared in ethanol/water (80:20 by volume) solutions. Concentrations of 0.016, 0.033, 0.065, and 0.13 M TILS were prepared and the solutions spotted onto Whatman No. 1 filter paper disks for the preparation of the "heavy-atom curves". All PAH standards were prepared daily in absolute ethanol by serial dilution of 1000 $\mu\text{g}/\text{mL}$ stock solutions. The preparation of Whatman No. 1 filter paper disks with TILS was described previously (17). The RTP intensity of the substrate, i.e., Whatman No. 1 treated with 5 μL of the appropriate concentration of TILS, was determined at the maximum excitation and emission wavelengths for each PAH; subsequently 3 μL of analyte was spotted onto the center of each substrate. Each PAH sample had its own blank whose intensity was subtracted from the total intensity measured for the analyte. All measurements were performed in triplicate in the presence of dry nitrogen.

RESULTS AND DISCUSSION

Whatman No. 1 filter paper treated with 0.065 M TILS produced a broad band of background emission from 400 to 600 nm. The excitation and emission maxima were 253 and 504 nm, respectively. The RTP emission intensity is approximately 10 times that of untreated Whatman No. 1 filter

* Author to whom correspondence should be addressed.

Table I. Room-Temperature Phosphorescence Spectral Properties of Several PAHs and PABA Examined on Whatman No. 1 Filter Paper Pretreated with TILS

compound	TILS, M	λ_{ex} , nm	λ_{em} , ^c nm
naphthalene	0.065	275	480, 513, (547)
pyrene	0.065	336	593, 653
1,2,3,4-DBA	0.065	292	567, 615, 670
carbazole	0.033	295	416, 440, (465)
PABA	0.033	286	430

^a Wavelength of maximum RTP emission is italicized when there is more than one band; the wavelengths of the shoulders are in parentheses; the precision for the wavelengths is ± 0.5 nm.

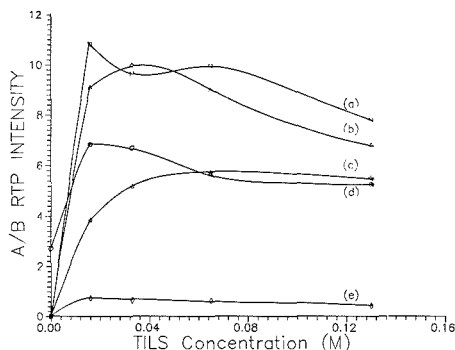


Figure 1. Ratio (*A/B*) of net analyte RTP signal intensity to the substrate background RTP emission intensity at the wavelengths of the particular analyte plotted versus the molar concentration of TILS to determine the effects of heavy-atom concentration on RTP emission of various PAHs and PABA: (a) 1,2,3,4-DBA; (b) carbazole; (c) pyrene; (d) PABA; (e) naphthalene.

paper under identical experimental conditions. The effect of the high background emission on the measurement of various PAHs was examined and is discussed below.

Table I lists the PAHs and their RTP excitation and emission characteristics chosen for examination on Whatman No. 1 pretreated with TILS, hereafter referred to as the substrate. These compounds were chosen because their emission maxima occurred on the broad background of the substrate and their excitation wavelengths were similar. PABA, carbazole, naphthalene, 1,2,3,4-DBA, and pyrene phosphorescence emission maxima were observed at 430, 440, 513, 567, and 593 nm, respectively. The relative emission maxima represent different situations for the measurement of these compounds. Since the naphthalene emission maximum at 513 nm is very near the RTP emission maximum of the substrate, its analytical figures of merit should be the most affected. Conversely, the other compounds should produce more favorable analytical results. Carbazole and PABA were specifically chosen because of their different polarities, in order to evaluate their interactions with the alkyl chains of the substrate.

The influence of heavy-atom concentration for each PAH was determined from a plot of the ratio (*A/B*) of the net analyte RTP signal intensity (*A*) to the substrate background RTP emission intensity (*B*) at the wavelengths of the particular analyte versus the molar concentration of TILS. From Figure 1, it can be seen that the *A/B* ratios for all the analytes changed little with TILS concentration. However, for all further studies, we chose the TILS concentrations given in Table I for the five analytes to achieve good signal to background ratios with little sensitivity to change in TILS concentration.

Table II. Reproducibility of Blanks at Excitation/Emission^a Maxima for Analytes

analyte	no. of substrates	av blank RTP response	RSD, %
PABA	37	11.8 \pm 0.7	6.1
carbazole	18	13.0 \pm 0.7	5.4
naphthalene	41	47.9 \pm 2.8	5.7
1,2,3,4-DBA	30	20.1 \pm 0.8	3.9
pyrene	18	6.9 \pm 0.3	4.3

^a Excitation and emission maxima reported in Table I.

Table III. Room-Temperature Phosphorescence of Several PAHs and PABA on Whatman No. 1 Pretreated with TILS

compound	LDR, ^a ng	slope log-log	corr coeff	LOD, ^{b,c} ng	precision ^d method, %
PABA	3-450	0.98	0.997	1.3	7.6
carbazole	1.5-300	0.99	0.996	0.8	7.8
naphthalene	15-900	1.02	0.998	8.8	13.9
1,2,3,4-DBA	1.5-75	1.03	0.996	0.5	5.8
pyrene	1.5-750	0.97	0.998	1.4	3.3

^a Linear dynamic range resulting from triplicate measurements of each analyte on Whatman No. 1 pretreated with TILS. ^b Limit of detection calculated by $3s_{\text{blank}}/m$, where s_{blank} is the standard deviation of 16 blanks and m is the slope of the analytical calibration curve plotted on linear-linear coordinates. ^c Values are detection limits in nanograms. ^d Precision for the method was obtained by the following formula: $P_{\text{method}} = (s_{A+B}^2 + s_B^2)^{1/2} / I_{A-B} \times 100$. Sixteen determinations of 10 ppm analyte and their respective blanks were utilized to determine s_{A+B} , standard deviation of analyte plus blank intensity; s_B , standard deviation of blank RTP intensity; and I_{A-B} , average net analyte RTP intensity.

The percent relative standard deviations (RSDs) of the RTP background emission signals of blanks pretreated with the optimum TILS concentrations and measured at the excitation/emission peaks for the five analytes (see Table I) are given in Table II. The percent relative standard deviations of the RTP background emissions of the substrate for all analytes were observed to be less than 7%. Additionally, the RTP background emissions of 4 disks of the same batch of substrates used for the analysis of naphthalene were measured at the naphthalene excitation and emission wavelengths at approximately a 1-month interval. There were no significant differences in the reproducibilities of the RTP background intensity observed over the monthly period as opposed to the reproducibilities obtained over a few hours.

The slopes (sensitivities) of the analytical calibration curves for the PAHs and the analytical figures of merit are summarized in Table III. The slopes of the log-log calibration plots are all close to unity (± 0.03) with excellent correlation coefficients. Pyrene, carbazole, naphthalene, and PABA show linearity over 2 decades, while 1,2,3,4-DBA was linear only over 1 decade. Nanogram detection limits were observed for all analytes. The precision of the method for each analyte was determined by using the 10 $\mu\text{g}/\text{mL}$ standard solution for each PAH. With the exception of naphthalene, the method precision for all analytes was observed to be less than 8%, which is statistically the same as the precision of the background emission. The poorer method precision (13.9%) for naphthalene can be mainly attributed to the high standard deviation of the substrate emission and to the high background emission at the peak wavelength for naphthalene. It should also be mentioned that the time for the naphthalene RTP signal to stabilize was more than twice that of the other compounds tested. The RTP intensity peaked at a maximum value after 10 min of drying in the sample compartment with dry N_2 and then rapidly degraded. Volatilization of the an-

alyte during the drying time (18) was, most likely, responsible for the unfavorable precision observed.

CONCLUSION

TILS was used as a matrix modifier for Whatman No. 1 filter paper. This new substrate was used successfully for nanogram detection of several PAHs. The analytical figures of merit compare favorably with those in literature reports (9, 18-22), which reveal a variety of filter papers and matrix modifiers utilized for such molecules.

This study suggests that Whatman No. 1 filter paper pretreated with TILS can be used as a general method for trace analysis of different kinds of PAHs. The substrate was stable over a long period of time, meaning it could be prepared ahead of time and stored for future use. The reproducibility of the substrates' background was less than 7%. As previously reported, the Tl(I) cation and the analyte were protected from source irradiation damage by the long alkyl chains of the anion (17). An additional advantage of the nonpolar environment was the protection of the analyte against quenching during the measurement (17). All of the analyte signals, with the exception of that of naphthalene, reached a steady state in less than 3 min as long as a N₂ purge was used. Although PABA and carbazole were chosen because of their polarity differences with respect to the other PAHs, these species were just as well behaved as the nonpolar PAHs.

ACKNOWLEDGMENT

A. D. Campiglia thanks the Coordenacao de Aperfeicoamento de Nivel Superior-Capes for the grant that is making possible his stay in Gainesville and the University of Brasilia (Brazil) for permission to leave.

Registry No. PABA, 150-13-0; 1,2,3,4-DBA, 215-58-7; TILS,

72925-49-6; naphthalene, 91-20-3; carbazole, 86-74-8; pyrene, 129-00-0.

LITERATURE CITED

- (1) Vo-Dinh, T. *Room Temperature Phosphorimetry for Chemical Analysis*; Elving, P. M., Winefordner, J. D., Eds.; John Wiley & Sons: New York, 1984.
- (2) Roth, M. J. *Chromatogr.* **1967**, *30*, 276-278.
- (3) Schulman, E. M.; Walling, C. J. *Phys. Chem.* **1973**, *77*, 902-905.
- (4) Schulman, E. M.; Walling, C. *Science* **1972**, *178*, 53-54.
- (5) Hurtubise, R. J. *Solid Surface Luminescence Analysis: Theory Instrumentation, Applications*; Marcel Dekker: New York, 1981.
- (6) Dalterio, R. A.; Hurtubise, R. J. *Anal. Chem.* **1982**, *54*, 224-228.
- (7) Burrell, G. J.; Hurtubise, R. J. *Anal. Chem.* **1989**, *60*, 564-568.
- (8) von Wandruszka, R. M. A.; Hurtubise, R. J. *Anal. Chem.* **1977**, *49*, 2164-2169.
- (9) Lue-Yen Bower, E.; Winefordner, J. D. *Anal. Chim. Acta* **1978**, *102*, 1-18.
- (10) Vo-Dinh, T.; Gammage, R. B.; Martinez, P. R. *Anal. Chem.* **1981**, *53*, 253-258.
- (11) Seybold, P. G.; White, W. *Anal. Chem.* **1975**, *47*, 1199, 1200.
- (12) Vo-Dinh, T.; Lue-Yen, E.; Winefordner, J. D. *Anal. Chem.* **1976**, *48*, 1186-1188.
- (13) Suter, G. W.; Kallir, A. J.; Wild, U. P. *Anal. Chem.* **1987**, *59*, 1644-1646.
- (14) Karnew, H. T.; Schulman, S. G.; Winefordner, J. D. *Anal. Chim. Acta* **1984**, *164*, 257-262.
- (15) Alak, A. M.; Vo-Dinh, T. *Anal. Chem.* **1988**, *60*, 596-600.
- (16) Parker, R. T.; Freeland, R. S.; Schulman, E. M.; Dunlap, R. B. *Anal. Chem.* **1979**, *51*, 1921-1926.
- (17) Perry, L. M.; Campiglia, A. D.; Winefordner, J. D. *Anal. Chim. Acta*, in press.
- (18) Ramis Ramos, G.; Khasawneh, I. M.; Garcia Alvarez-Coque, M. C.; Winefordner, J. D. *Talanta*, **1988**, *35*, 41-46.
- (19) Vo-Dinh, T.; Gammage, R. B. *Anal. Chim. Acta* **1979**, *107*, 261-271.
- (20) Vo-Dinh, T.; Hooymann, J. R. *Anal. Chem.* **1979**, *51*, 1915-1921.
- (21) Ramis Ramos, G.; Garcia Alvarez-Coque, M. C.; O'Reilly, A. M.; Khasawneh, I. M.; Winefordner, J. D. *Anal. Chem.* **1988**, *60*, 416-420.
- (22) Vo-Dinh, T.; Lue-Yen, E.; Winefordner, J. D. *Talanta* **1977**, *24*, 146-148.

RECEIVED for review March 24, 1989. Accepted June 19, 1989.
This research was supported by NIH-GM11373-27.

Apparatus for the Fabrication of Poly(chlorotrifluoroethylene) Composite Electrodes

Jeffrey E. Anderson,* Dale Hopkins, John W. Shadrick, and Yee Ren

Department of Chemistry, Murray State University, Murray, Kentucky 42071-3306

INTRODUCTION

Since the introduction of Kel-F graphite (Kelgraf) electrodes (1, 2), a number of papers have appeared dealing with the application (3-7) of these electrodes, as well as the characterization of their behavior (8, 9). The application of Kelgraf electrodes has primarily been as voltammetric detectors in liquid chromatography and flow injection analysis (2-5). Characterization studies indicate that they exhibit behavior typical of microelectrode ensembles and as such have the advantage of enhanced current densities leading to a higher signal to noise ratio than observed for other carbon electrodes such as glassy carbon.

Kelgraf electrodes that have been reported previously have been fabricated from Kel-F 81 brand plastic resin from 3M. The recommended fabrication techniques from the manufacturer (10) include compression molding of sheets and injection molding. In both cases, the physical properties of the resulting material are affected by the time and temperature of heating and cooling. For example, the degree of crystallinity is a function of the thermal history of the polymer. Rapid cooling of the Kel-F from above its crystalline melting point (212 °C) to below 150 °C yields a more amorphous material that is less dense, more elastic, more transparent, and tougher than its crystalline counterpart. The more amorphous material is also favored by minimizing the time that the plastic

is exposed to temperatures above 212 °C. This minimizes the thermal degradation of the polymer, which would lead to a lower molecular weight and more crystalline product. The denser translucent crystalline product is favored by slow cooling of the melt. It should be emphasized that under no conditions is the product purely crystalline or amorphous, which implies that the fabrication conditions must be strictly controlled to ensure a consistent product. An additional fabrication parameter that should be mentioned is the pressure. In the compression molding used to produce Kelgraf electrodes, it is important to maintain a pressure of at least 1000 psi during the cooling phase of the fabrication. If the pressure is not maintained, shrink voids may develop caused by shrinkage of the plastic during cooling.

Given the above considerations, an apparatus was designed to provide rapid heating of the Kel-F graphite mixture to above its melting point to decrease the fabrication time and minimize the time above 212 °C. In addition, provisions were made to simplify and provide control over the cooling time in an attempt to ensure a consistent product. Note that in the past, cooling was provided by squirting water on the fabrication die, a rather messy nonreproducible affair. This apparatus should be of interest given the more recent introduction of composite electrodes based on mixtures of Kel-F and silver (11) and anticipated extension of this work to other

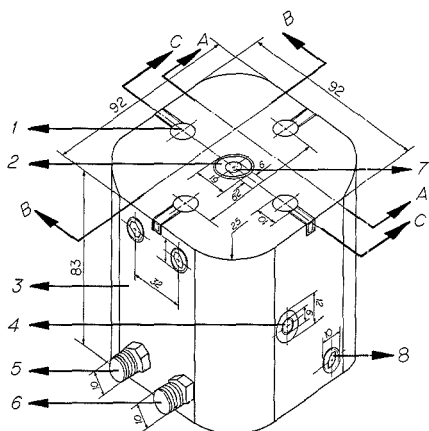


Figure 1. Illustration of apparatus for fabrication of Kelgraf electrodes. All units are in millimeters. Note that slices of the apparatus, A, B, and C, are shown in Figure 2. Key: 1, 500-W heater hole (10 mm); 2, stainless steel die; 3, aluminum block; 4, temperature probe hole; 5, cooling water inlet; 6, cooling water outlet; 7, die hole (6 mm); 8, cooling channel cap.

precious metals. In addition the apparatus should prove useful in the fabrication of electrodes using other inert binders such as Teflon (12, 13).

EXPERIMENTAL SECTION

Reagents and Materials. All chemicals used were of reagent grade. The Kel-F 81 resin was obtained from the 3M Commercial Chemicals Division, St. Paul, MN. The powdered graphite (UCP-2-325) was obtained from Ultra Carbon Corp. Bay City, MI. The Kel-F rod used in the electrode fabrication was from Plastic Profiles, Inc., East Hanover, NJ. The 120 V-500 W heaters were obtained from O.T.E., Inc., Henderson, KY. The temperature probe used (bimetallic dial thermometer, Model C) was from Omega Engineering Inc., Stanford, CT.

Instrumentation and Procedures. The potential step experiments were done on a solution that was 2 mM ferricyanide in 1.0 M KCl (pH 2.7). The potential was stepped from 0.6 to -0.2 V relative to an Ag/AgCl reference electrode (4 M KCl) using a Pt auxiliary electrode. The potentiostat used was homemade. The experiments were performed by using an Apple IIe computer equipped with a TM-AD213 (12-bit analog-to-digital converter) board and a TM-DA101 (12-bit digital-to-analog converter) board, both from TecMar, Inc. The software used was written in Applesoft basic and machine language. This system has been described previously (14).

The electrode fabrication procedure and the apparatus are described in the following section.

RESULTS AND DISCUSSION

Figures 1 and 2 provide a detailed illustration of the described apparatus. It consists of a block of aluminum into which water cooling channels were drilled. Figure 2 illustrates the route of the water through the aluminum block. A stainless steel sleeve (die) is centered in the middle of the block. Note that the die is screwed into the block to hold it in place when the resulting Kelgraf electrode is pressed out of the die. Placed symmetrically about the die in the aluminum block are four 120-V, 500-W heaters. These heaters are powered in parallel with a variable transformer. Finally, an additional hole was drilled for a temperature probe. Obviously this hole must be drilled such that it does not pass through a cooling channel yet comes as close as possible to the stainless steel die to ensure that the appropriate temperature is being measured.

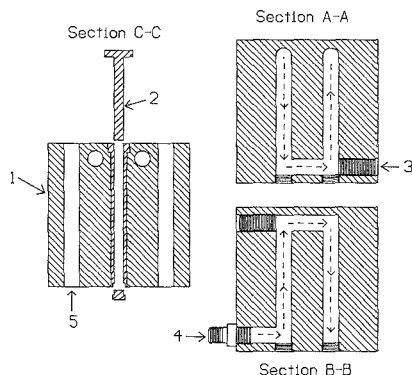


Figure 2. Slices of the apparatus illustrating the path of the water through the cooling channels. Also shown is a cross section of the stainless steel die and heater holes. Key: 1, aluminum block; 2, stainless steel die; 3, cooling channel cap; 4, cooling water inlet; 5, heater hole.

The fabrication process begins by placing approximately 2 g of the Kel-F-graphite mixture into the die. Preparation of the mixture has been described previously (1-3). We have found that manual mixing of the Kel-F and graphite is sufficient for obtaining a homogeneous mixture. In addition, we sieve the Kel-F obtained from the manufacturer and use resin with particle sizes less than 450 μm . It should also be noted that the graphite used in this work had particle sizes less than 45 μm as opposed to the less than 1 μm particle size graphite that has been used previously. Once the mixture is in the die, a pressure of approximately 2000 psi is applied. The temperature is then increased rapidly (100% power) to 200 $^{\circ}\text{C}$. The power is then adjusted to approximately 45%, providing an equilibrium temperature of 250 $^{\circ}\text{C}$. At this point, the pressure is again adjusted to 2000 psi and the system is maintained at this pressure and temperature for approximately 5 min. Cooling is then initiated by passing a slow stream of water through the cooling channel. Because of the steam produced, it is important that cooling line fittings be secure and copper tubing is recommended for the water input and output lines. The system is cooled from 250 to below 150 $^{\circ}\text{C}$ in about 30-60 s. Faster cooling results in shrink voids even with the pressure applied. Once the system is at room temperature, the Kel-F-graphite pellet may be pressed from the die. This often requires considerable pressure, and therefore, to minimize frustration and possible damage to the apparatus, we frequently treat the die with a parting agent. This amounts to coating the walls of the die with high-temperature silicon grease and heat treating the die at 300 $^{\circ}\text{C}$. It is important that the die then be wiped clean of excess grease before subsequent use of the apparatus.

The resulting Kel-F-graphite pellet can be easily machined to the desired diameter (3 mm in these studies). For testing of the product, we have found it convenient to press fit a 5 mm long pellet into a hole in a pure Kel-F rod. This eliminates the encapsulation procedure that has been used in the past, which can result in distortion of the Kel-F-graphite pellet. We have seen no evidence of seepage of the solution between the pure Kel-F and Kel-F-graphite mixture on the millisecond time scale provided the pellet is 1 to 2 thousandths of an inch bigger than the hole in the Kel-F rod. Electrical connection was made with a brass rod pushed through a hole in the opposite end of the rod. Polishing of the surface is accomplished by using progressively finer abrasives down to 1- μm alumina. Before the resulting electrode is used, the resistance

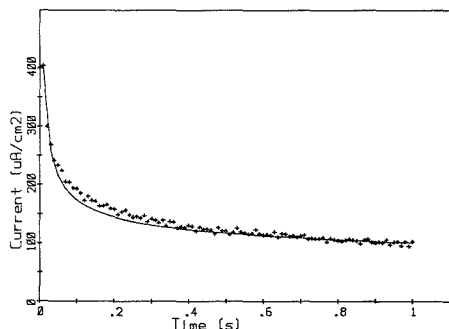


Figure 3. Potential step data (+) obtained after background subtraction when the potential of a 15% (w/w) graphite electrode was stepped from +0.6 V to -0.2 V vs Ag/AgCl (4.0 M KCl). The data shown is the average of four experiments on a single electrode with no polishing between runs. The solution contained 2 mM ferricyanide (1.0 M KCl, pH 2.8). Data collection was initiated at 10 ms after the step, with a total of 100 current measurements being made at 10-ms intervals. The solid line is the theoretical fit to the data.

is measured to ensure that it is below 100 Ω .

Chronoamperometric experiments have been used to characterize Kelgraf electrodes. In these experiments, the active surface area and the size of the active sites on the surface have been determined by fitting existing theory for microelectrode arrays to the experimental data. Weisshaar and Tallman (8) used this approach with the theory developed by Gueshi et al. (15). However, only after modification of the theory to include a distribution of two sizes of active sites were satisfactory results obtained. It was concluded that although the information obtained is useful, the model used to develop the theory is oversimplified with respect to the actual distribution and size of sites on the Kelgraf electrode surface. We have performed similar experiments with electrodes fabricated as described above. However, the theory of Shoup and Szabo (16) was used in the simplex optimization for the determination of the active area and site radii. This theoretical expression for the current has been shown to be more accurate than that used previously although it uses the same model for the distribution of active sites on the surface. Figure 3 shows the experimental potential step data obtained for the reduction of 2 mM ferricyanide at a 15% (w/w) graphite electrode after background subtraction. The experimental conditions are given in the caption. Also shown in Figure 3 is the theoretical fit (solid line), which is much better than that obtained in the study mentioned above when only one size of active site was considered. For one 15% (w/w) graphite electrode used in this study, the surface was found to be 18.0% active with a standard deviation of 0.15%. The active site radii determined were 25.0 μm (standard deviation 1.5). These

results are from four sets of experiments as described in the caption to Figure 3, with polishing between sets. This active site radius is in agreement with values determined previously by using chronoamperometry and scanning electron microscopy (8). In terms of reproducibility, results from another 15% electrode fabricated by a different individual yielded a percent active area and site radii of 21% and 30 μm , respectively. This variation between electrodes undoubtedly results from differences in the mixture preparation rather than from the compression molding step. It is this later step that we have attempted to refine, and its reproducibility is excellent with respect to the success rate and physical characteristics of the product. There are various reasons why our theoretical fit appears to be better than the results reported previously. Obviously the theory used was different. In addition, the fabrication technique is somewhat different as is the particle size of the graphite used to prepare the electrodes. Even though our results are rewarding, we agree with the previous conclusions that the model used to derive the theory is undoubtedly much simpler than the conditions that exist at the electrode surface. However, the percent active area and active site radii determined here are still useful in that they are important in determining the enhancement effects associated with microelectrode arrays in stationary solutions and flowing streams (17).

LITERATURE CITED

- (1) Anderson, J. E.; Tallman, D. E.; Chesney, D. J.; Anderson, J. L. *Anal. Chem.* **1978**, *50*, 1051-1056.
- (2) Anderson, J. E. Ph.D. Dissertation, North Dakota State University, 1979.
- (3) Chesney, D. J.; Anderson, J. L.; Weisshaar, D. E.; Tallman, D. E. *Anal. Chem.* **1981**, *53*, 321-331.
- (4) Weisshaar, D. E.; Tallman, D. E.; Anderson, J. L. *Anal. Chem.* **1981**, *53*, 1809-1813.
- (5) Tallman, D. E.; Weisshaar, D. E. *J. Liq. Chromatogr.* **1983**, *6*, 2157-2172.
- (6) Anderson, J. L.; Whiten, K. K.; Brewster, J. D.; Ou, T. Y.; Nonidez, W. K. *Anal. Chem.* **1985**, *57*, 1366-1373.
- (7) Cox, J. A.; Kulkarni, K. R. *Talanta* **1986**, *33*, 911-913.
- (8) Weisshaar, D. E.; Tallman, D. E. *Anal. Chem.* **1983**, *55*, 1146-1151.
- (9) Petersen, S. L.; Weisshaar, D. E.; Tallman, D. E.; Schulze, R. K.; Evans, J. F.; DesJarlais, S. E.; Engstrom, R. C. *Anal. Chem.* **1988**, *60*, 2385-2392.
- (10) Commercial Chemicals Division 3M, Technical Information, Y-IKCM (28.) RT.
- (11) Petersen, S. L.; Tallman, D. E. *Anal. Chem.* **1988**, *60*, 82-86.
- (12) Klatt, L. N.; Connell, D. R.; Adams, R. E.; Honigberg, I. L.; Price, J. C. *Anal. Chem.* **1975**, *47*, 2470-2472.
- (13) Shah, M. H.; Honigberg, I. L. *Anal. Lett.* **1983**, *16*(A15), 1149-1163.
- (14) Anderson, J. E. *Am. Lab. News* **1988**, December, 54, 55.
- (15) Gueshi, T.; Tokuda, K.; Matsuda, H. *J. Electroanal. Chem. Interfacial Electrochem.* **1978**, *89*, 247-260.
- (16) Shoup, D.; Szabo, A. J. *Electroanal. Chem. Interfacial Electrochem.* **1984**, *160*, 19-26.
- (17) Cope, D. K.; Tallman, D. E. *J. Electroanal. Chem. Interfacial Electrochem.* **1986**, *205*, 101-123.

RECEIVED for review May 9, 1989. Accepted July 18, 1989. The authors acknowledge financial support of this work by the Committee for Institutional Studies and Research at Murray State University.

Hollow Fiber Membrane Probes for the in Situ Mass Spectrometric Monitoring of Nitrogen Trichloride Formation during Wastewater Treatment

P. J. Savickas,* M. A. LaPack, and J. C. Tou

The Dow Chemical Company, Analytical Sciences, 1897 Building, Midland, Michigan 48667

The utility of mass spectrometry in the broad field of process analytical chemistry and in situ analysis has grown steadily over the past few years (1, 2) with concurrent re-

finements in mass spectrometers and their inlet systems. In our case, these mass spectrometers are used for a variety of analyses (3, 4). The characteristic role is to apply its excellent

sensitivity, good selectivity, and real time data capabilities. The challenge, in diverse applications, is the development of appropriate interfaces and inlet systems. They must be rugged, reliable, sensitive, and applicable to a wide range of sample environments.

This communication deals with the utility of a hollow fiber membrane interface developed several years ago in our laboratory (5) and since modified for this application. Other researchers have discovered its utility and have found numerous applications (6-9). However, some chemical processes in an industrial setting test the limits of any sampling technology. High temperatures, low or high pressures, corrosive or caustic environments, and rapidly changing dynamic processes, along with the sheer size of some of the processes, make for interesting research.

We have examined the utility of a hollow fiber membrane probe interface in the monitoring of potential NCl_3 (nitrogen trichloride) formation during bleach chlorinolysis treatment of chemical waste streams containing ammonia or other nitrogen-containing species. NCl_3 is an explosively unstable compound that will detonate above its boiling point of 71 °C, when catalyzed by light, and at concentrations above about 2000 ppm (10, 11).

Real-time monitoring of the process is necessitated by the transient stability of NCl_3 . Common trap and off-line analysis methods would prove difficult to use and since we do not know when to expect any formation to occur, we need to monitor the process during all of its stages. Off-line methods would only be able to provide time-averaged data, perhaps across several significant events. Self-evident safety factors also exist. In general, the unstable nature of NCl_3 necessitates a sensitive, real time monitoring method.

While this communication will discuss the application of mass spectrometry to chlorinolysis waste treatment, the intent is to demonstrate the general utility of a silicone hollow fiber membrane probe with in situ mass spectrometry, rather than specifying reaction conditions for successful wastewater treatment.

EXPERIMENTAL SECTION

In Situ Mass Spectrometer. The mass spectrometer is an in-house built unit based on a Balzers QMG-511 quadrupole mass spectrometer. The mass scanning range of the instrument is 1-1023 amu. An off axis 17-stage discrete dynode electron multiplier is used for ion detection after ion energy filtering through a 90° electrostatic sector. A Balzers gastight ion source was used for this work.

The quadrupole mass spectrometer vacuum housing is evacuated by a 270 L/s Balzers turbopump backed by a 310 L/min Alcatel direct drive pump, which is also used for system roughing. All of the MS control electronics, vacuum systems and auxiliary electronics are housed in a cabinet that can be purged with inert gas for hazardous area work. An explosion-proof roughing pump is located outside of the cabinet and cooling is provided by an external Neslab CFT-75 recirculating coolant refrigerator system (Forstmouth, NH). Cooling of the cabinet is necessary due to heat buildup by the electronics and turbopump.

The QMG-511 mass spectrometer is operated either by manual means or by computer. The data system is a DEC PDP 11/23 based system using two RL01 disk drives. In-house-written software was used to control all functions of the mass spectrometer. I/O between the computer and mass spectrometer occurred through a parallel communications cable which may be up to 300 m in length. In this study, due to the explosion potential of the experiment, the computer and operator were stationed in an office area about 15 m away from the mass spectrometer and chemical reactor. The separate coolant refrigerator was placed near the mass spectrometer. The mass spectrometer itself was positioned just outside the lab hood which houses the chemical reactor.

Chemical Reactor. The chlorinolysis experiments were performed with a bench scale reactor inside a flow hood. A 1-L round-bottomed flask reactor was equipped with a side arm

take-off, mechanical stirrer, reflux condenser, thermometer, combination pH electrode, and feed ports for adding waste feed, 10% NaOCl bleach solution, 15% NaOH, and 15% HCl. The acid and base provide pH control as needed. The pH was measured by the combination electrode and an automatic control circuit measured the caustic and acid into the reactor with calibrated FMI fluid metering pumps. An infrared heating lamp and temperature regulator circuit were also utilized to achieve temperature control.

Two modes of operations were studied, batch versus continuous chlorination. In the batch run, 350 mL of organic waste adjusted to pH 7 was heated to 100 °C. The pH control was started and adjusted to typically pH 5.5. The automatic pH controller maintains this value throughout the run. Normal operation involves the addition of caustic, as HCl was evolved during the process. At this point the bleach flow was started and added as fast as possible without venting any chlorine. Grab samples were taken at regular intervals to determine the chlorine concentration in solution by iodimetric titration. The bleach flow rate was adjusted accordingly to maintain a constant amount of chlorine, typically 1000 ppm, in solution. The reaction reached its end point when the chlorine concentration was seen to rise.

In the continuous mode of operation waste and bleach are added continuously. The feed rates are adjusted to allow several reactor turnovers before allowing the contents to flow out through a side port. Batch operations are usually preferred for small scale processes where not enough waste is being generated to sustain a continuous mode of operation.

Hollow Fiber Probe. Sampling of the chemical process occurred at two points. One monitor was set at the vent of the reflux condenser and the second was placed directly inside the reactor headspace. The reactor environment is 100 °C water saturated with high concentrations of Cl_2 and HCl gases along with CO_2 , chlorinated organics, and other byproducts of the chlorinolysis reaction. Due to the harsh operating conditions present during the reaction, research was performed to find a suitable sample inlet system, detailed below.

The species of prime interest was any detectable NCl_3 being formed. NCl_3 concentrations of a few thousand parts per million are explosive. To guarantee a suitable safety margin, our detection limit must be much lower. To ensure proper operation of the mass spectrometer, the large background from water vapor must be eliminated and high vacuum maintained.

A molecular leak probe, consisting of a quartz tube collapsed to a fine 10- μm hole size, was tried for sampling. However, too much water was let into the instrument vacuum system which raises the operating pressure and water background unacceptably high. The molecular leak probe suffered also from condensation of liquids on the probe tip. Drops formed or splashed there during reaction monitoring plugged the micrometer orifice and gave unstable signals.

With hollow fiber probes, factors such as the membrane material's area, thickness, and temperature can often be varied to find suitable characteristics. A non-cross-linked silicon polymer hollow fiber (Dow Corning non-cross-linked silicon medical tubing 0.008 in. o.d., 0.007 in. i.d.) has been found in the past (5) to provide fast response and excellent separation of organics from water. A sample probe was devised from this material. The open ends of two 3 cm lengths of tubing were looped and sealed into the end of a 1/4 in. o.d. Pyrex tube with Dow Corning 721 RTV silastic adhesive. The opposite end of the Pyrex tube was connected to the mass spectrometer ion source vacuum system via 1/4 in. o.d. Teflon tubing. In this manner the inside of the hollow fibers is held under vacuum while the exterior is exposed to the sample environment. Volatile organics soluble in the fiber materials pass through the probe and into the mass spectrometer ion source. Air and water, being generally less soluble in the polymer material, are thereby greatly excluded (5).

The non-cross-linked silicone polymer hollow fiber probe was initially evaluated by sampling air over an Erlenmeyer flask of boiling water. This would test the vacuum attainable as well as the stability of the probe which to date had only been used to sample systems up to 60 °C (12, 13). Vacuum system pressures from the non-cross-linked silicone polymer probe were totally unacceptable at temperatures higher than 75 °C. At 100 °C the probe material swells open to the point that pumping directly

Table I. Positive Ion Electron Impact Mass Spectrum of NCl_3

m/e	rel abund	ion species
49	54	N^{35}Cl^+
51	18	N^{37}Cl^+
84	100	$\text{N}^{35}\text{Cl}_2^+$
86	65	$\text{N}^{35}\text{Cl}^{37}\text{Cl}^+$
88	10	$\text{N}^{37}\text{Cl}_2^+$
119	5	$\text{N}^{35}\text{Cl}_3^+$
121	5	$\text{N}^{35}\text{Cl}^{37}\text{Cl}_2^+$

on the probe with a 195 L/min Alcatel vacuum pump could not keep the pressure below 100 Torr (uncorrected). Additionally the swelled hollow fibers were found to be easily broken; mild shocks tended to tear open the fiber material, venting the vacuum system. This system would be unlikely to survive any bumping, splattering, or explosions of NCl_3 potentially expected in this study.

Several different designs of supported hollow fiber probes were evaluated. The non-cross-linked material was dissolved in toluene and applied to a variety of frit glass and stainless steel screen probe designs. Although these systems did prove more physical stability to the probe, the problem of poor vacuum still existed. A much thicker material probe was considered, but rejected based on the conclusion that response times would be too slow compared to the real time needs of monitoring for an explosive material.

A cross-linked silicone polymer hollow fiber (Dow Corning Silastic medical grade tubing 0.02 in. i.d., 0.025 in. o.d.) was tried next in the above described loop design. Cross-linking is done by the manufacturer to add strength to the material. The cross-linked material response time was found in the past to be longer and, therefore, less desirable than for the non-cross-linked material (5, 14). But, a cross-linked silicone polymer probe was found to perform well in the water vapor test. Vacuum pressure at 100 °C over boiling water was about 10 μm (uncorrected) for a single loop design. This was very close to the absolute pressure attainable with this pump. The material was also seen to be physically tougher, able to resist knocks without tearing. To test stability to an acidic environment, the probe was exposed to concentrated vapors of HCl just inside the neck of an open bottle of HCl acid for 30 min. These experiments produced no noticeable effect on the probe. The RTV silastic adhesive used to seal the fiber into the probe body showed excellent sealing and stability properties under both of these tests and after a few days of curing, a negligible background. A double loop probe of the above design was built for insertion into the reaction vessel. A second probe was fashioned to sample the relatively low concentration sample region at the vent of the reflux condenser. At this point the headspace vapor should be near ambient temperature and most of the organic vapors condensed out. A non-cross-linked fiber was used here for its fast response and greater sensitivity. The probe was of similar design to the above concept. One end of five hollow fibers was set with adhesive into a $1/4$ in. stainless steel tube. The free ends were sealed with a dab of adhesive. Either probe could be sampled by a system of valves and a pump that kept the unsampled probe under vacuum.

DISCUSSION

Table I lists the mass spectrum of nitrogen trichloride obtained from an internal source. Since no provision is made for chromatographic separation of the various chemical species, we must choose characteristic ions to monitor. m/z 84 (NCl_2^+) is the base peak in the mass spectrum and is the logical choice for sensitive real time monitoring. However, it suffers from several direct mass interferences from chlorinated hydrocarbon fragments we would expect to see in the chlorinolysis of organic wastes (CH_2Cl_2^+ , $\text{C}^{35}\text{Cl}^{37}\text{Cl}^+$, etc). Lower mass fragments were considered but rejected due to the increased problems of interferences. The NCl_3 parent ions at m/z 119 and 121, though at weaker intensity than the base peak, could provide a unique pattern for identification. Most simple chlorinated hydrocarbon species would give a strong m/z 117 ion while NCl_3 would not. Thus the presence of m/z 84 and 119 peaks

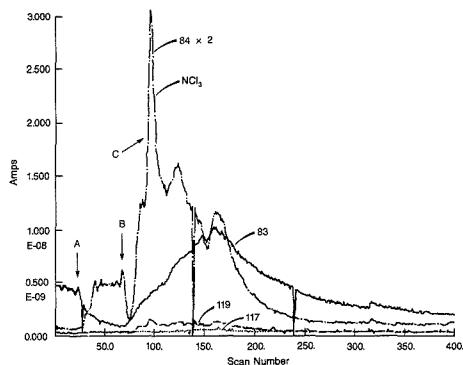


Figure 1. Selected ion plot for bleach reaction with 0.1% ammonia solution: (A) start of bleach flow; (B) end of oxidation reaction; (C) NCl_3 surge.

without corresponding increase of m/z 117 was used as a criterion for the presence of NCl_3 .

Those ions were monitored during the analysis, but to provide full information in case the spectra were complicated, the mass spectra were scanned from 10 to 300 amu. The data system allowed us to scan the low mass part of the spectrum, 10–75 amu, at low sensitivity and the 75–300 amu range at high sensitivity by changing the multiplier voltage in between.

Preliminary experiments, accomplished by injecting small amounts of chlorinated organics into the reactor vessel, showed system response time to be about 5–10 s and with part per million sensitivities. We saw no reason to pursue sensitivity studies with NCl_3 , lacking a new standard, and since the explosive concentration is reportedly a few percent in air. Relative sensitivity for NCl_3 is expected to be equivalent to similar chlorinated hydrocarbons.

The reactions of dilute aqueous solutions of chlorine and ammonia are very complex but have been studied extensively (15–17). In order to better understand the conditions under which NCl_3 might be formed under chlorinolysis of organic wastes in our system, several model experiments were performed using 0.5% ammonia solutions (from NH_4Cl) in water. A 350-mL aliquot of ammonia solution, in the previously described batch mode system, was substituted at pH 5.5 and 100 °C before the start of the mass spectral data accumulation. Figure 1 shows a selected ion plot of the reaction sequence obtained from the reaction flask probe. m/z 84 is plotted at 2 \times normal intensity to more clearly show its behavior above the other plotted ions. NCl_3 forms and degrades very rapidly in the headspace. At a molar ratio of bleach/ NH_3 equal to about 3, a surge of NCl_3 is seen. From the figure the m/z 84 and 119 peaks are seen to surge at point C while the m/z 117 peak remains flat. By the above criteria, this indicates the presence of NCl_3 .

Figure 2 shows a typical mass spectrum at the greatest yield of NCl_3 . The spectrum shows a good match for the earlier standard spectrum. The small, higher-mass peaks are identified to be from the decomposition of the exposed 1 cm^2 surface of a rubber stopper used to hold the pH probe. The stopper was only exposed to the headspace vapors but was severely corroded and was replaced by a glass feed-through in later experiments. This gives a feel for the severe conditions in the reactor.

Another series of trial runs was performed in which the reactor was run in a continuous feed mode. The 0.5% ammonia solution, used to represent a waste stream, was continuously fed into the reactor along with the bleach solution. The reactor was initially loaded with waste and adjusted to

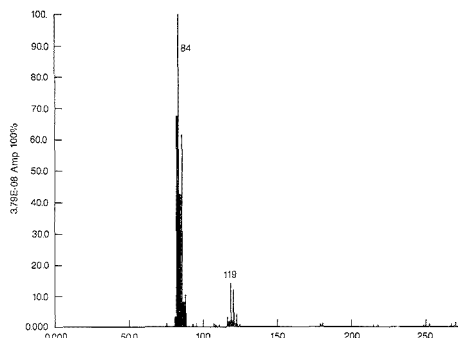


Figure 2. Mass spectrum of NCl_3 above m/z 75.

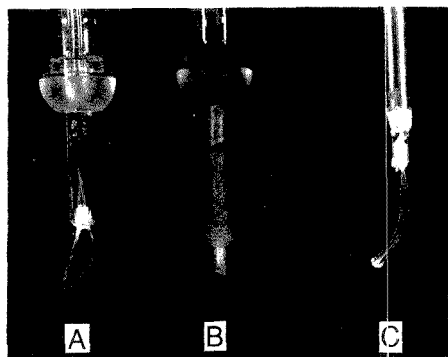


Figure 3. Photograph of probes used in chlorinolytic reaction: (A) Cross-linked probe from reactor headspace; (B) non-cross-linked probe from reactor vent exposure to reactor system; (C) non-cross-linked probe for comparison to B above.

pH 5.5 and 100 °C. The waste and bleach solutions were started simultaneously. Product was allowed to escape through the side arm of the reactor. Feed and exhaust rates were adjusted to ensure several reactor turnovers to occur. The chlorine concentration in solution was determined by periodic grab samples and the bleach flow was adjusted to keep the concentration at 1000 ppm. For this test the run continued at pH 5.5 for 2 h and was lowered to pH 4 for 20 min with a $[\text{Cl}_2] = 800$ ppm then to pH 2.0–2.5 $[\text{Cl}_2] = 100$ ppm for 30 min. The pH was then raised to pH 6 for 60 min $[\text{Cl}_2] = 1000$ ppm and then shut down. In situ monitoring of the entire sequence showed no build up of NCl_3 such as had been seen in the batch mode of operation. Since the solubility of chlorine in water is very low at a pH less than 4, the reactor headspace and vent were exposed to high concentrations of chlorine gas for an extended period of time. The cross-linked hollow fiber probe worked admirably under these conditions, and at the end of the experiment showed no signs of deterioration. The non-cross-linked probe above the condenser vent suffered traumatic failure however. Figure 3 is a photograph of the probes used in this experiment. Probe A with a body of Pyrex glass was the one used in the reactor headspace. No signs of deterioration were apparent, even after this work and dozens of more hours of testing. Probe B with a 316 stainless steel body was the one from the reactor vent after the above reaction sequence. For comparison a similar design probe, of the same material and makeup, though with a glass shaft, is shown as C. The non-cross-linked material had become stiff and fragile and indeed had snapped off upon removal from

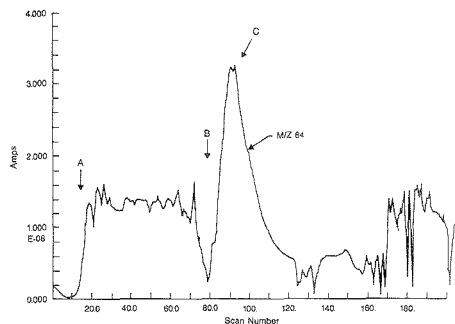


Figure 4. Selected ion plot chlorinolytic reaction: (A) start of bleach flow; (B) end of oxidation reaction; (C) NCl_3 buildup.

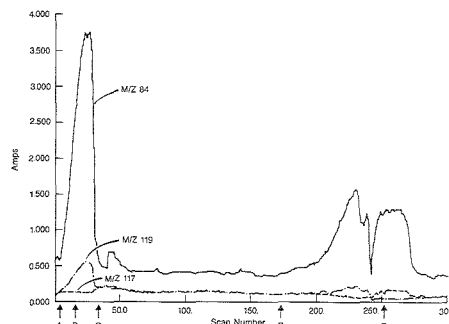


Figure 5. Selected ion plot of temperature upset during continuous bleach chlorinolytic: (A) heating lamp failure; (B) brine feed off; (C) heating lamp fixed, feed back on; (D) heating lamp turned off; (E) heating lamp turned back on.

the reactor. The RTV Silastic both in the vent and headspace showed good stability. The type 316 stainless steel body and the probe shows marked deteriorations too. Further probe bodies were made of glass.

Experiments were next performed that used synthetic waste samples containing 500–1000 ppm total organic carbon (TOC), mostly nitrogen-containing species. In a batch mode operation, Figure 4, similar to the experiment using an ammonia solution, a surge of NCl_3 is seen at a point when the oxidation reaction is essentially complete and the chlorine is building up in solution. Similarly, a test of the reactor in the continuous mode at pH values ranging from 2.0 to 10 showed no NCl_3 formation. The specific ion–time curve is essentially similar to the above model experiment.

A final experiment was performed to test the importance of the reactor temperature control and shows the utility of in situ monitoring. Figure 5 shows a specific ion–time curve from an intermediate time in a continuous chlorination reaction where the heating lamp was shut off to allow the temperature to drop to 85–90 °C. At around this point is seen a large upsurge of NCl_3 in the headspace. The reactor feed immediately was shut down and the lamp turned back on for fear of an explosion, though none occurred. After reequilibration of the system, the experiment was duplicated a few minutes later as shown in the figure. Again the NCl_3 concentration was seen to rise with a decrease in temperature and to fall when temperature equilibrium was again established. It is suggested that the phenomenon occurs due to a complex change in the solubilities of key intermediates in the NCl_3 formation. These complexities were forecast, thus necessitating the need for in situ monitoring. Regardless of the

mechanism, it can be seen that the hollow fiber probe and in situ mass spectrometer can be successfully used to monitor these harsh reactor conditions for an explosive material with good long-term performance from the probe and mass spectrometer.

ACKNOWLEDGMENT

The work of Karl Krümel in this project is gratefully acknowledged.

Registry No. NCI_3 , 10025-85-1; water, 7732-18-5.

LITERATURE CITED

- (1) Collis, J. B.; Illman, D. L.; Kowalski, B. R. *Anal. Chem.* **1987**, *59*, 624A.
- (2) Meuzelaar, H. L. C.; Windig, W.; Huff, S. M.; Richards, J. M. *Anal. Chim. Acta* **1988**, *190*, 119.
- (3) Kallos, G. J.; Tou, J. C. *Environ. Sci Technol.* **1977**, *11*, 1101.
- (4) Tou, J. C.; Reddy, D. Presented at 35th ASMS Conference on Mass Spectrometry and Allied Topics, Denver, 1987; *Anal. Chim. Acta*, in press.
- (5) Westover, L. B.; Tou, J. C.; Mark, J. H. *Anal. Chem.* **1974**, *46*, 568.
- (6) Bier, M. E.; Cooks, R. G. *Anal. Chem.* **1987**, *59*, 597.
- (7) Hwang, H.; Dasgupta, P. K. *Anal. Chem.* **1987**, *59*, 1356.
- (8) Brodbelt, J. S.; Cooks, R. G. *Anal. Chem.* **1985**, *57*, 153.
- (9) Brodbelt, J. S.; Cooks, R. G.; Tou, J. C.; Kallos, G. J.; Dryzga, M. R. *Anal. Chem.* **1987**, *59*, 454.
- (10) *Dangerous Properties of Industrial Materials*; Sax, N. I., Ed.; Von Nostrand Reinhold: New York, 1984.
- (11) Schliesinger, G. G. *Chem. Eng. News* **1966**, *44*, 46.
- (12) Tou, J. C.; Westover, L. B.; Sonnabend, L. F. *J. Phys. Chem.* **1974**, *78*, 1096.
- (13) Tou, J. C.; Westover, L. B.; Sonnabend, L. F. *Am. Ind. Hyg. Assoc. J.* **1975**, 374.
- (14) Crummett, W. B.; Tou, J. C.; Cortes, H. J.; Fawcett, T. G.; Kallos, G. J.; Martin, S. J.; Putzig, C. L.; Turkelson, V. T.; Yurga, L.; Zakett, D. *Talanta* **1989**, *36*, 63.
- (15) Frazier, S. E.; Sesler, H. H. *Chloramination Reactions, Benchmark Papers in Inorganic Chemistry/6*; Dowden, Hutchinson and Ross, Inc.: PA, 1977.
- (16) White, G. C. *Handbook of Chlorination*; Van Nostrand Reinhold: New York, 1972.
- (17) Corbett, R. E.; Metcalf, W. S.; Soper, F. G. *J. Chem. Soc.* **1953**, *45*, 1927.

RECEIVED for review March 16, 1989. Accepted July 19, 1989.

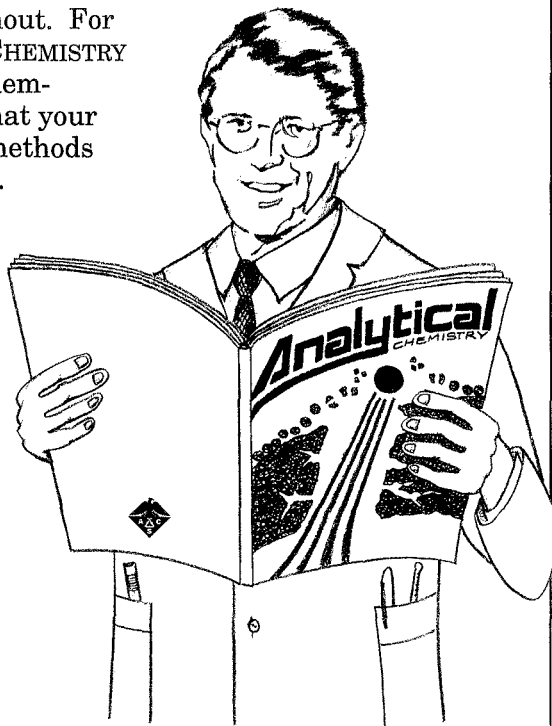
When you're confronted
with a specific "need to know"...

Analytical CHEMISTRY

Every chemist knows, having the most up to date information is essential for success. And, in the vital field of measurement science, ANALYTICAL CHEMISTRY is the one publication you cannot do without. For over sixty years, ANALYTICAL CHEMISTRY has proven to be a useful problem-solving resource, no matter what your specialty. And now, it covers methods used in the biotechnology field.

Publishing information that will help you deal more skillfully with problems such as sampling, data analysis and methodology—the papers in today's twice monthly ANALYTICAL CHEMISTRY cover real world problems involving trace analysis of air, water, soil, materials, drugs, and biopolymers.

Call now and reserve your own personal subscription.



Volume 61 (1989)	U.S.	Canada and Mexico	Europe Air-Service Included	All Other Countries Air-Service Included
ACS Member - 1 year	\$ 27	\$ 56	\$ 83	\$120
2 years	\$ 45	\$103	\$157	\$231
Nonmember	\$ 49	\$ 78	\$155	\$192

Member rates are for personal use only. Subscriptions may start any month of the year and expire one year later. Foreign payment must be made in U.S. currency by international money order, UNESCO coupons, or U.S. bank draft, or order through your subscription agency. For nonmember rates in Japan, contact Maruzen Co., Ltd. This publication is available on microfilm, microfiche, and the full text is available online on STN International.

**Call Toll-Free
1-800/227-5558
for credit card orders**

or write:

**American Chemical Society
Marketing Communication Dept.
1155 Sixteenth Street N.W.
Washington D.C. 20036**

Finally, a real GC/MS for under \$50,000!

HP 5890 Series II GC sets new industry standards with high temperature operation, cool-on-column injection and pressure programming.

MS ChemStation (DOS series) is 386-based to provide speed and multitasking for highest lab productivity.

Sensitive, universal and specific, the HP 5971A MSD produces true EI spectra even from dirty, complex matrices.



Complete quadrupole GC/MS system actually fits on a five-foot lab bench.

Mouse interface simplifies operation.

Now any lab can afford a GC/MS with an HP mass selective detector (MSD). Our new PC-controlled system costs only \$49,770*, yet gives you high performance.

There's multitasking for acquiring and analyzing data simultaneously. There's true, classical EI spectra that stand up to challenge. There's Microsoft® Windows software

for ease of use. Plus access to PC word processing, spreadsheets and desktop publishing. And for total automation, you can add an optional autosampler and bar-code reader.

Put the system to work in *any* size laboratory. Even network it to other vendors' data systems. Then enjoy the highest uptime in

the industry because HP is consistently rated number 1 for reliability, service and support. For more, call **1 800 556-1234, Ext. 10218**. In CA, **1 800 441-2345, Ext. 10218**.

*US list price
Microsoft® is a US registered trademark of Microsoft Corporation.



**HEWLETT
PACKARD**